

Cardiometabolic diseases and inflammatory responses

Edited by

Nadine Suffee, Wilfried Le Goff and
Jianmin Chen

Published in

Frontiers in Immunology



FRONTIERS EBOOK COPYRIGHT STATEMENT

The copyright in the text of individual articles in this ebook is the property of their respective authors or their respective institutions or funders. The copyright in graphics and images within each article may be subject to copyright of other parties. In both cases this is subject to a license granted to Frontiers.

The compilation of articles constituting this ebook is the property of Frontiers.

Each article within this ebook, and the ebook itself, are published under the most recent version of the Creative Commons CC-BY licence. The version current at the date of publication of this ebook is CC-BY 4.0. If the CC-BY licence is updated, the licence granted by Frontiers is automatically updated to the new version.

When exercising any right under the CC-BY licence, Frontiers must be attributed as the original publisher of the article or ebook, as applicable.

Authors have the responsibility of ensuring that any graphics or other materials which are the property of others may be included in the CC-BY licence, but this should be checked before relying on the CC-BY licence to reproduce those materials. Any copyright notices relating to those materials must be complied with.

Copyright and source acknowledgement notices may not be removed and must be displayed in any copy, derivative work or partial copy which includes the elements in question.

All copyright, and all rights therein, are protected by national and international copyright laws. The above represents a summary only. For further information please read Frontiers' Conditions for Website Use and Copyright Statement, and the applicable CC-BY licence.

ISSN 1664-8714
ISBN 978-2-8325-4265-1
DOI 10.3389/978-2-8325-4265-1

About Frontiers

Frontiers is more than just an open access publisher of scholarly articles: it is a pioneering approach to the world of academia, radically improving the way scholarly research is managed. The grand vision of Frontiers is a world where all people have an equal opportunity to seek, share and generate knowledge. Frontiers provides immediate and permanent online open access to all its publications, but this alone is not enough to realize our grand goals.

Frontiers journal series

The Frontiers journal series is a multi-tier and interdisciplinary set of open-access, online journals, promising a paradigm shift from the current review, selection and dissemination processes in academic publishing. All Frontiers journals are driven by researchers for researchers; therefore, they constitute a service to the scholarly community. At the same time, the *Frontiers journal series* operates on a revolutionary invention, the tiered publishing system, initially addressing specific communities of scholars, and gradually climbing up to broader public understanding, thus serving the interests of the lay society, too.

Dedication to quality

Each Frontiers article is a landmark of the highest quality, thanks to genuinely collaborative interactions between authors and review editors, who include some of the world's best academicians. Research must be certified by peers before entering a stream of knowledge that may eventually reach the public - and shape society; therefore, Frontiers only applies the most rigorous and unbiased reviews. Frontiers revolutionizes research publishing by freely delivering the most outstanding research, evaluated with no bias from both the academic and social point of view. By applying the most advanced information technologies, Frontiers is catapulting scholarly publishing into a new generation.

What are Frontiers Research Topics?

Frontiers Research Topics are very popular trademarks of the *Frontiers journals series*: they are collections of at least ten articles, all centered on a particular subject. With their unique mix of varied contributions from Original Research to Review Articles, Frontiers Research Topics unify the most influential researchers, the latest key findings and historical advances in a hot research area.

Find out more on how to host your own Frontiers Research Topic or contribute to one as an author by contacting the Frontiers editorial office: frontiersin.org/about/contact

Cardiometabolic diseases and inflammatory responses

Topic editors

Nadine Suffee — Sorbonne Universités, France

Wilfried Le Goff — Institut National de la Santé et de la Recherche Médicale (INSERM), France

Jianmin Chen — Queen Mary University of London, United Kingdom

Citation

Suffee, N., Le Goff, W., Chen, J., eds. (2024). *Cardiometabolic diseases and inflammatory responses*. Lausanne: Frontiers Media SA.

doi: 10.3389/978-2-8325-4265-1

Table of contents

- 05 **Association of the systemic immune-inflammation index (SII) and clinical outcomes in patients with stroke: A systematic review and meta-analysis**
Yong-Wei Huang, Xiao-Shuang Yin and Zong-Ping Li
- 18 **Role of inflammation, immunity, and oxidative stress in hypertension: New insights and potential therapeutic targets**
Zenglei Zhang, Lin Zhao, Xingyu Zhou, Xu Meng and Xianliang Zhou
- 36 **Single-cell atlas reveals different immune environments between stable and vulnerable atherosclerotic plaques**
Peicong Ge, Hao Li, Xiaolong Ya, Yiqiao Xu, Long Ma, Qiheng He, Rong Wang, Zechen Liu, Qian Zhang, Yan Zhang, Wenjing Wang, Dong Zhang and Jizong Zhao
- 47 **Leukocyte cell population data in patients with cardiac surgery and cardiopulmonary bypass: A potential readily available tool to monitor immunity**
Maxime Nguyen, Laure Stiel, Adrien Guilloteau, Pierre-Alain Bahr, David Masson, Charles Thomas, Mathieu Blot, Julien Guy, Cécile Fontaine, Bastien Durand, Belaid Bouhemad and Pierre-Grégoire Guinot
- 56 **Characterization of early myocardial inflammation in ischemia-reperfusion injury**
Qihong Wu, Rong Xu, Kun Zhang, Ran Sun, Mengxi Yang, Kuan Li, Hanrui Liu, Yiyuan Xue, Huayan Xu and Yingkun Guo
- 68 **CD4⁺ T cells expressing CX3CR1, GPR56, with variable CD57 are associated with cardiometabolic diseases in persons with HIV**
Celestine N. Wanjalla, Curtis L. Gabriel, Hubaida Fuseini, Samuel S. Bailin, Mona Mashayekhi, Joshua Simmons, Christopher M. Warren, David R. Glass, Jared Oakes, Rama Gangula, Erin Wilfong, Stephen Priest, Tecla Temu, Evan W. Newell, Suman Pakala, Spyros A. Kalams, Sara Gianella, David Smith, David G. Harrison, Simon A. Mallal and John R. Koethe
- 90 **Occlusion preconditioned mice are resilient to hypobaric hypoxia-induced myocarditis and arrhythmias due to enhanced immunomodulation, metabolic homeostasis, and antioxidants defense**
Gabriel Komla Adzika, Richard Mprah, Ruqayya Rizvi, Adebayo Oluwafemi Adekunle, Marie Louise Ndzie Noah, Prosperl Ivette Wowui, Seyram Yao Adzraku, Joseph Adu-Amankwaah, Fengli Wang, Yuwen Lin, Lu Fu, Xiaomei Liu, Jie Xiang and Hong Sun

- 104 **Interactions between PCSK9 and NLRP3 inflammasome signaling in atherosclerosis**
Yanan Wang, Dan Fang, Qinzhi Yang, Jingcan You, Liqun Wang, Jianbo Wu, Min Zeng and Mao Luo
- 117 **T lymphocyte characteristics and immune repertoires in the epicardial adipose tissue of heart failure patients**
Xu-Zhe Zhang, Xian-Li Chen, Ting-Ting Tang, Si Zhang, Qin-Lin Li, Ni Xia, Shao-Fang Nie, Min Zhang, Zheng-Feng Zhu, Zi-Hua Zhou, Nian-Guo Dong and Xiang Cheng
- 128 **Presence of tophi and carotid plaque were risk factors of MACE in subclinical atherosclerosis patients with gout: a longitudinal cohort study**
Yu Wang, Xuerong Deng, Xiaohui Zhang, Yan Geng, Lanlan Ji, Zhibo Song and Zhuoli Zhang
- 140 **The positive association between white blood cell count and metabolic syndrome is independent of insulin resistance among a Chinese population: a cross-sectional study**
ZhongYu Ren, Shi Luo and Lian Liu
- 149 **Analysis of immunogenic cell death in ascending thoracic aortic aneurysms based on single-cell sequencing data**
Zemin Tian, Peng Zhang, Xinyang Li and Delong Jiang
- 160 **The role of circadian clock-controlled mitochondrial dynamics in diabetic cardiomyopathy**
Zhenshuai Jin, Yanwei Ji, Wating Su, Lu Zhou, Xiaojing Wu, Lei Gao, Junfan Guo, Yutong Liu, Yuefu Zhang, Xinyu Wen, Zhong-Yuan Xia, Zhengyuan Xia and Shaoqing Lei
- 174 **Circulating levels of cytokines and risk of cardiovascular disease: a Mendelian randomization study**
Tao Wei, Zhanfang Zhu, Lin Liu, Bo Liu, Min Wu, Wei Zhang, Qianwei Cui, Fuqiang Liu and Ronghuai Zhang
- 183 **Gut lumen-leaked microbial DNA causes myocardial inflammation and impairs cardiac contractility in ageing mouse heart**
Hong Gao, Ke Wang, Jorge A. Suarez, Zhongmou Jin, Karina Cunha e Rocha, Dinghong Zhang, Andrea Farrell, Tyler Truong, Yasemin Tekin, Breanna Tan, Hyun Suh Jung, Julia Kempf, Sushil K. Mahata, Wolfgang H. Dillmann, Jorge Suarez and Wei Ying



OPEN ACCESS

EDITED BY

Jianmin Chen,
Queen Mary University of London,
United Kingdom

REVIEWED BY

Bing Han,
Ronald Reagan UCLA Medical Center,
United States
Zilong Hao,
West China Hospital, Sichuan
University, China

*CORRESPONDENCE

Yong-Wei Huang
525654934@qq.com

[†]These authors have share first
authorship

SPECIALTY SECTION

This article was submitted to
Inflammation,
a section of the journal
Frontiers in Immunology

RECEIVED 05 November 2022

ACCEPTED 29 November 2022

PUBLISHED 15 December 2022

CITATION

Huang Y-W, Yin X-S, Li Z-P (2022)
Association of the systemic immune-
inflammation index (SII) and clinical
outcomes in patients with stroke: A
systematic review and meta-analysis.
Front. Immunol. 13:1090305.
doi: 10.3389/fimmu.2022.1090305

COPYRIGHT

© 2022 Huang, Yin and Li. This is an
open-access article distributed under
the terms of the [Creative Commons
Attribution License \(CC BY\)](#). The use,
distribution or reproduction in other
forums is permitted, provided the
original author(s) and the copyright
owner(s) are credited and that the
original publication in this journal is
cited, in accordance with accepted
academic practice. No use,
distribution or reproduction is
permitted which does not comply with
these terms.

Association of the systemic immune-inflammation index (SII) and clinical outcomes in patients with stroke: A systematic review and meta-analysis

Yong-Wei Huang^{1*†}, Xiao-Shuang Yin^{2†} and Zong-Ping Li¹

¹Department of Neurosurgery, Mianyang Central Hospital, School of Medicine, University of Electronic Science and Technology of China, Mianyang, Sichuan, China, ²Department of Immunology, Mianyang Central Hospital, School of Medicine, University of Electronic Science and Technology of China, Mianyang, Sichuan, China

Introduction: A novel systemic immune-inflammation index (SII) has been proven to be associated with outcomes in patients with cancer. Although some studies have shown that the SII is a potential and valuable tool to diagnose and predict the adverse outcomes in stroke patients. Nevertheless, the findings are controversial, and their association with clinical outcomes is unclear. Consequently, we conducted a comprehensive review and meta-analysis to explore the relationship between SII and clinical outcomes in stroke patients.

Methods: A search of five English databases (PubMed, Embase, Cochrane Library, Scopus, and Web of Science) and four Chinese databases (CNKI, VIP, WanFang, and CBM) was conducted. Our study strictly complied with the PRISMA (the Preferred Reporting Items for Systematic Reviews and Meta-Analyses). We used the NOS (Newcastle-Ottawa Scale) tool to assess the possible bias of included studies. The endpoints included poor outcome (the modified Rankin Scale [mRS] ≥ 3 points or > 3 points), mortality, the severity of stroke (according to assessment by the National Institute of Health stroke scale [NIHSS] ≥ 5 points), hemorrhagic transformation (HT) were statistically analyzed.

Results: Nineteen retrospective studies met the eligibility criteria, and a total of 18609 stroke patients were included. Our study showed that high SII is significantly associated with poor outcomes (odds ratio [OR] 1.06, 95% confidence interval [CI] 1.02-1.09, $P = 0.001$, $I^2 = 93\%$), high mortality (OR 2.16, 95% CI 1.75-2.67, $P < 0.00001$, $I^2 = 49\%$), and the incidence of HT (OR 2.09, 95% CI 1.61-2.71, $P < 0.00001$, $I^2 = 42\%$). We also investigated the difference in SII levels in poor/good outcomes, death/survival, and minor/moderate-severe stroke groups. Our analysis demonstrated that the SII level of the poor outcome, death, and moderate-severe stroke group was much higher than that of the good outcome, survival, and minor stroke group, respectively (standard mean difference [SMD] 1.11, 95% CI 0.61-1.61, $P < 0.00001$ [poor/

good outcome]; MD 498.22, 95% CI 333.18–663.25, $P < 0.00001$ [death/survival]; SMD 1.35, 95% CI 0.48–2.23, $P = 0.002$ [severity of stroke]). SII, on the other hand, had no significant impact on recanalization (OR 1.50, 95% CI 0.86–2.62, $P = 0.16$).

Discussion: To the best of our knowledge, this may be the first meta-analysis to look at the link between SII and clinical outcomes in stroke patients. The inflammatory response after a stroke is useful for immunoregulatory treatment. Stroke patients with high SII should be closely monitored, since this might be a viable treatment strategy for limiting brain damage after a stroke. As a result, research into SII and the clinical outcomes of stroke patients is crucial. Our preliminary findings may represent the clinical condition and aid clinical decision-makers. Nonetheless, further research is needed to better understand the utility of SII through dynamic monitoring. To generate more robust results, large-sample and multi-center research are required.

Systematic review registration: <https://www.crd.york.ac.uk/prospero/>, identifier CRD42022371996.

KEYWORDS

systemic immune-inflammation index, stroke, SII, clinical outcome, meta-analysis

Introduction

Cerebrovascular disease is the second majority cause of death and disability worldwide. Stroke, including ischemic and hemorrhagic, is the leading component of it. More than 2.4 million newly diagnosed strokes occur in China yearly, and the mortality rate has risen to 22.3% (1, 2). Of these patients, 87% are ischemic stroke (3). Therefore, assessing stroke patients' risk and severity early and identifying risk factors that can be addressed through intervention can improve the dismal outcomes for stroke patients (4).

In recent two years, Scholars progressively recognize the secondary injury of the brain's inflammatory response after stroke. A study by Kim et al. (5) has shown that inhibiting inflammatory cells could alleviate brain injury. Therefore, inflammatory factor-related immunotherapy may become a potential treatment to improve the outcomes of stroke patients (6).

Systemic immune inflammatory index (SII) has been used as a prognostic marker for some diseases. A meta-analysis by Zhang et al. has shown that elevated pretreatment SII was significantly associated with worse overall survival and recurrence-free survival/progression-free survival in with biliary tract cancers (7). SII based on platelets \times neutrophils/lymphocytes ($P \times N/L$) was reported to accurately predict outcomes in patients with venous sinus thrombosis (8). Two studies have shown that SII is related to the severity of stroke at

admission (9, 10), but this index has no wide application to predict functional outcomes in stroke patients. Although some studies have shown that the SII is a potential and valuable tool to diagnose and predict the adverse outcomes in stroke patients. Nevertheless, the findings are controversial, and their association with clinical outcomes is unclear. Consequently, we conducted a comprehensive review and meta-analysis to explore the relationship between SII and clinical outcomes in stroke patients.

Methods

Aims and PICO statement

Our study strictly complied with the PRISMA (the Preferred Reporting Items for Systematic Reviews and Meta-Analyses) statement. We registered our study at PROSPERO with the identifier CRD42022371996 (<https://www.crd.york.ac.uk/PROSPERO/>) (11). The PRISMA checklist is presented in **Supplemental Table 1**. These were the PICO statements: 1) Population: patients who have had an ischemic or hemorrhagic stroke (also known as an ICH). 2) Intervention: mechanical thrombectomy, intravenous thrombolysis, or none of the above. 3) Comparisons: relative low SII vs. relative high SII, and the grouping definition is the same as our previous study (12). 4) Outcomes: the mRS ≥ 3 points or > 3 points at follow-up

was defined as poor outcome, and we categorized stroke severity as NIHSS ≥ 5 points. In AIS patients, symptomatic intracerebral hemorrhage was considered hemorrhagic transformation (HT). Besides, mortality and the SII level of the poor/good outcome and death/survival groups were also extracted.

Literature search strategy

In order to decrease the selectivity bias, a search of five English databases (PubMed, Embase, Cochrane Library, Scopus, and Web of Science) and four Chinese databases (CNKI, VIP, WanFang, and CBM) was conducted. Two reviewers (Huang YW and Yin XS) systematically screened the databases for the relevant studies published from databases inception to the end of November 2022. The following search strategy was applied: (“systemic immune-inflammation index” OR “SII”) AND (“stroke”) for English databases, and “(主题=全身炎症免疫指数) AND (主题=卒中)” for Chinese databases. The detailed search strategy is presented in [Supplemental Table 2](#). We also comprehensively searched the main clinical registry centers such as ClinicalTrials.gov, WHO-ICTRP, and ChiCTR for unpublished works and gray literature in GreyNet, OpenSIGLE, and HMIC databases. The purpose is to decrease the publication bias as far as possible.

Inclusion and exclusion criteria

After the inclusion and exclusion criteria, all potential studies were appraised independently by two reviewers (Huang YW and Yin XS). The reviewers assessed studies that met all the following criteria: 1) types of publication: articles published publicly without language restriction. 2) types of participants: stroke patients with complete data. 3) types of comparison: relative low SII vs. relative high SII. 4) types of outcome measure: poor outcome, the severity of the stroke, mortality, HT, and the SII level of poor/good outcome group, death/survival group. Case reports, reviews, notes, meta-analyses, editorials, letters to the editor, commentaries, and conference abstracts were excluded.

Data extraction

Two reviewers extracted data independently and used the same tables of data extraction. The extracted data were as follows: 1) essential characteristics: first author name, publication year, nation, study design, and participant count (n); 2) participant characteristics: age(y) (Mean \pm SD), male (%), type of stroke, medical history, medication history, time of blood sample, laboratory test method, type of intervention, cutoff of SII, primary endpoints, and clinical follow-up (d); 3) information on interesting results, etc.

Risk of bias assessment

To evaluate the possible bias of the included research, we used the NOS (Newcastle-Ottawa Scale) method ([13](#)). The three aspects of the method based on NOS were described in [Supplemental Table 3](#) and [Table 1](#), together with the specifics and outcomes for each. Studies were scored on a scale of one to nine, with over six scores being regarded to be of excellent quality. The evaluation was carried out separately by three reviewers (Huang YW, Yin XS, and Li ZP). Any disagreement was settled, if necessary, in a group investigation discussion.

Statistical analysis

For dichotomous variables, odds ratios (ORs) and their corresponding 95% confidence interval (CIs) were calculated. Mean difference (MD) and their corresponding 95% CIs were calculated for continuous variables. If the values of some continuous variable varied greatly, we utilized standard mean difference (SMD) to perform the meta-analysis. Besides, we extracted the ORs adjusted by confounding factors and their corresponding 95% CIs in some studies. The confounding factors of each study were provided in [Supplemental Table 4](#). We estimated the mean and standard deviation (SD) by the sample size, median, and interquartile range. The optional estimating methods were from Luo et al. ([31](#)) and Wan et al. ([32](#)). The website is <https://www.math.hkbu.edu.hk/~tongt/papers/median2mean.html>. To account for clinical heterogeneity, we conducted meta-analyses and subgroup analyses using the random-effects or fixed-effects model ([33](#)). The Cochrane Q test was used to evaluate the heterogeneity ($P < 0.1$ or $I^2 > 50\%$ was significant heterogeneity) ([34](#)). $P < 0.05$ was statistically significant. Specific data of the high SII and low SII groups were extracted from the studies based on our grouping definition. The publication bias was assessed by funnel plot. We performed the statistical analyses by Review Manager software (version 5.3.3; <https://training.cochrane.org/online-learning/core-softwarecochrane-reviews/revman>).

Results

The primary search in English databases yielded 469 records. Two hundred twenty-four duplicates were excluded, and 245 remained. Two hundred twenty-two records were further excluded after title/abstract and publication type screening. Then, 23 potentially eligible articles were retained for full-text assessment, and six were excluded for insufficient data, theme, endpoints, and groupings. Besides, we manually searched the Chinese databases, and two articles met the included criteria. Finally, 19 studies ([9, 10, 14–30](#)) met the eligibility criteria, and a number of 18609 stroke patients were involved. All the studies

TABLE 1 The baseline characteristics of included studies.

Author	Year	Nation	Study Design	Participants (n)	Age (y) (mean \pm SD)	Male (%)	Type of Stroke	Medical History	Medication History	Time of Blood Sample	Laboratory Test Method	Type of Intervention	Cutoff of SII	Primary Endpoints	Follow-up (d)	NOS
Chu et al. (14)	2020	Taiwan, China	Retrospective Single-center	415	70.7 \pm 13.5	61.69	AIS	①②③ ⑤⑥⑦⑧	–	On arrival in the emergency room	Full blood	–	651.00	PO	–	9
Trifan et al. (15)	2020	America	Retrospective Single-center	239	58.1 \pm 3.2	56.90	ICH	①② ⑪⑫⑬⑭⑮	Aspirin Clopidogrel Anti-hypertensive Statins	On arrival in the hospital	–	–	730.00	PO	discharge	8
Hou et al. (9)	2021	China	Retrospective Single-center	362	67.8 \pm 12.2	67.40	AIS	①②④	–	The following day (6:00 am), after admission	Full blood	–	–	Stroke severity	–	9
Li et al. (16)	2021	China	Retrospective Single-center	291	57.0 \pm 14.0	66.67	ICH	–	–	During hospitalization	–	–	1700.00	PO	90 d	7
Weng et al. (17)	2021	China	Retrospective Single-center	216	67.8 \pm 3.5	62.96	AIS	①②③ ④⑤⑥	–	The first 24 h	–	IVT	545.14	PO	90 d	8
Yang et al. (18)	2021	China	Retrospective Single-center	310	65.0 \pm 11.4	72.58	AIS	①②③⑫	Anti-platelet Anti-coagulation	Next morning (5:00 am) after admission	–	–	653.65	HT	–	9
Yi et al. (19)	2021	Korea	Retrospective Single-center	440	70.0 \pm 12.9	58.41	AIS	①②④ ③⑨⑫	–	On admission	Peripheral venous blood	MT	853.00	PO	90 d	8
Acar et al. (20)	2022	Turkey	Retrospective Single-center	123	66.5 \pm 12.0	52.85	AIS	①②④ ⑤⑨⑫	Anti-platelet Anti-coagulation	At admission to emergency room	Venous blood	EVENT	1690.00	PO Cerebral reperfusion	90 d	8
Adiguzel et al. (21)	2022	Turkey	Retrospective Single-center	205	71.0 \pm 15.0	41.46	AIS	①② ④⑫⑬⑭⑮	–	The first 14 days	–	–	–	Mortality PO Pneumonia	90 d	7
Chen et al. (22)	2022	Taiwan, China	Retrospective Single-center	3402	71.9 \pm 2.8	57.58	AIS	①②④⑤ ⑥⑦⑧⑫	–	Within 24 h of admission	–	IVT or EVT	2120.00 (IHIS) 1051.00 (OHIS)	Mortality PO	discharge	7
Hsu et al. (23)	2022	Taiwan, China	Retrospective Single-center	374	65.4 \pm 17.8	64.44	ICH	①②③⑥	–	On arrival at the emergency room	Full blood	–	–	PO Mortality	discharge	8
Huang et al. (10)	2022	China	Retrospective Single-center	234	68.9 \pm 3.7	50.43	AIS	①②④	Anti-platelet Anti-coagulation	Within 24 h of admission	Venous blood	–	1008.00	Stroke severity	discharge	9
Ji et al. (24)	2022	China	Retrospective Single-center	675	67.1 \pm 11.4	59.56	AIS	①②④	–	Within the first 24h after admission	–	EVENT	2140.00	PO	90 d	9
Wang et al. (25)	2022	China	Retrospective Multi-center	9107	61.9 \pm 11.1	69.65	AIS	①②④ ⑨⑫⑬⑭	–	Within 24 h after admission	venous blood	–	–	Mortality PO Recurrent stroke	90 d 1 y	7

(Continued)

TABLE 1 Continued

Author	Year	Nation	Study Design	Participants (n)	Age (y) (mean \pm SD)	Male (%)	Type of Stroke	Medical History	Medication History	Time of Blood Sample	Laboratory Test Method	Type of Intervention	Cutoff of SII	Primary Endpoints	Follow-up (d)	NOS
Wu et al. (26)	2022	China	Retrospective Multi-center	1181	69.1 \pm 15.6	50.80	AIS	①②③ ④⑧⑪②⑩	Warfarin NOAH Anti-platelet	The first test after entering the ICU	–	–	–	Mortality	30 d 90 d	7
Yang et al. (27)	2022	China	Retrospective Single-center	379	70.8 \pm 3.5	52.51	AIS	①②③④	Statin Anti-thrombotic	On admission	–	IVT & EVT	–	HT	–	8
Zhou et al. (28)	2022	China	Retrospective Single-center	208	63.3 \pm 11.3	68.75	AIS	①②④⑤	–	Within 24 h	Routine blood	–	802.8	Stroke severity PO	90 d	9
Zhu et al. (29)	2022	China	Retrospective Single-center	182	39.4 \pm 6.8	83.52	AIS	①②	–	Within 24 h of admission	Peripheral venous blood	–	781.40	Stroke severity PO	90 d	9
Liu et al. (30)	2022	China	Retrospective Single-center	266	65.0 \pm 10.9	60.15	AIS	①②④	–	Within 24 h of admission	Venous blood	–	728.03 (HT) 449.76 (PO)	HT PO	90 d	9

AIS, acute ischemic stroke; IS, ischemic stroke; ICH, intracerebral hemorrhage; CKD, chronic kidney disease; AF, atrial fibrillation; CAD, coronary artery disease; CHD, coronary heart disease; MI, myocardial infarct; CHF, congestive heart failure; PVD, peripheral vascular disease; CPD, chronic pulmonary disease; UTI, urinary tract infection; EVT, endovascular treatment; IVT, intravenous thrombolysis; MT, mechanical thrombectomy; IHIS, in-hospital ischemic stroke; NOAC, new oral anticoagulants. OHIS, out-of-hospital ischemic stroke; NOS, Newcastle-Ottawa Scale; HT, hemorrhagic transformation.

PO, poor outcome

①Hypertension; ②Diabetes; ③Hyperlipidemia; ④AF; ⑤Prior stroke; ⑥Heart disease; ⑦Uremia; ⑧Cancer; ⑨CAD; ⑩Hypercholesterolemia; ⑪CKD; ⑫Dyslipidemia; ⑬Uremia; ⑭CAD; ⑮CHD; ⑯IS; ⑰ICH; ⑱Pneumonia; ⑲UTI; ⑳MI, CHF, PVD, Dementia, CPD.

were retrospective. The literature search process is shown in **Figure 1**, and the systematic summary is summarized in **Table 1**.

Meta-Analysis and subgroup analysis of different outcomes

Table 2 provides a summary of the findings. When comparing the poor outcome between the low SII group and the high SII group, our analysis showed that high SII was significantly associated with poor outcome (OR 1.06, 95% CI 1.02-1.09, $P = 0.001$, $I^2 = 93\%$; **Figure 2**). When comparing the mortality between the low SII group and the high SII group, our analysis showed that high SII was significantly associated with high mortality (OR 2.16, 95% CI 1.75-2.67, $P < 0.00001$, $I^2 = 49\%$; **Figure 3**). When comparing the HT between the low SII group and the high SII group, our analysis showed that high SII was significantly associated with HT (OR 2.09, 95% CI 1.61-2.71, $P < 0.00001$, $I^2 = 42\%$; **Figure 4**). SII, on the other hand, had no significant impact on recanalization (OR 1.50, 95% CI 0.86-2.62, $P = 0.16$; **Figure 5**).

Because the other endpoints did not have enough included studies to perform subgroup analysis, we only performed the subgroup analysis of clinical heterogeneity of poor outcomes. In the Subgroup analysis, we identified that the different countries, types of stroke, and surgery intervention (IVT, EVT, or MT)

were associated with clinical heterogeneity of poor outcomes (**Figures 6A–C**).

When comparing the SII level between the poor outcome and good outcome groups, our study showed that poor outcomes had higher SII (SMD 1.11, 95% CI 0.61-1.61, $P < 0.00001$; **Figure 7A**). When comparing the SII between the death and survival groups, our study showed that the death group had higher SII (MD 498.22, 95% CI 333.18-663.25, $P < 0.00001$, $I^2 = 0\%$; **Figure 7B**). Our study compared the SII between the moderate-to-severe and minor groups and showed that the moderate-to-severe group had higher SII (SMD 1.35, 95% CI 0.48-2.23, $P = 0.002$; **Figure 7C**).

Some outcomes had substantial heterogeneity, and we could not decrease it by removing studies one by one. Therefore, the source of heterogeneity may be the studies themselves, the study design, the parameter measurement tool, the highly variable duration of follow-up, and so on. Although high heterogeneity influenced the robustness of our results, the preliminary findings were still worth paying attention to.

Risk of bias assessment and publication bias assessment

The NOS evaluated and assigned a median of 8 stars to all research, with an interquartile of (7-9) stars. The methodological

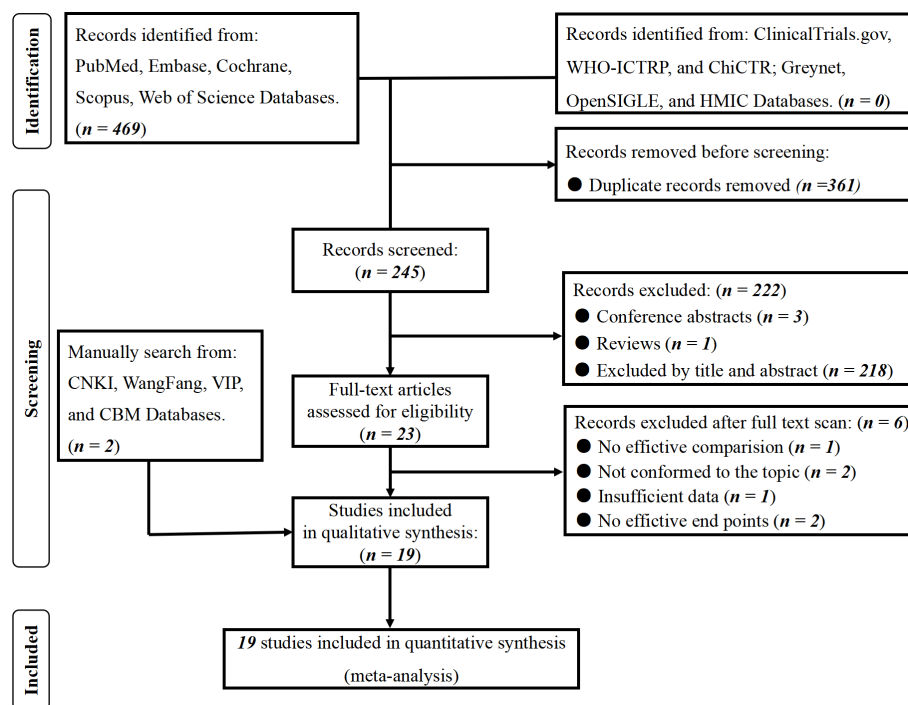


FIGURE 1
PRISMA flowchart of included studies.

TABLE 2 Meta-Analysis and subgroup analysis of Different Outcomes.

			Results	
Items	Studies, n	OR (95% CI)	P Value	Heterogeneity (I2, P for Cochran Q)
Poor Outcome				
Pooled	11	1.06 (1.02, 1.09)	P = 0.001	I2 = 93%, P < 0.00001
China	9	1.05 (1.01-1.08)	P = 0.005	I2 = 94%, P < 0.00001
Non-China	2	1.54 (0.97-2.43)	P = 0.06	I2 = 40%, P =0.19
AIS	9	1.05 (1.01-1.08)	P = 0.005	I2 = 94%, P < 0.00001
ICH	2	1.56 (0.95-2.57)	P = 0.08	I2 = 45%, P =0.18
NNo Surgery Intervention	8	1.04 (1.01-1.07)	P = 0.01	I2 = 94%, P < 0.00001
IVT, EVT, or MT	3	3.30 (2.27-4.81)	P < 0.00001	I2 = 0%, P =0.54
Mortality	2	2.16 (1.75-2.67)	P < 0.00001	I2 = 49%, P = 0.16
HT	4	2.09 (1.61-2.71)	P < 0.00001	I2 = 42%, P = 0.16
Recanalization	2	1.50 (0.86-2.62)	P = 0.16	I2 = 74%, P = 0.05

Results				
Items	Studies, n	SMD or MD (95% CI)	P Value	Heterogeneity (I2, P for Cochran Q)
PPoor outcome / Good outcome	9	1.11 (0.61-1.61)	P < 0.00001	I2 = 98%, P < 0.00001
Death / Survival	3	498.22 (333.18-663.25)*	P < 0.00001	I2 = 0%, P = 0.68
Severity of Stroke	3	1.35 (0.48-2.23)	P = 0.002	I2 = 96%, P < 0.00001

* The SII level did not vary greatly, so we utilized mean difference (MD) to perform the meta-analysis.

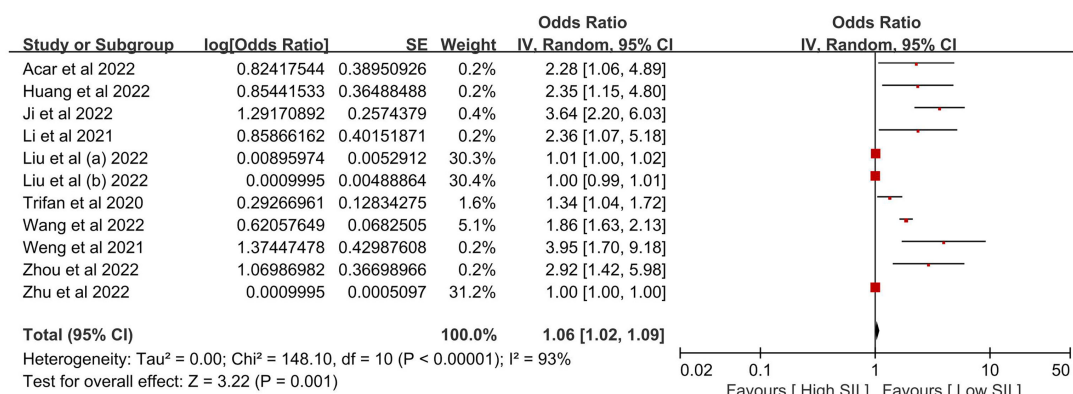


FIGURE 2

The poor outcome between the high SII and low SII groups. Liu et al. (a) and Liu et al. (b) were from the same study, Liu et al. (c) presented minor stroke patients, and Liu et al. (b) presented moderate-to-severe stroke patients. We regarded the two groupings as independent studies when performing a meta-analysis of poor outcomes.

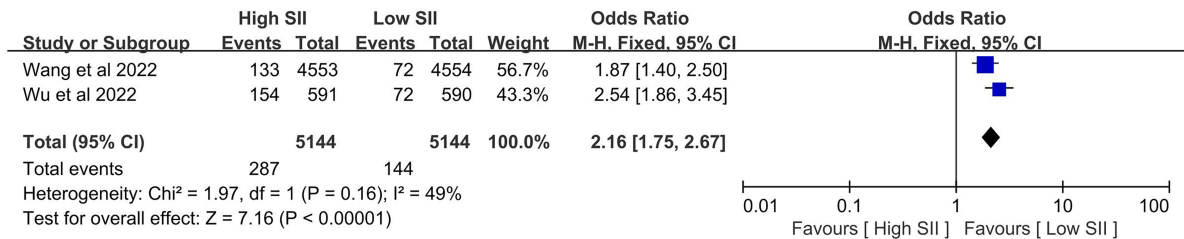


FIGURE 3
The mortality between the high SII and low SII groups.

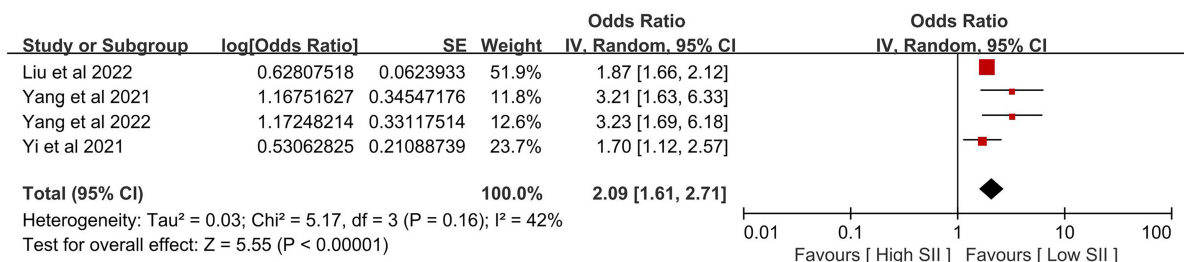


FIGURE 4
The HT between the high SII and low SII groups.

quality of the included studies is displayed in [Supplemental Table 3](#). The funnel plot results, which evaluated the probability of publication bias, are shown in [Supplemental Figure 1](#).

Discussion

Exploring the inflammatory response mechanism after stroke is beneficial for immunoregulatory therapy applications (10). The SII, calculated from neutrophils, lymphocytes, and platelets, is more reliable and representative than other leukocyte-based indicators of inflammation, including platelet-to-lymphocyte ratio (PLR) and lymphocyte-to-monocyte ratio (LMR). In addition, SII has the advantage of being easily

accessible and rapid, as routine blood analysis is essential for patients admitted to the hospital at no additional cost to the patient, thus improving compliance.

The relationship between high SII levels and the clinical outcome of stroke patients remains unclear. Possible mechanisms are as follows: first, in the leukocyte family of the peripheral circulation, neutrophils first infiltrate the lesion within hours after stroke, further leading to the release of inflammatory mediators that directly cause necrosis and apoptosis of cells in the ischemic zone (35, 36). Neutrophils are an essential source of cytokines, free radicals, and matrix metalloproteinase-9, which induce apoptosis of neuronal cells and disrupt the blood-brain barrier by directly damaging brain tissue (37). Leukocytes can penetrate a disrupted blood-brain barrier, which is linked to various stroke complications,

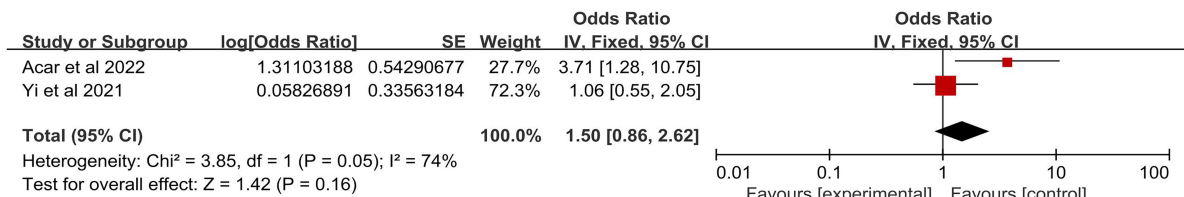


FIGURE 5
The recanalization between high SII and low SII groups.

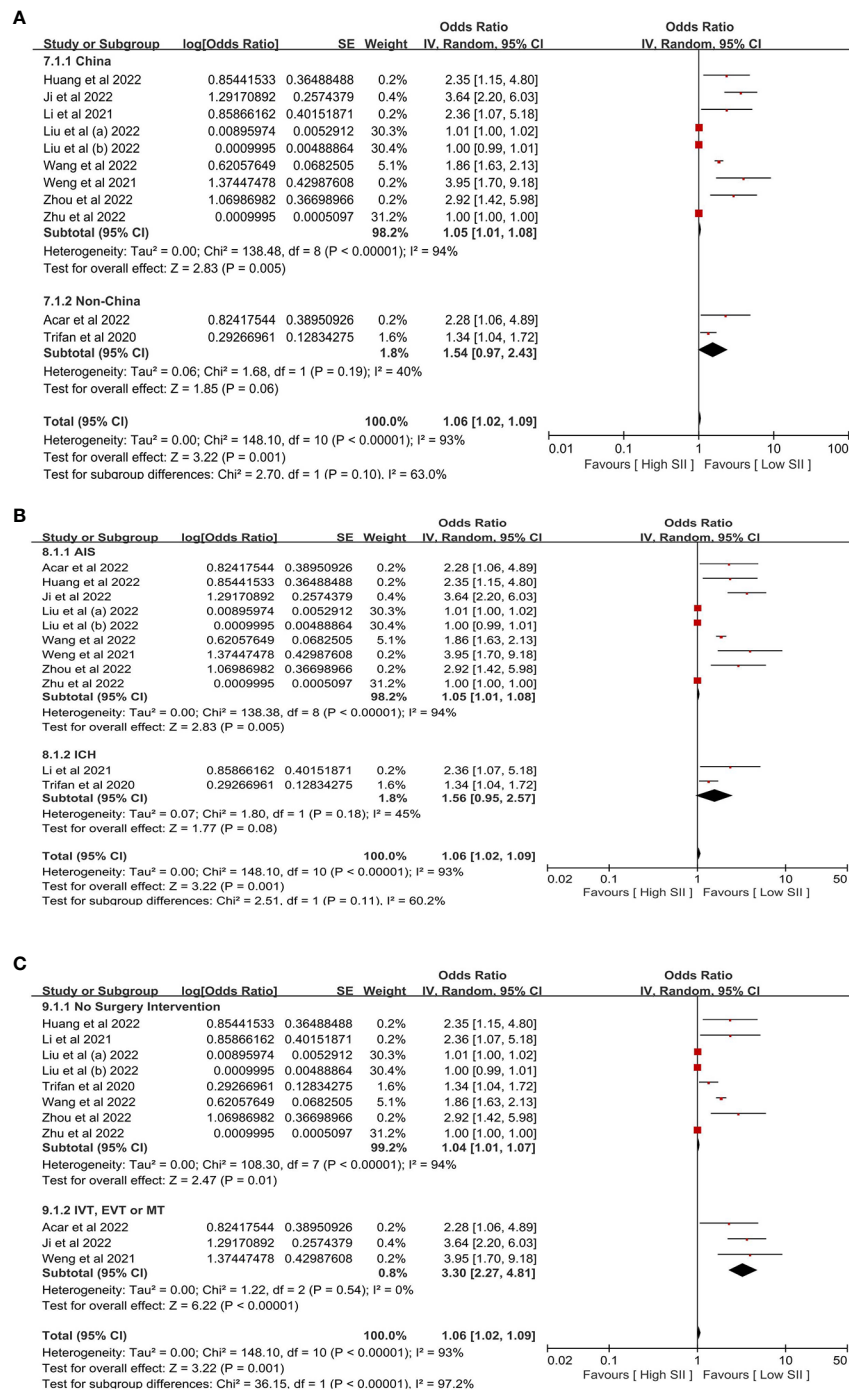


FIGURE 6

The subgroup analysis of poor outcomes is based on (A) different countries, (B) different types of stroke, and (C) surgery intervention.

including pathological cerebral edema, HT, and a decline in neurological function (38). Consequently, a rise in neutrophils is a crucial mediator of ischemic brain damage. More experimental data suggests that some specific lymphocyte subtypes, particularly CD4+ and CD8+ T cells, can release some cytotoxic chemicals and

pro-inflammatory cytokines, even if the involvement of lymphocytes in ischemic brain injury is debatable. However, according to other research, lymphocytes are the primary cerebral protective immunomodulators following AIS and play a critical role in inflammation-induced neuroprotection (39). Second, after an

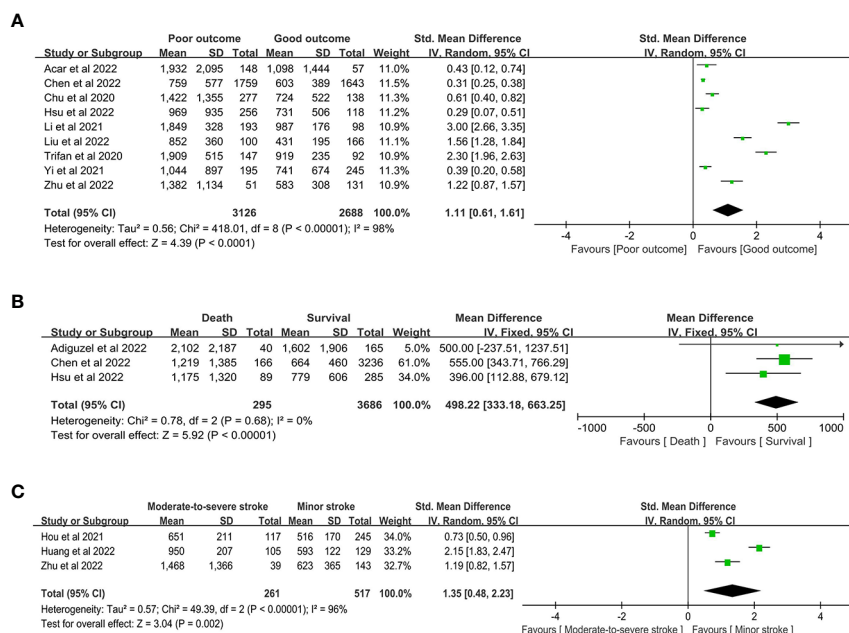


FIGURE 7

the SII level between the (A) poor outcome and good outcome group, (B) death and survival group, and (C) moderate-to-severe and minor stroke group.

ischemic stroke, platelets encourage brain damage (40–42). In mouse experiments, Ischemia-reperfusion in the brain causes platelet necrosis, which regulates injurious neutrophil recruitment and platelet-neutrophil aggregate formation and reduces cerebral blood flow (41). Platelets aggregate with circulating leukocytes when inflammation is activated *via* direct receptor-ligand interactions, activating platelet function and changing endothelial cell properties (43).

Up to now, some studies have reported the value of SII in cerebrovascular diseases and the association between high SII levels and clinical outcomes. Chu et al. (14) showed that SII increases dynamically from the onset of symptoms in AIS patients eligible for thrombolytic therapy. Higher levels of SII indicate more in-hospital complications and worse short-term prognoses. Another study from America demonstrated that in patients with supratentorial spontaneous ICH, the early SII was an independent predictor of poor outcomes at discharge (15). Hou et al. (9) investigated SII's effect on stroke severity and found that SII was independently associated with stroke severity. Li et al. (16) demonstrated that SII, particularly in the acute phase (day 1), is highly correlated with 90-day functional outcomes in ICH patients. This index can be used to predict the prognosis. Weng et al. (17) found similar results to Li et al. and Hou et al. in AIS patients treated with IVT. In 2021, Yang et al. (18) conducted a more in-depth and detailed study, and the results showed that in patients with acute ischemia of the anterior circulation due to significant artery atherosclerosis, higher SII was associated with a greater risk of HT, particularly in artery-to-artery embolism and *in situ* thrombosis. This is the first study on HT. Then

Yang et al. (27) and Yi et al. (19) continued to study this. Their findings demonstrated that admission SII is positively associated with HT in AIS due to large vessel occlusion patients treated with EVT, and higher SII meant more risk of HT. Besides, a study by Yi et al. (19) showed that a reduction in SII after mechanical thrombectomy (MT) was associated with favorable clinical outcomes. SII represents potential prognostic factors in patients undergoing MT for large artery occlusion. Acar et al. (20) considered SII a potential indicator to predict unsuccessful cerebral reperfusion and unfavorable clinical outcomes for patients with AIS undergoing EVT. Nevertheless, our analysis showed that no significant influence of SII for recanalization was observed. Further investigations were required. Adiguzel et al. (21) showed that significant variations of SII were observed during the first two weeks following the stroke. However, due to age and post-treatment clinical stroke severity, the discriminative capacity of these changes was limited. An investigation by Chen et al. (22) divided into two groups, one for in-hospital ischemic stroke (IHIS) and the other for out-of-hospital ischemic stroke (OHIS), and their study found that IHIS patients had more complicated clinical features, higher levels of SII and higher rates of mortality than OHIS patients. The underlying significance of the study was that IHIS patients should be paid more attention to in clinical practice. Hsu et al. (23) thought higher SII was associated with larger ICH volumes, poorer initial Glasgow Coma Scale, and unfavorable outcomes but was not an independent prognostic predictor. Furthermore, the association of SII and hematoma expansion in ICH patients requires further in-depth investigation. Huang et al.

(10) further identified that higher SII meant a greater risk of stroke severity and adverse clinical outcomes after AIS. Ji et al. (24) identified elevated SII as related to malignant brain edema after EVT. Wang et al. (25) findings further affirmed that SII was closely associated with the short- and long-term prognosis of patients with AIS, and higher SII were more likely to have poor outcomes. Wu et al. (26) elevated SII increased the rate of 30-day all-cause mortality as an available index to elucidate the role of thrombocytosis, inflammation, and immunity interaction in developing AIS. Zhou et al. (28) obtained similar findings to previous studies, and a nomogram based on the SII could predict the risk of adverse outcomes in patients with AIS with an accuracy of 80.2%.

SII is not only associated with functional prognosis but also with psychic disorders. Hu et al. (44) conducted a study based on a prospective stroke cohort, and their findings showed that increased SII, especially SII at admission, is significantly correlated with post-stroke depression. The findings may provide some diagnostic clues to determine the early discovery of post-stroke depression. Nevertheless, whether SII is correlated with other psychic disorders secondary to stroke or not, comparative studies are urgent, and this may be the point of future research. Another study by Li et al. (45) demonstrated that the SII was not associated with neurological recovery at three months. In contrast, a low neutrophil-to-lymphocyte ratio was an independent factor for predicting neurological recovery three months after stroke. Topcuoglu et al. (46) considered that SII only had moderate utility and was far from perfection. In patients with HT, SII increased after bleeding occurred, and the admission values are not very valuable in this regard. Additionally, according to Li et al. (47) findings, the SII at admission is an independent predictor for the requirement of decompressive craniectomy (DC) in patients with large artery occlusion-AIS after MT. Based on the findings, the authors created a unique SII-based nomogram that assisted neurosurgeons in making prompt and sensible judgments about whether DC was required, potentially improving the prognosis of these patients. In elderly patients who underwent non-cardiac surgery, preoperative SII was a potential prognostic biomarker for predicting perioperative IS. $SII > 583$ was an independent risk factor for perioperative IS (48). In like manner, this finding may assist surgeons in avoiding severe complications and improving clinical outcomes.

By comprehensively and systematically reviewing the currently available literature, this may be the first meta-analysis assessing the relationship between SII and clinical outcomes of stroke patients. We obtained three significant findings by analysis: firstly, high SII is significantly associated with poor outcome, high mortality, and the incidence of HT; secondly, the SII of poor outcome, death, and moderate-to-severe stroke group was much higher than that of the excellent outcome, survival, and minor stroke group, respectively; thirdly, no significant influence was observed of SII for recanalization in patients with stroke who was undergoing operation procedure. Nevertheless, limited studies on some endpoints restricted the prevalence of our findings. Consequently, more studies on mortality, HT,

recanalization, the difference of SII in the death/survival group, and stroke severity are urgent.

Limitations

There are some limitations: first, other than randomized controlled trials, the majority of available studies are retrospective, and the study design may limit the evidence level of our findings; second, the majority of scholars are from China, and most of the participants are Chinese, too. Consequently, studies from other countries are required, as well as the other races of participants; third, the high heterogeneity of some endpoints influenced the robustness of our results. Despite these limitations, the preliminary findings of our meta-analysis may be useful to clinicians in making treatment decisions for stroke patients.

Conclusion

To the best of our knowledge, this may be the first meta-analysis to look at the link between SII and clinical outcomes in stroke patients. The inflammatory response after a stroke is useful for immunoregulatory treatment. Stroke patients with high SII should be closely monitored, since this might be a viable treatment strategy for limiting brain damage after a stroke. As a result, research into SII and the clinical outcomes of stroke patients is crucial. Our preliminary findings may represent the clinical condition and aid clinical decision-makers. Nonetheless, further research is needed to better understand the utility of SII through dynamic monitoring. To generate more robust results, large-sample and multi-center research are required.

Data availability statement

The original contributions presented in the study are included in the article/**Supplementary Material**. Further inquiries can be directed to the corresponding author.

Author contributions

HY-W and YX-S developed the initial idea for this study. LZ-P developed and revised the search strategy. HY-W and YX-S formulated the study design. HY-W and YX-S contributed to the original draft. LZ-P was responsible for the revision of the draft. HY-W and YX-S contributed equally and are co-first authors. All authors contributed to the article and approved the submitted version.

Funding

This work was supported by the Project of Mianyang Central Hospital (2021YJ006).

Conflict of interest

The authors declare that the research was conducted in the absence of any commercial or financial relationships that could be construed as a potential conflict of interest.

Publisher's note

All claims expressed in this article are solely those of the authors and do not necessarily represent those of their affiliated

organizations, or those of the publisher, the editors and the reviewers. Any product that may be evaluated in this article, or claim that may be made by its manufacturer, is not guaranteed or endorsed by the publisher.

Supplementary material

The Supplementary Material for this article can be found online at: <https://www.frontiersin.org/articles/10.3389/fimmu.2022.1090305/full#supplementary-material>

References

- Ren H, Liu X, Wang L, Gao Y. Lymphocyte-to-monocyte ratio: a novel predictor of the prognosis of acute ischemic stroke. *J Stroke Cerebrovasc Dis* (2017) 26:2595–602. doi: 10.1016/j.jstrokecerebrovasdis.2017.06.019
- Wang Y, Li Z, Gu H, Zhai Y, Jiang Y, Zhao X, et al. China Stroke statistics 2019: a report from the national center for healthcare quality management in neurological diseases, China national clinical research center for neurological diseases, the Chinese stroke association, national center for chronic and non-communicable disease control and prevention, Chinese center for disease control and prevention and institute for global neuroscience and stroke collaborations. *Stroke Vasc Neurol* (2020) 5:211–39. doi: 10.1136/svn-2020-000457
- Zhu T, Wang L, Feng Y, Sun G, Sun X. Classical active ingredients and extracts of Chinese herbal medicines: pharmacokinetics, pharmacodynamics, and molecular mechanisms for ischemic stroke. *Oxid Med Cell Longev* (2021) 2021:8868941. doi: 10.1155/2021/8868941
- Slot K, Berge E, Dorman P, Lewis S, Dennis M, Sandercock P. Impact of functional status at six months on long-term survival in patients with ischaemic stroke: prospective cohort studies. *BMJ* (2008) 336:376–9. doi: 10.1136/bmj.39456.688333.BE
- Kim J, Kawabori M, Yenari M. Innate inflammatory responses in stroke: mechanisms and potential therapeutic targets. *Curr Med Chem* (2014) 21:2076–97. doi: 10.2174/0929867321666131228205146
- Program H, Bivard A, Linz L, Levi C. Peripheral immune cell counts and advanced imaging as biomarkers of stroke outcome. *Cerebrovasc Dis Extra* (2016) 6:120–8. doi: 10.1159/000450620
- Zhang BW, Yao WY. Prognostic role of the systemic immune inflammation index in biliary tract cancers: a meta-analysis of 3515 patients. *World J Surg Oncol* (2022) 20:320. doi: 10.1186/s12957-022-02783-z
- Li S, Liu K, Gao Y, Zhao L, Zhang R, Fang H, et al. Prognostic value of systemic immune-inflammation index in acute/subacute patients with cerebral venous sinus thrombosis. *Stroke Vasc Neurol* (2020) 5:368–73. doi: 10.1136/svn-2020-000362
- Hou D, Wang C, Luo Y, Ye X, Han X, Feng Y, et al. Systemic immune inflammation index (SII) but not platelet-albumin-bilirubin (PALBI) grade is associated with severity of acute ischemic stroke (AIS). *Int J Neurosci* (2020) 131:1203–8. doi: 10.1080/00207454.2020.1784166
- Huang L. Increased systemic immune-inflammation index predicts disease severity and functional outcome in acute ischemic stroke patients. *Neurologist* (2022). doi: 10.1097/NRL.0000000000000464
- Huang YW, Yin XS, Li ZP. Association of the systemic immune-inflammation index (SII) and clinical outcomes in patients with stroke: A systematic review and meta-analysis. In: *PROSPERO* (2022). identifier: CRD42022371996. Available at: https://www.crd.york.ac.uk/prospero/display_record.php?ID=CRD42022371996.
- Huang YW, Yin XS, Li ZP. Association of the stress hyperglycemia ratio and clinical outcomes in patients with stroke: A systematic review and meta-analysis. *Front Neurol* (2022) 13:999536. doi: 10.3389/fneur.2022.999536
- Wells GA, Shea B, O'Connell D, Peterson J, Welch V, Losos M, et al. *The Newcastle-Ottawa scale (NOS) for assessing the quality of nonrandomized studies in meta-analyses*. Available at: http://www.ohri.ca/programs/clinical_epidemiology/oxford.htm (Accessed February 27, 2020).
- Chu YW, Chen PY, Lin SK. Correlation between immune-inflammatory markers and clinical features in patients with acute ischemic stroke. *Acta neurol Taiwanica* (2020) 29:103–13.
- Trifan G, Testai FD. Systemic immune-inflammation (sii) index predicts poor outcome after spontaneous supratentorial intracerebral hemorrhage. *J stroke cerebrovasc Dis* (2020) 29:105057. doi: 10.1016/j.jstrokecerebrovasdis.2020.105057
- Li Y, Wen D, Cui W, Chen Y, Zhang F, Yuan M, et al. The prognostic value of the acute phase systemic immune-inflammation index in patients with intracerebral hemorrhage. *Front Neurol* (2021) 12:628557. doi: 10.3389/fneur.2021.628557
- Weng Y, Zeng T, Huang H, Ren J, Wang J, Yang C, et al. Systemic immune-inflammation index predicts 3-month functional outcome in acute ischemic stroke patients treated with intravenous thrombolysis. *Clin Interventions aging* (2021) 16:877–86. doi: 10.2147/CIA.S311047
- Yang Y, Han Y, Sun W, Zhang Y. Increased systemic immune-inflammation index predicts hemorrhagic transformation in anterior circulation acute ischemic stroke due to large-artery atherosclerotic. *Int J Neurosci* (2021), 1–7. doi: 10.1080/00207454.2021.1953021
- Yi HJ, Sung JH, Lee DH. Systemic inflammation response index and systemic immune-inflammation index are associated with clinical outcomes in patients treated with mechanical thrombectomy for large artery occlusion. *World neurosurg* (2021) 153:e282–9. doi: 10.1016/j.wneu.2021.06.113
- Acar BA, Acar T, Vatan MB, Aras YG, Ulaş SB, Eryılmaz HA, et al. Predictive value of systemic immune-inflammation index for cerebral reperfusion and clinical outcomes in patients with acute ischemic stroke undergoing endovascular treatment. *Eur Rev Med Pharmacol Sci* (2022) 26:5718–28. doi: 10.26355/eurrev_202208_29507
- Adiguzel A, Arsava EM, Topcuoglu MA. Temporal course of peripheral inflammation markers and indexes following acute ischemic stroke: Prediction of mortality, functional outcome, and stroke-associated pneumonia. *Neurol Res* (2022) 44:224–31. doi: 10.1080/01616412.2021.1975222
- Chen PY, Chen GC, Hsiao CL, Hsu PJ, Yang FY, Liu CY, et al. Comparison of clinical features, immune-inflammatory markers, and outcomes between patients with acute in-hospital and out-of-hospital ischemic stroke. *J Inflammation Res* (2022) 15:881–95. doi: 10.2147/JIR.S342830
- Hsu HT, Chen PY, Tzeng IS, Hsu PJ, Lin SK. Correlation of immune-inflammatory markers with clinical features and novel location-specific nomograms for short-term outcomes in patients with intracerebral hemorrhage. *Diagn (Basel)* (2022) 12:622. doi: 10.3390/diagnostics12030622
- Ji Y, Xu X, Wu K, Sun Y, Wang H, Guo Y, et al. Prognosis of ischemic stroke patients undergoing endovascular thrombectomy is influenced by systemic inflammatory index through malignant brain edema. *Clin Interventions aging* (2022) 17:1001–12. doi: 10.2147/CIA.S365553
- Wang N, Yang Y, Qiu B, Gao Y, Wang A, Xu Q, et al. Correlation of the systemic immune-inflammation index with short- and long-term prognosis after acute ischemic stroke. *Aging* (2022) 14:6567–78. doi: 10.18632/aging.204228
- Wu S, Shi X, Zhou Q, Duan X, Zhang X, Guo H. The association between systemic immune-inflammation index and all-cause mortality in acute ischemic stroke patients: Analysis from the mimic-iv database. *Emergency Med Int* (2022) 2022:4156489. doi: 10.1155/2022/4156489
- Yang Y, Cui T, Bai X, Wang A, Zhang X, Wan J, et al. Association between systemic immune-inflammation index and symptomatic intracranial hemorrhage in acute ischemic stroke patients undergoing endovascular treatment. *Curr neurovasc Res* (2022) 19:83–91. doi: 10.2174/1567202619666220406102429
- Zhou YX, Li WC, Xia SH, Xiang T, Tang C, Luo JL, et al. Predictive value of the systemic immune inflammation index for adverse outcomes in patients with

acute ischemic stroke. *Front Neurol* (2022) 13:836595. doi: 10.3389/fneur.2022.836595

29. Liu Z, Liu YY, Xu SF, Kang H. Immune-inflammation index with hemorrhagic transformation and prognosis of acute ischemic stroke. *Adv Clin Med* (2022) 12:1335–46. doi: 10.12677/ACM.2022.122194
30. Zhu LY, Liu J, Xiao CH. Study on the relationship between systemic immune inflammation index and d-dimer and the severity and prognosis of young acute cerebral infarction patients. *J Neurosci Ment Health* (2022) 22:363–8. doi: 10.3969/j.issn.1009-6574.2022.05.011
31. Luo D, Wan X, Liu J, Tong T. Optimally estimating the sample mean from the sample size, median, mid-range and/or mid-quartile range. *Stat Methods Med Res* (2018) 27:1785–805. doi: 10.1177/0962280216669183
32. Wan X, Wang W, Liu J, Tong T. Estimating the sample mean and standard deviation from the sample size, median, range and/or interquartile range. *BMC Med Res Method* (2014) 14:135. doi: 10.1186/1471-2288-14-135
33. DerSimonian R, Laird N. Meta-analysis in clinical trials. *Control Clin Trials* (1986) 7:177–88. doi: 10.1016/0197-2456(86)90046-2
34. Higgins JP, Thompson SG. Quantifying heterogeneity in a meta-analysis. *Stat Med* (2002) 21:1539–58. doi: 10.1002/sim.1186
35. Darbousset R, Thomas GM, Mezouar S, Frère C, Bonier R, Mackman N, et al. Tissue factor-positive neutrophils bind to injured endothelial wall and initiate thrombus formation. *Blood* (2012) 120:2133–43. doi: 10.1182/blood-2012-06-437772
36. Jin R, Yang G, Li G. Inflammatory mechanisms in ischemic stroke: role of inflammatory cells. *J Leukoc Biol* (2010) 87:779–89. doi: 10.1189/jlb.1109766
37. Chamorro Á, Dirnagl U, Urra X, Planas AM. Neuroprotection in acute stroke: targeting excitotoxicity, oxidative and nitrosative stress, and inflammation. *Lancet Neurol* (2016) 15:869–81. doi: 10.1016/S1474-4422(16)00114-9
38. Petty MA, Lo EH. Junctional complexes of the blood-brain barrier: permeability changes in neuroinflammation. *Prog Neurobiol* (2006) 68:311–23. doi: 10.1016/S0301-0082(02)00128-4
39. Liesz A, Suri-Payer E, Veltkamp C, Doerr H, Sommer C, Rivest S, et al. Regulatory T cells are key cerebroprotective immunomodulators in acute experimental stroke. *Nat Med* (2009) 15:192–9. doi: 10.1038/nm.1927
40. Nording HM, Seizer P, Langer HF. Platelets in inflammation and atherogenesis. *Front Immunol* (2015) 6:98. doi: 10.3389/fimmu.2015.00098
41. Denorme F, Manne BK, Portier I, Eustes AS, Kosaka Y, Kile BT, et al. Platelet necrosis mediates ischemic stroke outcome in mice. *Blood* (2020) 135:429–40. doi: 10.1182/blood.2019002124
42. Arevalo-Lorido JC, Carretero-Gomez J, Alvarez-Oliva A, Gutiérrez-Montaña C, Fernández-Recio JM, Najarro-Diez F, et al. Mean platelet volume in acute phase of ischemic stroke, as predictor of mortality and functional outcome after 1 year. *J Stroke Cerebrovasc Dis* (2013) 22:297–303. doi: 10.1016/j.jstrokecerebrovasdis.2011.09.009
43. Nawaz M, Langer H, May AE. Platelets in inflammation and atherogenesis. *J Clin Invest* (2005) 115:3378–84. doi: 10.1172/JCI27196
44. Hu J, Wang L, Fan K, Ren W, Wang Q, Ruan Y, et al. The association between systemic inflammatory markers and post-stroke depression: A prospective stroke cohort. *Clin Interv Aging* (2021) 16:1231–9. doi: 10.2147/CIA.S314131
45. Li LH, Chen CT, Chang YC, Chen YJ, Lee IH, How CK. Prognostic role of neutrophil-to-lymphocyte ratio, platelet-to-lymphocyte ratio, and systemic immune inflammation index in acute ischemic stroke: A STROBE-compliant retrospective study. *Med (Baltimore)* (2021) 100:e26354. doi: 10.1097/MD.00000000000026354
46. Topcuoglu MA, Pektezel MY, Yilmaz E, Arsava EM. Systemic inflammation indices in patients with acute ischemic stroke treated with intravenous tissue plasminogen activator: Clinical yield and utility. *Angiology* (2021) 72:279–84. doi: 10.1177/0003319720969997
47. Li WC, Zhou YX, Zhu G, Zeng KL, Zeng HY, Chen JS, et al. Systemic immune inflammatory index is an independent predictor for the requirement of decompressive craniectomy in large artery occlusion acute ischemic stroke patients after mechanical thrombectomy. *Front Neurol* (2022) 13:945437. doi: 10.3389/fneur.2022.945437
48. Zhang F, Niu M, Wang L, Liu Y, Shi L, Cao J, et al. Systemic-Immune-Inflammation index as a promising biomarker for predicting perioperative ischemic stroke in older patients who underwent non-cardiac surgery. *Front Aging Neurosci* (2022) 14:865244. doi: 10.3389/fnagi.2022.865244



OPEN ACCESS

EDITED BY

Jianmin Chen,
Queen Mary University of London,
United Kingdom

REVIEWED BY

Alberto N. Peón,
Sociedad Española
de Beneficencia, Mexico
Aisah Anisah Aubdool,
Queen Mary University of London,
United Kingdom

*CORRESPONDENCE

Xianliang Zhou
✉ zhouxianliang0326@hotmail.com
Xu Meng
✉ mengxu1219@hotmail.com

†These authors have contributed
equally to this work

SPECIALTY SECTION

This article was submitted to
Inflammation,
a section of the journal
Frontiers in Immunology

RECEIVED 15 November 2022

ACCEPTED 21 December 2022

PUBLISHED 10 January 2023

CITATION

Zhang Z, Zhao L, Zhou X, Meng X and
Zhou X (2023) Role of inflammation,
immunity, and oxidative stress in
hypertension: New insights and
potential therapeutic targets.
Front. Immunol. 13:1098725.
doi: 10.3389/fimmu.2022.1098725

COPYRIGHT

© 2023 Zhang, Zhao, Zhou, Meng and
Zhou. This is an open-access article
distributed under the terms of the
[Creative Commons Attribution License](#)
(CC BY). The use, distribution or
reproduction in other forums is
permitted, provided the original
author(s) and the copyright owner(s)
are credited and that the original
publication in this journal is cited, in
accordance with accepted academic
practice. No use, distribution or
reproduction is permitted which does
not comply with these terms.

Role of inflammation, immunity, and oxidative stress in hypertension: New insights and potential therapeutic targets

Zenglei Zhang[†], Lin Zhao[†], Xingyu Zhou, Xu Meng*
and Xianliang Zhou*

Department of Cardiology, Fuwai Hospital, National Center for Cardiovascular Diseases, Chinese Academy of Medical Sciences and Peking Union Medical College, Beijing, China

Hypertension is regarded as the most prominent risk factor for cardiovascular diseases, which have become a primary cause of death, and recent research has demonstrated that chronic inflammation is involved in the pathogenesis of hypertension. Both innate and adaptive immunity are now known to promote the elevation of blood pressure by triggering vascular inflammation and microvascular remodeling. For example, as an important part of innate immune system, classically activated macrophages (M1), neutrophils, and dendritic cells contribute to hypertension by secreting inflammatory cytokines. In particular, interferon-gamma (IFN- γ) and interleukin-17 (IL-17) produced by activated T lymphocytes contribute to hypertension by inducing oxidative stress injury and endothelial dysfunction. However, the regulatory T cells and alternatively activated macrophages (M2) may have a protective role in hypertension. Although inflammation is related to hypertension, the exact mechanisms are complex and unclear. The present review aims to reveal the roles of inflammation, immunity, and oxidative stress in the initiation and evolution of hypertension. We envisage that the review will strengthen public understanding of the pathophysiological mechanisms of hypertension and may provide new insights and potential therapeutic strategies for hypertension.

KEYWORDS

hypertension, inflammation, immunity, oxidative stress, cytokines, cardiovascular diseases

1 Introduction

Hypertension has become the leading global risk factor for cardiovascular diseases (CVDs) (1), and 1.15 billion adult individuals have been confirmed with hypertension according to related data (2). In addition, the American Heart Association and the American College of Cardiology formulated strict new diagnostic criteria that are

expected to extend the number of patients with hypertension by two–threefold (3, 4). Many common and effective drugs, including angiotensin-converting enzyme inhibitors (ACEIs)/angiotensin II (Ang II) type 1 receptor blockers (ARBs), beta-blockers, calcium channel blockers (CCBs), and diuretics, have been widely confirmed to control raised blood pressure (5), causing a significant reduction of mortality associated with hypertension; however, hypertension still remains a major public health problem and health care burden in both developed and developing countries. Blood pressure is still poorly controlled in approximately half of patients who are receiving treatment (6), so potential therapeutic targets are urgently needed.

The pathogenesis of hypertension is complex and there are many risk factors. Accumulating evidence confirms that an activated inflammatory response and immune system are an indispensable part in the genesis and evolution of hypertension and are associated with hypertensive complications, such as myocardial infarction, hemorrhagic stroke, and renal injury (7). The elevated level of inflammatory biomarkers, including C-reactive protein (CRP) and cytokines, have been detected in patients with hypertension, revealing that the immune system is involved in hypertension as a low-grade inflammatory condition which is a chronic and continuous process and is more characterized by the increase of inflammatory cells and inflammatory mediators compared with infectious diseases, and usually does not show significant symptoms (5, 8, 9). Elevated BP by many risk factors including genetic susceptibility and several environmental factors can induce organ injury promoting the formation of damage-associated molecular patterns (DAMPs) and new antigens which are regarded as the main impetus for the low-grade inflammation (10). Inappropriate immune activation may act in the kidney, microvascular, nervous system, and even gut microbiome to promote the elevation of blood pressure (11–17), especially salt-sensitive hypertension (18, 19). Inflammation is generally considered an immune response and thus, in the early stage, mainly engages the innate immune system (IIS) and is subsequently followed by the adaptive immune response. Although interactions occur between these responses, they have different effects on disease progression and clinical significance; therefore, we will discuss these separately in this review.

In 1967, Okuda and Grollman first reported there was a relationship between the immune and vascular systems based on the induction of artery hypertension in rats after they had received lymphocytes derived from rats with hypertension (20). According to the surface markers and functions, macrophages are classified into proinflammatory M1 macrophages and anti-inflammatory M2 macrophages. The recent study has confirmed the damage effect of M1 macrophages and the inconsiderably protective role of M2 macrophages in hypertension (10). Moreover, increasing

evidence showed that hypertension has a chronic inflammatory status characterized as the transmigration, accumulation, and activation of inflammatory cells, and the proinflammatory cytokines and free radicals produced by activated innate immune cells and endothelial cells (21). In the present review, we will discuss how the immune system and associated inflammation and oxidative stress affect the procession of hypertension and will summarize the potential therapeutic targets in hypertension.

2 The relationship of inflammation, immunity, and oxidative stress

Although numerous risk factors promote the genesis and progress of hypertension, the role of inflammation, immunity, and oxidative stress have been overwhelming confirmed by evidence from many laboratories worldwide (22–26). The causal state of circulating immune cells, such as monocytes, neutrophils, and lymphocytes, has been demonstrated (27), and the imbalanced activated immune system is known to produce an inflammatory condition with an increasing amount of proinflammatory cytokines. First, leukocytes gather *via* cytokine and chemokine signaling and roll on the vascular endothelium regulated by E and P selectin in the early phase of vascular inflammation. The interaction of leucocyte integrins and the intracellular adhesion molecules (ICAMs) 1–5 and vascular cell adhesion molecule 1 (VCAM-1) then play a crucial part in the subsequent processes (28). Cytokines and chemokines promote oxidative stress, a typical characteristic of essential hypertension. Reactive oxygen species (ROS) are the major effector of the oxidative stress injury and consequently may have a crucial role in connecting inflammation, immune system, and hypertension (10). A low inflammatory condition, resulting from massive production of the superoxide anion ($\cdot\text{O}_2$) and hydrogen peroxide (H_2O_2) by endothelial cells, monocytes, and macrophages, promotes oxidative stress and causes vascular dysfunction and target-organ damage in the process of hypertension (29). The activated renin-angiotensin-aldosterone system (RAAS) is a crucial regulator of oxidative stress, and results in the inflammatory damage of vessels (30). As the major component of the RAAS, Ang II promotes vascular inflammation by activating nicotinamide adenine dinucleotide phosphate oxidase oxidases (NOXs) and increasing the expression of endothelin-1 (ET-1), causing the production of a large number of proinflammatory mediators that contribute to the endothelial dysfunction. The main function of NOXs are producing ROS. For example, the low level of ROS produced by NOX2 in physiological state is closely related to the process of cell proliferation and differentiation. However, excessive ROS by activated NOXs is responsible for the CVDs, especially hypertension. Although 7 isoforms of NOXs have been reported, NOX2 and 4 are considered as having tight

association with CVDs. NOX 2 and 4 are mainly expressed in endothelial cells and cardiomyocytes (31). NOX2 causes vascular oxidative stress *via* producing superoxide directly, while NOX4 mainly depend on the production of H_2O_2 through the rapid dismutation of superoxide into H_2O_2 (32). The role that activated NOX2 contributes to hypertension *via* mediating oxidative stress injury and further promoting endothelial dysfunction has been observed (33, 34). According to the results from Toral M et al., the NOX2 inhibitor decreased vascular ROS production and restored endothelial dysfunction in the hypertensive mice (34). NOX4 facilitates vascular hyperproliferation and microvascular remodeling through the induced hyperoxidation and ER stress (35). Furthermore, Ang II, ET-1, and aldosterone may be responsible for impaired remodeling of vessels in a large extent *via* upregulating expression of chemokines in vascular smooth muscle cells and endothelial cells (36, 37). In addition, activated neutrophils can release ROS as well as proinflammatory cytokines, causing significant oxidative stress. The positive association between the concentration of CRP and the level of oxidative stress has been confirmed (38), and Savoia et al. reported that CRP may upregulate expression of angiotensin type 1 receptors, which could then modulate the formation of ROS (39).

The kidneys have an indispensable role in modulating blood pressure, and renal hypertension resulting from chronic kidney injury and renal artery stenosis is one of most common secondary hypertension diseases globally (40). ROS has been detected in the early stage of chronic kidney disease and exasperates renal function contributing to oxidative stress and chronic inflammation (41, 42), which further accelerates the process of hypertension.

In summary, oxidative stress may be a trigger as well as the result of both inflammation and imbalance in the immune system, contributing to the vascular injury and remodeling, and results in the progression of hypertension.

3 Pathophysiological mechanisms of essential hypertension

Essential hypertension is a disease of unknown etiology that includes the complex interaction of many factors, especially those of genetic and environmental origin. However, it is unclear how these factors increase blood pressure. Increasing evidence indicates that essential hypertension is not a homogeneous disease and that the etiology and pathogenesis vary among individuals. Furthermore, hypertension has a long course and generally slow progression. The mechanisms of initiation, maintenance, and acceleration are different in different stages, and there are interactions among various pathogenic mechanisms (e.g., oxidative stress and inflammation and the immune system) (43). Therefore, hypertension is a multi-factor, -link, and -stage disease that is

also affected by differences between individuals. In this section, we intend to briefly summarize the potential pathophysiological process of essential hypertension.

The main mechanisms of hypertension include microvascular remodeling, imbalance of the autonomic nervous system (ANS), and activation of the RAAS (43). The increase of peripheral resistance in small arteries, ranging from 100 to 300 μ m in diameter, is the central mechanism and the most significant characteristic in essential hypertension (44). As mentioned above, ROS, activated immune cells, and inflammation, can stimulate endothelial cells to produce and release large amounts of vasoactive substances, such as nitric oxide (NO), prostaglandin-I-2 (PGI₂), ET-1, and endothelium-dependent vasoconstrictor factor (EDGF) (44). Age and various cardiovascular risk factors, including dyslipidemia, elevated blood sugar, and smoking, lead to abnormal blood endothelial cell function, increase the production of oxygen free radicals, enhance NO inactivation, vascular inflammation, and oxidative stress response, and influence the elastic function and structure of arteries. With the decreased elasticity of the aorta, the pulse wave conduction velocity increases, and the phase of the reflected wave arriving at the central aorta advances from diastole to systole. The occurrence of a delayed systolic pressure peak can elevate systolic blood pressure and reduce diastolic blood pressure. Changes in the structure (sparse number of tubes or increased wall/lumen ratio) and function (decreased elasticity and increased resistance) and function of resistance arterioles affect peripheral pressure responses.

The position of the origin or the intensity of the reflected wave also has an important part in increasing the pulse pressure. In the nervous system, various reasons can cause changes in the function of the cerebral subcortical nerve center leading to abnormal concentrations and activities of various neuropeptides and neurotransmitters, including norepinephrine, epinephrine, dopamine, serotonin, vasopressin, enkephalin, and brain natriuretic peptide as well as changes in the central renin-angiotensin system. These changes eventually hyperactivate the sympathetic nerve system, increasing the concentrations of plasma catecholamines and constriction of arteries and causing resistance and increased blood pressure (45, 46).

AT-II is the main effector of the RAAS and is involved in a range of processes that can increase blood pressure. These include acting on angiotensin receptor 1, making arteriole smooth muscle contract, stimulating the glomerular zona of adrenal cortex to secrete aldosterone, and promoting the release of norepinephrine through the positive feedback in sympathetic nerve terminal presynaptic membrane. Recently, many tissues, including the blood vessel wall, heart, central nervous system, kidney, and adrenal gland, have been found to contain various components of the RAAS (47). The role of tissue RAAS in the function and structure of the heart and blood vessels may have a greater impact on the occurrence and maintenance of

hypertension (44). In addition, water and sodium retention and insulin resistance can contribute to elevating blood pressure.

4 Inflammation in hypertension

Inflammation is a rapid, nonspecific defense response of the body that acts to maintain hemostasis *via* monitoring and clearing of foreign bodies. This involves coordinating vascular endothelial cells and circulating inflammatory cells and cytokines (48). Although inflammation has beneficial effects, including eradicating pathogens and protecting organs from damage, imbalanced regulation may cause serious and sustained inflammatory response that can in turn cause progressive tissue injury, organ dysfunction, and fibrosis, and even systemic inflammatory response syndrome. Overwhelming evidence shows that low-grade chronic inflammation contributes to the initiation and maintenance of essential hypertension (49, 50). A recent study reported that the chronic inflammatory condition induced by excessive and prolonged stimulation of IIS could lead to vascular endothelial cell damage (51). In this section, we mainly discuss the role of inflammasomes and inflammatory cytokines and of neuroinflammation in the progress of essential hypertension.

4.1 Inflammasomes

The inflammasomes are cytosolic protein complexes, such as NLR-family pyrin domain-containing protein (NLRP1) and NLRP3 mainly expressed in innate immune cells (like monocytes and macrophages) and endothelial cells, that identify pathogens and activate inflammatory responses, including the intracellular IIS receptors (52, 53). As inflammasomes are major components of the IIS, they mediate important inflammatory responses and pyroptosis, which are tightly associated with endothelial dysfunction. Improperly activated inflammasomes are involved in the potential pathogenesis of many inflammations related diseases (54). NLRP3 is the most characteristic inflammasome among the pattern recognition receptors (PRRs) that recognize damage-associated molecular patterns (DAMPs) and pathogen-associated molecular patterns (PAMPs) to initiate and promote an inflammation response (55). Briefly, a wide range of DAMPs or PAMPs stimulate NLRP3 activation by inducing ion transporting (e.g., K^+ efflux and Ca^{2+} influx) and lysosomal leakage. The activated NLRP3 inflammasome then triggers caspases to induce cleavage of inactive proinflammatory cytokine precursors, such as pro-IL-1 β , pro-IL-18, and pro-IL-37 (Figure 1) (48). Numerous studies show that activated NLRP3 inflammasomes are tightly associated with many chronic inflammatory and metabolic diseases, such as ischemic heart diseases and diabetes mellitus, stroke, atherosclerosis, and

hypertension (56–59). Studies have suggested that inflammasomes and their related cytokines are tightly associated with raised blood pressure. According to Dalekos et al., an elevated serum concentration of IL-1 β was detected in patients with hypertension (60). Endothelial cells are not only the action target of IL-1 β but also produce IL-1 β (61). *In vitro* experiments show that monocytes derived from hypertensive patients can release a high level of IL-1 β in response to the stimulation of Ang II or lipopolysaccharide (LPS) (62). In addition, the production of mitochondrial ROS is a vital component of cellular oxidative stress, and NLRP3 activation is indispensable in this process. More and more agonists have been reported to produce vascular inflammation and injury by triggering NLRP3 inflammasome activation. According to Xie et al., the NLRP3 inflammasome is involved in visfatin-mediated vascular injury, which may cause atherosclerosis (63). IL-1 β and IL-18 would then be released into the blood flow to activate more inflammatory cells and thereby expand the inflammatory response when inflammasomes are activated.

Recent research suggests that endothelial dysfunction is associated with activated NLRP3 inflammasomes through the release of HMGB1. Activated NLRP3 inflammasome and subsequent release of HMGB1 have been considered as the underlying cause of cell-to-cell junction breaks in mouse vascular endothelial cells treated with high-glucose levels (64). Interestingly, NLRP3 deficiency has a significantly protective role *via* preventing tight junction disruption in diabetic mice and ameliorating endothelial permeability in endothelial cells *in vitro* (64), and inhibiting the NLRP3 inflammasome by pharmacological inhibition also produced potent therapeutic effects (65). More recently, knockdown of NLRP3 also exhibited remarkable effect on lowering blood pressure, improving vascular remodeling and insulin resistance, and ameliorating or delaying the atherosclerosis *via* regulating metabolism, relieving oxidative stress and reducing release of inflammatory cytokines (58, 66, 67). WEHD, a caspase-1 inhibitor, could significantly reduce inflammasome activity and prohibited ATP-induced hypertension in mice (68).

4.2 Role of cytokines in raising blood pressure

Traditionally, essential hypertension was thought to be caused by hemodynamic changes, but in recent years, numerous studies have revealed that inflammatory cytokines play a significant part in promoting the progression of hypertension *via* affecting vascular and renal function. Cytokines are a major component of the immune system and the main performer of inflammatory response, which connects them with vascular remodeling and hypertension. Until recently, the connection between how inflammation and immunity affect blood pressure levels was not well understood. According to

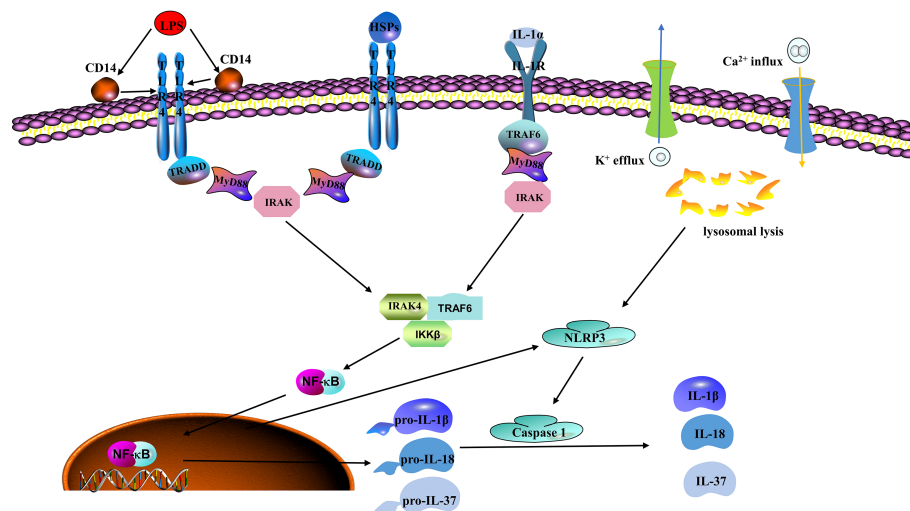


FIGURE 1

Classic mechanisms of inflammasome activation. Lipopolysaccharide (LPS), which is regarded as the prototype of pathogen associated molecular patterns (PAMPs) and heat shock proteins (HSPs) as a typical representative of damage associated molecular patterns (DAMPs), can be recognized by toll-like receptor 4 (TLR4). Nuclear factor kappa B (NFκB) mediates these signals to produce NOD-like receptor family pyrin domain containing 3 (NLRP3), pro-IL-1β, pro-IL-18, and pro-IL-37. Next, NLRP3 is activated by potassium (K⁺) efflux, calcium (Ca²⁺) influx, and lysosomal leakage to recruit cysteine-requiring aspartate protease-1 (caspase-1). Caspase-1 then induces the maturation and release of pro-IL-1β, pro-IL-18, and pro-IL-37 and other related inflammatory agents that cause the inflammatory reaction and participate in the occurrence and development of the disease.

previous observations, numerous T cells and monocytes/macrophages accumulated in vessels and kidneys in the mice model with renal ischemia-reperfusion injury (69). Based on other's and our own research, these cells have been shown to secrete potent cytokines that impair organs, especially the heart and kidneys. Modern experimental technologies have demonstrated that a variety of cytokines are involved in the initiation and progression of hypertension (Table 1).

4.2.1 Interleukin 17

IL-17 is derived from TH17 cells, an important subset of CD4⁺ T cells, and includes several isoforms, including IL-17A and IL-17F; several B cells and CD8⁺ cells also produce IL-17 (84). IL-17A is generally considered to act synergistically with other cytokines (e.g., TNF) during inflammatory response. IL-17A and TNF-α have been demonstrated to synergistically enhance lung inflammation and expression of C-C motif chemokine ligand 2 (CCL2) in an NADPH oxidase-dependent manner (70), which affects vascular functions by influencing gene expression (71). Moreover, IL-17A is reported to be involved in multiple inflammatory diseases, such as asthma, psoriasis, and systemic lupus erythematosus (84). Considering the important position of IL-17 in inflammation-related diseases, research on anti-IL-17 monoclonal antibodies (Ixekizumab and Secukinumab) and anti-IL-17 receptor antibodies (Brodalumab) has become a scientific hotspot in recent years, and these antibodies have shown satisfactory treatment effects in clinical trials (85, 86).

Growing evidence has linked IL-17A to increased blood pressure, although the exact mechanisms are unclear. Plasma IL-17A concentrations were significantly increased in Ang II-

induced animal models with hypertension. In contrast, Ang II infusion could not impair endothelial function or result in an elevation of blood pressure in IL-17A^{-/-} mice. A similar result was observed when the level of oxidative stress was lowered and infiltration of T cells decreased in IL-17A^{-/-} mice compared with that in the control group. Treatment with anti-IL-17 antibody was found to significantly lower blood pressure and reduce collagen deposition in mouse heart and kidneys. Consistent with these findings, when co-cultured human vascular smooth muscle cells (VSMCs) with TNF-α *in vitro*, IL-17A facilitate the expression of various cytokines and chemokines, such as CCL7 and 8, CXCL2 and CSF3, which could recruit more inflammatory cells. Subsequently, another exact role of IL-17A in hypertension has been demonstrated by Nguyen et al. that IL-17A could reduce the production of NO by phosphorylating threonine 495 of endothelial nitric oxide synthase (eNOS) in porcine aortic endothelial cells (87). And the study also showed intravenous administration of IL-17A could elevate the blood pressure modestly in the normal mice. Taking together, inhibition of IL-23/IL-17 axis has been regarded as promising therapeutic target in the future precise therapy of hypertension (72).

4.2.2 Interleukin 6

IL-6 is a 21 kDa glycoprotein secreted by monocytes, macrophages, and dendritic cells, which can activate related genes and upregulate expression of receptors involved in cell proliferation, differentiation, and apoptosis. Once the receptor recognizes the IL-6 signals, the related cellular events, such as

TABLE 1 Examples of inflammatory cytokines involved in hypertension.

Cytokines	Cell sources	Disease models	Mechanisms	Biological effects	Reference
IL-17	CD4 ⁺ T cells and some CD8 ⁺ cells	IL-17A ^{-/-} mice	Enhance CCL-2 in an NADPH oxidase-dependent manner, and altering gene expression in vascular smooth muscle cells	Promotes oxidative stress and increases the number of infiltrated T cells	(70–72)
IL-6	Monocytes, macrophages, dendritic cells, etc.	IL-6 ^{-/-} mice	polarizes the CD4 ⁺ cells and facilitates water and sodium retention	promotes the production of IL-17 and upregulates the expression and increase the activity of the epithelial sodium channel in duct cells	(73–75)
TNF- α	Monocytes and macrophages	rheumatoid arthritis patients	NF- κ B and NADPH oxidase activation	upregulates the expressions of chemokine and adhesion molecule in vessels, facilitates microvascular remodeling and sodium retention, and reduce NO production	(76–81)
IFN- γ	Th1 cells	Ang II-treated IFN- γ R knockout mice	Increases the angiotensinogen expression	Promotes renal fibrosis and decreases glomerular filtration rate	(82)
IL-1 β	Monocytes, T cells and neutrophils	Diabetic db/db mice	Polarize the naïve macrophages into M1 subtype	Releases a large amount of IL-6	(83)

CCL-2, C-C motif chemokine ligand 2; IL, interleukin; IFN- γ , interferon gamma; NADPH, nicotinamide adenine dinucleotide phosphate; NF- κ B, nuclear factor kappa-B; NO, nitric oxide; Th, T helper; TNF- α , tumor necrosis factor α .

activation of Janus kinases and Ras-mediated signal pathways, are initiated immediately (88). IL-6 is responsible for regulating the expression of the acute-phase plasma proteins in liver cells. In addition, IL-6 could facilitate the production of IL-17 *via* polarizing CD4⁺ T cells. Mounting evidence indicates that IL-6 has a crucial role in aspects of the chronic inflammatory response, such as hypertension, rheumatoid arthritis, and ischemic heart disease. Blocking IL-6-related signaling pathways by using the human monoclonal antibody Tocilizumab has shown considerable clinically therapeutic effect on rheumatoid and juvenile arthritis, and related clinical trials are being performed in other inflammatory diseases (89). Therefore, IL-6 may well have a potential therapeutic role in CVD treatment, especially with hypertension.

Accumulating evidence strongly indicates that IL-6 signaling pathways are a vital link in Ang II-induced hypertensive animal models, as the level of IL-6 had a positive relationship with blood pressure and was significantly lower when the Ang-II receptor was blocked (73). *In vivo* animal studies show that injection of Ang II can increase plasma IL-6 concentration and blood pressure, whereas the blood pressure-raising effect of Ang-II was clearly weakened in IL-6^{-/-} mice (74, 75), and was also blocked by spironolactone, suggesting the activation of mineralocorticoid receptors. In addition, evidence from *in vitro* experiments indicated that IL-6 promotes the expression and activity of sodium channels in mouse cortical collecting duct cells (90), implicating that IL-6 may have the ability to facilitate water and sodium retention *in vivo*. Thus, these research

suggested that IL-6 may a potential and promising therapeutic targets in lowering blood pressure leading to the inhibition of the activity of mineralocorticoid receptors and sodium channels in duct cells.

4.2.3 Tumor necrosis factor- α

TNF- α is a well-established inflammatory cytokine in the acute phase response, whose expression has been shown to increase in human and rodent hypertension studies (91). The role of TNF- α signaling in modulating many secondary inflammatory processes, such as cytokine secretion, cell differentiation, and apoptosis, is complex and cell-type and dose-dependent (92). Clinical trial data show that elevated plasma IL-6 concentrations are tightly associated with the severity of refractory hypertension and the six-year risk of death (93). In contrast, TNF- α inhibitors could lower the level of blood pressure in patients and animal models (76, 77). Although a variety of cells can secrete TNF- α , which can activate other immune cells through TNF- α receptors (TNFR1 and TNFR2), it is mainly secreted by monocytes and macrophages. The activation of TNF- α receptors is responsible for cell apoptosis, NADPH oxidase activation, and nuclear factor kappa B (NF κ B) activation (78). An accumulating body of studies suggest that NF κ B and NADPH oxidase activation promote hypertension by upregulating the expression of chemokines and adhesion molecules in blood vessels, facilitating microvascular remodeling and sodium retention (79). Superoxide production from NADPH oxidase could react

with endothelial NO to form the strong oxidant peroxynitrite. This can severely affect vasodilation and cause a significant elevation of blood pressure because of the decrease in NO levels. Moreover, TNF- α can affect the promoter of eNOS and help destabilize the eNOS mRNA structure, which eventually leads to the massive degradation of eNOS and reduction of NO synthesis (80, 81). In kidneys, TNF- α can inhibit eNOS activity in the renal medulla in a Rho-kinase dependent fashion, thereby reducing production of NO which inhibits sodium reabsorption at several sites along the renal tubule (94, 95), and can result in renal injury directly which shift the pressure natriuresis curve to promote the elevation of blood pressure. Thus, TNF- α plays an important role in elevating blood pressure. Unfortunately, TNF- α inhibitors are currently mainly used to treat autoimmune diseases, and there is no evidence that they can be used to lower blood pressure and improve cardiovascular prognosis, but that is worthy to explore and evaluate in the future.

4.2.4 Interferon gamma

IFN- γ is the only known member of the type II family of interferons and is mainly produced by T helper (Th) 1 cells. IFN- γ is not only an important part of adaptive immune responses but also indispensable in protecting hosts from infection. William et al. reported that IFN- γ -producing CD4⁺ and CD8⁺ T cells are consistently increased in hypertensive mice (21), but, according to the results from Ishimitsu et al., subcutaneous injections of IFN- γ could lower blood pressure and alleviate proteinuria and glomerular injury in Dahl salt sensitive rats (96). However, the effect on lowering blood pressure did not observe in the mice with essential hypertension (96). The study neglected the role of endogenous IFN- γ in hypertension, which might be responsible for the conflicting results. The previous study suggested that IFN- γ R deficiency can significantly attenuate ventricular hypertrophy and ventricular electrical remodeling (82). Although high doses of angiotensin were injected, blood pressure levels did not increase significantly, but the degree of renal fibrosis was reduced while the glomerular filtration rate was maintained in mice lacking the IFN- γ receptor 1 compared with that in wild-type mice (82). One of the most important mechanisms whereby IFN- γ triggers hypertension is that IFN- γ can increase the expression of angiotensinogen of rat renal proximal tubule cells in a JAK2/STAT3-dependent manner (97), which consequently increases blood volume. Therefore, it is reasonable to infer that interferon-secreting T cells may establish a link with RAAS by regulating the production of angiotensinogen, resulting in an increase in blood pressure.

4.2.5 Interleukin 1 beta

IL-1 β is known as an important component of the IL-1 family of interleukins and mainly derived from monocytes, T cells and neutrophils. A growing amount of evidence has confirmed the association between IL-1 β and hypertension (98). Specifically, it has been demonstrated that IL-1 β could

upregulate many proinflammatory genes, including IL-6, IL-17 and IFN- γ , resulting in further tissue injury and inflammation related events, like hypertension and myocardial infarction (99–101). High levels of IL-1 β have been detected in the serum of patients with essential hypertension in recent studies (102), indicating the role of IL-1 β in elevating blood pressure. Considering the tight association with hypertension and the essential role in inflammation, more and more studies on how the IL-1 β involves in pathophysiological mechanisms of hypertension have been performed and explored. According to a previous study, IL-1 β not only triggers the inflammatory response directly but also mediates the phenotype and functions of VSMCs and eventually leads to vascular remodeling on inflammatory-dependent or independent mechanisms (103). A recent study which aimed to evaluate the effect of an IL-1R1 receptor Inhibitor (Anakinra) on lowering the blood pressure in patients with obesity suggested Anakinra could significantly lower the systolic blood pressure and peripheral vascular resistance (104), which supported that the IL-1 β could affect the progression of hypertension. Another study suggests that IL-1 β derived from renal tubular epithelial cells of diabetic db/db mice could polarize the naïve macrophages into M1 subtype which releases a large amount of IL-6 resulting in salt-sensitive hypertension, but could be blunted when inhibited the synthesis of IL-1 β or knocked out the IL-1 R1 in immune cells (83). Thus collectively, IL-1 β plays a crucial role in the progression of essential hypertension and may be a novel promising therapeutic targets of hypertension.

4.3 Gut microbiota and neuroinflammation in hypertension

Recently, we have gained greater understanding of the role of gut microbiota and neuroinflammation in the pathogenesis of hypertension. Interaction between the gut microbiota and epithelial cells of the gut-brain axis is involved in regulating ANS activity to control blood pressure. The endocrine pathway of hypertension mainly involves the activation of the hypothalamus-pituitary-adrenal axis. The complex interactions of immune-regulatory organs such as bone marrow, gut, and spleen, which can enhance vascular tone and contraction, can contribute to increases in peripheral resistance and blood pressure.

In addition, increased neural activity may result in neuroinflammatory events, activating microglia, producing more proinflammatory molecules, and an inflammatory environment in autonomic brain regions. Disorder of the gut-brain axis, including gut microbiota dysbiosis, gut epithelial injury, and deranged brain input, is responsible for hypertension through inflammatory mediators, metabolites, circulating bacteria, and altered afferent information, causing neuroinflammation and disorder of the ANS. This in turn can

negatively impact gut functions and associated microflora to create a vicious spiral. In this section, we address the role of an impaired gut-brain axis in the pathophysiology of hypertension.

The ANS can regulate the arterial blood pressure by controlling the vasomotor activity of sympathetic and parasympathetic nerves. Numerous inflammatory cytokines, including IL-1 β (105), TNF- α , IL-6 (88), and IFN- γ (91), were detected in animal brains in hypertension models, and these cytokines have been demonstrated to raise blood pressure by increasing sympathetic nerve activity. Furthermore, the impaired blood-brain barrier is another important cause of neuroinflammation. For example, increasing evidence suggests that Ang-II as well as gut microbes and their metabolites affect the blood-brain barrier permeability, which allows more cytokines to enter the brain. Once the blood-brain barrier is disturbed, circulating inflammatory factors and toxins can enter autonomic brain regions, interfering with normal neural activity and causing hypertension (106). Microglial cells are the important part of the IIS in the brain, and responsible for homeostasis of the central nervous system *via* clearing senescent and apoptotic cells (107). Inhibition of microglia activation helps to decrease hypertension and alleviate sympathetic activation and peripheral inflammation (108). Interestingly, specific deletion of microglia could significantly relieve the Ang II-induced elevation of blood pressure and inflammation (109).

In recent years, the gut microbiota has become a hot research topic in CVDs and metabolic diseases and is considered as the most promising interventional target of chronic diseases in the coming decades. Rapid developments and major breakthroughs in sequencing technologies have helped recognize the important role of the gut microbiota on body homeostasis, especially regarding obesity, insulin resistance, and CVDs. Animal and human experiments consistently showed that patients with hypertension had significantly lower gut flora richness compared with that of normotensive subjects (110). Two concurrent studies have reported the relationship between gut microbiome composition and hypertension (111, 112). A recent study by Mell et al. highlighted differences in the cecal microflora between salt-sensitive and -tolerant strains in Dahl rats (111). Moreover, changes in the variety and abundance of several short chain fatty acids in the plasma were observed after cecal transplantation. Thus, there is reason to believe microbial composition may affect the levels of short chain fatty acids in the plasma *via* roles in metabolism. Significant dysbiosis due to decreased microbial richness, diversity, homogeneity, and increased Firmicutes/Bacteroides ratios in hypertensive animals have been observed by comparing changes in the fecal microflora in spontaneously hypertensive and chronic Ang II-infused hypertensive rats (112). Another difference between the microbiota of normotensive and hypertensive patients is the production of LPS. *Veillonellae* are enriched in gut microbes in human hypertensive patients and produce LPS. Biofilms encapsulate bacterial communities in an extracellular matrix

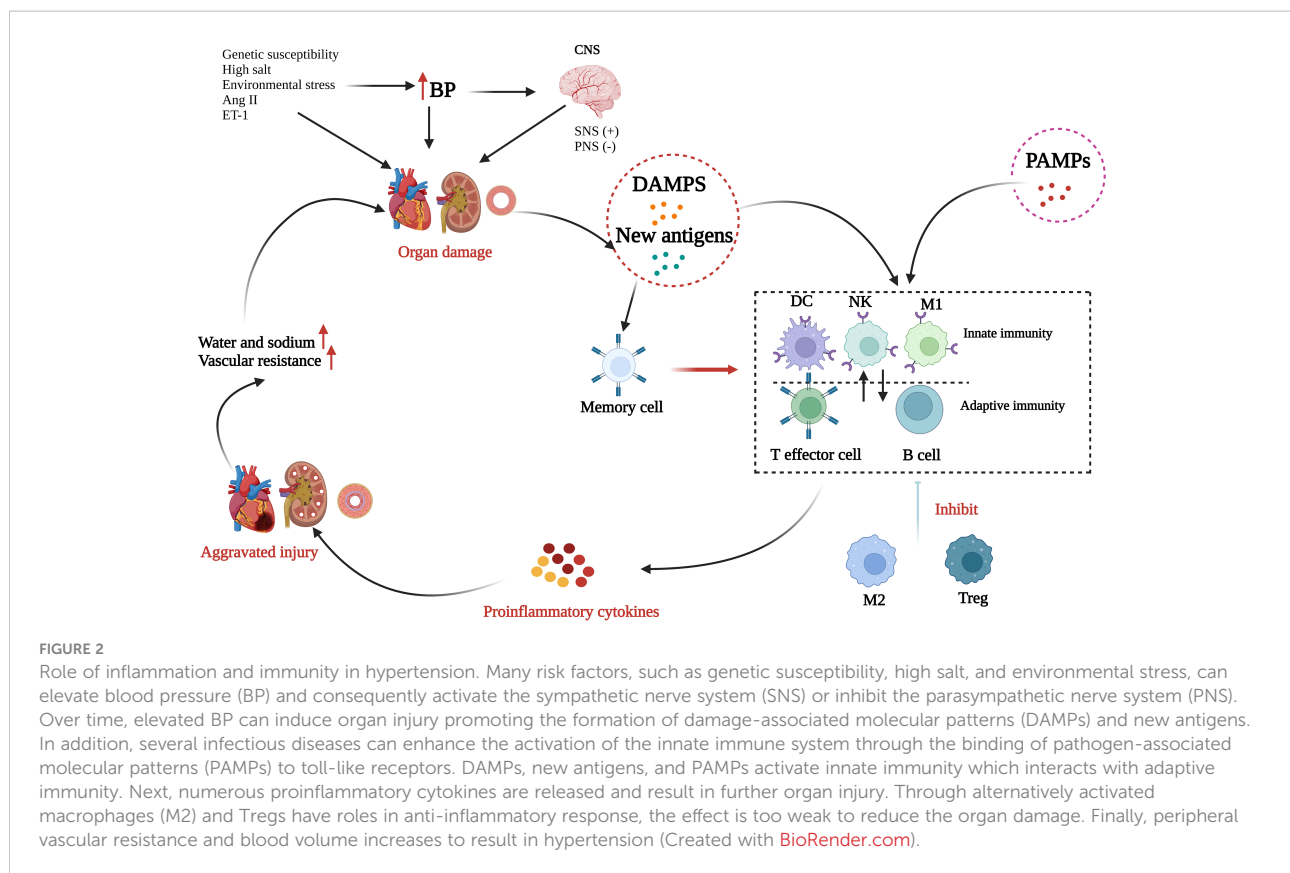
produced by bacteria, increasing their adhesion, and creating an environment that is more suitable for their growth. LPS-producing bacteria in biofilms were more inflammatory than Gram-negative bacteria without biofilm protection (113, 114). This shows that the hypertensive microbiota are more inflammatory throughout the body and, because of the arrival of LPS in the brain, are more responsible for the possibility of ANS activation and hypertension.

5 Immunity in hypertension

The human immune system includes the IIS and the adaptive immune system (AIS), and the components of these function in an extremely complex and complementary manner to exterminate invaders and rescue injured tissue, thereby maintaining homeostasis. Most immune cells become involved in the initiation, progress, and maintenance of hypertension (Figure 2). Briefly, in the presence of genetic susceptibility, several environmental factors, especially salt and environmental stress, can cause a small rise in arterial blood pressure responsible for activating sympathetic nerves or inhibiting parasympathetic nerves. Next, elevated blood pressure causes or aggravates tissue damage and together with oxidative stress damage caused by Ang II and ET-1 is conducive to the formation of DAMPs and new antigens, and thereby initiates subsequent inflammatory activation. DAMPs trigger the activation of the IIS by recognizing and activating the Toll-like receptors (TLRs) on antigen-presenting cells while the new antigens enhance the immunogenicity of dendritic cells and facilitate their production and release of proinflammatory cytokines, which not only enable the proliferation and activation of T cells but also further produce more cytokines. DAMPs and new antigens can activate $\gamma\delta$ T cells, which can activate T lymphocytes directly. Several infectious diseases can also enhance the activation of the IIS in a PAMP-dependent manner. Innate immune cells and $\gamma\delta$ T cells release proinflammatory cytokines as well as autoantibodies, directly or through the activated AIS, producing vascular and renal damage, which is a feedforward process contributing to a progressive rise in blood pressure. In addition, additional effects, such as high salt intake, may reactivate the T effector memory cells in the lymphoid organs, which will induce a more intense inflammatory response and cause more severe tissue damage. M2 macrophages and Treg cells have a role in anti-inflammatory response during this process, although their effect is very weak and not enough to reduce the organ damage.

5.1 Innate immune system

Innate immunity is the rapid, nonspecific defense response to a variety of exogenous stimuli that is often considered as the early stage of inflammation. The key effectors are mainly



monocytes, M1 macrophages, natural killer cells, and neutrophils. Monocytes/macrophages have been revealed to be tightly associated with the microvascular remodeling. In a rodent model with a deficiency in macrophage colony stimulating factor, Ang II failed to induce endothelial injury and vascular oxidative stress or elevate blood pressure (115). Consistently, removing lysozyme M-positive myelomonocytic cells prevented mice from suffering severe hypertension (116). As mentioned above, macrophages are crucial to the progress of hypertension and, although the exact mechanisms remain elusive, increasing evidence indicates that a large amount of ROS derived from activated macrophages may cause irreversible vascular endothelial cell damage and microvascular remodeling, causing increased peripheral arteriolar resistance (116, 117). Experiments have shown that activated monocytes can produce endothelial dysfunction. Chemokines become involved in the pathological process of hypertension by recruiting immune cells to the site of endothelial injury, causing further impairment of endothelial function. An increase in the number of monocytes and neutrophils with the CXCL1 receptor CCR2 can be clearly detected in patients with hypertension, suggesting that blocking CCR2 may alleviate inflammation and control blood pressure. Neutrophils are an important component of the IIS and produce large quantities of cytokines and superoxide anion when stimulated (118). Ang-II

could connect thromboinflammation with essential hypertension by inducing neutrophil to release extracellular traps. The use of plasma from untreated patients with hypertension to stimulate neutrophils in normal patients can facilitate the production of endothelial collagen, thereby causing vascular remodeling and injury (119). More recently, the gene *SH2B3* (*LNK*) that encodes SH2B adaptor protein 3 have been confirmed that regulate the immune cell (notably T cells and macrophages) development, differentiation, and signaling in the hypertension according to the genome-wide association studies (120). Therefore, elucidating molecular mechanisms where *SH2B3* regulating immune cells in hypertension may found novel therapeutic targets for hypertension.

5.2 Adaptive immune system

Increasing evidence suggests that the activated AIS promotes the pathogenesis of hypertension and aggravates targeted organ damage. The AIS executes a highly specific response and is regulated by activated T and B lymphocytes. According to specific markers on the cells, T lymphocytes are divided into two subpopulations: CD4⁺ and CD8⁺ T lymphocytes. Although it has been confirmed that both types of T cells are involved in the initiation and progression of hypertension, results based on

in vivo models showed that CD4⁺ T cells are likely to be the key factor in promoting hypertension (121). However, Trott et al. reported that CD8⁺ T cells can be a crucial motivating force in experimental hypertension. Once the endogenous or exogenous antigens presented by antigen-presenting cells are recognized, lymphocytes are activated and differentiated into T effector cells or Treg cells (122). Under the action of inflammatory cytokines or chemokines, these activated T lymphocytes target the site of inflammation. The balance among T cell subsets can influence inflammatory responses. Kassan et al. (123) described the relationship between Tregs and vascular dysfunction in patients with hypertension and found that endothelial damage, plaque rupture, and arterial occlusion mainly resulted from the imbalance of Treg cells.

The hypothesis that T lymphocytes are the important participant in the pathogenesis of hypertension was proposed many years ago but failed to receive enough attention initially. It was not until the past 20 years that experimental evidence confirmed the exact role of T lymphocytes in elevating blood pressure and promoting vascular injury (76). Elevated blood pressure may further activate the immune response *via* modifying self-antigens or generating new antigens. Studies have shown that several T lymphocyte subsets may promote the occurrence of hypertension and vascular remodeling (124). T- and B-lymphocyte-deficient mice, produced by silencing recombination-activated gene 1 (RAG1^{-/-}), exhibited a blunted hypertensive response compared with that in control mice in the Ang II-induced hypertension animal model. Adoptive transfer of effector T cells, but not B cells, to the RAG1^{-/-} mice restored the effects of Ang II (76). Moreover, in mice lacking T cells, there was insufficient infiltration of innate immune cells in vascular pathological sections, which was possibly related to the absence of cytokines derived from Th cells (76).

Studies have demonstrated that T lymphocyte-mediated immune responses can be induced by oxidative stress. The role of Th17, an important part of effector T cells, in hypertension has been identified by Madhur et al. (125). Th17 not only promotes but can also inhibit inflammation. Using the Ang II-induced hypertension animal model, improved vascular function, lowered oxidative stress levels, and decreased T lymphocyte infiltration have been observed in IL-17^{-/-} mice compared with these parameters in control mice (125). Madhur et al. revealed that the blood pressure level is positively correlated with the amount of circulating Th17 cells and that the inhibition of IL-17 contributes to the improvement of hypertension, which is consistent with previous research. In addition, enhanced acquired immunity due to genetic susceptibility, and vascular inflammation due to decreased Treg immunosuppressive function may contribute to hypertension (126). Viel et al. proposed a famous hypothesis that the genetic predisposition based on loci on chromosome 2 where many proinflammatory genes locate enhances adaptive immunity (127).

6 Oxidative stress in hypertension

Oxygen molecules can easily form free radicals because of their special electronic arrangement structure. These oxygen molecules are called oxygen free radicals (OFR) and include the superoxide anion, hydroxyl radical, and NO free radical. The hydroxyl radical is the most active OFR found so far. Furthermore, ROS, which includes H₂O₂ and O₃ as well as OFR, is a critical signaling molecule that mediates the activation of transcription factors, induction of immune response genes, and the phosphorylation of kinases (128). Cumulative evidence from humans and animals suggests that ROS plays an important part in regulating endothelial cell function and vascular remodeling (129, 130). In the development of hypertension, the interaction of ROS and humoral factors such as ET-1 and Ang-II increases the production of ROS, especially the superoxide anion produced by the uncoupling of NOXs family and eNOS (130). Recently, studies have suggested that hypertension is associated with the decrease in NO and the increase in oxidative stress (131). ROS directly inhibits the activity of NO (132). In addition, ROS can stimulate the PI3K/Akt-MAPK pathway related to redox transcription factors causing overexpression of redox genes and thereby inhibiting the expression of eNOS mRNA and eNOS activity, which reduces the availability of NO. NADPH oxidase is regarded as the most important provider of ROS in vascular walls and endothelial cells and has an indispensable role in the pathogenesis of endothelial dysfunction and vascular remodeling. There is another crucial source of eNOS, xanthine oxidase and mitochondrial uncoupling, that helps to explain the increase in ROS production in different vascular diseases (133, 134). Previous evidence demonstrated that ROS regulates the arrangement of various proteins and the role of signal pathways in cells and that this redox biology is precisely and spatially regulated to influence the individual healthy conditions. Moreover, disordered physiological ROS production can cause a variety of diseases, including hypertension. During hypertension, neurohumoral factors can stimulate receptors located on the cell membrane to activate NADPH oxidase and mitochondria to produce ROS, such as highly active superoxide anions, which can then initiate cellular phosphorylation pathways (135). This subsequently initiates gene expression of factors such as p53, activating protein-1 (AP-1), nuclear E2-related factor 2 (Nrf2), and NFκB. Eventually, these changes result in endothelial dysfunction and hypertension (136, 137).

7 Novel potentially therapeutic strategies in hypertension

Multiple animal experiments have proved that an insufficiency of vascular endothelial cells is closely related to the increase in arterial blood pressure. Considering the

pathogenesis, prevalence, and severity of hypertension, it is critical to find novel and potential therapeutic strategies to lower blood pressure. In this section, we will summarize and explore the role of anti-inflammation and antioxidant therapies for hypertension (Figure 3).

7.1 Anti-inflammation therapeutic role in hypertension

As mentioned above, chronic inflammation has a close association with elevated blood pressure. Clinical studies indicate that elevated CRP levels at baseline are more likely due to an increased risk of hypertension (138). Although inflammatory activation is closely associated with elevated blood pressure, so far there is no obvious data supporting that routine use of anti-inflammatory drugs can treat hypertension. Table 2 describes several drugs that may lower blood pressure *via* an anti-inflammatory effect. A preliminary analysis of one clinical study shows that minocycline, a broad-spectrum tetracycline antibiotic has a continuous antihypertensive effect in patients with hypertension (139). Mycophenolate mofetil is a well-known immunosuppressant, whose active metabolite inhibits the activation and synthesis of T and B lymphocytes by inhibiting dihydrolactate dehydrogenase and thereby decreases the synthesis of pyrimidine nucleotides, which can significantly lower blood pressure in salt-sensitive hypertension (140). In addition, a significant effect of mycophenolate mofetil on lowering blood pressure has been observed in patients

suffering from psoriasis and rheumatoid arthritis (141). Another observational study showed that long-term use of immunosuppressive drugs can alleviate arterial stiffness and lower blood pressure in patients with chronic kidney disease (142). A monoclonal antibody against IL-17A could lower baseline blood pressure in patients with psoriasis (143). In addition, an IL-1 receptor antagonist (anakinra) could significantly reduce the blood pressure after a 14-day treatment *via* specifically inhibiting the actions of IL-1 α and IL-1 β (145, 146), but no significant antihypertensive effect was observed with canakinumab (an IL-1 β antagonist) in large-scale randomized controlled trials in patients with previous myocardial infarction and elevated hsCRP (147). The study suggests that the mechanisms of reducing major adverse cardiovascular events are not associated with the change of blood pressure. The main reason that canakinumab does not lower the blood pressure may be related to the enrolled populations of whom 80% are patients with hypertension and were taking antihypertensive drugs, which may mask the real antihypertensive effect of canakinumab. Statins are widely used lipid-controlling drugs in clinics and can significantly reduce cholesterol levels, thereby reducing the risk of CVDs and improving prognosis. Statins also show multiple effects and have particular benefits on the cardiovascular system. Mounting evidence has demonstrated that statins have mild antihypertensive effects, especially in patients with intractable blood pressure and with hypertensive target organ damage (102, 144). The underlying mechanism whereby statins reduce blood pressure may be associated with the protective effect on the

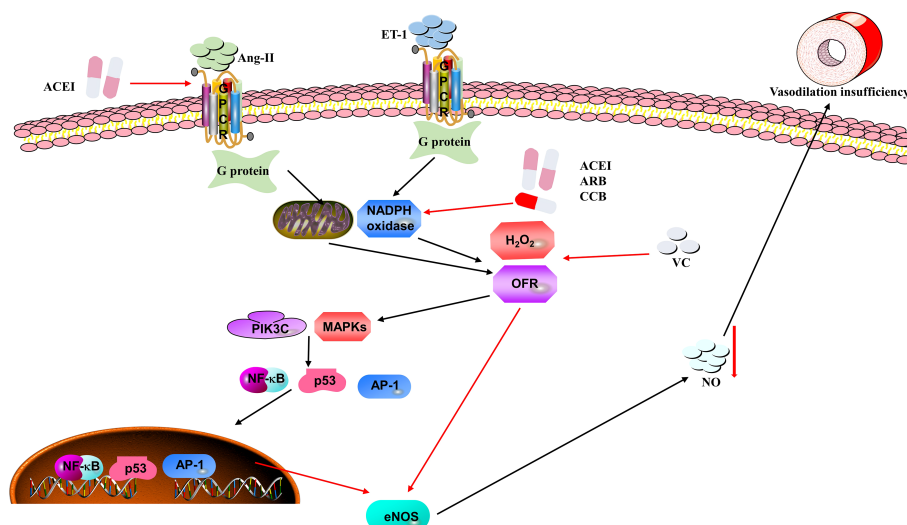


FIGURE 3

Mechanisms of oxidative stress causing hypertension in vascular endothelial cells. Ang II and ET-1 can stimulate NADPH oxidase and mitochondria to produce ROS (e.g., H₂O₂ and OFR), which are recognized by their receptors on the endothelial cells. ROS stimulate the PI3K/Akt-MAPK pathway to inhibit the expression of eNOS mRNA and eNOS activity, thus reducing the availability of NO, which results in vasodilation insufficiency and elevation of blood pressure. Moreover, angiotensin converting enzyme inhibitors (ACEIs), angiotensin receptor blockers (ARBs), calcium channel blockers (CCBs) and vitamin C (VC) may be potential therapeutic strategies in the process of oxidative stress.

TABLE 2 Anti-inflammation therapeutic strategies in hypertension.

Agents	Intervention objects	Mechanisms	Biological effects	Reference
Minocycline	A patient with resistant hypertension	Has direct effects on gut microbiota	May cause a large reduction in Firmicutes and Bacteroidetes and a corresponding dramatic increase in Proteobacteria	(139)
Mycophenolate mofetil	Ang-II induced hypertensive rat models or patients with autoimmune disease	Prevents the development of salt-sensitive hypertension	Significantly reduces tubulointerstitial injury, superoxide-producing cells and T-cell infiltration and activation	(140–142)
Anti-IL-17A antibody	Hypertension rat models or patients with psoriatic arthritis	Inhibits IL-17 receptor unit A	Blocks the transport pathway including sodium hydrogen exchanger 3, Na-K-2Cl-cotransporter, Na-Cl cotransporter, epithelial sodium channel of renal tubules stimulated or upregulated by IL-17A	(72, 85–87, 143)
Statins	Patients with intractable hypertension	Anti-inflammatory and antioxidant effects that could reduce arterial stiffening and protect vascular endothelium	Inhibits the production of ROS, reducing the circulating level of pro-inflammatory cytokines and inhibits the expression of adhesion molecules on vascular endothelial cells and smooth muscle cells	(102, 144)

vascular endothelium by inhibiting the production of ROS, reducing the circulating level of proinflammatory cytokines, and inhibiting the expression of adhesion molecules on vascular endothelial cells and smooth muscle cells.

7.2 The value of antioxidant therapy in hypertension

Antioxidants are substances that effectively trap ROS, so they can reduce oxidative damage and may lower blood pressure (Table 3). The use of antioxidants, such as vitamin C and E, have been confirmed as effective therapeutic strategies in lowering the level of blood pressure. Vitamin C as an enzyme manager, increases eNOS activity and reduces ROS, and has been proved to improve vasodilation in hypertensive patients (158). Studies from humans and animals have shown that vitamin C can enhance endothelial function in a variety of situations (159). The effect of antioxidants on lowering blood pressure and enhancing vascular function has been confirmed in the hypertensive animals (160). One possible reason is that the free contractile response to norepinephrine is increased in patients with hypertension, which can be reduced by vitamin C (148). However, in several large-scale clinical trials, the effect of supplementation of vitamin C on blood pressure was unpredictable and more experiments are needed to confirm the exact effect (161–163), which may result from the reduced bioavailability of NO. B-cell lymphoma 6 (BCL6) is known as a key intervention target for autoimmune diseases by inhibiting production of ROS and apoptosis (149); however, it is unclear whether this can reduce hypertension. Chen et al. recently reported that BCL6 can lower blood pressure by suppressing vascular smooth muscle cell proliferation, attenuating oxidative stress injury, and microvascular remodeling in the Ang-II induced hypertensive rats (150).

In addition, several antihypertensive drugs currently used in the clinic have a significant and specific effect on decreasing the incidence of hypertension independent of the expected mechanism. Next, we will mainly discuss the ACEI, ARB, beta-blockers, and CCBs. RAAS has a crucial part in the production of ROS during the process of hypertension. NOXs are recognized as one of most important sources of ROS in the endothelium and are mainly induced by Ang-II (149). Both ACEI and ARB can not only effectively inhibit the activity of NOXs but improve the superoxide dismutase activity (151). In addition, they can prevent eNOS from uncoupling and enhance NO activity (152, 153). The novel beta-blockers, nebivolol and carvedilol, have been reported to have antioxidant properties. According to the results from clinical and experimental studies, these drugs have favorable protective effects on endothelial function and do not depend on the activity of beta-blockers. The antioxidant effect of carvedilol is mainly based on reducing the ROS production from inflammatory cells and the oxidation of low-density lipoprotein (LDL). Carvedilol and nebivolol could improve endothelium dependent vasodilation performance in patients with hypertension (154). Moreover, nebivolol exhibits a protective effect in the endothelial function and lowers blood pressure through suppressing the activity and expression of NADPH oxidase, thereby preventing eNOS uncoupling and promoting eNOS activity to produce more NO (155, 156). CCBs, especially dihydropyridines (like nifedipine) could directly reduce production of ROS to protect the endothelial function. CCBs have been demonstrated to prevent oxidized LDL, which can promote ROS production to trigger oxidative damage from causing endothelial dysfunction (157). Therefore, in addition to the direct effect of lowering blood pressure, dihydropyridine, CCBs play an additional antihypertensive effect by improving the function of vascular endothelial cells through antioxidation.

TABLE 3 Antioxidant therapy in hypertension.

Agents	Intervention objects	Mechanisms	Biological effects	Reference
Vitamin C	Patients with hypertension	Have a beneficial effect on vasodilation	Antagonizing the free contraction induced by norepinephrine by antioxidation	(148)
BCL6	Ang-II induced hypertensive rats	Reduces producing of ROS and cell apoptosis	Inhibits vascular smooth muscle cells proliferation, attenuating oxidative stress injury and microvascular remodeling	(149, 150)
ACEIs/ ARBs	Diabetic rats or patients with coronary artery disease	Suppress the RAAS producing ROS	Effectively inhibit the activity of NADPH oxidase, improve the superoxide dismutase activity, prevent eNOS from uncoupling and enhance of NO activity	(149, 151–153)
Novel beta-blockers	Hypertensive patients	Protect endothelial function	Reduces the ROS production from inflammatory cells and the oxidation of LDL, improve endothelium dependent vasodilation performance, inhibit the activity and expression of NADPH oxidase and prevent eNOS uncoupling and promoting eNOS activity	(154–156)
CCBs	Human aortic endothelial cells	Prevent oxidized low density lipoprotein	Lower the ROS production to alleviate oxidative damage	(157)

ACEIs, angiotensin converting enzyme inhibitors; ARBs, angiotensin receptor blockers; BCL6, B-cell lymphoma 6; CCBs, calcium channel blockers; eNOS, endothelial nitric oxide synthase; LDL, low density lipoprotein; NADPH, nicotinamide adenine dinucleotide phosphate; NO, nitric oxide; ROS, reactive oxygen species.

8 Conclusion

Accumulating evidence shows that hypertension is a chronic inflammatory condition that involves the migration, accumulation, and activation of immune cells and the production of ROS. Although many studies have been performed, the specific molecular mechanisms of inflammation and immunity that affect elevated blood pressure remain unclear. Inflammatory or oxidative stress can damage vascular endothelial cells and cause microcirculation remodeling; however, whether this can increase blood pressure through other mechanisms requires more research. Although there are many drugs that can treat hypertension, a deeper understanding of the mechanism of elevated blood pressure and the discovery of more action targets will be more conducive to earlier detection and intervention of hypertension and thereby significantly reduce the occurrence of cardiovascular adverse events. As emphasized in this review, the occurrence of hypertension is complex, so it is necessary to understand the pathological mechanism of the different stages. In addition, there is also an urgent requirement for the research and development of new antihypertensive drugs for different targets.

Author contributions

(I) Conception and design: All authors. (II) Administrative support: None. (III) Provision of study materials or patients:

None. (IV) Collection and assembly of data: None. (V) Data analysis and interpretation: None. (VI) All authors contributed to the article and approved the submitted version.

Funding

This study was supported by grants from the National Key Research and Development Program of China (2016YFC1300100), Nonprofit Central Research Institute Fund of Chinese Academy of Medical Sciences (2019XK320057), CAMS Innovation Fund for Medical Science (CIFMS, 2022-I2M-C&T-A-010).

Acknowledgments

We thank Mike Herbert, PhD from Liwen Bianji (Edanz) (www.liwenbianji.cn) for editing the English text of a draft of this manuscript.

Conflict of interest

The authors declare that the research was conducted in the absence of any commercial or financial relationships that could be construed as a potential conflict of interest.

Publisher's note

All claims expressed in this article are solely those of the authors and do not necessarily represent those of their affiliated

organizations, or those of the publisher, the editors and the reviewers. Any product that may be evaluated in this article, or claim that may be made by its manufacturer, is not guaranteed or endorsed by the publisher.

References

- Global Burden of Metabolic Risk Factors for Chronic Diseases Collaboration. Cardiovascular disease, chronic kidney disease, and diabetes mortality burden of cardiometabolic risk factors from 1980 to 2010: A comparative risk assessment. *Lancet Diabetes Endocrinol* (2014) 2:634–47. doi: 10.1016/S2213-8587(14)70102-0
- NCD Risk Factor Collaboration (NCD-RisC). Worldwide trends in blood pressure from 1975 to 2015: A pooled analysis of 1479 population-based measurement studies with 19.1 million participants. *Lancet* (2017) 389 (10064):37–55. doi: 10.1016/S0140-6736(16)31919-5
- Whelton PK, Carey RM, Aronow WS, Casey DE Jr, Collins KJ, Dennison Himmelfarb C, et al. 2017 ACC/AHA/AAPA/ABC/ACPM/AGS/APHA/ASH/ASPC/NMA/PCNA guideline for the prevention, detection, evaluation, and management of high blood pressure in adults: Executive summary: A report of the American college of Cardiology/American heart association task force on clinical practice guidelines. *Hypertension* (2018) 71(6):1269–324. doi: 10.1161/HYP.0000000000000066
- Eljovich F, Laffer CL, Sahinoz M, Pitzer A, Ferguson JF, Kirabo A. The gut microbiome, inflammation, and salt-sensitive hypertension. *Curr Hypertens Rep* (2020) 22(10):79. doi: 10.1007/s11906-020-01091-9
- Lu X, Crowley SD. Inflammation in salt-sensitive hypertension and renal damage. *Curr Hypertens Rep* (2018) 20(12):103. doi: 10.1007/s11906-018-0903-x
- Egan BM, Zhao Y, Axon R. US Trends in prevalence, awareness, treatment, and control of hypertension, 1988–2008. *JAMA* (2010) 303(20):2043–50. doi: 10.1001/jama.2010.650
- Barrows IR, Ramezani A, Raj DS. Inflammation, immunity, and oxidative stress in hypertension-partners in crime? *Adv Chronic Kidney Dis* (2019) 26 (2):122–30. doi: 10.1053/j.ackd.2019.03.001
- Caillon A, Schiffrin EL. Role of inflammation and immunity in hypertension: Recent epidemiological, laboratory, and clinical evidence. *Curr Hypertens Rep* (2016) 18(3):21. doi: 10.1007/s11906-016-0628-7
- Norlander AE, Madhur MS, Harrison DG. The immunology of hypertension. *J Exp Med* (2018) 215(1):21–33. doi: 10.1084/jem.20171773
- Rizzoni D, De Ciuceis C, Szczepaniak P, Paradis P, Schiffrin EL, Guzik TJ. Immune system and microvascular remodeling in humans. *Hypertension* (2022) 79 (4):691–705. doi: 10.1161/HYPERTENSIONAHA.121.17955
- Muller DN, Shagdarsuren E, Park JK, Dechend R, Mervaala E, Hampich F, et al. Immunosuppressive treatment protects against angiotensin II-induced renal damage. *Am J Pathol* (2002) 161(5):1679–93. doi: 10.1016/S0002-9440(10)64445-8
- Rodríguez-Iturbe B, Pons H, Quiroz Y, Gordon K, Rincon J, Chavez M, et al. Mycophenolate mofetil prevents salt-sensitive hypertension resulting from angiotensin II exposure. *Kidney Int* (2001) 59(6):2222–32. doi: 10.1046/j.1523-1755.2001.00737.x
- Ko EA, Amiri F, Pandey NR, Javeshghani D, Leibovitz E, Touyz RM, et al. Resistance artery remodeling in deoxycorticosterone acetate-salt hypertension is dependent on vascular inflammation: Evidence from m-CSF-deficient mice. *Am J Physiol Heart Circ Physiol* (2007) 292(4):H1789–95. doi: 10.1152/ajpheart.01118.2006
- Kossmann S, Hu H, Steven S, Schonfelder T, Fraccarollo D, Mikhed Y, et al. Inflammatory monocytes determine endothelial nitric-oxide synthase uncoupling and nitro-oxidative stress induced by angiotensin II. *J Biol Chem* (2014) 289 (40):27540–50. doi: 10.1074/jbc.M114.604231
- Wiig H, Schroder A, Neuhofer W, Jantsch J, Kopp C, Karlsen TV, et al. Immune cells control skin lymphatic electrolyte homeostasis and blood pressure. *J Clin Invest* (2013) 123(7):2803–15. doi: 10.1172/JCI60113
- Xiao L, Kirabo A, Wu J, Saleh MA, Zhu L, Wang F, et al. Renal denervation prevents immune cell activation and renal inflammation in angiotensin II-induced hypertension. *Circ Res* (2015) 117(6):547–57. doi: 10.1161/CIRCRESAHA.115.306010
- Zaldivia MTK, Rivera J, Hering D, Marusic P, Sata Y, Lim B, et al. Renal denervation reduces monocyte activation and monocyte-platelet aggregate formation: An anti-inflammatory effect relevant for cardiovascular risk. *Hypertension* (2017) 69(2):323–31. doi: 10.1161/HYPERTENSIONAHA.116.08373
- O'Donnell M, Mente A, Yusuf S. Sodium intake and cardiovascular health. *Circ Res* (2015) 116(6):1046–57. doi: 10.1161/CIRCRESAHA.116.303771
- Wright JT Jr, Rahman M, Scarpa A, Fathollahi M, Griffin V, Jean-Baptiste R, et al. Determinants of salt sensitivity in black and white normotensive and hypertensive women. *Hypertension* (2003) 42(6):1087–92. doi: 10.1161/01.HYP.0000101687.89160.19
- Okuda T, Grollman A. Passive transfer of autoimmune induced hypertension in the rat by lymph node cells. *Texas Rep Biol Med* (1967) 25:257–64.
- McMaster WG, Kirabo A, Madhur MS, Harrison DG. Inflammation, immunity, and hypertensive end-organ damage. *Circ Res* (2015) 116(6):1022–33. doi: 10.1161/CIRCRESAHA.116.303697
- Kamat NV, Thabet SR, Xiao L, Saleh MA, Kirabo A, Madhur MS, et al. Renal transporter activation during angiotensin-II hypertension is blunted in interferon- γ -/- and interleukin-17A-/- mice. *Hypertension* (2015) 65(3):569–76. doi: 10.1161/HYPERTENSIONAHA.114.04975
- Vinh A, Chen W, Blinder Y, Weiss D, Taylor WR, Goronzy JJ, et al. Inhibition and genetic ablation of the B7/CD28 T-cell costimulation axis prevents experimental hypertension. *Circulation* (2010) 122(24):2529–37. doi: 10.1161/CIRCULATIONAHA.109.930446
- Wu KL, Chan SH, Chan JY. Neuroinflammation and oxidative stress in rostral ventrolateral medulla contribute to neurogenic hypertension induced by systemic inflammation. *J Neuroinflamm* (2012) 9:212. doi: 10.1186/1742-2094-9-212
- Wang H, Yu M, Ochani M, Amella CA, Tanovic M, Susarla S, et al. Nicotinic acetylcholine receptor $\alpha 7$ subunit is an essential regulator of inflammation. *Nature* (2003) 421(6921):384–8. doi: 10.1038/nature01339
- Wenzel P, Knorr M, Kossmann S, Stratmann J, Hausding M, Schuhmacher S, et al. Lysozyme m-positive monocytes mediate angiotensin II-induced arterial hypertension and vascular dysfunction. *Circulation* (2011) 124(12):1370–81. doi: 10.1161/CIRCULATIONAHA.111.034470
- Siedlinski M, Jozefczuk E, Xu X, Teumer A, Evangelou E, Schnabel RB, et al. White blood cells and blood pressure: A mendelian randomization study. *Circulation* (2020) 141:1307–17. doi: 10.1161/CIRCULATIONAHA.119.045102
- Xiao L, Harrison DG. Inflammation in hypertension. *Can J Cardiol* (2020) 36:635–47. doi: 10.1016/j.cjca.2020.01.013
- Muñoz M, López-Oliva ME, Rodríguez C, Martínez MP, Sáenz-Medina J, Sánchez A, et al. Differential contribution of Nox1, Nox2 and Nox4 to kidney vascular oxidative stress and endothelial dysfunction in obesity. *Redox Biol* (2020) 28:101330. doi: 10.1016/j.redox.2019.101330
- Schiffrin EL. Vascular remodeling in hypertension: mechanisms and treatment. *Hypertension* (2012) 59:367–74. doi: 10.1161/HYPERTENSIONAHA.111.187021
- Zhang Y, Murugesan P, Huang K, Cai H. NADPH oxidases and oxidase crosstalk in cardiovascular diseases: Novel therapeutic targets. *Nat Rev Cardiol* (2020) 17(3):170–94. doi: 10.1038/s41569-019-0260-8
- Takac I, Schröder K, Zhang L, Lardy B, Anilkumar N, Lambeth JD, et al. The e-loop is involved in hydrogen peroxide formation by the NADPH oxidase Nox4. *J Biol Chem* (2011) 286(15):13304–13. doi: 10.1074/jbc.M110.192138
- Ma MM, Gao M, Guo KM, Wang M, Li XY, Zeng XL, et al. TMEM16A contributes to endothelial dysfunction by facilitating Nox2 NADPH oxidase-derived reactive oxygen species generation in hypertension. *Hypertension* (2017) 69(5):892–901. doi: 10.1161/HYPERTENSIONAHA.116.08874
- Toral M, Romero M, Rodríguez-Nogales A, Jiménez R, Robles-Vera I, Algieri F, et al. Lactobacillus fermentum improves tacrolimus-induced hypertension by restoring vascular redox state and improving eNOS coupling. *Mol Nutr Food Res* (2018):e1800033. doi: 10.1002/mnfr.201800033
- Camargo LL, Harvey AP, Rios FJ, Tsiropoulou S, Da Silva RNO, Cao Z, et al. Vascular nox (NADPH oxidase) compartmentalization, protein hyperoxidation, and endoplasmic reticulum stress response in hypertension. *Hypertension* (2018) 72(1):235–46. doi: 10.1161/HYPERTENSIONAHA.118.10824
- Mikolajczyk TP, Szczepaniak P, Vidler F, Maffia P, Graham GJ, Guzik TJ. Role of inflammatory chemokines in hypertension. *Pharmacol Ther* (2021) 223:107799. doi: 10.1016/j.pharmthera.2020.107799

37. Mikolajczyk TP, Nosalski R, Szczepaniak P, Budzyn K, Osmenda G, Skiba D, et al. Role of chemokine RANTES in the regulation of perivascular inflammation, T-cell accumulation, and vascular dysfunction in hypertension. *FASEB J* (2016) 30:1987–99. doi: 10.1096/fj.201500088R
38. Yasunari K, Maeda K, Nakamura M, Yoshikawa J. Oxidative stress in leukocytes is a possible link between blood pressure, blood glucose, and c-reacting protein. *Hypertension* (2002) 39(3):777–80. doi: 10.1161/hy0302.104670
39. Savoia C, Schiffrin EL. Inflammation in hypertension. *Curr Opin Nephrol Hypertens* (2006) 15:152–8. doi: 10.1097/01.mnh.0000203189.57513.76
40. Foley RN, Collins AJ. End-stage renal disease in the united states: An update from the united states renal data system. *J Am Soc Nephrol* (2007) 18(10):2644–8. doi: 10.1681/ASN.2007020220
41. Dounousi E, Papavasiliou E, Makedou A, Ioannou K, Katopodis KP, Tselepis A, et al. Oxidative stress is progressively enhanced with advancing stages of CKD. *Am J Kidney Dis* (2006) 48(5):752–60. doi: 10.1053/j.ajkd.2006.08.015
42. Stuvling EM, Hillege HL, Bakker SJ, Gans RO, De Jong PE, De Zeeuw D. C-reactive protein is associated with renal function abnormalities in a non-diabetic population. *Kidney Int* (2003) 63(2):654–61. doi: 10.1046/j.1523-1755.2003.00762.x
43. Li Y, Wei B, Liu X, Shen XZ, Shi P. Microglia, autonomic nervous system, immunity and hypertension: Is there a link? *Pharmacol Res* (2020) 155:104451. doi: 10.1016/j.phrs.2019.104451
44. Usui T, Okada M, Hara Y, Yamawaki H. Death-associated protein kinase 3 mediates vascular inflammation and development of hypertension in spontaneously hypertensive rats. *Hypertension* (2012) 60(4):1031–9. doi: 10.1161/HYPERTENSIONAHA.112.200337
45. Valensi P. Autonomic nervous system activity changes in patients with hypertension and overweight: Role and therapeutic implications. *Cardiovasc Diabetol* (2021) 20(1):170. doi: 10.1186/s12933-021-01356-w
46. Noll G, Wenzel RR, Binggeli C, Corti C, Lüscher TF. Role of sympathetic nervous system in hypertension and effects of cardiovascular drugs. *Eur Heart J* (1998) 19 Suppl F:F32–8.
47. Ferrario CM, Mullick AE. Renin angiotensin aldosterone inhibition in the treatment of cardiovascular disease. *Pharmacol Res* (2017) 125(pt A):57–71. doi: 10.1016/j.phrs.2017.05.020
48. Olivares-Silva F, De Gregorio N, Espitia-Corredor J, Espinoza C, Vivar R, Silva D, et al. Resolvin-D1 attenuation of angiotensin II-induced cardiac inflammation in mice is associated with prevention of cardiac remodeling and hypertension. *Biochim Biophys Acta Mol Basis Dis* (2021) 1867(12):166241. doi: 10.1016/j.bbdis.2021.166241
49. Zewinger S, Reiser J, Jankowski V, Alansary D, Hahm E, Triem S, et al. Apolipoprotein C3 induces inflammation and organ damage by alternative inflammasome activation. *Nat Immunol* (2020) 21(1):30–41. doi: 10.1038/s41590-019-0548-1
50. Guzik TJ, Touyz RM. Oxidative stress, inflammation, and vascular aging in hypertension. *Hypertension* (2017) 70:660–7. doi: 10.1161/HYPERTENSIONAHA.117.07802
51. Drummond GR, Vinh A, Guzik TJ, Sobey CG. Immune mechanisms of hypertension. *Nat Rev Immunol* (2019) 19(8):517–32. doi: 10.1038/s41577-019-0160-5
52. Próchnicki T, Latz E. Inflammasomes on the crossroads of innate immune recognition and metabolic control. *Cell Metab* (2017) 26(1):71–93. doi: 10.1016/j.cmet.2017.06.018
53. Bai B, Yang Y, Wang Q, Li M, Tian C, Liu Y, et al. NLRP3 inflammasome in endothelial dysfunction. *Cell Death Dis* (2020) 11(9):776. doi: 10.1038/s41419-020-02985-x
54. Franchi L, Eigenbrod T, Muñoz-Planillo R, Nuñez G. The inflammasome: A caspase-1-activation platform that regulates immune responses and disease pathogenesis. *Nat Immunol* (2009) 10(3):241–7. doi: 10.1038/ni.1703
55. Zhang Z, Tang J, Cui X, Qin B, Zhang J, Zhang L, et al. New insights and novel therapeutic potentials for macrophages in myocardial infarction. *Inflammation* (2021) 44(5):1696–712. doi: 10.1007/s10753-021-01467-2
56. Strowig T, Henao-Mejia J, Elinav E, Flavell R. Inflammasomes in health and disease. *Nature* (2012) 481(7381):278–86. doi: 10.1038/nature10759
57. Rheinheimer J, de Souza BM, Cardoso NS, Bauer AC, Crispim D. Current role of the NLRP3 inflammasome on obesity and insulin resistance: A systematic review. *Metabolism* (2017) 74:1–9. doi: 10.1016/j.metabol.2017.06.002
58. Sun HJ, Ren XS, Xiong XQ, Chen YZ, Zhao MX, Wang JJ, et al. NLRP3 inflammasome activation contributes to VSMC phenotypic transformation and proliferation in hypertension. *Cell Death Dis* (2017) 10:e3074. doi: 10.1038/cddis.2017.470
59. Zhao Z, Wang Y, Zhou R, Li Y, Gao Y, Tu D, et al. A novel role of NLRP3-generated IL-1 β in the acute-chronic transition of peripheral lipopolysaccharide-elicited neuroinflammation: Implications for sepsis-associated neurodegeneration. *J Neuroinflamm* (2020) 17(1):64. doi: 10.1186/s12974-020-1728-5
60. Dalekos GN, Elisaf M, Bairaktari E, Tsolas O, Siamopoulos KC. Increased serum levels of interleukin-1 β in the systemic circulation of patients with essential hypertension: Additional risk factor for atherogenesis in hypertensive patients? *J Lab Clin Med* (1997) 129:300–8. doi: 10.1016/S0022-2143(97)90178-5
61. Wang JG, Williams JC, Davis BK, Jacobson K, Doerschuk CM, Ting JP, et al. Monocytic microparticles activate endothelial cells in an IL-1 β -dependent manner. *Blood* (2011) 118(8):2366–74. doi: 10.1182/blood-2011-01-330878
62. Dörfel Y, Franz S, Pruss A, Neumann G, Rohde W, Burmester GR, et al. Preactivated monocytes from hypertensive patients as a factor for atherosclerosis? *Atherosclerosis* (2001) 157(1):151–60. doi: 10.1016/S0021-9150(00)00674-2
63. Xia M, Boini KM, Abais JM, Xu M, Zhang Y, Li PL. Endothelial NLRP3 inflammasome activation and enhanced neointima formation in mice by adipokine visfatin. *Am J Pathol* (2014) 184(5):1617–28. doi: 10.1016/j.ajpath.2014.01.032
64. Chen Y, Wang L, Pitzer AL, Li X, Li PL, Zhang Y. Contribution of redox-dependent activation of endothelial Nlrp3 inflammasomes to hyperglycemia-induced endothelial dysfunction. *J Mol Med (Berl)* (2016) 94(12):1335–47. doi: 10.1007/s00109-016-1481-5
65. Toldo S, Mezzaroma E, Buckley LF, Potere N, Di Nisio M, Biondi-Zoccai G, et al. Targeting the NLRP3 inflammasome in cardiovascular diseases. *Pharmacol Ther* (2022) 236:108053. doi: 10.1016/j.pharmthera.2021.108053
66. Orecchioni M, Kobiyama K, Winkels H, Ghosh Y, McArdle S, Mikulski Z, et al. Olfactory receptor 2 in vascular macrophages drives atherosclerosis by NLRP3-dependent IL-1 production. *Science* (2022) 375(6577):214–21. doi: 10.1126/science.abg3067
67. Sharma BR, Kanneganti TD. NLRP3 inflammasome in cancer and metabolic diseases. *Nat Immunol* (2021) 22(5):550–9. doi: 10.1038/s41590-021-00886-5
68. Xia M, Abais JM, Koka S, Meng N, Gehr TW, Boini KM, et al. Characterization and activation of NLRP3 inflammasomes in the renal medulla in mice. *Kidney Blood Press Res* (2016) 41(2):208–21. doi: 10.1159/000443424
69. Tang PM, Nikolic-Paterson DJ, Lan HY. Macrophages: Versatile players in renal inflammation and fibrosis. *Nat Rev Nephrol* (2019) 15(3):144–58. doi: 10.1038/s41581-019-0110-2
70. Sharma AK, Mulloy DP, Le LT, Laubach VE. NADPH oxidase mediates synergistic effects of IL-17 and TNF- α on CXCL1 expression by epithelial cells after lung ischemia-reperfusion. *Am J Physiol Lung Cell Mol Physiol* (2014) 306:L69–79. doi: 10.1152/ajplung.00205.2013
71. Oh S, Yang JY, Park CH, Son KH, Byun K. Dieckol reduces muscle atrophy by modulating angiotensin type II type 1 receptor and NADPH oxidase in spontaneously hypertensive rats. *Antioxid (Basel)* (2021) 10(10):1561. doi: 10.3390/antiox10101561
72. Higaki A, Mahmoud AUM, Paradis P, Schiffrin EL. Role of interleukin-23/interleukin-17 axis in T-cell-mediated actions in hypertension. *Cardiovasc Res* (2021) 117:1274–83. doi: 10.1093/cvr/cvaa257
73. Vázquez-Oliva G, Fernández-Real JM, Zamora A, Vilaseca M, Badimón L. Lowering of blood pressure leads to decreased circulating interleukin-6 in hypertensive subjects. *J Hum Hypertens* (2005) 19(6):457–62. doi: 10.1038/sj.jhh.1001845
74. Lee DL, Sturgis LC, Labazi H, Osborne JB Jr, Fleming C, Pollock JS, et al. Angiotensin II hypertension is attenuated in interleukin-6 knockout mice. *Am J Physiol Heart Circ Physiol* (2006) 290(3):H935–40. doi: 10.1152/ajpheart.00708.2005
75. Brands MW, Banes-Berceli AK, Inscho EW, Al-Azawi H, Allen AJ, Labazi H. Interleukin 6 knockout prevents angiotensin II hypertension: Role of renal vasoconstriction and janus kinase 2/signal transducer and activator of transcription 3 activation. *Hypertension* (2010) 56(5):879–84. doi: 10.1161/HYPERTENSIONAHA.110.158071
76. Guzik TJ, Hoch NE, Brown KA, McCann LA, Rahman A, Dikalov S, et al. Role of the T cell in the genesis of angiotensin II induced hypertension and vascular dysfunction. *J Exp Med* (2007) 204(10):2449–60. doi: 10.1084/jem.20070657
77. Yoshida S, Takeuchi T, Kotani T, Yamamoto N, Hata K, Nagai K, et al. Infliximab, a TNF- α inhibitor, reduces 24-h ambulatory blood pressure in rheumatoid arthritis patients. *J Hum Hypertens* (2014) 28(3):165–9. doi: 10.1038/jhh.2013.80
78. Kleinbongard P, Heusch G, Schulz R. TNF α in atherosclerosis, myocardial ischemia/reperfusion and heart failure. *Pharmacol Ther* (2010) 127(3):295–314. doi: 10.1016/j.pharmthera.2010.05.002
79. Landry DB, Couper LL, Bryant SR, Linder V. Activation of the NF- κ B and I κ B system in smooth muscle cells after rat arterial injury. induction of vascular cell adhesion molecule-1 and monocyte chemoattractant protein-1. *Am J Pathol* (1997) 151(4):1085–95.
80. Neumann P, Gertzberg N, Johnson A. TNF- α induces a decrease in eNOS promoter activity. *Am J Physiol Lung Cell Mol Physiol* (2004) 286:L452–9. doi: 10.1152/ajplung.00378.2002

81. Alonso J, Sanchez de Miguel L, Monton M, Casado S, Lopez-Farre A. Endothelial cytosolic proteins bind to the 3' untranslated region of endothelial nitric oxide synthase mRNA: Regulation by tumor necrosis factor alpha. *Mol Cell Biol* (1997) 17:5719–26. doi: 10.1128/MCB.17.10.5719
82. Markó L, Kvakan H, Park JK, Qadri F, Spallek B, Binger KJ, et al. Interferon- γ signaling inhibition ameliorates angiotensin II-induced cardiac damage. *Hypertension* (2012) 60(6):1430–6. doi: 10.1161/HYPERTENSIONAHA.112.199265
83. Veiras LC, Bernstein EA, Cao D, Okwan-Duodu D, Khan Z, Gibb DR, et al. Tubular IL-1 β induces salt sensitivity in diabetes by activating renal macrophages. *Circ Res* (2022) 131(1):59–73. doi: 10.1161/CIRCRESAHA.121.320239
84. Gu C, Wu L, Li X. IL-17 family: Cytokines, receptors and signaling. *Cytokine* (2013) 64:477–85. doi: 10.1016/j.cyt.2013.07.022
85. Langley RG, Elewski BE, Lebwohl M, Reich K, Griffiths CE, Papp K, et al. Secukinumab in plaque psoriasis—results of two phase 3 trials. *N Engl J Med* (2014) 371(4):326–38. doi: 10.1056/NEJMoa1314258
86. Mease PJ, Genovese MC, Greenwald MW, Ritchlin CT, Beaulieu AD, Deodhar A, et al. Brodalumab, an anti-IL17RA monoclonal antibody, in psoriatic arthritis. *N Engl J Med* (2014) 370(24):2295–306. doi: 10.1056/NEJMoa1315231
87. Fleming I, Fisslthaler B, Dimmeler S, Kemp BE, Busse R. Phosphorylation of Thr(495) regulates Ca(2+)/calmodulin-dependent endothelial nitric oxide synthase activity. *Circ Res* (2001) 88(11):E68–75. doi: 10.1161/hh1101.092677
88. Heinrich PC, Behrmann I, Müller-Newen G, Schaper F, Graeve L. Interleukin-6-type cytokine signalling through the gp130/Jak/STAT pathway. *Biochem J* (1998) 334(Pt 2):297–314. doi: 10.1042/bj3340297
89. Ogata A, Tanaka T. Tocilizumab for the treatment of rheumatoid arthritis and other systemic autoimmune diseases: Current perspectives and future directions. *Int J Rheumatol* (2012) 2012:946048. doi: 10.1155/2012/946048
90. Li K, Guo D, Zhu H, Hering-Smith KS, Hamm LL, Ouyang J, et al. Interleukin-6 stimulates epithelial sodium channels in mouse cortical collecting duct cells. *Am J Physiol Regul Integr Comp Physiol* (2010) 299(2):R590–5. doi: 10.1152/ajpregu.00207.2009
91. Segiet A, Smykiewicz P, Kwiatkowski P, Żera T. Tumour necrosis factor and interleukin 10 in blood pressure regulation in spontaneously hypertensive and normotensive rats. *Cytokine* (2019) 113:185–94. doi: 10.1016/j.cyt.2018.07.003
92. Aggarwal BB. Signalling pathways of the TNF superfamily: A double-edged sword. *Nat Rev Immunol* (2003) 3(9):745–56. doi: 10.1038/nri1184
93. Barbaro NR, Harrison DG. Markers or makers: Inflammatory cytokines in treatment-resistant hypertension. *Hypertension* (2019) 73(4):767–9. doi: 10.1161/HYPERTENSIONAHA.119.12604
94. Ramseyer VD, Hong NJ, Garvin JL. Tumor necrosis factor alpha decreases nitric oxide synthase type 3 expression primarily via Rho/Rho kinase in the thick ascending limb. *Hypertension* (2012) 59:1145–50. doi: 10.1161/HYPERTENSIONAHA.111.189761
95. Garvin JL, Herrera M, Ortiz PA. Regulation of renal NaCl transport by nitric oxide, endothelin, and ATP: Clinical implications. *Annu Rev Physiol* (2011) 73:359–76. doi: 10.1146/annurev-physiol-012110-142247
96. Ishimitsu T, Uehara Y, Numabe A, Tsukada H, Ogawa Y, Iwai J, et al. Interferon gamma attenuates hypertensive renal injury in salt-sensitive Dahl rats. *Hypertension* (1992) 19(6 Pt 2):804–8. doi: 10.1161/01.HYP.19.6.804
97. Satou R, Miyata K, Gonzalez-Villalobos RA, Ingelfinger JR, Navar LG, Kobori H. Interferon- γ biphasically regulates angiotensinogen expression via a JAK-STAT pathway and suppressor of cytokine signaling 1 (SOCS1) in renal proximal tubular cells. *FASEB J* (2012) 26(5):1821–30. doi: 10.1096/fj.11-195198
98. Krishnan SM, Ling YH, Huuskens BM, Ferens DM, Saini N, Chan CT, et al. Pharmacological inhibition of the NLRP3 inflammasome reduces blood pressure, renal damage, and dysfunction in salt-sensitive hypertension. *Cardiovasc Res* (2019) 115(4):776–87. doi: 10.1093/cvr/cvy252
99. Sims JE, Smith DE. The IL-1 family: Regulators of immunity. *Nat Rev Immunol* (2010) 10(2):89–102. doi: 10.1038/nri2691
100. Xu D, Mu R, Wei X. The roles of IL-1 family cytokines in the pathogenesis of systemic sclerosis. *Front Immunol* (2019) 10:2025. doi: 10.3389/fimmu.2019.02025
101. Dinarello C, Arend W, Sims J, Smith D, Blumberg H, O'Neill L, et al. IL-1 family nomenclature. *Nat Immunol* (2010) 11(11):973. doi: 10.1038/nri1110-973
102. Krishnan SM, Sobey CG, Latz E, Mansell A, Drummond GR. IL-1 β and IL-18: Inflammatory markers or mediators of hypertension? *Br J Pharmacol* (2014) 171(24):5589–602. doi: 10.1111/bph.12876
103. Postlethwaite AE, Raghov R, Stricklin GP, Poppleton H, Seyer JM, Kang AH. Modulation of fibroblast functions by interleukin 1: Increased steady-state accumulation of type I procollagen messenger RNAs and stimulation of other functions but not chemotaxis by human recombinant interleukin 1 alpha and beta. *J Cell Biol* (1988) 106(2):311–8. doi: 10.1083/jcb.106.2.311
104. Urwyler SA, Ebrahimi F, Burkard T, Schuetz P, Poglitsch M, Mueller B, et al. IL (Interleukin)-1 receptor antagonist increases ang (Angiotensin [1-7]) and decreases blood pressure in obese individuals. *Hypertension* (2020) 75(6):1455–63. doi: 10.1161/HYPERTENSIONAHA.119.13982
105. Shi P, Diez-Freire C, Jun JY, Qi Y, Katovich MJ, Li Q, et al. Brain microglial cytokines in neurogenic hypertension. *Hypertension* (2010) 56:297–303. doi: 10.1161/HYPERTENSIONAHA.110.150409
106. Santisteban MM, Kim S, Pepine CJ, Raizada MK. Brain-Gut-Bone marrow axis: Implications for hypertension and related therapeutics. *Circ Res* (2016) 118(8):1327–36. doi: 10.1161/CIRCRESAHA.116.307709
107. Kettenmann H, Kirchhoff F, Verkhratsky A. Microglia: New roles for the synaptic stripper. *Neuron* (2013) 77(1):10–8. doi: 10.1016/j.neuron.2012.12.023
108. Cui C, Xu P, Li G, Qiao Y, Han W, Geng C, et al. Vitamin D receptor activation regulates microglia polarization and oxidative stress in spontaneously hypertensive rats and angiotensin II-exposed microglial cells: Role of renin-angiotensin system. *Redox Biol* (2019) 26:101295. doi: 10.1016/j.redox.2019.101295
109. Shen XZ, Li Y, Li L, Shah KH, Bernstein KE, Lyden P, et al. Microglia participate in neurogenic regulation of hypertension. *Hypertension* (2015) 66:309–16. doi: 10.1161/HYPERTENSIONAHA.115.05333
110. Li J, Zhao F, Wang Y, Chen J, Tao J, Tian G, et al. Gut microbiota dysbiosis contributes to the development of hypertension. *Microbiome* (2017) 5(1):14. doi: 10.1186/s40168-016-0222-x
111. Mell B, Jala VR, Mathew AV, Byun J, Waghulde H, Zhang Y, et al. Evidence for a link between gut microbiota and hypertension in the dahl rat. *Physiol Genomics* (2015) 47:187–97. doi: 10.1152/physiolgenomics.00136.2014
112. Yang T, Santisteban MM, Rodriguez V, Li E, Ahmari N, Carvajal JM, et al. Gut dysbiosis is linked to hypertension. *Hypertension* (2015) 65:1331–40. doi: 10.1161/HYPERTENSIONAHA.115.05315
113. Hetemäki I, Jian C, Laakso S, Mäkitie O, Pajari AM, de Vos WM, et al. Fecal bacteria implicated in biofilm production are enriched and associate to gastrointestinal symptoms in patients with APECED - a pilot study. *Front Immunol* (2021) 12:668219. doi: 10.3389/fimmu.2021.668219
114. Srivastava A, Gupta J, Kumar S, Kumar A. Gut biofilm forming bacteria in inflammatory bowel disease. *Microb Pathog* (2017) 112:5–14. doi: 10.1016/j.micpath.2017.09.041
115. De Ciuceis C, Amiri F, Brassard P, Endemann DH, Touyz RM, Schiffrin EL. Reduced vascular remodeling, endothelial dysfunction, and oxidative stress in resistance arteries of angiotensin II-infused macrophage colony-stimulating factor-deficient mice: Evidence for a role in inflammation in angiotensin-induced vascular injury. *Arterioscler Thromb Vasc Biol* (2005) 25(10):2106–13. doi: 10.1161/01.ATV.0000181743.28028.57
116. Wenzel P, Rossmann H, Müller C, Kossmann S, Oelze M, Schulz A, et al. Heme oxygenase-1 suppresses a pro-inflammatory phenotype in monocytes and determines endothelial function and arterial hypertension in mice and humans. *Eur Heart J* (2015) 36(48):3437–46. doi: 10.1093/eurheartj/ehv544
117. Harrison DG, Marvar PJ, Titze JM. Vascular inflammatory cells in hypertension. *Front Physiol* (2012) 3:128. doi: 10.3389/fphys.2012.00128
118. Higaki A, Caillon A, Paradis P, Schiffrin EL. Innate and innate-like immune system in hypertension and vascular injury. *Curr Hypertens Rep* (2019) 21:4. doi: 10.1007/s11906-019-0907-1
119. Chrysanthopoulou A, Gkaliagkousi E, Lazaridis A, Arelaki S, Pateinakis P, Ntinopoulou M, et al. Angiotensin II triggers release of neutrophil extracellular traps, linking thromboinflammation with essential hypertension. *JCI Insight* (2021) 6:e148668. doi: 10.1172/jci.insight.148668
120. Rudemiller N, Lund H, Jacob HJ, Geurts AM, Mattson DL. PhysGen Knockout Program. CD247 modulates blood pressure by altering T-lymphocyte infiltration in the kidney. *Hypertension* (2014) 63:559–64. doi: 10.1161/HYPERTENSIONAHA.113.02191
121. Itani HA, McMaster WG Jr, Saleh MA, Nazarewicz RR, Mikolajczyk TP, Kaszuba AM, et al. Activation of human T cells in hypertension: Studies of humanized mice and hypertensive humans. *Hypertension* (2016) 68:123–32. doi: 10.1161/HYPERTENSIONAHA.116.07237
122. Leibowitz A, Schiffrin EL. Immune mechanisms in hypertension. *Curr Hypertens Rep* (2011) 13:465–72. doi: 10.1007/s11906-011-0224-9
123. Kassan M, Wecker A, Kadowitz P, Trebak M, Matrougui K. CD4+CD25+Foxp3 regulatory T cells and vascular dysfunction in hypertension. *J Hypertens* (2013) 31:1939–43. doi: 10.1097/HJH.0b013e328362feb7
124. Schiffrin EL. Mechanisms of remodelling of small arteries, antihypertensive therapy and the immune system in hypertension. *Clin Invest Med* (2015) 38:E394–402. doi: 10.25011/cim.v38i6.26202
125. Madhur MS, Lob HE, McCann LA, Iwakura Y, Blinder Y, Guzik TJ, et al. Interleukin 17 promotes angiotensin II-induced hypertension and vascular dysfunction. *Hypertension* (2010) 55:500–7. doi: 10.1161/HYPERTENSIONAHA.109.145094

126. Schiffrin EL. T Lymphocytes: A role in hypertension? *Curr Opin Nephrol Hypertens* (2010) 19:181–6. doi: 10.1097/MNH.0b013e3283360a2e
127. Viel EC, Lemarié CA, Benkirane K, Paradis P, Schiffrin EL. Immune regulation and vascular inflammation in genetic hypertension. *Am J Physiol Heart Circ Physiol* (2010) 298:H938–44. doi: 10.1152/ajpheart.00707.2009
128. Dröge W. Free radicals in the physiological control of cell function. *Physiol Rev* (2002) 82(1):47–95. doi: 10.1152/physrev.00018.2001
129. Montezano AC, Touyz RM. Oxidative stress, noxs, and hypertension: Experimental evidence and clinical controversies. *Ann Med* (2012) 44:S2–16. doi: 10.3109/07853890.2011.653393
130. Rodrigo R, González J, Paoletto F. The role of oxidative stress in the pathophysiology of hypertension. *Hypertens Res* (2011) 34(4):431–40. doi: 10.1038/hr.2010.264
131. Touyz RM. Reactive oxygen species, vascular oxidative stress, and redox signaling in hypertension: What is the clinical significance? *Hypertension* (2004) 44:248–52. doi: 10.1161/01.HYP.0000138070.47616.9d
132. Cai H, Harrison DG. Endothelial dysfunction in cardiovascular diseases: The role of oxidant stress. *Circ Res* (2000) 87:840–4. doi: 10.1161/01.RES.87.10.840
133. Rochette L, Lorin J, Zeller M, Guillard JC, Lorgis L, Cottin Y, et al. Nitric oxide synthase inhibition and oxidative stress in cardiovascular diseases: possible therapeutic targets? *Pharmacol Ther* (2013) 140(3):239–57. doi: 10.1016/j.pharmthera.2013.07.004
134. Moens AL, Kass DA. Tetrahydrobiopterin and cardiovascular disease. *Arterioscler Thromb Vasc Biol* (2006) 26(11):2439–44. doi: 10.1161/01.ATV.0000243924.00970.cb
135. Majzunova M, Dovinova I, Barancik M, Chan JY. Redox signaling in pathophysiology of hypertension. *J BioMed Sci* (2013) 20(1):69. doi: 10.1186/1423-0127-20-69
136. Balakumar P, Jagadeesh G. Multifarious molecular signaling cascades of cardiac hypertrophy: Can the muddy waters be cleared? *Pharmacol Res* (2010) 62(5):365–83. doi: 10.1016/j.phrs.2010.07.003
137. Griendling KK, Sorensen D, Lassègue B, Ushio-Fukai M. Modulation of protein kinase activity and gene expression by reactive oxygen species and their role in vascular physiology and pathophysiology. *Arterioscler Thromb Vasc Biol* (2000) 20(10):2175–83. doi: 10.1161/01.ATV.20.10.2175
138. Sesso HD, Buring JE, Rifai N, Blake GJ, Gaziano JM, Ridker PM. C-reactive protein and the risk of developing hypertension. *JAMA* (2003) 290(22):2945–51. doi: 10.1001/jama.290.22.2945
139. Qi Y, Aranda JM, Rodriguez V, Raizada MK, Pepine CJ. Impact of antibiotics on arterial blood pressure in a patient with resistant hypertension—a case report. *Int J Cardiol* (2015) 201:157–8. doi: 10.1016/j.ijcard.2015.07.078
140. Fanouriakis A, Tziolos N, Bertsias G, Boumpas DT. Update on the diagnosis and management of systemic lupus erythematosus. *Ann Rheum Dis* (2021) 80(1):14–25. doi: 10.1136/annrheumdis-2020-218272
141. Herrera J, Ferrebuz A, MacGregor EG, Rodríguez-Iturbe B. Mycophenolate mofetil treatment improves hypertension in patients with psoriasis and rheumatoid arthritis. *J Am Soc Nephrol* (2006) 17(12 Suppl 3):S218–25. doi: 10.1681/ASN.2006080918
142. Ferro CJ, Edwards NC, Hutchison C, Cockwell P, Steeds RP, Savage CO, et al. Does immunosuppressant medication lower blood pressure and arterial stiffness in patients with chronic kidney disease? An observational study. *Hypertens Res* (2011) 34(1):113–9. doi: 10.1038/hr.2010.193
143. Makavos G, Ikonomidis I, Andreadou I, Varoudi M, Kapniari I, Loukeri E, et al. Effects of interleukin 17A inhibition on myocardial deformation and vascular function in psoriasis. *Can J Cardiol* (2020) 36(1):100–11. doi: 10.1016/j.cjca.2019.06.021
144. Boutouyrie P, Chowienczyk P, Humphrey JD, Mitchell GF. Arterial stiffness and cardiovascular risk in hypertension. *Circ Res* (2021) 128(7):864–86. doi: 10.1161/CIRCRESAHA.121.318061
145. Morton AC, Rothman AM, Greenwood JP, Gunn J, Chase A, Clarke B, et al. The effect of interleukin-1 receptor antagonist therapy on markers of inflammation in non-ST elevation acute coronary syndromes: The MRC-ILA heart study. *Eur Heart J* (2015) 36(6):377–84. doi: 10.1093/eurheartj/ehu272
146. Alfaidi MA, Chamberlain J, Rothman A, Crossman D, Villa-Urriol MC, Hadoke P, et al. Dietary docosahexaenoic acid reduces oscillatory wall shear stress, atherosclerosis, and hypertension, most likely mediated via an IL-1-Mediated mechanism. *J Am Heart Assoc* (2018) 7(13):e008757. doi: 10.1161/JAHA.118.008757
147. Rothman AM, MacFadyen J, Thuren T, Webb A, Harrison DG, Guzik TJ, et al. Effects of interleukin-1 β inhibition on blood pressure, incident hypertension, and residual inflammatory risk: A secondary analysis of CANTOS. *Hypertension* (2020) 75(2):477–82. doi: 10.1161/HYPERTENSIONAHA.119.13642
148. Li Y, Zafar S, Salih Ibrahim RM, Chi HL, Xiao T, Xia WJ, et al. Exercise and food supplement of vitamin c ameliorate hypertension through improvement of gut microflora in the spontaneously hypertensive rats. *Life Sci* (2021) 269:119097. doi: 10.1016/j.lfs.2021.119097
149. Cardenas MG, Oswald E, Yu W, Xue F, MacKerell AD Jr, Melnick AM. The expanding role of the BCL6 oncoprotein as a cancer therapeutic target. *Clin Cancer Res* (2017) 23(4):885–93. doi: 10.1158/1078-0432.CCR-16-2071
150. Chen D, Zang YH, Qiu Y, Zhang F, Chen AD, Wang JJ, et al. BCL6 attenuates proliferation and oxidative stress of vascular smooth muscle cells in hypertension. *Oxid Med Cell Longev* (2019) 2019:5018410. doi: 10.1155/2019/5018410
151. Griendling KK, Sorensen D, Ushio-Fukai M. NAD(P)H oxidase: Role in cardiovascular biology and disease. *Circ Res* (2000) 86(5):494–501. doi: 10.1161/01.RES.86.5.494
152. Wenzel P, Schulz E, Oelze M, Müller J, Schuhmacher S, Alhamdani MS, et al. AT1-receptor blockade by telmisartan upregulates GTP-cyclohydrolase I and protects eNOS in diabetic rats. *Free Radic Biol Med* (2008) 45(5):619–26. doi: 10.1016/j.freeradbiomed.2008.05.009
153. Hornig B, Landmesser U, Kohler C, Ahlersmann D, Spiekermann S, Christoph A, et al. Comparative effect of ace inhibition and angiotensin II type 1 receptor antagonism on bioavailability of nitric oxide in patients with coronary artery disease: Role of superoxide dismutase. *Circulation* (2001) 103(6):799–805. doi: 10.1161/01.CIR.103.6.799
154. Zepeda RJ, Castillo R, Rodrigo R, Prieto JC, Aramburu I, Brugere S, et al. Effect of carvedilol and nebivolol on oxidative stress-related parameters and endothelial function in patients with essential hypertension. *Basic Clin Pharmacol Toxicol* (2012) 111(5):309–16. doi: 10.1111/j.1742-7843.2012.00911.x
155. Mollnau H, Schulz E, Daiber A, Baldus S, Oelze M, August M, et al. Nebivolol prevents vascular NOS III uncoupling in experimental hyperlipidemia and inhibits NADPH oxidase activity in inflammatory cells. *Arterioscler Thromb Vasc Biol* (2003) 23(4):615–21. doi: 10.1161/01.ATV.0000065234.70518.26
156. Münzel T, Gori T. Nebivolol: The somewhat-different beta-adrenergic receptor blocker. *J Am Coll Cardiol* (2009) 54(16):1491–9. doi: 10.1016/j.jacc.2009.05.066
157. Matsubara M, Hasegawa K. Benidipine, a dihydropyridine-calcium channel blocker, prevents lysophosphatidylcholine-induced injury and reactive oxygen species production in human aortic endothelial cells. *Atherosclerosis* (2005) 178(1):57–66. doi: 10.1016/j.atherosclerosis.2004.08.020
158. Ulker S, McKeown PP, Bayraktutan U. Vitamins reverse endothelial dysfunction through regulation of eNOS and NAD(P)H oxidase activities. *Hypertension* (2003) 41(3):534–9. doi: 10.1161/01.HYP.0000057421.28533.37
159. Duffy SJ, Gokce N, Holbrook M, Hunter LM, Biegelsen ES, Huang A, et al. Effect of ascorbic acid treatment on conduit vessel endothelial dysfunction in patients with hypertension. *Am J Physiol Heart Circ Physiol* (2001) 280(2):H528–34. doi: 10.1152/ajpheart.2001.280.2.H528
160. Atarashi K, Ishiyama A, Takagi M, Minami M, Kimura K, Goto A, et al. Vitamin e ameliorates the renal injury of Dahl salt-sensitive rats. *Am J Hypertens* (1997) 10(5 Pt 2):116S–9S. doi: 10.1016/S0895-7061(97)00088-5
161. Duffy SJ, Gokce N, Holbrook M, Huang A, Frei B, Keaney JF Jr, et al. Treatment of hypertension with ascorbic acid. *Lancet* (1999) 354(9195):2048–9. doi: 10.1016/S0140-6736(99)04410-4
162. Block G, Mangels AR, Norkus EP, Patterson BH, Levander OA, Taylor PR. Ascorbic acid status and subsequent diastolic and systolic blood pressure. *Hypertension* (2001) 37(2):261–7. doi: 10.1161/01.HYP.37.2.261
163. Mullan BA, Young IS, Fee H, McCance DR. Ascorbic acid reduces blood pressure and arterial stiffness in type 2 diabetes. *Hypertension* (2002) 40(6):804–9. doi: 10.1161/01.HYP.0000039961.13718.00

Glossary

ACEIs	angiotensin converting enzyme inhibitors
Ang II	angiotensin II
AP-1	activating protein-1
ARBs	angiotensin receptor blockers
BCL6	B-cell lymphoma 6
CCBs	calcium channel blockers
CCL-2	C-C motif chemokine ligand 2
CVD	cardiovascular disease
DAMPs	damage-associated molecular patterns
EDGF	endothelium-dependent vasoconstrictor factor
eNOS	endothelial nitric oxide synthase
ET-1	endothelin-1
H ₂ O ₂	hydrogen peroxide
IL	interleukin
IFN- γ	interferon gamma
LDL	low density lipoprotein
M1	classic activated macrophages
M2	alternatively activated macrophages
MMF	mycophenolate mofetil
NADPH	nicotinamide adenine dinucleotide phosphate
NADPH-Ox	nicotinamide adenine dinucleotide phosphate oxidase
NF κ B	nuclear factor kappa-B
NO	nitric oxide
PAMPs	pathogen-associated molecular patterns
PPRs	pattern recognition receptors
RAAS	Activated renin-angiotensin-aldosterone system
RAG1	recombination-activated gene 1
ROS	reactive oxygen species
Nrf2	nuclear E2-related factor 2
Th	T helper
TLR	Toll-like receptors
TNF- α	tumor necrosis factor α
TNFR	TNF- α receptor
Treg	T regulatory cells
VCDM	vascular cell adhesion molecule



OPEN ACCESS

EDITED BY
Nadine Suffee,
Sorbonne Universités, France

REVIEWED BY
Haocheng Lu,
Southern University of Science and
Technology, China
Sijia Liang,
Zhongshan School of Medicine, Sun
Yat-sen University, China

*CORRESPONDENCE
Wenjing Wang
✉ wangwenjing85321@ccmu.edu.cn
Dong Zhang
✉ zhangdong0660@aliyun.com
Jizong Zhao
✉ zhaojizong@bjtth.org

[†]These authors have contributed
equally to this work

SPECIALTY SECTION
This article was submitted to
Inflammation,
a section of the journal
Frontiers in Immunology

RECEIVED 31 October 2022
ACCEPTED 20 December 2022
PUBLISHED 18 January 2023

CITATION
Ge P, Li H, Ya X, Xu Y, Ma L, He Q,
Wang R, Liu Z, Zhang Q, Zhang Y,
Wang W, Zhang D and Zhao J (2023)
Single-cell atlas reveals different
immune environments between stable
and vulnerable atherosclerotic
plaques.
Front. Immunol. 13:1085468.
doi: 10.3389/fimmu.2022.1085468

Single-cell atlas reveals different immune environments between stable and vulnerable atherosclerotic plaques

Peicong Ge^{1,2†}, Hao Li^{1,2†}, Xiaolong Ya^{1,2†}, Yiqiao Xu³,
Long Ma^{1,2}, Qiheng He^{1,2}, Rong Wang^{1,2}, Zechen Liu⁴,
Qian Zhang^{1,2}, Yan Zhang^{1,2}, Wenjing Wang^{5*},
Dong Zhang^{1,2,6*} and Jizong Zhao^{1,2*}

¹Department of Neurosurgery, Beijing Tiantan Hospital, Beijing, China, ²China National Clinical Research Center for Neurological Diseases, Beijing, China, ³Capital Medical University, Beijing, China, ⁴Department of Biostatistics, Harvard School of Public Health, Huntington Avenue, Boston, MA, United States, ⁵Beijing Institute of Hepatology, Beijing YouAn Hospital, Capital Medical University, Beijing, China, ⁶Department of Neurosurgery, Beijing Hospital, Beijing, China

Introduction: Regardless of the degree of stenosis, vulnerable plaque is an important cause of ischemic stroke and thrombotic complications. The changes of the immune microenvironment within plaques seem to be an important factor affecting the characteristics of the plaque. However, the differences of immune microenvironment between stable and vulnerable plaques were remained unknown.

Methods: In this study, RNA-sequencing was performed on superficial temporal arteries from 5 traumatic patients and plaques from 3 atherosclerotic patients to preliminary identify the key immune response processes in plaques. Mass cytometry (CyTOF) technology was used to explore differences in immune composition between 9 vulnerable plaques and 12 stable plaques. Finally, immunofluorescence technique was used to validate our findings in the previous analysis.

Results: Our results showed that more CD86+CD68+ M1 pro-inflammatory macrophages were found in vulnerable plaques, while CD4+T memory cells were mainly found in stable plaques. In addition, a CD11c+ subset of CD4+T cells with higher IFN- γ secretion was found within the vulnerable plaque. In two subsets of B cells, CD19+CD20-B cells in vulnerable plaques secreted more TNF- α and IL-6, while CD19-CD20+B cells expressed more PD-1 molecules.

Conclusion: In conclusion, our study suggested that M1-like macrophages are the major cell subset affecting plaque stability, while functional B cells may also contribute to plaque stability.

KEYWORDS

Vulnerable plaques, single-cell, immune environments, CyTOF/mass cytometry, RNA-seq analysis

Introduction

The latest Global Burden of Disease report showed that ischemic heart disease and stroke had become the leading causes of mortality. The common pathological basis was atherosclerosis, a disease of vascular stenosis, in which subendothelial resident LDL undergoes a series of oxidations to produce ox-LDL with immune effects (1–3). On the one hand, ox-LDL can be endocytosed by macrophages from the innate immune system through scavenger receptors. On the other hand, these antigens can be taken up by antigen-presenting cells. Then, it is processed and presented to lymphocytes, activating the adaptive immune response (4, 5). Multiple types of cells and the complex immune microenvironment in plaques lead to the puzzle of plaque formation and development, which are even now not fully understood.

The bifurcation of the carotid artery is the most common site of atherosclerosis. About 10% to 15% of patients with carotid artery stenosis will experience an ischemic stroke, mainly related to local thrombosis caused by plaque rupture (6–9). Usually, atherosclerotic plaques progress slowly and silently, but some plaques can rupture suddenly, leading to acute vascular events. Therefore, the concept of vulnerable plaque was introduced to identify these high-risk plaques (9). Pathological studies suggested that vulnerable plaques were often manifested as a thin fibrous cap and large eccentric necrotic core occupying approximately one-quarter of the plaque area (10, 11). The difference in the clinical process and pathological feature implies that the two types of plaques may have different changes in the immune microenvironment. In recent years, anti-inflammatory programs have successfully treated atherosclerosis (12, 13). Therefore, researchers have paid more attention to immunotherapy. Exploring the differences in immune microenvironment composition in different plaque types and finding key intervention targets will help guide the precision immunotherapy.

In this study, we used Mass Cytometry (Mass Cytometry, CyTOF), a precise, high-dimensional approach, to identify the differences in immune microenvironment between stable and vulnerable plaques. The results showed that more M1 pro-inflammatory macrophages were found in vulnerable plaques, while CD4+T memory cells were mainly found in stable plaques. In contrast, B-cell subsets and T-cells within vulnerable plaques showed higher activity. These clusters may be important for plaque vulnerability. Our study revealed the surface characteristics of these clusters in detail, which may help identify vulnerable plaque cells and understand the relevant mechanisms of rupture.

Materials and methods

Human specimens and ethics statements

From August 2021 to November 2021, 21 atherosclerotic patients undergoing carotid atherectomy at Beijing Tiantan

Hospital were enrolled in this study after informed consent provided. The detailed clinical data of the enrolled patients are shown in Table 1. Plaques were obtained from each patient. According to the imaging results (CTA/MRA/CU), plaque vulnerability was determined based on imaging biomarkers (Intraplaque haemorrhage, Lipid-rich necrotic core, Neovascularisation, Carotid plaque thickness, Surface morphology and Carotid plaque volume) (14). Normal superficial temporal arteries were obtained from other 5 patients undergoing craniocerebral trauma surgery for RNA-seq analysis (See Figure 2 for details). This research was approved by the Institutional Review Board (IRB) and Ethics Committee of Beijing Tiantan Hospital. Written informed consent was obtained from all patients.

RNA extraction and library construction

Peripheral blood and plaque tissues from 3 patients were used for RNA-seq analysis. In addition, superficial temporal artery samples from 5 patients undergoing craniocerebral trauma surgery were used as blank controls. The plaque tissues and artery samples were washed with DPBS (Sigma-Aldrich, United States) within 1 hour after surgical resection. Then, TRIzol method was also adopted. Sequencing libraries were generated using rRNA-depleted RNA with an NEBNext Ultra Directional RNA Library Prep Kit for Illumina (NEB, MA) following the manufacturer's recommendations. We then performed the paired-end sequencing on illumina NovaSeq 6000(illumina, USA) as recommended by the supplier. After cluster generation, the libraries were sequenced on the Illumina HiSeq platform, and 150-bp paired-end reads were generated.

Quality control and data analysis

In order to obtain clean data, raw data in fastq format were first processed through in-house Perl scripts. Reference genome and gene model annotation files were downloaded directly from the genome website. The index of the reference genome was built using bowtie2 v2.2.8, and paired-end clean reads were aligned to the reference genome using Hisat2 v2.0.5. Hg19 RefSeq (RNA sequences, GRCh38) was downloaded from the UCSC Genome Browser (<http://genome.ucsc.edu>). The clean reads were aligned with both genome hg19 and transcript reference using STAR v2.2.1, and gene expression was calculated by RSEM v1.3.0 using FPKM (fragments per kilobase of exon per million fragments mapped). We then compared RNA-seq in peripheral blood between healthy individuals and atherosclerotic patients. $P < 0.05$ indicated statistically significant difference in expression. R was used for analysis of the gene expression data.

TABLE 1 Clinical characteristics of the patients.

	Stable Plaque	Vulnerable Plaque	p-value
Gender (male/female)	9/3	8/1	0.810
Age (Mean \pm SD)	64.76 \pm 4.94	65.15 \pm 4.76	0.492
Hypertension	8	6	1.000
Diabetes	5	2	0.640
Hyperlipidemia	1	0	1.000
Smoking	10	6	0.712
Drinking	8	5	0.293
Degree of stenosis			0.681
Severe stenosis (70~100%)	8	6	
Moderate stenosis (50~69%)	4	3	

Plaque tissue and superficial temporal arteries single-cell dissociation

Atherosclerotic plaque tissues were washed with Dulbecco's phosphate-buffered saline (DPBS, Sigma-Aldrich, United States) within 1h after surgery. Each specimen was digested at 37°C for 1h using miscible liquids that contain collagenase type IV (GIBCO, Gaithersburg, United States), DNase (Sigma, DN25), hyaluronidase (Sigma, H3506), collagenase type XI (Sigma, C7657) and collagenase type II (Sigma, C6885). The mixture was filtered through a 70 μ m cell strainers with DPBS and washed with red blood cell (RBC) lysis buffer (BD Biosciences, United States). The dissociated cell suspension was then washed once with DPBS and resuspended in 1 mL of staining buffer (DPBS containing 5% fetal bovine serum, ScienCell, United States).

Mass cytometry

A panel of 39 antibodies designed to distinguish a broad range of immune cells was used. Antibodies were either purchased in a preconjugated form from Fluidigm (South San Francisco, United States) or purchased from Biolegend (San Diego, United States) in a purified form and conjugated inhouse using the Maxpar X8 Multimetal Labeling Kit (Fluidigm, United States) according to the manufacturer's instructions. The antibodies and reporter isotopes are included in [Supplementary Table 1](#). The samples were then washed and stained with cisplatin-195Pt (Fluidigm, 201064) as a viability dye. Cell samples were then washed and stained with cell surface antibodies for 30 min on ice. Subsequently, the samples were permeabilized at 4°C overnight and stained with intracellular antibodies for 30 min on ice. The antibody-labeled samples were washed and incubated in 0.125 nM intercalator-Ir (Fluidigm, United States) diluted in phosphate-buffered saline (PBS, Sigma-

Aldrich, United States) containing 2% formaldehyde and stored at 4°C until mass cytometry examination. Before acquisition, the samples were washed with deionized water and then resuspended at a concentration of 1×10^6 cells/mL in deionized water containing a 1:20 dilution of EQ Four Element Beads (Fluidigm, United States). The samples were then examined by CyTOF2 mass cytometry (Fluidigm, United States).

CyTOF data analysis

CyTOF data were acquired in the form of .fcs files from the CyTOF2 system. The addition of EQ Four Element Beads allowed us to use the MATLAB-based normalization technique. The obtained data were uploaded to Cytobank. Firstly, beads are filtered and active cells were selected from the specific gate. Then, CD45+ cells were gated (see [Supplementary Figure 1](#) for details). Further analysis using the automated dimensionality reduction algorithm FlowSom by R language. The results were shown by viSNE, a visual dimensionality reduction algorithm.

Histology and immunofluorescence staining

Plaques from 9 patients (4 vulnerable plaques and 5 stable plaques) were fixed overnight in 4% formalin (4°C) and embedded in paraffin blocks for paraffin sections. Three paraffin sections (4 μ m) were cut from each specimen. Hematoxylin and eosin (H&E) staining was performed. For immunofluorescence, paraffin sections were washed twice 15 min in PBS (Sigma-Aldrich, United States), permeabilized in 0.2%-0.5% Triton X-100 (Solarbio, China) and blocked in 5% normal donkey serum (Jackson Lab, United States) for 1 h and

stained with primary antibody overnight. Primary antibody was detected using fluorescent-conjugated second antibodies (ZSGB-BIO, China). Primary antibodies were: anti-CD68 (Abcam, United States), anti-CD86 (Abcam, United States), and anti-HLA_DR (Abcam, United States). Sections were mounted with fluorescence mounting medium (Glostrup, Denmark). Fluorescent images were acquired on a Zeiss LSM880 NLO microscope and Zeiss Axio Scope A1 was used to obtain H&E images. Three fields were randomly selected from each staining and the number of fusion particles of CD68, CD86 and HLA_DR in each field was counted. The Wilcoxon rank test was used and $P < 0.05$ indicated statistically significant difference.

Results

RNA-seq data from plaques and normal superficial temporal artery was analyzed to preliminarily explore the immune microenvironment in plaques

In order to explore the composition of immune microenvironment in plaques, RNA sequencing data from plaques of 3 atherosclerotic patients and data from superficial temporal artery of 5 patients undergoing craniocerebral trauma surgery were analyzed. A total of 16036 differentially expressed genes (defined as $|\log_2\text{FoldChange}| > 1$ and $\text{FDR} < 0.05$) were identified. Among them, 3656 genes were upregulated in the atherosclerosis plaques (Figure 1A). To elucidate the functional implications of the differentially expressed genes, we performed pathway enrichment analyses of the upregulated and downregulated genes. For genes upregulated in plaques, NF- κ B signaling and B cell activation were found to be significantly by Gene Ontology analysis and T cell receptor signaling pathway and B cell receptor signaling pathway were found to be significantly by Kyoto Encyclopedia of Genes and Genomes analysis. These results suggested immune responses involved T lymphocyte and B lymphocyte were existed in plaques (Figure 1C). Some of the up-regulated genes in plaques were also enriched in the biological processes associated with TNF signaling pathway. This suggested the TNF- α mediated immune responses within the plaques (Figure 1D) (Complete GO and KEGG enrichment data were shown in Supplementary Tables 2 and 3).

Finally, based on these RNA-Seq data, we used xCell (R package, Aran Dvir, 2017) to infer the type and proportion of cells contained in atherosclerotic plaques. The results showed that endothelial cells, smooth muscle cells and fibrous cells were composed of superficial temporal artery (Figure 1E). In addition to these cells, atherosclerotic plaques also contain a large number of macrophages, dendritic cells, T and B lymphocytes

(Figure 1E). The results of immune infiltration analysis provided guidance for the subsequent selection of CyTOF antibody profiles.

Composition of immune cells in atherosclerotic plaque

According to the imaging (CTA/MRA/UTA) results, we divided the enrolled specimens into 12 stable plaques and 9 vulnerable plaques (Typical H&E images of stable and vulnerable plaques were shown in Supplementary Figure 2). Specific metal antibodies were selected on the basis of RNA-seq analysis (Detailed information of antibodies panel was shown in Supplementary Table 1). FlowSOM, an unsupervised clustering method, was used to analyze the cellular composition of atherosclerotic plaques from 21 patients (Figure 2). Finally, 15 clusters were found. Each cell type was identified by specific markers on the its surface (Figure 3A). We found that macrophages and lymphocytes were the main components of plaques (Figure 3B). Macrophages were composed of 6 clusters, accounting for 63.9%. Lymphocytes consisted of T lymphocytes and B lymphocytes. While 7 clusters made up T lymphocytes, accounting for 31.9%. B lymphocytes were composed of two clusters, accounting for 4.2% (Figure 3B). T-SNE was employed to convert high-dimensional CyTOF data and was used to map the immune compartments of all samples.

T cells were dominant in stable plaques, and macrophages were dominant in vulnerable plaques

The composition of the two plaques was compared to explore differences in immune composition between stable and vulnerable plaques. Overall, each cell subset was distributed in both types of plaques. T cells were predominant in stable plaques, accounting for 57.2%. Macrophages accounted for 39.1%. However, macrophages were the most abundant cell group in vulnerable plaques, accounting for 56.4%. T cells only accounted for 36.7% (Figure 4C). These seemed to suggest differences in immune environments between the two plaques.

CD4+T memory cells were more abundant in stable plaques, while CD11c+CD4+T cells in vulnerable plaques secreted higher IFN- γ

The type of T cells in plaques was diverse. CD4+T cells dominate the plaques. There were 5 clusters of CD4+T lymphocytes, including

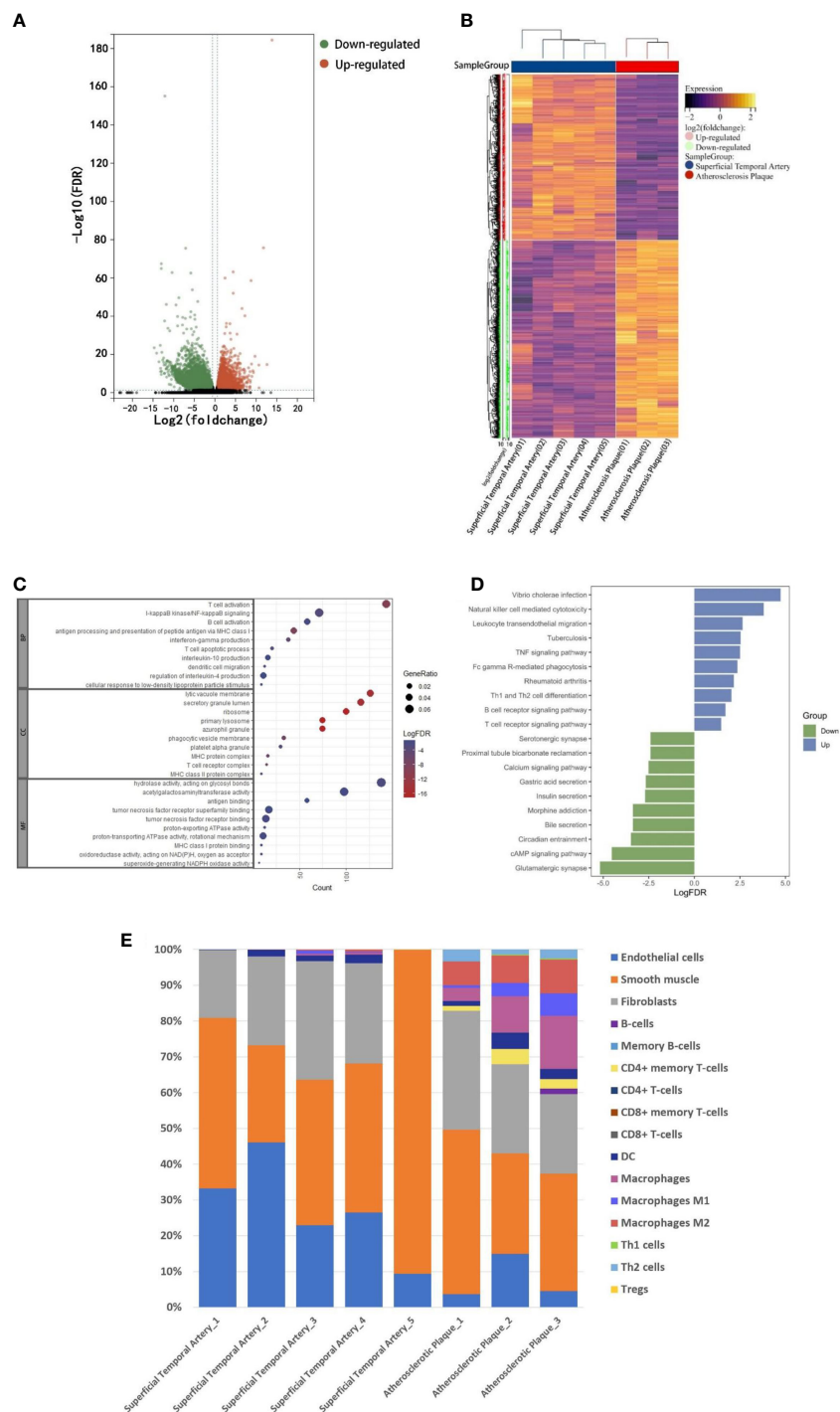


FIGURE 1 RNA-seq analysis. **A:** The RNA-seq data of normal superficial temporal arteries and plaques were compared. The differential genes were shown by volcano map **(A)** and heatmap **(B)**. **(C)** Bubble map shown the GO enrichment results of up-regulated genes in plaques. **(D)** Histogram shown KEGG pathway enrichment results of up-regulated and down-regulated genes in plaques. **(E)** Immune infiltration analysis revealed the composition of superficial temporal arteries and atherosclerotic plaques.

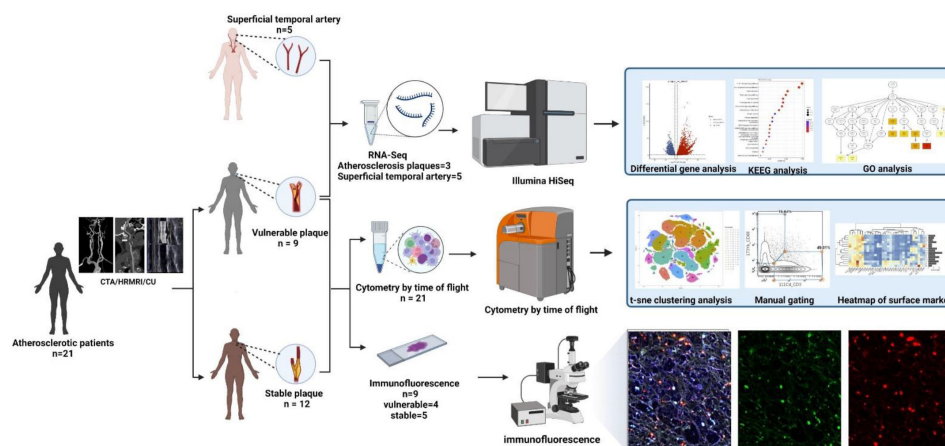


FIGURE 2

Workflow: According to preoperative imaging data, 21 enrolled atherosclerotic patients were divided into the vulnerable plaque group (n=9) and the stable plaque group (n=12). All plaques were examined by Mass Cytometry after special treatment. Among them, 9 remaining plaque samples were paraffin-embedded and were stained with immunofluorescent antibodies. Atherosclerotic plaques from 3 additional patients were performed for RNA-seq analysis. In addition, superficial temporal artery from 5 patients undergoing craniocerebral trauma surgery were also used for RNA-seq analysis as control groups (This Figure was created by [BioRender](#)).

memory cells and effector cells. Comparing the percentage of cell subsets in the two plaques, CD4+T cells of cluster10 were the only group of cells more abundant in stable plaques ($p < 0.05$) (Figures 4B, D). CD45RO+ and CD127, surface markers of memory cells, co-exist on the surface of cells from this cluster (15, 16). There was no difference in the content of other subsets between the two types of plaque. However, Cluster2 (CD11c+CD4+T cells) in vulnerable plaques secreted a higher level of IFN- γ than in stable plaques ($p < 0.05$) (Figure 4E-1). It was suggested that this group of cells in vulnerable plaques might also play a unique function.

CD19+CD20-B cells in vulnerable plaques secreted more TNF- α and IL-6, while CD19-CD20+B cells expressed more PD-1 molecules

Two types of B cells existed in samples. These B cells have different surface molecular patterns. Cluster9 expressed CD19+, whereas Cluster8 expressed CD20 but not CD19 (Figure 3D). Cluster9 also expressed surface markers HLA-DR and CCR7, which were involved in cell activation and migration, suggesting that this cluster may be a group of activated B subsets cells (17, 18). There was no difference in the number of these clusters between the two types of plaque. Functional analysis showed that cluster8 expressed a higher level of PD-1 molecule in vulnerable

plaques ($p < 0.05$) (Figure 4E-2). Cluster9 showed a higher level of TNF- α and IL-6 ($p < 0.05$) (Figure 4E-3 and 4E-4).

Vulnerable plaques contain more CD86+CD68+ M1 pro-inflammatory macrophages

Macrophages were the most abundant cluster in plaques and contained multiple cell subsets (Figure 4C). However, compared with stable plaques, cluster14 was the only cluster that was more abundant in vulnerable plaques (Figures 4B, D). These clusters expressed CD68 and HLA-DR, typical macrophage surface markers (19). In addition, CD86, corresponding to M1-like macrophages, existed on the surface of cluster14 (20, 21). Polychromatic immunofluorescence showed that there were more M1 macrophages in vulnerable plaques (Figures 5A, B). Functional analysis showed that this cluster also expressed IL-6 and IFN- γ (pro-inflammatory cytokines), and functional analysis did not reveal a significant difference (Figure 4E-4).

Discussion

Stroke has become a severe disease endangering human health, and its high mortality and disability rate have increased the global burden of disease (22, 23). Many of these diseases are

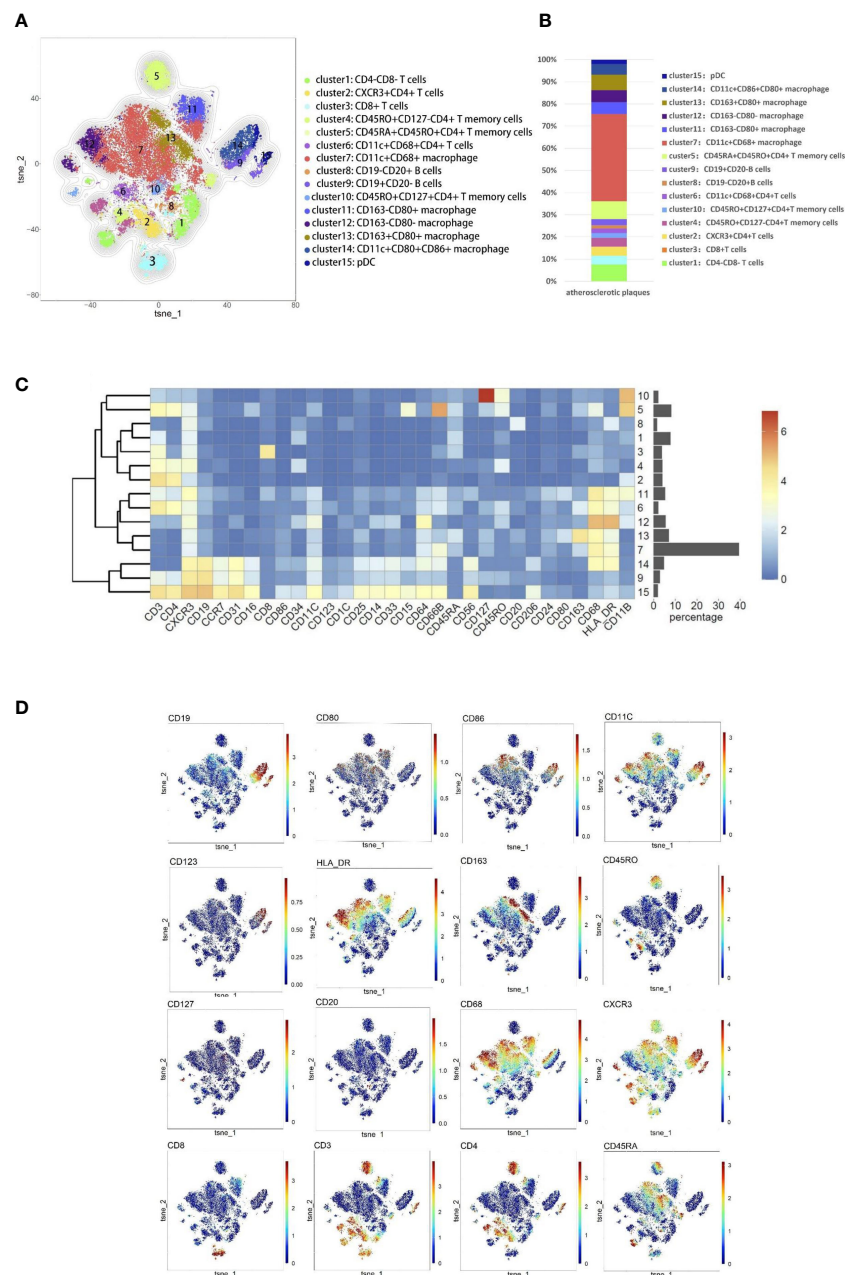
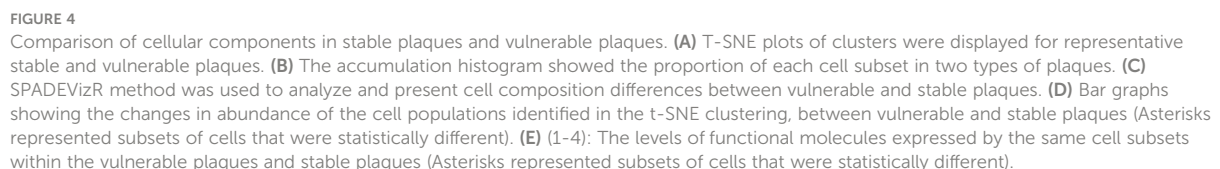


FIGURE 3

Cellular components within atherosclerotic plaques. **(A)** The analysis identified 15 populations, including T lymphocyte cells and macrophages. High-dimensional characterization of the mononuclear cell was shown by t-SNE. **(B)** The accumulation histogram presented the proportion of cell subsets within the plaques. **(C)** Heatmap showing the relative expression level of the chosen markers within the 15 cell subsets identified by the t-SNE clustering shown in **(A)**. **(D)** Markers of the particular cell were displayed by spectral colors on t-SNE maps.

caused by plaque shedding in the carotid artery that blocked the distal blood vessels. Deciduous plaques (often referred to as vulnerable plaques) are more likely to cause distal vascular obstruction than stable plaques (14, 24). Therefore, it is particularly important to explore the differences in immune microenvironment composition between stable plaques and

vulnerable plaques. In this study, we used CyTOF technology to analyze the cell composition between two types of plaques. It was found that CD4+T memory cells were mainly present in stable plaques, while M1 macrophages were mainly existed in vulnerable plaques. Polychromatic immunofluorescence and RNA-seq analysis further confirmed this finding that was



As an important cell type in plaques, T lymphocytes are widely involved in the development of atherosclerotic lesions

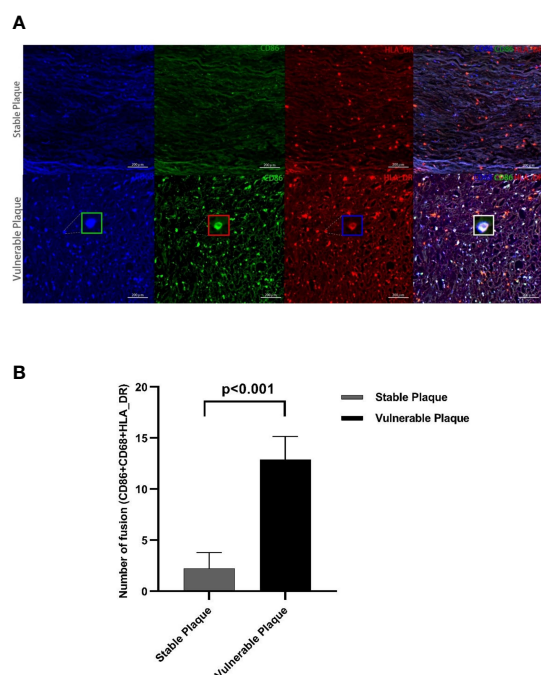


FIGURE 5

Polychromatic immunofluorescence. A larger amount of activated M1 macrophages were expressed in vulnerable plaques than in stable plaques. Typical multicolor immunofluorescence images of stable and vulnerable plaques are shown in Figure (A). Statistical difference in CD68+CD80+HLA_DR+ particles between two groups were shown in Figure (B).

(25, 26). Comparative analysis showed that cluster2, a CD4+T cell subset, was highly secreted IFN- γ in vulnerable plaques. IFN- γ is the main effector molecule of Th1 cells (26–28), suggesting that cluster 2 cells in vulnerable plaques were more inclined to the pro-inflammatory Th1 activation state. IFN- γ , as an important proatherogenic cytokine, plays an important role in the development of atherosclerosis (29, 30). IFN- γ could promote the formation of foam cells and lead to plaque instability by affecting endothelial cell function (31–33). This implied that CD11c+ CD4+T cells with high secreted IFN- γ in vulnerable plaques might be the primary cell subsets causing vulnerable transformation of plaques.

Although B cells are less abundant in plaque tissue, they are also considered important in the immune microenvironment of plaques (34, 35). We found two clusters of B lymphocytes in plaques, and there was no difference in the amount of B lymphocytes between the two types. Our study suggested that the two subsets of B cells in vulnerable plaques may play a role in plaque vulnerability in different ways. CD19+CD20- B cells from vulnerable plaques expressed the pro-inflammatory cytokines IL-6 and TNF- α . IL6 generally was considered to be a pro-atherogenic cytokine that had a strong regulatory effect on the

extracellular matrix (36, 37). IL-6 stimulates the synthesis of matrix-degrading enzymes that erode the matrix within plaques, leading to the rupture of plaques (38, 39). In addition, TNF- α derived from B cells can activate macrophages within plaques to produce more TNF- α , further leading to apoptosis and causing rupture (40). This subset of B cells may influence plaque stability via these proinflammatory cytokines. The other CD19-CD20+ B cells from vulnerable plaques expressed higher level of PD-1. Studies have found that high expression of PD-1 by innate-type B cells after their activation by antigens and PD-1 molecule on the surface of B cells facilitate the adaptive responses through longer-lived plasma cells and memory cells generated (41). Animal experiments have also found that B2 cells involved in adaptive immune response can promote the progression of atherosclerotic plaques (42). This suggests that CD19-CD20+B cells in vulnerable plaques may mediate local adaptive immune response through PD-1 molecules on their surface and trigger plaque progression. Differences in expression levels of functional molecules expressed by the same clusters reflected the difference in immune microenvironment between stable and vulnerable plaques. These differences may be an important cause of plaque instability.

Macrophages are key players in atherosclerotic disease and their polarization states have a role in atherogenesis (43). Phagocytosis, clearance of ox-LDL, secretion of a variety of cytokines and antigen presentation were the important functions of macrophages involved in plaque lesions (44). These macrophages can change the phenotype expression, depending on the location and microenvironment. Previous studies have found that the lesions of stable plaques were mainly composed of M2-like macrophages, while M1-like macrophages primarily existed in vulnerable plaques (45). This is consistent with our findings. In this study, we found that a variety of macrophage subpopulations existed in plaques, among which cluster14 content was higher in vulnerable plaques. This subgroup expressed the surface marker of CD86 and CD68, which were surface markers of M1-like pro-inflammatory macrophages. Functional analysis showed that these cells secreted pro-inflammatory cytokines and the functional status were consistent in different type of environments. The small number of these cells in the stable plaques suggested that a weak proinflammatory response was also present in the stable plaque. The change in the number of CD86+CD68+ M1-like macrophages may disrupt the original homeostasis and promote plaque vulnerability.

This also reflected the dynamic association between vulnerable and stable plaques. Further multicolor immunofluorescence revealed the presence of more MMP2 and MMP9 within the vulnerable plaques (see Supplementary Figure 3 for details). It is generally believed that M1 macrophages degraded the extracellular matrix by secreting proteolytic enzymes, thus causing the rupture of fibrous caps (25). This may also be a reason for the vulnerable transformation.

Compared with vulnerable plaques, the immune environment in stable plaques was relatively mild. The same subsets of cells presented in stable plaques were not as active as those in vulnerable plaques. In contrast, only CD4⁺T memory cells were more abundant in stable plaques. Memory cells are generally considered the evidence of a prior adaptive immune response. This evidence also suggested that atherosclerotic plaque was a chronic progressive disease. In response to reappeared antigen stimulation, memory T cells may trigger the next inflammatory response within the plaque, promoting further plaque progression.

There are also some limitations to our study. Firstly, only 32 antibodies were selected, and some subsets could not be effectively distinguished. Secondly, mononuclear cells were extracted from the specimen as a whole, which could not reflect the immune changes in different parts of the plaque. In future study, spatial single-cell technology could effectively solve this problem. Finally, atherosclerotic plaques from patients undergoing surgery may be in the terminal stage of lesion evolution, so it is necessary to analyze the immune components of plaques in different periods, and reflect the dynamic changes in plaque immune environment more comprehensively. Further and more refined exploration is needed.

Data availability statement

The data presented in the study are deposited in the National Genomics Data Center repository, accession number OMIX002548.

Ethics statement

The studies involving human participants were reviewed and approved by Institutional Review Board (IRB) and Ethics Committee of Beijing Tiantan Hospital. The patients/participants provided their written informed consent to participate in this study.

References

- Hansson GK, Hermansson A. The immune system in atherosclerosis. *Nat Immunol* (2011) 12(3):204–12. doi: 10.1038/ni.2001
- Hansson GK. Inflammation, atherosclerosis, and coronary artery disease. *New Engl J Med* (2005) 352(16):1685–95. doi: 10.1056/NEJMra043430
- Christopher JLM, Cristiana A, Kaja MA, Mohammad A, Mohsen A, Foad A. Five insights from the global burden of disease study 2019. *Lancet (London England)* (2020) 396(10258):1135–59. doi: 10.1016/S0140-6736(20)31404-5
- Ampomah PB, Cai B, Sukka SR, Gerlach BD, Yurdagul A Jr, Wang X, et al. Macrophages use apoptotic cell-derived methionine and Dnmt3a during efferocytosis to promote tissue resolution. *Nat Metab* (2022) 4(4):444–57. doi: 10.1038/s42255-022-00551-7
- Guo Y, Qin J, Zhao Q, Yang J, Wei X, Huang Y, et al. Plaque-targeted rapamycin spherical nucleic acids for synergistic atherosclerosis treatment. *Advanced Sci* (Weinheim Baden-Wuerttemberg Germany) (2022) 9(16):e2105875. doi: 10.1002/advs.202105875
- Song P, Fang Z, Wang H, Cai Y, Rahimi K, Zhu Y, et al. Global and regional prevalence, burden, and risk factors for carotid atherosclerosis: A systematic review, meta-analysis, and modelling study. *Lancet Global Health* (2020) 8(5):e721–e9. doi: 10.1016/S2214-109X(20)30117-0
- Joh JH, Cho S. Cardiovascular risk of carotid atherosclerosis: Global consensus beyond societal guidelines. *Lancet Global Health* (2020) 8(5):e625–e6. doi: 10.1016/S2214-109X(20)30132-7

Author contributions

PG conducted the experiment and wrote this article. HL designed the experiment and collected the data. XY provided the surgical specimen and analysis data. YX, QH, LM helped organize some of the data. QZ and XY performed the atherectomy. WW provided the guidance for this experiment. DZ and JZ supervised this experiment. All authors contributed to the article and approved the submitted version.

Acknowledgments

Thanks to Zechen Liu for his help with the language of this article.

Conflict of interest

The authors declare that the research was conducted in the absence of any commercial or financial relationships that could be construed as a potential conflict of interest.

Publisher's note

All claims expressed in this article are solely those of the authors and do not necessarily represent those of their affiliated organizations, or those of the publisher, the editors and the reviewers. Any product that may be evaluated in this article, or claim that may be made by its manufacturer, is not guaranteed or endorsed by the publisher.

Supplementary material

The Supplementary Material for this article can be found online at: <https://www.frontiersin.org/articles/10.3389/fimmu.2022.1085468/full#supplementary-material>

8. Tomaniak M, Katagiri Y, Modolo R, de Silva R, Khamis RY, Bourantas CV, et al. Vulnerable plaques and patients: State-of-the-Art. *Eur Heart J* (2020) 41(31):2997–3004. doi: 10.1093/eurheartj/ehaa227
9. Muller JE, Tofler GH, Stone PH. Circadian variation and triggers of onset of acute cardiovascular disease. *Circulation* (1989) 79(4):733–43. doi: 10.1161/01.CIR.79.4.733
10. Yang WJ, Wong KS, Chen XY. Intracranial atherosclerosis: From microscopy to high-resolution magnetic resonance imaging. *J stroke* (2017) 19(3):249–60. doi: 10.5853/jos.2016.01956
11. Verjans JW, Osborn EA, Ughi GJ, Calfon Press MA, Hamidi E, Antoniadis AP, et al. Targeted near-infrared fluorescence imaging of atherosclerosis: Clinical and intracoronary evaluation of indocyanine green. *JACC Cardiovasc Imaging* (2016) 9(9):1087–95. doi: 10.1016/j.jcmg.2016.01.034
12. Ridker PM, Everett BM, Thuren T, MacFadyen JG, Chang WH, Ballantyne C, et al. Antiinflammatory therapy with canakinumab for atherosclerotic disease. *New Engl J Med* (2017) 377(12):1119–31. doi: 10.1056/NEJMoa1707914
13. Tardif JC, Kouz S, Waters DD, Bertrand OF, Diaz R, Maggioni AP, et al. Efficacy and safety of low-dose colchicine after myocardial infarction. *New Engl J Med* (2019) 381(26):2497–505. doi: 10.1056/NEJMoa1912388
14. Saba L, Saam T, Jäger HR, Yuan C, Hatsukami TS, Saloner D, et al. Imaging biomarkers of vulnerable carotid plaques for stroke risk prediction and their potential clinical implications. *Lancet Neurol* (2019) 18(6):559–72. doi: 10.1016/S1474-4422(19)30035-3
15. Liu Q, Sun Z, Chen L. Memory T cells: Strategies for optimizing tumor immunotherapy. *Protein Cell* (2020) 11(8):549–64. doi: 10.1007/s13238-020-00707-9
16. Crawley AM, Angel JB. The influence of hiv on Cd127 expression and its potential implications for il-7 therapy. *Semin Immunol* (2012) 24(3):231–40. doi: 10.1016/j.smim.2012.02.006
17. Beverley PC. Functional analysis of human T cell subsets defined by Cd45 isoform expression. *Semin Immunol* (1992) 4(1):35–41.
18. Cossarizza A, Chang HD, Radbruch A, Abrignani S, Addo R, Akdis M, et al. Guidelines for the use of flow cytometry and cell sorting in immunological studies (Third edition). *Eur J Immunol* (2021) 51(12):2708–3145. doi: 10.1002/eji.202170126
19. Chávez-Galán L, Ollerios ML, Vesin D, García I. Much more than M1 and M2 macrophages, there are also Cd169(+) and tcr(+) macrophages. *Front Immunol* (2015) 6:263. doi: 10.3389/fimmu.2015.00263
20. Gordon S, Plüddemann A. The mononuclear phagocytic system: generation of diversity. *Front Immunol* (2019) 10:1893. doi: 10.3389/fimmu.2019.01893
21. Akinrinmade OA, Chetty S, Daramola AK, Islam MU, Thepen T, Barth S. Cd64: An attractive immunotherapeutic target for M1-type macrophage mediated chronic inflammatory diseases. *Biomedicine* (2017) 5(3):56. doi: 10.3390/biomedicine5030056
22. Falk E. Pathogenesis of atherosclerosis. *J Am Coll Cardiol* (2006) 47(8 Suppl):C7–12. doi: 10.1016/j.jacc.2005.09.068
23. Hafiane A. Vulnerable plaque, characteristics, detection, and potential therapies. *J Cardiovasc Dev Dis* (2019) 6(3):26. doi: 10.3390/jcdd6030026
24. Naghavi M, Libby P, Falk E, Casscells SW, Litovsky S, Rumberger J, et al. From vulnerable plaque to vulnerable patient: A call for new definitions and risk assessment strategies: Part I. *Circulation* (2003) 108(14):1664–72. doi: 10.1161/01.CIR.0000087480.94275.97
25. Tabas I, Lichtman AH. Monocyte-macrophages and T cells in atherosclerosis. *Immunity* (2017) 47(4):621–34. doi: 10.1016/j.immuni.2017.09.008
26. Winkels H, Wolf D. Heterogeneity of T cells in atherosclerosis defined by single-cell rna-sequencing and cytometry by time of flight. *Arteriosclerosis thrombosis Vasc Biol* (2021) 41(2):549–63. doi: 10.1161/ATVBAHA.120.312137
27. Li H, Nam Y, Huo R, Fu W, Jiang B, Zhou Q, et al. De novo germline and somatic variants convergently promote endothelial-to-Mesenchymal transition in simplex brain arteriovenous malformation. *Circ Res* (2021) 129(9):825–39. doi: 10.1161/CIRCRESAHA.121.319004
28. Foulds KE, Wu CY, Seder RA. Th1 memory: Implications for vaccine development. *Immunol Rev* (2006) 211:58–66. doi: 10.1111/j.0105-2896.2006.00400.x
29. Yu XH, Zhang J, Zheng XL, Yang YH, Tang CK. Interferon- γ in foam cell formation and progression of atherosclerosis. *Clinica chimica acta; Int J Clin Chem* (2015) 441:33–43. doi: 10.1016/j.cca.2014.12.007
30. Goossens P, Gijbels MJ, Zernecke A, Eijgelar W, Vergouwe MN, van der Made I, et al. Myeloid type I interferon signaling promotes atherosclerosis by stimulating macrophage recruitment to lesions. *Cell Metab* (2010) 12(2):142–53. doi: 10.1016/j.cmet.2010.06.008
31. Weng X, Cheng X, Wu X, Xu H, Fang M, Xu Y. Sin3b mediates collagen type I gene repression by interferon gamma in vascular smooth muscle cells. *Biochem Biophys Res Commun* (2014) 447(2):263–70. doi: 10.1016/j.bbrc.2014.03.140
32. Yeh JL, Hsu JH, Liang JC, Chen JJ, Liou SF. Lercanidipine and labeledipinedilol-a attenuate Lipopolysaccharide/Interferon- γ -Induced inflammation in rat vascular smooth muscle cells through inhibition of Hmgb1 release and mmp-2, 9 activities. *Atherosclerosis* (2013) 226(2):364–72. doi: 10.1016/j.atherosclerosis.2012.12.005
33. Nakagawa T, Nozaki S, Nishida M, Yakub JM, Tomiyama Y, Nakata A, et al. Oxidized ldl increases and interferon-gamma decreases expression of Cd36 in human monocyte-derived macrophages. *Arteriosclerosis thrombosis Vasc Biol* (1998) 18(8):1350–7. doi: 10.1161/01.ATV.18.8.1350
34. Ma X, Deng J, Han L, Song Y, Miao Y, Du X, et al. Single-cell rna sequencing reveals b cell-T cell interactions in vascular adventitia of hyperhomocysteinemiaaccelerated atherosclerosis. *Protein Cell* (2022) 13(7):540–547. doi: 10.1007/s13238-021-00904-0
35. Zhang S, Zhang S, Lin Z, Zhang X, Dou X, Zhou X, et al. Deep sequencing reveals the skewed b-cell receptor repertoire in plaques and the association between pathogens and atherosclerosis. *Cell Immunol* (2021) 360:104256. doi: 10.1016/j.cellimm.2020.104256
36. Fernández-Ruiz I. Promising anti-IL-6 therapy for atherosclerosis. *Nat Rev Cardiol* (2021) 18(8):544. doi: 10.1038/s41569-021-00575-8
37. Bernberg E, Ulleryd MA, Johansson ME, Bergström GM. Social disruption stress increases il-6 levels and accelerates atherosclerosis in apoe-/- mice. *Atherosclerosis* (2012) 221(2):359–65. doi: 10.1016/j.atherosclerosis.2011.11.041
38. Falk E, Shah PK, Fuster V. Coronary plaque disruption. *Circulation* (1995) 92(3):657–71. doi: 10.1161/01.CIR.92.3.657
39. Tyrrell DJ, Goldstein DR. Ageing and atherosclerosis: Vascular intrinsic and extrinsic factors and potential role of il-6. *Nat Rev Cardiol* (2021) 18(1):58–68. doi: 10.1038/s41569-020-0431-7
40. Tay C, Liu YH, Hosseini H, Kanellakis P, Cao A, Peter K, et al. B-Cell-Specific depletion of tumour necrosis factor alpha inhibits atherosclerosis development and plaque vulnerability to rupture by reducing cell death and inflammation. *Cardiovasc Res* (2016) 111(4):385–97. doi: 10.1093/cvr/cvw186
41. Okazaki T, Chikuma S, Iwai Y, Fagarasan S, Honjo T. A rheostat for immune responses: The unique properties of pd-1 and their advantages for clinical application. *Nat Immunol* (2013) 14(12):1212–8. doi: 10.1038/ni.2762
42. Kyaw T, Tay C, Khan A, Dumouchel V, Cao A, To K, et al. Conventional B2 b cell depletion ameliorates whereas its adoptive transfer aggravates atherosclerosis. *J Immunol (Baltimore Md 1950)* (2010) 185(7):4410–9. doi: 10.4049/jimmunol.1000033
43. Libby P, Buring JE, Badimon L, Hansson GK, Deanfield J, Bittencourt MS, et al. Atherosclerosis. *Nat Rev Dis Primers* (2019) 5(1):56. doi: 10.1038/s41572-019-0106-z
44. Moore KJ, Sheedy FJ, Fisher EA. Macrophages in atherosclerosis: A dynamic balance. *Nat Rev Immunol* (2013) 13(10):709–21. doi: 10.1038/nri3520
45. Mehu M, Narasimulu CA, Singla DK. Inflammatory cells in atherosclerosis. *Antioxidants (Basel Switzerland)* (2022) 11(2):233. doi: 10.3390/antiox11020233

COPYRIGHT

© 2023 Ge, Li, Ya, Xu, Ma, He, Wang, Liu, Zhang, Zhang, Wang, Zhang and Zhao. This is an open-access article distributed under the terms of the [Creative Commons Attribution License \(CC BY\)](https://creativecommons.org/licenses/by/4.0/). The use, distribution or reproduction in other forums is permitted, provided the original author(s) and the copyright owner(s) are credited and that the original publication in this journal is cited, in accordance with accepted academic practice. No use, distribution or reproduction is permitted which does not comply with these terms.



OPEN ACCESS

EDITED BY
Nadine Suffee,
Sorbonne Universités, France

REVIEWED BY
Antoine Roquilly,
Université de Nantes, France
Akram M. Zaaqoq,
MedStar Washington Hospital Center,
United States
Celestine Wanjalla,
Vanderbilt University Medical Center,
United States

*CORRESPONDENCE
Maxime Nguyen
✉ maxime.nguyensoenen@gmail.com

SPECIALTY SECTION
This article was submitted to
Inflammation,
a section of the journal
Frontiers in Immunology

RECEIVED 18 November 2022
ACCEPTED 30 December 2022
PUBLISHED 19 January 2023

CITATION
Nguyen M, Stiel L, Guilloteau A, Bahr P-A,
Masson D, Thomas C, Blot M, Guy J,
Fontaine C, Durand B, Bouhemad B
and Guinot P-G (2023) Leukocyte cell
population data in patients with cardiac
surgery and cardiopulmonary bypass:
A potential readily available tool to
monitor immunity.
Front. Immunol. 13:1101937.
doi: 10.3389/fimmu.2022.1101937

COPYRIGHT
© 2023 Nguyen, Stiel, Guilloteau, Bahr,
Masson, Thomas, Blot, Guy, Fontaine,
Durand, Bouhemad and Guinot. This is an
open-access article distributed under the
terms of the [Creative Commons Attribution
License \(CC BY\)](https://creativecommons.org/licenses/by/4.0/). The use, distribution or
reproduction in other forums is permitted,
provided the original author(s) and the
copyright owner(s) are credited and that
the original publication in this journal is
cited, in accordance with accepted
academic practice. No use, distribution or
reproduction is permitted which does not
comply with these terms.

Leukocyte cell population data in patients with cardiac surgery and cardiopulmonary bypass: A potential readily available tool to monitor immunity

Maxime Nguyen^{1,2,3,4*}, Laure Stiel^{3,4,5}, Adrien Guilloteau⁶,
Pierre-Alain Bahr¹, David Masson^{2,3,4}, Charles Thomas^{2,3,4},
Mathieu Blot^{2,3,4,7}, Julien Guy⁸, Cécile Fontaine¹,
Bastien Durand¹, Belaid Bouhemad^{1,2,3,4}
and Pierre-Grégoire Guinot^{1,2,3,4}

¹Department of Anaesthesiology and Intensive Care, Dijon University Hospital, Dijon, France,

²University of Burgundy and Franche-Comté, LNC UMR1231, Dijon, France, ³INSERM, LNC UMR1231, Dijon, France, ⁴LipSTIC LabEx, Dijon, France, ⁵Service de Réanimation Médicale, Groupe Hospitalier de la Région Mulhouse Sud Alsace, Mulhouse, France, ⁶Clinical Research Support Unit, Dijon University Hospital, Dijon, France, ⁷Department of Infectiology, Dijon University Hospital, Dijon, France,

⁸Cytometry Core Facility, University of Burgundy Franche-Comté, Dijon, France

Purpose: Cardiac surgery with cardiopulmonary bypass triggers sterile inflammation that is responsible for post-operative morbidity. Automated flow cytometry devices used for leukocyte count provide cell population data (CPD) regarding fluorescence intensity, size and granularity of leukocytes that have never been studied in the context of sterile inflammation. Our objective was to explore leukocyte cell population data in patients undergoing cardiac surgery with cardiopulmonary bypass in order to determine whether CPD could be used to monitor immune cell activation.

Methods: This is an ancillary study of a cohort of patients undergoing cardiac surgery with cardiopulmonary bypass. Cell population data (CPD) extracted from a routine automated flow cytometer were analyzed (Fluorescence targeted to nucleic acids). The time points of interest were: pre-operative, postoperative and 5 days after surgery. The variations in those parameters were studied. Data were then compared between patients according to the occurrence of a composite criteria (supra-ventricular arrhythmia, stroke, acute renal failure, and/or death).

Results: Data from 1453 patients were analyzed. The neutrophil count, fluorescence granularity (NE-SCC), intensity (NE-SFL) and size (NE-FSC) increased with surgery. Heterogeneity of neutrophils decreased in terms of fluorescence granularity (NE-WX) and size (NE-WZ) but increased in terms of intensity (NE-WY). The lymphocyte count decreased with surgery. While fluorescence granularity (LY-X) and size increased (LY-Z), Lymphocyte intensity decreased (LY-Y). Lymphocytes were less heterogeneous in terms of their granularity, size and intensity after surgery (LY-WX, LY-WY, LY-WZ). Patients who developed the composite complication criteria had a higher pre-operative neutrophil count (5.08 [3.89;6.95] vs 4.76 [3.60;6.13], $p = 0.02$; AUC = 0.56

[0.51;0.60]), and more heterogeneous neutrophils in terms of fluorescence granularity (NE-WX, AUC = 0.57 [0.52;0.62]) and intensity (NE-WY, AUC 0.61 [0.56;0.65]). Those patients also had lower pre-operative lymphocyte count (1.49 [1.10;1.14] vs 1.81 [1.39;2.39], $p < 0.01$, AUC = 0.61 [0.57;0.66]) and fluorescence granularity (LY-X, AUC = 0.57 [0.53;0.62]). NE-WX, NE-WY and LY-X were associated with post-operative complications after adjustment on the EuroSCORE 2 (adjusted odd ratio of 1.01 [1.00;1.02]; 1.01 [1.00;1.01] and 1.08 [1.02;1.15] respectively).

Conclusion: Cardiac surgery with cardiopulmonary bypass was associated with substantial alterations of CPD probably reflecting leukocytes activation in sterile inflammation. Pre-operative NE-WX, NE-WY and LY-X biomarkers levels were associated with post-operative complications, independently of the EuroSCORE 2. Such routine, unexploited and low cost parameters might represent useful tools likely to monitor immune function and predict outcomes for patients undergoing cardiac surgery. Our findings requires validation on a larger external cohort.

KEYWORDS

biomarker, cell population data, cardiac surgery, cardiopulmonary bypass, inflammation, post-operative outcome, immunity, acute kidney injury

Introduction

Immune dysregulation is a major issue in critically ill patients and biomarkers for the monitoring of the immune function are urgently needed in order to implement therapies targeting immunity (1). Cardiac surgery with cardiopulmonary bypass (CPB) is performed daily for the treatment of cardiovascular conditions. Although the procedure of CPB has been improved, this surgery is associated with high incidences of complications and mortality. Cardiac surgery with CPB represents a major aggression (to the human body) and the sterile inflammatory response triggered by CPB drives post-operative complications (2).

In addition to cell count, automated hematology analyzers measure cell population data (CPD) that do not appear on traditional reports, meaning this information remains unused. These parameters are directly linked to leukocyte characteristics (granularity, size and fluorescence) and in patients with sepsis (3) it has been suggested that these CPD reflect leukocyte activation (4). However, they have never been studied in the context of sterile inflammation such as cardiac surgery with CPB.

The objective of the present study was to explore CPD as a potential marker of immune function in sterile inflammation by following the changing patterns of leukocyte CPD in patients undergoing cardiac surgery and cardiopulmonary bypass and by reporting associations between leukocyte CPD and post-operative complications.

We hypothesized that CPD would be highly modified by cardiac surgery and cardiopulmonary bypass (reflecting the activation of leukocytes) and that pre-operative levels of those parameters reflecting a pre-operative pro-inflammatory state would be associated with post-operative complications.

Material and methods

Patients

This is an ancillary analysis of a prospective cohort that aimed to study risk factor for vasoplegia in patients undergoing cardiac surgery with cardiopulmonary bypass. Patients were recruited between October 2017 and July 2021. The inclusion criteria were as follows: all adult patients undergoing cardiac surgery with cardiopulmonary bypass, covered by a social insurance system, who have given oral consent to participate after receiving full information and with at least one blood count at any of the time points of interest. Exclusion criteria were: cardiac graft, pre-operative extracorporeal life support or membrane oxygenation, mechanical cardiac assistance and patient deprived of liberty. Only patients included in Dijon university hospital were considered for the present analysis.

This report was drafted in accordance with the STROBE statement (5). This study was approved by the Institutional Review Board (IRB 00010254 - 2022 - 034). All patients received written information of their inclusion in the study.

Protocol

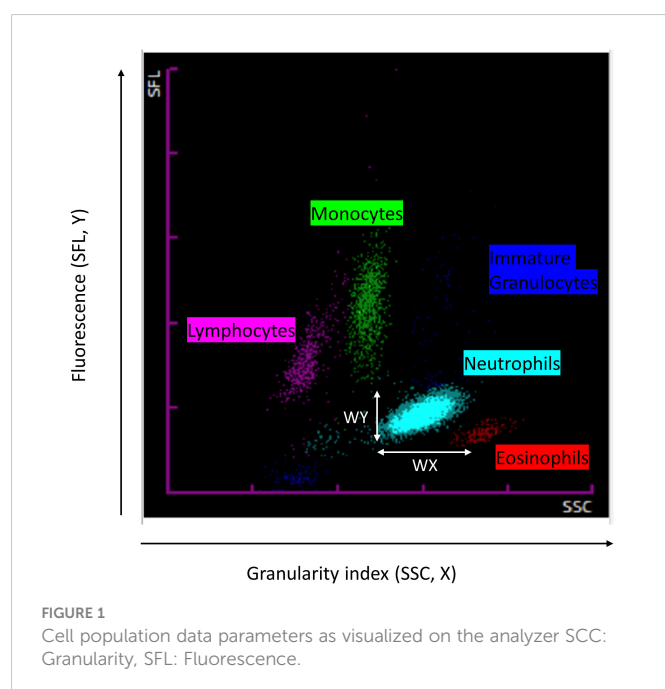
Cytometry data were retrospectively extracted from the automated hematology analyzer (Sysmex XN-200, Sysmex, France). No blood sampling was mandatory for the study as blood cell count is usually monitored daily after cardiac surgery in our centre. Those data were merged with the data from the prospective cohort (ClinicalTrials.gov Identifier: NCT03281317). Three time points of interest were defined: pre-operative, post-operative (on the day of

surgery) and 5 days after surgery. We choose the pre-operative and post-operative time points to capture the modifications of CPD induce by the surgery. Day 5 was chosen because it allowed to describe the evolution of CPD with the resolution of inflammation without too many lost too follow-up patients.

Blood cell count (CBC) was measured on an automated Sysmex XN2000 analyzer equipped with impedance and fluorescence flow cytometry devices. The optical system of the XN2000 employs a red diode laser producing a light beam. Cell permeabilization is performed by treatment with specific lysis reagents allowing specific dyes to enter the cells, where they bind to nucleic acids in the cytoplasmic organelles and the nucleus. Three mains signals are recorded (Figure 1): forward-scattered light (FSC, cell size), side-scattered light (SSC, internal cell structure and granularity), and side fluorescence light intensity (SFL, reflecting DNA/RNA content). Based on the resulting fluorescence and scattered light characteristics, the cells can be separated. For each type of leukocyte (neutrophil, lymphocyte and monocyte), the cell count and CPD were extracted. Neutrophil to lymphocyte ratio (NLR) was calculated.

The CPD included:

- Neutrophil cell complexity (NE-SCC), heterogeneity in cell complexity (NE-WX)
- Fluorescence intensity (NE-SFL), heterogeneity in fluorescence intensity (NE-WY)
- Neutrophil size (NE-FSC) and heterogeneity in size (NE-WZ)
- Lymphocytes cell complexity (LY-X), heterogeneity in cell complexity (LY-WX)
- Fluorescence intensity (LY-Y), heterogeneity in fluorescence intensity (LY-WY)
- Monocytes size (LY-Z) and heterogeneity in size (LY-WZ).
- Monocytes cell complexity (MO-X), heterogeneity in cell complexity (MO-WX)



- Fluorescence intensity (MO-Y), heterogeneity in fluorescence intensity (MO-WY)
- Monocytes size (MO-Z) and heterogeneity in size (MO-WZ).

Endpoints

The primary endpoint was inflammation-related complication or death occurring during the hospitalisation (6, 7). This endpoint was defined by a composite criteria (8) that included *de novo* supra-ventricular arrhythmia, stroke, acute renal failure (defined according to KDIGO guidelines (9)) and/or death.

Data collection

Baseline demographic data, per-operative and ICU data presented were collected prospectively. The EuroSCORE 2, a validated score for post-operative morbimortality of patients undergoing cardiac surgery was calculated (10). The American Society of Anesthesiologists physical status (ASA score) has been evaluated during the pre-operative consultation (11). Complications were monitored until hospital discharge. All those data were recorded in a data base (Excel, Microsoft). Cell population data are recorded prospectively by the automated hematology analyzer and were extracted retrospectively. The two data bases were merged in order to perform this analysis.

Statistical analysis

Normality was assessed graphically; quantitative data were presented as means (standard deviation/SD) or medians (interquartile range/IQR) and were compared using the Student t-test and the Kruskal-Wallis nonparametric test. Categorical, ordinal, and binary data were presented as frequencies and percentages and were compared using Chi-squared or Fisher's exact tests if the conditions of validity were not fulfilled. A Bonferroni correction was applied to compensate for alpha risk inflation with repeated measurements. For longitudinal data, changing patterns of CPD with time were assessed using mixed linear modeling. ROC curve analyses were carried out for cell line parameters of interest. Optimal cut-off values were calculated using Youden's method. An adjusted logistic regression analysis based on the EuroSCORE 2 was also carried out in order to determine whether those associations were independent of classical risks factors of post-operative morbi-mortality included in this validated score. Last, we developed a multivariable model combining the CPD variable of interest with the EuroSCORE 2 to predict post-operative complications. Data were split into a training set (60%) and a validation set (40%). The model was developed using logistic regression on the training data set. Variable selection was stepwise, AIC based. Then the model accuracy and area under the curve were calculated on the validation set. The Hosmer-Lemeshow Goodness-of-fit Test was also carried out. Missing data were considered to be missing at random and were omitted from the analysis. All analyses were performed using R software.

Results

Population and baseline characteristics

After exclusion of 121 patients (Figure 2) data from 1453 patients had CPD available for at least one of the time points of interest and were analyzed. Out of those 1453 patients, CPD data were available for 639 patients at the pre-operative time point, 907 patients at the post-operative time points and 651 patients 5 days after surgery. Patients' characteristics are described in Table 1. Median age was 69 [IQR 61;75], most patients were men (76%) with an ASA score of 3 (71.6%) and the median EuroSCORE 2 was 2.23 [IQR 1.19;4.60]. Sixty eight (4.68%) patients had sepsis, mostly due to endocarditis (76%). Among the 636 (43.8%) patients that developed the composite criteria, 342 (23.6%) developed renal failure, 384 (26.4%) *de novo* supra ventricular arrhythmia, 58 (4.0%) stroke and 81 (5.6%) died.

Neutrophil cell data are modified by cardiac surgery

The neutrophil count (Figure 3A), fluorescence granularity (NE-SCC), intensity (NE-SFL) and size (NE-FSC) increased with surgery (Figures 4A, C, E respectively). Heterogeneity of neutrophils decreased in terms of fluorescence granularity (NE-WX) and size (NE-WZ) but increased in terms of intensity (NE-WY) (Figures 4B, D, F respectively).

Neutrophil cell data are associated with post-operative complications

Patients who developed the composite complication score had higher pre-operative neutrophil counts (5.08 [3.89;6.95] vs 4.76 [3.60;6.13] $p = 0.02$) and more heterogeneous neutrophils in terms of fluorescence granularity (NE-WX, $p < 0.01$) and intensity (NE-WY, $p < 0.01$) (Figures 4B, D and Table 2). Immature granulocytes and the neutrophil to lymphocyte ratio (NLR) increased with cardiac surgery, and pre-operative NLR was associated with occurrence of post-operative complications ($p < 0.01$ for both) (Supplementary Table 1). Using multivariate analysis, NE-WX and NE-WY were associated with post-

TABLE 1 Characteristics of the patients.

	N= 1453
Baseline	
Age (year)	69.0 [61.0;75.0]
Male (n,%)	1105 (76%)
BMI (Kg/m ²)	26.7 [24.2;30.2]
ASA score n,%)	
1	4 (0.28%)
2	173 (11.9%)
3	1039 (71.6%)
4	220 (15.2%)
5	16 (1.10%)
EuroSCORE II	2.23 [1.19;4.60]
Sepsis (n,%)	68 (4.68%)
Per-operative	
Emergent surgery (n,%)	283 (19.5%)
Valvular surgery (n,%)	777 (53.5%)
CABP (n,%)	755 (52.0%)
Combined surgery (n,%)	489 (33.7%)
CPB duration (minutes)	116 [92.0;147]
ICU admission	
SOFA (ICU admission)	5.00 [3.00;6.00]
SAPS-2 (ICU admission)	32.0 [24.0;41.0]
Norepinephrine (ICU admission) (n,%)	1080 (74.3%)
Dobutamine (ICU admission) (n,%)	229 (15.8%)
Outcome	
ICU length of stay (days)	2.00 [1.00;4.00]
Hospital length of stay (days)	9.00 [7.00;12.0]
In hospital mortality (n,%)	81 (5.57%)

(Continued)

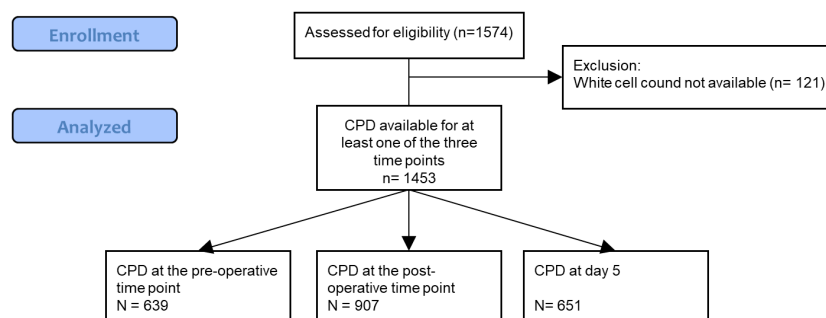


FIGURE 2
Study flow chart. CPD, Cell Population Data.

TABLE 1 Continued

	N= 1453
Supra-ventricular arrhythmia (n,%)	384 (26.4%)
Stroke (n,%)	58 (3.99%)
Acute kidney injury (n,%)	342 (23.5%)

BMI, Body mass index; ASA, American Society of Anesthesiologists; CABP, Coronary artery bypass; CPB, Cardiopulmonary bypass; SOFA, Sequential organ failure assessment; SAPS-2, Simplified acute physiology score-2; ICU, Intensive care unit.

operative complications independently of the EuroSCORE 2 (adjusted odd ratio of 1.01 [1.00;1.02] and 1.01 [1.00;1.01] respectively) (Table 2).

Lymphocyte cell data are modified by cardiac surgery

The lymphocyte count decreased with surgery (Figure 3B). While fluorescence granularity (LY-X) and size (LY-Z) increased, lymphocyte fluorescence intensity decreased (LY-Y) (Figures 5A, C, E). Lymphocytes were less heterogeneous in terms of their granularity, intensity and size after surgery (i.e., lower LY-WX, LY-WY and LY-WZ respectively).

Lymphocyte cell data are associated with post-operative complications

Patients who developed post-operative complications had lower pre-operative lymphocyte counts (1.49 [1.10;1.14] vs 1.81 [1.39;2.39], $p<0.01$) and fluorescence granularity (LY-X, $p<0.01$) (Figure 5).

Using multivariate analysis, LY-X was associated with the occurrence of post-operative complications, independently of the EuroSCORE 2 (adjusted odd ratio of 1.08 [1.02;1.15]) (Table 2).

Monocyte cell data are not associated with post-operative complications

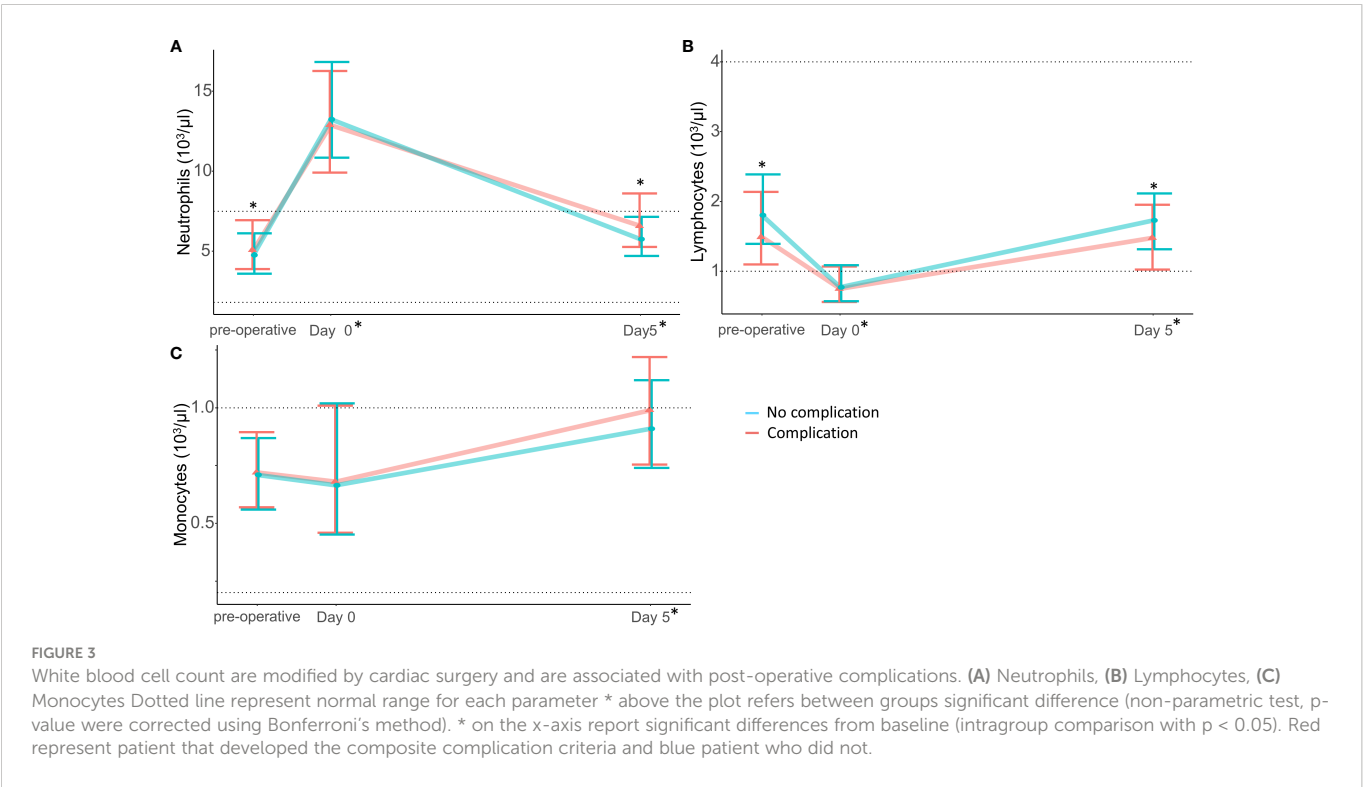
The monocyte count was unchanged after cardiac surgery (Figure 3C). There was no difference between patients developing complications and others in terms of pre-operative monocyte cell parameters (Supplementary Table 2).

Multivariate model for post-operative complications

After stepwise variable selection (training data set), EuroSCORE 2, NE-WY and LY-X were kept in the model (Supp file 3). The accuracy of this model (testing data set) was of 0.65 [0.59;0.71] and the Area under the curve (AUC) of 0.63 [0.58;0.68]. The p-value of the Hosmer-Lemeshow Goodness-of-fit Test was of 0.33. For the EuroSCORE 2 alone the accuracy was of 0.63 [0.56;0.69] and the AUC of 0.60 [0.55;0.65].

Discussion

Our main finding is that CPD were highly modified by the systemic aggression caused by cardiac surgery and cardiopulmonary bypass. In addition, we were able to identify pre-operative differences in CPD associated with post-operative complications. In particular: a



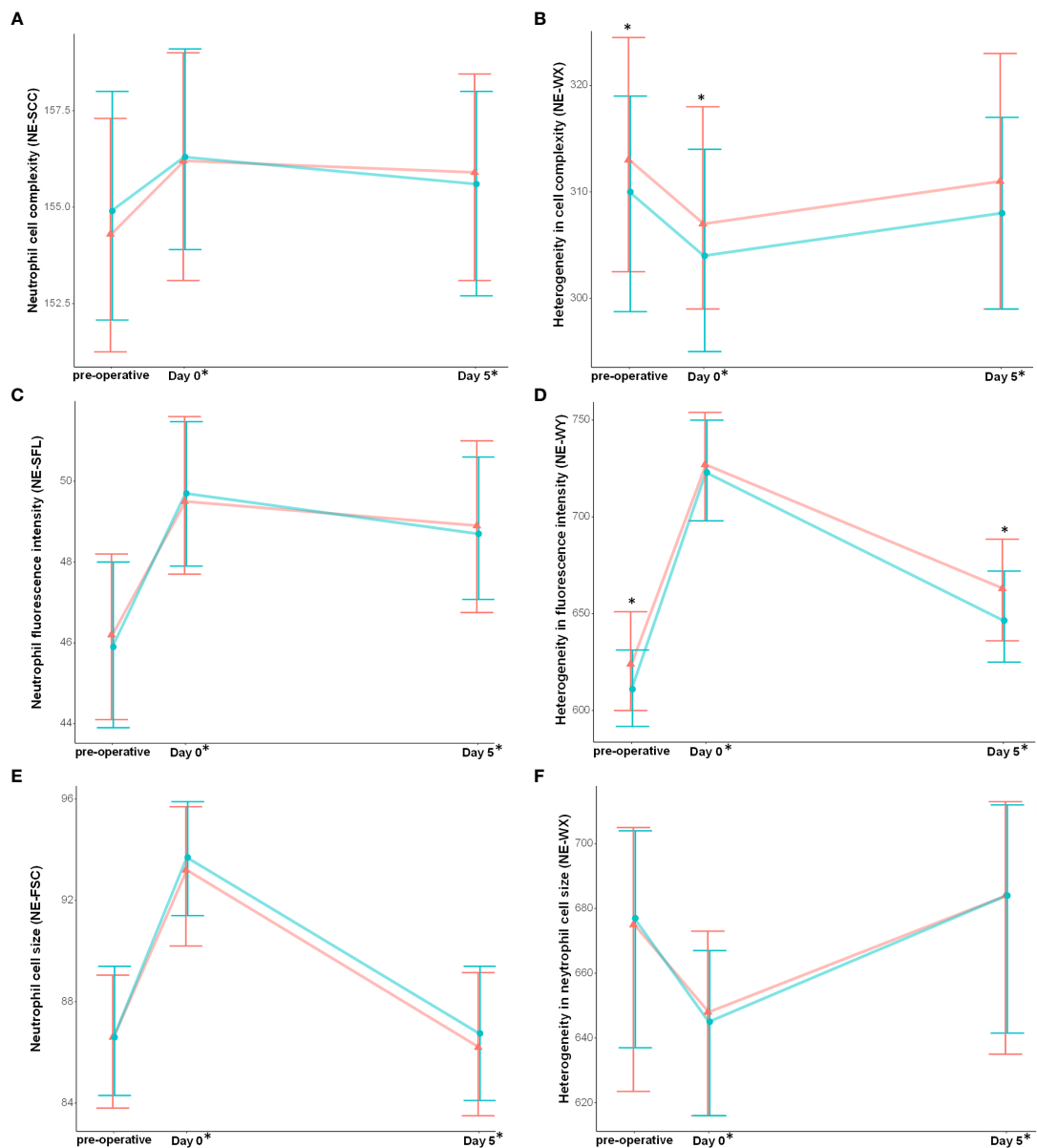


FIGURE 4 Neutrophil cell populations data are modified with cardiac surgery and are associated with post-operative complications. **(A)** Neutrophil cell complexity, **(B)** Heterogeneity in cell complexity, **(C)** Neutrophil fluorescence intensity, **(D)** Heterogeneity in fluorescence intensity, **(E)** Neutrophil cell size, **(F)** Heterogeneity in neutrophil cell size. Results are presented as median and interquartile range. * above the plot refers between groups significant difference (non-parametric test, p-value were corrected using Bonferroni's method). * on the x-axis report significant differences from baseline (intragroup comparison with $p < 0.05$). Red represent patient that developed the composite complication criteria and blue patient who did not.

TABLE 2 Area under the curve, threshold and odd ratio adjusted for EuroSCORE 2.

Variable	AUC (95% CI)	Optimal threshold	Accuracy	OR adjusted for the EuroSCORE 2
Neutrophil count	0.56 [0.51;0.60]	6.65	0.52 [0.50;0.54]	1.02 [0.97;1.08]
NE-WX	0.57 [0.52;0.62]	320	0.52 [0.50;0.54]	1.01 [1.00;1.02]*
NE-WY	0.61 [0.56;0.65]	636	0.53 [0.51;0.55]	1.01 [1.00;1.01]*
Lymphocyte count	0.61 [0.57;0.66]	1.52	0.53 [0.51;0.56]	0.93 [0.80;1.08]
LY-X	0.57 [0.53;0.62]	80.2	0.52 [0.50;0.54]	1.08 [1.02;1.15]*
Immature granulocyte	0.57 [0.53;0.61]	0.06	0.52 [0.50;0.54]	2.27 [0.67;15.24]
Neutrophyl to Lymphocyte ratio	0.61 [0.57;0.66]	3.5	0.53 [0.51;0.55]	1.05 [1.01;1.10]*

OR, Odd ratio. For adjusted OR, each parameter was individually adjust on the EuroSCORE 2. Accuracy is given for the optimal threshold. * $p < 0.05$.

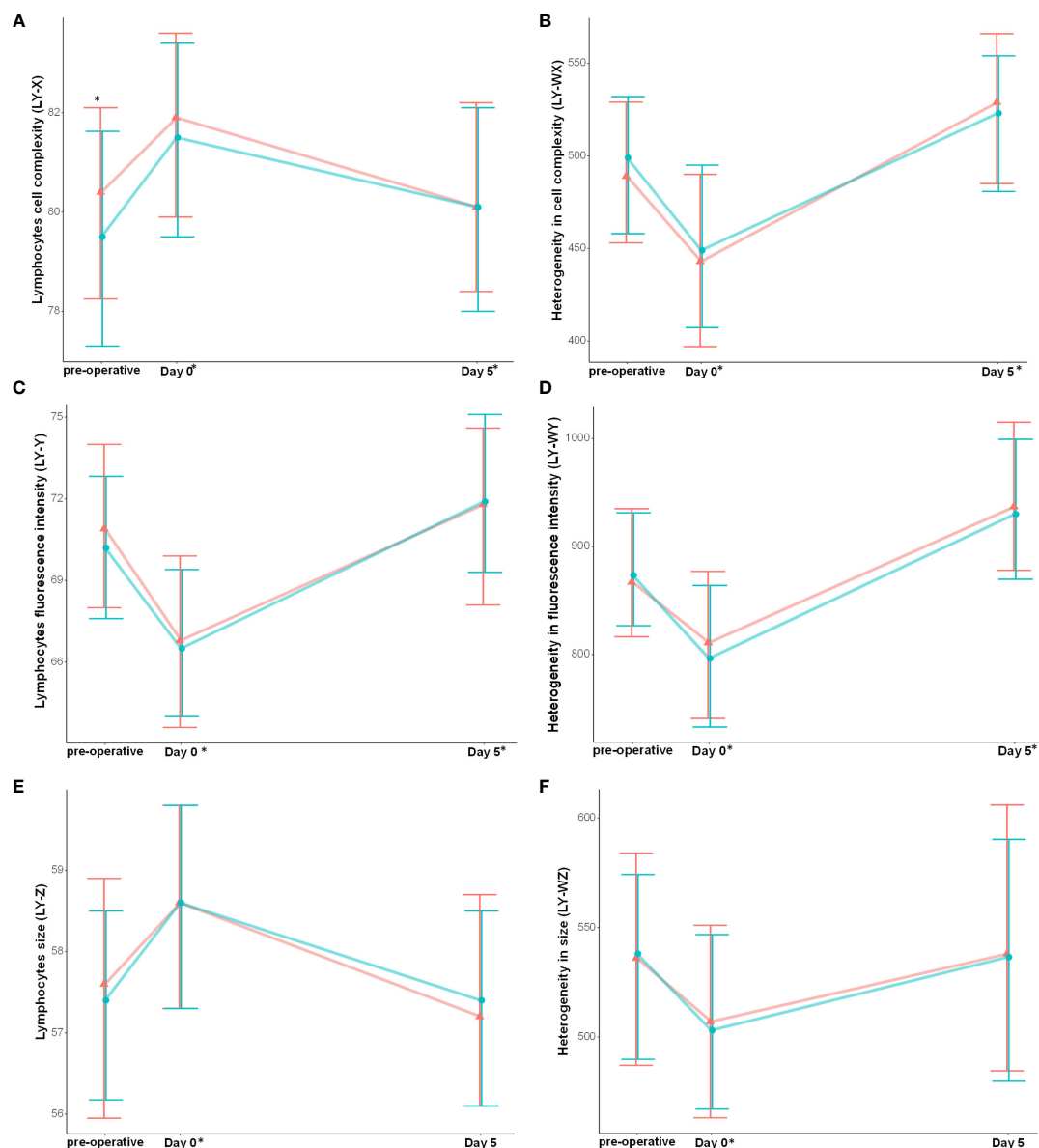


FIGURE 5
Lymphocyte cell populations data are modified with cardiac surgery and are associated with post-operative complications. (A) Lymphocytes cell complexity, (B) Heterogeneity in cell complexity, (C) Lymphocytes fluorescence intensity, (D) Heterogeneity in fluorescence intensity, (E) Lymphocytes cell size, (F) Heterogeneity in lymphocytes cell size. Results are presented as median and interquartile range. *: between groups significant difference (non-parametric test, p-value were corrected using Bonferroni's method). * on the x-axis report significant differences from baseline (intragroup comparison with $p < 0.05$). Red represent patient that developed the composite complication criteria and blue patient who did not.

high pre-operative neutrophil count, a low per-operative lymphocyte count, and a high immature granulocyte count were associated with the occurrence of post-operative complications. Neutrophils were also more heterogenous in granularity and intensity and lymphocytes had lower granularity in patients who developed complications. CPD are highly modified in the context of sterile inflammation, further supporting the use of CPD as a marker of immune response during critical illness.

In patients undergoing cardiac surgery, the pre-operative inflammatory status is a major concern and influences clinical outcome (12). Among the traditional blood cell count data reported, high neutrophil and low lymphocyte counts have been related to adverse outcomes following coronary graft surgery (13, 14).

In addition to a pro-inflammatory state, a low lymphocyte count has also been suggested to reflect poorer general health (15) which might also link lymphopenia to worse outcome. In line with this, by combining these two markers, the neutrophil to lymphocyte ratio (NLR) has been reported as a predictor of morbidity and mortality in patients undergoing cardiac surgery (15, 16). Our results are consistent with those findings and further support the importance of the pre-operative inflammatory status.

In addition to the traditional quantitative leukocyte count, the automated blood analyzer provides data that give qualitative information about leukocytes (cell fluorescence intensity, granularity, size and the heterogeneity of these three parameters among each cell line (17)) that could be used to greater advantage.

Neutrophil fluorescence intensity (NE-SFL) and the heterogeneity in fluorescence (NE-WY) have been demonstrated to discriminate sepsis with a good accuracy, leading to hypothesize that these parameters indicate neutrophil activation or immaturity (18). NE-SFL is related to the degree of chromatin, DNA and RNA condensation and thus is likely to indicate neutrophil cell activation, i.e., in transcriptional activity. The increase in neutrophil size observed in our cohort could indicate increased neutrophil heterogeneity that could be linked to bone marrow release of immature granulocytes. The increase of NE-WY, reflecting the fluorescent light distribution width of the neutrophil area may also indicate neutrophil immaturity. Using multivariate analysis, the heterogeneity of neutrophils (NE-WX, NE-WY) and Lymphocytes cell complexity (LY-X) were associated with the occurrence of complications after adjustment on the EuroSCORE 2, suggesting that these parameters could bring additional information to traditional complication scores and be useful in early detection of complications.

Cardiac surgery with cardiopulmonary bypass triggers inflammation by multiple mechanisms (19). As in sepsis, during cardiac surgery, inflammation drives adverse clinical outcome (20, 21). However, this inflammation is unrelated to pathogen aggression and involves different pathways (22). Leucocytes counts modifications induced by CPB (increased neutrophil, decrease lymphocyte and similar monocyte) reported in our study are in line with previous results (23). Nevertheless, our study provides new additional information on blood cell properties and activation induced by cardiac surgery with cardiopulmonary bypass. In our data, whereas baseline NE-SFL and NE-WY were in the same range of values as healthy controls, the post-operative values increased but were not as elevated as those reported in patients with sepsis (4, 18). The heterogeneity in neutrophil CPD probably reflects different states of leukocyte activation, further underlying the separate immune pathways of sterile and septic inflammation. Thus, CPD may represent a new tool for a better understanding of immune cell activation during critical illness. As blood counts are widely available, CPD could provide interesting additional information for the monitoring of immunity.

This study has some limitations. Firstly, this is an observational study and only association could be inferred. Secondly, as leukocyte count is not routinely performed daily, there was a large amount of missing data which might introduce a selection bias. Indeed, patients with a pre-operative blood cell count seemed to be more severe at baseline than patients with missing data (Supplementary Table 3). Blood transfusion might induce significant modification of CPD kinetics. Complications were only monitored until hospital discharge, thus only “early” complications are reported in this analysis. Lastly, biomarkers of inflammation were not measured in those post-operative patients and could have provided interesting additional information.

In conclusion, CPD were highly modified by cardiac surgery with cardiopulmonary bypass and some of those modifications were associated with post-operative complications, suggesting that CPD reflect the activation of leukocytes in sterile inflammation. Before surgery: NE-WX, NE-WY and LY-X were associated with post-operative complication independently of the EuroSCORE 2. Those parameters measured with traditional blood cell counts might represent a readily available and low cost tool for the monitoring of

immune function during critical illness. Our findings requires validation on a larger external cohort.

Data availability statement

The raw data supporting the conclusions of this article will be made available by the authors, without undue reservation.

Ethics statement

The studies involving human participants were reviewed and approved by “Comité d’Ethique pour la Recherche en Anesthésie-Réanimation”. Written informed consent for participation was not required for this study in accordance with the national legislation and the institutional requirements.

Author contributions

MN, MB, AG, DM, LS, P-GG contributed to the study design. MN, BD, AG, MB, P-AB, CF collected the data. MN, BB P-GG, LS analysed the data. MN, LS drafted the manuscript. MN, LS, AG, P-AB, DM, CT, MB, JG, CF, BD, BB, P-GG reviewed and edited the manuscript. All authors contributed to the article and approved the submitted version.

Acknowledgments

The authors wish to acknowledge the ICU staff who contributed to this research.

Conflict of interest

The authors declare that the research was conducted in the absence of any commercial or financial relationships that could be construed as a potential conflict of interest.

Publisher’s note

All claims expressed in this article are solely those of the authors and do not necessarily represent those of their affiliated organizations, or those of the publisher, the editors and the reviewers. Any product that may be evaluated in this article, or claim that may be made by its manufacturer, is not guaranteed or endorsed by the publisher.

Supplementary material

The Supplementary Material for this article can be found online at: <https://www.frontiersin.org/articles/10.3389/fimmu.2022.1101937/full#supplementary-material>

References

1. Venet F, Lukaszewicz AC, Payen D, Hotchkiss R, Monneret G. Monitoring the immune response in sepsis: A rational approach to administration of immunoadjuvant therapies. *Curr Opin Immunol* (2013) 25:477–83. doi: 10.1016/j.coi.2013.05.006
2. Wan S, LeClerc JL, Vincent JL. Inflammatory response to cardiopulmonary bypass: Mechanisms involved and possible therapeutic strategies. *Chest* (1997) 112:117–32. doi: 10.1378/CHEST.112.3.676
3. Urrechaga E, Bóveda O, Aguirre U. Role of leucocytes cell population data in the early detection of sepsis. *J Clin Pathol* (2018) 71:259–66. doi: 10.1136/JCLINPATH-2017-204524
4. Stiel L, Delabranche X, Galois AC, Severac F, Toti F, Mauvieux L, et al. Neutrophil fluorescence: A new indicator of cell activation during septic shock-induced disseminated intravascular coagulation. *Crit Care Med* (2016) 44:e1132–6. doi: 10.1097/CCM.0000000000001851
5. von Elm E, Altman DG, Egger M, Pocock SJ, Gøtzsche PC, Vandenbroucke JP, et al. The strengthening of reporting of observational studies in epidemiology (STROBE) statement: Guidelines for reporting observational studies. *PloS Med* (2007) 4:e296. doi: 10.1371/journal.pmed.0040296
6. Kumar AB, Suneja M. Cardiopulmonary bypass-associated acute kidney injury. *Anesthesiology* (2011) 114:964–70. doi: 10.1097/ALN.0b013e318210f86a
7. Bruins P, Te Velthuis H, Yazdanbakhsh AP, Jansen PGM, Van Hardevelt FWJ, De Beaumont EMFH, et al. Activation of the complement system during and after cardiopulmonary bypass surgery: Postsurgery activation involves c-reactive protein and is associated with postoperative arrhythmia. *Circulation* (1997) 96:3542–8. doi: 10.1161/01.CIR.96.10.3542
8. Nguyen M, Tavernier A, Gautier T, Aho S, Morgant MC, Bouhemad B, et al. Glucagon-like peptide-1 is associated with poor clinical outcome, lipopolysaccharide translocation and inflammation in patients undergoing cardiac surgery with cardiopulmonary bypass. *Cytokine* (2020) 133:155182. doi: 10.1016/j.cyt.2020.155182
9. Khwaja A. KDIGO clinical practice guidelines for acute kidney injury. *Nephron* (2012) 120:c179–84. doi: 10.1159/000339789
10. Nashef SAM, Roques F, Sharples LD, Nilsson J, Smith C, Goldstone AR, et al. EuroSCORE II. *Eur J Cardio-Thoracic Surg* (2012) 41:734–45. doi: 10.1093/EJCTS/EZS043
11. Doyle DJ, Goyal A, Garmon EH. American Society of anesthesiologists classification, in: *StatPearls* (2022). Available at: <https://www.ncbi.nlm.nih.gov/books/NBK441940/> (Accessed December 6, 2022).
12. D'Agostino D, Cappabianca G, Rotunno C, Castellana F, Quagliara T, Carozzo A, et al. The preoperative inflammatory status affects the clinical outcome in cardiac surgery. *Antibiotics* (2019) 8:176. doi: 10.3390/ANTIBIOTICS8040176
13. Dacey LJ, DeSimone J, Braxton JH, Leavitt BJ, Lahey SJ, Klemperer JD, et al. Preoperative white blood cell count and mortality and morbidity after coronary artery bypass grafting. *Ann Thorac Surg* (2003) 76:760–4. doi: 10.1016/S0003-4975(03)00675-1
14. Aghdaii N, Ferasatkish R, Jouryabi AM, Hamidi SH. Significance of preoperative total lymphocyte count as a prognostic criterion in adult cardiac surgery. *Anesthesiol Pain Med* (2014) 4:20331. doi: 10.5812/AAPM.20331
15. Perry LA, Liu Z, Loth J, Penny-Dimri JC, Plummer M, Segal R, et al. Perioperative neutrophil-lymphocyte ratio predicts mortality after cardiac surgery: Systematic review and meta-analysis. *J Cardiothorac Vasc Anesth* (2022) 36:1296–303. doi: 10.1053/JJVCA.2021.07.001
16. Tan TP, Arekapudi A, Metha J, Prasad A, Venkatraghavan L. Neutrophil-lymphocyte ratio as predictor of mortality and morbidity in cardiovascular surgery: A systematic review. *ANZ J Surg* (2015) 85:414–9. doi: 10.1111/ANS.13036/SUPPINFO
17. Park SH, Park CJ, Lee BR, Kim MJ, Han MY, Cho YU, et al. Establishment of age- and gender-specific reference ranges for 36 routine and 57 cell population data items in a new automated blood cell analyzer, sysmex XN-2000. *Ann Lab Med* (2016) 36:244–9. doi: 10.3343/ALM.2016.36.3.244
18. Park SH, Park CJ, Lee BR, Nam KS, Kim MJ, Han MY, et al. Sepsis affects most routine and cell population data (CPD) obtained using the sysmex XN-2000 blood cell analyzer: neutrophil-related CPD NE-SFL and NE-WY provide useful information for detecting sepsis. *Int J Lab Hematol* (2015) 37:190–8. doi: 10.1111/IJLH.12261
19. Paparella D, Yau TM, Young E. Cardiopulmonary bypass induced inflammation: pathophysiology and treatment. *update. Eur J Cardio-Thoracic Surg* (2002) 21:232–44. doi: 10.1016/S1010-7940(01)01099-5
20. Asimakopoulos G. Systemic inflammation and cardiac surgery: An update. *Perfusion* (2001) 16:353–60. doi: 10.1177/026765910101600505
21. Day JRS, Taylor KM. The systemic inflammatory response syndrome and cardiopulmonary bypass. *Int J Surg* (2005) 3:129–40. doi: 10.1016/j.ijssu.2005.04.002
22. Chen GY, Nuñez G. Sterile inflammation: sensing and reacting to damage. *Nat Rev Immunol* (2010) 10:826–37. doi: 10.1038/nri2873
23. Mossanen JC, Jansen TU, Pracht J, Liepelt A, Buendgens L, Stoppe C, et al. Elevated circulating CD14++CD16+ intermediate monocytes are independently associated with extracardiac complications after cardiac surgery. *Sci Rep* 2020 101 (2020) 10:1–11. doi: 10.1038/s41598-020-57700-9



OPEN ACCESS

EDITED BY
Nadine Suffee,
Sorbonne Universités, France

REVIEWED BY
Guiyou Liang,
Guizhou Medical University, China
Niek J. Pluijmert,
Heart Center, Amsterdam UMC,
Netherlands
Amie Moyes,
Queen Mary University of London,
United Kingdom

*CORRESPONDENCE
Yingkun Guo
✉ gykpanda@163.com
Huayan Xu
✉ xuhuayan89@sina.com

[†]These authors have contributed
equally to this work and share
first authorship

SPECIALTY SECTION
This article was submitted to
Inflammation,
a section of the journal
Frontiers in Immunology

RECEIVED 27 October 2022
ACCEPTED 30 December 2022
PUBLISHED 06 February 2023

CITATION
Wu Q, Xu R, Zhang K, Sun R, Yang M, Li K,
Liu H, Xue Y, Xu H and Guo Y (2023)
Characterization of early
myocardial inflammation in
ischemia-reperfusion injury.
Front. Immunol. 13:1081719.
doi: 10.3389/fimmu.2022.1081719

COPYRIGHT
© 2023 Wu, Xu, Zhang, Sun, Yang, Li, Liu,
Xue, Xu and Guo. This is an open-access
article distributed under the terms of the
Creative Commons Attribution License
(CC BY). The use, distribution or
reproduction in other forums is permitted,
provided the original author(s) and the
copyright owner(s) are credited and that
the original publication in this journal is
cited, in accordance with accepted
academic practice. No use, distribution or
reproduction is permitted which does not
comply with these terms.

Characterization of early myocardial inflammation in ischemia-reperfusion injury

Qihong Wu^{1†}, Rong Xu^{2†}, Kun Zhang¹, Ran Sun¹, Mengxi Yang³,
Kuan Li¹, Hanrui Liu¹, Yiyuan Xue⁴, Huayan Xu^{2*}
and Yingkun Guo^{1,2*}

¹Department of Radiology, Development and Related Diseases of Women and Children Key Laboratory of Sichuan Province, West China Second University Hospital, Sichuan University, Chengdu, Sichuan, China, ²Department of Radiology, West China Second University Hospital, Sichuan University, Chengdu, Sichuan, China, ³Department of Radiology, Sichuan Cancer Hospital, Chengdu, Sichuan, China, ⁴Department of Prosthodontics, West China Hospital of Stomatology, Sichuan University, Chengdu, China

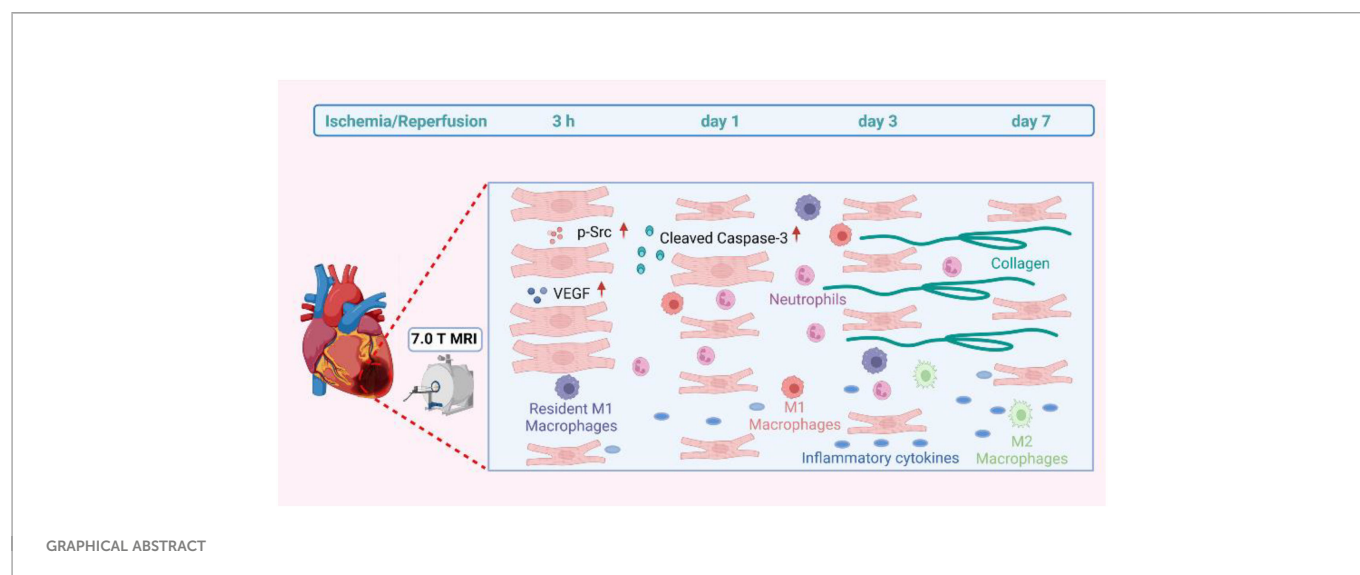
Background: Myocardial injury may be caused by myocardial ischemia-reperfusion (IR), and salvaging such an injury is still a great challenge in clinical practice. This study comprehensively characterized the physiopathologic changes of myocardial injury after IR to explore the underlying mechanism in the early reperfusion phase with particular emphasis on early myocardial inflammation.

Methods and Results: The experimental IR model was obtained by the left anterior descending artery's transient ligation of C57BL/6 mice. T2W signals of all mice showed increased signal at different IR stages. It was positively correlated with inflammatory cytokines and cells. T2W imaging by 7.0 T MRI surprisingly detected signal enhancement, but histopathology and flow cytometry did not reveal any inflammatory cells infiltration within 3 h after IR. Cardiomyocyte swelling and increased vascular permeability were observed by WGA staining and ultrastructural analysis, respectively. The 3 h IR group showed that the cardiomyocytes were severely affected with disintegrating myofilaments and mitochondria. Both VEGF and phosphorylated Src protein were markedly expressed in the 3 h IR group in comparison with the sham group, and TUNEL staining displayed little positive cells. Cleaved caspase-3 apoptin also has similar expression levels with that of the sham group. Resident macrophages had notably become M1 phenotype. The T2W signal was still elevated, and we observed that collagen deposition occurred from 1 to 7 days.

Conclusions: The inflammation response during the first week after reperfusion injury gradually increase 3 h later, but the main manifestation before that was edema. This study indicated that the first 3 h may be crucial to the early rescue process for reperfusion-induced myocardial injury due to inflammatory cell infiltration absence and apoptosis.

KEYWORDS

myocardial ischemia reperfusion injury, MRI, inflammation, edema, apoptosis



1 Introduction

Acute myocardial infarction (AMI) and the associated heart failure are the leading causes of death and disability worldwide (1, 2). Timely myocardial reperfusion using primary percutaneous coronary intervention (PCI) is the most effective treatment. However, the myocardial reperfusion process itself can induce cardiomyocyte death and myocardial injury, resulting in up to 50% final volume myocardial infarction (3). The ischemia-reperfusion (IR) injury rescue after reperfusion is still a great challenge in clinical practice, although the preferred reperfusion strategy time is within 2 h of ST-segment elevation MI diagnosis (4, 5).

The main mechanisms of myocardium IR injury involve inflammation, oxidative stress, mitochondrial damage, apoptosis, and autophagy (6, 7). Inflammation is significantly increased during reperfusion (8), which is activated at the stage of myocardial ischemia and plays a critical role in determining the AMI size and subsequent post-MI adverse left ventricular (LV) remodeling (9–12). The inflammatory process response includes inflammatory cell infiltration, and cytokine synthesis and secretion during myocardium IR (13). Previous findings have documented early neutrophils infiltration into the ischemia zone from 6 to 24 h post-AMI, followed by the accumulation of pro-inflammatory macrophages over the next 48–72 h, both of which contribute to cardiomyocyte death and myocardial IR injury (14). However, whether the inflammatory response was initiated in the very early reperfusion stage and its underlying mechanism still needs to be further investigated.

To recognize the myocardial pathophysiological changes *in vivo*, cardiac magnetic resonance imaging (MRI) has been identified as a promising imaging modality (15). And T2-weighted (T2W) imaging has particularly outstanding ability to determine edema with specific high signal (16) and has potential specificity for myocardial inflammation (17). Therefore, the present study focused on the myocardial inflammatory response and post reperfusion related tissue cellular changes in IR mouse model by 7.0 T MRI imaging and pathological analysis, spanning from the very early to late reperfusion stages, to provide new insight for myocardium rescue.

2 Methods

2.1 Mouse cardiac IR model induction

The experimental design is shown in Figure 1A. All animal procedure were approved by the Animal Experimentation Ethics Committee of West China Second Hospital of Sichuan University and conformed to the NIH Guide for the Care and Use of Laboratory Animals. C57BL/6 wild-type male mice of 8–10 weeks were used in this study. All mice were kept in the same room in a light-controlled environment with a 12:12 h light-dark cycle and with free access to standard mouse chow and water. The myocardial IR model was established as described in a previous study (18). Briefly, mice were anesthetized by isoflurane inhalation (1.5%–2%). Under a stereomicroscope, left thoracotomy was performed between the third and fourth ribs, and then the left anterior descending coronary artery was identified and ligated with a 8-0 polypropylene suture. A slipknot was tied over the vessel to create the occlusion. Ischemia was deemed successful when the myocardium supplied by the vessel turned pale. Mice of sham group were identically except that the ligature was not tied. After 30 minutes of ischemia, the slipknot was released by gently pulling the slipknot sutures in opposite directions. At this time, reperfusion began and lasted for 7 days. All mice were euthanized by inhaling 3%–5% isoflurane.

2.2 MR imaging study

Magnetic resonance images were acquired using a NOVA 7.0 T preclinical horizontal MRI system (Time Medical Ltd). Mice were imaged on 3 h, day 1, day 3, day 7 after reperfusion. Baseline MRI scan was performed immediately before myocardial IR induction. All MRI images were acquired with ECG and respiration double-gating. Gated multi-slice IntraGate Fast Low Angle Shot-cine was performed to confirm the heart position in three planes (short-axis, and 2- and 4-chamber long axis) to determine the location of LV. The echo signals of mice were measured with a T2W imaging sequence: TR = 800 ms,

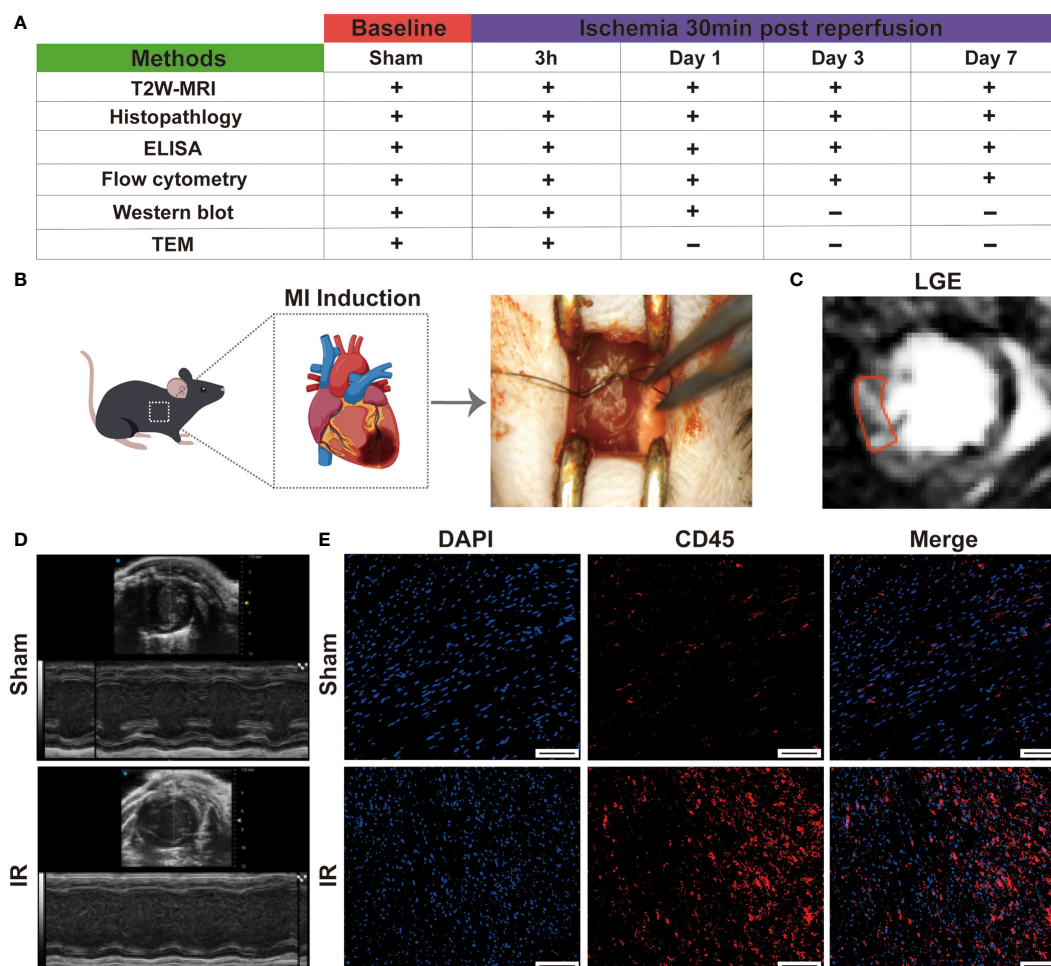


FIGURE 1

Establishment of mouse IR model. (A), schema of *in vivo* protocol. The present study population comprised 60 mice which were used for the characterization of myocardial inflammation during the first week after IR. (B), graphic image of myocardial IR injury induction. (C), typical LGE image on day 7 in IR group. (D), representative echocardiography on day 1 in sham and experimental group. (E), immunofluorescence staining detect the infiltration of leukocytes (Bar=150 μ m).

TE = 10.16 ms, slice thickness = 1.0 mm, matrix = 192 x 192, field of view = 40 x 40 mm, number of signal averages = 2. Successful IR induction was confirmed by late gadolinium enhancement (LGE) sequence (TR_{ir} = ~1 s depending upon respiratory rate, TE = 2.21 ms, slice thickness = 1.0 mm, matrix = 128 x 128, field of view = 40 x 40 mm, flip angle = 90°) starting 15 min after intraperitoneal injection of 0.5 mmol/Kg Gd-DPTA. T2W signal and LGE area were evaluated using cvi42 software (Circle Cardiovascular Imaging) or ImageJ software.

2.3 Echocardiography

To assess LV physiology, echocardiography was performed using a Vevo 3100 system (VisualSonics, Toronto, ON, Canada) with a 30 MHz image transducer. Images were acquired prior to IR surgery (baseline) and at day 1 post-reperfusion. Mice were anesthetized with 1.5% isoflurane in an oxygen mix. Heart rate, body temperature, and electrocardiogram were monitored throughout the imaging procedure. Measurements were taken from the LV parasternal long axis (B-mode) and short axis (M-mode) views. For analysis, three images from consecutive cardiac cycles were

included. Percent fractional shortening (FS) and ejection fraction (EF) were calculated as described previously (19).

2.4 Histological analysis

At indicated time points, hearts were fixed through trans-cardiac perfusion with saline followed by 4% paraformaldehyde (PFA), subsequently, the heart samples were immersed into 4% PFA and fixed over 24 h. Latter, the heart samples were embedded into paraffin blocks and cut into 5 μ m thickness sections. Hematoxylin Eosin (H&E) staining, Masson trichrome staining (Solarbio[®]) and WGA staining (VectorLabs) were performed following a standard protocol. The cell apoptosis was detected by using TUNEL System (Roche) according to the operating manual, after which the sections were incubated with DAPI for nucleus staining. For immunohistochemistry staining, the sections were rehydrated and heat-mediated antigen retrieval was performed using Target Retrieval Solution (S1699, Dako). The sections were incubated with 3% H₂O₂ (Sigma) to block endogenous peroxidase activity, followed by blocking with normal serum. A primary antibody specific for macrophages (CD68, Abcam; 1:400) was used at 4°C

overnight, followed by incubation with rabbit anti-rat IgG and ABC reagent (VectorLabs). For immunofluorescence staining, the sections were blocked with goat serum at room temperature for 1 h. The primary antibodies (CD45, Servicebio; F4/80, Abcam; Ki67, Abcam) diluted in goat serum were then dropped to cover sections and incubated overnight at 4°C. Then the sections were washed three times with PBS, followed by incubating with a second primary antibody (Alexa Fluor 594, Abcam; Alexa Fluor 488, Life). DAPI was used for nucleus staining. Images were acquired on the Olympus IX73 imaging microscope. All histological analysis were quantified using ImageJ software.

2.5 Ultrastructural analysis by transmission electron microscopy

Cardiac tissue was prepared from sham group and 3 h group following reperfusion, and the infarct regions were sectioned. Tissue was fixed in 0.1 M sodium cacodylate buffer (pH 7.3) containing 4% paraformaldehyde and 1.5% glutaraldehyde for 2 hours, transferred to 5% glutaraldehyde overnight, then to 1% osmium tetroxide for 1 hour. Blocks were washed, dehydrated in a graded ethanol series, and embedded in Epon/Araldite resin. Ultrathin sections were stained with uranyl acetate and lead citrate and were viewed using a Hitachi HT7700 transmission electron microscope.

2.6 Cell preparation for flow cytometry

Samples were obtained from Left ventricular at indicated time points. Single cell suspensions were prepared as described previously, with some modifications (20). Briefly, hearts were cut into small pieces and digested with 0.3 mg/ml collagenase II (Invitrogen, USA), 0.3 mg/ml dispase II (Sigma, USA), DNase I (Biosharp, China) and 2.5 mM CaCl₂ (Mackin, china) in HBSS solution (Invitrogen, USA) for 45 min at 37°C with gentle agitation. After the digestion, primary cardiac cells were obtained using Percoll (Solarbio[®]) gradient separation and passed through 70-μm cell strainer. The obtained cells were washed with RPMI-1640 cell culture medium for further analysis.

2.7 Flow cytometric analysis

To block the nonspecific binding of antibodies to Fcγ receptors, isolated single cell suspensions were incubated first with anti-CD16/32 antibody (101302, Biolegend) at 4°C for 10 min. Subsequently, the cells were incubated with a mixture of antibodies at 4°C for 25 min. Anti-CD11b-PE (Cat: 101208, Biolegend), anti-Gr1-FITC (Cat: 108406, Biolegend), anti-F4/80-BV421 (Cat: 123132, Biolegend) and anti-CD206-Alexa674 (Cat: 565250, BD Pharmingen) were used for flow cytometric analysis. The obtained results were expressed as the percent. Flow cytometric data was analyzed using official FlowJo software.

2.8 Western blotting analysis

Left ventricles were homogenized in ice-cold RIPA lysis buffer containing 1% PMSF. The protein concentration was determined using

Bradford BCA method (Beyotime, China). Total protein (30 μg) of each samples was separated by SDS-PAGE, transferred to 0.2 μm PVDF membrane (Millipore, USA) and probed with primary antibodies against VEGF (Cat: ET1604-28, HUABIO), p-Src (Cat: ET1609-15, HUABIO), Cleaved-caspase 3 (Cat: ab32042, Immunoway), CCL2 (Cat: HA500267, HUABIO) and GAPDH (Cat: ET1601-4, HUABIO). The ECL system was used for detection. GAPDH was used as an internal control and results expressed as the mean value.

2.9 ELISA assay

Blood samples were collected from the ophthalmic vein and kept 4 °C overnight before centrifugation for 15 min at 1000x g. Levels of IL-1β, TNF-α, TGF-β and Arg-1 in serum were measured with mouse ELISA kits (All from Animalunion, China) according to the manufacture's instruction respectively.

2.10 Statistical analysis

The mice were randomized to experimental groups. All statistical data analyses were conducted using GraphPad prism 9.3.1 software. All experiments were performed independently at least three times, and the results were presented as the mean ± SD. Two group means were compared by two-tailed independent samples student's *t*-tests, while means of more than two groups were compared by one-way ANOVA. Correlation analysis was performed using Pearson's or Spearman's method, as appropriate. For all comparisons, **p* < 0.05, ***p* < 0.01 and ****p* < 0.001.

3 Results

3.1 Establishment of IR model in mice

The study design is showed in **Figures 1A, B**. Firstly, to evaluate the success of the model, we measured the cardiac function by performing echocardiography on day 1 post- myocardial IR induction. Following IR, the experimental mice displayed cardiac dysfunction and left chamber dilation, while the sham group exhibited a normal physiology (**Figure 1D**). Moreover, left ventricular EF and FS were significantly reduced in the experimental mice, as compared to those of the sham group (**Figure S1**). After 7 days, late gadolinium enhancement (LGE) magnetic resonance imaging revealed an obviously high light signal intensity in the experimental mice (**Figure 1C**), indicating the presence of cardiomyocyte necrosis. The infiltration of leukocytes is also a sign of successful modelling. Subsequently, the CD45 immunofluorescence staining revealed that more inflammatory cell infiltration was observed in the IR group (**Figure 1E** and **Figure S2**). These results suggested that the IR mice models were successful and could be used for subsequent experiments.

3.2 MRI evaluation of myocardial inflammation during the first week after IR

Myocardial IR is characterized by inflammation, which contributes to myocardial injury. To noninvasively evaluate inflammation, cardiac

MRI was used. We utilized a small animal 7.0 T MRI to detect myocardial inflammation post-IR, specifically at baseline and at 3 h, 1 day, 3 days and 7 days post-IR. All MRI scans were acquired with an electrocardiogram and respiration double-gating method (Figures 2A, B). Baseline T2W image was relatively black in the LV anterior wall (Figure 2C). Initial reperfusion (3 h) was associated with a significant increase in T2W signal above that of the baseline, which subsequently increased progressively, reaching peak values on day 7 (Figure 2D). Figure 2C shows a representative example of one mouse serially scanned at all time-points.

3.3 Inflammatory response induced by myocardial IR injury

The inflammatory response after IR was subsequently evaluated via a histological analysis. H&E staining demonstrated an increase in leukocyte infiltration from day 1 to day 7 (Figure 3A). Monocyte/macrophage recruitment in the ischemic hearts was further investigated by immunostaining with CD68, and the number of

infiltrated macrophages was evaluated (Figure 3B and Figure S3). Interestingly, the inflammatory cells before 3 h were absent, indicating that, although IR injury causes an inflammatory response, activated leukocytes have not reached the ischemic area yet in the very early stage (3 h). It is possible that increased macrophages may come from recruitment of peripheral monocytes or from proliferation of residential macrophages. As shown in Figure S4A, F4/80 and Ki67 were co-located in several cells (Person's correlation coefficient: 0.14) at the site of myocardial ischemia after 1 day reperfusion, but this was absent in the sham group and post-reperfusion 3 h group. Additionally, we detected that CCL2 chemokine was highly expressed in post-reperfusion 1 day group (Figure S4B). At the same time, the ELISA results indicated that both anti-inflammatory cytokines IL-1 β and TNF- α and pro-inflammatory cytokines Arg-1 and TGF- β were improved after IR induction in the peripheral blood in mice (Figures 3C-F). Additionally, the expression level of myocardial IL-6 mRNA was significantly elevated in 3 h group (Figure S5). Collectively, these data indicated that the inflammatory response was induced and gradually increased after myocardial IR injury.

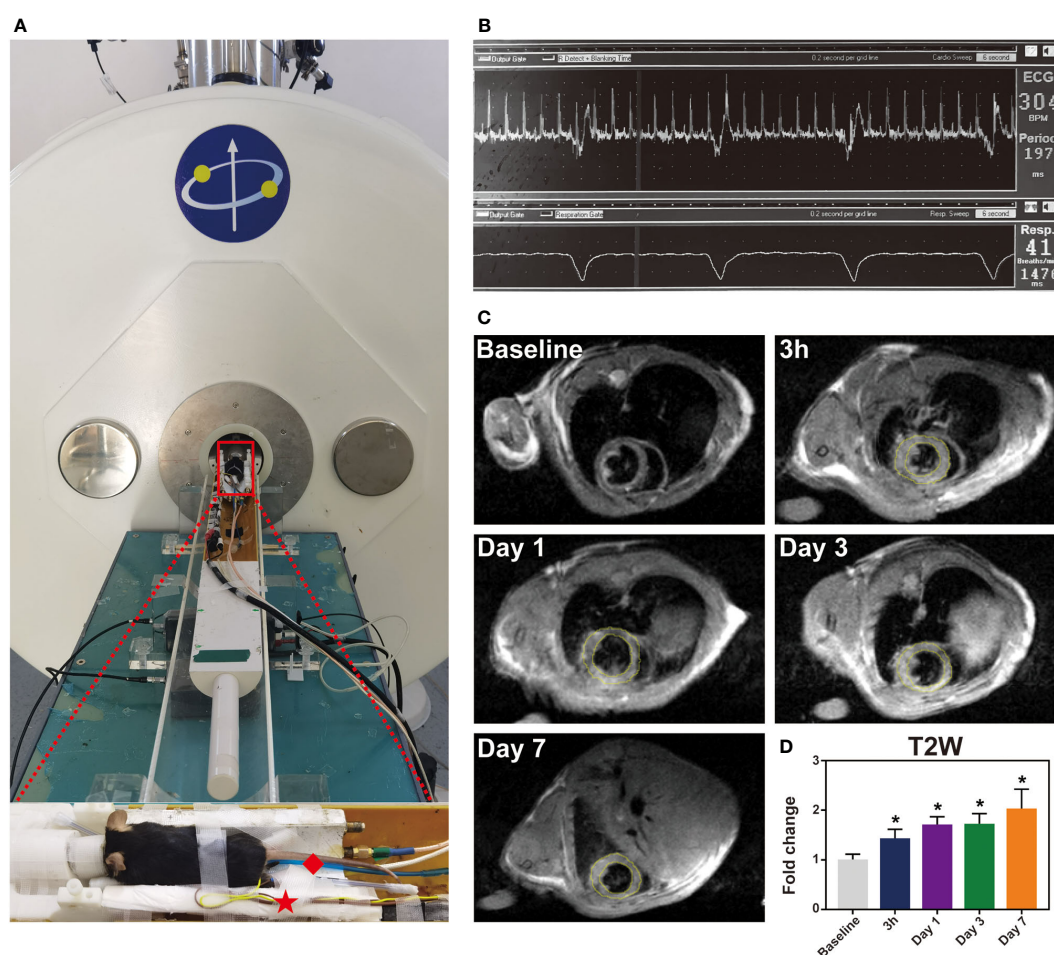


FIGURE 2

The immune response induced by IR injury at the first week. Representative images of histological changes in the ischemic myocardium. (A), for each time point, images are shown of staining with H&E (Bar=1mm, 50 μ m). (B), macrophages in mice post-IR were evaluated by CD68 staining (Bar=50 μ m). (C-F), plasma levels of IL-1 β (C), TNF- α (D), Arg-1 (E) and TGF- β (F) were also determined by ELISA (n = 3-5). *p < 0.05 VS. Sham.

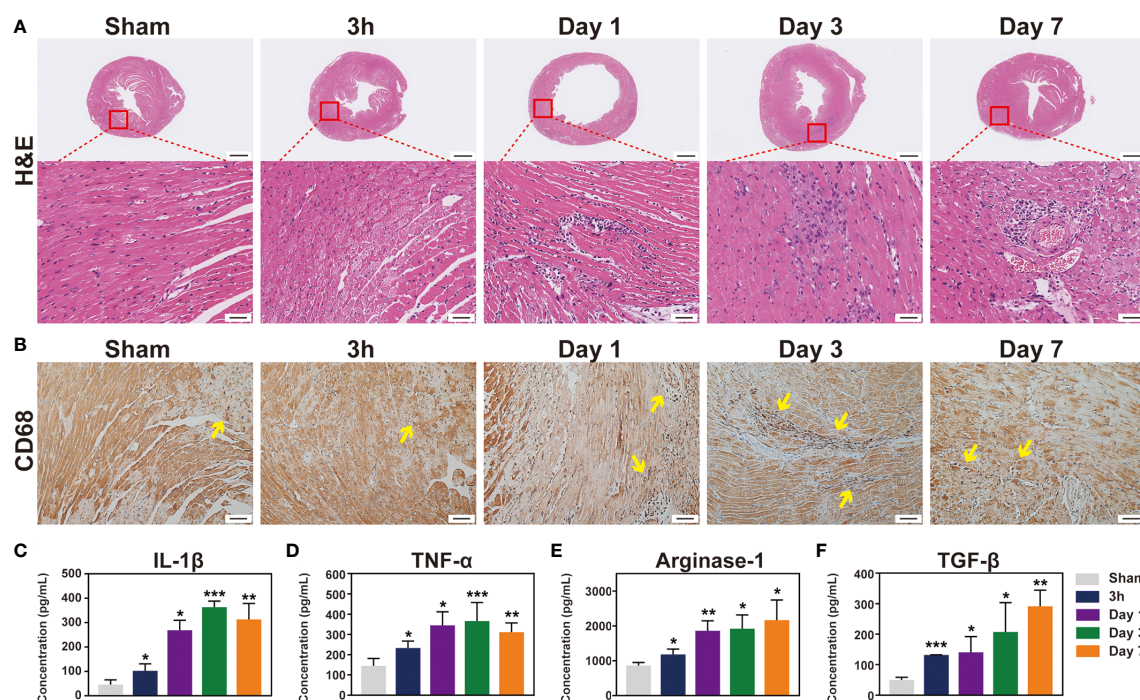


FIGURE 3

T2-weighted imaging sequence detect inflammation signal in the mouse heart during the first week post-IR. (A), one mouse equipped with ECG (☆) and respiratory (◇) are being prepared to scan under 7.0 T MRI. (B), real-time ECG and respiratory rate in a mouse. (C), the typical T2W images from the same mouse before and after IR. (D), quantitative the mean T2W signal intensity of the LV myocardium in each group, (n = 5). *p < 0.05 VS. Sham, ** p < 0.01, *** p < 0.001.

3.4 Temporal dynamic of the main cellular subsets of infiltration after IR

To detect major cellular components associated with inflammation, flow cytometry was conducted at 3 h and 1, 3, and 7 days following IR. Given the relatively low number of macrophages in the mouse heart, we used standard negative and positive magnetic beads (BD™ Comp Beads) to calibrate fluorescence compensation (Figure S6). The CD11b⁺ and F4/80⁺ double positive cells were defined as macrophages; pro-inflammatory M1 macrophages were labelled with CD206⁻ (CD11b⁺F4/80⁺Gr1⁺CD206⁻), whereas CD206⁺ was used to identify M2 macrophages (CD11b⁺F4/80⁺Gr1⁺CD206⁺) (Figure 4A). Neutrophils were defined as CD11b⁺Gr1⁺. After the IR injury, neutrophils accumulated in the ischemic heart, peaking at day 1 and then notably, continuing to accumulate in the myocardium over 3 days (Figure 4E). Moreover, macrophages began to infiltrate on day 1 and peaked on day 3 in the ischemic myocardium (Figure 4B), and these cells showed a biphasic pattern of activation. M1 macrophages increased gradually and dominated at 3 days post-IR, whereas the M2 macrophages represented the predominant cell subset after 3 days post-IR (Figures 4C, D). Consistent with the histopathological findings, flow cytometry also did not detect infiltrating inflammatory cells at 3 h after the IR injury. From these results, we found that neutrophils and macrophages were the major cellular components during the first week of IR injury, although inflammatory cell infiltration did not occur in the first 3 h post-IR.

3.5 Correlation of T2W signal with inflammatory components

To further prove whether T2W imaging can detect inflammation after myocardial IR in mice, a correlation analysis between T2W signal and inflammatory components was performed. Inflammatory cytokine activity in the serum of IR mice was significantly correlated with the T2W signal from 3 h to 7 days post-reperfusion (Figures 5A-D). In addition, both macrophage and neutrophil contents were also obviously correlated with the T2W signal. Interestingly, regarding macrophage phenotype, the pro-inflammatory M1 macrophages showed a moderate correlation with T2W signal rather than anti-inflammatory M2 macrophages (Figure 5E). These results indicate that T2W imaging could help detect myocardium inflammation in the IR mice models.

3.6 Myocardial edema occurs in the first 3 h after myocardial IR

Considering the signal enhancement detected by T2W imaging, histopathology and flow cytometry did not reveal any infiltration of inflammatory cells during the first 3 h after reperfusion. Therefore, we turned our attention to myocardial edema. Firstly, the cross-sectional area of cardiomyocytes at the ischemia zone was determined by WGA staining, and the 3 h IR group showed a marked cardiomyocyte

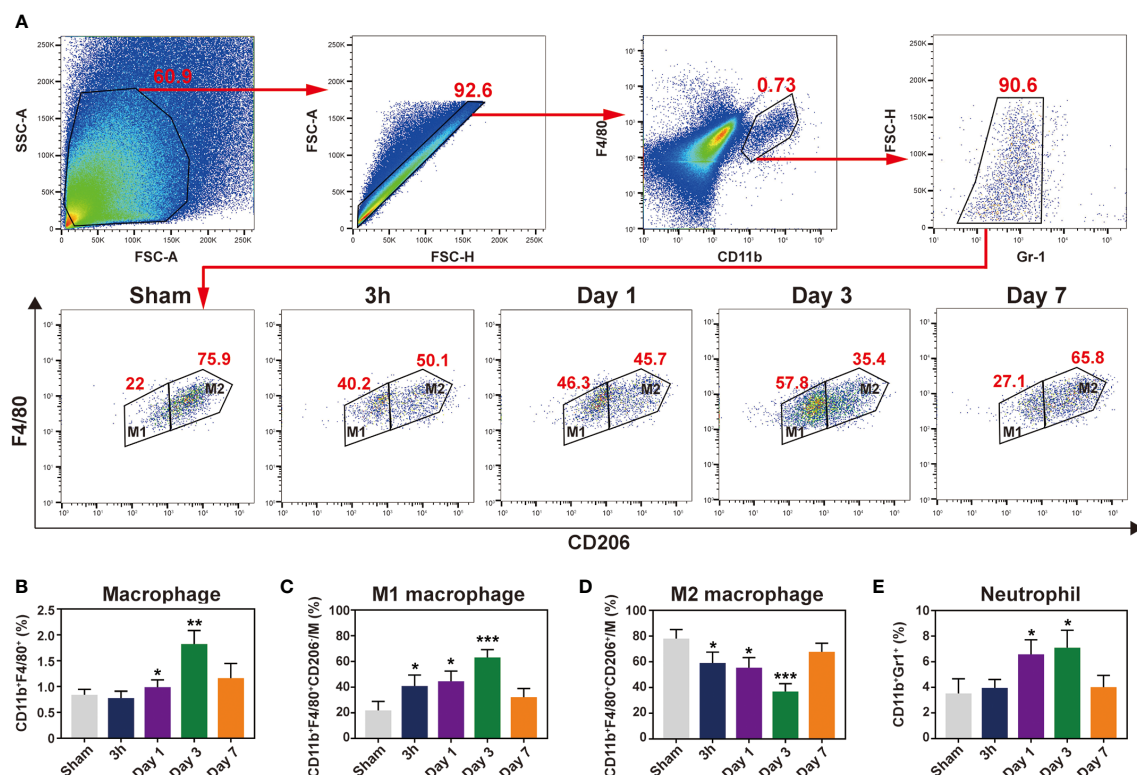


FIGURE 4

Characterization of temporal dynamic of the macrophages and neutrophil in the heart after IR. (A), gating strategy for cardiac macrophages, M1 (CD11b⁺F4/80⁺Gr1⁺CD206⁺) and M2 (CD11b⁺F4/80⁺Gr1⁺CD206⁺) macrophages at indicated time point after myocardial IR injury. Represent flow cytometric images of M1 and M2 macrophages in the post-IR heart. (B–E), the percentages of macrophages (B), M1 (C), M2 (D) and neutrophils (E) were determined in the hearts of sham group and reperfusion groups (n = 5–6, each). *p < 0.05 VS. Sham, **p < 0.01, ***p < 0.001.

expansion compared with the sham group (Figures 6A, F). And the myocardial water content in 3 h group was higher than sham group (Figure S7). Subsequently, we evaluated the cardiac tissues at the ultrastructural level at 3 h after reperfusion. In the sham group, the section transverse to cardiomyocytes showed normal myofilament

architecture and mitochondria (Figure 6B-1). In contrast to the normal myocardial tissue, the cardiomyocytes in the 3 h IR group were severely affected with disintegrating myofilaments and mitochondria (Figure 6B-2). At the same time, the blood vessels appear to be damaged and contained many large vacuoles

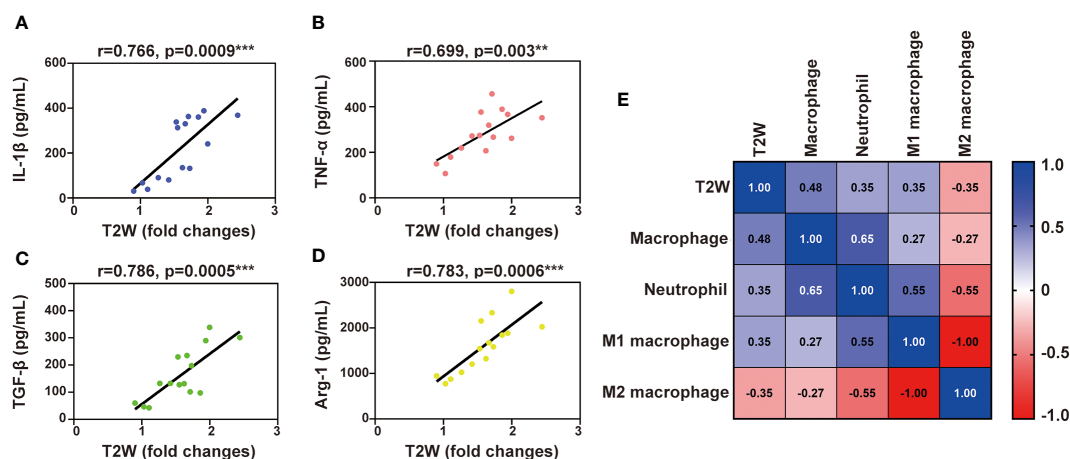


FIGURE 5

Liner correlation between myocardial T2W signal and inflammation mediator. (A–D), scatter plot of myocardial T2W signal and IL-1 β (A), TNF- α (B), TGF- β (C) and Arg-1 (D). (E), heat map of neutrophils, M1 macrophages, M2 macrophages and macrophages among myocardial T2W signal, **p < 0.01, ***p < 0.001.

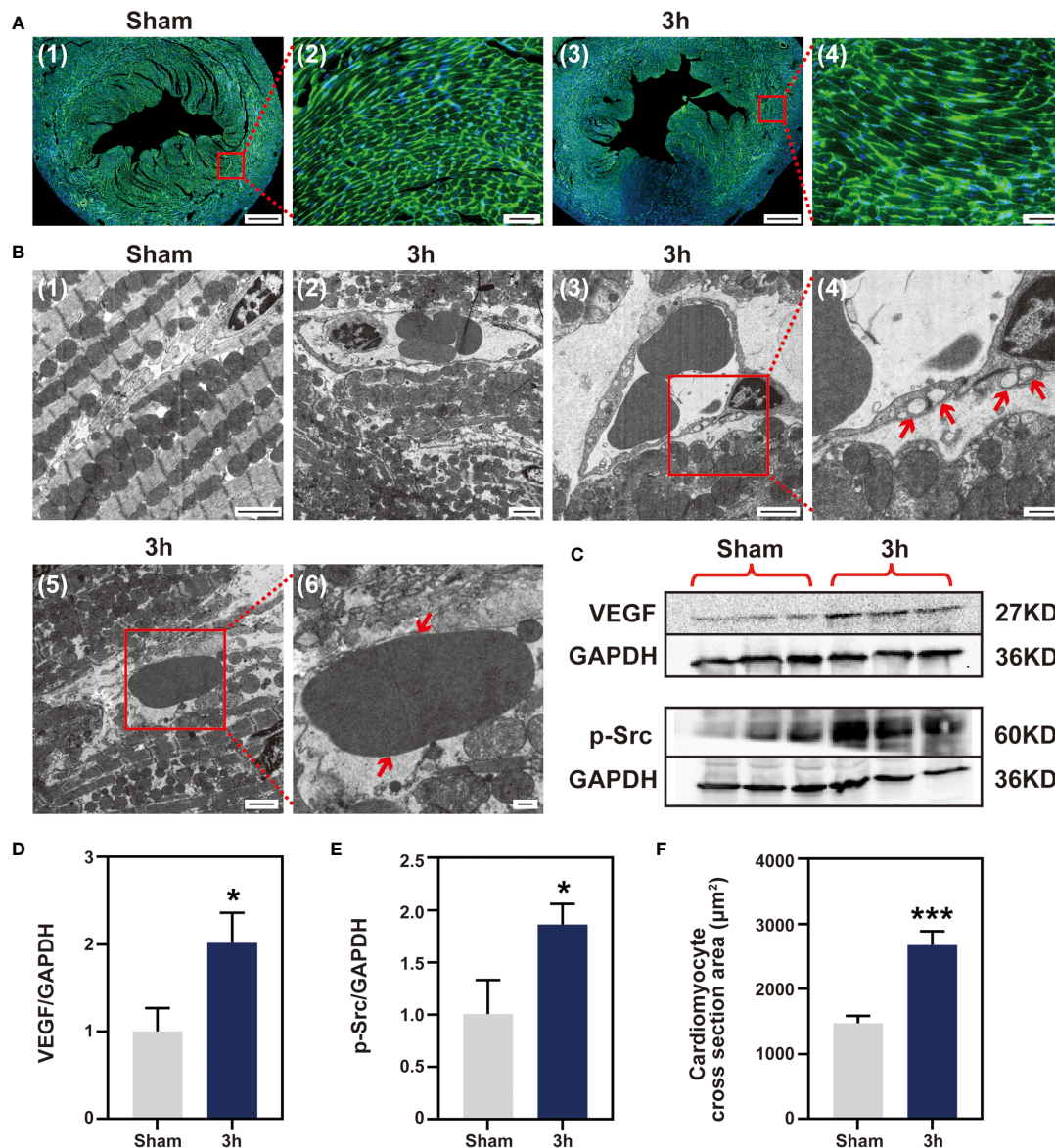


FIGURE 6 Myocardial IR induced edema at 3 h post-IR. (A), WGA staining cardiomyocyte hypertrophy, (n = 3) (Bar=400 μm, 50μm). (B) (1–6), ultrastructural changes in mouse myocardium. (1), sham group ventricular myocardium showing normal myofilament architecture and mitochondria (Bar=2μm). (2), anomalous myofilaments and mitochondria are displayed after IR 3 h (Bar=2μm). (3–4), Vessel with no apparent gaps, but several large vacuoles apparent (Bar=2μm, 500nm). (5–6), section transverse to myocardium showing an RBC in the extracellular space (Bar=2μm, 500nm). (C), western blotting detect VEGF and p-Src protein expression, (n = 3). Quantitative of VEGF protein (D), p-Src protein (E) and cardiomyocytes area (F). RBC, red blood cell; VEGF, vascular endothelial growth factor; p-Src, phosphor-Src, *p < 0.05 VS Sham, ***p < 0.001.

(Figure 6B-3). Moreover, extravasated red blood cells were present in the interstitium (Figure 6B-5), which apparently escaped from the nearby vessels. The vascular endothelial growth factor (VEGF), first described as the “vascular permeability factor”, likely contributes to the development of myocardial edema (21), and VEGF-mediated Src signaling had been proved to be involved in disease progression following MI (22). To further explore the possible mechanism of IR-induced edema, we evaluated the expression of VEGF-mediated Src signaling pathway. As shown in Figures 6C-E, in comparison with the sham group, both VEGF and phosphorylated Src proteins were markedly expressed in the 3 h IR group. These data showed that edema obviously appear at 3 h post-IR, and was probably mediated by the VEGF-Src signaling pathway.

3.7 No cell apoptosis occurs at 3 h post-IR

Myocardial cell apoptosis has been reported to contribute significantly to IR-induced myocardial injury, which motivated us to determine whether apoptosis occurs at the very early stage of injury. Firstly, detection of apoptosis by TUNEL staining was performed in ischemic tissue sections. Little TUNEL positive cells were found in the 3 h IR group. On the contrary, the number of TUNEL positive cells in the day 1 IR group was significantly increased when compared with that of the sham group (Figure 7B and Figure S8). Subsequently, the extracts of cleaved-caspase 3 apoptin isolated from the ischemic zone in the three groups were examined *via* Western blotting analysis. As shown in Figures 7C, D,

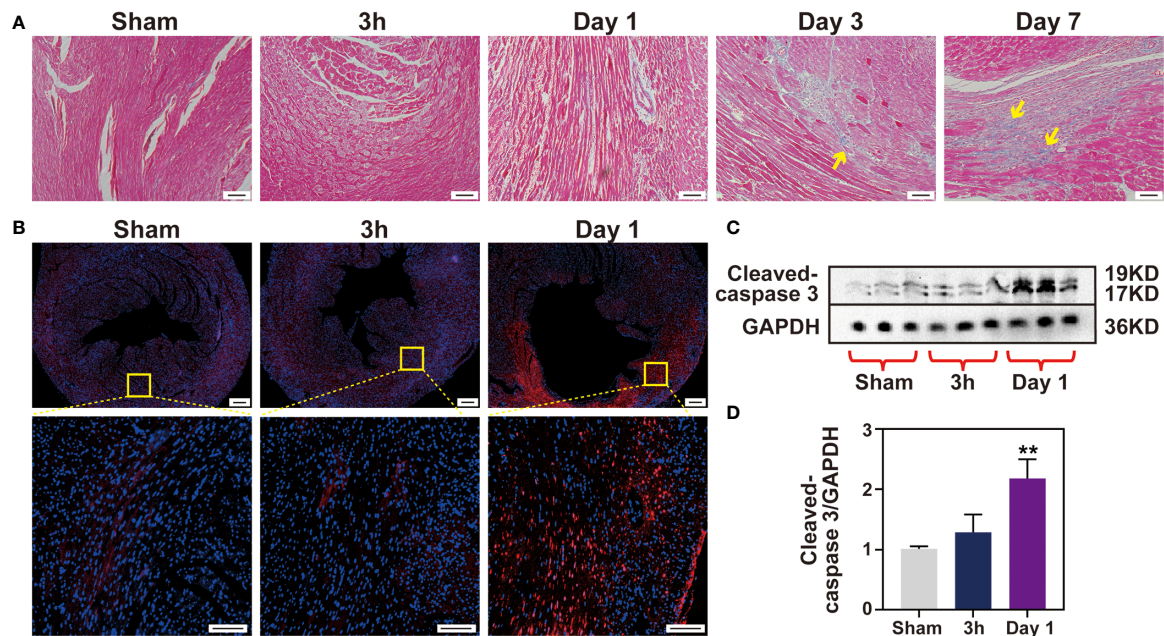


FIGURE 7

No cell apoptosis happens after 3 h IR. (A), Masson staining of heart sections was performed for each time point (Bar 100 μ m). (B), cell apoptosis was measured by TUNEL assay (Bar =200 μ m, 50 μ m) and Western blotting (C) in sham group and 3 h, 1 day after IR induction. Quantitative of cleaved-caspase 3 protein expression level (D), (n = 3). **p < 0.01 VS. Sham.

the cleaved-caspase 3 protein in the 3 h IR group has similar expression levels with that of the sham group, although an obviously higher expression level was observed in the day 1 IR group. Likewise, caspase 3 mRNA expression in the 3 h group displayed no obvious difference with sham group (Figure S9). In addition, we found that collagen was gradually deposited in the ischemia myocardium post-IR (Figure 7A and Figure S10). The trend is similar to the performance of inflammatory cytokines, implying that IR-induced inflammatory response may be involved in the tissue healing processes.

4 Discussion

Characterization of the time course of the myocardium IR-induced inflammation and its determinants is critically important for the development of diagnostic and therapeutic applications. In the present longitudinal experiment study, we explored the inflammatory response of myocardial post-IR and the possible underlying mechanisms by performing a comprehensive histopathological cellular and advanced MRI serial analysis using a widely used small animal model.

MRI allows *in vivo* myocardial characterization and cardiac MRI has been identified as a promising imaging modality (15). T2W imaging techniques have been widely used to detect edema and are potentially specific for myocardial inflammation (17). Recently, our team has demonstrated that cardiac MRI could help detect inflammation in the remote myocardium in MI porcine models (23). In this study, we first utilized a 7.0 T magnetic resonance T2W imaging sequence to detect post- myocardial IR inflammation in a widely used small animal model. As expected, the T2W signals

were positively correlated with inflammatory cytokines and cells. We found that the T2W signals were abnormal at 3 h of perfusion and then increased gradually, suggesting that myocardial edema or inflammation had started very early.

Macrophages and neutrophils secrete pro-inflammatory cytokines in the early stage of MI, which leads to sustained inflammation and myocardial injury (24). The neutrophils peak shifted from day 3 to day 1, while the macrophages infiltration peak switched from day 7 to day 3 in mice IR model, compared with permanent ligation MI (25). Reperfusion temporally shifted the innate immune cell to an earlier time point, indicating that timely reperfusion may benefit from ischemic myocardial recovery by preventing the transition from acute to persistent inflammation. Macrophages are composed of two populations, including pro-inflammatory M1 and reparative M2 macrophages. The M1 macrophages predominate at the early stage after myocardial IR, followed by a gradual increase of the M2 subset (26). Macrophages undergo a rapid shift to an M1 subset and elicit inflammatory cytokine secretion, lowering the CD206 expression. At 7 days after reperfusion, the M2 subset became the predominant macrophage. The pro-inflammatory M1 macrophages showed moderate correlation with the T2W signals rather than the anti-inflammatory M2 macrophages combined with our MR imaging results, suggesting that T2W imaging may tend to reflect pro-inflammatory cell infiltration.

Interestingly, there was no infiltration of inflammatory cells, including neutrophils and macrophages, at 3 h post-reperfusion. A previous study reported that the neutrophils in the myocardium subjected to 45 minutes of ischemia followed by 4 h of reperfusion significantly increased in comparison with the normal myocardium from the same hearts (27). Thus, we speculate that 3 h may be the critical time point for inflammatory cells to reach ischemic

myocardium. It is reported that IL-6 expression is obvious after reperfusion 3 h (28). Indeed, we also detected IL6 changed obviously after 3 h reperfusion in the heart (Figure S5). This is consistent with our ELISA and T2W results that detected inflammation at 3 h reperfusion. After carefully examining our flow cytometry data, we found that the resident macrophages had already become M1 phenotype at 3 h post-reperfusion (Figure S11), despite the absence of infiltration of inflammatory cells, which not only contribute to the source of inflammatory cytokines (such as IL-1 β and IL-6) but partly explain the enhancement of T2W signal. The changes in the phenotype of resident macrophages preceded the infiltration of inflammatory cells, suggesting that they may play a vital role in the initiation of myocardial reperfusion-induced injury. Owing to the abundance and phenotypic plasticity of macrophages, they are well fit for mediating the repair response after IR. Most of the previous studies have made great progress in the treatment of IR-induced injury by regulating the recruited macrophage polarization (29). According to our data, we believed that more attention should be paid to resident macrophages.

As with most organs, water is the primary component of cardiac tissues. In homeostasis, myocardial water is stable and nearly intracellular, with only a little interstitial component. In the context of MI, edema appears initially in the form of cardiomyocyte swelling during the early stages of ischemia (30). Myocardial edema is then obviously exacerbated upon reperfusion of blood flow to the ischemic region. This increase is due to the enhancement of interstitial edema, due to water permeability and protein leakage (31). Given that there was no infiltration of inflammatory cells, but rather a clear signal was detected on T2W imaging at 3 h post-reperfusion. We therefore shift our focus on myocardial edema. As expected, myocardial water content in the 3 h group was higher than sham group (Figure S7). Our results indicated that early edema was partly due to cardiomyocyte swelling and increased vascular permeability, while the intracellular and extracellular edema were undetermined. A method based on MRI has been developed to differentiate intracellular and extracellular myocardial water compartments, but the intracellular water distribution does not accurately reflect intracellular edema (32). Further studies are needed to discriminate between intracellular and extracellular edema. Notably, a comprehensive work has observed that the myocardial edema after IR is not stable and follows a bimodal pattern in the pig model (33). However, we did not see a drop in T2W signal during the reperfusion in a small animal model. The absence of bimodal in the mouse heart and the apparent presence of bimodal in the pig heart after IR may be associated with species differences.

After MI, an increase in VEGF levels occurs and contributes to detrimental myocardial edema (34). Genetics interferes with the ability of VEGF to mediate the increased vascular permeability, which is correlated with reduced LV edema in mice and improved survival after MI (35). Src is implicated as the tyrosine kinase responsible for phosphorylation of vascular endothelial-cadherin and the elevated vascular permeability (36). Constitutive Src gene inactivation is accompanied by reduced edema and improved long-term outcome after MI (22). We thus concluded that the VEGF/Src-mediated pathway may be a key signal molecule in the very early reperfusion stages; however, additional works are needed, in particular, to assess whether a combined treatment of myocardium

edema and inflammation can accelerate the recovery of heart function.

It has been investigated that myocardial edema induced by reperfusion may contribute to cell death. Cell apoptosis is obviously initiated at 6 h reperfusion, which progressively progressed into myocardial apoptotic cell death during the late phase of reperfusion in a canine model (37). Gottlieb et al. (27), however found that apoptosis was detected in the ischemia myocardium after 30 min of ischemia and 4 h of reperfusion in a rabbit model. In the current mouse model, we observed that there was no obvious cell apoptosis in the ischemic myocardium at 3 h of reperfusion. Given that apoptosis represents a potentially preventable form of cell death, identifying its timing may help in developing potential treatment strategies for alleviating myocardial IR injury by regulating apoptosis. Both inflammatory cell infiltration and apoptosis are involved in the early myocardial IR injury, and they greatly affect cardiac repair and healing. The data presented here implicate that the first 3 h of reperfusion, when inflammatory cell infiltration and apoptosis have not been initiated yet, may be crucial to perform rescue procedures for the ischemia myocardium.

In clinical practice, timely PCI is an essential step to rescue the ischemic myocardium to restore reperfusion in patients with ischemic cardiomyopathy. However, a substantial number of patients could experience severe myocardial IR injury and these complications may be associated with an increased risk of major adverse cardiac events (MACE). Therefore, early identification and myocardial IR injury intervention after PCI is an important reason for improving the prognosis. Recent clinical guidelines suggest that cTn monitoring should be performed at least once 3–6 h after PCI to determine the myocardial injury extent and determine subsequent management strategies (38). However, it remains a challenge for new treatment or appropriate time window to reduce the risk of MACE. This study comprehensively characterized the myocardial injury process after IR in mice *in vitro* and *in vivo*. It is feasible to develop new strategies to reduce the myocardial IR injury by targeting myocardial edema, resident macrophages, apoptosis and inflammatory cell infiltration collectively in the first 3 h after reperfusion. However, further interventions and population cohort studies are needed to clarify the importance of myocardial rescue within 3 h of IR injury due to the differences in animal experiments and clinical scenarios.

We proved that the inflammatory response during the first week after reperfusion gradually increase at 3 hours later, and before that, the main manifestation was edema probably induced by the activation of VEGF/Src signaling pathway. Meanwhile, the infiltrating inflammatory cells and apoptosis are absent in the very early reperfusion stage. These data reveals that the first 3 h of reperfusion may be the vital for ischemia myocardial recovery, especially when developing anti-inflammatory strategies. We investigated the critical time point for changes in cardiac pathophysiology in IR myocardium, a finding with potentially important implications for managing patients with reperfusion after MI.

Data availability statement

The raw data supporting the conclusions of this article will be made available by the authors, without undue reservation.

Ethics statement

The animal study was reviewed and approved by Animal Experimentation Ethics Committee of West China Second Hospital of Sichuan University.

Author contributions

QW and RX: conceptualization, methodology, software. KZ, RS and MY: data curation, statistical. KL, HL and YX: visualization, experimental studies. HX and YG: manuscript preparation, reviewing and editing, validation. All authors contributed to the article and approved the submitted version.

Funding

This work was supported by National Natural Science Foundation of China (82120108015, 82102020, 82071874, 81971586) and Sichuan Science and Technology Program (2020YJ0029, 2017TD0005).

References

- He L, Nguyen NB, Ardehali R, Zhou B. Heart regeneration by endogenous stem cells and cardiomyocyte proliferation: Controversy, fallacy, and progress. *Circulation* (2020) 142:275–91. doi: 10.1161/CIRCULATIONAHA.119.045566
- Benjamin EJ, Virani SS, Callaway CW, Chamberlain AM, Chang AR, Cheng S, et al. Heart disease and stroke statistics-2018 update: a report from the American heart association. *Circulation* (2018) 137:e67–492. doi: 10.1161/CIR.0000000000000558
- Yellow DM, Hausenloy DJ. Myocardial reperfusion injury. *N Engl J Med* (2007) 357:1121–35. doi: 10.1056/NEJMra071667
- Gara PTO, Kushner FG, Ascheim DD, Jr DEC, Chung MK, de Lemos JA, et al. AHA guideline for the management of ST-elevation myocardial infarction: executive summary: A report of the American college of cardiology Foundation/American heart association task force on practice guidelines. *J Am Coll Cardiol* (2013) 61:484–510. doi: 10.1161/CIR.0b013e3182742c84
- Step PG, James SK, Atar D, Badano LP, Carina BL, Borger MA, et al. ESC Guidelines for the management of acute myocardial infarction in patients presenting with ST-segment elevation. *Eur Heart J* (2012) 33:2569–619. doi: 10.1093/eurheartj/ehs215
- Wei B, Lin Q, Ji YG, Zhao YC, Ding LN, Zhou WJ, et al. Luteolin ameliorates rat myocardial ischemia-reperfusion injury through activation of peroxiredoxin II. *Br J Pharmacol* (2018) 175:3315–32. doi: 10.1111/bph.14367
- Cheng G, Zhang J, Jia S, Feng PP, Chang FG, Yan L, et al. Cardioprotective effect of gossypin against myocardial ischemic/reperfusion in rats via alteration of oxidative stress, inflammation and gut microbiota. *J Inflammation Res* (2022) 15:1637–51. doi: 10.2147/JIR.S348883
- Haan JJ, Bosch L, Borgman A, Bastemeijer M, Brans MAD, van de Weg SM, et al. Complement 5a receptor deficiency does not influence adverse cardiac remodeling after pressure-overload in mice. *Sci Rep* (2017) 7:17045. doi: 10.1038/s41598-017-16957-3
- Buckley LF, Abbate A. Interleukin-1 blockade in cardiovascular diseases: A clinical update. *Eur Heart J* (2018) 39:2063–9. doi: 10.1093/eurheartj/ehy128
- Dai Y, Song J, Li W, Yang TL, Yue XJ, Lin X, et al. RhoE fine-tunes inflammatory response in myocardial infarction. *Circulation* (2019) 139:1185–98. doi: 10.1161/CIRCULATIONAHA.118.033700
- Martini E, Stirparo GG, Kourdis MK. Immunotherapy for cardiovascular disease. *J Leukoc Biol* (2018) 103:493–500. doi: 10.1002/JLB.5MR0717-306R
- Westman PC, Lipinski MJ, Luger D, Waksman R, Bonow RO, Wu E, et al. Inflammation as a driver of adverse left ventricular remodeling after acute myocardial infarction. *J Am Coll Cardiol* (2016) 67:2050–60. doi: 10.1016/j.jacc.2016.01.073
- Wu X, Shen A, Bao L, Wu MZ, Lin XY, Wang H, et al. Qingda granules attenuate hypertensive cardiac remodeling and inflammation in spontaneously hypertensive rats. *BioMed Pharmacother* (2020) 129:110367. doi: 10.1016/j.biopha.2020.110367
- Ioanna A, Hector CF, Yvan AD, Frangogiannis NG, Frantz S, Guzik T, et al. Immune cells as targets for cardioprotection: new players and novel therapeutic opportunities. *Cardiovasc Res* (2019) 115:1117–30. doi: 10.1093/cvr/cvz050

Conflict of interest

The authors declare that the research was conducted in the absence of any commercial or financial relationships that could be construed as a potential conflict of interest.

Publisher's note

All claims expressed in this article are solely those of the authors and do not necessarily represent those of their affiliated organizations, or those of the publisher, the editors and the reviewers. Any product that may be evaluated in this article, or claim that may be made by its manufacturer, is not guaranteed or endorsed by the publisher.

Supplementary material

The Supplementary Material for this article can be found online at: <https://www.frontiersin.org/articles/10.3389/fimmu.2022.1081719/full#supplementary-material>

- Ibanez B, Aletras AH, Arai AE, Arheden H, Bax Jeroen Berry C, et al. Cardiac MRI endpoints in myocardial infarction experimental and clinical trials: JACC scientific expert panel. *J Am Coll Cardiol* (2019) 74:238–56. doi: 10.1016/j.jacc.2019.05.024
- Tada Y, Yang PC. Myocardial edema on T2-weighted MRI: New marker of ischemia reperfusion injury and adverse myocardial remodeling. *Circ Res* (2017) 121:326–8. doi: 10.1161/CIRCRESAHA.117.311494
- Ferreira VM, Schulz-Menger J, Holmvang G, Kramer CM, Carbone I, Sechtem U, et al. Cardiovascular magnetic resonance in nonischemic myocardial inflammation: Expert recommendations. *J Am Coll Cardiol* (2018) 72:3158–76. doi: 10.1016/j.jacc.2018.09.072
- Zhao Y, Zheng Z, Pi Y, Liang X, Jin SQ. Cardioprotective effects of transfusion of late phase preconditioned plasma may be induced by activating the reperfusion injury salvage kinase pathway but not the survivor activating factor enhancement pathway in rats. *Oxid Med Cell Longev* (2017) 2017:8526561. doi: 10.1155/2017/8526561
- Wu C, Chen R, Wang Y, Wu WY, Li G. Acacetin alleviates myocardial ischemia/reperfusion injury by inhibiting oxidative stress and apoptosis via the nrf-2/HO-1 pathway. *Pharm Biol* (2022) 60:553–61. doi: 10.1080/13880209.2022.2041675
- Meng X, Zhang P, Zhang L. Fetal hypoxia impacts on proliferation and differentiation of sca-1⁺ cardiac progenitor cells and maturation of cardiomyocytes: A role of MicroRNA-210. *Genes (Basel)* (2020) 11:328. doi: 10.3390/genes11030328
- Senger DR, Perruzzi CA, Feder J, Dvorak HF. A highly conserved vascular permeability factor secreted by a variety of human and rodent tumor cell lines. *Cancer Res* (1986) 46:5629–32.
- Weis S, Shintani S, Weber A, Kirchmair R, Wood M, Cravens A, et al. Src blockade stabilizes a FAK/cadherin complex, reducing edema and tissue injury following myocardial infarction. *J Clin Invest* (2004) 113:885–94. doi: 10.1172/JCI20702
- Yang MX, Shi K, Xu HY, He Y, Ma M, Zhang L, et al. Inflammation in remote myocardium and left ventricular remodeling after acute myocardial infarction: A pilot study using T2 mapping. *J Magn Reson Imaging* (2022) 55:555–64. doi: 10.1002/jmri.27827
- Hayashidani S, Tsutsui H, Shiomi T, Ikeuchi M, Matsusaka H, Suematsu N, et al. Anti-monocyte chemoattractant protein-1 gene therapy attenuates left ventricular remodeling and failure after experimental myocardial infarction. *Circulation* (2003) 108:2134–40. doi: 10.1161/01.CIR.0000092890.29552.22
- Yan X, Anzai A, Katsumata Y, Matsuhashi T, Ito K, Endo J, et al. Temporal dynamics of cardiac immune cell accumulation following acute myocardial infarction. *J Mol Cell Cardiol* (2013) 62:24–35. doi: 10.1016/j.jmcc.2013.04.023
- Fan Q, Tao R, Zhang H, Xie HY, Lu L, Wang T, et al. Dectin-1 contributes to myocardial ischemia/reperfusion injury by regulating macrophage polarization and neutrophil infiltration. *Circulation* (2019) 139:663–78. doi: 10.1161/CIRCULATIONAHA.118.036044
- Gottlieb RA, Burleson KO, Kloner RA, Babior BM, Engler RL. Reperfusion injury induces apoptosis in rabbit cardiomyocytes. *J Clin Invest* (1994) 94:1621–8. doi: 10.1172/JCI117504

28. Chandrasekar B, Mitchell DH, Coilton JT, Freeman GL. Regulation of CCAAT/Enhancer binding protein, interleukin-6, interleukin-6 receptor, and gp130 expression during myocardial ischemia/reperfusion. *Circulation* (1999) 99:427–33. doi: 10.1161/01.cir.99.3.427
29. Margarida V, de Jager SCA, Sluijter JPG. Target inflammation after myocardial infarction: A therapeutic opportunity for extracellular vesicles? *Int J Mol Sci* (2021) 22:7831. doi: 10.3390/ijms22157831
30. Whalen DAJ, Hamilton DG, Ganote CE, Jennings RB. Effect of a transient period of ischemia on myocardial cells. i. effects on cell volume regulation. *Am J Pathol* (1974) 74:381–97.
31. David GD, Mireia AV, Marisol RM, Inserte J, Barba I. Myocardial edema: A translational view. *J Mol Cell Cardiol* (2012) 52:931–9. doi: 10.1016/j.yjmcc.2012.01.010
32. Mireia AV, Ignasi B, Marcos P, Javier I, Jose RP, Victor P, et al. Measuring water distribution in the heart: Preventing edema reduces ischemia-reperfusion injury. *J Am Heart Assoc* (2016) 5:e003843. doi: 10.1161/JAHA.116.003843
33. Rodrigo FJ, Javier SG, Jaume A, Jaime GP, Gonzalo JLM, Jose MGR, et al. Myocardial edema after ischemia/reperfusion is not stable and follows a bimodal pattern: imaging and histological tissue characterization. *J Am Coll Cardiol* (2015) 65:315–23. doi: 10.1016/j.jacc.2014.11.004
34. Weis SM, Cheresh DA. Pathophysiological consequences of VEGF-induced vascular permeability. *Nature* (2005) 437:497–504. doi: 10.1038/nature03987
35. Li X, Redfors B, Miguel SJ, Shi SJ, Martinsson P, Padhan N, et al. Suppressed vascular leakage and myocardial edema improve outcome from myocardial infarction. *Front Physiol* (2020) 11:763. doi: 10.3389/fphys.2020.00763
36. Wessel F, Winderlich M, Holm M, Maïke F, Ronmy RG, Vockel M, et al. Leukocyte extravasation and vascular permeability are each controlled *in vivo* by different tyrosine residues of VE-cadherin. *Nat Immunol* (2014) 15:223–30. doi: 10.1038/ni.2824
37. Zhao ZQ, Velez DA, Wang NP, Hewan-Lowe KO, Nakamura M, Guyton RA, et al. Progressively developed myocardial apoptotic cell death during late phase of reperfusion. *Apoptosis* (2001) 6:279–90. doi: 10.1023/a:1011335525219
38. Bulluck H, Paradies V, Barbato E, Baumbach A, Hans EB, Davide C, et al. Prognostically relevant periprocedural myocardial injury and infarction associated with percutaneous coronary interventions: a consensus document of the ESC working group on cellular biology of the heart and European association of percutaneous cardiovascular interventions (EAPCI). *Eur Heart J* (2021) 42:2630–42. doi: 10.1093/eurheartj/ehab271



OPEN ACCESS

EDITED BY
Wilfried Le Goff,
INSERM, France

REVIEWED BY
Sarah Elizabeth Jackson,
University of Cambridge, United Kingdom
Gabriela Silveira-Nunes,
Juiz de Fora Federal University, Brazil

*CORRESPONDENCE
Celestine N. Wanjalla
✉ celestine.wanjalla@vumc.org

SPECIALTY SECTION
This article was submitted to
Inflammation,
a section of the journal
Frontiers in Immunology

RECEIVED 15 November 2022

ACCEPTED 18 January 2023

PUBLISHED 14 February 2023

CITATION

Wanjalla CN, Gabriel CL, Fuseini H, Bailin SS, Mashayekhi M, Simmons J, Warren CM, Glass DR, Oakes J, Gangula R, Wilfong E, Priest S, Temu T, Newell EW, Pakala S, Kalams SA, Gianella S, Smith D, Harrison DG, Mallal SA and Koethe JR (2023) CD4⁺ T cells expressing CX3CR1, GPR56, with variable CD57 are associated with cardiometabolic diseases in persons with HIV.
Front. Immunol. 14:1099356.
doi: 10.3389/fimmu.2023.1099356

COPYRIGHT

© 2023 Wanjalla, Gabriel, Fuseini, Bailin, Mashayekhi, Simmons, Warren, Glass, Oakes, Gangula, Wilfong, Priest, Temu, Newell, Pakala, Kalams, Gianella, Smith, Harrison, Mallal and Koethe. This is an open-access article distributed under the terms of the [Creative Commons Attribution License \(CC BY\)](https://creativecommons.org/licenses/by/4.0/). The use, distribution or reproduction in other forums is permitted, provided the original author(s) and the copyright owner(s) are credited and that the original publication in this journal is cited, in accordance with accepted academic practice. No use, distribution or reproduction is permitted which does not comply with these terms.

CD4⁺ T cells expressing CX3CR1, GPR56, with variable CD57 are associated with cardiometabolic diseases in persons with HIV

Celestine N. Wanjalla^{1*}, Curtis L. Gabriel², Hubaida Fuseini¹, Samuel S. Bailin¹, Mona Mashayekhi³, Joshua Simmons¹, Christopher M. Warren¹, David R. Glass⁴, Jared Oakes¹, Rama Gangula¹, Erin Wilfong^{5,6}, Stephen Priest¹, Tecla Temu⁷, Evan W. Newell⁴, Suman Pakala¹, Spyros A. Kalams¹, Sara Gianella⁸, David Smith⁸, David G. Harrison⁹, Simon A. Mallal¹ and John R. Koethe^{1,10}

¹Division of Infectious Diseases, Vanderbilt University Medical Center, Nashville, TN, United States,

²Division of Gastroenterology, Vanderbilt University Medical Center, Nashville, TN, United States,

³Division of Endocrinology, Vanderbilt University Medical Center, Nashville, TN, United States,

⁴Vaccine and Infectious Diseases Division, Fred Hutchinson Cancer Center, Seattle, WA, United States,

⁵Division of Rheumatology, Vanderbilt University Medical Center, Nashville, TN, United States,

⁶Division of Allergy, Pulmonary and Critical Care Medicine, Vanderbilt University Medical Center, Nashville, TN, United States, ⁷Department of Global Health, University of Washington, Seattle, WA, United States, ⁸Department of Medicine, University of California, San Diego, CA, United States,

⁹Division of Clinical Pharmacology, Vanderbilt University Medical Center, Nashville, TN, United States,

¹⁰Infectious Disease Section, Veterans Affairs Tennessee Valley Healthcare System, Nashville, TN, United States

Persons with HIV (PWH) on long-term antiretroviral therapy (ART) have a higher incidence and prevalence of cardiometabolic diseases attributed, in part, to persistent inflammation despite viral suppression. In addition to traditional risk factors, immune responses to co-infections such as cytomegalovirus (CMV) may play an unappreciated role in cardiometabolic comorbidities and offer new potential therapeutic targets in a subgroup of individuals. We assessed the relationship of CX3CR1⁺, GPR56⁺, and CD57^{+/−} T cells (termed CGC⁺) with comorbid conditions in a cohort of 134 PWH co-infected with CMV on long-term ART. We found that PWH with cardiometabolic diseases (non-alcoholic fatty liver disease, calcified coronary arteries, or diabetes) had higher circulating CGC⁺CD4⁺ T cells compared to metabolically healthy PWH. The traditional risk factor most correlated with CGC⁺CD4⁺ T cell frequency was fasting blood glucose, as well as starch/sucrose metabolites. While unstimulated CGC⁺CD4⁺ T cells, like other memory T cells, depend on oxidative phosphorylation for energy, they exhibited higher expression of carnitine palmitoyl transferase 1A compared to other CD4⁺ T cell subsets, suggesting a potentially greater capacity for fatty acid β -oxidation. Lastly, we show that CMV-specific T cells against multiple viral epitopes are predominantly CGC⁺. Together, this study suggests that among PWH, CGC⁺ CD4⁺ T cells are frequently CMV-specific and are associated with diabetes,

coronary arterial calcium, and non-alcoholic fatty liver disease. Future studies should assess whether anti-CMV therapies could reduce cardiometabolic disease risk in some individuals.

KEYWORDS

HIV, CD4 T cells, cardiometabolic disease, cytomegalovirus, CGC

Introduction

Persons with HIV (PWH) are at increased risk of cardiovascular and metabolic diseases compared to the general population (1), which has been attributed to persistent systemic inflammation despite the effective suppression of plasma viremia on antiretroviral therapy (ART) (2–4). Among PWH, co-infection with other viruses, such as cytomegalovirus (CMV) and hepatitis B and C, increases the risk of diabetes, cardiovascular disease, and cerebrovascular events, as well as other non-AIDS illnesses (5–8). The adaptive immune system devotes a relatively large proportion of memory CD4⁺ and CD8⁺ T cells to the anti-CMV response as compared to other viruses (9–12), and this disproportionate inflation is further exaggerated in PWH compared to age-matched individuals without HIV (10, 13). As such, HIV presents an important natural model to investigate how sustained exposure to CMV affects various aspects of the immune response and contributes to other aging-related disease processes.

CMV is a herpesvirus that co-evolved with mammals and infects many individuals at a young age, and CMV is highly prevalent in some groups including adult PWH (14, 15). Growing evidence suggests that anti-CMV T cell responses have a role in metabolic dysregulation in both animal models (16) and humans (17–22). CMV-seropositivity has been shown to predict severe non-AIDS-related illnesses and is an independent risk factor for cardiovascular and cerebrovascular disease in PWH (8, 23, 24). In PWH, the high prevalence of CMV is such that CMV-seropositivity alone does not stratify individuals at risk of developing these comorbidities. However CMV antibody titers were not associated with cardiovascular mortality in HIV-negative community-dwelling adults, suggesting antibody titers alone may not fully reflect the impact of anti-CMV immune responses on disease risk. (25).

Prior studies from our group suggest that an increase in CMV-specific CD4⁺ T cells in PWH may serve as a novel marker of metabolic and cardiovascular disease risk. We previously showed that adipose tissue CD4⁺ T cells co-expressing CX3CR1, GPR56, and CD57 (termed ‘CGC⁺’ cells), a surface marker combination suggestive of antiviral activity, increased with progressive glucose intolerance (26) and with carotid plaque burden in PWH (18). Furthermore, we showed that CMV-specific CD4⁺ T cells that recognized an immunodominant peptide epitope (DYSNTHSTRYV from glycoprotein B (gB)) restricted through HLA-DR7 were predominantly CGC⁺ (17, 18). Further, we demonstrated that CGC⁺ CD4⁺ T cells were cytotoxic and oligoclonal (17). Despite several studies describing a role for CMV-seropositivity in morbidity and mortality in PWH (8), little is known

about the role of CMV-specific CD4⁺ and CD8⁺ T cells, target viral epitopes, and the basic mechanisms that mediate these pathologies.

A study of pneumococcal vaccine responses in persons with antineutrophil cytoplasmic antibody-associated vasculitis showed that treatment with valgancyclovir reduced subclinical CMV and the proportion of CD4⁺ CD28[−] T cells, and improved responses to the vaccine (27). The expansion of CD4⁺ CD28[−] T cells was thought to have reduced the functional capacity of the CD4⁺ T cell memory compartment, and thereby reduced responses to vaccines. Although valgancyclovir is not a recommended first-line therapy against CMV, this study suggests the possible role of anti-CMV therapy in reducing the proportion of CD4⁺ CD28[−] T cells, a population with considerable overlap with CGC⁺ CD4⁺ T cells (26). A similar study in PWH showed that treatment with valgancyclovir reduced detectable CMV DNA levels and reduced CD8⁺ T cell activation, defined by CD38 and HLA-DR expression, at 8 weeks and 12 weeks of treatment (28). Notably, there was no difference in soluble inflammation biomarkers between the placebo group and those treated with valgancyclovir, suggesting this effect was primarily on circulating T cells. These findings are important clinically, as they suggest that the anti-CMV T cell response is malleable, and if CD4⁺ CD28[−] or CGC⁺ T cells contribute to cardiometabolic disease pathogenesis the use of antiviral agents could serve as a novel therapeutic strategy.

The goal of the current study was to (1) characterize the CMV specificity of CGC⁺ cells using a broader range of tetramer staining, (2) evaluate the relationship between peripheral blood CGC⁺ T cells with cardiovascular and metabolic diseases among a large cohort of PWH on ART, and (3) determine the relationships between CGC⁺ T cells and traditional cardiovascular disease risk factors. Using a wide array of class I and II CMV tetramers, we show that CMV-specific T cells are CX3CR1⁺ and GPR56⁺ with variable expression of CD57, and are among the cluster defined as CGC⁺. We show that circulating CGC⁺ CD4⁺ T cells and CGC⁺ CD8⁺ T cells in PWH are associated with prevalent cardiometabolic conditions (diabetes, subclinical atherosclerosis, and liver disease). Among individual disease risk factors, CGC⁺ T cells are related most strongly to fasting blood glucose and hemoglobin A1C. CGC⁺ T cells are also correlated with starch and sucrose metabolites measured in the plasma of PWH. Notably, total memory CD4⁺ and CD8⁺ T cells do not have a similar relationship with starch and sucrose metabolites. The relationship between circulating CGC⁺ T cells and fasting blood glucose does not appear to be driven by a greater dependence on glucose metabolism as a source of energy when compared to other memory T cell subsets. However, higher expression of carnitine palmitoyl transferase 1A

(CPT1A) by CGC⁺ T cells may be due to a greater capacity for fatty acid β -oxidation CPT1A. These findings suggest that CGC⁺ T cell expansion associated with cardiometabolic disease in PWH may be driven by CMV co-infection. Additional prospective studies defining the antigen specificity of CGC⁺ T cells and their mechanistic role in cardiometabolic disease pathogenesis are underway.

Methods

Study participants

From August 2017 and November 2019, we recruited 134 adults PWH without diabetes (fasting blood glucose (FBG) <100 mg/dl and/or hemoglobin A1c (HbA1c) <5.7%), with pre-diabetes (FBG 100-125

mg/dl and/or HbA1c 5.7-6.4%) or with diabetes (FBG \geq 126 mg/dl and/or HbA1c \geq 6.5% or on anti-diabetic medications) to the *HIV, Adipose Tissue Immunology and Metabolism* (HATIM) study from the Vanderbilt Comprehensive Care Clinic, an academic, urban HIV treatment facility (17). All participants were on ART combination therapy for \geq 18 months, with a minimum of 12 months of sustained plasma viral suppression, a CD4⁺ T cell count >350 cells/ μ l, and no known inflammatory or rheumatologic conditions. Exclusion criteria were self-reported heavy alcohol use (>11 drinks/week), known liver cirrhosis, active hepatitis B or C, cocaine or amphetamine use, and use of corticosteroids or growth hormones. Anthropometric measurements including waist circumference, height, weight, and body mass index (BMI) were obtained on the day of recruitment (Table 1). Diabetic PWH were older, with significantly fewer smokers. Participants provided written informed consent, and the study was

TABLE 1 Clinical and demographic characteristics of the study cohort.

	N	Non-Diabetic PWH N=51	Pre-Diabetic PWH N=44	Diabetic PWH N=39	Test Statistic
Age, yrs	134	45 [36, 52]	44 [36, 56]	54 [49, 58]	0.001
Sex, male	134	0.80 ^{41/51}	0.80 ^{35/44}	0.72 ^{28/39}	0.6
Race, Caucasian	134	0.59 ^{30/51}	0.52 ^{23/44}	0.46 ^{18/39}	0.5
Smoker status, yes	131	0.36 ^{18/50}	0.30 ^{13/44}	0.11 ^{4/37}	0.001
Hepatitis C ab status	134	0.20 ^{10/51}	0.09 ^{4/44}	0.13 ^{5/39}	0.3
HTN, yes	134	0.63 ^{32/51}	0.57 ^{25/44}	0.67 ^{26/39}	0.9
BMI (Kg/m ²)	134	30.7 [28.1, 34.1]	31.8 [29.0, 35.3]	33.8 [30.3, 39.2]	0.01
Waist circumference (cm)	132	104 [92, 109]	106 [95, 113]	112 [107, 120]	0.001
Laboratory values					
Hemoglobin A1C, %	132	5.3 [4.9, 5.4]	5.6 [5.2, 5.9]	6.8 [6.2, 8.9]	<0.001
FBG, mg/dL	131	90 [83, 94]	111 [104, 118]	161 [128, 234]	0.001
Creatinine, mg/dL	132	1.0 [0.9, 1.1]	1.0 [0.8, 1.1]	1.0 [0.9, 1.3]	0.3
LDL, mg/dL	131	96 [84, 120]	110 [93, 127]	90 [80, 105]	0.03
Cholesterol, mg/dL	133	170 [149, 202]	180 [166, 212]	175 [150, 196]	0.3
HDL, mg/dL	133	44 [36, 54]	41 [34, 50]	40 [34, 46]	0.5
Triglycerides, mg/dL	133	104 [77, 170]	128 [90, 196]	165 [114, 262]	0.006
HsCRP, mg/dL	131	2.7 [1.2, 5.1]	2.7 [1.1, 4.1]	3.0 [2.1, 7.7]	0.2
Statin use, yes	124	0.22 ^{10/45}	0.32 ^{14/44}	0.63 ^{22/35}	<0.001
Non-contrast CT imaging					
Pericardial fat, cm ³	112	55 [35, 80]	75 [45, 108]	91 [64, 202]	0.008
Visceral fat, cm ³	113	143 [90, 163]	169 [120, 215]	200 [130, 280]	<0.001
Liver mean density, hu	112	63.0 [58.6, 65.6]	62.3 [55.0, 67.2]	60.5 [46.2, 63.0]	0.04
CAC prevalence, yes	113	0.02 ^{1/41}	0.33 ^{12/36}	0.44 ^{16/36}	<0.001
HIV-related Laboratory Values					
CD4 at ART start, cells/ml	130	508 [342, 652]	424 [310, 554]	462 [249, 620]	0.6
CD4 T count at enrollment, cells/ml	134	799 [596, 942]	832 [627, 1016]	945 [732, 1154]	0.08
CD4 cell percentage	134	37.0 [31.5, 41.0]	34.5 [28.8, 38.5]	40.0 [35.0, 45.5]	0.004
Duration ART, yrs	131	6.7 [4.3, 11.6]	7.1 [3.1, 11.2]	8.9 [5.0, 16.2]	0.2

N is the number of non-missing values. Statistical tests used: Kruskal-Wallis test for continuous variables; Pearson chi-square test for categorical variable. Bold values indicate p-values <0.05.

approved by the Vanderbilt University Institutional Review Board. The study is registered at [ClinicalTrials.gov](https://clinicaltrials.gov/ct2/show/study/NCT04451980) (NCT04451980).

Sample collection

Subcutaneous adipose tissue was obtained from participants by liposuction and the stromal vascular fraction (SVF) was processed within 30 minutes to 1 hour of the procedure as previously published in detail (17). Peripheral blood mononuclear cells (PBMCs) were processed by Ficoll gradient. PBMCs and SVF from all participants were cryopreserved and subsequent assays were performed at a later date in batches. We also re-analyzed data single-cell metabolic profiling of T cells obtained from healthy human donors at the Stanford Blood Center, according to the guidelines of the Stanford Institutional Review Board (29).

Computed tomography imaging

We performed non-contrast computed tomography (CT) imaging within 1 week of blood collection and anthropometric measurements. This was performed using a Siemens Somatom Force multidetector scanner (Erlangen, Germany). Total coronary arterial calcium (Agatston units, Au) was measured in the left anterior descending (LAD), left main (LM), left circumflex (LCX), and right coronary artery (RCA). For our analysis, coronary arterial calcium (CAC) was treated as a categorical variable (presence or absence of coronary CAC). The mean coronary cross-sectional area (external diameter of the outer walls) was measured at three equidistant points of the LAD. The mean coronary cross-sectional area (corCSA) was derived from the mean of three points and used as a surrogate for arterial remodeling. Non-alcoholic fatty liver disease was defined by liver attenuation, which was averaged from nine total regions using the open-source OsiriX software field (30). Perivascular adipose tissue (PAT) volume (adipose tissue around the LM coronary, LAD, circumflex, and RCA) and epicardial adipose were measured as previously described (30).

Flow cytometry

A multiparameter flow cytometry antibody panel was used to stain PBMCs (17, 18, 26). The panel used to define CGC⁺ cells included anti-CD3, CD4, CD8, CCR7, CD45RO, GPR56, CX3CR1, CD57, CD14, CD19, and LIVE/DEAD Aqua (Supplemental Table 1). We included Class I and Class II CMV tetramers with this panel to identify virus-specific T cells. CMV Class I (pp65 [HLA-A02 NLVPMVATV (NLV)]) and Class II tetramers (gB [HLA DR1:07 DYSNTHSTRYV (DYS)], pp65 [HLA DR1:03 EFFWDANDIYRIF (EFF)], IE2 [HLA DR1:03 TRRGVRKIDEVSRMF (TRR)], IE1 [HLA DR1:03 VKQIKVRVDMVRHRI (VKQ)] and pp65 [HLADQB1*06:02 LLQTGIHVRSQPSL (LLQ)]) were obtained from the NIH tetramer facility supported by contract 75N93020D00005 from the National Institute of Allergy and Infectious Diseases. The analysis was performed using the BD FACS Aria II flow cytometer. Bulk and single-cell sorting was

performed using a 70µm nozzle into 96 well plates or Eppendorf tubes, respectively, as previously published (17). An additional panel with fluorescently tagged antibodies was used to further characterize KLRG1, CD27, and CD28 expression on CGC⁺ T cells (anti-GPR56, CCR7, CD38, KLRG1, CD14, CX3CR1, CD45RO, CXCR3, PD1, CD27, CD57, CD3, Live/Dead stain, CD8, CD4, CD28, and CXCR5) (Supplemental Table 1). These samples were run on a Cytex/Aurora. We used Cytobank to analyze the flow cytometry and mass cytometry data (31). The gating strategy used to define the immune subsets is shown in the Supplemental Material (Supplemental Figure 1).

Metabolomics sample extraction

Plasma samples were aliquoted at 25 µL and spiked with 5 µL of metabolomics internal standards solution. Extraction of metabolites was performed by protein precipitation by adding 200 µL of 8:1:1 Acetonitrile: Methanol: Acetone (Fisher Scientific, San Jose, CA) to each sample. Samples were mixed thoroughly, incubated at 4°C for 30 min to allow protein precipitation, and centrifuged at 20,000xg to pellet the proteins. After centrifugation, 190 µL supernatant was transferred into a clean microcentrifuge tube and dried under a gentle stream of nitrogen at 30°C (Organomation Associates, Inc., Berlin, MA). Samples were reconstituted with 25 µL of injection standards solution, mixed, and incubated at 4°C for 10-15 min. Reconstituted samples were centrifuged at 20,000xg and supernatants were transferred into LC-vials for LC-MS analysis.

Metabolomics LC-MS analysis

LC-MS untargeted metabolomics was performed on a Thermo Q-Exactive Orbitrap mass spectrometer equipped with a Dionex UPLC system (Thermo, San Jose, CA). Separation was achieved on an ACE 18-pfp 100 x 2.1 mm, 2 µm column (Mac-Mod Analytical, Inc., Chaddsford, PA) with mobile phase A as 0.1% formic acid in water and mobile phase B as acetonitrile (Fisher Scientific, San Jose, CA). The gradient was run at a flow rate of 350 µL/min and consisted of: 0-3 min, 0% B; 3-13 min, 80% B, 13-16 min, 80% B, 16-16.5 min, 0% B. The total run time was 20.5 min. The column temperature was set at 25°C. The injection volume was 4 µL for negative and 2 µL for positive polarity. All samples were analyzed in positive and negative heated electrospray ionization with a mass resolution of 35,000 at m/z 200 as separate injections. The heated-electrospray conditions are 350°C capillary temperature, 3.5 kV capillary voltage, 50 sheath, and 10 arbitrary units of auxiliary gas. LC-MS injection was done following a sequence of 3 blanks, neat QC, pooled QC, 10 randomized samples, blank, neat QC, pooled QC, 10 randomized samples, and so on.

Metabolomics data processing

The percent relative standard deviation of internal standard peak areas was calculated to evaluate extraction and injection reproducibility. The raw files were then converted to mzXML using MS Convert (ProteoWizard, Palo Alto, CA). Mzmine 2 was used to identify features, deisotope, align features and perform a gap filling to

fill in any features that may have been missed in the first alignment algorithm. The data were searched against an internal retention time metabolite library. All adducts and complexes were identified and removed from the data set.

Mass cytometry by time of flight

We used cytometry by time of flight (CyTOF) to further define cell surface markers expressed on CGC⁺ T cells. In brief, cryopreserved PBMCs were thawed and treated with Nuclease S7. After two washes, the cells were stained with LIVE/DEAD Cisplatin stain for 3 minutes, followed by quenching, and then stained with a master mix of CyTOF antibodies against surface markers. Sixteen percent PFA was used to fix cells for 15 minutes at room temperature. After one wash, we resuspended cells in 1mL cold methanol, and caps were sealed with parafilm before incubating overnight at -20°C. On the day the cells were to be analyzed, we washed them with 1X PBS/1% BSA. They were then stained with the intracellular marker CTLA4 for 20 minutes at room temperature. This was followed by staining with a 25μM DNA intercalator (Ir) in the presence of 1.6% PFA for 20 minutes at room temperature and then transferred to 4°C until analyzed. Just before analysis on Helios, we washed cells with PBS followed by a wash with Millipore H₂O. We resuspended 500,000 cells/ml (in minimum 500μL) ddH₂O for the CyTOF run. We added 1/10th volume of equilibration beads to the cells and filtered the cells immediately before running. The Cytof panel included antibodies that define T cells (CD3, CD4, CD8) and memory subsets (CD45RA, CD45RO, CCR7).

For the metabolic profiling, cryopreserved PBMCs from healthy donors were thawed in a cell culture medium (CCM; RPMI 1640 containing 10% FBS, and GlutaMAX; Thermo Fisher Scientific) supplemented with 1:10000x Benzodase (Sigma-Aldrich). Cells from different donors were live cell barcoded using CD45 antibodies as previously described (32), then washed and combined for downstream cell staining. Cells were suspended in TruStain FcX Fc blocker (BioLegend) for 10 min at RT and washed in cell staining media (CSM: PBS with 0.5% BSA and 0.02% sodium azide) before staining. Surface staining was performed in CSM for 30 min at RT. Cells were resuspended in monoisotopic cisplatin-195 for 5 min to label non-viable cells (Fluidigm, 0.5 μM final concentration in PBS). Cells were washed in CSM and fixed and permeabilized using the Foxp3/Transcription Factor Staining Buffer Set (eBiosciences). Intracellular staining was performed in a permeabilization buffer for 30 min at RT. Cells were then washed and resuspended in intercalator solution (1.6% PFA in PBS and 0.5 mM rhodium-intercalator (Fluidigm)) for 1 hr at RT. Cells were washed and resuspended in CSM + 10% DMSO and cryopreserved. Before the acquisition, cells were thawed in CSM and washed twice in Cell Acquisition Solution (CAS; Fluidigm). All samples were filtered through a 35 mm nylon mesh cell strainer, resuspended in CAS supplemented with 1x EQ four-element calibration beads (Fluidigm), and acquired on a Helios mass cytometer (Fluidigm).

Primary CD4 and CD8 T cell expansion

CGC⁺ and non-CGC⁺ CD4⁺ and CD8⁺ T cells were sorted from PBMCs stained with the multiparameter flow cytometry panel. Greater than 90% purity was confirmed by spot checks of sorted cells. The CGC⁺ T cells were expanded using the ImmunoCultTM Human CD3/CD28 T Cell Activator (Stem Cell Technologies, #10991). Cells were expanded per the manufacturer's protocol with the replacement of media supplemented with human interleukin (IL)-2 (10 to 50ng/ml) every 2-3 days, depending on the density of the cells. Cells were expanded past 14 days and were re-stimulated once more by the addition of CD3/CD28.

Plasma CMV IgG levels

CMV IgG levels were measured in the plasma by ELISA per the manufacturer's protocol (Genway, # GWB-BQK12C).

Single-cell TCR sequencing

Single-cell T cell receptor (TCR) sequencing was performed as published (17). In brief, we stained PBMCs and index-sorted CGC⁺CD4⁺ T cells by flow cytometry into 96-well plates containing 3μL of lysis buffer with a ribonuclease inhibitor (33, 34). We used uniquely tagged primers (TSOend primer and the constant region primers, TCRA or TCRB) for reverse transcription, which tags the cDNA with well-specific barcodes coupled with a unique molecular identifier (UMI) to allow for multiplexing. Samples from each well were then pooled and amplified using the KAPA HiFi HotStart ReadyMix (Roche, Basel, Switzerland). Nested polymerase chain reactions were performed to target the TCR region specifically. We purified the PCR products using Agencourt AMPure XP (Beckman Coulter, CA, UWA) and indexed libraries were created for sequencing using Truseq adapters. The prepared libraries were quantified using the KAPA Universal qPCR Library Quantification Kit (Kapa Biosystems Inc., MA, USA). The products were sequenced on an Illumina MiSeq using a 2×300bp paired-end chemistry kit (Illumina Inc., CA, USA). Reads were quality-filtered and passed through a demultiplexing tool to assign reads to individual wells and mapped to the TCRB and TCRA loci. We used the MIXCR software package to assign TCR clonotypes. We used the visual genomics analysis studio (VGAS), an in-house program for visualizing and analyzing TCR data (<http://www.iiid.com.au/software/vgas>).

RNA transcriptomic analysis

Our group previously sorted CGC⁺CD4⁺ and CGC⁺CD8⁺ T cells, as well as other memory T cells, for RNA transcriptomic analysis as published (17). Here, we performed a secondary differential expression analysis to assess differences in 475 genes involved in metabolic pathways between cell types (Supplemental Table 3).

Cytokine assays

We measured interleukin (IL)-4, IL-10, IL-6, and highly sensitive reactive protein (hs-CRP) in plasma using a multiplex assay (Meso Scale Diagnostics, Rockville, MD) as previously published (35).

Cellular metabolic assays

We analyzed the metabolic profile of CGC⁺CD4⁺ T cells and CGC⁺CD8⁺ T cells *ex vivo* using the SCENITH assay as published (36). In brief, cryopreserved PBMCs were rapidly thawed and resuspended in RPMI media supplemented with 10% fetal bovine serum. After two washes, the cells were stained with antibodies against CCR7 and CX3CR1 at 37°C for 15 minutes. The cells were added in duplicate per condition to 96-well plates at about 1 million cells per well in 180ul R10 media. They were rested for 15–30 minutes at 37°C. 2-Deoxy-D-glucose (2mM), oligomycin (3mM), and DGO (1mM 2DG and 1.5mM oligomycin) were added to the cells, which were incubated at 37°C for 30 minutes. This was followed by the addition of puromycin (10μM) to each well, incubated at 37°C. We included samples without puromycin as controls. The cells were incubated at 37°C for 30 minutes. Cells were spun down and washed with PBS twice. These were then stained with surface antibodies for 15 minutes at room temperature. The cells were washed twice and fixed using the Foxp3/Transcription factor fixation fix/perm solution (20 minutes) and then washed with the Foxp3/Transcription factor permeabilization buffer. This buffer was used to dilute the anti-puromycin antibody. Cells were incubated with the anti-puromycin antibody for 20 minutes at room temperature. Cells were then washed with PBS and immediately analyzed by flow cytometry.

We sorted CGC⁺ and non-CGC⁺ CD4⁺ and CD8⁺ T cells and expanded them as above to obtain enough cells for the Seahorse assay. After 12 days of expansion, 100,000 cells per well were plated on Cell-Tak (Corning) coated plates in Seahorse XF Base Medium (Agilent, 102353-100) supplemented with 1 mM L-glutamine and 1 mM pyruvate at pH 7.4. Seeded cells were centrifuged at 200 g without break and incubated for 1 h at 37°C in a non-CO₂ (2) chamber. ECAR measurements were taken using the Agilent Seahorse XF96 analyzer under basal conditions and after consecutive injections with 10 mM Glucose, 1.5 μM Oligomycin, and 50 mM 2-deoxy-glucose (2-DG). Control wells with assay medium lacking cells were used for background measurements.

Statistical analysis

Continuous variables/clinical demographics are presented as median values [25th and 75th percentiles], and statistical analyses comparing the three metabolic groups were performed using the Kruskal-Wallis test. Differences between categorical variables, represented as proportions, were analyzed using the Chi-squared test. TCR and RNA transcriptomic analyses were performed using the visual genomics analytics studio tool (VGAS) (37). Differential gene expression between CGC⁺ T cells and non-CGC⁺ T cells was performed using Kruskal Wallis tests, and adjustment for multiple

corrections using the Benjamini Hochberg (BH) method. The top differentially expressed genes, *p*-value < 0.1, were included in the KEGG pathway and Gene Ontology pathway enrichment analysis using Enrichr and Appster (38–40). The relationship between CGC⁺ T cells and plasma metabolites was analyzed using Spearman's rank correlation. Metabolomic pathways represented by metabolites correlated with CGC⁺ T cells were analyzed using MetaboAnalyst 5.0. Over Representation Analysis (ORA) of the significant plasma metabolites was performed using the hypergeometric test. One-tailed adjusted *p* values are provided after correcting for multiple testing (FDR). We used the Kruskal-Wallis test to analyze differences in the proportions of immune cell subsets between two groups/treatments, and Wilcoxon tests when there were more than two groups. Relationships between immune subsets and anthropometric or clinical laboratory measurements were determined using Spearman's rank correlation analysis. We also measured relationships between the immune subsets and other factors after adjustment for potential confounders using partial Spearman's rank analysis. Statistical analysis was performed using R version 4.1.0 (41) and Prism version 9.

Data and code availability

The data presented in the study are deposited in the NIH GeneExpression Omnibus repository, accession number GenBank: GSE159759. Differential gene expression was performed using custom software, Visual genomics analysis studio (VGAS) (37).

Results

CMV-specific CD8⁺ T cells co-express CX3CR1 and GPR56 with variable CD57

We previously defined CMV-specific CD4⁺ T cells that bind the DYSNTHSTRYV epitope (DYS, HLA-DR7, glycoprotein B (gB)) as CGC⁺, however the extent to which this subset of cells is CMV-specific is unknown (18). We characterized CGC⁺ T cells using additional markers that have been associated with CMV-specific T cells. Two-dimensional plots show CX3CR1, GPR56, and CD57 expression on CD8⁺ T cells in two HIV-negative donors (CMV-negative and CMV-positive) and four CMV-positive PWH (Figure 1A). We used the Uniform Manifold Approximation and Projection (UMAP) algorithm to visualize clusters of CD8⁺ T cells related by marker expression. The CGC⁺ cluster on CD8⁺ T cells had variable CD57 expression (Figure 1A, UMAPs) and expressed the killer-cell lectin-like receptor G1 (KLRG1, a marker associated with senescence) (Figure 1B). Additional markers included in the panel defined the CGC⁺ CD8⁺ T cell cluster as largely made up of T effector memory RA-revertant (TEMRA) cells (CD45RO⁺ CCR7⁻), CD28⁻, CD27^{+/−} and CD38⁺ (Supplemental Figures 2A, B).

We characterized the CMV-specificity of CD8⁺ T cells from a subset of HLA-typed individuals (Supplemental Table 2). In participant #1, we evaluated CMV-specific CD8⁺ T cells in the peripheral blood and adipose tissue using a class I tetramer against the HLA-A*02-01 binding CMV 65 kilodalton phosphoprotein

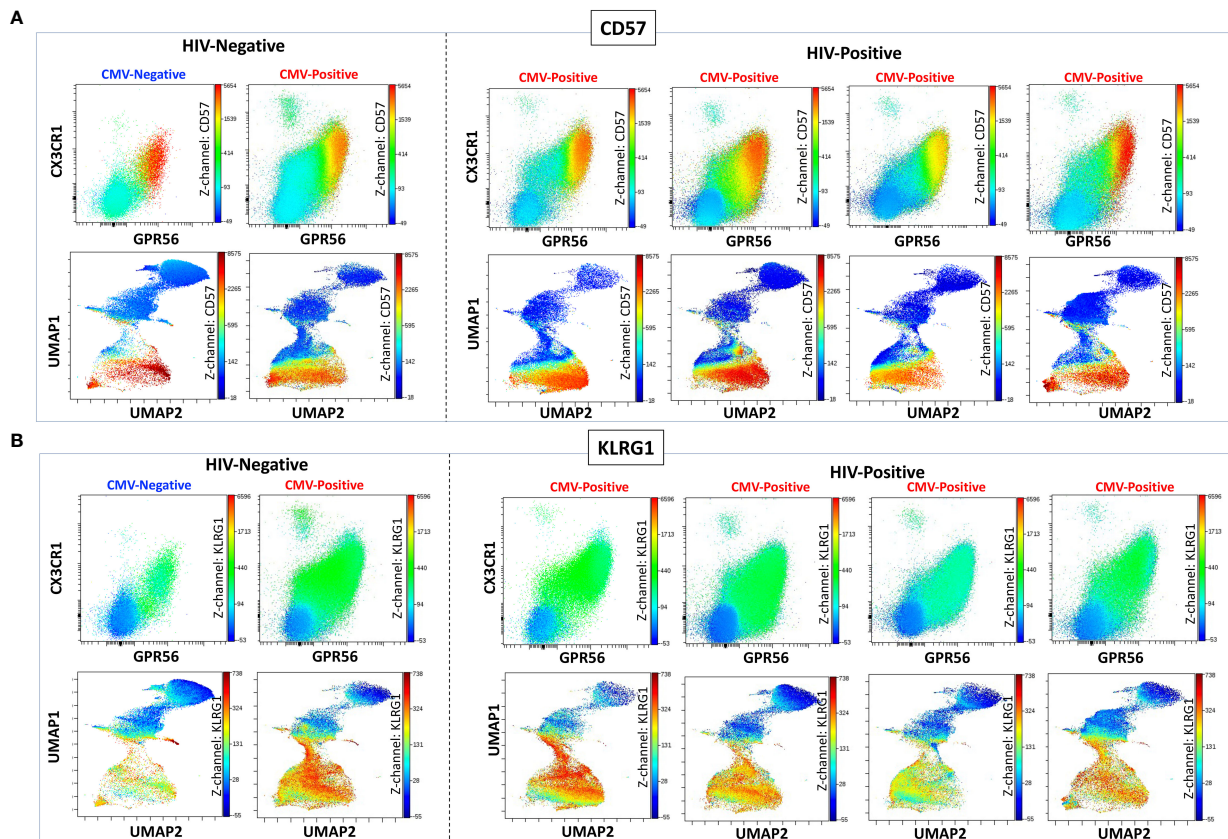


FIGURE 1

CGC⁺ CD8⁺ T cells express CX3CR1 and GPR56 with variable expression of CD57. The two-dimensional flow cytometry panel shows the co-expression of CX3CR1 and GPR56 and highlights CD57 expression on these cells compared to non-CGC⁺ T cells. UMAP shows CGC⁺ CD8⁺ cluster and variable expression of CD57 (A). KLRG1 expression on CGC⁺ CD8⁺ T cells is demonstrated by two-dimensional plots and UMAP (B). Participants in this analysis included two HIV-negative persons with and without CMV, and four CMV-positive PWH.

(pp65) epitope₄₉₅₋₅₀₃ NLVPMVATV (NLV). NLV tetramer⁺ cells constituted 2.0% of total CD3⁺ T cells and 3.8% of total CD8⁺ T cells in the peripheral blood of participant #1 (Figures 2A, B). Two-dimensional flow cytometry plots show that NLV-tetramer⁺ CD8⁺ T cells co-express CX3CR1 and GPR56 with variable expression of CD57 (Figure 2C). 65.7% of the NLV-tetramer⁺ CD8⁺ T cells are TEMRA and the rest effector memory T cells (TEM) (Figure 2D). NLV tetramer⁺ cells were present in the cluster of CX3CR1⁺ and GPR56⁺ cells with variable expression of CD57 (Figure 2E). We gated on the CGC⁺ CD8⁺ cluster and show the expression of the NLV tetramer, CX3CR1, GPR56 and CD57 (Figure 2F). The coloring channel highlights NLV-tetramer⁺ cells (bright red) and shows that 8.4% of the CGC⁺ CD8⁺ T cell cluster from participant #1 express TCRs that bind the NLV tetramer. For this participant #1, we also analyzed NLV tetramer⁺ CD8⁺ T cells in the adipose tissue, given the contribution of adipose tissue inflammation to the development of cardiometabolic disease. 1.2% of total CD3⁺ T cells and 3.4% of total CD8⁺ T cells expressed the NLV TCR (Figures 2G, H). These NLV-specific CD8⁺ T cells present in the adipose tissue also co-expressed CX3CR1 and GPR56, with variable CD57⁺ expression. Like the matched peripheral blood, 54.1% of the NLV-tetramer⁺ T cells in

adipose were TEMRA and the rest were TEM (Figures 2I, J). UMAPs show that NLV-tetramer⁺ CD8⁺ T cells present in the adipose tissue from participant #1 cluster with CGC⁺ CD8⁺ T cells, with a proportion of ~ 6.0% (Figures 2K, L).

To assess the heterogeneity among individuals, we analyzed CMV-specific responses in the peripheral blood of additional donors. Participant #2 had NLV⁺ tetramer cells that constituted 0.6% of total CD3⁺ T cells (Figure 2M) and 1.4% of total CD8⁺ T cells (Figure 2N). In this participant, NLV-specific CD8⁺ T cells were CX3CR1⁺ and GPR56⁺, with much less CD57 expression (Figure 2O). There was also a higher proportion of TEM cells among the gated NLV tetramer⁺ cells (Figure 2P). NLV tetramer-specific cells in participant #2 did not form a tight cluster as seen with participant #1 (Figure 2Q), and 1.9% of CGC⁺ CD8⁺ T cells were NLV-tetramer specific (Figure 2R). Two additional HLA-A*02:01 PWH were also evaluated: participant #3 with 2.1% NLV tetramer⁺ cells as a proportion of total CD3⁺ T cells (Supplemental Figures 3A-F) and participant #4 with 0.8% NLV tetramer⁺ cells as a proportion of total CD3⁺ T cells (Supplemental Figures 3G-L). In summary, despite heterogeneity in immune cell markers, NLV-tetramer⁺ CD8⁺ T cells are largely present within the CGC⁺ cluster.

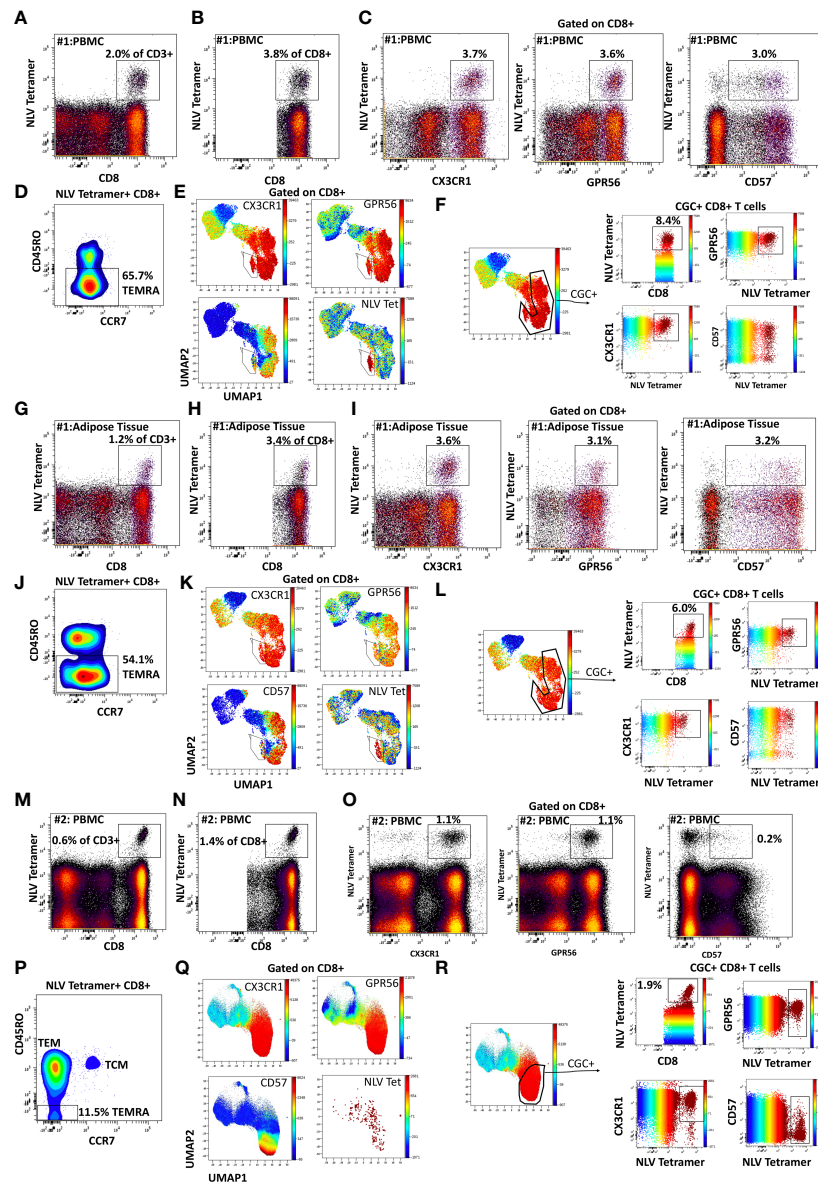


FIGURE 2

CMV-specific CD8⁺ T cells are predominantly CGC⁺. Phenotypic expression of CX3CR1, GPR56, and CD57 by NLV-specific CD8⁺ T cells in two participants. Peripheral blood NLV-specific CD8⁺ T cells as a proportion of CD3⁺ T cells (A) and total CD8⁺ T cells (B). Two-dimensional plots show the co-expression of CX3CR1, GPR56, and CD57 by NLV-specific CD8⁺ T cells (C). Memory cell phenotypes were classified as TEM (CD45RO⁺ CCR7⁺) and TEMRA (CD45RO⁺ CCR7⁺) (D). UMAP of CD8⁺ T cells showing the CD8⁺ T cells with NLV tetramers among the CGC cells (E, F). The proportion of NLV-tetramer⁺ CD8⁺ T cells in matched SVF fraction (G, H). Co-expression of CGC markers (I) and memory T cell subsets (J) within UMAPs as the proportion of total CGC⁺ CD8⁺ T cells (K, L). A representative sample from the blood of a second participant sample is shown (M–R).

CMV-specific CD4⁺ T cells co-express CX3CR1 and GPR56 with variable CD57

Like CGC⁺ CD8⁺ T cells, we also characterized markers expressed on CGC⁺ CD4⁺ T cells. The two-dimensional plots show CX3CR1 and GPR56 expression on the y and x-axis and highlight CD57 expression on the z-channel (Figure 3A). The CMV-negative donor had very few CGC⁺ CD4⁺ T cells, unlike CGC⁺ CD8⁺ T cells. The UMAP shows the separation of the CGC⁺ CD4⁺ T cell cluster from the rest of the CD4⁺ T cells. In addition, CGC⁺ CD4⁺ T cells also express KLRG1, which may be less variable than CD57 (Figure 3B). With additional markers, we can define CGC⁺ CD4⁺ T cells as TEM (CD45RO⁺ CCR7⁺) and TEMRA (CD45RO⁺ CCR7⁺) cells that are

CD28⁺, CD27⁺, PD1⁺ and CD38⁺ (Supplemental Figure 5). We used MHC Class II tetramers to identify CD4⁺ T cells recognizing two immunodominant CMV epitopes: DYS and LLQTGIHVRSQPSL (LLQ, HLA-DQ06:02, pp65 protein) as previously published (10, 13). Participants with HLA-DR7 and HLA-DQ6 were selected (Supplemental Table 2). 12.1% of the total CD4⁺ T cells in participant #2 were DYS tetramer⁺ (Figure 4A). Two-dimensional flow cytometry plots show that DYS-tetramer⁺ CD4⁺ T cells also express CX3CR1 and GPR56 with variable CD57 (Figure 4B). 88.7% of the DYS-tetramer⁺ CD4⁺ T cells were TEM, and the rest were TEMRA (Figure 4C). Visualization using the UMAP technique showed that the majority of the DYS tetramer⁺ cells were within the CGC⁺ CD4⁺ cluster (Figures 4D, E). Analysis of the DYS tetramer

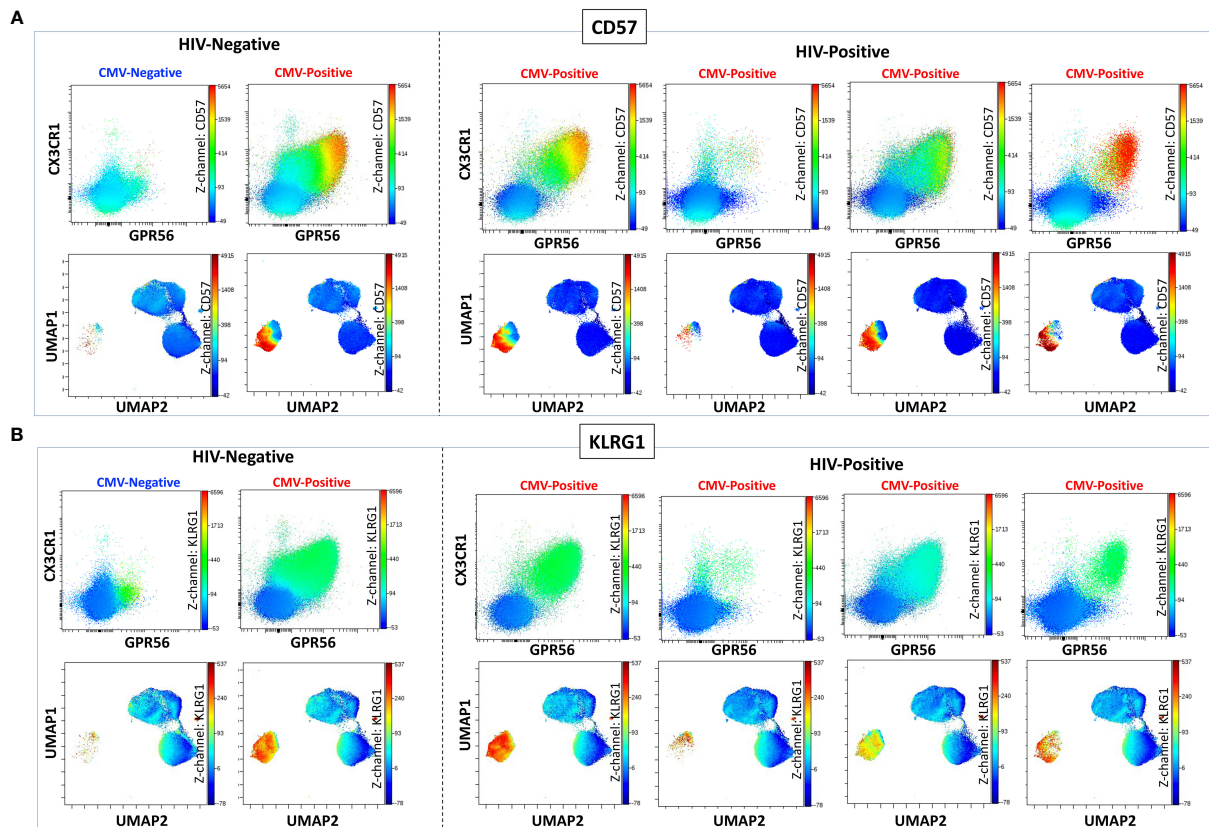


FIGURE 3

CGC⁺ CD4⁺ T cells express CX3CR1 and GPR56 with variable expression of CD57. The two-dimensional flow cytometry panel shows the co-expression of CX3CR1 and GPR56 and highlights CD57 expression on these cells compared to non-CGC⁺ T cells. UMAP shows CGC⁺ CD4⁺ cluster and variable expression of CD57 (A). KLRG1 expression on CGC⁺ CD4⁺ T cells is demonstrated by two-dimensional plots and UMAP (B). Participants in this analysis included two HIV-negative persons with and without CMV, and four CMV-positive PWH.

on the CGC⁺ CD4⁺ cluster showed that 42.0% of CGC⁺ CD4⁺ T cells in participant #1 had TCRs that recognized the DYS epitope (Figure 4F). In participant #5 (Supplemental Table 2, HLA-DQ6+) LLQ-specific CD4⁺ T cells comprised 0.28% of CD4⁺ T cells (Figure 4G). LLQ tetramer⁺ T cells co-expressed CX3CR1, and GPR56 with variable CD57 expression (Figure 4H). 93.6% tetramer⁺ cells fell within the CGC⁺ cluster (Figures 4I–K). 1.3% of CGC⁺ CD4⁺ T cells in participant #5 were specific for the LLQ epitope (Figure 4L). In summary, the majority of the CD4⁺ T cells with TCRs that recognize two different immunodominant CMV epitopes are CGC⁺. CMV-specific CD4⁺ T cells in PWH are significantly inflated compared to matched HIV-negative controls (13). These data suggest that in PWH without evidence of acute CMV infection at the time of the study, a large proportion of CGC⁺ T cells may be CMV-specific.

Detection of low-frequency CMV-specific CD4⁺ T cells among expanded CGC⁺ T cells

To characterize CMV-specific T cells with TCRs to less immunodominant epitopes with a lower frequency of tetramer⁺ T cells in PBMCs, we flow-sorted and expanded CGC⁺ and non-CGC⁺ T cells as depicted in the schematic (Figure 5A). We made attempts to expand CGC⁺ CD8⁺ T cells but could not analyze this population due to a high proportion of cell death. (Photos of expanded cell subsets on

day 10 of culture are shown in Figure 5B). The morphology of the expanded CGC⁺ CD4⁺ T cells in some participants was distinct from the non-CGC⁺ CD4⁺ and CD8⁺ T cells, with satellite clusters that we speculate may represent clonal expansion. Control MHC class II tetramers (HLA-DR3 and HLA-DQ6) with the CLIP peptides were also used to stain CGC⁺ CD4⁺ T cells from expanded cell lines (Figure 5C). We used the CMV tetramers to identify CD4⁺ T cells with TCRs to less dominant epitopes (TRRGRVKIDEVSRMF (TRR, HLA-DRB1*03:01, IE2 protein) and VKQIKVRVDMVRHRI (VKQ, HLA-DRB1*03:01, IE1 protein)). We measured tetramer⁺ CD4⁺ T cells (DYS, TRR, and VKQ) after a 10-day expansion of sorted CGC⁺ CD4⁺ T cells and compared them to unsorted PBMCs (Figure 5D). For some of the less dominant epitopes, we had improved detection after expansion in culture (TRR and VKQ). Sorted non-CGC⁺ CD4⁺ T cells expanded in culture for 10 days also had some CMV-specific CD4⁺ T cells by tetramer analysis (Figure 5E). Expanded CGC⁺ CD4⁺ cells maintained CX3CR1, GPR56, and CD57 expression on the tetramer⁺ cells (Supplemental Figures 5A, C, E). The tetramer⁺ CD4⁺ T cells that we detected in the expanded T cells from the non-CGC⁺ CD4⁺ sort also expressed CX3CR1 and GPR56 compared to the other cells in the same pool. This may suggest that some CGC⁺ T cells were among the non-CGC⁺ T cells obtained by sorting before expansion, or that CGC⁺ CD4⁺ T cells may be derived from non-CGC⁺ T cells (Supplemental Figures 5B, D, F). In general, CGC⁺ CD4⁺ T cells maintained higher levels of CX3CR1, GPR56, and CD57

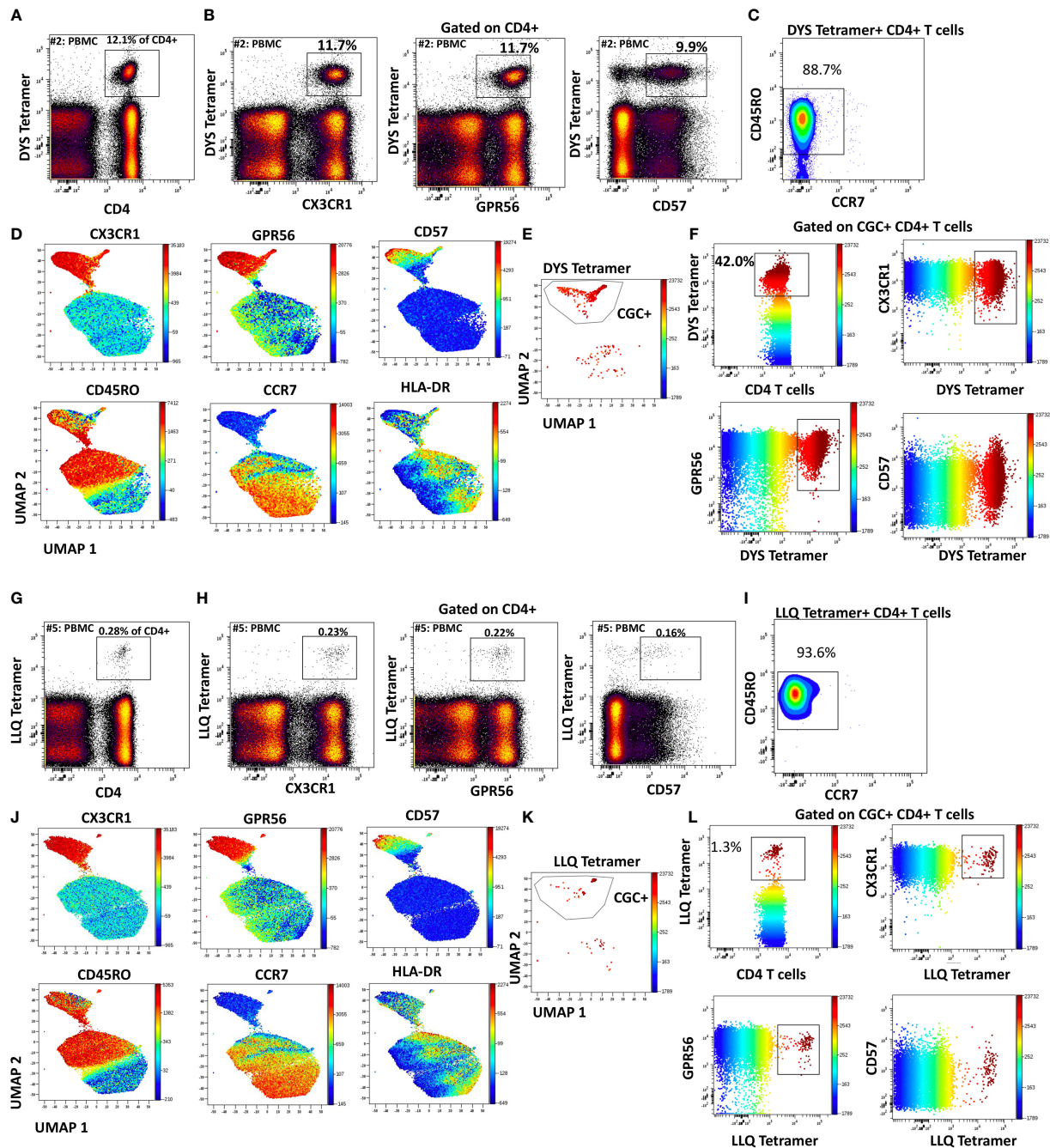


FIGURE 4

CMV-specific CD4⁺ T cells are predominantly CGC⁺. Phenotypic expression of CX3CR1, GPR56, and CD57 by CMV-specific CD4⁺ T cells that recognize two different epitopes (DYS and LLQ). Peripheral blood DYS-specific CD4⁺ T cells as a proportion of CD3⁺ T cells (A). Two-dimensional plots show the co-expression of CX3CR1, GPR56, and CD57 by DYS-specific CD4⁺ T cells (B). Memory cell phenotypes were classified as TEM (CD45RO⁺ CCR7⁻) and TEMRA (CD45RO⁻ CCR7⁻) (C). UMAP of CD4⁺ T cells showing the CD4⁺ T cells with DYS tetramers among the CGC cells. Each panel shows the distribution of CX3CR1, GPR56, CD57, CD45RO, CCR7, and HLA-DR expression on the clusters (D-F). A second participant with LLQ-specific CD4⁺ T cells is shown (G-L).

in culture (Supplemental Figures 5G, H). Notably, there was no significant difference in the mean fluorescence intensity of the CX3CR1 and GPR56 between the tetramer⁺ cells in the CGC⁺ CD4⁺ population versus tetramer⁺ cells in the non-CGC⁺ CD4⁺ expanded T cells, while CD57 expression trended towards being higher in the expanded CGC⁺ CD4⁺ T cells (Supplemental Figure 5I). Taken together, CGC⁺ CD4⁺ T cells as we have defined

them can proliferate in culture after CD3/CD28 stimulation with IL-2 supplementation. This is different from previous studies that failed to show the proliferation of CD57⁺ CD4⁺ T cells after stimulation with PHA (42) or HIV antigens (43). In our studies, the CGC⁺ CD4⁺ T cell cluster appears to be driven by CX3CR1 and GPR56, which includes CD4⁺ T cells with variable CD57⁺ T cell expression that may undergo several rounds of replication. In summary, CMV-tetramer⁺ CD4⁺ T

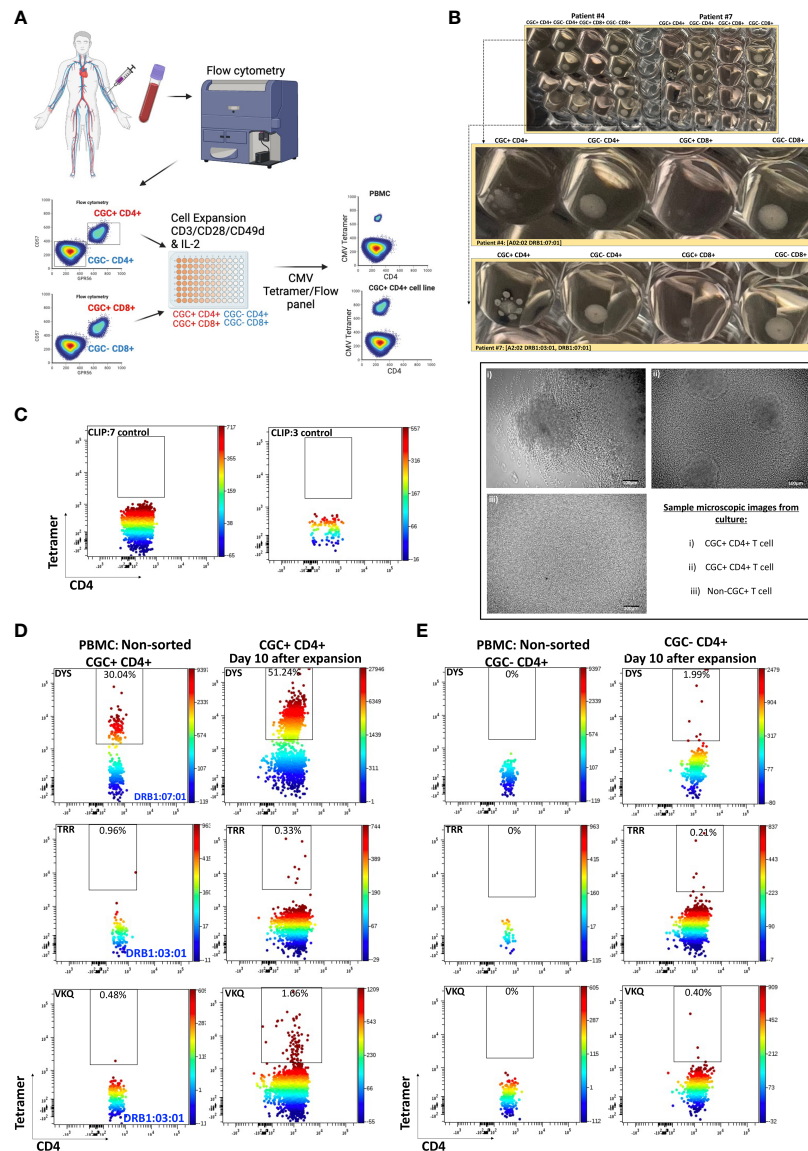


FIGURE 5

CMV-specific T cells among expanded CGC⁺ CD4⁺ and non-CGC⁺ CD4⁺ T cells. Schematic showing workflow for sorting and expansion of CGC⁺ and non-CGC⁺ cells (A). Cell expansion cultures from two participants (Supplemental Table 2, participants #4 & #7) on day 10 of expansion. The top figure shows duplicate wells, with the middle panel showing an enlarged image to highlight the satellite cultures in CGC⁺ CD4⁺ T cells by direct observation and by light microscopy (B). Tetramer staining controls on expanded cells (DRB1:07:01 and DRB1:03:01) with CLIP peptide (C). Two-dimensional flow cytometry plots showing CMV-specific T cells using tetramers against three different CMV MHC class II epitopes (DR7:DYS) and (DR3:TRR, DR3:VKQ) in non-sorted PBMCs and expanded CGC⁺ CD4⁺ T cells (D). Similar analysis on non-CGC⁺ CD4⁺ T cells gated from PBMCs and on expanded non-CGC⁺ CD4⁺ T cell line (E).

cells in PWH are mainly CX3CR1⁺ GPR56⁺ with variable expression of CD57, while similar cells present in the non-CGC⁺ cells have low expression of CD57.

CGC⁺ CD4⁺ T cells have a large proportion of clonal TCRs and are largely CMV-specific

While we observed that CGC⁺ CD4⁺ T cells can recognize several CMV epitopes, it remains unclear the extent to which the CGC⁺ T cell cluster of cells is CMV-specific as a whole. To understand whether starting with CGC⁺ CD4⁺ T cells can help define CMV-specific T cells

agnostic to HLA typing, we sorted single CGC⁺ CD4⁺ T cells into 96-well plates from two participants (#4 and #6, both HLA-DR7) as shown (Figure 6A). Two-dimensional plots show that 5.5% of CD4⁺ T cells in participant #4 are DYS tetramer⁺ (Figures 6B, C) and largely TEM cells (Figure 6D). UMAPs show DYS tetramer⁺ T cells within the CGC⁺ T cell cluster (Figures 6E, F). Paired $\alpha\beta$ TCR sequences from the sorted CGC⁺ CD4⁺ T cells are shown in Circos plots (Figure 6G). Clonal TCRs that did not have paired $\alpha\beta$ pairs are not shown on the Circos plots. Out of a total of 41 TCRs with paired $\alpha\beta$ pairs, 26.8% had the CDR3 (CASSGGTGGGADTQYF). Other clonal TCRs are shown. Participant #6 was selected because of known DYS-specific CD4⁺ TCRs identified by bulk sequencing apriori (13). We

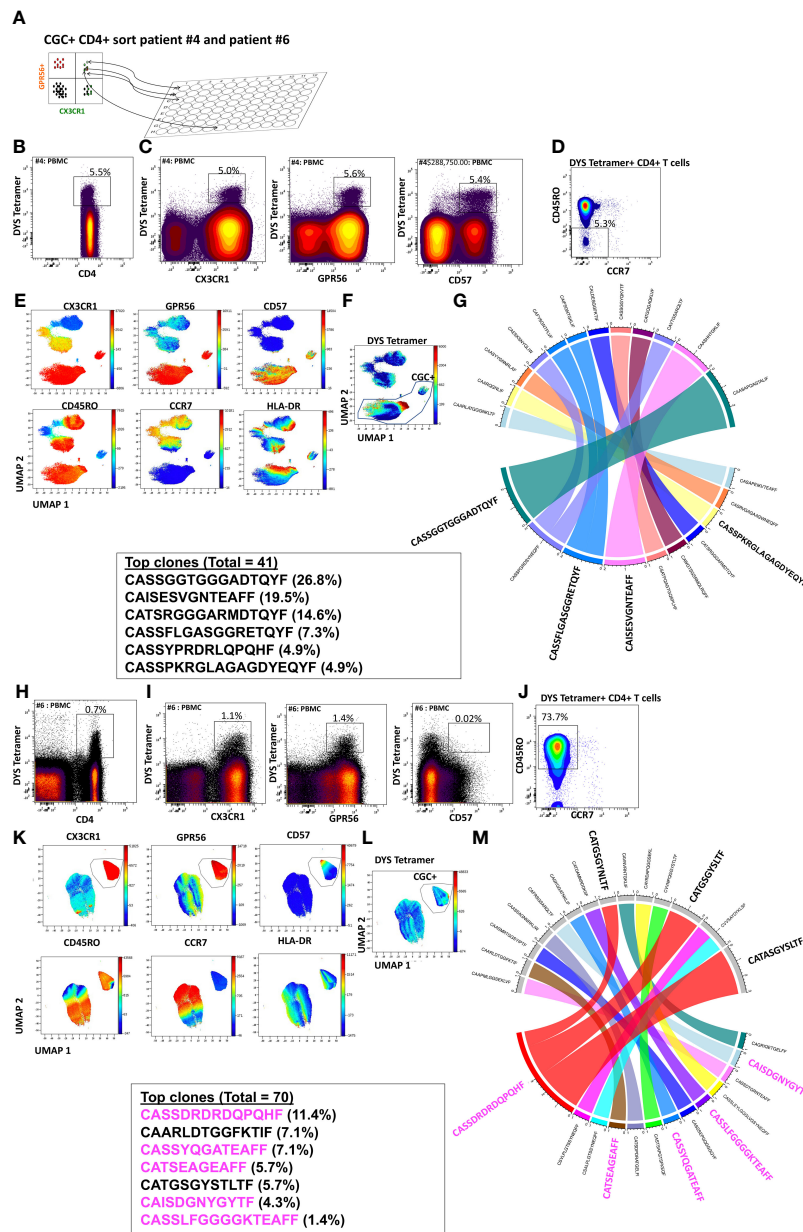


FIGURE 6

CGC⁺ CD4⁺ T cells express clonal TCRs and are largely CMV-specific. Single CGC⁺ CD4⁺ T cells were sorted into 96 well plates as shown (A). Two-dimensional plots from participant #4 show DYS tetramer-specific T cells as a proportion of CD4⁺ T cells (B). CX3CR1, GPR56, and CD57 expression on DYS tetramer⁺ cells (C) and memory distribution of the tetramer⁺ cells are shown (D). UMAPs show the distribution of markers (E, F). A total of 40 paired TCRs had identifiable sequences. The Circos plot shows paired $\alpha\beta$ TCR CDR3 sequences, and TRBV and paired TCRJ genes are shown (G). A similar analysis was done with participant #6 (H-M). CDR3 sequences in magenta have previously been shown to be DYS-specific, by tetramer staining.

also sorted CGC⁺CD4⁺ T cells from participant #6 (Figures 6H-M). Out of a total of 70 TCR sequences with matched $\alpha\beta$ TCR pairs, 5 of the top 10 clones among the CGC⁺ CD4⁺ T cells (n=21) had been previously identified as CMV-DYS specific by sequencing TCRs from DYS tetramer⁺ CD4⁺ T cells (13). This suggests CGC⁺ CD4⁺ T cells in PWH co-infected with CMV may be largely CMV-specific.

The frequency of peripheral blood CGC⁺ CD4⁺ T cells from participants in the full cohort of PWH was positively correlated with plasma anti-CMV IgG titers ($p=0.21$, $p=0.03$), while CGC⁺ CD8⁺ T cells were not significant ($p=0.18$, $p=0.07$) (Supplemental Figures 6A,

B). Finally, CGC⁺ CD4⁺ T cells and CGC⁺ CD8⁺ T cells were strongly correlated with each other (Supplemental Figure 6C).

CGC⁺ CD4⁺ T cells are higher in PWH with cardiometabolic disease

To investigate the extent to which CGC⁺ CD4⁺ and CGC⁺ CD8⁺ T cells differ in cardiometabolic disease conditions (diabetes, pre-diabetes, hypertension, coronary arterial calcium, nonalcoholic fatty

liver disease, and pericardial fat volume), we measured the frequencies of CGC⁺ T cells in PBMCs as a proportion of total CD4⁺ and CD8⁺ T cells. We found similar proportions of CGC⁺ CD4⁺ and CGC⁺ CD8⁺ T cells in participants with and without hypertension (Figure 7A), while CGC⁺ CD4⁺ T cells were higher in participants with coronary arterial calcium (CAC) on CT imaging ($p=0.0009$), (Figure 7B), and non-alcoholic fatty liver disease (NAFLD, defined as absolute liver attenuation less than 58 Hounsfield units [HU] on CT imaging [$p=0.04$; Figure 7C]). Both CGC⁺ CD4⁺ and CGC⁺ CD8⁺ T cells were significantly higher among participants with prediabetes and diabetes as compared to non-diabetics (Figure 7D). Notably, the frequency of CGC⁺ CD8⁺ T cells was positively correlated with pericardial fat volume as measured by CT imaging ($p=0.02$), which was mainly driven by diabetic participants ($p=0.0008$) (Figure 7E). A similar relationship was not observed for CGC⁺ CD4⁺ T cells and pericardial fat volume

($p=0.3$). Collectively, these results indicate that there are more circulating CGC⁺ CD4⁺ and CGC⁺ CD8⁺ T cells in persons with HIV with subclinical atherosclerosis, NAFLD, pre-diabetes, and diabetes.

Circulating CGC⁺ CD4⁺ and CGC⁺ CD8⁺ T cells are associated with fasting blood glucose and hemoglobin A1C

Prior murine studies showed the adoptive transfer of peripheral senescent CD8⁺ T cells (CD8⁺ CD44⁺ CD153⁺) from spleens of mice on a high-fat chow diet to mice on a normal chow diet was followed by insulin resistance in the recipient animals, suggesting a role for circulating T cells in the development of metabolic dysregulation (44). This concept is further supported by epidemiologic analyses in PWH

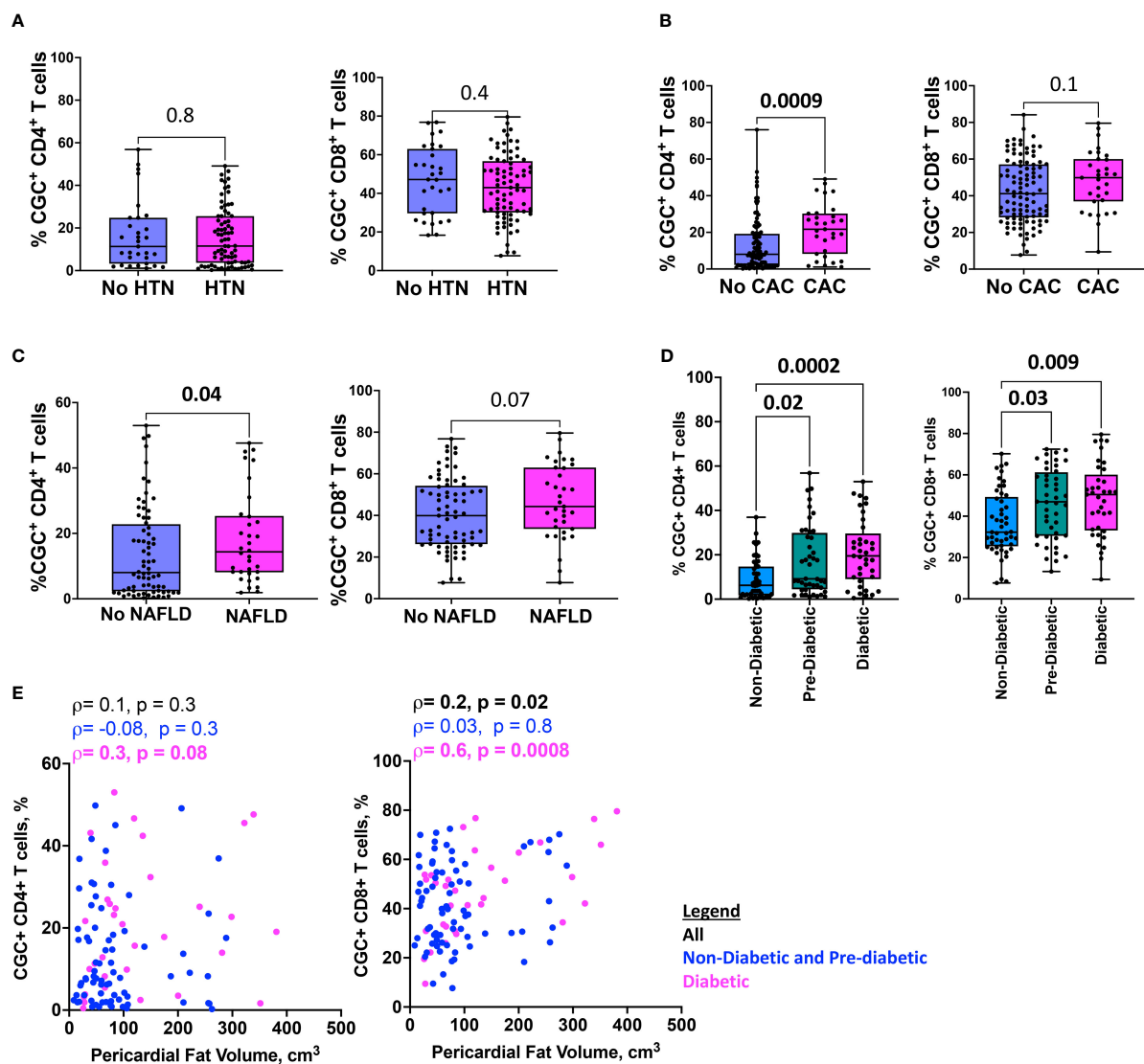


FIGURE 7

Higher CGC⁺ CD4⁺ T cells are associated with cardiometabolic disease. Box plots showing CGC⁺ CD4⁺ and CGC⁺ CD8⁺ T cells in the presence or absence of hypertension (HTN) (A), coronary arterial calcium (CAC) (B), non-alcoholic fatty liver disease (NAFLD) (C), and diabetes (D). Correlation plots show the relationship between CGC⁺ T cells and pericardial fat volume (E). Statistical analysis by Mann Whitney, Kruskal Wallis, and Spearman's rank correlation tests.

showing an association between a higher circulating CD4⁺ TEMRA cell frequency and the subsequent development of diabetes mellitus (45). In light of these findings, we assessed the relationship between peripheral CGC⁺ CD4⁺ T cells (as a proportion of total CD4⁺ T cells) and CGC⁺ CD8⁺ T cells (as a proportion of total CD8⁺ T cells) with several cardiometabolic disease risk factors. CGC⁺ CD4⁺ T cells were correlated with waist circumference, and there was a trend towards a correlation with age and BMI (Figures 8A–C). These cells were most

strongly correlated with fasting blood glucose in non-diabetic and pre-diabetic individuals ($p=0.002$) (Figure 8D). The correlation with fasting blood glucose was stratified by the metabolic group because of the effect of diabetes medications on glucose levels (all diabetic participants were receiving anti-diabetes medications and had a fasting blood glucose range of 73–416 mg/dL). We did not observe a significant relationship between CGC⁺ CD4⁺ T cells and fasting blood glucose in diabetic PWH ($=-0.13$, $p=0.47$). T cells can mediate

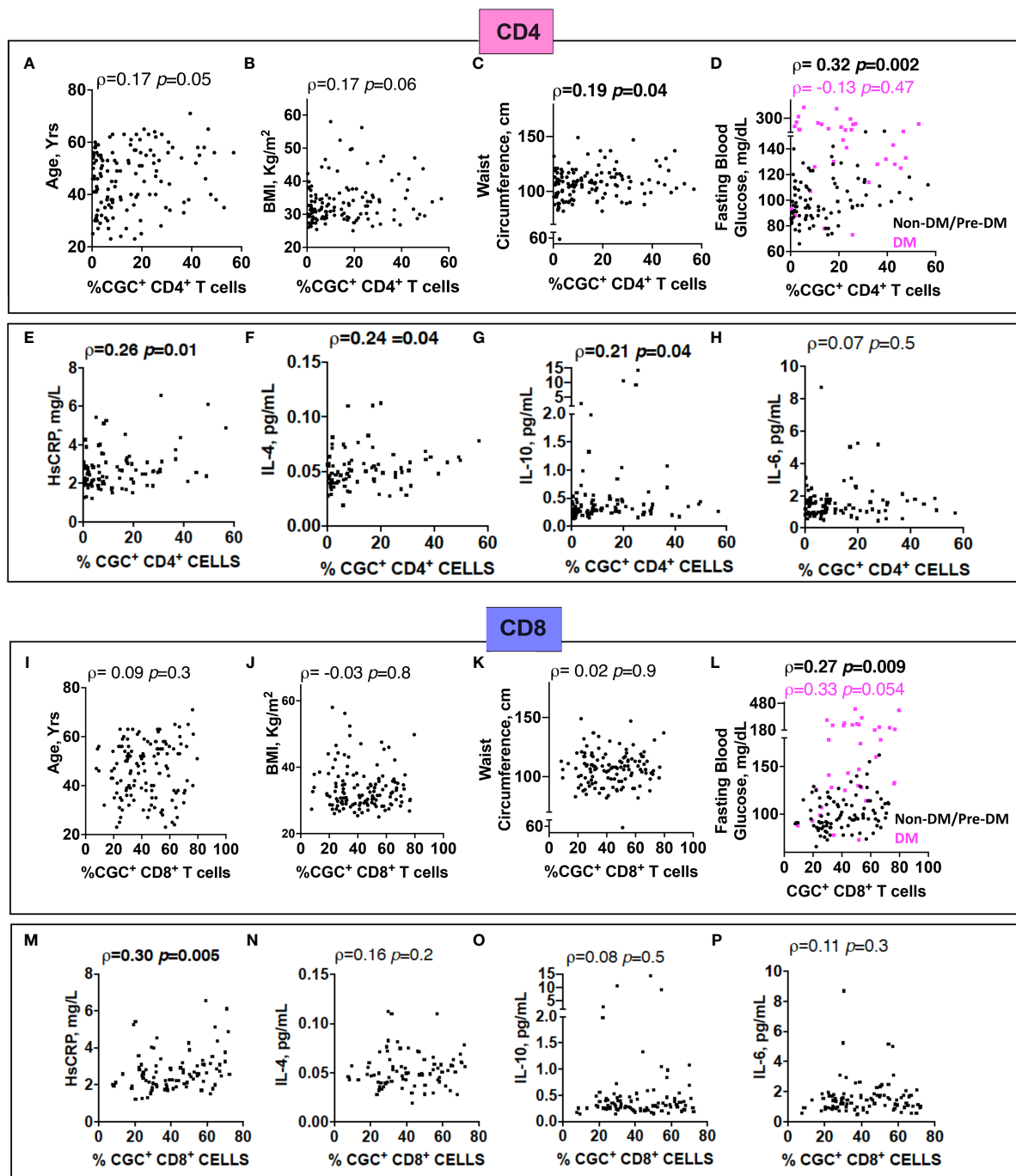


FIGURE 8

The proportion of circulating CGC⁺ T cells in peripheral blood is correlated with fasting blood glucose. Spearman's rank correlation analysis shows relationships between CGC⁺ CD4⁺ T cells and age (A), body mass index (BMI) (B), waist circumference (C), and fasting blood glucose stratified by non-diabetic and prediabetic (black) and diabetic (magenta) (D). Correlation plots showing relationships between % CGC⁺ CD4⁺ T cells and inflammatory markers including high sensitivity C-reactive protein (HsCRP) (E), IL-4 (F), IL-10 (G), and IL-6 (H). Similar analyses were performed with CGC⁺ CD8⁺ T cells (I–P). Statistical analysis by Spearman's rank test.

inflammatory and anti-inflammatory effects through plasma cytokines. Therefore, we also assessed whether CGC⁺ T cells were related to inflammatory markers and anti-inflammatory cytokines important in cardiometabolic disease (35). The frequency of CGC⁺ CD4⁺ T cells correlated with hsCRP ($p=0.01$), IL-4 ($p=0.04$), IL-10 ($p=0.04$) but not IL-6 ($p=0.5$) (Figures 8E-H). On the other hand, CGC⁺ CD8⁺ T cells were not correlated with age, BMI, or waist circumference, and had a modest correlation with fasting blood glucose in non-diabetic/pre-diabetic PWH ($r=0.27$, $p=0.009$), and a trend toward significance in diabetic PWH ($r=0.33$, $p=0.05$) (Figures 8I-L). CGC⁺ CD8⁺ T cells were also correlated with hsCRP ($p=0.30$, $p=0.005$) (Figure 8M) but not IL-4, IL-10, or IL-6 (Figures 8N-P). Both CGC⁺ CD4⁺ T cells ($p=0.23$, $p=0.01$) and CGC⁺ CD8⁺ T cells ($p=0.27$, $p=0.003$) were correlated with hemoglobin A1C in a partial Spearman's correlation analysis adjusted for age, sex, body mass index (BMI), hypertension, statin use, and smoking status (Figure 9, top). CGC⁺ CD4⁺ T cells had a stronger association with hemoglobin A1C when BMI was removed from the model ($p=0.27$, $p=0.004$), while the relationship between

CGC⁺ CD8⁺ T cells and hemoglobin A1C attenuated ($p=0.24$, $p=0.01$) (Figure 9, bottom).

CGC⁺ CD4⁺ and CGC⁺ CD8⁺ T cells are correlated with circulating concentrations of starch/sucrose metabolites and branch-chain amino acids

Both fasting blood glucose and HbA1c can be influenced by multiple factors, including the time of day, hydration status, medications, red blood cell survival, genetics, and vitamin deficiencies, among others. Plasma metabolites offer an additional profile of metabolic status, and changes in metabolites are frequently present before the development of overt disease (46). Therefore, we next assessed whether the observed association between CGC⁺ T cells and blood glucose measurements was also present for other plasma metabolites. We found that frequencies of CGC⁺ CD4⁺ T cells and CGC⁺ CD8⁺ T cells were positively correlated with plasma levels of

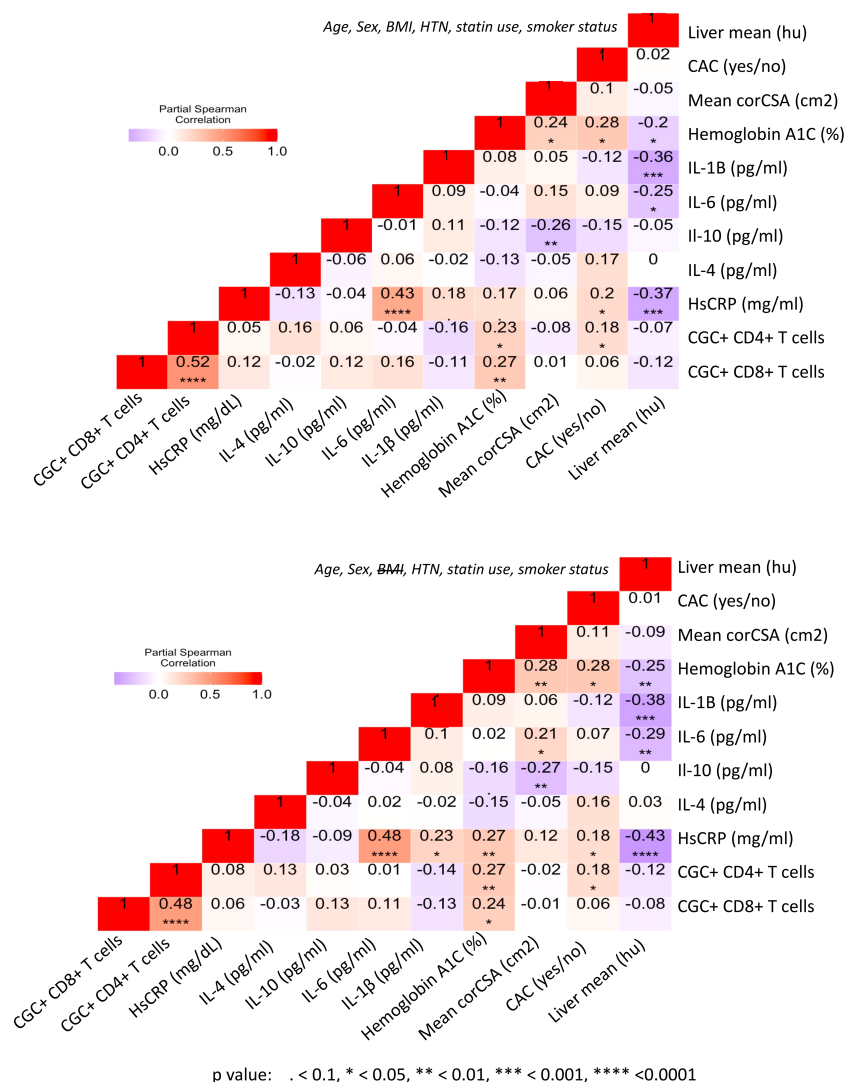


FIGURE 9

CGC⁺ T cells are associated with higher hemoglobin A1C levels in adjusted analyses. Partial Spearman's rank correlation analysis adjusted for age, sex, HTN, BMI, statin use, and smoking status (top), and after removal of BMI from the model (bottom).

branch chain amino acids (isoleucine and norleucine), carbohydrate metabolites (glucose/fructose, glucosamine, galactosamine, and fumarate), acetoacetate, and 2-beta-hydroxybutyric acid among others (Figure 10A). On the other hand, phosphocholine, L-Anserine, 3-Methylhistamine, Sulfinio-L-Alanine, and Hydroxy-L-Tryptophan were inversely correlated with the frequencies of CGC⁺ CD4⁺ and CGC⁺ CD8⁺ T cells. Most of these correlations were not present for total memory CD4⁺ or CD8⁺ T cells (Supplemental Figures 7A, B). The frequency of CGC⁺ CD4⁺ cells positively correlated with metabolites that enriched for the starch and sucrose metabolism pathways (FDR 0.02) (Figure 10B), and negatively with other metabolites from the taurine and hypotaurine metabolism pathways (FDR 0.09, data not shown). Metabolites that were positively correlated with CGC⁺ CD8⁺ cells enriched for the pentose and glucuronate conversions, starch, and sucrose metabolism pathways but were not statistically significant (FDR 0.16) (Figure 10C). Similarly, metabolites that were negatively correlated with CGC⁺ CD8⁺ enriched for taurine and hypotaurine metabolism pathways but they were not significant (FDR 0.33, data not shown). Taken together, these results demonstrate that CGC⁺ T cells are related to starch and sucrose metabolites in plasma, as well as

branched-chain amino acids (BCAA) which have been linked with the development of diabetes and cardiovascular disease (46–48).

CGC⁺ CD4⁺ and CGC⁺ CD8⁺ T cells are predominantly mitochondrial-dependent

CD4⁺ TEMRA cells are senescent and bioenergetically flexible compared to CD8⁺ TEMRA cells, partly due to their ability to effectively engage both glucose metabolism and oxidative phosphorylation (49). One possible explanation is that CD8⁺ TEMRA cells may have dysfunctional mitochondria (49). Given the observed relationship between the frequency of CGC⁺ T cells with starch and sucrose metabolites, we studied their metabolic profile as a way to understand their functional capacity in PWH. We analyzed the mitochondrial and glucose dependence of T cells using SCENITH, Single Cell ENergetIc metabolism by profiling Translation in inHibition. Puromycin uptake by CGC⁺ CD4⁺ and CGC⁺ CD8⁺ T cells after incubation with inhibitors was measured by geometric mean fluorescence (Figures 11A, C). In general, naïve cells (CD4⁺ and CD8⁺) had lower levels of puromycin uptake compared to T cell

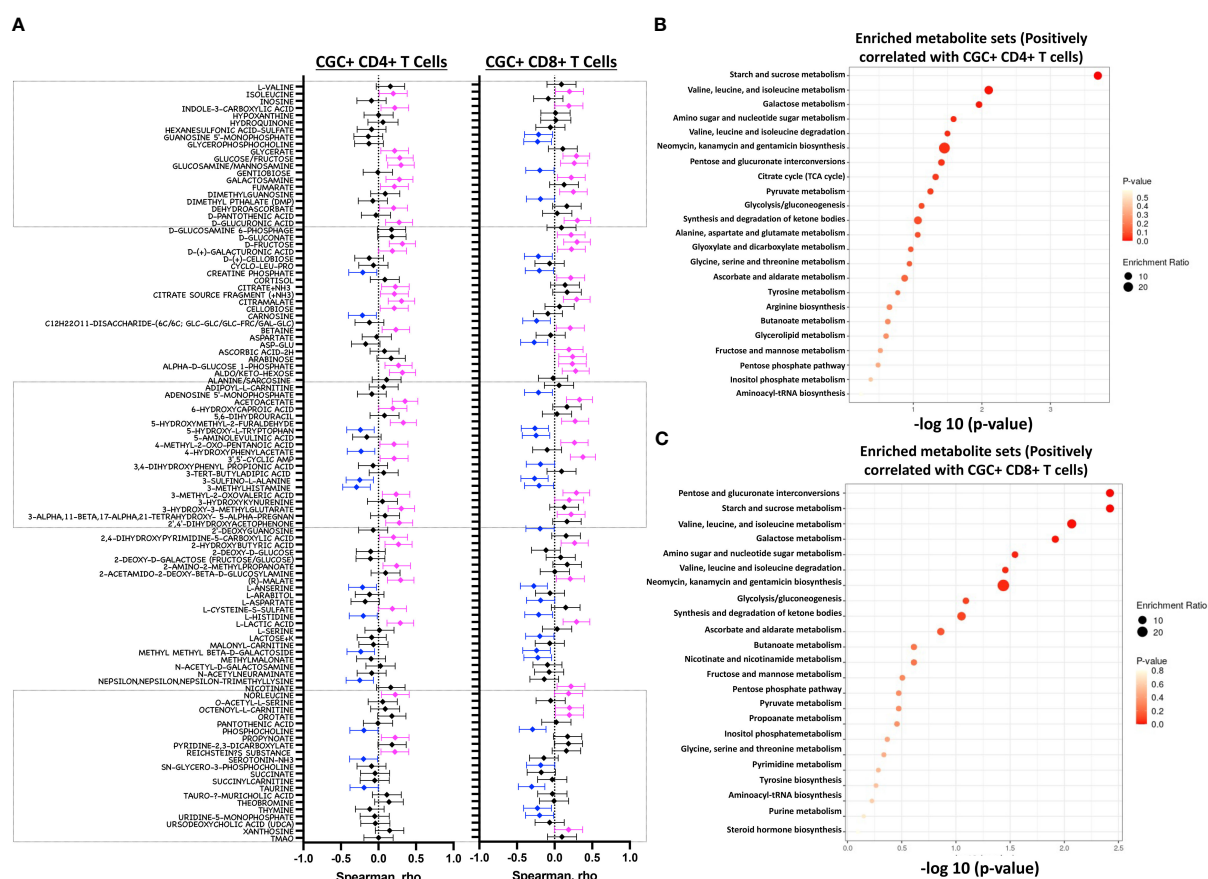


FIGURE 10

Starch and sucrose metabolism pathways are enriched among plasma metabolites positively correlated with CGC⁺ T cells. Forest plots showing Spearman's rank correlation coefficients between plasma metabolites and the proportion of CGC⁺ CD4⁺ T cells over total CD4⁺ T cells (left panel) and % CGC⁺ CD8⁺ T cells over total CD8⁺ T cells (right panel) (A). The top twenty-five metabolite sets in the enrichment analysis (number of metabolites/expected metabolites per set) were determined based on metabolites that were positively correlated with % CGC⁺ CD4⁺ T cells (B) and % CGC⁺ CD8⁺ T cells (C). Statistical analysis by Spearman's rank correlation. Color code: Blue, negative correlation $p < 0.05$; Magenta, positive correlation $p < 0.05$; black, non-significant correlation. Over Representation Analysis (ORA) of plasma metabolites that were associated with CGC⁺ T cells was performed using MetaboAnalyst 5.0 with the hypergeometric test. One-tailed adjusted p values are provided after correcting for multiple comparisons.

memory subsets (Figures 11A, C). We found that unstimulated CD4⁺ memory (TCM, TEM, TEMRA, and CGC⁺) T cell subsets were predominantly mitochondrial-dependent (Figure 11B). CD4⁺ naïve T cells had higher mitochondrial dependence compared to CD4⁺ TEM ($p=0.006$). Although not significant, CGC⁺ CD4⁺ T cells had lower mitochondrial dependence and higher glycolytic capacity when compared to CD4⁺ naïve T cells ($p=0.05$) (Figure 11B). CD8⁺ T cell memory subsets also had higher mitochondrial dependence. However, CD8⁺ TEM ($p=0.02$) and TEMRA ($p=0.01$) cells showed significantly higher glycolytic dependence than central memory CD8⁺ T cells (TCM) (Figure 11D). Unstimulated CGC⁺ CD8⁺ T cells also had higher glucose dependence than CD8⁺ TCM but this was not significant ($p=0.07$) (Figure 11D). CGC⁺ CD4⁺ T cells that we expanded in culture using CD3/CD28/CD49d did not utilize glycolysis as effectively as non-CGC⁺ T cells (Supplemental

Figures 8A, B). Notably, expanded CGC⁺ CD8⁺ T cells utilized glycolysis more than CGC⁺ CD4⁺ T cells (Supplemental Figure 8C). Taken together, since T cells are known to be bioenergetically flexible and can undergo metabolic reprogramming to utilize the more abundant nutrition sources in the local environment, it is possible that CGC⁺ T cells can meet their bioenergetic demands using abundant nutrient sources other than glucose.

Transcriptionally, unstimulated CGC⁺ CD4⁺ T cells were enriched for cytotoxic RNA transcripts (*GNLY*, *CD244*, *GZMH*, *CTLA4*) and were deficient in transcripts that form the aerobic/mitochondrial electron transport chain [*SDHC* (complex II), *UQCRI0* (complex III), *COX5B* (complex IV)] when compared to non-CGC⁺ CD4⁺ memory T cells (Figure 11E and Supplemental Tables 4, 5). CGC⁺ CD8⁺ T cells, on the other hand, displayed higher *CPT1A* (fatty acid β oxidation), *GRIN1* (glutamate receptor), and

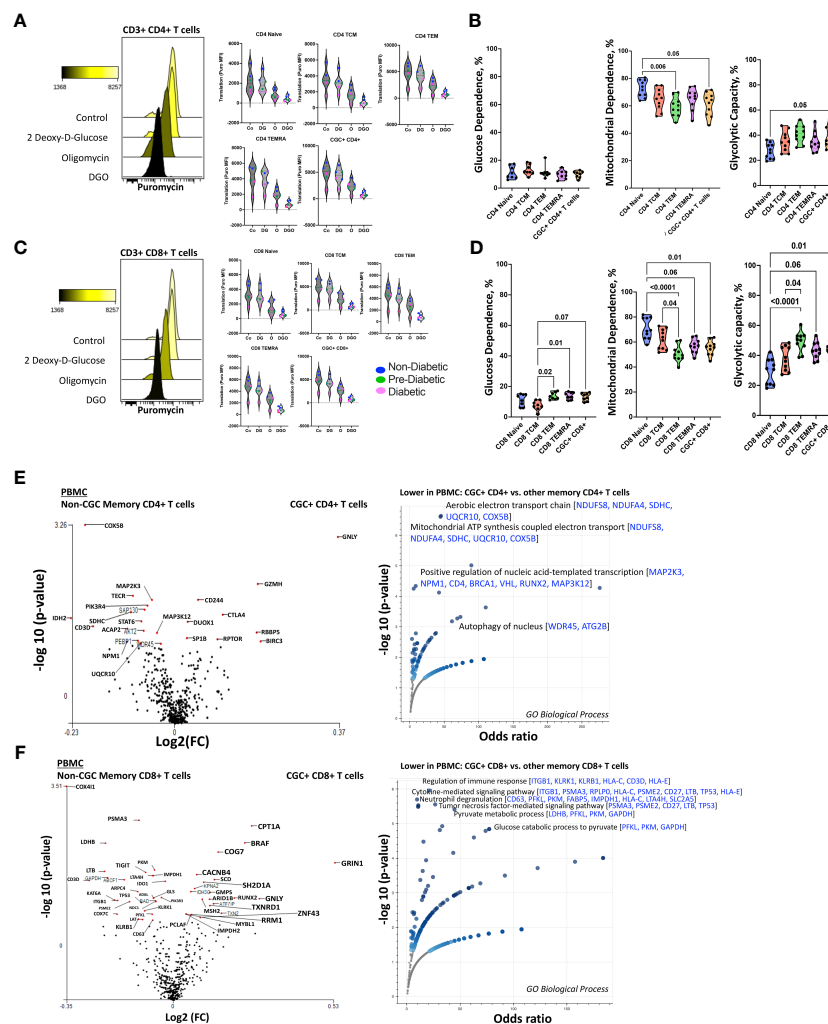


FIGURE 11

Unstimulated CGC⁺ CD4⁺ and CGC⁺ CD8⁺ T cells are dependent on oxidative phosphorylation. Overlapping histograms showing puromycin geometric mean fluorescence in CD4⁺ T cells after treatment with 2 deoxy-d-glucose (2DG), oligomycin (o), 2DG and oligomycin (DGO), and media (Co). Adjacent violin plots show the geometric mean fluorescence (MFI) of puromycin in different memory subsets for the different experimental conditions (Co, DG, O, and DGO groups), and participants by color-coded by diabetes status (A). Truncated violin plots showing the glucose dependence, mitochondrial dependence, and glycolytic capacity in all memory subsets including CGC⁺ CD4⁺ T cells (B). Similar analyses were done with CD8⁺ T cells showing differences in puromycin uptake in all memory subsets (C) and differences in glucose dependence, mitochondrial dependence, and glycolytic capacity (D). Volcano plots show differential gene expression of metabolic genes between CGC⁺ CD4⁺ and non-CGC CD4⁺ T cells (E), and CGC⁺ CD8⁺ and non-CGC CD8⁺ T cells (F). Statistical analysis (B, D) was performed using the Mann-Whitney U test and differential gene expression by the Kruskal-Wallis test. GO Biological Processes (GO) enrichment was performed using Enrichr with multiple comparisons correction (Supplemental Tables S5, S7) (38–40).

lower *COX4I1* and *COX7C* transcripts than non-CGC⁺ CD8⁺ T cells (Figure 11F and Supplemental Tables 6, 7). Some studies have suggested that long-chain fatty acid oxidation modulated by CPT1A is important for CD8⁺ T cell memory development, while knockout studies in mice suggest that CPT1A is dispensable (50).

We performed a direct comparison of CGC⁺ CD4⁺ and CGC⁺ CD8⁺ T cell transcriptomes to try and explain why CGC⁺ CD4⁺ T cells appeared to have a stronger relationship with cardiometabolic disease conditions and risk factors. We found that CGC⁺ CD8⁺ T cells were enriched for genes involved in mitochondrial ATP synthesis coupled electron transport [*SDHC*, *UQCRI0*, *COX5B*] and fatty-acyl-CoA biosynthetic process [*TECR*] (Supplemental Figures 8A–C and Supplemental Table 6). Notably, three genes, *SDHC*, *UQCRI0*, and *COX5B*, were consistently lower in CGC⁺ CD4⁺ T cells as compared to other memory CD4⁺ T cells and CGC⁺ CD8⁺ T cells. While CGC⁺ CD4⁺ T cells had higher expression of several genes including *SLC16A1*, *BCL2*, *BIRC3*, *ICOS*, *CTLA4*, and *IDO1* which enriched several pathways including the pyruvate metabolic process. Taken together, the RNA transcriptomes of both CGC⁺ CD4⁺ and CGC⁺ CD8⁺ T cells show lower expression of transcripts that encode for mitochondrial complexes than non-CGC⁺ T cells. However, a direct comparison between CGC⁺ CD8⁺ and CGC⁺ CD4⁺ T cells suggests differences in bioenergetic sustenance. Notably, CGC⁺ T cells are largely TEM and TEMRA, compared to other memory cells which would include cells that are TCM, TEM, and TEMRA. Differences that may be driven by TCM in the non-CGC⁺ memory T cells have not been accounted for in this analysis.

CGC⁺ T cells express higher levels of carnitine palmitoyl transferase than other memory T cells

Although CGC⁺ CD4⁺ and CGC⁺ CD8⁺ T cells were modestly correlated with fasting blood glucose, we did not find significant differences in glucose dependence compared to other memory T cells. Transcriptional analysis suggested that CGC⁺ CD8⁺ T cells may rely on long-chain fatty acid oxidation mediated by CPT1A. A previous study showed that PD-1 ligation of T cells induced CPT1A expression leading to an increased rate of fatty acid β oxidation (FAO) while limiting glycolysis (51). Some CGC⁺ CD4⁺ T cells and CGC⁺ CD8⁺ T cells express PD-1 (Supplemental Figures 2, 4), and our differential gene expression analysis suggests that CGC⁺ CD8⁺ T cells may use FAO as an energy source. We leveraged a separate cohort of HIV-negative donors that had undergone single-cell metabolic profiling of CD4⁺ and CD8⁺ T cells by mass cytometry (29). In this prior cohort, study, we defined CGC⁺ T cells based on the expression of killer cell lectin-like receptor G1 (KLRG1), and lack of expression of CD27 and CD28 (Figure 12A). Select previously validated metabolic antibodies (29) were used to characterize metabolic proteins/enzymes in CGC⁺ CD4⁺ and CGC⁺ CD8⁺ T cells. These included metabolic proteins involved in fatty acid metabolism (CPT1A), the tricarboxylic acid cycle and the electron transfer chain (ATP synthase (ATP5A)), mitochondrial expression (voltage-dependent ion channel 1 (VDAC1)), glycolysis and fermentation (hexokinase 2 (HK2)), signaling and transcription (ribosomal protein S6, pS6)) and amino

acid metabolism (CD98) (Figure 12B). Of all the metabolic proteins tested, CPT1A expression was higher on CGC⁺ CD4⁺ T cells than all other CD4 subsets (Figure 12C), and when compared to all other non-CGC⁺ CD4⁺ T cells, both CPT1A and CD98 were higher while pS6 was lower (Figure 12D). CGC⁺ CD8⁺ T cells also had higher CPT1A than other CD8⁺ T cell subsets, while pS6 was significantly lower (Figures 12E, F). Taken together, higher levels of CPT1A in both CGC⁺ CD4⁺ and CGC⁺ CD8⁺ T cells implicate FAO as a potential source of energy in CGC⁺ T cells. Lower pS6 compared to other T cells may indicate that CGC⁺ cells have a lower basal level of translation than other memory subsets.

Discussion

In PWH, systemic inflammation remains chronically elevated despite consistent suppression of plasma viremia on ART and reconstitution of total CD4⁺ T cells. CMV co-infection contributes to inflammation by engaging cells from both the innate and adaptive immune arms (52, 53). Importantly, latent CMV infection permanently alters the immune repertoire in aging individuals regardless of their HIV status, inducing a unique T cell response characterized by an increase in TEM and TEMRA cells (9, 54, 55). While doing so, CMV alters the responses to other viruses such as the impaired CD8⁺ T cell response to Epstein Barr virus (11). In PWH, the memory CD4⁺ T cell pool against CMV is significantly inflated, but the exact mechanism is unknown (13, 56). It has been proposed that higher CMV viral replication at the tissue level may be an important driver of this T cell expansion; however, the tissue(s) responsible for the inflation of T cell responses has not been identified (10). To date, we lack a clear mechanism that explains the role of CMV in the pathogenesis of cardiometabolic diseases.

Unlike the innate immune system, cells of the adaptive immune system appear more prone to influence by environmental and physiologic factors (54). To our knowledge, this is the first study to show a correlation between CGC⁺ CD4⁺ T cells and plasma metabolites, including several amino acid and carbohydrate metabolism pathways. Notably, despite the modest relationship between CGC⁺ CD4⁺ T cells and fasting blood glucose or starch metabolites, unstimulated CGC⁺ CD4⁺ T cells exhibited low glucose and high mitochondrial dependence ex-vivo. This was also observed in primary CGC⁺ CD4⁺ T cells expanded ex-vivo. Hence, the relationship between CGC⁺ CD4⁺ T cells and fasting blood glucose does not appear to stem from higher glucose dependence. While circulating CGC⁺ CD8⁺ and CGC⁺ CD4⁺ T cells were strongly correlated, they differed in their relationships with CAC, NAFLD, diabetes, and pericardial fat volume. This suggests that although CGC⁺ CD4⁺ and CGC⁺ CD8⁺ T cells are likely related by their response to CMV antigens, and the circulating proportion of both increases with progressive glucose intolerance, the role or interaction of these cells with the processes contributing to end-organ disease may differ.

CMV-specific T cells can be identified using tetramers, or by the functional expression of inflammatory cytokines after exposure to antigen-presenting cells infected with CMV or pulsed with CMV

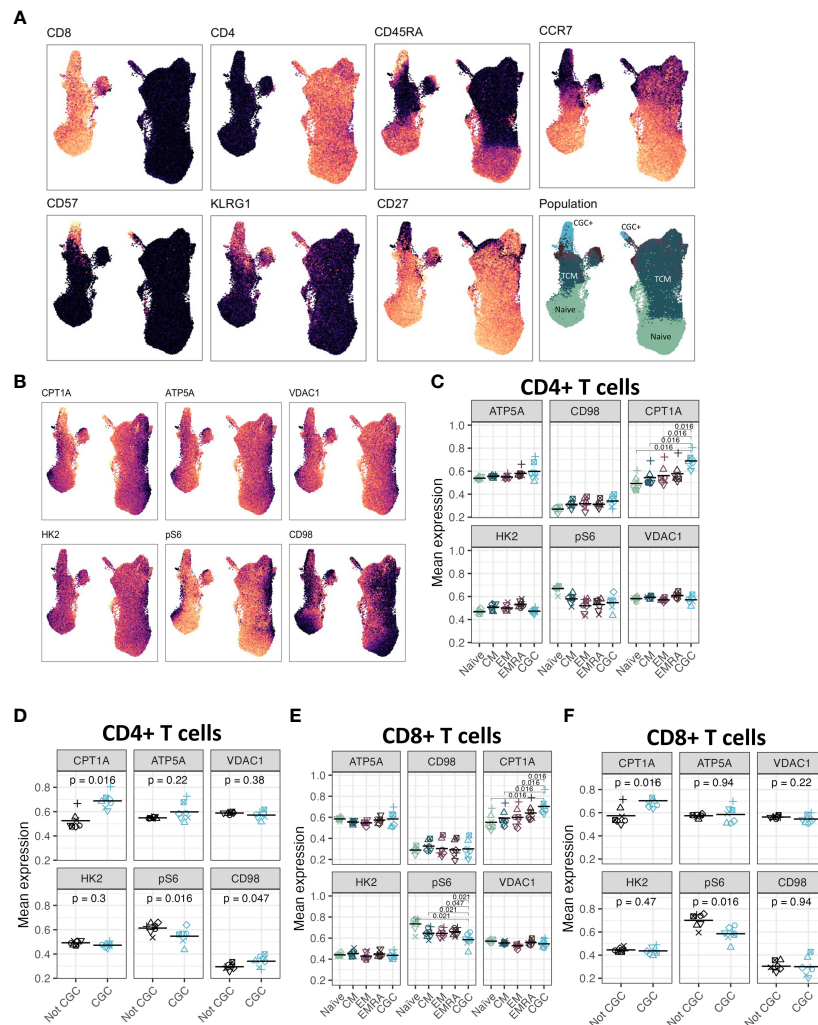


FIGURE 12

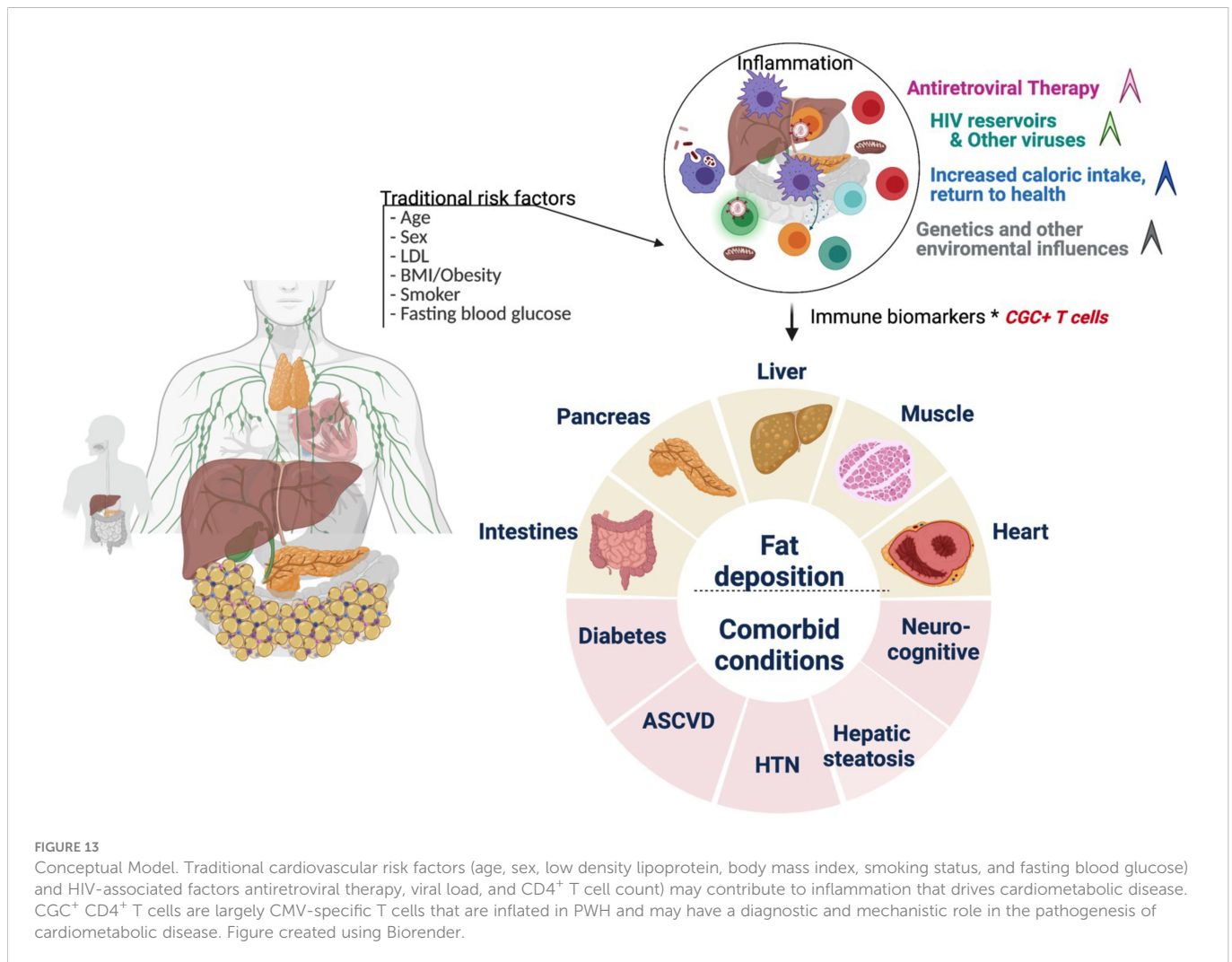
CGC⁺ CD4⁺ T cells have higher expression of carnitine palmitoyl transferase (CPT1A), a rate-limiting enzyme of fatty acid oxidation. UMAPs showing markers used to define the CGC⁺ T cells (CD28⁺ KLRG1⁺ CD27⁺) (A). CPT1A, ATP5A, VDAC1, HK2, pS6, and CD98 expression were measured by mass cytometry (B). Dot plots show the expression of each of the metabolic markers between CD4⁺ naive, central memory (CM), effector memory (EM), TEMRA (EMRA), and CGC T cells (C), as well as a comparison of CGC⁺ CD4⁺ T cells and non-CGC⁺ T cells [every other CD4⁺ T cell] (D). A similar analysis is shown with CD8⁺ T cell subsets (E, F). Statistical analysis (C, E) was performed using pairwise comparisons between the CGC subset and each of the other four populations for each marker, followed by local FDR for multiple hypothesis correction within each marker for the four population comparisons. We only show comparisons with q value < 0.05. Statistical analysis of (D, F) was by paired Wilcoxon signed rank test, with no multiple hypothesis testing.

peptides (13, 57, 58). Other surface marker combinations including CX3CR1, CD57, KLRG1, and a lack of expression of CD28, have also been used to define CD4⁺ and CD8⁺ T cell subsets associated with CMV seropositivity (27, 59–63). However, technical challenges to defining T cell responses to CMV include the size of its genome and HLA restriction of T cell responses. In this study, we showed that CMV-specific T cells in individuals with HIV were predominantly CGC⁺. Further studies are underway to define the breadth of TCRs that are recognized by the CGC⁺ subset of CD4⁺ T cells among PWH and HIV-negative individuals, to further understand the extent to which these cells react to CMV epitopes.

CD4⁺ CD28⁺ T cells are a subset of cytotoxic cells that are increased in autoimmune diseases and with persistent infections such as HIV (64, 65). Specifically, high proportions of CD4⁺ CD28⁺ T cells have been reported in individuals with unstable angina (66),

within unstable plaques (67), and in persons with recurrent coronary events (68). Our group has previously shown that CD4⁺ CD28⁺ T cells are also increased prior to the development of incident diabetes in PWH (45). Although CD4⁺ CD28⁺ T cells are oligoclonal (67), different antigens may stimulate CD4⁺ CD28⁺ T cells including HIV and CMV. However, studies in which treatment of individuals with anti-CMV therapies has reduced the proportion of CD4⁺ CD28⁺ T cells in circulation suggest that targeting the CMV viral burden may be a feasible therapeutic approach (27).

Although our study suggests a role for CGC⁺ CD4⁺ T cells in the pathogenesis of cardiometabolic disease in PWH, the cross-sectional design precludes an assessment of causality. Following longitudinal cohorts to correlate changes between frequencies of CGC⁺ CD4⁺ T cells and cardiometabolic clinical endpoints may define a threshold to



classify a subset of persons in which residual inflammation from CMV is a risk factor for the development of comorbidities. Second, our study did not include matched controls without HIV and with metabolic diseases (non-diabetic, pre-diabetic, and diabetic), which would be necessary to understand whether CGC⁺ CD4⁺ T cells demonstrate a similar role in HIV-negative individuals. Third, the mechanism by which CGC⁺ T cells could alter metabolic health is an area of ongoing investigation. Further studies are underway by our group to understand how CGC⁺ CD4⁺ T cells impact the pathogenesis of cardiometabolic diseases given their cytotoxic capacity, particularly within adipose tissue and vascular structures (17). One intriguing possibility is that these cells could be stimulated by non-viral antigens that mimic CMV epitopes and contribute to the development of metabolic disease. The model figure (Figure 13) summarizes the traditional and HIV-specific risk factors that contribute to ectopic fat distribution and the increased prevalence of cardiometabolic disease in PWH. The role of CGC⁺ cells in cardiometabolic disease risk stratification and its potential role in identifying individuals with a higher risk of developing comorbidities needs to be explored in detail. Eventually, treating CMV or targeting CGC⁺CD4⁺ T cells may provide a target that can improve outcomes in PWH and possibly extend to a subset of individuals in the general population.

Data availability statement

The original contributions presented in the study are included in the article/Supplementary Material. Further inquiries can be directed to the corresponding author.

Ethics statement

The studies involving human participants were reviewed and approved by Vanderbilt University Institutional Review Board. The patients/participants provided their written informed consent to participate in this study.

Author contributions

CNW and JK contributed to the conception of the study. CNW, CG, HF, DG, JO, EN, SK, SM, JK contributed to the design of the study. CG, HF, DG, JS, CMW, JO, RG, SPa, SPr contributed to data collection and analysis. SG, DS, DH, MM, SB, TT, SK, SM, JK contributed to the integration of concepts. CNW performed the statistical analysis. CNW and JK wrote the first draft of the manuscript. All authors contributed to manuscript revision, read, and approved the submitted version.

Funding

National Institutes of Health (NIH) grants R01 DK112262 (JK and CNW), K23 HL156759 (CMW), U19 AI128914 (EN), UM1 AI068618 (EN) and the NIH Tennessee Center for AIDS Research grant P30 AI110527 (SM), Doris Duke CSDA grant 2021193 (CMW), Burroughs Wellcome Fund grant 1021480 (CMW). DG was supported by a Fred Hutchinson Cancer Center Mahan Fellowship and a Cancer Research Institute Irvington Postdoctoral Fellowship.

Conflict of interest

The authors declare that the research was conducted in the absence of any commercial or financial relationships that could be construed as a potential conflict of interest.

References

- Bourgi K, Wanjalla C, Koethe JR. Inflammation and metabolic complications in HIV. *Curr HIV/AIDS Rep* (2018) 15(5):371–81. doi: 10.1007/s11904-018-0411-2
- Hsue PY, Waters DD. HIV Infection and coronary heart disease: Mechanisms and management. *Nat Rev Cardiol* (2019) 16(12):745–59. doi: 10.1038/s41569-019-0219-9
- Armah KA, McGinnis K, Baker J, Gibert C, Butt AA, Bryant KJ, et al. HIV Status, burden of comorbid disease, and biomarkers of inflammation, altered coagulation, and monocyte activation. *Clin Infect Dis* (2012) 55(1):126–36. doi: 10.1093/cid/cis406
- Freiberg MS, Bebu I, Tracy R, So-Armah K, Okulicz J, Ganesan A, et al. D-dimer levels before HIV seroconversion remain elevated even after viral suppression and are associated with an increased risk of non-AIDS events. *PLoS One* (2016) 11(4):e0152588. doi: 10.1371/journal.pone.0152588
- Béténé A, Dooko C, De Wit S, Neuhaus J, Palfreeman A, Pepe R, Pankow JS, et al. Interleukin-6, high sensitivity c-reactive protein, and the development of type 2 diabetes among HIV-positive patients taking antiretroviral therapy. *J Acquir Immune Defic Syndr* (2014) 67(5):538–46. doi: 10.1097/QAI.0000000000000354
- Freiberg MS, Cheng DM, Kraemer KL, Saitz R, Kuller LH, Samet JH. The association between hepatitis c infection and prevalent cardiovascular disease among HIV-infected individuals. *AIDS* (2007) 21(2):193–7. doi: 10.1097/QAD.0b013e3280118a0d
- Ishizaka N, Ishizaka Y, Takahashi E, Tooda E, Hashimoto H, Nagai R, et al. Association between hepatitis c virus seropositivity, carotid-artery plaque, and intima-media thickening. *Lancet* (2002) 359(9301):133–5. doi: 10.1016/S0140-6736(02)07339-7
- Lichtner M, Cicconi P, Vita S, Cozzi-Lepri A, Galli M, Lo Caputo S, et al. Cytomegalovirus coinfection is associated with an increased risk of severe non-AIDS-defining events in a large cohort of HIV-infected patients. *J Infect Dis* (2015) 211(2):178–86. doi: 10.1093/infdis/jiu417
- Wetevrede M, Eilers R, de Melker HE, van Baarle D. Cytomegalovirus persistence and T-cell immunosenescence in people aged fifty and older: A systematic review. *Exp Gerontol* (2016) 77:87–95. doi: 10.1016/j.exger.2016.02.005
- Pachnio A, Ciauriz M, Begum J, Lal N, Zuo J, Beggs A, et al. Cytomegalovirus infection leads to development of high frequencies of cytotoxic virus-specific CD4+ T cells targeted to vascular endothelium. *PLoS Pathog* (2016) 12(9):e0150583. doi: 10.1371/journal.ppat.1005832
- Khan N, Hislop A, Gudgeon N, Cobbold M, Khanna R, Nayak L, et al. Herpesvirus-specific CD8 T cell immunity in old age: Cytomegalovirus impairs the response to a co-released EBV infection. *J Immunol* (2004) 173(12):7481–9. doi: 10.4049/jimmunol.173.12.7481
- Crompton L, Khan N, Khanna R, Nayak L, Moss PA. CD4+ T cells specific for glycoprotein b from cytomegalovirus exhibit extreme conservation of T-cell receptor usage between different individuals. *Blood* (2008) 111(4):2053–61. doi: 10.1182/blood-2007-04-079863
- Abana CO, Pilkinton MA, Gaudieri S, Chopra A, McDonnell WJ, Wanjalla C, et al. Cytomegalovirus (CMV) epitope-specific CD4(+) T cells are inflated in HIV(+) CMV(+) subjects. *J Immunol* (2017) 199(9):3187–201. doi: 10.4049/jimmunol.1700851
- Bate SL, Dollard SC, Cannon MJ. Cytomegalovirus seroprevalence in the united states: the national health and nutrition examination surveys, 1988–2004. *Clin Infect Dis* (2010) 50(11):1439–47. doi: 10.1086/652438
- Parry HM, Zuo J, Frumento G, Mirajkar N, Inman C, Edwards E, et al. Cytomegalovirus viral load within blood increases markedly in healthy people over the age of 70 years. *Immun Ageing* (2016) 13:1. doi: 10.1186/s12979-015-0056-6
- Contreras NA, Sitnik KM, Jettif I, Copen CP, Čičin-Šain L, Nikolic-Žugich J. Life-long control of cytomegalovirus (CMV) by T resident memory cells in the adipose

Publisher's note

All claims expressed in this article are solely those of the authors and do not necessarily represent those of their affiliated organizations, or those of the publisher, the editors and the reviewers. Any product that may be evaluated in this article, or claim that may be made by its manufacturer, is not guaranteed or endorsed by the publisher.

Supplementary material

The Supplementary Material for this article can be found online at: <https://www.frontiersin.org/articles/10.3389/fimmu.2023.1099356/full#supplementary-material>

- tissue results in inflammation and hyperglycemia. *PLoS Pathog* (2019) 15(6):e1007890. doi: 10.1371/journal.ppat.1007890
- Wanjalla CN, McDonnell WJ, Ram R, Chopra A, Gangula R, Leary S, et al. Single-cell analysis shows that adipose tissue of persons with both HIV and diabetes is enriched for clonal, cytotoxic, and CMV-specific CD4+ T cells. *Cell Rep Med* (2021) 2(2):100205. doi: 10.1016/j.xcrm.2021.100205
- Wanjalla CN, Mashayekhi M, Bailin S, Gabriel CL, Meenderink LM, Temu T, et al. Anticytomegalovirus CD4+ T cells are associated with subclinical atherosclerosis in persons with HIV. *Arterioscler Thromb Vasc Biol* (2021) 41(4):1459–73. doi: 10.1161/ATVBAHA.120.315786
- Yen YF, Jen I, Chen M, Chuang PH, Liu YL, Sharp GB, et al. Association of cytomegalovirus end-organ disease with stroke in people living with HIV/AIDS: A nationwide population-based cohort study. *PLoS One* (2016) 11(3):e0151684. doi: 10.1371/journal.pone.0151684
- Sorlie PD, Adam E, Melnick SL, Folsom A, Skelton T, Chambless LE, et al. Cytomegalovirus/herpesvirus and carotid atherosclerosis: the ARIC study. *J Med Virol* (1994) 42(1):33–7. doi: 10.1002/jmv.1890420107
- Nieto FJ, Adam E, Sorlie P, Farzadegan H, Melnick JL, Comstock GW, et al. Cohort study of cytomegalovirus infection as a risk factor for carotid intimal-medial thickening, a measure of subclinical atherosclerosis. *Circulation* (1996) 94(5):922–7. doi: 10.1161/01.CIR.94.5.922
- Smieja M, Gnarpe J, Lonn E, Gnarpe H, Olsson G, Yi Q, et al. Multiple infections and subsequent cardiovascular events in the heart outcomes prevention evaluation (HOPE) study. *Circulation* (2003) 107(2):251–7. doi: 10.1161/01.cir.0000044940.65226.1f
- Spyridopoulos I, Martin-Ruiz C, Hilken S, Yadegarfar ME, Isaacs J, Jagger C, et al. CMV seropositivity and T-cell senescence predict increased cardiovascular mortality in octogenarians: Results from the Newcastle 85+ study. *Aging Cell* (2016) 15(2):389–92. doi: 10.1111/acer.12430
- Solana R, Tarazona R, Aiello AE, Akbar AN, Appay V, Beswick M, et al. CMV and immunosenescence: from basics to clinics. *Immun Ageing* (2012) 9(1):23. doi: 10.1186/1742-4933-9-23
- Chen S, Pawelec G, Trompet S, Goldeck D, Mortensen LH, Slagboom PE, et al. Associations of cytomegalovirus infection with all-cause and cardiovascular mortality in multiple observational cohort studies of older adults. *J Infect Dis* (2021) 223(2):238–46. doi: 10.1093/infdis/jiaa480
- Wanjalla CN, McDonnell WJ, Barnett L, Simmons JD, Furch BD, Lima MC, et al. Adipose tissue in persons with HIV is enriched for CD4. *Front Immunol* (2019) 10:408. doi: 10.3389/fimmu.2019.00408
- Chanouzas D, Sagmeister M, Faustini S, Nightingale P, Richter A, Ferro CJ, et al. Subclinical reactivation of cytomegalovirus drives CD4+CD28null T-cell expansion and impaired immune response to pneumococcal vaccination in antineutrophil cytoplasmic antibody-associated vasculitis. *J Infect Dis* (2019) 219(2):234–44. doi: 10.1093/infdis/jiy493
- Hunt PW, Martin JN, Sinclair E, Epling L, Teague J, Jacobson MA, et al. Valganciclovir reduces T cell activation in HIV-infected individuals with incomplete CD4+ T cell recovery on antiretroviral therapy. *J Infect Dis* (2011) 203(10):1474–83. doi: 10.1093/infdis/jir060
- Hartmann FJ, Mrdjen D, McCaffrey E, Glass DR, Greenwald NF, Bharadwaj A, et al. Single-cell metabolic profiling of human cytotoxic T cells. *Nat Biotechnol* (2021) 39(2):186–97. doi: 10.1038/s41587-020-0651-8
- Gabriel CL, Ye F, Fan R, Nair S, Terry JG, Carr JJ, et al. Hepatic steatosis and ectopic fat are associated with differences in subcutaneous adipose tissue gene expression in people with HIV. *Hepatol Commun* (2021) 5(7):1224–37. doi: 10.1002/hep4.1695

31. Kotecha N, Krutzik PO, Irish JM. Web-based analysis and publication of flow cytometry experiments. *Curr Protoc Cytom* (2010) Chapter 10:Unit10.17. doi: 10.1002/0471142956.cy1017s53
32. Hartmann FJ, Simonds EF, Bendall SC. A universal live cell barcoding-platform for multiplexed human single cell analysis. *Sci Rep* (2018) 8(1):10770. doi: 10.1038/s41598-018-28791-2
33. Jaitin DA, Kenigsberg E, Keren-Shaul H, Elefant N, Paul F, Zaretsky I, et al. Massively parallel single-cell RNA-seq for marker-free decomposition of tissues into cell types. *Science* (2014) 343(6172):776–9. doi: 10.1126/science.1247651
34. Picelli S, Faridani OR, Björklund AK, Winberg G, Sagasser S, Sandberg R. Full-length RNA-seq from single cells using smart-seq2. *Nat Protoc* (2014) 9(1):171–81. doi: 10.1038/nprot.2014.006
35. Wanjalla CN, Temu TM, Mashayekhi M, Warren CM, Shepherd BE, Gangula R, et al. Interleukin-17A is associated with flow-mediated dilation and interleukin-4 with carotid plaque in persons with HIV. *Aids* (2022) 36(7):963–73. doi: 10.1097/qad.0000000000003196
36. Argüello RJ, Combes AJ, Char R, Gigan JP, Baaziz AI, Bousiquot E, et al. SCENITH: A flow cytometry-based method to functionally profile energy metabolism with single-cell resolution. *Cell Metab* (2020) 32(6):1063–75.e7. doi: 10.1016/j.cmet.2020.11.007
37. Hertzman RJ, Deshpande P, Leary S, Li Y, Ram R, Chopra A, et al. Visual genomics analysis studio as a tool to analyze multiomic data. *Front Genet* (2021) 12:642012. doi: 10.3389/fgene.2021.642012
38. Chen EY, Tan CM, Kou Y, Duan Q, Wang Z, Meirelles GV, et al. Enrichr: interactive and collaborative HTML5 gene set enrichment analysis tool. *BMC Bioinf* (2013) 14:128. doi: 10.1186/1471-2105-14-128
39. Xie Z, Bailey A, Kuleshov MV, Clarke DJB, Evangelista JE, Jenkins SL, et al. Gene set knowledge discovery with enrichr. *Curr Protoc* (2021) 1(3):e90. doi: 10.1002/cpz1.90
40. Kuleshov MV, Jones MR, Rouillard AD, Fernandez NF, Duan Q, Wang Z, et al. Enrichr: a comprehensive gene set enrichment analysis web server 2016 update. *Nucleic Acids Res* (2016) 44(W1):W90–7. doi: 10.1093/nar/gkw377
41. R Core Team. R: A language and environment for statistical computing. R Foundation for Statistical Computing. Vienna, Austria (2021). Available at: <https://www.R-project.org/>.
42. Palmer BE, Blyveis N, Fontenot AP, Wilson CC. Functional and phenotypic characterization of CD57+CD4+ T cells and their association with HIV-1-induced T cell dysfunction. *J Immunol* (2005) 175(12):8415–23. doi: 10.4049/jimmunol.175.12.8415
43. Brenchley JM, Karandikar NJ, Betts MR, Ambrozak DR, Hill BJ, Crotty LE, et al. Expression of CD57 defines replicative senescence and antigen-induced apoptotic death of CD8+ T cells. *Blood* (2003) 101(7):2711–20. doi: 10.1182/blood-2002-07-2103
44. Yi HS, Kim SY, Kim JT, Lee YS, Moon JS, Kim M, et al. T-Cell senescence contributes to abnormal glucose homeostasis in humans and mice. *Cell Death Dis* (2019) 10(3):249. doi: 10.1038/s41419-019-1494-4
45. Bailin SS, Kundu S, Wellons M, Freiberg MS, Doyle MF, Tracy RP, et al. Circulating CD4+ TEMRA and CD4+ CD28- T cells and incident diabetes among persons with and without HIV. *Aids* (2022) 36(4):501–11. doi: 10.1097/qad.0000000000003137
46. Wang TJ, Larson MG, Vasan RS, Cheng S, Rhee EP, McCabe E, et al. Metabolite profiles and the risk of developing diabetes. *Nat Med* (2011) 17(4):448–53. doi: 10.1038/nm.2307
47. Felig P, Marliss E, Cahill GF Jr. Plasma amino acid levels and insulin secretion in obesity. *N Engl J Med* (1969) 281(15):811–6. doi: 10.1056/nejm196910092811503
48. Würtz P, Havulinna AS, Soininen P, Tyynkynen T, Prieto-Merino D, Tillin T, et al. Metabolite profiling and cardiovascular event risk: A prospective study of 3 population-based cohorts. *Circulation* (2015) 131(9):774–85. doi: 10.1161/circulationaha.114.013116
49. Callender LA, Carroll EC, Bober EA, Akbar AN, Solito E, Henson SM. Mitochondrial mass governs the extent of human T cell senescence. *Aging Cell* (2020) 19(2):e13067. doi: 10.1111/accel.13067
50. Raud B, McGuire PJ, Jones RG, Sparwasser T, Berod L. Fatty acid metabolism in CD8. *Immunol Rev* (2018) 283(1):213–31. doi: 10.1111/imr.12655
51. Patoukian N, Bardhan K, Chatterjee P, Sari D, Liu B, Bell LN, et al. PD-1 alters T-cell metabolic reprogramming by inhibiting glycolysis and promoting lipolysis and fatty acid oxidation. *Nat Commun* (2015) 6:6692. doi: 10.1038/ncomms7692
52. Rossini G, Cerboni C, Santoni A, Landini MP, Landolfi S, Gatti D, et al. Interplay between human cytomegalovirus and intrinsic/innate host responses: A complex bidirectional relationship. *Mediators Inflamm* (2012) 2012:607276. doi: 10.1155/2012/607276
53. Jackson SE, Mason GM, Wills MR. Human cytomegalovirus immunity and immune evasion. *Virus Res* (2011) 157(2):151–60. doi: 10.1016/j.virusres.2010.10.031
54. Patin E, Hasan M, Bergstedt J, Rouilly V, Libri V, Urrutia A, et al. Natural variation in the parameters of innate immune cells is preferentially driven by genetic factors. *Nat Immunol* (2018) 19(3):302–14. doi: 10.1038/s41590-018-0049-7
55. Klennerman P, Oxenius A. T Cell responses to cytomegalovirus. *Nat Rev Immunol* (2016) 16(6):367–77. doi: 10.1038/nri.2016.38
56. Naeger DM, Martin JN, Sinclair E, Hunt PW, Bangsberg DR, Hecht F, et al. Cytomegalovirus-specific T cells persist at very high levels during long-term antiretroviral treatment of HIV disease. *PLoS One* (2010) 5(1):e8886. doi: 10.1371/journal.pone.0008886
57. Bitmansour AD, Waldrop SL, Pitcher CJ, Khatamzas E, Kern F, Maino VC, et al. Clonotypic structure of the human CD4+ memory T cell response to cytomegalovirus. *J Immunol* (2001) 167(3):1151–63. doi: 10.4049/jimmunol.167.3.1151
58. Lindau P, Mukherjee R, Gutschow MV, Vignali M, Warren EH, Riddell SR, et al. Cytomegalovirus exposure in the elderly does not reduce CD8 T cell repertoire diversity. *J Immunol* (2019) 202(2):476–83. doi: 10.4049/jimmunol.1800217
59. Chen B, Morris SR, Panigrahi S, Michaelson GM, Wyrick JM, Komissarov AA, et al. Cytomegalovirus coinfection is associated with increased vascular-homing CD57. *J Immunol* (2020) 204(10):2722–33. doi: 10.4049/jimmunol.1900734
60. Siero S, Rothkopf R, Klennerman P. Evolution of diverse antiviral CD8+ T cell populations after murine cytomegalovirus infection. *Eur J Immunol* (2005) 35(4):1113–23. doi: 10.1002/eji.200425534
61. Stone SF, Price P, Khan N, Moss PA, French MA. HIV Patients on antiretroviral therapy have high frequencies of CD8 T cells specific for immediate early protein-1 of cytomegalovirus. *AIDS* (2005) 19(6):555–62. doi: 10.1097/01.aids.0000163931.68907.7e
62. Bano A, Pera A, Almoukayed A, Clarke THS, Kirmani S, Davies KA, et al. CD28null CD4 T-cell expansions in autoimmune disease suggest a link with cytomegalovirus infection. *F1000Res* (2019) 8(F1000 Faculty Rev):327. doi: 10.12688/f1000research.17119.1
63. Bajwa M, Vita S, Vescovini R, Larsen M, Sansoni P, Terrazzini N, et al. CMV-specific T-cell responses at older ages: Broad responses with a Large central memory component may be key to long-term survival. *J Infect Dis* (2017) 215(8):1212–20. doi: 10.1093/infdis/jix080
64. Vallejo AN, Weyand CM, Goronzy JJ. T-Cell senescence: A culprit of immune abnormalities in chronic inflammation and persistent infection. *Trends Mol Med* (2004) 10(3):119–24. doi: 10.1016/j.molmed.2004.01.002
65. Gerli R, Schillaci G, Giordano A, Bocci EB, Bistoni O, Vaudo G, et al. CD4+CD28- T lymphocytes contribute to early atherosclerotic damage in rheumatoid arthritis patients. *Circulation* (2004) 109(22):2744–8. doi: 10.1161/01.cir.0000131450.66017.b3
66. Liuzzo G, Kopecky SL, Frye RL, O'Fallon WM, Maseri A, Goronzy JJ, et al. Perturbation of the T-cell repertoire in patients with unstable angina. *Circulation* (1999) 100(21):2135–9. doi: 10.1161/01.cir.100.21.2135
67. Liuzzo G, Goronzy JJ, Yang H, Kopecky SL, Holmes DR, Frye RL, et al. Monoclonal T-cell proliferation and plaque instability in acute coronary syndromes. *Circulation* (2000) 101(25):2883–8. doi: 10.1161/01.cir.101.25.2883
68. Liuzzo G, Biasucci LM, Trotta G, Brugaletta S, Pinnelli M, Digianuario G, et al. Unusual CD4+CD28null T lymphocytes and recurrence of acute coronary events. *J Am Coll Cardiol* (2007) 50(15):1450–8. doi: 10.1016/j.jacc.2007.06.040



OPEN ACCESS

EDITED BY
Nadine Suffee,
Sorbonne Universités, France

REVIEWED BY
Xuanyou Liu,
University of Missouri, United States
Haifu Li,
University of Southern California,
United States

*CORRESPONDENCE
Hong Sun
✉ sunh@xzhmu.edu.cn
Jie Xiang
✉ 18052268386@163.com

[†]These authors have contributed equally to this work

SPECIALTY SECTION
This article was submitted to
Inflammation,
a section of the journal
Frontiers in Immunology

RECEIVED 15 December 2022
ACCEPTED 27 January 2023
PUBLISHED 15 February 2023

CITATION
Adzika GK, Mprah R, Rizvi R, Adekunle AO, Ndzie Noah ML, Wowui PI, Adzraku SY, Adu-Amankwaah J, Wang F, Lin Y, Fu L, Liu X, Xiang J and Sun H (2023) Occlusion preconditioned mice are resilient to hypobaric hypoxia-induced myocarditis and arrhythmias due to enhanced immunomodulation, metabolic homeostasis, and antioxidants defense. *Front. Immunol.* 14:1124649. doi: 10.3389/fimmu.2023.1124649

COPYRIGHT
© 2023 Adzika, Mprah, Rizvi, Adekunle, Ndzie Noah, Wowui, Adzraku, Adu-Amankwaah, Wang, Lin, Fu, Liu, Xiang and Sun. This is an open-access article distributed under the terms of the [Creative Commons Attribution License \(CC BY\)](#). The use, distribution or reproduction in other forums is permitted, provided the original author(s) and the copyright owner(s) are credited and that the original publication in this journal is cited, in accordance with accepted academic practice. No use, distribution or reproduction is permitted which does not comply with these terms.

Occlusion preconditioned mice are resilient to hypobaric hypoxia-induced myocarditis and arrhythmias due to enhanced immunomodulation, metabolic homeostasis, and antioxidants defense

Gabriel Komla Adzika^{1†}, Richard Mprah^{1†}, Ruqayya Rizvi^{2†}, Adebayo Oluwafemi Adekunle^{1†}, Marie Louise Ndzie Noah^{1†}, Prosper Ivette Wowui¹, Seyram Yao Adzraku³, Joseph Adu-Amankwaah¹, Fengli Wang⁴, Yuwen Lin⁵, Lu Fu¹, Xiaomei Liu⁶, Jie Xiang^{4*} and Hong Sun^{1*}

¹Department of Physiology, Xuzhou Medical University, Xuzhou, Jiangsu, China, ²Department of Clinical Medicine, Xuzhou Medical University, Xuzhou, Jiangsu, China, ³Department of Hematology, Key Laboratory of Bone Marrow Stem Cell, The Affiliated Hospital of Xuzhou Medical University, Xuzhou, China, ⁴Department of Rehabilitation Medicine, The Affiliated Xuzhou Rehabilitation Hospital of Xuzhou Medical University, Xuzhou, Jiangsu, China, ⁵Jiangsu Key Laboratory of New Drug Research and Clinical Pharmacy, Xuzhou Medical University, Xuzhou, Jiangsu, China, ⁶Jiangsu Key Laboratory of Immunity and Metabolism, Department of Pathogen Biology and Immunology and Laboratory of Infection and Immunity, Xuzhou Medical University, Xuzhou, Jiangsu, China

Background: Sea-level residents experience altitude sickness when they hike or visit altitudes above ~2,500 m due to the hypobaric hypoxia (HH) conditions at such places. HH has been shown to drive cardiac inflammation in both ventricles by inducing maladaptive metabolic reprogramming of macrophages, which evokes aggravated proinflammatory responses, promoting myocarditis, fibrotic remodeling, arrhythmias, heart failure, and sudden deaths. The use of salidroside or altitude preconditioning (AP) before visiting high altitudes has been extensively shown to exert cardioprotective effects. Even so, both therapeutic interventions have geographical limitations and/or are inaccessible/unavailable to the majority of the population as drawbacks. Meanwhile, occlusion preconditioning (OP) has been extensively demonstrated to prevent hypoxia-induced cardiomyocyte damage by triggering endogenous cardioprotective cascades to mitigate myocardial damage. Herein, with the notion that OP can be conveniently applied anywhere, we sought to explore it as an alternative therapeutic intervention for preventing HH-induced myocarditis, remodeling, and arrhythmias.

Methods: OP intervention (6 cycles of 5 min occlusion with 200 mmHg for 5 min and 5 min reperfusion at 0 mmHg – applying to alternate hindlimb daily for 7 consecutive days) was performed, and its impact on cardiac electric activity, immunoregulation, myocardial remodeling, metabolic homeostasis, oxidative stress responses, and behavioral outcomes were assessed before and after

exposure to HH in mice. In humans, before and after the application of OP intervention (6 cycles of 5 min occlusion with 130% of systolic pressure and 5 min reperfusion at 0 mmHg – applying to alternate upper limb daily for 6 consecutive days), all subjects were assessed by cardiopulmonary exercise testing (CPET).

Results: Comparing the outcomes of OP to AP intervention, we observed that similar to the latter, OP preserved cardiac electric activity, mitigated maladaptive myocardial remodeling, induced adaptive immunomodulation and metabolic homeostasis in the heart, enhanced antioxidant defenses, and conferred resistance against HH-induced anxiety-related behavior. Additionally, OP enhanced respiratory and oxygen-carrying capacity, metabolic homeostasis, and endurance in humans.

Conclusions: Overall, these findings demonstrate that OP is a potent alternative therapeutic intervention for preventing hypoxia-induced myocarditis, cardiac remodeling, arrhythmias, and cardiometabolic disorders and could potentially ameliorate the progression of other inflammatory, metabolic, and oxidative stress-related diseases.

KEYWORDS

hypobaric hypoxia, myocarditis, myocardial remodeling, arrhythmias, remote ischemic preconditioning, immunomodulation, metabolic homeostasis, antioxidant responses

Introduction

Sea-level residents suffer from altitude sickness when they hike or visit altitudes above ~2,500 m due to the hypobaric hypoxia (HH) conditions at such places. Altitude sickness typically presents clinical manifestations such as shortness of breath, headache, dizziness, tiredness, mental confusion, and loss of appetite (1). Meanwhile, recent studies have shown that besides the aforementioned symptoms, individuals experiencing altitude sickness have underlying myocarditis and arrhythmias that were either induced or aggravated by HH (2, 3). Evidently, HH has been shown to drive cardiac inflammation in both ventricles by inducing maladaptive metabolic reprogramming of macrophages which evokes hypersecretion of the proinflammatory mediator – inducible nitric oxide synthase (iNOS) and cytokines (C-Reactive Proteins, Interleukin (IL)-1 β and IL-18). HH-induced hyperactive proinflammatory responses expedite adverse cardiac remodeling by activating and sustaining fibrosis cascades, ultimately resulting in heart failure and sudden cardiac death (4, 5).

Therapeutic approaches developed against altitude sickness over the years have mainly been preventive interventions targeted at circumventing or mitigating the adverse outcomes of HH exposure. Notably, the use of salidroside (a phenylethanoid glycoside found in *Rhodiola* genus plants) and altitude preconditioning (AP) (as known as intermittent HH preconditioning) prior to visiting high altitudes have been extensively shown to exert cardioprotective effects (6, 7). The efficacies of salidroside and AP interventions have been attributed to their abilities to decrease reactive oxygen species

(ROS), induce adaptive regulation of antioxidants and anti-inflammatory-related pathways as well as enhance tissue oxygenation to prevent necrosis and apoptosis of cardiomyocytes (6–9). However, the availability of *Rhodiola* plants or salidroside is geographically limited to Europe, North America, and low-Arctic to high-temperature regions of Asia (10). Similarly, hypoxia chambers for AP are inaccessible/unavailable to the majority of the population, and the intervention cannot be applied at one's convenience before hiking or visiting high altitudes.

Meanwhile, remote ischemic preconditioning [hereafter referred to as occlusion preconditioning (OP)] has been extensively demonstrated to prevent hypoxia-induced cardiomyocyte damage by triggering endogenous cardioprotective cascade (11–13). These generally positive outcomes of OP have encouraged its application in clinical trials and settings to reduce the severity of ischemic injuries and myocardial damage, even though the underlying mechanisms of the intervention are still being elucidated.

Here, with the notion that OP can be conveniently applied anywhere, we sought to explore it as an alternative therapeutic intervention for preventing HH-induced myocarditis and cardiac arrhythmia. Herein, we demonstrate the cardioprotective potentials of OP in HH by comparing its impact on cardiac electric activity, hypertrophy and injury, immunoregulation, oxidative stress responses, and behavioral outcomes, with AP's in HH. Also, we showed that OP enhances respiratory and oxygen-carrying capacity in humans. In addition, numerous studies have shown that the β_2 -adrenergic receptor (β_2 AR) confers cardioprotection in stressful conditions, including hypoxia (14, 15). Hence, we utilized β_2 AR-

knockout (β_2 AR-KO) mice and uncovered that β_2 AR is involved in mediating OP-induced cardioprotection in HH. These findings illustrate OP as a potent alternative therapeutic intervention for preventing hypoxia-induced myocarditis and as well suggest its potential to ameliorate other oxidative stress-related diseases.

Methods

Experimental animal model protocols

Eight- to twelve-week-old wild-type (*Adrb2*^{+/+}) and β_2 AR-knockout (*Adrb2*^{-/-}) FVB male mice were used in this study. The mice were kept and fed in a hypoxia chamber (Guizhou Fenglei Aviation Machinery Co., Ltd., Guizhou, China: FLYDWC50-IIA), and hypobaric hypoxia (HH) was induced by increasing altitude to 3000 m for 10 min, then to 4500 m for 10 min, followed by 5500 m for 20 min before finally increasing to 6000 m altitude for 7 days. Mice in the control group were kept and fed in a normobaric normoxia (NN) environment at sea level (with ambient oxygen percentage) for 7 days.

To explore the therapeutic potentials of limb occlusion ischemic preconditioning, hair was removed from mice's hindlimbs. Limb occlusion preconditioning (OP) was performed by applying a 200 mmHg pressure tourniquet for 5 min and allowing 5 min reperfusion at 0 mmHg. Six cycles of OP were performed daily on alternate hindlimbs for 7 days. Next, the mice were randomized into two groups; the first group, (OP) mice, were sacrificed, and the second group was exposed to HH stepwise as previously described for 7 days. The latter group was designated as OP prior to HH exposure (OPHH) (Supplementary Figure 1A). Additionally, we sought to compare the experimental outcomes from OP and OPHH with altitude preconditioning (AP) prior to HH exposure (APHH) models; hence, AP was done by exposing wild-type FVB to HH at 3500 altitudes for 30 min daily, for 7 days. Afterward, the mice were randomized into two groups; the first group (AP) mice were sacrificed, and the second group (APHH) mice were exposed to HH in a stepwise manner as previously described for 7 days (Supplementary Figure 1B).

At the end of all experimental models, electrocardiography (EKG) data acquisitions were performed with PowerLab (ADInstruments, North America), and the mice were euthanatized by cervical dislocation. Hearts were excised, quickly wet-weighted for morphometric analysis, and processed for further investigations. The performed experiments were approved by the Experimental Animal Centre of Xuzhou Medical University and the Animal Ethics Committee of the Medical University (permit number: xz11-12541) and conform to the Guide for the Care and Use of Laboratory Animals published by the US National Institutes of Health (NIH Publication, 8th Edition, 2011).

Electrocardiography

Electrocardiography (EKG) data acquisitions were performed with the 3-lead monopolar needle electrode from PowerLab systems (ADInstruments, North America), as previously described (16).

Assays

Enzyme-linked immunosorbent assay (ELISA)

Myocardia lysates were used to examine the concentration of proinflammatory (iNOS, IL-1 β , and IL-18) and anti-inflammatory biomarkers (Arg-1, IL-10, and TGF- β) and cardiac hypertrophy/injury markers (ANP and BNP). Sera were used to assess cardiac troponin I (cTnI) and C-reactive protein (CRP) concentrations. IL-1 β (JL18442; Jianglai Bio. Tech.), IL-18 (JL20253; Jianglai Bio. Tech.), iNOS (JL20675; Jianglai Bio. Tech.), IL-10 (JL20242; Jianglai Bio. Tech.), TGF- β (JL13959; Jianglai Bio. Tech.), Arg-1 (JL13668; Jianglai Bio. Tech.), ANP (JL20612; Jianglai Bio. Tech.), BNP (JL12884; Jianglai Bio. Tech.), CRP (JL13196; Jianglai Bio. Tech.) and cTnI (JL31923; Jianglai Bio. Tech.) ELISAs were done in triplicates and as per the manufacturer's instructions.

NAD/NADH content assay

Using equal weights (0.1 g) of myocardia, the coenzyme I NAD/NADH contents were assessed using assay kits (BC0310; Solarbio) and following the manufacturer's instructions.

Total antioxidant capacity assay

Equal weights (0.1 g) of myocardia were used to evaluate the total antioxidant capacity (T-AOC). Assay kits (BC1310; Solarbio) were used according to the manufacturer's instructions.

Behavioral assessments

Open field test (OFT)

Locomotor activity and exploratory and anxiety-related behavior of the mice were examined before and after preconditioning or exposure to HH or NN by using the OFT apparatus. Briefly, the apparatus consists of a squared box (50cm x 50 cm) with its base divided into 9 squares; 1 central (zone C), 4 corners (zone B), and 4 peripheries (zone A). Before the initial and subsequent tests, fecal pellets or urine were cleaned, and the chamber was wiped-dry with 95% ethanol to remove any clues and scent left by the last tested mouse. The mice were individually placed in zone C and left undisturbed to explore for 5 min while their locomotion activities were tracked with video tracking software (ANY-maze version 7.00).

Elevated plus maze (EPM)

Utilizing the EPM apparatus, anxiety-related behaviors were examined before and after preconditioning or exposure to HH or NN. In brief, the EPM consists of a plus (+) shaped apparatus with a central point, two opposite arms enclosed, and the other opposite arms opened. Before the initial and subsequent tests, fecal pellets or urine were cleaned, and the arms were wiped-dry with 95% ethanol to remove any clues and scent left by the last tested mouse. During testing, the plus maze was elevated ~ 1 m from the floor, and each mouse was placed at the central point of the open and closed arms, with their head facing the open arm. The mice were allowed to explore the maze for 5 min while their locomotion activities and entries into either arm were tracked and recorded by video tracking software (ANY-maze version 7.00).

Myocardial macrophage isolations

Mice were euthanized by cervical dislocation; hearts were exposed and perfused-blanch with iced-cold PBS through the right and left ventricle by using a 5 mL syringe and 25 G needle. Hearts were then transferred in 12-well plates containing 1 mg/mL collagenase IV (Gibco™: 17104019) in 3 mL Hanks' Balanced Salt Solution (HBSS) kept on ice and minced with sterile scissors. Minced myocardia were digested for 45 min at 37°C on a shaker (50 rpm). Next, the plates were vortexed, kept on ice, and new Pasteur pipettes were used to dissociate cells mechanically. Obtained suspensions were filtered through 35 µm strainers into 15 ml tubes containing 10 ml cold HBSS, centrifuged at 1500 rpm for 5 min, and the supernatants were discarded. Red blood cells in the pellet were hemolyzed with ACK buffer (Gibco™: A1049201) and washed twice with PBS. Myocardial macrophage phenotypes were identified and sorted with FACS (BD FACSAria™ III) after resuspension and incubation with Fc Blocker (Invitrogen; 14-9161-73; 1:100), PE-Cy5 anti-CD45 (BD Pharmingen™; 553082; 1:100), APC anti-F4/80 (BioLegend; 123116; 1:100), FITC anti-CD11b (BioLegend; 101206; 1:100), PerCP anti-CD86 (BioLegend; 105028; 1:100) and PE anti-CD206 (BioLegend; 141706; 1:100).

Histology, immunohistochemistry, and biochemical staining

Wheat germ agglutinin (WGA) staining

Cryopreserved heart sections were fixed with 4% formaldehyde for 30 min at room temperature (RT), washed thrice with PBS, and primed with HBSS for 15 min. Next, without permeabilization, the myocardial sections were incubated with WGA staining (Thermo Fisher Scientific; W11261) in the dark for 10 min at RT – followed by three times wash with PBS and DAPI counterstaining. Imaging was done at X60 magnification, and ImageJ (1.52a version; National Institute of Health USA) was used to assess cardiomyocyte surface area.

Masson's trichrome staining

Myocardial sections were trichrome stained according to the manufacturer's (Solarbio; G1340) instructions. Microscopy was done at X40 magnification, and collagen volume fractions (CVF) were analyzed with ImageJ.

Immunohistochemical (IHC) staining

CD86 (Abcam; ab53004; 1:1000) and CD206 (Abcam; ab8918; 1:1000) IHC staining were done as previously described (17), but with few optimizations. Briefly, frozen sections were used; hence, the antigen retrieval step in the described experiment was skipped, and myocardial sections were fixed with 4% formaldehyde for 15 min prior to staining. Infiltrated CD86+ and CD206+ macrophages were observed at X40 magnification and quantified with ImageJ.

Oil Red O (ORO) staining

To investigate the metabolic state of the hearts, lipid depositions in myocardia were assessed by performing ORO staining described by

the manufacturer (Solarbio; G1261). Lipid depositions were observed at X40 magnification and quantified with ImageJ.

Periodic Acid Schiff (PAS) staining

To examine the hearts' metabolic state, glycogen and other polysaccharide contents of the myocardia were assessed by performing PAS staining described by the manufacturer (Solarbio; G1281). PAS-positive areas were observed at X40 magnification and quantified with ImageJ.

Western blot

Hearts were washed with cold PBS, homogenized, and cocktails of RIPA buffer, protease, and phosphatase inhibitor (ratio 100:1:1) were added to extract proteins. Protein sample concentrations were normalized, electrophoresed on 10–12% gels, and transferred onto 0.45 µm PVDF membrane (Millipore Immobilon®-P; IPVH08100). Membranes were blocked with 2% BSA in TBST, and proteins of interest were blotted with the following antibodies: anti-HIF-1α (Proteintech; 20960-1-AP; 1:1000), anti-HIF-2α (Abcam; ab199; 1:1000), anti-Nrf2 (Proteintech; 16396-1-AP; 1:1000), anti-β₂AR (Abcam; ab182136; 1:1000), anti-Scarb3 (Abcam; ab133625; 1:1000), anti-Slc2a1 (Abcam; ab115730; 1:1000), anti-GATA4 (Abcam; ab84593; 1:1000), GAPDH (Proteintech; 10494-1-AP; 1:1000) and HRP-conjugated Goat Anti-Rabbit IgG(H+L) (Proteintech; SA00001-2; 1:1000). Membranes were imaged using enhanced chemiluminescence (Tanon, China).

Quantitative RT-PCR

mRNAs were isolated from myocardial macrophages with TRIzol™ Reagent (Invitrogen™; 15596026), cDNAs synthesized using a reverse transcription kit (FSQ107; Toyobo), and qPCR analysis was conducted by utilizing SYBR Green Master Mix (Q111-02; Vazyme) according to manufacturer instructions. The assessed macrophage metabolic genes (Gcdh, Adcd1, Acaa2, Decr1, Hsd17b4, Hadha, Cpt2, Etfb, Echdc2, Scarb3, mTOR, Slc2a1, Hk2, Ldha, Aldoc, Fbp1, Pgm2, Gpi1, Pgl1, and Pfkfb3) and their respective primer sequences are tabulated here (Supplementary Table 1). GAPDH was utilized as the housekeeping gene, and mRNAs fold changes were computed by the $2^{-\Delta\Delta C_t}$ method.

Cardiopulmonary exercise test in humans

Before and after the application of OP intervention (6 cycles of 5 min occlusion with 130% of systolic pressure and reperfusion at 0 mmHg – alternating upper limb daily for 6 consecutive days), all human subjects were assessed by cardiopulmonary exercise testing (CPET) (Vyaire Medical; Vyntus® CPX) on a bicycle ergometer (Stex Fitness; S25U) using the ramp 10 Watts protocol (10 W increment in workload per 1 min). Data analysis included the following physiological indexes; heart rate (HR), systolic (Psys) and diastolic (Pdia) pressures, expiratory reserve, inhalation and exhalation vital capacities, minute ventilation (V'E), carbon dioxide output (V'CO₂), oxygen uptake (V'O₂), oxygen pulse (V'O₂/HR),

metabolic equivalent of task (MET) and respiratory exchange ratio (RER). Additionally, oxygen saturation (SPO₂) was measured with an ear sensor probe (Integrated NoninTM).

Statistics

All results in this study are presented as mean \pm standard error of the mean. Statistical analyses were done using GraphPad Prism (Software version 8.0.2). Unpaired t-test was used for comparing two groups, one-way ANOVA was used for comparing three or more groups, and two-way ANOVA was used for grouped data statistical analyses. P-values less than 0.05 were deemed statistically significant.

Result

OP preserves cardiac electric activity during hypobaric hypoxia

Electrocardiograms (EKG) of mice post-HH exposure showed overt distortions in their cardiac electric activity (cEA) in comparison with the normobaric normoxia (NN) mice (control group). A detailed look at the EKG parameters revealed HH mice had modest increments in their heart rates (HRs) but with significant prolongations of QT, QTc, JT, and Tpeak-Tend intervals, and ST height, P duration, and R and T amplitudes (Figures 1A–G; Supplementary Table 2). Taken together, the aforementioned EKG alterations indicate that HH mice had severe arrhythmias resulting from chronic exposure to hypoxia. To determine the efficacy of OP's impact on OPHH mice, we employed AP and APHH mice groups for comparison. The EKG data indicated that, similar to AP, OP prevents disruption of cEA with initial slight elevations of HRs and its normalization when exposed to HH. However, we uncovered that OP

preserved cEA better than AP because unlike in OPHH mice – QT, QTc, JT, and Tpeak-Tend intervals, and ST height remained significantly increased in APHH compared to NN mice.

OP mitigates myocardial hypertrophy, injury, and fibrosis during hypobaric hypoxia

Mice exposed to HH without any preconditioning exhibited significant body weight (BW) loss and increased heart weight/body weight ratio (Figures 2A, B), depicting cardiac hypertrophy. Next, cardiomyocyte surface area, atrial natriuretic peptide (ANP), brain natriuretic peptide (BNP), and GATA4 expressions were ascertained to validate the incidence of cardiac hypertrophy (Figures 2C–H). These indexes and biomarkers were substantially increased in HH mice. Also, the extent of ANP, BNP, and GATA4 upregulation in HH heart revealed the incidence of cardiac injury. Compared with HH and APHH mice, OPHH mice showed the least weight loss and moderate increases in the prior mentioned cardiac hypertrophy and cardiac injury indexes. In addition, utilizing trichrome staining, we observed massive fibrosis in HH hearts (Figures 2I, J). Meanwhile, like APHH, OPHH mice had only modest collagen depositions with no significant differences in comparison to the NN mice. These findings indicated that employing the OP intervention before exposure to chronic HH confers cardioprotection by mitigating excessive myocyte hypertrophy, injury, and myocardial fibrosis.

OP induces adaptive immunomodulation and metabolic homeostasis during hypobaric hypoxia

To understand how severe hypoxia affects immunoregulation in the myocardia, we investigated the phenotype of macrophages infiltrating

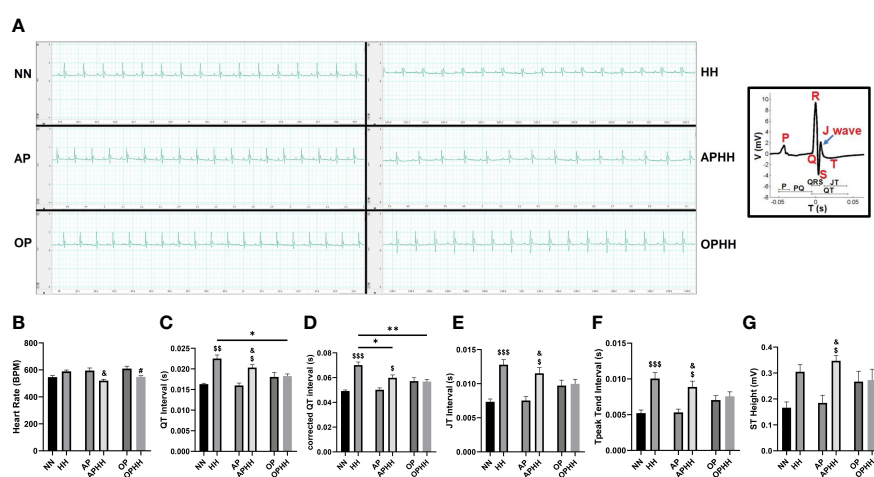


FIGURE 1

OP preserves cardiac electric activity during hypobaric hypoxia. (A) Representative electrocardiography (EKG) of Normobaric Normoxia (NN), Hypobaric Hypoxia (HH), Altitude Preconditioned (AP), Altitude Preconditioned before HH exposure (APHH), Occlusion Preconditioned (OP) and Occlusion Preconditioned before HH exposure (OPHH) mice. P wave: atrial depolarization; Q wave: Interventricular septum depolarization; R wave: Ventricular depolarization; S wave: Purkinje fibres depolarization; J wave: Early ventricular repolarization; T wave: End of ventricular repolarization. (B–G) Graphical presentation of EKG parameters including: Heart Rate (HR), QT Interval, corrected QT Interval (QTc), JT Interval, Tpeak Tend Interval, and ST Height. (n= 5–9 mice per experimental group). [#]p<0.05, ^{SS}p<0.01, ^{SSS}p<0.001 HH vs NN; [&]p<0.05 APHH vs AP; [#]p<0.05 OPHH vs OP; ^{*}p<0.05, ^{**}p<0.01. Data are expressed as mean \pm SEM. Data were analyzed using one-way ANOVA, followed by Tukey's *post hoc* analysis.

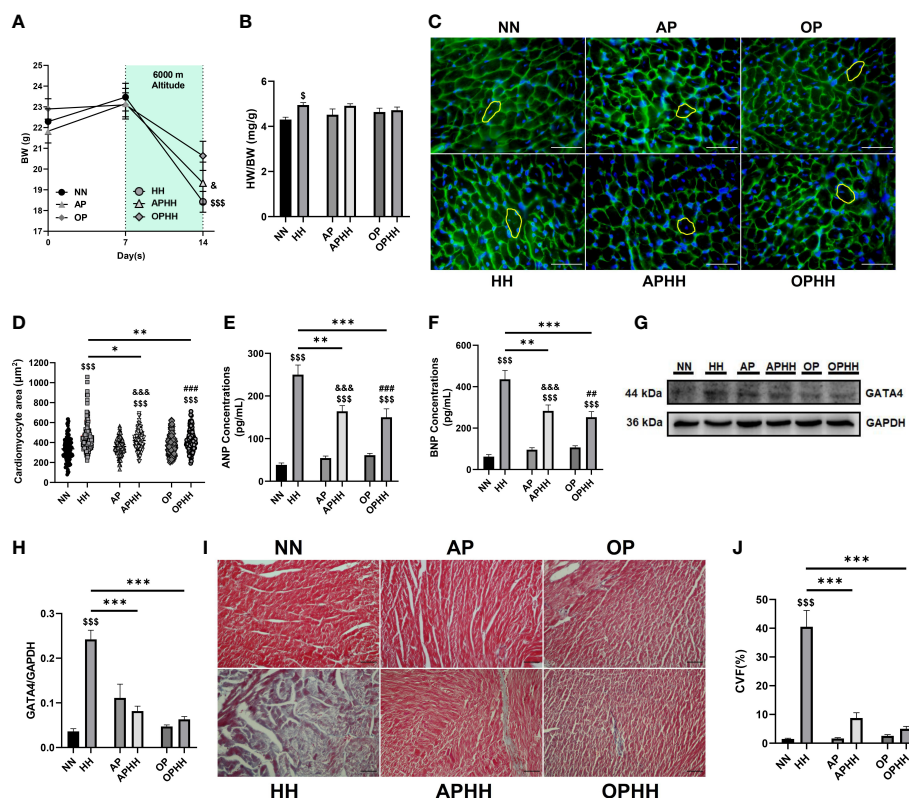


FIGURE 2

OP mitigates myocardial hypertrophy, injury, and fibrosis during hypobaric hypoxia. (A) Graphical representation of Body Weight (BW) trends of 14 days period by Normobaric Normoxia (NN), Hypobaric Hypoxia (HH), Altitude Preconditioned (AP), Altitude Preconditioned before HH exposure (APHH), Occlusion Preconditioned (OP) and Occlusion Preconditioned before HH exposure (OPHH) mice (n= 7-15 mice per experimental group). (B) Graphical presentation of Heart Weight (HW)/BW ratio (n= 5-10 mice per experimental group). (C-H) Indexes for cardiac hypertrophy assessment, including; Representative Wheat germ agglutinin (WGA) staining and Graphical presentation of Cardiomyocyte surface area (n=8-12 cells per section per 4-6 heart per group), Atrial natriuretic peptide (ANP) and Brain natriuretic peptide (BNP) concentrations (n=6-8 hearts per group), Representative Immunoblotting of GATA4 and its Graph plot (n= 3 hearts per group). ELISA were performed in triplicates. Immunoblots were performed in triplicates, and each blot band in the representative blot is an independent biological sample. (I, J) Representative Masson's trichrome staining and Graphical presentation of collagen volume fraction (CVF) showing the extent of fibrosis among experimental groups (n= 3-6 sections per 4,5 hearts per group). ^sp<0.05, ^{sss}p<0.001 HH vs NN; ^sp<0.05, ^{sss}p<0.001 APHH vs AP; ^{##}p<0.01, ^{###}p<0.001 OPHH vs OP; ^{*}p<0.05, ^{**}p<0.01, ^{***}p<0.001. Data are expressed as mean \pm SEM. Data were analyzed using one-way anova, followed by Tukey's *post hoc* analysis.

the heart after chronic exposure to HH. We observed a substantial influx of CD86+ (proinflammatory) macrophages into the myocardial of HH mice, while the CD206+ (anti-inflammatory) populations were repressed (Figures 3A, B; Supplementary Figures 2A-C). Contrarily, CD206+ macrophages outnumbered the CD86+ cells when AP and OP interventions were applied prior to HH exposure. Remarkably, the degree of CD86+ macrophage infiltrations across all the groups corresponded to sera levels of the damage-associated molecular pattern (DAMP) – cardiac troponin I (cTnI) (Figure 3C). Further investigations assessed the concentrations of inflammatory mediators and cytokines in the hearts. The proinflammatory response mediator – iNOS, was overtly upregulated in HH mice but modestly in AP and OP hearts and without any significant alterations in APHH and OPHH hearts; meanwhile, the contrast was observed for the anti-inflammatory mediator, arginase (Arg)-1 (Figures 3D, E). Similarly, we found that proinflammatory cytokines (IL-1 β and IL-18) were significantly upregulated in HH but only moderately in APHH and OPHH mice hearts (Figures 3F, G). Additionally, the systemic inflammatory mark (CRP) was prominently upregulation in HH but not in APHH and OPHH mice (Supplementary Figure 2D). However, like Arg-1, the anti-inflammatory cytokines (IL-10 and TGF- β) secretions were repressed

in HH but modestly increased in APHH and OPHH hearts (Figures 3H, I). These findings demonstrated that just like AP, the OP intervention circumvents HH-induced myocarditis by minimizing cardiomyocyte necrosis and DAMP secretions – ultimately preventing the induction of hyperactive proinflammatory responses.

Furthermore, besides cardiac fibroblast activation, hypoxia-induced glycolysis shift orchestrates immune cells reprogramming toward proinflammatory phenotypes (18–20). Hence, the metabolic states of the infiltrated CD45⁺F4/80⁺CD11b⁺ cells and the entire myocardial were assessed. We observed that lipid metabolism-related gene expressions (Gcdh, Adcd1, Acaa2, Decr1, Hsd17b4, Hadha, Cpt2, Etfb, Echdc2, and Scarb3) in the macrophages isolated from HH hearts were mostly downregulated. In contrast, glycolysis-related genes (Slc2a1, Hk2, Ldha, Aldoc, Fbp1, Pgm2, Gpi1, Pgk1, and Pfkfb3) and the cellular metabolic regulator – mechanistic target of rapamycin (mTOR) mRNA levels were upregulated. Intriguingly, we found only modest downregulation of the lipid metabolism-related genes and slight increases in mRNA levels of the glycolysis-related and mTOR genes in CD45⁺F4/80⁺CD11b⁺ cells obtained from APHH and OPHH hearts (Supplementary Figure 2E). Consistently, Oil red O and PAS staining showed HH mice myocardial had abundant lipid

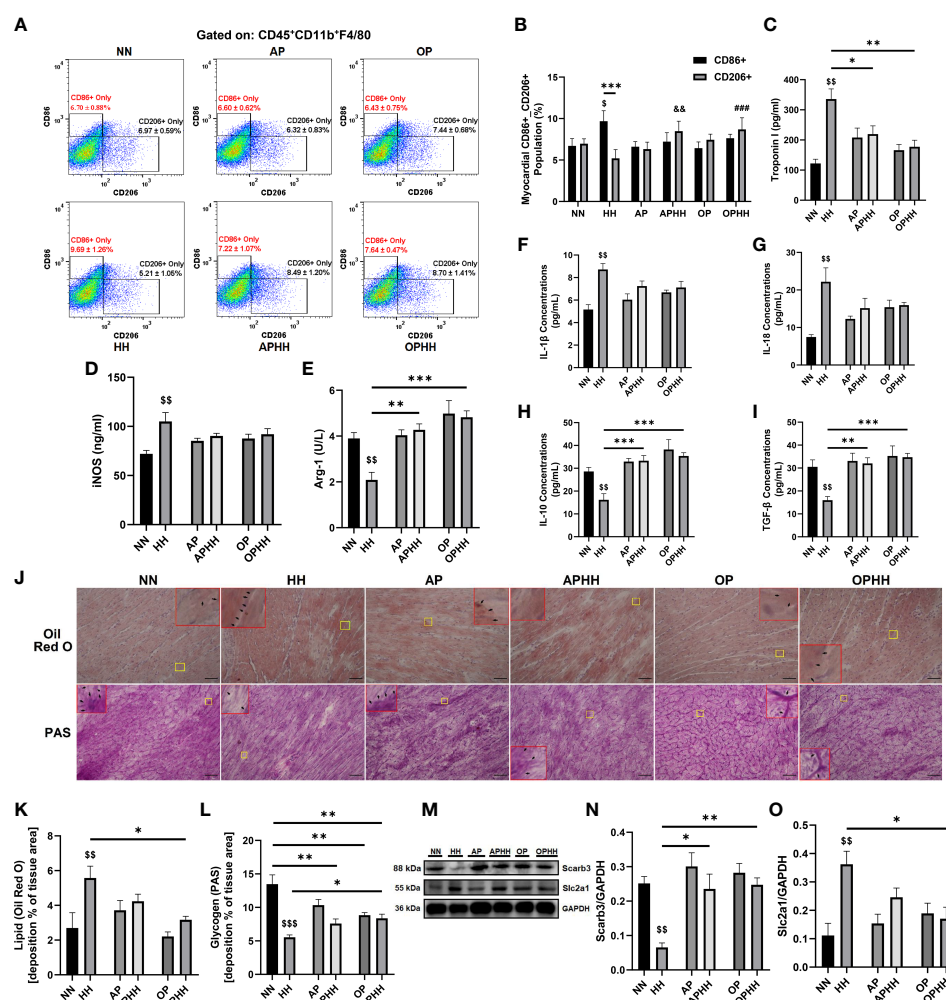


FIGURE 3

OP induces adaptive immunomodulation and metabolic homeostasis during hypobaric hypoxia. (A, B) Representative flow cytometry of myocardial macrophages gated on CD45⁺CD11b⁺F4/80 and Graphical plots of CD86⁺ and CD206⁺. Normobaric Normoxia (NN), Hypobaric Hypoxia (HH), Altitude Preconditioned (AP), Altitude Preconditioned before HH exposure (APHH), Occlusion Preconditioned before HH exposure (OPHH) mice hearts (n=4 hearts per group). $^{\circ}p<0.05$ vs NN_{CD86⁺}; $^{##}p<0.01$, $^{###}p<0.001$ vs HH_{CD206⁺}. (C) Graphical presentation of sera cardiac troponin I (cTnI) concentrations. (D, E) Inflammatory mediators; Inducible nitric oxide synthase (iNOS) and Arginase-1 (Arg-1) concentrations assessed by ELISA using myocardia lysates. (F-I) Inflammatory cytokines; Interleukin (IL)-1β, IL-18, IL-10, and transforming growth factor (TGF)-β concentrations assessed by ELISA using myocardia lysates. All ELISA were performed in triplicates (n= 5-8 mice per group). (J-L) Representative Oil Red O (ORO) and Periodic Acid Schiff (PAS) staining of myocardial sections and their respective graphical presentations showing lipid and glycogen depositions percentages (n=4-6 sections per 4-6 mice per group). Yellow outlined boxes are original myocardial portions and red outline boxes are their zoomed-in (5x) inserts to show positive stained area (indicated with black arrows). (M-O) Representative Immunoblotting of Scarb3 and Slc2a1 and their respective Graphical plots; each blot band in the representative blot is an independent biological sample (n= 3 hearts per group). $^{ss}p<0.01$, $^{sss}p<0.001$ HH vs NN; $^{ss}p<0.01$ APHH vs AP; $^{*}p<0.05$, $^{**}p<0.01$, $^{***}p<0.001$. Data are expressed as mean ± SEM. Data were analyzed using one-way ANOVA, followed by Tukey's *post hoc* analysis.

depositions compared to the NN mice, while glycogen and other polysaccharide contents were substantially depleted. Meanwhile, OPHH mice myocardial revealed a balance constitution of lipid metabolism and glycolysis substrates, as similarly observed in APHH hearts (Figures 3J-L). These phenomena were validated by immunoblotting myocardial protein lysate, which revealed that HH hearts had decreased expression of the fatty acid transporter (Scarb3). In contrast, the glucose transporter protein (Slc2a1) was increased – indicating a glycolysis shift in HH hearts but not entirely in APHH and OPHH hearts (Figures 3M-O). Overall, these findings indicate that the OP intervention exerts immunomodulation by adaptively regulating metabolic shifts to prevent glycolytic reprogramming of macrophages towards proinflammatory phenotypes during HH.

OP induces adaptive modulation of oxidative stress responses

Redox homeostasis (balance between ROS and antioxidants) signaling are major alterations occurring during chronic hypoxia (7). Hence, to elucidate the underlying mechanisms employed by the OP intervention during HH, we investigated its impact on oxidative stress regulators – hypoxia-inducible factors (HIF-1α and HIF-2α) and antioxidant response element-dependent genes regulator, nuclear factor erythroid 2-related factor 2 (Nrf2). Compared to the control group (NN), we observed significant decreases of HIF-1α expression in HH mice hearts and further sharp declines in the protein levels when AP or OP interventions

were applied before HH exposure. Conversely, we observed that HIF-2 α and Nrf2 expressions were reduced substantially in HH but modestly upregulated in APHH and OPHH mice hearts (Figures 4A–D). Nicotinamide adenine dinucleotide (NAD⁺) and NADH ratio are good predictors of the redox homeostasis state (21); as such, NAD⁺ and NADH contents in the heart were assessed. The outcomes demonstrated that AP and OP increased NAD⁺/NADH ratio modestly compared to NN. Secondly, HH hearts had a ~60% decrease in NAD⁺ and ~35% increase in NADH contents, thereby decreasing the NAD⁺/NADH ratio compared with NN, APHH, and OPHH hearts (Figures 4E–G). This indicated increased ROS with deficient antioxidant defenses in HH hearts but not in APHH and OPHH hearts which employed AP and OP interventions, respectively. The total antioxidant capacity assays (T-AOC) performed with myocardial lysates validated the prior statement. T-AOC of HH hearts reduced significantly but remained unaltered in APHH and OPHH, compared to NN hearts (Figure 4H). Thus, similar to AP, the OP intervention reinforces antioxidant responses to confer protection

against hypoxia-induced oxidative stress damage – improving survival rates of OPHH compared to HH mice (Figure 4I).

OPHH mice are resilient to HH-associated maladaptive behavioral outcomes

Since OP intervention prevented myocarditis and distortion of cEA in OPHH mice, we next tested whether it influenced behavioral outcomes. We observed that HH mice exhibited the most dullness among the experimental groups. Utilizing the open field test (OFT) to validate our observation, it was determined that the HH mice had the most decreases in locomotive function – with the least total distance moved, average velocity, and mobile duration compared to NN, APHH, and OPHH mice. Also, HH mice exhibited significant immobile duration in the OFT, but this was not the case for APHH and OPHH mice (Figures 5A–F). Thus, similar to AP in APHH, the OP intervention resulted in only modest reductions of locomotive functions in OPHH mice.

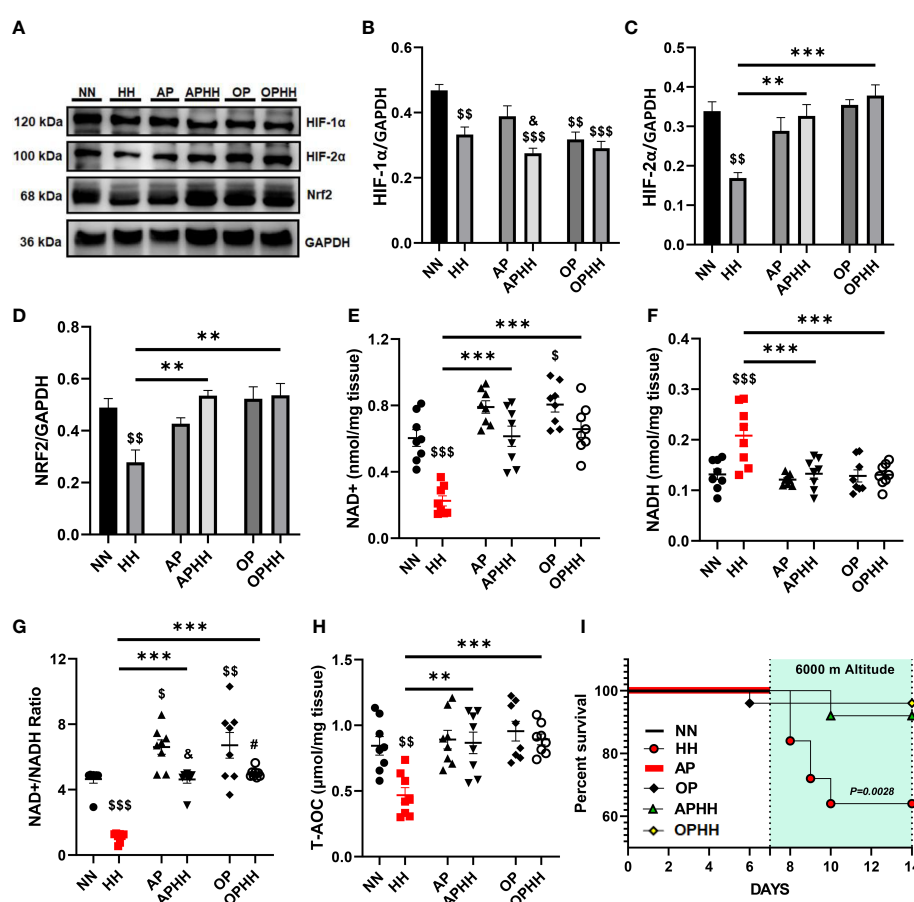


FIGURE 4

OP induces adaptive modulation of oxidative stress responses. (A–D) Representative Immunoblotting of Hypoxia-inducible factors (HIF)-1 α , HIF-2 α , and nuclear factor erythroid 2-related factor 2 (Nrf2), and their respective Graphical plots; each blot band in the representative blot is an independent biological sample ($n = 4$ hearts per group). Normobaric Normoxia (NN), Hypobaric Hypoxia (HH), Altitude Preconditioned (AP), Altitude Preconditioned before HH exposure (APHH), Occlusion Preconditioned (OP), and Occlusion Preconditioned before HH exposure (OPHH) mice hearts. (E–H) Antioxidant state indexes; Graphical plots of the concentrations of redox cofactors, Nicotinamide adenine dinucleotide (NAD)+hydrogen (NADH) and their ratio, as well as the Total antioxidant capacity (T-AOC) of the myocardia ($n = 8$ hearts per group). (I) Graphical plot of survival data in Kaplan-Meier estimator ($n = 18$ mice per group). $^{\$}p < 0.05$, $^{\$\$}p < 0.01$, $^{$$$}p < 0.001$ HH vs NN; $^{\&}p < 0.05$ APHH vs AP; $^{\#}p < 0.05$ OPHH vs OP; $^{*}p < 0.01$, $^{***}p < 0.001$. Data are expressed as mean \pm SEM. Data were analyzed using one-way ANOVA, followed by Tukey's *post hoc* analysis. Survival curves were analyzed with the Kaplan-Meier estimator.

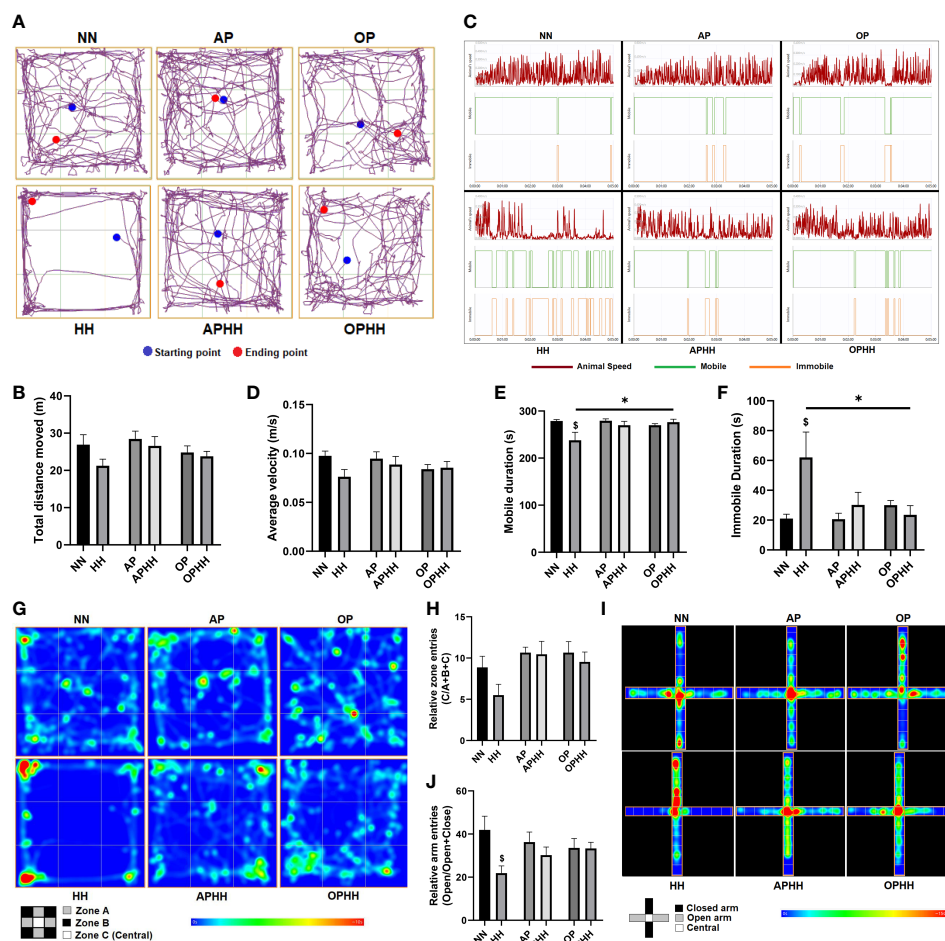


FIGURE 5

OPHH mice are resilient to HH-associated maladaptive behavioral outcomes. (A–H) Locomotive and exploratory behavioral assessment indexes from Open field test (OFT), including; Representative plots of Total distance moved and its graphical presentation, Representative plots of Average velocity, Mobile duration, and Immobile duration, and their graphical presentations and Representative heat-maps of Relative zone entries and its graphical presentation (n=6–10 mice per group). Normobaric Normoxia (NN), Hypobaric Hypoxia (HH), Altitude Preconditioned (AP), Altitude Preconditioned before HH exposure (APHH), Occlusion Preconditioned (OP), and Occlusion Preconditioned before HH exposure (OPHH) mice. (I, J) Anxiety-related and exploratory behavioral assessment indexes from Elevated plus maze (EPM), including; Representative heat-maps of Relative arm entries and its graphical presentation (n=6–10 mice per group). $^{\$}p<0.05$ HH vs NN; $^*p<0.05$. Data are expressed as mean \pm SEM. Data were analyzed using one-way ANOVA, followed by Tukey's *post hoc* analysis.

In addition, most HH mice were observed to restrict their movement to the peripheries (zone A) and corners (zone B) but avoided the central (zone C) of the OFT apparatus, thereby, had the least relative entries into zone C (Figures 5G, H) – a phenomenon shown to depict an increase in anxiety-related behaviors (22). Intriguingly, neither APHH nor OPHH mice exhibited the same exploratory behavior as HH mice, although they were all exposed to chronic hypoxia. The elevated plus maze (EPM) was used to confirm increased anxiety-related behaviors in HH mice. Most HH mice refrained from exploring the EPM apparatus's open arms and mostly limited their movement to within the closed arm; hence, they had the least relative open arm entries (Figures 5I, J). Conversely, APHH and OPHH mice still demonstrated exploratory patterns in both open and closed arms similar to NN and the respective preconditioning groups. Taken together, the findings from OFT and EPM indicated that chronic hypoxia exposure increased susceptibility to developing anxiety-related behavior, as reported previously (22). Meanwhile, like AP to APHH, OP intervention

makes OPHH mice resilient to hypoxia-induced negative behavioral outcomes.

OP enhances respiratory and oxygen-carrying capacity in humans

Still, in attempts to elucidate the underlying mechanism employed by the OP intervention, we assessed its impact on respiratory and oxygen-carrying capacity in humans. Cardiopulmonary exercise tests were performed on the healthy human subjects before (BOP) and after (AOP) the application of OP for 6 consecutive days. We found that HRs and diastolic and systolic blood pressures were slightly decreased in AOP compared to BOP (Figures 6A–C). Also, the inhalation and exhalation vital capacities were increased substantially while expiratory reserve volume elevated modestly in AOP compared to BOP (Figures 6D–F). The changes observed in the aforementioned indexes suggest that OP induces adaptive respiratory

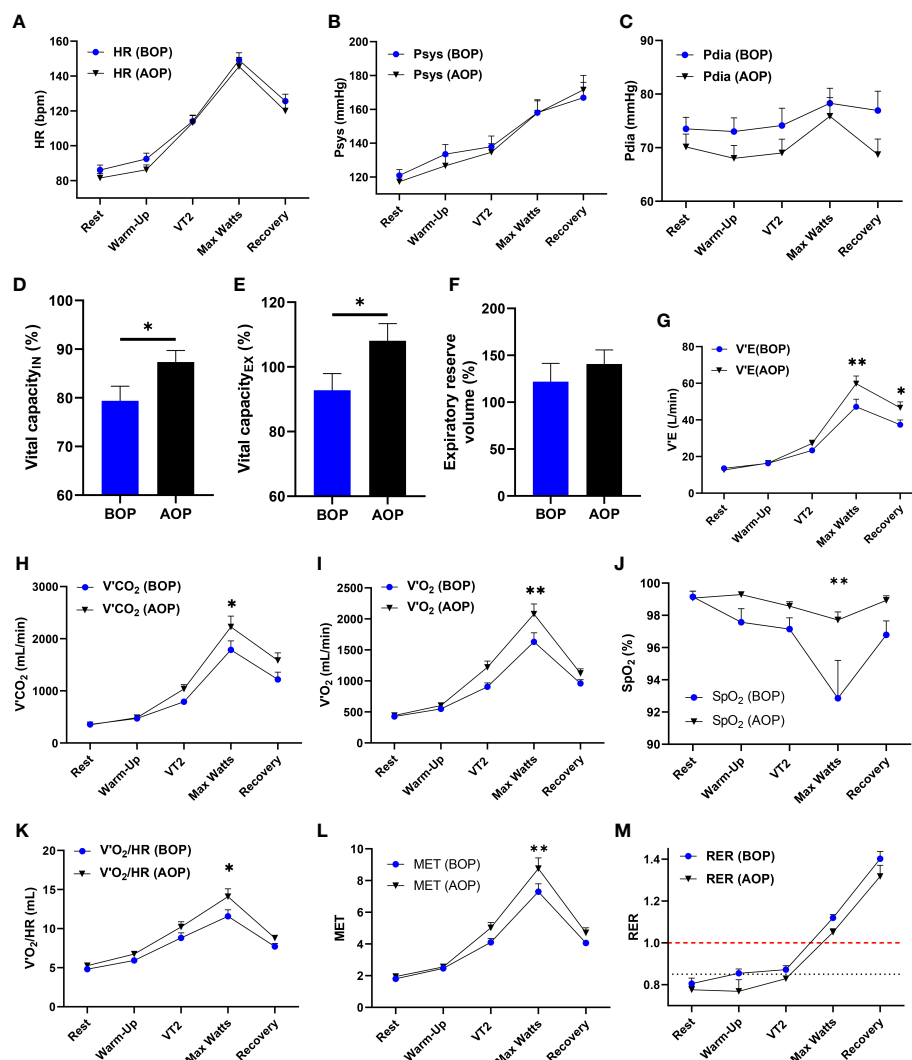


FIGURE 6

OP enhances respiratory and oxygen-carrying capacity in humans. (A–M) Cardiopulmonary Exercise Test (CPET) indexes for respiratory and oxygen carrying capacity in humans (n=14 human volunteers), Before occlusion preconditioning (BOP) and After occlusion preconditioning (AOP), including; Graphical plots of Heart Rates (HR), Systolic blood pressures (Psys), Diastolic blood pressures (Pdia), Vital capacity of inhalation (IN), Vital capacity of exhalation (EX), Expiratory reserve volume, Minute ventilation (V'E), Carbon dioxide output (V'CO₂), Oxygen uptake (V'O₂), Oxygen saturation (SpO₂), Oxygen pulse (V'O₂/HR), Metabolic equivalent of task (MET) and Respiratory exchange ratio (RER). Rest, Warm-up, Second ventilation threshold (VT2), Maximal workload (Max Watts) and Recovery are timepoints of interest during the CPET. *p<0.05, **p<0.01 AOP vs BOP. Data are expressed as mean ± SEM. Data were analyzed using an unpaired t-test for comparing two groups and two-way ANOVA for grouped analysis.

response and lowers the risk of pulmonary injuries and complications. Additionally, we found that after performing OP, minute ventilation (V'E), carbon dioxide output (V'CO₂), oxygen uptake (V'O₂), oxygen saturation (SpO₂), oxygen pulse (V'O₂/HR), and the metabolic equivalent of task (MET) were all significantly improved during the maximal workload (Max Watts) phase of exercising with the cycle ergometer (Figures 6G–L). Thus, OP enhanced the oxygen-carrying capacity and endurance in humans – an adaptation shown to mitigate the deleterious effects of severe hypoxia (23). Lastly, we observed that in AOP, the respiratory exchange ratio (RER) was lowered and took more time to reach ≥1.00 compared to BOP (Figure 6M). Consolidating our observation in the mice myocardia and macrophages, the lowered RER in AOP showed that OP induces mechanisms that mitigate the extent of metabolic shift to glycolysis.

β₂AR is implicated in OP-induced adaptive responses against hypobaric hypoxia

The pleiotropic nature of β₂AR makes it an essential mediator for most adaptive responses to stressful conditions in the heart and immunoregulation (14). Concordant with previous reports, we found β₂AR overexpressed in HH compared to NN (24). Meanwhile, AP, APHH, OP, and OPHH hearts had modest upregulation of β₂AR (Supplementary Figure 3A, B). By utilizing β₂AR knockout (Adrb2^{-/-}) mice, we explored the β₂AR's involvement in HH-induced myocarditis and arrhythmias and OP-induced cardioprotective against HH. Consistently, the OP intervention prevented significant body weight loss due to hypoxia in the OPHH_{Adrb2+/+} mice; however, the contrast was observed in the OPHH_{Adrb2-/-} mice (Figure 7A). While the HRs remained similar in

FIGURE 7
 β_2 AR is implicated in OP-induced adaptive responses against hypobaric hypoxia **(A)** Graphical presentation of Body weight (BW) alteration trends among Wild type ($Adrb2^{+/+}$) and β_2 AR knockout ($Adrb2^{-/-}$) mice in experiment groups; Normobaric Normoxia (NN), Hypobaric Hypoxia (HH), Altitude Preconditioned (AP), Altitude Preconditioned before HH exposure (APHH), Occlusion Preconditioned (OP) and Occlusion Preconditioned before HH exposure (OPHH) (n=5-15 mice per group). **(B-D)** Graphical presentation of electrocardiogram (EKG) indexes, including; Heart Rate, QT Interval, and JT interval (n=5-9 mice per group). **(E-G)** Inflammatory biomarker; C-reactive protein, Inducible nitric oxide synthase (iNOS), and Arginase-1 (Arg-1) concentrations assessed by ELISA. Assays were performed in triplicates (n=4 mice per group). **(H-K)** Representative Immunoblotting of Hypoxia-inducible factors (HIF)-1 α , HIF-2 α , and nuclear factor erythroid 2-related factor 2 (Nrf2), and their respective Graphical plots; each blot band in the representative blot is an independent biological sample (n= 3 hearts per group). **(L)** Graphical plots of the concentrations of Total antioxidant capacity (T-AOC) of myocardia (n=4 hearts per group). ^Sp<0.05, ^{SS}p<0.01, ^{SSS}p<0.001 vs NN_{Adrb2+/+}; ^Pp<0.05, ^{PP}p<0.01, ^{PPP}p<0.001 vs HH_{Adrb2+/+}; ^{##}p<0.01 vs OP_{Adrb2+/+}; ^{*}p<0.05, ^{YY}p<0.01, ^{YYY}p<0.001 vs OPHH_{Adrb2+/+}; ^{!!!}p<0.001 vs NN_{Adrb2-/-}; [%]p<0.001 vs HH_{Adrb2-/-}; [£]p<0.05, ^{££}p<0.01, ^{£££}p<0.001 vs OP_{Adrb2-/-}. Data are expressed as mean \pm SEM. Data were analyzed using two-way ANOVA.

arrhythmia, and ultimately heart failure due to adverse cardiac remodeling has made clinicians to advised those prone to cardiovascular complications and physiologically unprepared individuals against visiting high altitudes (25–27). Studies over the years have made attempts at elucidating the underlying pathomechanisms of altitude sickness and have generally demonstrated that the clinical manifestations observed are due to HH-induced maladaptive oxidative stress responses (imbalance between ROS and antioxidants), metabolic dysregulation and dampened anti-inflammatory defenses (7, 28, 29). Currently, AP and salidroside are the primary preventive therapeutic interventions being employed to circumvent or mitigate the adverse effects of HH exposure. Even so, inaccessibility to hypoxic chambers and unavailability of salidroside due to geographical limitations are the respective drawbacks of these interventions. Our study aimed to explore OP – which is potent in preventing hypoxia-induced damages (11–13), as an alternative therapeutic intervention for HH-induced myocarditis and arrhythmias. To ascertain the efficacy of OP intervention (in OPHH), its impacts on EKG, cardiac architecture, immunomodulation, oxidative stress regulation, and behavior outcomes were compared with APHH.

Concordant with previous studies (30, 31), we found that HH-induced tachycardia and prolongations of QT, QTc, JT, and Tpeak-Tend intervals, and ST height, P duration, and R and T amplitudes. Reportedly, these observations are because at HH; there is an increase in sympathetic activity, which triggers prolongation of repolarization, resulting in arrhythmia, heart failure, and sudden death (30). However, AP has been demonstrated to prevent significant disruption of cEA (32); consistently, our findings showed similar outcomes. Intriguingly, we observed that OPHH mice had fewer alterations in the EKG indexes than APHH mice compared to the NN mice. This led to the conclusion that OP preserved cEA modestly better than AP during HH exposure.

Furthermore, unlike in HH mice, we observed that BW losses were only modest, and the extent of cardiomyocyte hypertrophies, injury, and fibrosis were mitigated in APHH and OPHH hearts. Lippl et al. and others have similarly shown that at high altitudes, there is a loss of appetite hence the excessive BW (33, 34). Also, to compensate for oxygen demand, hypertrophy cascades are induced, resulting in excessive enlargement of cardiomyocytes and their apoptosis/necrosis, which in turn drives proinflammatory and fibrotic responses (33, 35). Interestingly, both AP and OP have been shown to lessen adverse cardiac remodeling during hypoxic or ischemic events, just as we observed – and it has also been suggested that both interventions might have similar underlying mechanisms (32, 36). While OP's cardiac cardioprotection has been demonstrated mainly against ischemia/reperfusion injury, we show here for the first time that OP intervention is potent against HH-induced myocardial hypertrophy, injury, and fibrosis.

Myocarditis scaffolded by unresolved proinflammatory responses drives the maladaptive remodeling of the heart in HH (5); hence we investigated OP's effect on immunomodulation. Typically observed at injured tissues or inflamed sites (37), we found massive infiltrations of proinflammatory (CD86+) macrophages in HH myocardia, while the reparative (CD206+) macrophage populations were significantly less. Also, inflammatory cytokines concentrations were altered in a similar fashion in the HH myocardia. In contrast, employing the OP intervention facilitated anti-inflammatory defenses while minimizing the

proinflammatory responses in OPHH, as AP did in APHH. While we demonstrated OP's immunoregulation in OPHH; Gorjipour et al.'s earlier works had shown similar observations where the OP intervention enhanced the elevation of IL-10 while downregulating the circulation IL-8 to confer cardioprotection in coronary artery bypass graft surgery (38). The metabolic state of inflammatory cells crucially influences their immune responses and functions (39); as such, we sought to ascertain the metabolic state of infiltrated macrophages and the entire myocardia in further investigations. Interestingly, we found that glycolysis-related genes had increased ~3 folds while that lipid metabolism-related genes were downregulated in macrophages isolated from HH hearts. These findings are consistent with metabolic shifts, which facilitate biased reprogramming of macrophages toward proinflammatory phenotypes (19, 39). Similarly, we observed that the entire HH myocardia had increased lipid deposition while glycogen and other polysaccharide contents were substantially depleted – all of which are consistent with glycolysis shift (40). Contrarily, OP intervention modulated metabolic homeostasis by preventing complete glycolysis shift (41), thereby impeding the reprogramming of macrophages towards proinflammatory phenotypes in OPHH, as similarly done by AP in APHH.

Also, disruption in redox homeostasis is a cofactor in HH-induced cardiac dysfunction (7), and our findings consolidated this fact, as HIF-1 α , HIF-2 α and Nrf2 expression were declining in HH mice hearts. Even so, it was observed that by employing OP intervention, HIF-2 α and Nrf2 but not HIF-1 α expressions were rescued and sustained in OPHH mice hearts. Similar outcomes were found in APHH mice hearts. These findings indicated that, like AP, OP stimulates adaptive oxidative stress regulation by reinforcing antioxidant responses. Consistently, OP has been shown to improve antioxidant defenses by enhancing NAD⁺ levels, which directly promotes Nrf2 antioxidant activities (42, 43). Next, we investigated OP's impact on the NAD⁺/NADH ratio. We found that the OP intervention had increased the NAD⁺/NADH ratio and prevented significant decreases in OPHH hearts, which contributed to sustaining their T-AOC like in APHH hearts, while we observed declines in HH hearts. In line with our finding, Morris-Blanco et al. previously demonstrated that OP did increase NAD⁺/NADH ratio *via* protein kinase C epsilon (PKC ϵ) in neuronal-glial (42), hence it is suggestive that similar mechanisms might be involved here. Overall, compared to HH, survival rates improved in OPHH and APHH.

Cardiovascular events promote anxiety-related behavior and vice versa; as such, it has become imperative to assess the behavioral outcomes of interventions targeted at improving cardiac health (44, 45). Typically, HH has been shown decrease locomotive functions while increasing the levels of anxiety and depression in humans (1). These were confirmed in the HH mice model as they had decreased total distance moved, average velocity, and mobile duration and mostly refrained from the central zone and open arms in the OFT and EPM apparatuses, respectively, during their locomotive and exploratory activities. Contrarily, like APHH mice, OPHH mice combed throughout zones and arms of the OFT and EPM apparatuses – indicating that similar to AP (22), the OP intervention makes mice resilient to HH-induced anxiety-related behavior and decreased locomotive functions.

To have prevented HH-induced cardiac remodeling, it was hypothesized that the OP intervention must have induced mechanisms to facilitate adequate tissue oxygenation. Surprisingly and in validating our hypothesis, CPET parameters in AOP showed enhanced respiratory and

oxygen-carrying capacity and endurance in humans as $\dot{V}E$, $\dot{V}CO_2$, $\dot{V}O_2$, SpO_2 , $\dot{V}O_2/HR$, and MET were all substantially improved at Max Watts (Maximal workload). Concordantly, it has been shown that OP mitigates declines in regional oxygenation to confer cardioprotection when exposed to HH (46). Also, OP modestly delayed the time for $RER=1$ in AOP compared to BOP; hence, indicating that the intervention induces mechanisms that mitigate the extent of metabolic shift to glycolysis, just as shown earlier and reported by others (41).

Lastly, we had previously demonstrated the adaptive roles of β_2AR in cardioprotection and immunoregulation during stressful conditions (14); hence we sought to investigate its implication in OP-induced cardioprotection against HH. We observed that HH mice characterized with arrhythmias had β_2AR expressions drastically increased in their hearts. Consistent with our observation, Lang et al. demonstrated that the overexpression of β_2AR significantly increases the predisposition to the occurrence of arrhythmias (47). Surprisingly, β_2AR deletion prevented long QT, QTc, JT, and Tpeak-Tend intervals in $HH_{A\delta rb2-/-}$ mimicking the effect of β -blockers in preventing long QT syndrome (48). Meanwhile, most of the adaptive responses we observed in $OPHH_{A\delta rb2+/+}$ mice were abolished in $OPHH_{A\delta rb2-/-}$ mice as their BW losses were substantial, arrhythmia worsened, proinflammatory responses heightened against anti-inflammatory responses, and antioxidant defenses declined significantly. Consistent with our observations, carvedilol (a β -blockers) was shown to have abolished the cardioprotection conferred by OP during cardiac surgery (49).

In conclusion, by preserving cEA, mitigating cardiac remodeling, facilitating adaptive immunomodulation and oxidative stress responses, sustaining homeostasis in metabolic shifts, causing resilient against anxiety-related behaviors, and enhancing respiratory and oxygen-carrying capacity, OP demonstrates as a potent alternative therapeutic intervention for preventing HH-induced adverse effects on cardiac and overall health. Even so, OP is not recommended as an intervention for individuals on β -blocker medications prior to their visit to high altitudes/HH environments, as these medications blunt the cardioprotection conferred by the intervention and conversing aggravates myocarditis and arrhythmias. Lastly, immunoregulatory and metabolism homeostasis induced by OP is suggestive of its potential to ameliorate the progression of other inflammatory, metabolic and oxidative stress-related diseases.

Data availability statement

The original contributions presented in the study are included in the article/supplementary material. Further inquiries can be directed to the corresponding authors.

Ethics statement

The studies involving human participants were reviewed and approved by Ethics Committee of the Xuzhou Medical University. The patients/participants provided their written informed consent to participate in this study. The animal study was reviewed and approved by Experimental Animal Centre of Xuzhou Medical

University and the Animal Ethics Committee of the Xuzhou Medical University.

Author contributions

GKA and HS conceived and designed the project. GA, RM, RR, AA, MN, and PW performed animal models. GA, RM, RR, AA, and MN performed most experiments and analyzed data. GA, RR, AA, MN, PW, SA and JA-A performed assays. Cardiopulmonary Exercise Test was facilitated by JX, and FW, GA, LF, and JX conducted examinations and analyses. GA, SA, and XL performed flow cytometry experiments and analysis. GA, YL, and RM conducted behavioral experiments and analyses. GA wrote the manuscript with input from all authors and was approved by JX and HS. All authors contributed to the article and approved the submitted version.

Funding

This research was supported by the National Natural Science Foundation of China (81971179) and the Postgraduate Research & Practice Innovation Program of Jiangsu Province, China (KYCX17-1712), and Priority Academic Program Development of Jiangsu Higher Education Institutions (PAPD).

Acknowledgments

We thank all MBBS students of Xuzhou Medical University (Rethabile Montleesi Morake, Chellah Chanda, Lindani Mcondisi Mabuza, Kimberley Tawanda Gunguwo, and Given Michael Kihaga) and members of the Department of Physiology, Xuzhou Medical University (Xi Tao, Tao Li, Xin Meng Zuo, Chun Yang Liu, and Shi Jie Zhang) – who volunteered as subjects to explore the impact of the OP intervention in Humans.

Conflict of interest

The authors declare that the research was conducted in the absence of any commercial or financial relationships that could be construed as a potential conflict of interest.

Publisher's note

All claims expressed in this article are solely those of the authors and do not necessarily represent those of their affiliated organizations, or those of the publisher, the editors and the reviewers. Any product that may be evaluated in this article, or claim that may be made by its manufacturer, is not guaranteed or endorsed by the publisher.

Supplementary material

The Supplementary Material for this article can be found online at: <https://www.frontiersin.org/articles/10.3389/fimmu.2023.1124649/full#supplementary-material>

References

- Neuhaus C, Hinkelbein J. Cognitive responses to hypobaric hypoxia: Implications for aviation training. *Psychol Res Behav Manag* (2014) 7:297–302. doi: 10.2147/prbm.s51844
- Faulhaber M, Flatz M, Gatterer H, Schoberberger W, Burtscher M. Prevalence of cardiovascular diseases among alpine skiers and hikers in the Austrian Alps. *High Alt Med Biol* (2007) 8(3):245–52. doi: 10.1089/ham.2007.1005
- Mrakic-Spota S, Gussoni M. Effects of acute and sub-acute hypobaric hypoxia on oxidative stress: a field study in the Alps. *Eur J Appl Physiol* (2021) 121(1):297–306. doi: 10.1007/s00421-020-04527-x
- Abe H, Semba H, Takeda N. The roles of hypoxia signaling in the pathogenesis of cardiovascular diseases. *J Atheroscler Thromb* (2017) 24(9):884–94. doi: 10.5551/jat.RV17009
- Chouvarine P, Legchenko E, Geldner J, Riehle C, Hansmann G. Hypoxia drives cardiac miRNAs and inflammation in the right and left ventricle. *J Mol Med (Berl)* (2019) 97(10):1427–38. doi: 10.1007/s00109-019-01817-6
- Wang N, Song J, Zhou G, Li W, Ma H. Mechanism of salidroside relieving the acute hypoxia-induced myocardial injury through the PI3K/Akt pathway. *Saudi J Biol Sci* (2020) 27(6):1533–7. doi: 10.1016/j.sbs.2020.04.035
- González-Candia A, Candia AA, Paz A, Mobarec F, Urbina-Varela R, Campo AD. Cardioprotective antioxidant and anti-inflammatory mechanisms induced by intermittent hypobaric hypoxia. *Antioxidants (Basel)* (2022) 11(6):1043. doi: 10.3390/antiox11061043
- Chen CY, Hou CW, Bernard JR, Chen CC, Hung TC, Cheng LL, et al. Rhodiola crenulata- and cordyceps sinensis-based supplement boosts aerobic exercise performance after short-term high altitude training. *High Alt Med Biol* (2014) 15(3):371–9. doi: 10.1089/ham.2013.1114
- Xiong Y, Wang Y, Xiong Y. Protective effect of salidroside on hypoxia-related liver oxidative stress and inflammation via Nrf2 and JAK2/STAT3 signaling pathways. *Food Sci Nutr* (2021) 9(9):5060–9. doi: 10.1002/fsn.3.2459
- Kubentayev SA, Zhumagul MZ. Current state of populations of rhodiola rosea L. (Crassulaceae) in East Kazakhstan. *Bot Stud* (2021) 62(1):19. doi: 10.1186/s40529-021-00327-4
- Murry CE, Jennings RB, Reimer KA. Preconditioning with ischemia: A delay of lethal cell injury in ischemic myocardium. *Circulation* (1986) 74(5):1124–36. doi: 10.1161/01.cir.74.5.1124
- Hausenloy DJ, Yellon DM. Remote ischaemic preconditioning: underlying mechanisms and clinical application. *Cardiovasc Res* (2008) 79(3):377–86. doi: 10.1093/cvr/cvn114
- Lau JK, Roy P, Javadzadegan A, Moshfegh A, Fearon WF, Ng M, et al. Remote ischemic preconditioning acutely improves coronary microcirculatory function. *J Am Heart Assoc* (2018) 7(19):e009058. doi: 10.1161/jaha.118.009058
- Hou H, Adzika GK, Wu Q, Ma T, Ma Y, Geng J, et al. Estrogen attenuates chronic stress-induced cardiomyopathy by adaptively regulating macrophage polarizations via β_2 -adrenergic receptor modulation. *Front Cell Dev Biol* (2021) 9: 737003. doi: 10.3389/fcell.2021.737003
- Song Y, Xu C, Liu J, Li Y, Wang H, Shan D, et al. Heterodimerization with 5-HT (2B)R is indispensable for β_2 AR-mediated cardioprotection. *Circ Res* (2021) 128(2):262–77. doi: 10.1161/circresaha.120.317011
- Doggett TM, Tur JJ, Alves NG, Yuan SY, Tipparaju SM, Breslin JW. Assessment of cardiovascular function and microvascular permeability in a conscious rat model of alcohol intoxication combined with hemorrhagic shock and resuscitation. *Methods Mol Biol* (2018) 1717:61–81. doi: 10.1007/978-1-4939-7526-6_6
- Zhang L, Li C, Yang L, Adzika GK, Machuki JO, Shi M, et al. Estrogen protects vasomotor functions in rats during catecholamine stress. *Front Cardiovasc Med* (2021) 8:679240. doi: 10.3389/fcvm.2021.679240
- Jing C, Castro-Dopico P. Macrophage metabolic reprogramming presents a therapeutic target in lupus nephritis. *Proc Natl Acad Sci USA* (2020) 117(26):15160–71. doi: 10.1073/pnas.2000943117
- Sun L, Yang X, Yuan Z, Wang H. Metabolic reprogramming in immune response and tissue inflammation. *Arterioscler Thromb Vasc Biol* (2020) 40(9):1990–2001. doi: 10.1161/atvbaha.120.314037
- Chen ZT, Gao QY, Wu MX, Wang M, Sun RL, Jiang Y, et al. Glycolysis inhibition alleviates cardiac fibrosis after myocardial infarction by suppressing cardiac fibroblast activation. *Front Cardiovasc Med* (2021) 8:701745. doi: 10.3389/fcvm.2021.701745
- Zhang Z, Xu HN, Li S, Antonio DJr, Chellappa K, Davis JG, et al. Rapamycin maintains NAD(+)/NADH redox homeostasis in muscle cells. *Aging (Albany NY)* (2020) 12(18):17786–99. doi: 10.18632/aging.103954
- Kushwah N, Jain V, Deep S, Prasad D, Singh SB, Khan N. Neuroprotective role of intermittent hypobaric hypoxia in unpredictable chronic mild stress induced depression in rats. *PloS One* (2016) 11(2):e0149309. doi: 10.1371/journal.pone.0149309
- Zhang J, Wu Y, Peng XY, Li QH, Xiang XM, Zhu Y, et al. The protective effect of a novel cross-linked hemoglobin-based oxygen carrier on hypoxia injury of acute mountain sickness in rabbits and goats. *Front Physiol* (2021) 12:690190. doi: 10.3389/fphys.2021.690190
- Cheong HI, Asosingh K, Stephens OR, Queisser KA, Xu W, Willard B, et al. Hypoxia sensing through β -adrenergic receptors. *JCI Insight* (2016) 1(21):e90240. doi: 10.1172/jci.insight.90240
- Bärtsch P, Gibbs JS. Effect of altitude on the heart and the lungs. *Circulation* (2007) 116(19):2191–202. doi: 10.1161/circulationaha.106.650796
- Messerli-Burgy N, Meyer K, Steptoe A, Laederach-Hofmann K. Autonomic and cardiovascular effects of acute high altitude exposure after myocardial infarction and in normal volunteers. *Circ J* (2009) 73(8):1485–91. doi: 10.1253/circj.cj-09-0004
- Louis Hofstetter US, Stefano F, Rimoldi. Going to high altitude with heart disease. *Cardiovasc Med* (2017) 20((04):87–95. doi: 10.4414/cvm.2017.00478
- Pham K, Parikh K, Heinrich EC. Hypoxia and inflammation: Insights from high-altitude physiology. *Front Physiol* (2021) 12:676782. doi: 10.3389/fphys.2021.676782
- Xu J, Chen WJ, Wang Z, Xin MY, Gao SH, Liu WJ, et al. Profiles of transcriptome and metabolic pathways after hypobaric hypoxia exposure. *Proteome Sci* (2022) 20(1):16. doi: 10.1186/s12953-022-00198-y
- Roche F, Reynaud C, Pichot V, Duverney D, Costes F, Garet M, et al. Effect of acute hypoxia on QT rate dependence and corrected QT interval in healthy subjects. *Am J Cardiol* (2003) 91(7):916–9. doi: 10.1016/s0002-9149(03)00040-7
- Mikolajczak K, Czerwińska K, Pilecki W, Poręba R, Gać P. The impact of temporary stay at high altitude on the circulatory system. *J Clin Med* (2021) 10(8):1622. doi: 10.3390/jcm10081622
- Estrada JA, Williams AG Jr., Sun J, Gonzalez L, Downey HF, Caffrey JL, et al. δ -opioid receptor (DOR) signaling and reactive oxygen species (ROS) mediate intermittent hypoxia induced protection of canine myocardium. *Basic Res Cardiol* (2016) 111(2):17. doi: 10.1007/s00395-016-0538-5
- Chouabe C, Ricci E, Amsellem J, Blaineau S, Dalmaz Y, Favier R, et al. Effects of aging on the cardiac remodeling induced by chronic high-altitude hypoxia in rat. *Am J Physiol Heart Circ Physiol* (2004) 287(3):H1246–1253. doi: 10.1152/ajpheart.00199.2004
- Lippl FJ, Neubauer S, Schipfer S, Lichter N, Tufman A, Otto B, et al. Hypobaric hypoxia causes body weight reduction in obese subjects. *Obes (Silver Spring)* (2010) 18(4):675–81. doi: 10.1038/oby.2009.509
- Pena E, Brito J. Oxidative stress, kinase activity and inflammatory implications in right ventricular hypertrophy and heart failure under hypobaric hypoxia. *Int J Mol Sci* (2020) 21(17):. doi: 10.3390/ijms21176421
- Surendra H, Diaz RJ, Harvey K, Tropak M, Callahan J, Hinek A, et al. Interaction of δ and κ opioid receptors with adenosine A1 receptors mediates cardioprotection by remote ischemic preconditioning. *J Mol Cell Cardiol* (2013) 60:142–50. doi: 10.1016/j.yjmcc.2013.04.010
- Krzyszczak P, Schloss R, Palmer A, Berthiaume F. The role of macrophages in acute and chronic wound healing and interventions to promote pro-wound healing phenotypes. *Front Physiol* (2018) 9:419. doi: 10.3389/fphys.2018.00419
- Gorjipour F, Saeedzadeh T, Toloueitabar Y, Kachouei N, Bahloul Ghashghaei S, Mortazian M, et al. Remote ischemic preconditioning effects on inflammatory markers and myocardial protection in coronary artery bypass graft surgery. *Perfusion* (2022) 37(1):56–61. doi: 10.1177/0267659120979293
- Shirai T, Nazarewicz RR, Wallis BB, Yanes RE, Watanabe R, Hilhorst M, et al. The glycolytic enzyme PKM2 bridges metabolic and inflammatory dysfunction in coronary artery disease. *J Exp Med* (2016) 213(3):337–54. doi: 10.1084/jem.20150900
- Yan J, Young ME, Cui L, Lopaschuk GD, Liao R, Tian R. Increased glucose uptake and oxidation in mouse hearts prevent high fatty acid oxidation but cause cardiac dysfunction in diet-induced obesity. *Circulation* (2009) 119(21):2818–28. doi: 10.1161/circulationaha.108.832915
- Geng J, Zhang Y, Li S, Li S, Wang J, Wang H, et al. Metabolomic profiling reveals that reprogramming of cerebral glucose metabolism is involved in ischemic preconditioning-induced neuroprotection in a rodent model of ischemic stroke. *J Proteome Res* (2019) 18(1):57–68. doi: 10.1021/acs.jproteome.8b00339
- Morris-Blanco KC, Cohan CH, Neumann JT, Sick TJ, Perez-Pinzon MA. Protein kinase c epsilon regulates mitochondrial pools of namp1 and NAD following resveratrol and ischemic preconditioning in the rat cortex. *J Cereb Blood Flow Metab* (2014) 34(6):1024–32. doi: 10.1038/jcbfm.2014.51
- Xie N, Zhang L, Gao W, Huang C. NAD(+) metabolism: Pathophysiologic mechanisms and therapeutic potential. *Signal Transduct Target Ther* (2020) 5(1):227. doi: 10.1038/s41392-020-00311-7
- Abed MA, Kloub MI, Moser DK. Anxiety and adverse health outcomes among cardiac patients: a biobehavioral model. *J Cardiovasc Nurs* (2014) 29(4):354–63. doi: 10.1097/JCN.0b013e318292b235
- Pino EC, Zuo Y, Borba CP, Henderson DC, Kalesan B. Clinical depression and anxiety among ST-elevation myocardial infarction hospitalizations: Results from nationwide inpatient sample 2004–2013. *Psychiatry Res* (2018) 266:291–300. doi: 10.1016/j.psychres.2018.03.025
- Zhong Z, Dong H, Wu Y, Zhou S, Li H, Huang P, et al. Remote ischemic preconditioning enhances aerobic performance by accelerating regional oxygenation and improving cardiac function during acute hypobaric hypoxia exposure. *Front Physiol* (2022) 13:950086. doi: 10.3389/fphys.2022.950086
- Lang D, Holzem K, Kang C, Xiao M, Hwang HJ, Ewald GA, et al. Arrhythmogenic remodeling of β_2 versus β_1 adrenergic signaling in the human failing heart. *Circ Arrhythm Electrophysiol* (2015) 8(2):409–19. doi: 10.1161/circp.114.002065
- Vincent GM, Schwartz PJ, Denjoy I, Swan H, Bithell C, Spazzolini C, et al. High efficacy of beta-blockers in long-QT syndrome type 1: contribution of noncompliance and QT-prolonging drugs to the occurrence of beta-blocker treatment “failures”. *Circulation* (2009) 119(2):215–21. doi: 10.1161/circulationaha.108.772533
- Cho YJ, Nam K, Kim TK, Choi SW, Kim SJ, Hausenloy DJ, et al. Sevoflurane, propofol and carvedilol block myocardial protection by limb remote ischemic preconditioning. *Int J Mol Sci* (2019) 20(2):269. doi: 10.3390/ijms20020269



OPEN ACCESS

EDITED BY

Wilfried Le Goff,
Institut National de la Santé et de la
Recherche Médicale (INSERM), France

REVIEWED BY

Charles Thomas,
Université de Bourgogne, France
Fausto Chiazza,
University of Eastern Piedmont, Italy
Mathilde Varret,
Institut National de la Santé et de la
Recherche Médicale (INSERM), France

*CORRESPONDENCE

Mao Luo

✉ luomao20050908@163.com

Min Zeng

✉ zengminlz@163.com

†These authors have contributed equally to
this work

SPECIALTY SECTION

This article was submitted to
Inflammation,
a section of the journal
Frontiers in Immunology

RECEIVED 18 December 2022

ACCEPTED 08 February 2023

PUBLISHED 22 February 2023

CITATION

Wang Y, Fang D, Yang Q, You J, Wang L,
Wu J, Zeng M and Luo M (2023)
Interactions between PCSK9 and NLRP3
inflammasome signaling in atherosclerosis.
Front. Immunol. 14:1126823.
doi: 10.3389/fimmu.2023.1126823

COPYRIGHT

© 2023 Wang, Fang, Yang, You, Wang, Wu,
Zeng and Luo. This is an open-access article
distributed under the terms of the [Creative
Commons Attribution License \(CC BY\)](#). The
use, distribution or reproduction in other
forums is permitted, provided the original
author(s) and the copyright owner(s) are
credited and that the original publication in
this journal is cited, in accordance with
accepted academic practice. No use,
distribution or reproduction is permitted
which does not comply with these terms.

Interactions between PCSK9 and NLRP3 inflammasome signaling in atherosclerosis

Yanan Wang^{1,2,3†}, Dan Fang^{1,2,3†}, Qinzhi Yang^{1,2,3†},
Jingcan You^{1,2,3}, Liqun Wang^{1,2,3}, Jianbo Wu^{1,2,3}, Min Zeng^{4*}
and Mao Luo^{1,2,3,4*}

¹Key Laboratory of Medical Electrophysiology, Ministry of Education, Drug Discovery Research Center, Southwest Medical University, Luzhou, Sichuan, China, ²Laboratory for Cardiovascular Pharmacology, Department of Pharmacology, School of Pharmacy, Southwest Medical University, Luzhou, Sichuan, China, ³Metabolic Vascular Disease Key Laboratory of Sichuan Province, Luzhou Municipal Key Laboratory of Thrombosis and Vascular Biology, Luzhou, Sichuan, China, ⁴Department of Pharmacy, The Affiliated Hospital of Southwest Medical University, Luzhou, Sichuan, China

Atherosclerosis is an early pathological basis of numerous cardiovascular events that result in death or disability. Recent studies have described PCSK9 as a novel target for the treatment of atherosclerosis; PCSK9 is capable of degrading LDLR on the surface of hepatocytes through the regulation of lipid metabolism, and it can function as a novel inflammatory modulator in atherosclerosis. Inflammasomes are important intracellular multiprotein complexes that promote the inflammatory response in atherosclerosis. Among inflammasomes, the NLRP3 inflammasome is particularly notable because of its important role in the development of atherosclerotic disease. After activation, NLRP3 forms a complex with ASC and pro-caspase-1, converting pro-caspase-1 into activated caspase-1, which may trigger the release of IL-1 β and IL-18 and contribute to the inflammatory response. Several recent studies have indicated that there may be interactions between PCSK9 and the NLRP3 inflammasome, which may contribute to the inflammatory response that drives atherosclerosis development and progression. On the one hand, the NLRP3 inflammasome plays an important role via IL-1 β in regulating PCSK9 secretion. On the other hand, PCSK9 regulates caspase-1-dependent pyroptosis by initiating mtDNA damage and activating NLRP3 inflammasome signaling. This paper reviews the mechanisms underlying PCSK9 and NLRP3 inflammasome activation in the context of atherosclerosis. Furthermore, we describe the current understanding of the specific molecular mechanism underlying the interactions between PCSK9 and NLRP3 inflammasome signaling as well as the drug repositioning events that influence vascular cells and exert beneficial antiatherosclerotic effects. This review may provide a new therapeutic direction for the effective prevention and treatment of atherosclerosis in the clinic.

KEYWORDS

PCSK9, NLRP3 inflammasome signaling, interactions, atherosclerosis, therapy

Introduction

Inflammation is an important driver of atherosclerosis, which is an early pathological basis of cardiovascular disease (1). Atherosclerosis is characterized by the excessive accumulation of lipids, extracellular matrix, and cholesterol-laden macrophages under the arterial endothelium, resulting in the formation of atherosclerotic plaques (2, 3). LDL-cholesterol (C) is considered to be a major risk factor for the development of atherosclerotic diseases (4). The mechanism by which proprotein convertase subtilisin/kexin type 9 (PCSK9) regulates LDLR degradation involves both extracellular and intracellular pathways. On the one hand, extracellular PCSK9 can act as a companion protein and bind to LDL-receptor (R) on the cell surface, thus causing the formation of a complex and directing LDLR to lysosomes where the PCSK9/LDLR complex is degraded, thereby promoting further LDL-C accumulation (5). On the other hand, intracellular PCSK9 can also directly bind with LDLR in the Golgi network to induce the lysosomal degradation of LDLR (6). PCSK9 is closely associated with the indirect regulation of lipid metabolism (5) and participates in the direct regulation of atherosclerosis *via* the accumulation of foam cells and inflammatory mediators as well as apoptosis in vascular walls (7). If PCSK9 inhibition is reduced, there is more PCSK9, more degraded LDLRs and therefore an increase in LDL levels (8). Persistent accumulation of LDL results in not only the formation of foam cells but also the chronic amplification of inflammatory responses, which are major causes of plaque rupture and vascular thrombosis (9). NOD-like receptor thermal protein domain associated protein 3 (NLRP3) inflammasomes are classical receptors of intracellular innate immunity that closely regulate inflammatory responses (10). NLRP3 inflammasome activation is a powerful mediator of the inflammatory response *via* caspase-1 activation (11). The NLRP3 inflammasome can activate caspase-1 and cleave pro-IL-1 β and IL-18 to generate IL-1 β and IL-18, which further promote inflammatory responses and play crucial roles in regulating atherosclerotic lesions (12).

Recently, several studies have reported that PCSK9 activates the NLRP3 inflammasome signaling pathway and the associated inflammation (13–15). Conversely, the NLRP3 inflammasome signaling pathway can regulate PCSK9 secretion (16). However, the regulatory mechanisms are still not fully understood, especially in the context of atherosclerosis. In this review, we summarize the current findings related to the interactions between PCSK9 and the NLRP3 inflammasome in atherosclerosis. Furthermore, we describe the specific molecular mechanism underlying the PCSK9 and NLRP3 inflammasome signaling pathway in atherosclerosis and cells related to inflammation, including vascular smooth muscle cells (VSMCs), endothelial cells (ECs) and macrophages (M Φ). These findings may provide a novel theoretical basis and important targets for clinical application in the treatment of atherosclerosis.

PCSK9 biology and its role in atherothrombosis

PCSK9 biology

In 2003, Abifadel M et al. first reported that PCSK9 is highly expressed in the liver and contributes to cholesterol homeostasis (17). Similar to other proprotein convertases, PCSK9 is synthesized as a soluble proenzyme and undergoes autocatalytic cleavage in the endoplasmic reticulum (ER) at residue 152 between its prodomain and catalytic domains (18). Then, a stable heterodimer consisting of a prodomain of approximately 14 kDa and a mature fragment of approximately 57 kDa is formed, as shown in Figure 1. After transportation to the Golgi apparatus, the protein is modified by acetylation and subsequently secreted (18). PCSK9 is mainly secreted by the liver, small intestine, kidney, skin, and cerebrospinal fluid, while PCSK9 in blood is almost exclusively secreted from the liver (19). PCSK9 and LDLR form a tight complex and are targeted to lysosomes for degradation, thereby reducing the level of LDLR on the surface of hepatocytes and decreasing hepatic clearance of LDL-C (20).

Through its function of degrading the LDLR, PCSK9 is a key player in lipid metabolism by regulating the LDL level in blood responsible for hypercholesterolemia, which is associated with the risk of atherosclerosis (21). Overexpression of PCSK9 was found to inversely downregulate the expression of LDLR and reduce the clearance of cholesterol from plasma, so inhibiting PCSK9 overexpression is significant in the prevention and treatment of atherosclerosis. Moreover, Tavori et al. found that PCSK9 expression is involved in regulating the size and composition of atherosclerotic plaques and significantly enlarges atherosclerotic lesion areas (8). Giunzioni et al. further showed that PCSK9 directly increases the inflammation of atherosclerotic lesion in an LDLR-dependent but cholesterol-independent manner, suggesting that therapeutic PCSK9 inhibition may have vascular benefits that are secondary to reductions in the LDL levels (22). Overall, PCSK9 is expressed at high levels at the sites of atherosclerotic lesions, particularly in intimal plaques (23). PCSK9 inhibition has emerged as a potential novel therapeutic approach to treat hypercholesterolemia and associated diseases, such as atherosclerosis.

PCSK9 is a key modulator of atherosclerosis

It has been clearly established that PCSK9 plays a crucial role in the development of atherosclerosis. While the liver is the major source of circulating PCSK9, PCSK9 is also expressed in various cellular components of atherosclerotic plaques, including monocytes/M Φ s, VSMCs, and ECs, that directly participate in the

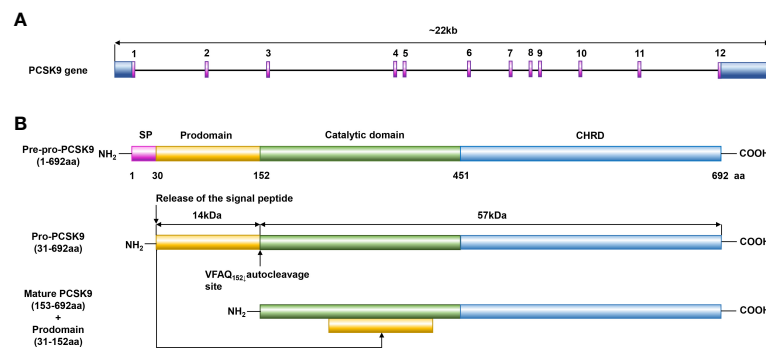


FIGURE 1

Structure diagram of PCSK9. (A) PCSK9 is the ninth member of the subtilisin serine protease family, and its gene is located on human chromosome 1p32.3, is 22 kb in length, includes 12 exons, and encodes 692 amino acids. (B) PCSK9 consists of a signal peptide (residues 1–30), a prodomain (residues 31–152), a catalytic domain (residues 153–451), and a C-terminal domain (residues 452–692). Similar to other proprotein convertases, PCSK9 is synthesized as a soluble proenzyme and undergoes autocatalytic cleavage in the ER at residue 152 between its prodomain and catalytic domains. Then, a stable heterodimer consisting of a prodomain of approximately 14 kDa and a mature fragment of approximately 57 kDa is formed, and after transportation to the Golgi apparatus, the protein is modified by acetylation and subsequently secreted.

progression of atherosclerotic lesions by exacerbating vascular inflammation (Figure 2 and Table S1) (24–31). Moreover, the secretion of PCSK9 in ECs, SMCs and MΦs were strongly induced by LPS treatment with or without ATP compared with the control (23, 32). PCSK9 secreted by VSMCs, which express more PCSK9 than ECs in a paracrine manner, downregulating LDLR expression on the cell surface of MΦs and preventing the formation of foam cells, thus reducing atherosclerosis progression. However, native LDL molecules are not the major source of cholesterol accumulation in macrophages and LDLR is not the

main receptor for lipoprotein uptake in cells within the atherosclerotic plaque (5). Scavenger receptors expressed by MΦ in vessel walls take up LDL-cholesterol, resulting in the transformation of MΦs into foam cells that secrete a large amount of proinflammatory cytokines and mature into activated MΦ, contributing to the acceleration of arterial inflammation and atherosclerosis (33, 34). Cluster of differentiation 36(CD36) is a scavenger receptor that is highly expressed in macrophages and macrophage-derived foam cells in atherosclerotic plaques. Levy et al. found that gain-of-function PCSK9 mutants could

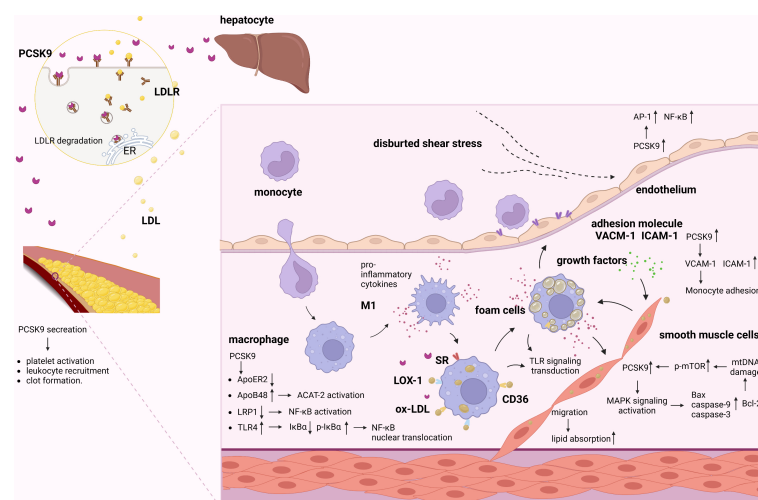


FIGURE 2

Role of PCSK9 in atherosclerosis. PCSK9 and LDLR form a complex and are targeted to lysosomes for degradation. Secreted PCSK9 by the liver reduces the level of LDLR not only on hepatocytes surface but also on other cells. PCSK9 promotes platelet activation, leukocyte recruitment and clot formation both in the plasma and in vascular cells. Proinflammatory stimuli activate ECs and increase adhesion molecules, promoting the adhesion and migration of monocytes. Migrated monocytes and ox-LDL-C accumulate in the subintimal region. Meanwhile, migrated monocytes transform into MΦs. In inflammatory milieu, PCSK9 increases scavenger receptors to increase ox-LDL uptake. In addition, PCSK9 mediated inflammation via activating LRP1, TLR4/NF-κB pathway. PCSK9 increased cholesterol synthesis by activating ACAT-2/ApoB48. Furthermore, migrated SMCs can absorb lipid and exacerbate the inflammatory responses and myogenic foam cell formation caused by the effects of growth factors and proinflammatory cytokines. In VSMCs, PCSK9 is enhanced by mtDNA damage via the upregulation of p-mTOR. In turn, PCSK9 increases mtDNA damage by regulating the apoptotic proteins via MAPK signaling pathway. Besides, low shear stress increases PCSK9, which induces EC dysfunction and upregulates AP-1 and NF-κB.

significantly increase CD36 expression (35). In addition, Ding et al. also showed that PCSK9 can enhance the uptake of ox-LDL in MΦs by targeting lectin-like ox-LDL receptor 1 (LOX-1) (23). Moreover, Giunzioni et al. found that PCSK9 exerts a direct effect on the monocyte/MΦ phenotype during the progression of atherosclerosis (22). Given that LDL-R-related protein 1 (LRP1) deficiency induces nuclear factor kappa-B (NF-κB) activation and promotes a proinflammatory phenotype in MΦs, some studies have suggested that PCSK9 induces macrophage inflammation by targeting LRP1 for degradation. Tang et al. found that PCSK9 overexpression upregulates toll-like receptors 4 (TLR4) expression and promotes inhibitor kappa B alpha (IκBα) degradation, p-IκBα expression, and NF-κB nuclear translocation (36). The findings show that PCSK9 enhances inflammatory cytokine secretion through TLR4/NF-κB pathway activation in MΦs. Another mechanism underlying the PCSK9-mediated promotion of inflammation might involve the PCSK9-induced LDLR-independent degradation of apolipoprotein E receptor 2 (ApoER2) (37), which plays a critical role in maintaining the anti-inflammatory phenotype of MΦs; these results indicate that PCSK9 can regulate macrophage inflammation through inflammasome activation.

VSMCs are important for the maintenance of vascular homeostasis and play a key role in atherosclerosis (38). PCSK9 is reported to be expressed in VSMCs in atherosclerotic plaques (39), and its expression is markedly increased by inflammatory stimuli, indicating that proinflammatory factors that are associated with atherosclerosis stimulate PCSK9 expression in VSMCs and suggesting a critical role for PCSK9 in the development of atherosclerotic lesions (40). For example, migration of SMCs from the tunica media of the vessel wall can lead to increased lipid absorption and exacerbate the inflammatory responses and myogenic foam cell formation caused by the effects of growth factors and proinflammatory cytokines on the fatty streak (41). Previous studies have shown that there is a positive feedback interplay between VSMC-derived PCSK9 and mitochondrial DNA (mtDNA) damage in the proinflammatory milieu that involves mitochondrial reactive oxygen species (mtROS); this feedback loop results in inflammation, oxidative stress, and apoptosis, which directly contribute to atherosclerosis (42). In VSMCs, PCSK9, which increases mtDNA damage by upregulating the expression of the pro-apoptotic proteins Bax, caspase-9, and caspase-3 and downregulating the expression of Bcl-2, is correlated with the activation of the MAPK signaling pathway. Moreover, PCSK9 expression is enhanced by mtDNA damage *via* the upregulation of p-mTOR expression in a dose-dependent manner, while inhibition of PCSK9 reduces mammalian target of rapamycin (mTOR) phosphorylation and decreases VSMC autophagy.

Vascular endothelial dysfunction and the inflammatory response contribute to the initiation and progression of atherosclerosis (43). Landlinger et al. found that treatment of mice with AT04A obviously suppressed the inflammatory response and activated ECs and stimulated monocyte/macrophage migration, suggesting that PCSK9 inhibition also suppresses endothelial inflammation (44). Although PCSK9 expression and secretion by ECs may be lower than that by VSMCs, the effects of PCSK9 on EC biology in atherosclerosis

cannot be ignored. The development of atherosclerosis is caused by a variety of factors, including biochemical factors and physical factors. Hemodynamic shear stress regulates EC functions and influences the pathobiology of atherosclerosis (45). Laminar shear stress is thought to exert atheroprotective effects (46). Conversely, low shear stress significantly increases PCSK9 expression, induces EC dysfunction, and upregulates the expression of transcription factors, including AP-1 and NF-κB, that promote pro-oxidant and proinflammatory states (40, 46); these results indicate that PCSK9 may play an important role in the EC inflammation that is induced by low shear stress.

NLRP3 inflammasome signaling pathway

Hosts regulate the release of intracellular inflammatory mediators and the initiation of inflammatory responses mainly through two types of pattern recognition receptors (PRRs), namely, membrane-bound Toll-like receptors (TLRs) and nucleotide-binding oligomerization domain (NOD)-like receptors (NLRs) (47, 48); these receptors recognize pathogen-associated molecular patterns (PAMPs) and danger-associated molecular patterns (DAMPs) and thus promote the maturation and release of tightly regulated, highly inflammatory cytokines. NLRP3 is a recognized PRR, and it is a cytoplasmic receptor that responds to danger signals and can be activated to form the NLRP3 inflammasome (49).

The NLRP3 inflammasome is a multimolecular protein complex that comprises the NOD-like receptor NLRP3, the adaptor ASC and the effector pro-caspase-1, which play fundamental roles in inflammation (50). Among these components, the NOD-like receptor NLRP3 contains a leucine-rich repeat (LRR) domain, nucleotide triphosphatase (NACHT) domain, and pyrin domain (PYD), and it plays fundamental roles in inflammation (51). ASC is composed of the N-terminal PYD domain and the C-terminal CARD domain, which promote oligomeric homotypic interactions (52). Pro-caspase-1 is composed of a CARD and catalytic domain, including p10 and p20 (53). The sensing of various stimuli by TLRs on the cell membrane can induce the activation of the TRIF/NF-κB and TLR4/MyD88 signaling pathways and upregulate the transcription of NLRP3 receptor proteins and proinflammatory cytokines (54, 55). Moreover, the LRR domain of NLRP3 senses stimuli, which leads to NACHT domain oligomerization, most likely by promoting a PYD-ASC interaction, and these processes result in the formation of the NLRP3 inflammasome *via* the binding of pro-caspase-1, which is another component of the NLRP3 inflammasome, to CARD and ASC (56, 57). Upon activation, the NLRP3 inflammasome results in the proteolytic activation of caspase-1, which facilitates the cleavage of pro-IL-1β and pro-IL-18 and the secretion of the proinflammatory cytokines IL-1β and IL-18 (58) (Figure 3).

Additionally, the caspase-1-dependent cleavage of gasdermin-D (GSDMD) is thought to be the classic initiator pyroptotic cell death (59). Pyroptosis is a novel form of cell death that is induced in

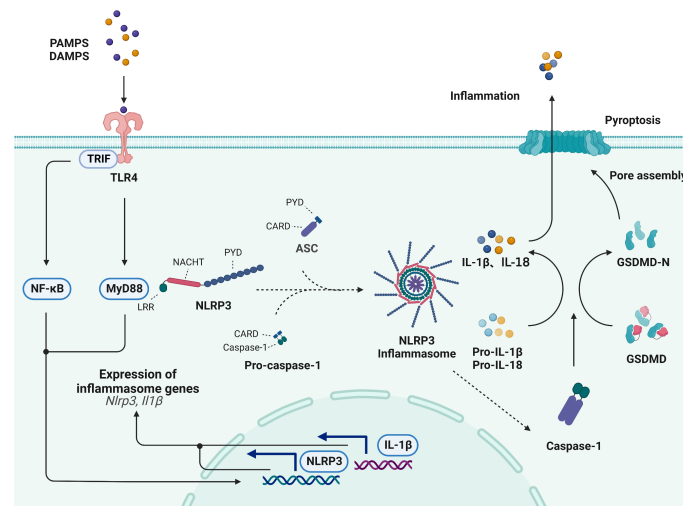


FIGURE 3

Activation of the NLRP3 inflammasome signaling pathway. The NLRP3 inflammasome is comprised of the NLRP3, ASC and pro-caspase-1. The sensing of various stimuli by TLRs on the cell membrane can induce the activation of the TRIF/NF- κ B, the activation of TLR4/MyD88 signaling, the transcription of NLRP3 receptor proteins and lead to formation of NLRP3 inflammasome. Upon activation, NLRP3 induces the proteolytic activation of caspase-1, which facilitates the cleavage of pro-IL-1 β and pro-IL-18. Additionally, activated caspase-1 cleaves GSDMD and generates an active GSDMD-NT, which translocates to the plasma membrane and oligomerizes to form a pore that allows the secretion of IL-1 β and IL-18, subsequently inducing pyroptotic cell death.

response to cell disruption by the inflammasome-induced GSDMD protein, which promotes the release of proinflammatory cytokines, such as IL-1 β and IL-18 (60). Previous studies have revealed that pyroptosis is involved in atherosclerotic plaque formation. Activated caspase-1 cleaves GSDMD and generates an active N-terminal cleaving product (GSDMD-NT), which translocates to the plasma membrane and oligomerizes to form a pore that allows the release of IL-1 β and IL-18, subsequently inducing pyroptotic cell death and promoting the occurrence and development of atherosclerosis (61).

The role of the NLRP3 inflammasome signaling pathway in atherosclerosis

Recently, it has been shown that NLRP3 inflammasome/IL-1 β signaling-mediated inflammation plays an important role in the development of atherosclerosis (12), as is shown in Table S2 (62–73) and Figure 4. The inflammatory process starts with inflammasome activation, which leads to the release of mature IL-1 β . Various PAMPs and DAMPs have been shown to activate macrophages (74). Upon activation, macrophages exacerbate the vascular inflammatory response by releasing cytokines, and activated macrophages are the main source of IL-1 β (75). For example, Orecchioni et al. recently found that macrophages express the olfactory receptor Olfr2 and all associated trafficking and signaling molecules, which drive atherosclerosis via NLRP3-dependent IL-1 β secretion (76). In addition, a study by Zhang et al. reported that desmosterol suppressed inflammasome activation in macrophages and protected against vascular inflammation and atherosclerosis (77). Decreased desmosterol accumulation in mitochondria promotes mtROS production and NLRP3-dependent

inflammasome activation. NLRP3 or ASC deficiency can reverse the increase in inflammasome activity and atherogenesis that is observed in desmosterol-depleted macrophages.

Endothelium dysfunction is involved in the development of atherosclerotic vascular lesions. It has been shown that ECs synthesize IL-1 β in response to inflammatory stimuli; moreover, the atherosclerotic endothelium exhibits increased expression of IL-1 β (78). Wilson et al. found that HUVECs express P2X (4) R and P2X (7)R subtypes, and both were significantly upregulated under inflammatory conditions (79). Activation of P2X(7)Rs results in the release of low levels of bioactive IL-1 β and the simultaneous release of IL-1Ra (79). Wu et al. demonstrated that cytotoxin-associated gene A (CagA) promotes aortic endothelial inflammation and accelerates atherosclerosis through the NLRP3/caspase-1/IL-1 β axis (80). In addition, the activation of the vascular endothelium and the infiltration of circulating monocytes into the vessel wall are considered to be key factors in the occurrence and development of atherosclerosis (81). Hettwer et al. revealed that IL-1 β suppression reduces inflammatory leukocyte production and uptake in atherosclerosis (82). When the NLRP3 inflammasome is inhibited in ECs from atherosclerotic aortas, these cells show decreased expression of leukocyte chemoattractants and adhesion molecules, indicating that NLRP3 inflammasome- and IL-1 β -targeted therapies may reduce blood leukocyte recruitment to atherosclerotic aortas.

The inflammatory response that is induced by VSMC apoptosis accounts for approximately 15% of the systemic inflammatory response in atherosclerosis. Apoptotic VSMCs are phagocytosed by normal endothelial cells *in vivo*, which does not require the involvement of macrophages, leading to the inhibition of inflammation and slowing the progression of atherosclerosis (83). In addition, Clarke et al. found that necrotic VSMCs release IL-1 α , whereas apoptotic VSMCs undergoing secondary necrosis release

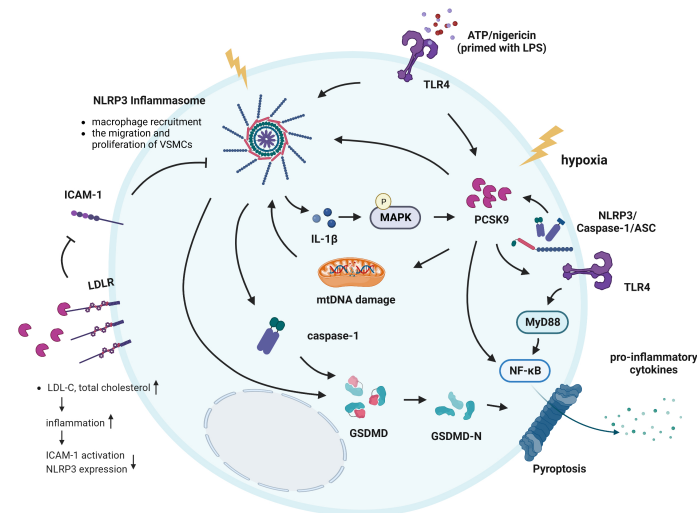


FIGURE 5

Interactions between PCSK9 and the NLRP3 inflammasome signaling pathway. ATP and nigericin simultaneously induced the NLRP3 inflammasome in cells primed with LPS and induced PCSK9 expression. In addition, hypoxia induces PCSK9 expression and NLRP3 inflammasome activation. The NLRP3 inflammasome and its downstream signals all regulate PCSK9 secretion, while MAPKs play a key role in regulating IL-1 β -mediated PCSK9 secretion. PCSK9 can directly activate the NLRP3 inflammasome and promote the secretion of pro-inflammatory cytokines via NF- κ B signaling. PCSK9 knockout inhibits macrophage recruitment, suppresses the migration and proliferation of VSMCs; these effects are related to NLRP3 inflammasome. PCSK9 initiates mtDNA damage, activates NLRP3 inflammasome signaling and subsequently induces pyroptosis. Another mechanism underlying the effects of PCSK9 on NLRP3 inflammasome activation involves TLR4/MyD88/NF- κ B signaling. PCSK9 binds to LDLR, causing an increase in the total cholesterol and LDL-C levels, inducing inflammation, resulting in ICAM expression and NLRP3 inflammasome activation.

activates NLRP3 inflammasome signaling (NLRP3, ASC, Caspase-1, IL-1 β , and IL-18), and subsequently induces Caspase-1-dependent pyroptosis, with intense expression of PCSK9 and the pyroptosis marker GSDMD-NT in the zone bordering the infarct area. Moreover, PCSK9 knockout significantly decreases the NLRP3 inflammasome signaling, GSDMD-NT expression, and LDH release (13, 15). These results suggest that PCSK9 regulates Caspase-1-dependent pyroptosis *via* mtDNA damage and may reveal proinflammatory processes, including NLRP3 inflammasome signaling and pyroptosis, as potential targets for the treatment of PCSK9-related cardiovascular diseases (13). Additionally, PCSK9 binds to the LDLR and enhances its degradation, which leads to the reduced clearance of LDL-C and a higher risk of atherosclerosis. Landlinger et al. found that AT04A immunization induced high and persistent levels of antibodies against PCSK9, significantly reducing the total cholesterol and LDL-C levels in plasma, decreasing vascular inflammation, and ultimately reducing ICAM expression in activated endothelial cells and caspase-1-activating NLRP3 inflammasome-related protein expression in proinflammatory macrophages (44).

Effects of the NLRP3 inflammasome signaling pathway on PCSK9

Notably, the expression of NLRP3 inflammasome-related proteins and secretion of PCSK9 were particularly evident when mouse peritoneal macrophages were exposed to LPS, ATP or nigericin, indicating that the NLRP3 inflammasome is connected to PCSK9 secretion (16, 96). Macrophage-derived PCSK9 may also play an important role in atherogenesis *via* its local effects on atherosclerotic plaques (36). Ding et al. revealed that NLRP3 and its

downstream signaling proteins ASC, Caspase-1, IL-18, and IL-1 β all regulate PCSK9 secretion by macrophages as well as in a host of tissues, including the liver, small intestine and kidney; on the other hand, MAPKs play a key role in regulating IL-1 β -mediated PCSK9 secretion, particularly in the context of high-fat diet consumption (16). The study pointed out that macrophages secrete large amounts of PCSK9 *via* NLRP3 inflammasome activation. PCSK9 expression is downstream of NLRP3 and IL-1 β , which are the major regulators of PCSK9 secretion. Furthermore, HFD-C results in the robust secretion of PCSK9, and this PCSK9 secretion is dependent on IL-1 β upregulation, providing a strong link between IL-1 β and PCSK9 in the proatherosclerotic and proinflammatory milieu (97, 98).

Recent advances in the use of PCSK9 and NLRP3 inflammasome signaling as therapeutic targets for atherosclerosis

Inhibiting PCSK9 with inhibitors has been studied as a potential therapeutic approach in the field of atherosclerotic treatment (99). Different forms of PCSK9 inhibitors and their targets, including monoclonal antibodies (mAbs), small interfering RNAs (siRNAs), and vaccines, have recently been explored (100–102). At present, two mAbs against human PCSK9, alirocumab and evolocumab, are approved for listing and are available for use in clinical treatment (103). Ongoing clinical trials have shown that these PCSK9 mAbs are well tolerated, enhance the clearance of LDL-C, and decrease cardiovascular events in patients (104). Therapeutic monoclonal antibodies target PCSK9 in the plasma, while siRNA selective silences the translation of messenger RNA (mRNA) molecules, thus preventing the intracellular translation of PCSK9 mRNA to

protein (105). Inclisiran is an siRNA and was discovered several years ago (106). The positive results of the ORION series provide strong supporting evidence for the clinical application of inclisiran in the treatment of atherosclerosis (107, 108). Compared with therapeutic mAbs, siRNA treatment shows a more sustained efficacy and requires fewer injections, thus overcoming some known barriers to treatment compliance compared with mAbs (109). The basic characteristic of a PCSK9 vaccine is the capacity to trigger the generation of anti-PCSK9 antibodies by the host (110). However, research on PCSK9 vaccines, such as PCSK9Q β -003, AT04A and L-IFPTA+, is still in the animal experimental stage (44, 111, 112).

In terms of NLRP3 inhibitors, currently available clinical agents are targeting IL-1 β (113). Although targeting IL-1 β is an effective method for treating inflammatory diseases, it seems to have limitations. First, the activated NLRP3 inflammasome produces various inflammatory cytokines, including IL-1 β , IL-18 secretion. All of cytokines play crucial roles in the occurrence and development of related diseases (114, 115). Second, IL-1 β is produced not only by the NLRP3 inflammasome but also by other inflammasomes or in an inflammasome-independent manner, so inhibition of NLRP3 may have more immunosuppressive effects than inhibition of IL-1 β (116, 117). Additionally, MCC950 can specific inhibit classical and nonclassical NLRP3 inflammasome activation and pro-inflammatory cytokines secretion to significantly decrease the maximum degree of aortic stenosis as well as the mean plaque size and volume and increase plaque stability (118–120). Several studies have revealed that MCC950 can directly interact with the Walker B motif in the NACHT domain to block ATP hydrolysis and inhibit NLRP3 inflammasome activation and formation (121, 122). In addition, CY-09, which is an analog of C172, was also found to directly bind to the ATP-binding site of the NLRP3 NACHT domain and inhibit its ATPase activity, inhibiting NLRP3 inflammasome oligomerization and activation (123). Besides, Song et al. revealed that blocking NLRP3 phosphorylation at S194 significantly decreased NLRP3 inflammasome activation, suggesting that the inhibition of NLRP3 phosphorylation may be a potential approach for treating NLRP3-related diseases (124). Melatonin has proven to be effective in treating atherosclerosis by inhibiting NLRP3 inflammasome signaling pathway (125, 126).

Collectively, the research on novel methods for inhibiting PCSK9 and NLRP3 inflammasome is still in an early stage, and the efficacy, safety and feasibility of these approaches require further study.

Conclusions and perspective

In summary, PCSK9 can promote the occurrence and development of atherosclerosis by inhibiting the metabolism of LDL-C, enhancing the formation of foam cells and thus promoting the progression of vascular wall inflammation, suggesting that PCSK9 is an important intervention target in the occurrence and development of atherosclerosis. NLRP3 inflammasome activation contributes to the vascular inflammatory response driving atherosclerosis development and progression. Significantly, the effect of PCSK9 and the NLRP3 inflammasome on atherosclerosis

seems to be synergistic. Interactions between PCSK9 and the NLRP3 inflammasome may form a positive feedback loop, acting together to drive the inflammatory response and lipid accumulation and thus promoting atherosclerosis. On the one hand, the NLRP3 inflammasome signaling pathway has been shown to promote PCSK9 secretion by regulating IL-1 β , and this may be mediated by MAPK signaling. On the other hand, PCSK9 directly induces inflammatory responses in VSMCs as well as the expression and secretion of inflammatory factors and cytokines, including NLRP3 and its downstream molecules ASC, Caspase-1, IL-6, IL-18, and IL-1 β , in macrophages. Collectively, these findings suggest a bidirectional positive correlation between the NLRP3 inflammasome signaling pathway and PCSK9. Therapeutic options that target PCSK9 and NLRP3 inflammasome may play an important role in the future treatment of atherosclerosis-related diseases. For example, inclisiran not only decreases LDL-C levels but also reduces Lp(a) concentrations. Given that Lp(a) is an independent risk factor for atherosclerosis, early treatment with inclisiran might result in extensive benefits for patients and decrease the damage caused by atherosclerosis *via* multiple mechanisms. Additionally, the inhibitors of NLRP3 inflammasome signaling that are currently available are agents that target IL-1 β and caspase-1 as well as antagonists of the receptor P2X7.

It is noteworthy that knockout of the PCSK9 gene without inflammatory activation does not affect the levels of inflammatory proteins under physiological conditions; only the presence of factors that induce inflammatory responses, such as a high-fat diet, significantly decrease the levels of inflammatory cytokines. Besides, although the deficiency of the PCSK9 gene partially decreased inflammation in mice with atherosclerosis, it failed to diminish the inflammatory response completely. First, activation of the NLRP3 inflammasome during apoptosis is closely associated with mtROS-mediated mtDNA damage. Second, activated NLRP3-mediated IL-1 β secretion in turn serves as a proinflammatory stimulant that can promote inflammatory responses. In addition, Chen et al. indicated that NLRP3, NLRP12 and NLRC4 exerted a significant synergistic effect, suggesting that NLRP3, NLRP12 and NLRC4 could be mutually regulated (127). This synergistic effect can promote caspase-1-dependent GSDMD cleavage-induced pyroptosis during vascular damage and accelerate the secretion of IL-1 β . Finally, the synthesis of inflammatory factors and cytokines, such as ASC, Caspase-1, and IL-1 β , may not be fully dependent on the NLRP3 inflammasome. NLRP6, NLRP7, NLRP12, NLRC4 and AIM2 have been shown to contribute to proinflammatory cytokine expression. As shown in the study by Liu et al., overexpression of NLRP6 enhanced the activation of caspase-1 and gasdermin-D, induced the pyroptosis of human gingival fibroblasts, and promoted the release of the proinflammatory mediator IL-1 β (128).

In conclusion, the NLRP3 inflammasome signaling pathway and PCSK9 play critical roles in atherosclerosis and show promise as essential targets for the prevention and treatment of atherosclerosis. However, the precise mechanisms by which interactions between the NLRP3 inflammasome and PCSK9 affect atherosclerosis have largely remained unclear. Further research is needed to reveal the functions of PCSK9 and NLRP3 inflammasome signaling in atherosclerosis by revealing the underlying molecular mechanisms. Moreover, long-term clinical follow-up with a large sample size will still be necessary for

studying PCSK9 and NLRP3 inhibitors since these inhibitors may increase the risk of diabetes and neurological diseases.

Author contributions

YW and DF conceived the idea, analysis of literature, and writing of the manuscript. QY, JY, LW, and JW collected and read the literature and revised the article. MZ and ML read through and corrected the manuscript. All authors contributed to the article and approved the submitted version.

Funding

This work was supported by the National Natural Science Foundation of China [grant numbers 81800434], Grant of Sichuan Province Science and Technology Agency Grant [2019YJ0487].

Acknowledgments

Figures were created with BioRender software, ©biorender.com.

References

- Ruparelia N, Chai JT, Fisher EA, Choudhury RP. Inflammatory processes in cardiovascular disease: A route to targeted therapies. *Nat Rev Cardiol* (2017) 14(3):133–44. doi: 10.1038/nrcardio.2016.185
- Wu M-Y, Li C-J, Hou M-F, Chu P-Y. New insights into the role of inflammation in the pathogenesis of atherosclerosis. *Int J Mol Sci* (2017) 18(10):2034. doi: 10.3390/ijms18102034
- Souilhol C, Harmsen MC, Evans PC, Krenning G. Endothelial-mesenchymal transition in atherosclerosis. *Cardiovasc Res* (2018) 114(4):565–77. doi: 10.1093/cvr/cvx253
- Sandesara PB, Virani SS, Fazio S, Shapiro MD. The forgotten lipids: Triglycerides, remnant cholesterol, and atherosclerotic cardiovascular disease risk. *Endocr Rev* (2019) 40(2):537–57. doi: 10.1210/er.2018-00184
- Barale C, Melchionda E, Morotti A, Russo I. Pcsk9 biology and its role in atherothrombosis. *Int J Mol Sci* (2021) 22(11):5880. doi: 10.3390/ijms22115880
- Poirier S, Mayer G, Poupon V, McPherson PS, Desjardins R, Ly K, et al. Dissection of the endogenous cellular pathways of Pcsk9-induced low density lipoprotein receptor degradation: Evidence for an intracellular route. *J Biol Chem* (2009) 284(42):28856–64. doi: 10.1074/jbc.M109.037085
- Stoekenbroek RM, Lambert G, Cariou B, Hovingh GK. Inhibiting Pcsk9 - biology beyond ldl control. *Nat Rev Endocrinol* (2018) 15(1):52–62. doi: 10.1038/s41574-018-0110-5
- Tavori H, Giunzioni I, Predazzi IM, Plubell D, Shivinsky A, Miles J, et al. Human Pcsk9 promotes hepatic lipogenesis and atherosclerosis development Via apoe- and ldlr-mediated mechanisms. *Cardiovasc Res* (2016) 110(2):268–78. doi: 10.1093/cvr/cvw053
- Calara F, Silvestre M, Casanada F, Yuan N, Napoli C, Palinski W. Spontaneous plaque rupture and secondary thrombosis in apolipoprotein e-deficient and ldl receptor-deficient mice. *J Pathol* (2001) 195(2):257–63. doi: 10.1002/path.915
- Jo E-K, Kim JK, Shin D-M, Sasakawa C. Molecular mechanisms regulating Nlrp3 inflammasome activation. *Cell Mol Immunol* (2016) 13(2):148–59. doi: 10.1038/cmi.2015.95
- Olsen MB, Gregersen I, Sandanger Ø, Yang K, Sokolova M, Halvorsen BE, et al. Targeting the inflammasome in cardiovascular disease. *JACC Bas Transl Sci* (2022) 7(1):84–98. doi: 10.1016/j.jacbs.2021.08.006
- Grebe A, Hoss F, Latz E. Nlrp3 inflammasome and the il-1 pathway in atherosclerosis. *Circ Res* (2018) 122(12):1722–40. doi: 10.1161/CIRCRESAHA.118.311362
- Wang X, Li X, Liu S, Brickell AN, Zhang J, Wu Z, et al. Pcsk9 regulates pyroptosis Via mtDNA damage in chronic myocardial ischemia. *Bas Res In Cardiol* (2020) 115(6):66. doi: 10.1007/s00395-020-00832-w
- Huang L, Li Y, Cheng Z, Lv Z, Luo S, Xia Y. Pcsk9 promotes endothelial dysfunction during sepsis via the Tlr4/Myd88/Nf-Kb and Nlrp3 pathways. *Inflammation* (2022). doi: 10.1007/s10753-022-01715-z
- Zou Y, Chen Z, Zhang X, Yu J, Xu H, Cui J, et al. Targeting Pcsk9 ameliorates graft vascular disease in mice by inhibiting Nlrp3 inflammasome activation in vascular smooth muscle cells. *Front Immunol* (2022) 13:894789. doi: 10.3389/fimmu.2022.894789
- Ding Z, Wang X, Liu S, Zhou S, Kore RA, Mu S, et al. Nlrp3 inflammasome il-1β regulates Pcsk9 secretion. *Theranostics* (2020) 10(16):7100–10. doi: 10.7150/thno.45939
- Sundström C, Nilsson K. Cytochemical profile of human haematopoietic biopsies and derived cell lines. *Br J Haematol* (1977) 37(4):489–501. doi: 10.1111/j.1365-2141.1977.tb01022.x
- Seidah NG, Benjannet S, Wickham L, Marcinkiewicz J, Jasmin SB, Stifani S, et al. The secretory proprotein convertase neural apoptosis-regulated convertase 1 (Narc-1): Liver regeneration and neuronal differentiation. *Proc Natl Acad Sci U.S.A.* (2003) 100(3):928–33. doi: 10.1073/pnas.0335507100
- Moreau F, Thédrez A, Garçon D, Ayer A, Sotin T, Dijk W, et al. Pcsk9 is not secreted from mature differentiated intestinal cells. *J Lipid Res* (2021) 62:100096. doi: 10.1016/j.jlr.2021.100096
- Wang Y, Liu Z-P. Pcsk9 inhibitors: Novel therapeutic strategies for lowering ldl cholesterol. *Mini Rev Med Chem* (2019) 19(2):165–76. doi: 10.2174/1389557518666180423111442
- Lin X-L, Xiao L-L, Tang Z-H, Jiang Z-S, Liu M-H. Role of Pcsk9 in lipid metabolism and atherosclerosis. *Biomed Pharmacother = Biomed Pharmacother* (2018) 104:36–44. doi: 10.1016/j.biopha.2018.05.024
- Giunzioni I, Tavori H, Covarrubias R, Major AS, Ding L, Zhang Y, et al. Local effects of human Pcsk9 on the atherosclerotic lesion. *J Pathol* (2016) 238(1):52–62. doi: 10.1002/path.4630
- Ding Z, Liu S, Wang X, Deng X, Fan Y, Shahanawaz J, et al. Cross-talk between lox-1 and Pcsk9 in vascular tissues. *Cardiovasc Res* (2015) 107(4):556–67. doi: 10.1093/cvr/cvv178
- Kong N, Xu Q, Cui W, Feng X, Gao H. Pcsk9 inhibitor inclisiran for treating atherosclerosis Via regulation of endothelial cell pyroptosis. *Ann Transl Med* (2022) 10(22):1205. doi: 10.21037/atm-22-4652
- Zeng J, Tao J, Xi L, Wang Z, Liu L. Pcsk9 mediates the oxidative Low-Density Lipoprotein-Induced pyroptosis of vascular endothelial cells Via the Uqcrc1/Ros pathway. *Int J Mol Med* (2021) 47(4):53. doi: 10.3892/ijmm.2021.4886
- Schuster S, Rubil S, Endres M, Princen HMG, Boeckel J-N, Winter K, et al. Anti-Pcsk9 antibodies inhibit pro-atherogenic mechanisms in Apoe⁻³leiden.Cetp mice. *Sci Rep* (2019) 9(1):11079. doi: 10.1038/s41598-019-47242-0
- Ferri N, Tibolla G, Pirillo A, Cipollone F, Mezzetti A, Pacia S, et al. Proprotein convertase subtilisin kexin type 9 (Pcsk9) secreted by cultured smooth muscle cells reduces macrophages ldl levels. *Atherosclerosis* (2012) 220(2):381–6. doi: 10.1016/j.atherosclerosis.2011.11.026

Conflict of interest

The authors declare that the research was conducted in the absence of any commercial or financial relationships that could be construed as a potential conflict of interest.

Publisher's note

All claims expressed in this article are solely those of the authors and do not necessarily represent those of their affiliated organizations, or those of the publisher, the editors and the reviewers. Any product that may be evaluated in this article, or claim that may be made by its manufacturer, is not guaranteed or endorsed by the publisher.

Supplementary material

The Supplementary Material for this article can be found online at: <https://www.frontiersin.org/articles/10.3389/fimmu.2023.1126823/full#supplementary-material>

28. Ricci C, Ruscica M, Camera M, Rossetti L, Macchi C, Colciago A, et al. Pcsk9 induces a pro-inflammatory response in macrophages. *Sci Rep* (2018) 8(1):2267. doi: 10.1038/s41598-018-20425-x
29. Adorni MP, Cipollari E, Favari E, Zanotti I, Zimetti F, Corsini A, et al. Inhibitory effect of Pcsk9 on Abca1 protein expression and cholesterol efflux in macrophages. *Atherosclerosis* (2017) 256:1–6. doi: 10.1016/j.atherosclerosis.2016.11.019
30. Jin P, Gao D, Cong G, Yan R, Jia S. Role of Pcsk9 in homocysteine-accelerated lipid accumulation in macrophages and atherosclerosis in apoe mice. *Front Cardiovasc Med* (2021) 8:746989. doi: 10.3389/fcvm.2021.746989
31. Ragusa R, Basta G, Neglia D, De Caterina R, Del Turco S, Caselli C. Pcsk9 and atherosclerosis: Looking beyond ldl regulation. *Eur J Clin Invest* (2021) 51(4):e13459. doi: 10.1111/eci.13459
32. Ding Z, Wang X, Liu S, Zhou S, Kore RA, Mu S, et al. Nlrp3 inflammasome *Via* il-1 β regulates Pcsk9 secretion. *Theranostics* (2020) 10(16):7100–10. doi: 10.7150/thno.45939
33. Ding Z, Liu S, Wang X, Theus S, Deng X, Fan Y, et al. Pcsk9 regulates expression of scavenger receptors and ox-ldl uptake in macrophages. *Cardiovasc Res* (2018) 114(8):1145–53. doi: 10.1093/cvr/cvy079
34. Badimon L, Luquero A, Crespo J, Peña E, Borrell-Pages M. Pcsk9 and Lrp5 in macrophage lipid internalization and inflammation. *Cardiovasc Res* (2021) 117(9):2054–68. doi: 10.1093/cvr/cvaa254
35. Levy E, Ben Djoudi Ouadda A, Spahis S, Sane AT, Garofalo C, Grenier É, et al. Pcsk9 plays a significant role in cholesterol homeostasis and lipid transport in intestinal epithelial cells. *Atherosclerosis* (2013) 227(2):297–306. doi: 10.1016/j.atherosclerosis.2013.01.023
36. Tang Z-H, Peng J, Ren Z, Yang J, Li T-T, Li T-H, et al. New role of Pcsk9 in atherosclerotic inflammation promotion involving the Tlr4/Nf-Kb pathway. *Atherosclerosis* (2017) 262:113–22. doi: 10.1016/j.atherosclerosis.2017.04.023
37. Poirier S, Mayer G, Benjannet S, Bergeron E, Marcinkiewicz J, Nassoury N, et al. The proprotein convertase Pcsk9 induces the degradation of low density lipoprotein receptor (Ldlr) and its closest family members vldlr and Apoer2. *J Biol Chem* (2008) 283(4):2363–72. doi: 10.1074/jbc.M708098200
38. Bennett MR, Sinha S, Owens GK. Vascular smooth muscle cells in atherosclerosis. *Circ Res* (2016) 118(4):692–702. doi: 10.1161/CIRCRESAHA.115.306361
39. Ferri N, Marchianò S, Tibolla G, Baetta R, Dhyani A, Ruscica M, et al. Pcsk9 knock-out mice are protected from neointimal formation in response to perivascular carotid collar placement. *Atherosclerosis* (2016) 253:214–24. doi: 10.1016/j.atherosclerosis.2016.07.910
40. Ding Z, Liu S, Wang X, Deng X, Fan Y, Sun C, et al. Hemodynamic shear stress *Via* ros modulates Pcsk9 expression in human vascular endothelial and smooth muscle cells and along the mouse aorta. *Antioxid Redox Signal* (2015) 22(9):760–71. doi: 10.1089/ars.2014.6054
41. Zhang M-J, Zhou Y, Chen L, Wang X, Pi Y, Long C-Y, et al. Impaired Sirt1 promotes the migration of vascular smooth muscle cell-derived foam cells. *Histochem Cell Biol* (2016) 146(1):33–43. doi: 10.1007/s00418-016-1408-9
42. Ding Z, Liu S, Wang X, Mathur P, Dai Y, Theus S, et al. Cross-talk between Pcsk9 and damaged mtDNA in vascular smooth muscle cells: Role in apoptosis. *Antioxid Redox Signal* (2016) 25(18):997–1008. doi: 10.1089/ars.2016.6631
43. Martínez GJ, Celermajer DS, Patel S. The Nlrp3 inflammasome and the emerging role of colchicine to inhibit atherosclerosis-associated inflammation. *Atherosclerosis* (2018) 269:262–71. doi: 10.1016/j.atherosclerosis.2017.12.027
44. Landlinger C, Pouwer MG, Juno C, van der Hoorn JWA, Pieterman EJ, Jukema JW, et al. The At04a vaccine against proprotein convertase Subtilisin/Kexin type 9 reduces total cholesterol, vascular inflammation, and atherosclerosis in ApoE³leiden.Cetp mice. *Eur Heart J* (2017) 38(32):2499–507. doi: 10.1093/eurheartj/ehx260
45. Chistiakov DA, Orekhov AN, Bobryshev YV. Effects of shear stress on endothelial cells: Go with the flow. *Acta Physiol (Oxf)* (2017) 219(2):382–408. doi: 10.1111/apha.12725
46. Ding Z, Pothineni NVK, Goel A, Lüscher TF, Mehta JL. Pcsk9 and inflammation: Role of shear stress, pro-inflammatory cytokines, and ldx-1. *Cardiovasc Res* (2020) 116(5):908–15. doi: 10.1093/cvr/cvz313
47. Takeuchi O, Akira S. Pattern recognition receptors and inflammation. *Cell* (2010) 140(6):805–20. doi: 10.1016/j.cell.2010.01.022
48. Brubaker SW, Bonham KS, Zanon I, Kagan JC. Innate immune pattern recognition: A cell biological perspective. *Annu Rev Immunol* (2015) 33:257–90. doi: 10.1146/annurev-immunol-032414-112240
49. Song N, Li T. Regulation of Nlrp3 inflammasome by phosphorylation. *Front Immunol* (2018) 9:2305. doi: 10.3389/fimmu.2018.02305
50. Zahid A, Li B, Kombe AJK, Jin T, Tao J. Pharmacological inhibitors of the Nlrp3 inflammasome. *Front Immunol* (2019) 10:2538. doi: 10.3389/fimmu.2019.02538
51. Abbate A, Toldo S, Marchetti C, Kron J, Van Tassel BW, Dinarello CA. Interleukin-1 and the inflammasome as therapeutic targets in cardiovascular disease. *Circ Res* (2020) 126(9):1260–80. doi: 10.1161/CIRCRESAHA.120.315937
52. Shiohara M, Taniguchi Si, Masumoto J, Yasui K, Koike K, Komiyama A, et al. Asc, which is composed of a pyd and a card, is up-regulated by inflammation and apoptosis in human neutrophils. *Biochem Biophys Res Commun* (2002) 293(5):1314–8. doi: 10.1016/S0006-291X(02)00384-4
53. Boucher D, Monteleone M, Coll RC, Chen KW, Ross CM, Teo JL, et al. Caspase-1 self-cleavage is an intrinsic mechanism to terminate inflammasome activity. *J Exp Med* (2018) 215(3):827–40. doi: 10.1084/jem.20172222
54. Zhang H, Du Y, Guo Y, Wang Z, Li H, Lv Z, et al. Tlr4-Nlrp3-Gsdmd-Mediated pyroptosis plays an important role in aggravated liver injury of Cd38 sepsis mice. *J Immunol Res* (2021) 2021:6687555. doi: 10.1155/2021/6687555
55. Palová-Jelínková L, Dáňová K, Drašarová H, Dvořák M, Funda DP, Fundová P, et al. Pepsin digest of wheat gliadin fraction increases production of il-1 β *Via* Tlr4/Myd88/Trif/Mapk/Nf-Kb signaling pathway and an Nlrp3 inflammasome activation. *PLoS One* (2013) 8(4):e62426. doi: 10.1371/journal.pone.0062426
56. Lu A, Magupalli VG, Ruan J, Yin Q, Atianand MK, Vos MR, et al. Unified polymerization mechanism for the assembly of asc-dependent inflammasomes. *Cell* (2014) 156(6):1193–206. doi: 10.1016/j.cell.2014.02.008
57. Fernandes-Alnemri T, Wu J, Yu JW, Datta P, Miller B, Jankowski W, et al. The pyroptosome: A supramolecular assembly of asc dimers mediating inflammatory cell death *Via* caspase-1 activation. *Cell Death Different* (2007) 14(9):1590–604. doi: 10.1038/sj.cdd.4402194
58. Chen G, Shaw MH, Kim Y-G, Nuñez G. Nod-like receptors: Role in innate immunity and inflammatory disease. *Annu Rev Pathol* (2009) 4:365–98. doi: 10.1146/annurev.pathol.4.110807.092239
59. Wang K, Sun Q, Zhong X, Zeng M, Zeng H, Shi X, et al. Structural mechanism for gsdmd targeting by autoprocessed caspases in pyroptosis. *Cell* (2020) 180(5):941–955.e20. doi: 10.1016/j.cell.2020.02.002
60. Wang C, Yang T, Xiao J, Xu C, Alippe Y, Sun K, et al. Nlrp3 inflammasome activation triggers gasdermin d-independent inflammation. *Sci Immunol* (2021) 6(64):eab3859. doi: 10.1126/sciimmunol.abj3859
61. Qian Z, Zhao Y, Wan C, Deng Y, Zhuang Y, Xu Y, et al. Pyroptosis in the initiation and progression of atherosclerosis. *Front Pharmacol* (2021) 12:652963. doi: 10.3389/fphar.2021.652963
62. Liu Y, Tie L. Apolipoprotein m and sphingosine-1-Phosphate complex alleviates tnF-A-Induced endothelial cell injury and inflammation through P13k/Akt signaling pathway. *BMC Cardiovasc Disord* (2019) 19(1):279. doi: 10.1186/s12872-019-1263-4
63. Jin H, Zhu Y, Wang X-D, Luo E-F, Li Y-P, Wang B-L, et al. Bdnf corrects Nlrp3 inflammasome-induced pyroptosis and glucose metabolism reprogramming through Klf2/HK1 pathway in vascular endothelial cells. *Cell Signal* (2021) 78:109843. doi: 10.1016/j.cellsig.2020.109843
64. Li Y, Niu X, Xu H, Li Q, Meng L, He M, et al. Vx-765 attenuates atherosclerosis in apoe deficient mice by modulating vsmcs pyroptosis. *Exp Cell Res* (2020) 389(1):111847. doi: 10.1016/j.yexcr.2020.111847
65. Wen C, Yang X, Yan Z, Zhao M, Yue X, Cheng X, et al. Nalp3 inflammasome is activated and required for vascular smooth muscle cell calcification. *Int J Cardiol* (2013) 168(3):2242–7. doi: 10.1016/j.ijcard.2013.01.211
66. Schönbeck U, Mach F, Bonnefoy JY, Loppnow H, Flad HD, Libby P. Ligation of Cd40 activates interleukin 1 β -converting enzyme (Caspase-1) activity in vascular smooth muscle and endothelial cells and promotes elaboration of active interleukin 1 β . *J Biol Chem* (1997) 272(31):19569–74. doi: 10.1074/jbc.272.31.19569
67. Lin S-J, Yen H-T, Chen Y-H, Ku H-H, Lin F-Y, Chen Y-L. Expression of interleukin-1 β and interleukin-1 receptor antagonist in oxdl-treated human aortic smooth muscle cells and in the neointima of cholesterol-fed endothelial-denuded rabbits. *J Cell Biochem* (2003) 88(4):836–47. doi: 10.1002/jcb.10431
68. Gage J, Hasu M, Thabet M, Whitman SC. Caspase-1 deficiency decreases atherosclerosis in apolipoprotein e-null mice. *Can J Cardiol* (2012) 28(2):222–9. doi: 10.1016/j.cjca.2011.10.013
69. Zheng F, Xing S, Gong Z, Mu W, Xing Q. Silence of Nlrp3 suppresses atherosclerosis and stabilizes plaques in apolipoprotein e-deficient mice. *Mediators Inflammation* (2014) 2014:507208. doi: 10.1155/2014/507208
70. Liu W, Yin Y, Zhou Z, He M, Dai Y. Oxdl-induced il-1 β secretion promoting foam cells formation was mainly *Via* Cd36 mediated ros production leading to Nlrp3 inflammasome activation. *Inflammation Res* (2014) 63(1):33–43. doi: 10.1007/s00011-013-0667-3
71. Ding Z, Liu S, Wang X, Dai Y, Khaidakov M, Deng X, et al. Lox-1, mtdna damage, and Nlrp3 inflammasome activation in macrophages: Implications in atherogenesis. *Cardiovasc Res* (2014) 103(4):619–28. doi: 10.1093/cvr/cvu114
72. Niemi K, Teirilä L, Lappalainen J, Rajamäki K, Baumann MH, Öörni K, et al. Serum amyloid a activates the Nlrp3 inflammasome *Via* P2x7 receptor and a cathepsin b-sensitive pathway. *J Immunol* (2011) 186(11):6119–28. doi: 10.4049/jimmunol.1002843
73. Duewell P, Kono H, Rayner KJ, Sirois CM, Vladimer G, Bauernfeind FG, et al. Nlrp3 inflammasomes are required for atherogenesis and activated by cholesterol crystals. *Nature* (2010) 464(7293):1357–61. doi: 10.1038/nature08938
74. Di Gioia M, Spreafico R, Springstead JR, Mendelson MM, Joehanes R, Levy D, et al. Endogenous oxidized phospholipids reprogram cellular metabolism and boost hyperinflammation. *Nat Immunol* (2020) 21(1):42–53. doi: 10.1038/s41590-019-0539-2
75. Zhu L, Zhao Q, Yang T, Ding W, Zhao Y. Cellular metabolism and macrophage functional polarization. *Int Rev Immunol* (2015) 34(1):82–100. doi: 10.3109/08830185.2014.969421
76. Orecchioni M, Kobayama K, Winkels H, Ghosh H, McArdle S, Mikulski Z, et al. Olfactory receptor 2 in vascular macrophages drives atherosclerosis by Nlrp3-

dependent il-1 production. *Sci (New York NY)* (2022) 375(6577):214–21. doi: 10.1126/science.abg3067

77. Zhang X, McDonald JG, Aryal B, Canfrán-Duque A, Goldberg EL, Araldi E, et al. Desmosterol suppresses macrophage inflammasome activation and protects against vascular inflammation and atherosclerosis. *Proc Natl Acad Sci U.S.A.* (2021) 118(47):e2107682118. doi: 10.1073/pnas.2107682118

78. Galea J, Armstrong J, Gadsdon P, Holden H, Francis SE, Holt CM. Interleukin-1 beta in coronary arteries of patients with ischemic heart disease. *Arteriosclerosis Thrombosis Vasc Biol* (1996) 16(8):1000–6. doi: 10.1161/01.ATV.16.8.1000

79. Wilson HL, Varcoe RW, Stokes L, Holland KL, Francis SE, Dower SK, et al. P2x receptor characterization and il-1/Il-1ra release from human endothelial cells. *Br J Pharmacol* (2007) 151(1):115–27. doi: 10.1038/sj.bjp.0707213

80. Li B-W, Liu Y, Zhang L, Guo X-Q, Wen C, Zhang F, et al. Cytotoxin-associated gene a (Caga) promotes aortic endothelial inflammation and accelerates atherosclerosis through the Nlrp3/Caspase-1/Il-1 β axis. *FASEB J* (2021) 35(11):e21942. doi: 10.1096/fj.202100695RR

81. Tedgui A, Mallat Z. Cytokines in atherosclerosis: Pathogenic and regulatory pathways. *Physiol Rev* (2006) 86(2):515–81. doi: 10.1152/physrev.00024.2005

82. Hettwer J, Hinterdobler J, Miritsch B, Deutsch M-A, Li X, Mauersberger C, et al. Interleukin-1 β suppression dampens inflammatory leucocyte production and uptake in atherosclerosis. *Cardiovasc Res* (2022) 118(13):2778–91. doi: 10.1093/cvr/cvab337

83. Clarke MCH, Talib S, Figg NL, Bennett MR. Vascular smooth muscle cell apoptosis induces interleukin-1-Directed inflammation: Effects of hyperlipidemia-mediated inhibition of phagocytosis. *Circ Res* (2010) 106(2):363–72. doi: 10.1161/CIRCRESAHA.109.208389

84. Hallenbeck WH, Markey DR, Dolan DG. Analyses of tissue, blood, and urine samples from a baboon gavaged with chrysotile and crocidolite asbestos. *Environ Res* (1981) 25(2):349–60. doi: 10.1016/0013-9351(81)90037-2

85. Burger F, Baptista D, Roth A, da Silva RF, Montecucco F, Mach F, et al. Nlrp3 inflammasome activation controls vascular smooth muscle cells phenotypic switch in atherosclerosis. *Int J Mol Sci* (2021) 23(1):340. doi: 10.3390/ijms23010340

86. Ruscica M, Ferri N, Macchi C, Corsini A, Sirtori CR. Lipid lowering drugs and inflammatory changes: An impact on cardiovascular outcomes? *Ann Med* (2018) 50(6):461–84. doi: 10.1080/07853890.2018.1498118

87. Cyr Y, Bissonnette S, Lamantia V, Wassef H, Loizon E, Ngo Sock ET, et al. White adipose tissue surface expression of ldlr and Cd36 is associated with risk factors for type 2 diabetes in adults with obesity. *Obes (Silver Spring)* (2020) 28(12):2357–67. doi: 10.1002/oby.22985

88. Cyr Y, Lamantia V, Bissonnette S, Burnette M, Besse-Patin A, Demers A, et al. Lower plasma Pcsk9 in normocholesterolemic subjects is associated with upregulated adipose tissue surface-expression of ldlr and Cd36 and Nlrp3 inflammasome. *Physiol Rep* (2021) 9(3):e14721. doi: 10.14841/phy2.14721

89. Grune J, Meyborg H, Bezhaeva T, Kappert K, Hillmeister P, Kintscher U, et al. Pcsk9 regulates the chemokine receptor Ccr2 on monocytes. *Biochem Biophys Res Commun* (2017) 485(2):312–8. doi: 10.1016/j.bbrc.2017.02.085

90. Hoseini Z, Sepahvand F, Rashidi B, Sahebkar A, Masoudifar A, Mirzaei H. Nlrp3 inflammasome: Its regulation and involvement in atherosclerosis. *J Cell Physiol* (2018) 233(3):2116–32. doi: 10.1002/jcp.25930

91. Yang C-L, Zeng Y-D, Hu Z-X, Liang H. Pcsk9 promotes the secretion of pro-inflammatory cytokines by macrophages to aggravate H/R-induced cardiomyocyte injury Via activating nf-kb signalling. *Gen Physiol Biophys* (2020) 39(2):123–34. doi: 10.4149/gpb-2019057

92. Cheng S-B, Nakashima A, Huber WJ, Davis S, Banerjee S, Huang Z, et al. Pyroptosis is a critical inflammatory pathway in the placenta from early onset preeclampsia and in human trophoblasts exposed to hypoxia and endoplasmic reticulum stressors. *Cell Death Dis* (2019) 10(12):927. doi: 10.1038/s41419-019-2162-4

93. Ding Z, Wang X, Liu S, Shahanaawaz J, Theus S, Fan Y, et al. Pcsk9 expression in the ischaemic heart and its relationship to infarct size, cardiac function, and development of autophagy. *Cardiovasc Res* (2018) 114(13):1738–51. doi: 10.1093/cvr/cvy128

94. Zhaolin Z, Guohua L, Shiyuan W, Zuo W. Role of pyroptosis in cardiovascular disease. *Cell Prolif* (2019) 52(2):e12563. doi: 10.1111/cpr.12563

95. Wang Y, Shi P, Chen Q, Huang Z, Zou D, Zhang J, et al. Mitochondrial ros promote macrophage pyroptosis by inducing gsdmd oxidation. *J Mol Cell Biol* (2019) 11(12):1069–82. doi: 10.1093/jmcb/mjz020

96. Wu N-Q, Shi H-W, Li J-J. Proprotein convertase Subtilisin/Kexin type 9 and inflammation: An updated review. *Front Cardiovasc Med* (2022) 9:763516. doi: 10.3389/fcvm.2022.763516

97. Kumar S, Kang D-W, Rezvan A, Jo H. Accelerated atherosclerosis development in C57bl6 mice by overexpressing aav-mediated Pcsk9 and partial carotid ligation. *Lab Invest* (2017) 97(8):935–45. doi: 10.1038/labinvest.2017.47

98. Frostegård J, Ahmed S, Hafström I, Ajejanova S, Rahman M. Low levels of Pcsk9 are associated with remission in patients with rheumatoid arthritis treated with anti-Tnf-A: Potential underlying mechanisms. *Arthritis Res Ther* (2021) 23(1):32. doi: 10.1186/s13075-020-02386-7

99. O'Donoghue ML, Fazio S, Giugliano RP, Stroes ESG, Kanevsky E, Gouni-Berthold I, et al. Lipoprotein(a), Pcsk9 inhibition, and cardiovascular risk. *Circulation* (2019) 139(12):1483–92. doi: 10.1161/CIRCULATIONAHA.118.037184

100. Mullard A. Nine paths to Pcsk9 inhibition. *Nat Rev Drug Discovery* (2017) 16(5):299–301. doi: 10.1038/nrd.2017.83

101. Oyama K, Furtado RHM, Fagundes A, Zelniker TA, Tang M, Kuder J, et al. Effect of evolucumab on complex coronary disease requiring revascularization. *J Am Coll Cardiol* (2021) 77(3):259–67. doi: 10.1016/j.jacc.2020.11.011

102. Schwartz GG, Steg PG, Szarek M, Bittner VA, Diaz R, Goodman SG, et al. Peripheral artery disease and venous thromboembolic events after acute coronary syndrome: Role of lipoprotein(a) and modification by alirocumab: Prespecified analysis of the odyssey outcomes randomized clinical trial. *Circulation* (2020) 141(20):1608–17. doi: 10.1161/CIRCULATIONAHA.120.046524

103. Guedeney P, Giustino G, Sorrentino S, Claessen BE, Camaj A, Kalkman DN, et al. Efficacy and safety of alirocumab and evolucumab: A systematic review and meta-analysis of randomized controlled trials. *Eur Heart J* (2019) 43(2):e17–125. doi: 10.1093/eurheartj/ehz430

104. Xu S, Luo S, Zhu Z, Xu J. Small molecules as inhibitors of Pcsk9: Current status and future challenges. *Eur J Med Chem* (2019) 162:212–33. doi: 10.1016/j.ejmech.2018.11.011

105. Fitzgerald K, Frank-Kamenetsky M, Shulga-Morskaya S, Liebow A, Bettencourt BR, Sutherland JE, et al. Effect of an rna interference drug on the synthesis of proprotein convertase Subtilisin/Kexin type 9 (Pcsk9) and the concentration of serum ldl cholesterol in healthy volunteers: A randomised, single-blind, placebo-controlled, phase 1 trial. *Lancet* (2014) 383(9911):60–8. doi: 10.1016/S0140-6736(13)61914-5

106. Warden BA, Duell PB. Inclisiran: A novel agent for lowering apolipoprotein b-containing lipoproteins. *J Cardiovasc Pharmacol* (2021) 78(2):e157–e74. doi: 10.1097/FJC.0000000000001053

107. Fitzgerald K, White S, Borodovsky A, Bettencourt BR, Strahs A, Clausen V, et al. A highly durable rna therapeutic inhibitor of Pcsk9. *New Engl J Med* (2017) 376(1):41–51. doi: 10.1056/NEJMoa1609243

108. Ray KK, Wright RS, Kallend D, Koenig W, Leiter LA, Raal FJ, et al. Two phase 3 trials of inclisiran in patients with elevated ldl cholesterol. *New Engl J Med* (2020) 382(16):1507–19. doi: 10.1056/NEJMoa1912387

109. Hardy J, Niman S, Pereira E, Lewis T, Reid J, Choksi R, et al. A critical review of the efficacy and safety of inclisiran. *Am J Cardiovasc Drugs* (2021) 21(6):629–42. doi: 10.1007/s40256-021-00477-7

110. Ataei S, Momtazi-Borojeni AA, Ganjali S, Banach M, Sahebkar A. The immunogenic potential of Pcsk9 peptide vaccine in mice. *Curr Med Chem* (2023) 30:1–8. doi: 10.2174/0929867329666220930114429

111. Wu D, Pan Y, Yang S, Li C, Zhou Y, Wang Y, et al. Pcsk9q9b-003 vaccine attenuates atherosclerosis in apolipoprotein e-deficient mice. *Cardiovasc Drugs Ther* (2021) 35(1):141–51. doi: 10.1007/s10557-020-07041-6

112. Momtazi-Borojeni AA, Jaafari MR, Badiie A, Banach M, Sahebkar A. Therapeutic effect of nanoliposomal Pcsk9 vaccine in a mouse model of atherosclerosis. *BMC Med* (2019) 17(1):223. doi: 10.1186/s12916-019-1457-8

113. Dinarello CA, Simon A, van der Meer JWM. Treating inflammation by blocking interleukin-1 in a broad spectrum of diseases. *Nat Rev Drug Discovery* (2012) 11(8):633–52. doi: 10.1038/nrd3800

114. Nowarski R, Jackson R, Gagliani N, de Zoete MR, Palm NW, Bailis W, et al. Epithelial il-18 equilibrium controls barrier function in colitis. *Cell* (2015) 163(6):1444–56. doi: 10.1016/j.cell.2015.10.072

115. Lu B, Nakamura T, Inouye K, Li J, Tang Y, Lundback P, et al. Novel role of pkr in inflammasome activation and Hmgbl release. *Nature* (2012) 488(7413):670–4. doi: 10.1038/nature11290

116. Coll RC, Robertson AAB, Chae JJ, Higgins SC, Muñoz-Planillo R, Inerra MC, et al. A small-molecule inhibitor of the Nlrp3 inflammasome for the treatment of inflammatory diseases. *Nat Med* (2015) 21(3):248–55. doi: 10.1038/nm.3806

117. Davis BK, Wen H, Ting JP. The inflammasome nlrs in immunity, inflammation, and associated diseases. *Annu Rev Immunol* (2011) 29:707–35. doi: 10.1146/annurev-immunol-031210-101405

118. Wu D, Chen Y, Sun Y, Gao Q, Li H, Yang Z, et al. Target of Mcc950 in inhibition of Nlrp3 inflammasome activation: A literature review. *Inflammation* (2020) 43(1):17–23. doi: 10.1007/s10753-019-01098-8

119. van der Heijden T, Kritikou E, Venema W, van Duijn J, van Santbrink PJ, Slütter B, et al. Nlrp3 inflammasome inhibition by Mcc950 reduces atherosclerotic lesion development in apolipoprotein e-deficient mice-brief report. *Arteriosclerosis Thrombosis Vasc Biol* (2017) 37(8):1457–61. doi: 10.1161/ATVBAHA.117.309575

120. Zeng W, Wu D, Sun Y, Suo Y, Yu Q, Zeng M, et al. The selective Nlrp3 inhibitor Mcc950 hinders atherosclerosis development by attenuating inflammation and pyroptosis in macrophages. *Sci Rep* (2021) 11(1):19305. doi: 10.1038/s41598-021-98437-3

121. MacDonald JA, Wijekoon CP, Liao K-C, Muruve DA. Biochemical and structural aspects of the atp-binding domain in inflammasome-forming human nlrp proteins. *IUBMB Life* (2013) 65(10):851–62. doi: 10.1002/iub.1210

122. Coll RC, Hill JR, Day CJ, Zamoshnikova A, Boucher D, Massey NL, et al. Mcc950 directly targets the Nlrp3 atp-hydrolysis motif for inflammasome inhibition. *Nat Chem Biol* (2019) 15(6):556–9. doi: 10.1038/s41589-019-0277-7

123. Jiang H, He H, Chen Y, Huang W, Cheng J, Ye J, et al. Identification of a selective and direct Nlrp3 inhibitor to treat inflammatory disorders. *J Exp Med* (2017) 214(11):3219–38. doi: 10.1084/jem.20171419

124. Song N, Liu Z-S, Xue W, Bai Z-F, Wang Q-Y, Dai J, et al. Nlrp3 phosphorylation is an essential priming event for inflammasome activation. *Mol Cell* (2017) 68(1):185–197.e6. doi: 10.1016/j.molcel.2017.08.017

125. Ma S, Chen J, Feng J, Zhang R, Fan M, Han D, et al. Melatonin ameliorates the progression of atherosclerosis Via mitophagy activation and Nlrp3 inflammasome inhibition. *Oxid Med Cell Longevity* (2018) 2018:9286458. doi: 10.1155/2018/9286458
126. Zhang Y, Liu X, Bai X, Lin Y, Li Z, Fu J, et al. Melatonin prevents endothelial cell pyroptosis Via regulation of long noncoding rna Meg3/Mir-223/Nlrp3 axis. *J Pineal Res* (2018) 64(2):e12449. doi: 10.1111/jpi.12449
127. Chen H, Deng Y, Gan X, Li Y, Huang W, Lu L, et al. Nlrp12 collaborates with Nlrp3 and Nlrc4 to promote pyroptosis inducing ganglion cell death of acute glaucoma. *Mol Neurodegenerat* (2020) 15(1):26. doi: 10.1186/s13024-020-00372-w
128. Liu W, Liu J, Wang W, Wang Y, Ouyang X. Nlrp6 induces pyroptosis by activation of caspase-1 in gingival fibroblasts. *J Dental Res* (2018) 97(12):1391–8. doi: 10.1177/0022034518775036

Glossary

PCSK9	proprotein convertase subtilisin/kexin type 9
ER	endoplasmic reticulum
LDLR	low-density lipoprotein receptor
LDL-C	low-density lipoprotein cholesterol
MΦ	macrophage
ox-LDL	oxidative low-density lipoprotein
LRP1	LDL-R-related protein 1
TLR4	toll-like receptors 4
NF-κB	nuclear factor kappa-B
IκBα	inhibitor kappa B alpha
ApoER2	apolipoprotein E receptor-2
ApoB48	apolipoprotein B-48
ACAT-2	acyl-coA cholesteryl acyl transferases 2
VSMCs	vascular smooth muscle cells
Bax	BCL2-associated X
Bcl-2	B-cell lymphoma-2
MAPK	mitogen-activated protein kinases
mTOR	mammalian target of rapamycin
VCAM-1	vascular cell adhesion molecule-1
ICAM-1	intercellular adhesion molecule-1
EC	endothelial cells
AP-1	activator protein-1
PRR	pattern recognition receptor
NLRP3	NOD-like receptor thermal protein domain associated protein 3
PAMPs	pathogen-associated molecular pattern
DAMPs	damage associated molecular patterns
LRR	leucine-rich repeat domain
NACHT	nucleotide triphosphatase domain
PYD	pyrin domain
CARD	caspase recruitment domain
TRIF	TRI domain-containing adaptor inducing interferon.β
MyD88	myeloid differentiation factor 88
IL-1β	interleukin-1β
IL-18	interleukin-18
GSDMD	gasdermin-D
GSDMD-NT	N-terminal cleaving product
Olf2	olfactory receptor 2
mtROS	mitochondrial reactive oxygen species

(Continued)

Continued

HUVECs	human umbilical vein endothelial cells
P2X (4) R	purinergic receptor P2X4
P2X (7) R	purinergic receptor P2X7
IL-1Ra	interleukin-1 receptor antagonist
CagA	cytotoxin-associated protein
Oct-4	POU class 5 homeobox 1
KLF4	kruppel-like factor 4
ATP	adenosine-triphosphate
LPS	lipopolysaccharide
mtDNA	mitochondrial deoxyribonucleic acid
MAECs	mouse aortic endothelial cells
BMDCs	bone marrow-derived dendritic cells
HAoSMCs	human aortic smooth muscle cells
BMDMs	primary bone marrow-derived macrophages
HEK293T	human embryonic kidney 293T
ACS	acute coronary syndrome
PBMC	peripheral blood mononuclear cells
GLP-1R	glucagon like peptide 1 receptor
PKC	protein kinase C
NOX-4	NADPH oxidase 4
LDH	lactate dehydrogenase
CCL-2	chemokine ligand 2
CC	cholesterol crystals
UQCRC1	ubiquinol-cytochrome c reductase core protein 1
MI	myocardial infarct
HeFH	heterozygous familial hypercholesterolemia
SREBP-2	sterol element binding protein 2
CAT	a catalytic domain
CHD	coronary heart disease
ASCVD	atherosclerotic cardiovascular disease
IgG1	immunoglobulin G1
WAT	White Adipose Tissue
CVD	cardiovascular disease
NAFLD	non-alcoholic fatty liver diseases
NASH	non-alcoholic steatohepatitis
CD36	cluster of differentiation 36
LOX-1	lectin-like ox-LDL receptor 1
TNF-α	tumor necrosis factor-α
T2D	Type 2 diabetes
MI	myocardial infarction.



OPEN ACCESS

EDITED BY

Jianmin Chen,
Queen Mary University of London,
United Kingdom

REVIEWED BY

Hongxu Xian,
University of California, San Diego,
United States
Han Zhu,
Stanford University, United States

*CORRESPONDENCE

Xiang Cheng
✉ nathanxc@hust.edu.cn

Nian-Guo Dong
✉ dongnianguo@hotmail.com

Zi-Hua Zhou
✉ zhouzihua@hust.edu.cn

[†]These authors have contributed equally to this work

SPECIALTY SECTION

This article was submitted to
Inflammation,
a section of the journal
Frontiers in Immunology

RECEIVED 19 December 2022

ACCEPTED 20 February 2023

PUBLISHED 07 March 2023

CITATION

Zhang X-Z, Chen X-L, Tang T-T, Zhang S,
Li Q-L, Xia N, Nie S-F, Zhang M, Zhu Z-F,
Zhou Z-H, Dong N-G and Cheng X (2023)
T lymphocyte characteristics and immune
repertoires in the epicardial adipose tissue
of heart failure patients.
Front. Immunol. 14:1126997.
doi: 10.3389/fimmu.2023.1126997

COPYRIGHT

© 2023 Zhang, Chen, Tang, Zhang, Li, Xia,
Nie, Zhang, Zhu, Zhou, Dong and Cheng.
This is an open-access article distributed
under the terms of the [Creative Commons
Attribution License \(CC BY\)](#). The use,
distribution or reproduction in other
forums is permitted, provided the original
author(s) and the copyright owner(s) are
credited and that the original publication in
this journal is cited, in accordance with
accepted academic practice. No use,
distribution or reproduction is permitted
which does not comply with these terms.

T lymphocyte characteristics and immune repertoires in the epicardial adipose tissue of heart failure patients

Xu-Zhe Zhang^{1,2,3†}, Xian-Li Chen^{1,2,3†}, Ting-Ting Tang^{1,2,3†},
Si Zhang^{1,2,3}, Qin-Lin Li^{1,2,3}, Ni Xia^{1,2,3}, Shao-Fang Nie^{1,2,3},
Min Zhang^{1,2,3}, Zheng-Feng Zhu^{1,2,3}, Zi-Hua Zhou^{1,2,3*},
Nian-Guo Dong^{4*} and Xiang Cheng^{1,2,3*}

¹Department of Cardiology, Union Hospital, Tongji Medical College, Huazhong University of Science and Technology, Wuhan, China, ²Hubei Key Laboratory of Biological Targeted Therapy, Union Hospital, Tongji Medical College, Huazhong University of Science and Technology, Wuhan, China, ³Hubei Provincial Engineering Research Center of Immunological Diagnosis and Therapy for Cardiovascular Diseases, Union Hospital, Tongji Medical College, Huazhong University of Science and Technology, Wuhan, China, ⁴Department of Cardiovascular Surgery, Union Hospital, Tongji Medical College, Huazhong University of Science and Technology, Wuhan, China

Background: Epicardial adipose tissue (EAT) acts as an active immune organ and plays a critical role in the pathogenesis of heart failure (HF). However, the characteristics of immune cells in EAT of HF patients have rarely been elucidated.

Methods: To identify key immune cells in EAT, an integrated bioinformatics analysis was performed on public datasets. EAT samples with paired subcutaneous adipose tissue (SAT), heart, and peripheral blood samples from HF patients were collected in validation experiments. T cell receptor (TCR) repertoire was assessed by high-throughput sequencing. The phenotypic characteristics and key effector molecules of T lymphocytes in EAT were assessed by flow cytometry and histological staining.

Results: Compared with SAT, EAT was enriched for immune activation-related genes and T lymphocytes. Compared with EAT from the controls, activation of T lymphocytes was more pronounced in EAT from HF patients. T lymphocytes in EAT of HF patients were enriched by highly expanded clonotypes and had greater TCR clonotype sharing with cardiac tissue relative to SAT. Experiments confirmed the abundance of IFN- γ^+ effector memory T lymphocytes (T_{EM}) in EAT of HF patients. CCL5 and GZMK were confirmed to be associated with T lymphocytes in EAT of HF patients.

Conclusion: EAT of HF patients was characterized by pronounced immune activation of clonally expanded IFN- γ^+ T_{EM} and a generally higher degree of TCR clonotypes sharing with paired cardiac tissue.

KEYWORDS

epicardial adipose tissue, heart failure, immune infiltration, T lymphocytes, TCR immune repertoires, bioinformatics analyses

Introduction

Due to its unique anatomic and functional features (1), epicardial adipose tissue (EAT) and its critical role in the pathogenesis of cardiovascular diseases have received increasing attention in recent years. EAT covers nearly 80% of the heart's surface and accounts for approximately 15% of the total heart mass (2). EAT is mainly located in the atrioventricular and the interventricular sulcus (3). EAT is in direct contact with the myocardium without fascial interruption, allowing mutual crosstalk. Under normal conditions, EAT is cardio-protective by maintaining lipid homeostasis and providing mechanical protection to the adjacent myocardium. Under pathological conditions, however, EAT transforms into a pro-inflammatory and pro-fibrotic phenotype and is cardiac deleterious (4).

Heart failure (HF) is a complex clinical condition with a poor prognosis characterized by cardiac diastolic or systolic dysfunction (5). Emerging evidence has linked EAT to the pathogenesis of HF (4, 6). Sodium-glucose cotransporter 2 (SGLT2) inhibitors is a novel agent for the treatment of HF (7). A reduction in EAT volume has been linked to the beneficial effects of SGLT2 inhibitor in HF patients (8). The mechanisms by which EAT contributes to HF remain unclear, but likely involve enhanced inflammation. EAT is populated by immune cells including macrophages, T lymphocytes, mast cells, etc., and serves as the source of pro-inflammatory mediators (9–11). Pro-inflammatory cytokines and pro-fibrotic factors, such as leptin, TNF- α , IL-1 β , and IL-6 are up-regulated in EAT under pathological conditions (12, 13) and may diffuse into the adjacent myocardium to promote cardiac dysfunction. However, a better understanding of the relationship between EAT and HF requires a full-scale knowledge of the changes in the immune microenvironment within EAT in HF. Here, we performed integrated bioinformatics and immune cell infiltration analyses on public datasets to characterize the immune features and immune cell profiles of EAT in HF patients. The results suggested

that EAT of HF patients was characterized by pronounced immune activation, particularly by the accumulation of T lymphocytes. Further analyses indicated that T lymphocytes in EAT of HF patients were highly expanded, closely related to those in cardiac tissue, and dominated by IFN- γ ⁺ effector memory T lymphocytes (T_{EM}). GZMK and CCL5 identified by bioinformatics analyses may act as the key effector molecules of T lymphocytes in EAT of HF patients. The overall flowchart of this study is shown in Figure 1.

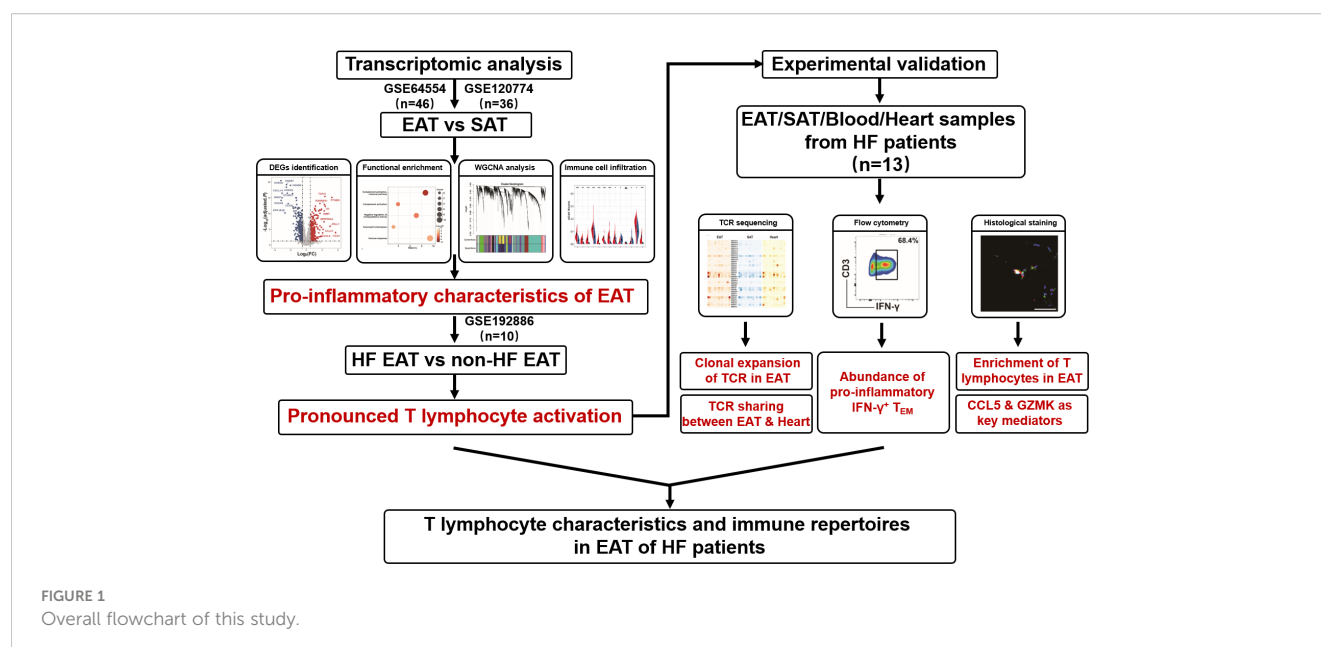
Materials and methods

Public datasets in transcriptomic analysis

GSE64554 (14), GSE120774 (15), GSE192886 (16) and GSE24425 (17) were obtained from Gene Expression Omnibus (GEO, <https://www.ncbi.nlm.nih.gov/geo>). Array or sequencing data of paired EAT and SAT in GSE64554 (n=46), GSE120774 (n=36), and GSE24425 (n=12) were from patients undergoing cardiac valve or coronary artery bypass graft surgery. GSE192886 contained sequencing data of EAT from HF patients (n=5) and non-HF patients (n=5) undergoing coronary artery bypass graft surgery. Clinical characteristics for analyzed patients can refer to the original citations of these datasets and Tables S1–S3.

Patients and samples in the experimental validation

In the validation experiments, fresh EAT with paired SAT, heart, and peripheral blood samples were collected from HF patients undergoing heart transplantation in Wuhan Union Hospital. Peripheral blood samples were obtained before surgery. SAT samples were obtained from the suprasternal region, heart and EAT samples were obtained from the left ventricle. We obtained



informed consent from all enrolled subjects. The experimental protocol and sample collection were in accordance with the Declaration of Helsinki and approved by the Medical Ethics Committee of Wuhan Union Hospital of Huazhong University of Science and Technology (METC number: 20200462). Information on the involved subjects was listed in [Table S4](#).

Identification of differentially expressed genes, functional enrichment analysis, PPI network construction, and identification of hub genes

The data obtained from GSE64554 and GSE120774 were processed by \log_2 transformation and quantile normalization *via* limma package (18) using R separately. The differential expression matrixes of the datasets were also identified by the limma package separately and *P* values were adjusted by the Benjamini-Hochberg method. We then applied the Robust Rank Aggregation (RRA) method (19) to filter the differential expression matrixes, so as to obtain the comprehensive differentially expressed genes (DEGs) across two different microarray platforms. DEGs with RRA score less than 0.05 were selected for further analyses.

Functional enrichment analyses were performed using the DAVID (20) by inputting the official gene symbols of obtained DEGs. Figures for functional enrichment analyses were plotted by R and Sangerbox (<http://www.sangerbox.com/tool>). Construction of the protein-protein interaction (PPI) network and identification of hub genes were performed as the previous description (21).

Weighted gene co-expression network analysis

To explore the gene modules responsible for the phenotypic differences between EAT and SAT, we performed the Weighted gene co-expression network analysis (WGCNA) to identify co-expressed gene modules (22). First, we screened the top 25% of the genes in the variance variability between samples in a pooled matrix and used them as input data. Next, we obtained the soft threshold and set the minimum gene number in the module to 30 to get gene co-expression modules. By analyzing the correlation between each module with the EAT/SAT phenotypes, we screened out the gene modules that need further exploration. Finally, functional enrichment analyses were performed on the obtained modules, and the modules significantly related to the immune process were identified. By taking the intersection of immune-related key modules and DEGs identified by RRA, we obtained a set of key immune-related genes.

Immune cell infiltration and correlation analyses

xCell (23) and CIBERSORT (24) are signature-based methods to infer the immune cell landscape according to expressional profiling. We

performed immune cell infiltration analyses and obtained the immune cell landscapes for EAT and SAT based on the pooled matrix. “Lymphoid cells” and “myeloid cells and others” were categorized. Results were evaluated by t-test to determine the significance of differences. The correlation relationship between immune cell types, WGCNA modules, and target genes was evaluated by Pearson correlation coefficients.

T cell receptor repertoires sequencing and analyses

Paired EAT, SAT, and heart samples were used for T cell receptor (TCR) repertoire sequencing. Tissue genomic DNA was extracted using Universal Genomic DNA Kit (CWBio, China). DNA quality was evaluated using Nanodrop2000 (Thermo, USA) with concentration >20ng/uL and OD260/280 between 1.7 and 2.0. Multiplex PCR reactions were run to specifically amplify the third complementarity-determining region (CDR3) of the TCR β chain for libraries construction. The constructed libraries were deeply sequenced by Illumina NextSeq500. Primers and sequencing were provided by SEQHealth (China).

Raw sequences filtered by SOAPnuke (version 1.6.0) were used for TCR sequencing analyses, and the sequencing data were mapped to the ImMunoGeneTics (IMGT) database using MiXCR (version 3.0.3) to define the V, D, and J fragments and CDR3 sequence (25). The terms TCR clonotype and TCR clone describe the CDR3 sequence composed of a unique amino acid sequence and CDR3 sequence composed of unique V, D, and J fragments, respectively. Antigen matching analysis was performed *via* the IEDB database (<http://www.iedb.org/>).

Flow cytometry

Peripheral blood mononuclear cells (PBMCs) were isolated by density gradient centrifugation using lymphocyte separation medium (MPbio, USA). Fresh EAT samples were digested at 37°C in Hepes buffer containing collagenase D (1mg/mL, Sigma, USA) and dispase II (2mg/mL, Sigma, USA), and then filtered by 100 μ m and 40 μ m filters (Falcon, USA) sequentially to collect the stromal vascular fraction (SVF) for subsequent flow cytometric analyses. Memory phenotypes of T lymphocytes were categorized into naïve T cell (T_N, CD62L⁺CD45RA⁺), central memory T cell (T_{CM}, CD62L⁺CD45RA⁻), effector memory T cell (T_{EM}, CD62L⁻CD45RA⁻) and CD45RA⁺ effector memory T cell (T_{EMRA}, CD62L⁻CD45RA⁺). For the detection of interferon (IFN)- γ , cells were re-suspended in RPMI-1640 medium (Gibco, USA) with 10% heat-inactivated FBS (Gibco, USA) at a concentration of 10⁶ cells/ml and stimulated with Cell Stimulation Cocktail (eBioscience, USA). After 6 hours of stimulation, cells were harvested, permeabilized, and then stained with fluorescence-conjugated antibodies. Used antibodies were as follows: PE-Cy7-anti-human CD3 (BD Biosciences, USA), PE-anti-human IFN- γ (BD Biosciences, USA), BV421-anti-human CD45RA (BD Biosciences, USA), APC-anti-human-CD62L (Biolegend, USA), Fixable Viability Stain 510 (BD Biosciences, USA). The stained cells were washed with Flow Cytometry Staining Buffer (eBioscience, USA) and fixed with IC

Fixation Buffer (eBioscience, USA). Flow cytometry analyses were performed with a FACS Calibur flow cytometer (BD Biosciences, USA) and analyzed by FlowJo software.

Histological staining

For immunohistological or immunofluorescence staining, paired EAT and SAT samples were fixed in 4% paraformaldehyde at 25 °C for 24 hours and embedded in paraffin. Slides were sectioned in 5µm and blocked with 1% BSA PBS buffer and then stained with target antibodies and DAPI following routine procedures. The slides were scanned with a digital scanner (3D-HISTECH, Hungary). CaseViewer software was used for observation and statistics. For immunohistological statistics, 3 areas under the 20x field of view from each slide were randomly selected, and the average number of positive cells per mm² was calculated (3 slides included for each sample). Used antibodies were as follows: human CD3 antibody (Servicebio, China), human CCL5 antibody (R&D systems, USA), and human GZMK antibody (R&D systems, USA).

Statistical analysis

Data processing and analyses were performed using SPSS 22.0, GraphPad Prism, and R. Normality were evaluated by the Shapiro-Wilk test. Differences were evaluated using Student's t-test and $P < 0.05$ was considered statistically significant unless indicated otherwise.

Results

Integrated bioinformatics analyses revealed pro-inflammatory characteristics of EAT

The DEGs between EAT and SAT in GSE64554 and GSE120774 were identified separately and shown in [Figure 2A](#). Next, we applied the RRA algorithm to integrate DEGs of the two datasets and obtain a more comprehensive DEGs list. The RRA method identified 131 genes that were up-regulated in EAT compared to SAT, while 159 genes were down-regulated. DEGs identified by RRA presented significant differences (adjusted P value < 0.05 and $|\log_2FC| \geq 0.5$) in at least one dataset, most of which (90%) showed consistent expressing trends across datasets. The top10 up- and down-regulated DEGs recognized by RRA were shown in [Figure 2B](#). Next, we applied Gene Ontology (GO) enrichment analysis on the DEGs identified by RRA that were up- and down-regulated in EAT versus SAT to explore their potential functions, respectively. As shown in [Figure 2C](#), the up-regulated DEGs in EAT were mainly enriched in complement activation and immune response, while the down-regulated DEGs were mainly related to embryonic skeletal system morphogenesis, suggesting immune activation in EAT compared to paired SAT. The PPI network of DEGs identified by STRING was further analyzed by cytoHubba to identify hub genes. As shown in [Figure S2](#) and [Table S5](#), we obtained the top 10 hub genes including *COL1A1*, *FGF2*, *BGN*, *C3*, *TIMP1*, *CD44*, *POSTN*, *COL3A1*, *CCL2* and *APOB*.

Further, we applied the WGCNA method to identify immune-related key gene modules associated with EAT. By filtering the expression profiles of the top 25% variance in all EAT and SAT samples, a total of 3869 highly variable genes were included in WGCNA. Then, filtered genes were clustered into 18 different modules based on WGCNA clustering ([Figure 2D](#)). The correlation analyses between all modules and EAT/SAT phenotype were carried out and 7 modules were found to be significantly associated with the EAT/SAT phenotype ([Figure 2E](#)). Functional enrichment analyses suggested that the blue and greenyellow modules were closely related to immune response ([Figure 2F](#)). The overlap of DEGs and the two modules were identified and 9 key genes were obtained for further analyses. Of the 9 key genes, all were up-regulated DEGs in EAT and listed in [Table S6](#), including *SLCO2B1*, *F13A1*, *C1QA*, *C1QB*, and *C1QC* from the blue module and *IGLL1*, *GZMK*, *CCL5*, and *SLC38A1* from the greenyellow module.

Immune cell infiltration analyses showed a potential enrichment of lymphocytes in EAT

We used xCell to explore the differences in the immune cell landscape between EAT and SAT. As shown in [Figure 3A](#), EAT was infiltrated by more lymphocytes and dendritic cells (DC), while the abundance of macrophages and M1 macrophages showed no significant difference. In SAT, M2 macrophages, basophils, and mast cells showed higher degrees of infiltration. The correlation between different cell subtypes was calculated to infer their potential interaction. In [Figure 3B](#), CD4⁺ T cells and CD8⁺ T cells presented a strong positive correlation ($r=0.82$), indicating that the two subtypes of T cells had a consistent tendency of infiltration.

Next, we analyzed the correlation between the infiltrated immune cells with hub genes, key genes and key modules identified in EAT from the previous PPI network and WGCNA analyses. As shown in [Figure 3C](#), the expression of *GZMK*, *CCL5*, *IGLL1*, and *SLC38A1* presented a strong positive correlation with CD4⁺ T cells, CD8⁺ T cells, and B cells, while the expression of *SLCO2B1*, *BGN*, *C3*, *TIMP1*, *C1QA*, *C1QB* and *C1QC* showed a strong positive correlation with DC. As shown in [Figure 3D](#), the 7 key modules related to EAT and SAT obtained by WGCNA were all related to different subtypes of immune cells. In particular, the blue and greenyellow modules closely related to the immune process presented a strong positive correlation with lymphocyte abundance. The correlation coefficients between the greenyellow module and T or B cells were more than 0.8. Based on the above analyses, we concluded that EAT acts as a pro-inflammatory adipose tissue characterized by abundant lymphocyte infiltration compared with SAT.

More activated T lymphocytes in EAT from HF patients

To further explore the characteristics of EAT from HF patients, we analyzed a public dataset GSE192886 containing transcriptome profiles of EAT from 5 HF patients and 5 patients

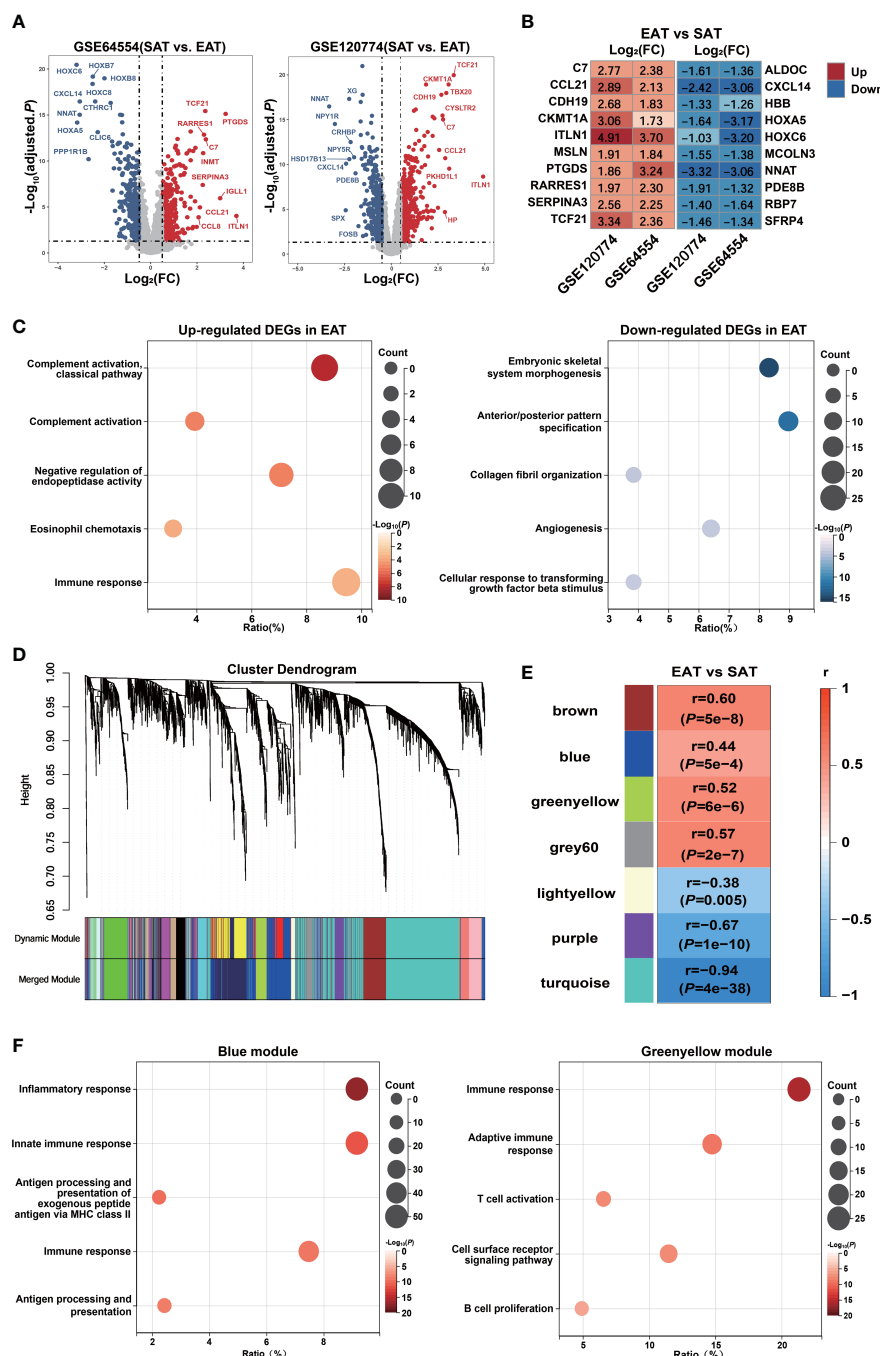


FIGURE 2

Bioinformatics analyses reveal pro-inflammatory characteristics and key genes of EAT. (A) Volcano plot of DEGs between EAT and SAT in GSE64554 and GSE120774. (B) Top 10 up- and down-regulated DEGs identified by RRA method. (C) GO-BP functional enrichment analyses of up- and down-regulated DEGs in EAT compared to SAT. (D) Cluster dendrogram of WGCNA. (E) WGCNA key modules and EAT/SAT phenotype correlation. (F) GO-BP functional enrichment analyses of WGCNA-identified blue and greenyellow gene modules.

without HF as controls (CON). We obtained 196 up-regulated and 261 down-regulated DEGs in EAT from HF patients versus that from controls. Function enrichment analysis of up-regulated DEGs suggested immune activation, particularly lymphocyte activation in EAT from HF patients (Figure 4A). Up-regulated DEGs were mainly enriched in the lymphocyte activation pathway relative to the myeloid leukocyte activation pathway (Figure 4B). Next, we used CIBERSORT to compare the immune cell

composition between EAT from HF patients and non-HF controls. As shown in Figure 4C, the frequencies of T cells and B cells were higher in EAT from HF patients compared to non-HF controls, indicating lymphocyte activation as the hallmark of EAT from HF patients.

We examined the expression levels of genes associated with the inflammatory characteristics of EAT (10 hub genes and 9 key genes identified above). As shown in Figure 4D and Figures S3, S4 (Mann-

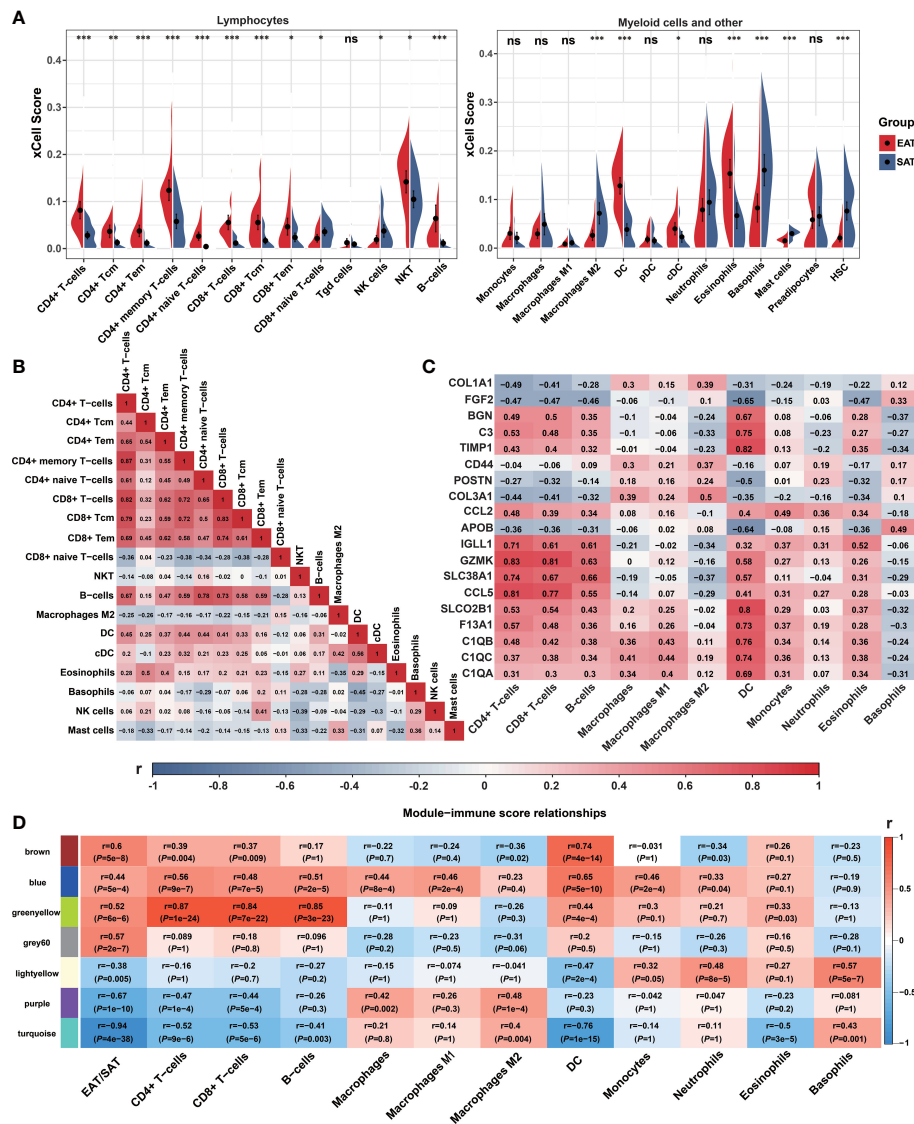


FIGURE 3

Immune cell infiltration and correlation analyses. (A) Violin charts of xCell immune infiltration score between EAT and SAT. (B) Correlation matrix of immune cell subtypes (Pearson correlation coefficients are displayed in the box). (C) Correlation matrix of immune cell infiltration scores with 19 identified key genes (Pearson correlation coefficients are displayed in the box). (D) Correlation matrix of immune cell infiltration scores with WGCNA key modules. * $P < 0.05$, ** $P < 0.01$, *** $P < 0.001$ and ns refers to no significance.

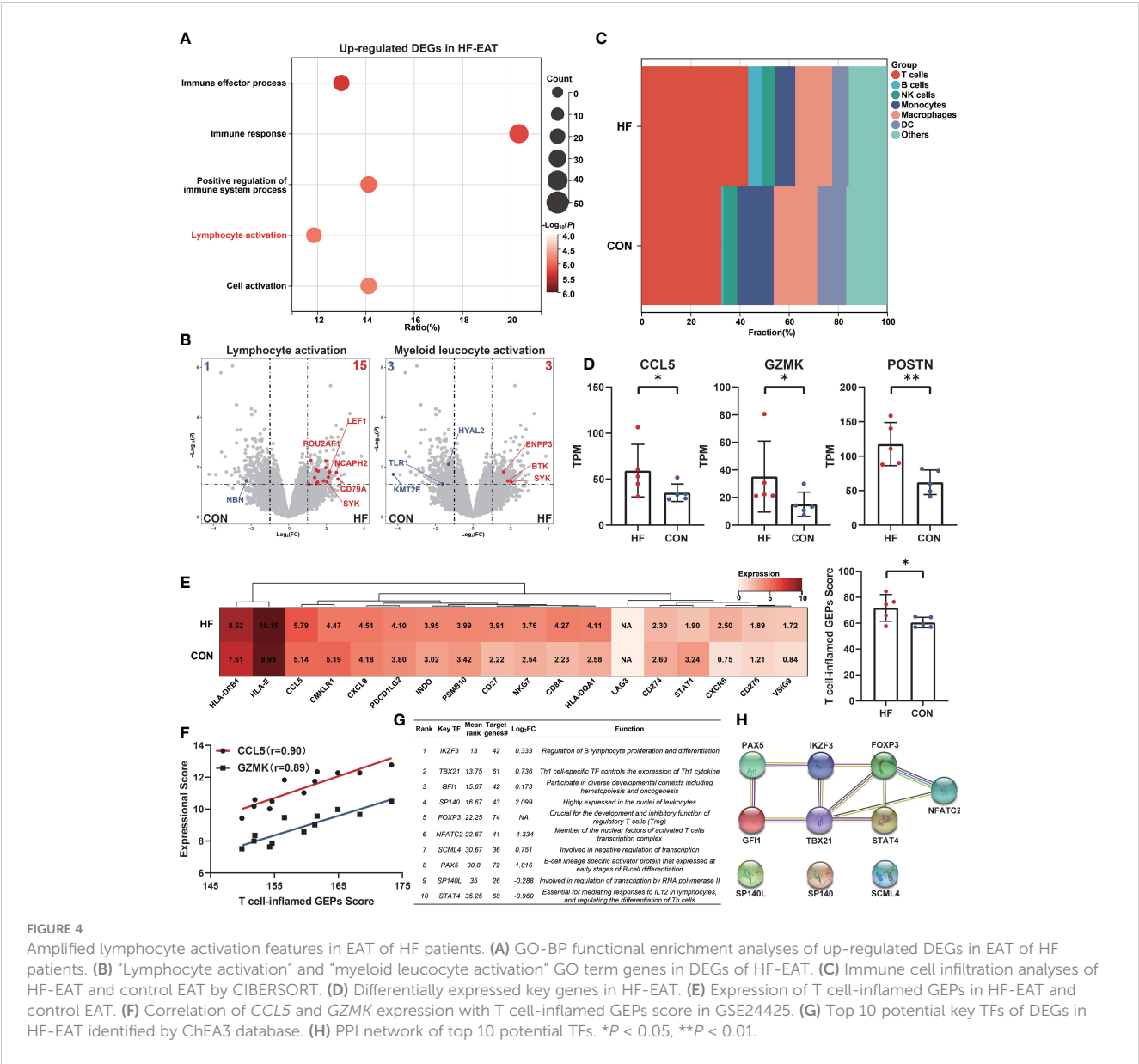
Whitney test), of these genes (*IGLL1* not included), the expression of *CCL5*, *GZMK*, and *POSTN* showed a further increase in EAT from HF patients indicating an enhanced degree of inflammation and fibrosis while *CCL5* and *GZMK* presented the strongest positive correlation with infiltrated T lymphocytes in previous analyses (Figure 3C). Next, we examined the expressions of T cell-inflamed gene expression profiles (GEPs) between EAT from HF patients and non-HF controls. T cell-inflamed GEPs (composite genes listed in Table S7) has been reported to be associated with inflammatory T-lymphocyte infiltration and prediction of sensitivity to immunotherapy in tumors (26, 27). As shown in Figure 4E (Mann-Whitney test), the expressions of T cell-inflamed GEPs were higher in EAT of HF patients, providing further evidence of an enhanced T-lymphocyte response. In addition, the expression of *CCL5* and *GZMK* were also strongly positively

correlated with T cell-inflamed GEPs in EAT and SAT samples from validation dataset GSE24425 (Figure 4F).

Next, we identified the potential key TFs regulating the phenotypic transition of EAT from HF patients using the ChEA3 database (28) (Figure 4G). The PPI network of top 10 predicted key TFs suggested a crucial role of lymphocyte-specific TFs in EAT of HF patients, especially for those were differentially expressed including *TBX21*, *PAX5*, *NFATC2*, and *STAT4* (Figure 4H).

Characteristics of TCR repertoires in EAT from HF patients

The numbers of TCR clones and TCR clonotypes were higher in EAT than in paired SAT from HF patients, indicating enhanced T



lymphocyte infiltration in EAT (Figure 5A). Next, we compared the distribution of the low (fraction>0.1%), middle (fraction>0.5%), and high (fraction>1%) frequency TCR clonotypes between EAT and paired SAT. The results suggested the enrichment of highly expanded TCR clonotypes in EAT compared to paired SAT (Figure 5B). Accordingly, the proportion of top 10 TCR clonotypes was higher in EAT than in SAT (Figures 5C, D). These results suggested that T lymphocytes from EAT of HF patients exhibited higher clonal expansion than those from SAT. TCR clones with high frequency in EAT were listed and evaluated by antigen matching analysis *via* the IEDB database (Tables S8, S9).

A relatively low proportion of shared TCR clonotypes was observed between EAT and paired SAT (Figure 5E). However, the degree of TCR clonotype sharing between cardiac tissue and EAT was higher than that between cardiac tissue and SAT (Figure 5F). Further, we found the Spearman's correlation coefficients between frequencies of TCR clonotypes in cardiac tissue and paired EAT was higher compared to that of SAT (Figure 5G). Next, we examined the usages of TRBV-TRBJ fragments in EAT, SAT, and cardiac tissue (Figure 5H). For the frequency distribution of V-J fragments with an average frequency >1% in the heart (19 V-J fragments ranked in Figure S5), the correlation between cardiac tissue and EAT was greater than that between EAT and SAT while no obvious correlation was observed between cardiac tissue and SAT (Figure 5I). Thus, the above results suggested a similar antigenic microenvironment between the heart and adjacent EAT.

Characteristics of T lymphocytes functional phenotypes in EAT from HF patients

In order to verify the accumulation of T lymphocytes in EAT and the role of key genes, we collected EAT together with paired SAT and peripheral blood samples from HF patients undergoing

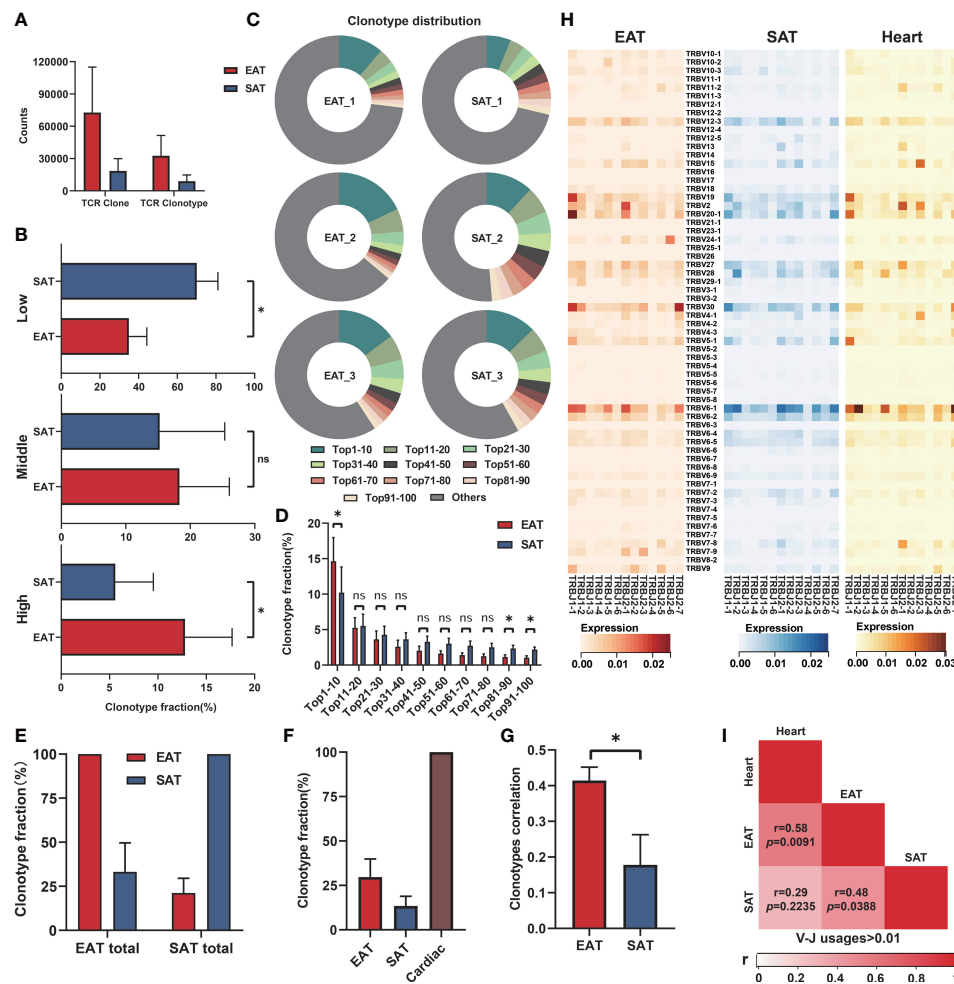


FIGURE 5

Characteristics of TCR repertoires in EAT. (A) TCR clone counts and TCR clonotype counts in EAT and paired SAT. (B) Fraction of low (proportion>0.1%), middle (proportion>0.5%) and high (proportion>1%) frequency TCR clonotypes between EAT and paired SAT. (C, D) The ratio and difference of the top 100 TCR clonotypes in EAT and paired SAT. (E) Total TCR clonotypes sharing between paired EAT and SAT. (F) Total cardiac TCR clonotypes sharing in paired EAT and SAT. (G) Spearman's correlation of cardiac TCR clonotypes with paired EAT and SAT. (H) Heat map of V-J usage between EAT, paired SAT and heart. (I) Spearman's correlation of V-J combination (average usage>0.01) in EAT, SAT and heart. * $P < 0.05$ and ns refers to no significance.

heart transplantation. Immunohistological staining showed abundant CD3-positive T lymphocytes in EAT compared to SAT (Figures 6A, B). Further flow cytometry showed that enriched T lymphocytes in EAT were mainly composed of T_{EM} expressing high levels of IFN- γ (Figures 6C–F). Further immunofluorescence staining results confirmed that CCL5 and GZMK were co-localized with CD3-positive T lymphocytes (Figure 6G). Taken together, we concluded that EAT from HF patients were populated by inflammatory T_{EM} cells expressing high levels of effector molecules including IFN- γ , CCL5, and GZMK and thus contributing to EAT pro-inflammatory conversion in HF patients.

Discussion

Previous understanding of the pro-inflammatory characteristics of EAT was limited to the paracrine and endocrine effects of adipokines and cytokines produced by EAT. The profiles of immune cells in EAT

have rarely been elucidated. A pioneering work by Hirata et al. (10) suggested that macrophages in EAT from patients with coronary artery disease tend to be polarized towards the pro-inflammatory M1 phenotype. Recently, Vyas et al. (9) found that EAT was highly enriched in adaptive immune cells. Given the relatively simple cellular composition of adipose tissue, integrated bioinformatics analyses based on the high-throughput array or sequencing data could expand our knowledge of the roles and characteristics of immune cells in EAT.

Based on our analyses, EAT was enriched in immune activation-related pathways and T lymphocytes compared to paired SAT and this trait was more pronounced in EAT from HF patients. Further, we used high-throughput TCR sequencing to explore the characteristics of TCR repertoires in EAT and found enrichment of highly expanded TCR clonotypes in EAT from HF patients. In addition, we found a higher degree of TCR clonotypes sharing between EAT and paired cardiac tissue from HF patients relative to SAT, suggesting a similar antigenic microenvironment between the heart and adjacent EAT. Furthermore, we

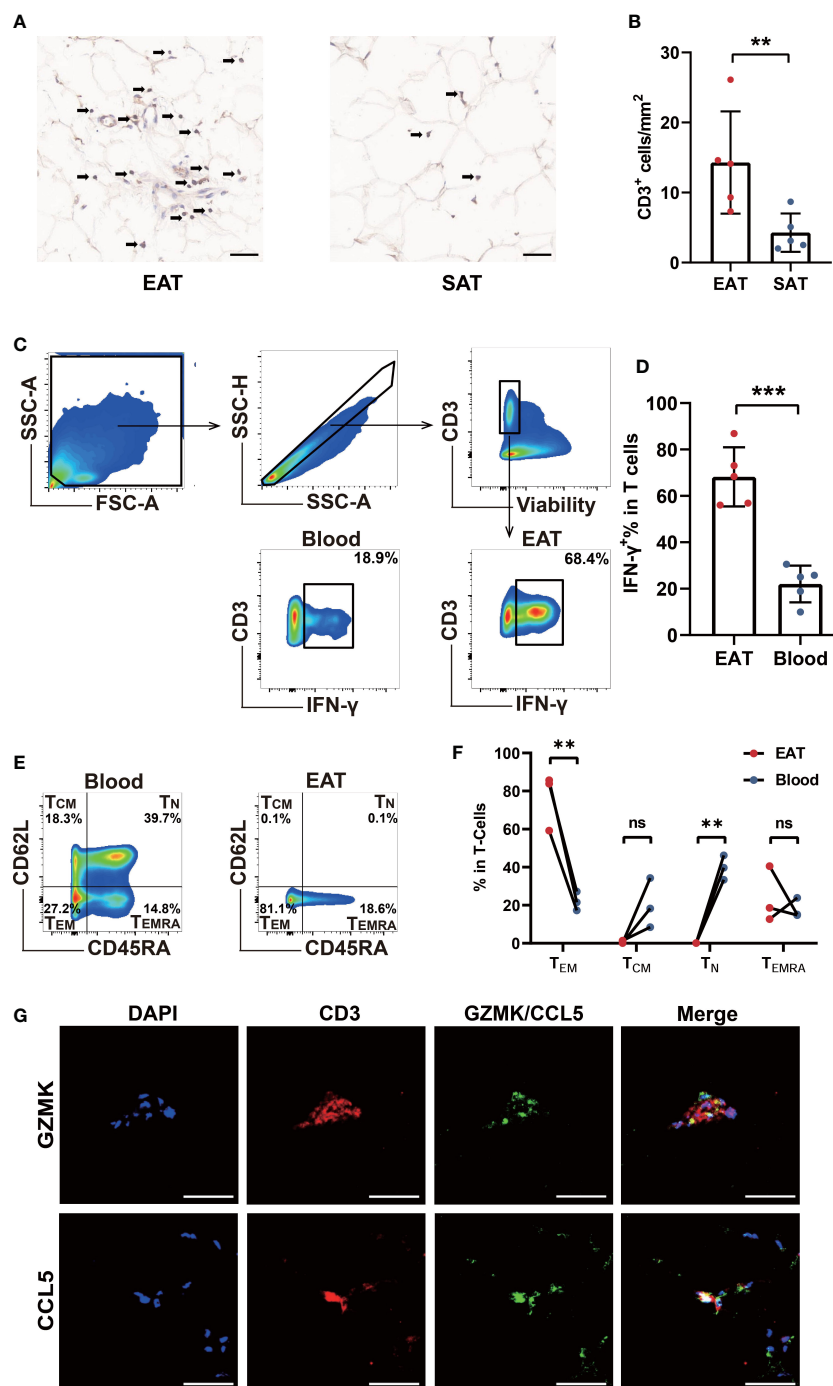


FIGURE 6

Verification of T cells infiltration and key molecules in EAT. (A, B) CD3-specific immunohistochemical staining in EAT and SAT. (C, D) Gating strategy and representative flow cytometry results of IFN- γ ⁺ T lymphocytes in EAT. (E, F) Representative flow cytometry results for proportion of T lymphocytes memory subtypes in EAT. (G) Representative fluorescent staining images of CCL5 and GZMK with CD3 from EAT of HF patients (scale: 50 μ m). ** P < 0.01, *** P < 0.001 and ns refers to no significance.

demonstrated the dominance of pro-inflammatory IFN- γ ⁺ effector memory T lymphocytes in EAT from HF patients. Considering our previous work has revealed a tissue-specific T-cell response predominated by clonally expanded Th1 and cytotoxic CD8⁺T lymphocytes in failing human hearts (29), the present work may provide further evidence of a similar immune microenvironment at the cellular level between EAT and heart.

CCL5 and GZMK may be the key effector molecules of T lymphocytes in EAT. GZMK produced by cytotoxic T lymphocytes mediates cell death by displaying tryptase-like activity (30). It has been reported that GZMK assists transcellular diapedesis of T_{EM} by inducing the expression of *ICAM1* in endothelial cells (31). CCL5 belongs to the C-C motif chemokine family and binds to its receptor CCR5 (32). CCL5 can be produced by a variety of cells including T lymphocytes,

macrophages, fibroblasts, and epithelial cells, and regulates the migration of T lymphocytes and monocytes (32). CCL5 expression was found to be higher in visceral adipose tissue (VAT) compared to SAT and positively correlated with CD3 and CD11b expression (33), while Zhou et al. (34) further identified CD8⁺ T lymphocytes as the major cellular sources of CCL5 in the VAT of obese mice. A recent study showed that clonally expanded GZMK⁺CD8⁺ T cells producing a high level of CCL5 may promote the recruitment of pro-inflammatory immune cells and elevate tissue inflammation (35). Taken together, GZMK and CCL5 may act as key effectors in mediating the adaptive immune response of T lymphocytes in EAT of HF patients.

Existing evidence suggest that increased EAT volume was associated with an increased risk of HF with preserved ejection fraction (HFpEF) (36). However, EAT volume was reduced in HF patients with reduced ejection fraction (HFrEF) (37). In HFpEF patients, increased EAT volume was associated with higher concentrations of troponin T, hs-CRP, IL-6, and increased risk of cardiovascular death and hospitalization, while these associations were reversed in HFrEF patients (6). The reason for the discrepancy may be due to the increased intra-myocardial fat energy requirement in patients with HFrEF because of the progression to cachexia state (38). The reduction of EAT may exacerbate the progression of HFrEF by diminishing the ability of the myocardium to nourish from adjacent EAT. Since the pro-inflammatory conversion of EAT often precedes the clinical diagnosis of HF (4), the specific causal relationship between EAT and different types or stages of HF remains unclear.

To conclude, EAT of HF patients was characterized by pronounced immune activation, particularly by the accumulation of IFN- γ ⁺ T_{EM} and a generally higher degree of TCR clonotypes sharing with paired cardiac tissue. GZMK and CCL5 may act as the key effector molecules of T lymphocytes in EAT of HF patients. Our study has certain limitations. First, we used expression profiles from public datasets to infer immune cell infiltration scenarios of EAT, which may have discordance with actual situations. Second, the samples were obtained from end-stage HF patients and the sample size was small in the validation experiments. More detailed exploration of immune cell profiles in EAT from different stages of HF patients is deserved in the future.

Conclusion

EAT of HF patients was characterized by pronounced immune activation of clonally expanded IFN- γ ⁺ T_{EM} and a generally higher degree of TCR clonotypes sharing with paired cardiac tissue.

Data availability statement

The datasets presented in this study can be found in online repositories. The names of the repository/repositories and accession number(s) can be found below: PRJNA925305 (SRA).

Ethics statement

The studies involving human participants were reviewed and approved by Medical Ethics Committee of Wuhan Union Hospital

of Huazhong University of Science and Technology. The patients/participants provided their written informed consent to participate in this study.

Author contributions

XC, X-ZZ, X-LC, and T-TT contributed to experiments design, data analyses, and manuscript writing. SZ and Q-LL contributed to reviewing the bioinformatics analyses. NX, S-FN, MZ, and Z-FZ contributed to reviewing the manuscript. Z-HZ contributed to reviewing and revising the manuscript. N-GD contributed to collecting clinical samples. All authors contributed to the article and approved the submitted version.

Funding

This work was supported by grants from the National Natural Science Foundation of China (No. 82030016, 82230011 to XC; No. 81974037, 82170394 to T-TT) and Hubei Key Laboratory of Biological Targeted Therapy (No. 2022swbx002 to X-ZZ). All the funders had no role in the study design, data collection, data analysis, interpretation, writing of the manuscript, or the decision to submit the paper for publication.

Acknowledgments

The authors acknowledge the Gene Expression Omnibus (GEO) database and contributors of used datasets in this study for providing public expressional data of EAT and SAT.

Conflict of interest

The authors declare that the research was conducted in the absence of any commercial or financial relationships that could be construed as a potential conflict of interest.

Publisher's note

All claims expressed in this article are solely those of the authors and do not necessarily represent those of their affiliated organizations, or those of the publisher, the editors and the reviewers. Any product that may be evaluated in this article, or claim that may be made by its manufacturer, is not guaranteed or endorsed by the publisher.

Supplementary material

The Supplementary Material for this article can be found online at: <https://www.frontiersin.org/articles/10.3389/fimmu.2023.1126997/full#supplementary-material>

References

- Sacks HS, Fain JN. Human epicardial adipose tissue: A review. *Am Heart J* (2007) 153(6):907–17. doi: 10.1016/j.ahj.2007.03.019
- Corradi D, Maestri R, Callegari S, Pastorì P, Goldoni M, Luong TV, et al. The ventricular epicardial fat is related to the myocardial mass in normal, ischemic and hypertrophic hearts. *Cardiovasc Pathol* (2004) 13(6):313–6. doi: 10.1016/j.carpath.2004.08.005
- Iacobellis G, Corradi D, Sharma AM. Epicardial adipose tissue: Anatomic, biomolecular and clinical relationships with the heart. *Nat Clin Pract Cardiovasc Med* (2005) 2(10):536–43. doi: 10.1038/npcardio0319
- Packer M. Epicardial adipose tissue may mediate deleterious effects of obesity and inflammation on the myocardium. *J Am Coll Cardiol* (2018) 71(20):2360–72. doi: 10.1016/j.jacc.2018.03.509
- Ziaiean B, Fonarow GC. Epidemiology and aetiology of heart failure. *Nat Rev Cardiol* (2016) 13(6):368–78. doi: 10.1038/nrcardio.2016.25
- Pugliese NR, Paneni F, Mazzola M, De Biase N, Del Punta L, Gargani L, et al. Impact of epicardial adipose tissue on cardiovascular haemodynamics, metabolic profile, and prognosis in heart failure. *Eur J Heart Fail* (2021) 23(11):1858–71. doi: 10.1002/ehf.2337
- McMurray JJV, Solomon SD, Inzucchi SE, Kober L, Kosiborod MN, Martinez FA, et al. Dapagliflozin in patients with heart failure and reduced ejection fraction. *N Engl J Med* (2019) 381(21):1995–2008. doi: 10.1056/NEJMoa1911303
- Sato T, Aizawa Y, Yuasa S, Kishi S, Fuse K, Fujita S, et al. The effect of dapagliflozin treatment on epicardial adipose tissue volume. *Cardiovasc Diabetol* (2018) 17(1):6. doi: 10.1186/s12933-017-0658-8
- Vyas V, Blythe H, Wood EG, Sandhar B, Sarker SJ, Balmforth D, et al. Obesity and diabetes are major risk factors for epicardial adipose tissue inflammation. *JCI Insight* (2021) 6(16):e145495. doi: 10.1172/jci.insight.145495
- Hirata Y, Tabata M, Kurobe H, Motoki T, Akaike M, Nishio C, et al. Coronary atherosclerosis is associated with macrophage polarization in epicardial adipose tissue. *J Am Coll Cardiol* (2011) 58(3):248–55. doi: 10.1016/j.jacc.2011.01.048
- Baker AR, Silva NF, Quinn DW, Harte AL, Pagano D, Bonser RS, et al. Human epicardial adipose tissue expresses a pathogenic profile of adipocytokines in patients with cardiovascular disease. *Cardiovasc Diabetol* (2006) 5:1. doi: 10.1186/1475-2840-5-1
- Cheng KH, Chu CS, Lee KT, Lin TH, Hsieh CC, Chiu CC, et al. Adipocytokines and proinflammatory mediators from abdominal and epicardial adipose tissue in patients with coronary artery disease. *Int J Obes (Lond)*. (2008) 32(2):268–74. doi: 10.1038/sj.ijo.0803726
- Gruzdeva O, Uchasova E, Dyleva Y, Borodkina D, Akbasheva O, Antonova L, et al. Adipocytes directly affect coronary artery disease pathogenesis via induction of adipokine and cytokine imbalances. *Front Immunol* (2019) 10:2163. doi: 10.3389/fimmu.2019.02163
- Vacca M, Di Eusanio M, Cariello M, Graziano G, D'Amore S, Petridis FD, et al. Integrative miRNA and whole-genome analyses of epicardial adipose tissue in patients with coronary atherosclerosis. *Cardiovasc Res* (2016) 109(2):228–39. doi: 10.1093/cvr/cvv266
- Fitzgibbons TP, Lee N, Tran KV, Nicoloso S, Kelly M, Tam SK, et al. Coronary disease is not associated with robust alterations in inflammatory gene expression in human epicardial fat. *JCI Insight* (2019) 4(20):e124859. doi: 10.1172/jci.insight.124859
- Zheng ML, Du XP, Zhao L, Yang XC. Expression profile of circular RNAs in epicardial adipose tissue in heart failure. *Chin Med J (Engl)* (2020) 133(21):2565–72. doi: 10.1097/CM9.0000000000001056
- Guaque-Olarte S, Gaudreault N, Piche ME, Fournier D, Mauriege P, Mathieu P, et al. The transcriptome of human epicardial, mediastinal and subcutaneous adipose tissues in men with coronary artery disease. *PLoS One* (2011) 6(5):e19908. doi: 10.1371/journal.pone.0019908
- Ritchie ME, Phipson B, Wu D, Hu Y, Law CW, Shi W, et al. Limma powers differential expression analyses for RNA-sequencing and microarray studies. *Nucleic Acids Res* (2015) 43(7):e47. doi: 10.1093/nar/gkv007
- Kolde R, Laur S, Adler P, Vilo J. Robust rank aggregation for gene list integration and meta-analysis. *Bioinformatics* (2012) 28(4):573–80. doi: 10.1093/bioinformatics/btr709
- Huang DW, Sherman BT, Tan Q, Collins JR, Alvord WG, Roayaei J, et al. The DAVID gene functional classification tool: A novel biological module-centric algorithm to functionally analyze large gene lists. *Genome Biol* (2007) 8(9):R183. doi: 10.1186/gb-2007-8-9-r183
- Zhang XZ, Zhang S, Tang TT, Cheng X. Bioinformatics and immune infiltration analyses reveal the key pathway and immune cells in the pathogenesis of hypertrophic cardiomyopathy. *Front Cardiovasc Med* (2021) 8:696321. doi: 10.3389/fcvm.2021.696321
- Langfelder P, Horvath S. WGCNA: An R package for weighted correlation network analysis. *BMC Bioinf* (2008) 9:559. doi: 10.1186/1471-2105-9-559
- Aran D, Hu Z, Butte AJ. xCell: Digitally portraying the tissue cellular heterogeneity landscape. *Genome Biol* (2017) 18(1):220. doi: 10.1186/s13059-017-1349-1
- Newman AM, Liu CL, Green MR, Gentles AJ, Feng W, Xu Y, et al. Robust enumeration of cell subsets from tissue expression profiles. *Nat Methods* (2015) 12(5):453–7. doi: 10.1038/nmeth.3337
- Bolotin DA, Poslavsky S, Mitrophanov I, Shugay M, Mamedov IZ, Putintseva EV, et al. MiXCR: software for comprehensive adaptive immunity profiling. *Nat Methods* (2015) 12(5):380–1. doi: 10.1038/nmeth.3364
- Ayers M, Luncford J, Nebozhyn M, Murphy E, Loboda A, Kaufman DR, et al. IFN-gamma-related mRNA profile predicts clinical response to PD-1 blockade. *J Clin Invest*. (2017) 127(8):2930–40. doi: 10.1172/JCI91190
- Cristescu R, Mogg R, Ayers M, Albright A, Murphy E, Yearley J, et al. Pan-tumor genomic biomarkers for PD-1 checkpoint blockade-based immunotherapy. *Science* (2018) 362(6411):eaar3593. doi: 10.1126/science.aar3593
- Keenan AB, Torre D, Lachmann A, Leong AK, Wojciechowski ML, Utti V, et al. ChEA3: transcription factor enrichment analysis by orthogonal omics integration. *Nucleic Acids Res* (2019) 47(W1):W212–W24. doi: 10.1093/nar/gkz446
- Tang TT, Zhu YC, Dong NG, Zhang S, Cai J, Zhang LX, et al. Pathologic T-cell response in ischaemic failing hearts elucidated by T-cell receptor sequencing and phenotypic characterization. *Eur Heart J* (2019) 40(48):3924–33. doi: 10.1093/eurheartj/ehz516
- Voskoboinik I, Whistock JC, Trapani JA. Perforin and granzymes: Function, dysfunction and human pathology. *Nat Rev Immunol* (2015) 15(6):388–400. doi: 10.1038/nri3839
- Herich S, Schneider-Hohendorf T, Rohlmann A, Khaleghi Ghadiri M, Schulte-Mecklenbeck A, Zondler L, et al. Human CCR5high effector memory cells perform CNS parenchymal immune surveillance via GZMK-mediated transendothelial diapedesis. *Brain* (2019) 142(11):3411–27. doi: 10.1093/brain/awz301
- Appay V, Rowland-Jones SL. RANTES: A versatile and controversial chemokine. *Trends Immunol* (2001) 22(2):83–7. doi: 10.1016/S1471-4906(00)01812-3
- Wu H, Ghosh S, Perrard XD, Feng L, Garcia GE, Perrard JL, et al. T-Cell accumulation and regulated on activation, normal T cell expressed and secreted upregulation in adipose tissue in obesity. *Circulation* (2007) 115(8):1029–38. doi: 10.1161/CIRCULATIONAHA.106.638379
- Zhou H, Liao X, Zeng Q, Zhang H, Song J, Hu W, et al. Metabolic effects of CCL5 deficiency in lean and obese mice. *Front Immunol* (2022) 13:1059687. doi: 10.3389/fimmu.2022.1059687
- Mogilenko DA, Shpynov O, Andhey PS, Arthur L, Swain A, Esaulova E, et al. Comprehensive profiling of an aging immune system reveals clonal GZMK(+) CD8(+) T cells as conserved hallmark of inflammaging. *Immunity* (2021) 54(1):99–115 e12. doi: 10.1016/j.immuni.2020.11.005
- Kenchaiah S, Ding J, Carr JJ, Allison MA, Budoff MJ, Tracy RP, et al. Pericardial fat and the risk of heart failure. *J Am Coll Cardiol* (2021) 77(21):2638–52. doi: 10.1016/j.jacc.2021.04.003
- Doesch C, Haghi D, Fluchter S, Suselbeck T, Schoenberg SO, Michaeli H, et al. Epicardial adipose tissue in patients with heart failure. *J Cardiovasc Magn Reson* (2010) 12:40. doi: 10.1186/1532-429X-12-40
- Wu CK, Lee JK, Hsu JC, Su MM, Wu YF, Lin TT, et al. Myocardial adipose deposition and the development of heart failure with preserved ejection fraction. *Eur J Heart Fail* (2020) 22(3):445–54. doi: 10.1002/ehf.1617



OPEN ACCESS

EDITED BY

Miguel Angel González-Gay,
University of Cantabria, Spain

REVIEWED BY

Santos Castañeda,
Hospital de La Princesa, Spain
Javier Rueda,
Hospital Sierrallana, Spain

*CORRESPONDENCE

Zhuoli Zhang
✉ zhuoli.zhang@126.com

SPECIALTY SECTION

This article was submitted to
Inflammation,
a section of the journal
Frontiers in Immunology

RECEIVED 26 January 2023

ACCEPTED 28 March 2023

PUBLISHED 18 April 2023

CITATION

Wang Y, Deng X, Zhang X, Geng Y, Ji L,
Song Z and Zhang Z (2023) Presence of
tophi and carotid plaque were risk factors
of MACE in subclinical atherosclerosis
patients with gout: a longitudinal
cohort study.
Front. Immunol. 14:1151782.
doi: 10.3389/fimmu.2023.1151782

COPYRIGHT

© 2023 Wang, Deng, Zhang, Geng, Ji, Song
and Zhang. This is an open-access article
distributed under the terms of the [Creative
Commons Attribution License \(CC BY\)](#). The
use, distribution or reproduction in other
forums is permitted, provided the original
author(s) and the copyright owner(s) are
credited and that the original publication in
this journal is cited, in accordance with
accepted academic practice. No use,
distribution or reproduction is permitted
which does not comply with these terms.

Presence of tophi and carotid plaque were risk factors of MACE in subclinical atherosclerosis patients with gout: a longitudinal cohort study

Yu Wang, Xuerong Deng, Xiaohui Zhang, Yan Geng, Lanlan Ji,
Zhibo Song and Zhuoli Zhang*

Department of Rheumatology and Clinical Immunology, Peking University First Hospital,
Beijing, China

Background: Patients with gout carry an excess risk for cardiovascular disease (CVD), but the contribution of subclinical atherosclerosis to the CVD risk has never been reported. In this study, we aimed to explore the predictive factors for incident major adverse cardiovascular events (MACE) in gout patients without a previous history of CVD or cerebral vascular disease.

Methods: A single-center, long-term follow-up cohort analysis was performed to assess subclinical atherosclerosis at baseline since 2008. Patients with a previous history of CVD or cerebrovascular disease were excluded. The outcome of the study was the first MACE. The presence of subclinical atherosclerosis was assessed by carotid plaque (CP), and carotid intima-media thickness (CMIT) was determined by ultrasound. An ultrasound scan of bilateral feet and ankles was performed at baseline. The association between tophi, carotid atherosclerosis, and the risk of developing incident MACE was evaluated using Cox proportional hazards models with adjustment for the CVD risk scores.

Results: A total of 240 consecutive patients with primary gout were recruited. Their mean age was 44.0 years, with male predominance (238, 99.2%). During a median follow-up of 10.3 years, incident MACE was ascertained in 28 (11.7%) patients. In a Cox hazards model, controlling for the CV risk scores, the presence of at least two tophi (HR, 2.12–5.25, $p < 0.05$) and carotid plaque (HR, 3.72–4.01, $p < 0.05$) were identified as independent predictors of incident MACE in gout patients.

Conclusions: The presence of at least two tophi and carotid plaque on an ultrasound could independently predict MACE in addition to conventional cardiovascular risk factors in gout patients.

KEYWORDS

gout, tophi, crystal arthritis, cardiovascular disease, ultrasonography

Introduction

Gout is a common chronic disorder resulting from the sustained elevation of serum urate acid (SUA) and gradual deposition of monosodium urate crystals in joints, tendons, and other tissues. Both the prevalence and incidence of gout seem to be rising globally, especially in developing countries (1). A meta-analysis of 44 studies published from 2000 to 2014 revealed that the pooled prevalence of gout was 1.1% in the adult Chinese population (2).

Gout is associated with a 17% increase in all-cause mortality risk, with cardiovascular disease (CVD) as the leading cause of death (3). A previous study found that patients with asymptomatic hyperuricemia and silent monosodium urate deposits suffered from a more severe form of coronary atherosclerosis (4). Atheroma plaque was observed by carotid ultrasound in 46.5% of gout patients with newly proven crystal deposition. Importantly, they were classified as having a very high risk of cardiovascular (CV) risk (5). To be noted, the cardiovascular risk in gout patients may be even higher than what has already been shown based on the standard evaluation. Moreover, the rationale for early and effective treatment of gout also greatly depends on the consideration of CV consequences.

Hyperuricemia is also closely associated with CVD, although whether this is due to covariation with the traditional risk factors or a causative role of its own has not been definitively elucidated. Hyperuricemia has also been identified as an independent risk factor for hypertension and impaired kidney function (6). A recent study showed that SUA level was associated with the coronary artery calcification score in male patients but not with carotid intima-media thickness (cIMT) or carotid plaque score (7). Of note, psoriasis is often associated with elevated serum uric acid levels. In this regard, in a cohort of patients with psoriatic arthritis without clinically evident cardiovascular disease, a correlation was found between the serum uric acid concentration and subclinical atherosclerosis measured by the thickness of the carotid intima-media (8).

Early recognition and intervention with risk factors for CVD may be beneficial in reducing CV events in patients with gout. Existing tools, such as the Framingham risk score (FRS), QRISK3, or Systematic Coronary Risk Evaluation (SCORE), have been validated in general population-based large cohorts with long follow-ups (9). It is noted that all these risk scores are based on the traditional CVD parameters, which may underestimate the real CVD risk in patients with rheumatic diseases. Therefore, EULAR recommends a 1.5 multiplication factor for the risk scores of patients with rheumatoid arthritis (10). In 2022, EULAR also recommended using these cardiovascular prediction tools for patients with gout. However, no study has been conducted to investigate the accuracy of these tools, and it is unclear to what extent the elevated risk for cardiovascular disease in gout patients is caused by an increased prevalence of traditional or disease-specific risk factors.

To address these important questions, we conducted this 10-year prospective study. The aims of the study were (1) to investigate

whether subclinical atherosclerosis evaluated by carotid ultrasound could predict incident MACE in patients with gout; (2) to identify whether crystal deposition evaluated by ultrasound could improve the prediction of MACE and whether it is positively adjudicated by traditional clinical cardiovascular algorithms (11).

Methods

Study design and population

This study is based on a prospective cohort of gout patients established in the Department of Rheumatology and Clinical Immunology, Peking University First Hospital (PKU-GOUT) in 2008. Patients in the cohort are followed up at regular intervals, and the treatment decisions at each visit are made at the discretion of the attending rheumatologist based on assessment.

In this study, we enrolled those patients from the PKU-GOUT cohort who satisfied the following inclusion criteria: (1) fulfilled the 2015 American College of Rheumatology/European League Against Rheumatism (ACR/EULAR) Classification Criteria or 1977 ACR criteria for gout (12); (2) >18 years old; (3) with available ultrasound data of carotid artery as well as urate acid deposition in bilateral feet and ankles at the first visit to our clinic; (4) being naïve to urate-lowering therapy (ULT) or with previous ULT treatment 3 months ago; and (5) experienced flare of gouty arthritis at least once within the last 3 months before enrollment.

Patients with any of the following conditions were further excluded: diagnosed stroke or CVD, including a history of myocardial infarction, coronary artery bypass graft surgery, or abnormalities on cardiac tests (exercise treadmill testing, echocardiography, myocardial perfusion, abnormal cardiac computed tomography, or coronary angiography), surgery for ischemic heart disease, transient ischemic attack (TIA), carotid endarterectomy, peripheral arterial reconstructive surgery, or limb amputation.

All the patients were followed up until the occurrence of an endpoint event, 31 January 2022, or loss of follow-up, whichever came first.

The study was performed in accordance with the Helsinki Declaration and approved by the Clinical Research Ethics Committees of Peking University First Hospital (No. 2016-083). The entire research scheme was explained in detail to each participant, and informed consent was obtained.

Clinical assessment at baseline

A structured series of clinical assessments were performed for all the enrolled patients at the baseline visit, including demographics, gout history, comorbidities, smoking status, alcohol consumption, blood pressure, treatment, and laboratory tests, for instance, the concentrations of fasting blood glucose, SUA, urea, creatinine, total cholesterol, high-density lipoprotein cholesterol (HDL-C), low-density lipoprotein cholesterol (LDL-

C), and triglycerides. They were performed using the standard protocols at Peking University First Hospital by an auto-analyzer (Beckman Coulter AU 680 Chemistry Analyzer, Tokyo, Japan).

Smoking status was self-reported by patients, and those with a lifetime consumption of more than 100 cigarettes were defined as smokers (13). Alcohol consumption was defined as an intake of more than or equal to 100 ml/day for over 1 year. Hypertension was defined when a patient had a history of hypertension (blood pressure $\geq 140/90$ mmHg) or was currently taking antihypertensive medications continuously (14). Diabetes mellitus was diagnosed if the subject had a history of diabetes or was currently using antidiabetic drugs (15). Dyslipidemia was defined as a history of dyslipidemia satisfying any one of the following: total cholesterol, ≥ 6.2 mmol/L; triglycerides, ≥ 1.7 mmol/L; LDL-C, ≥ 4.14 mmol/L; or HDL-C, <1.0 mmol/L, or currently using lipid-lowering drugs (16). The estimated glomerular filtration rate was calculated using the Chronic Kidney Disease Epidemiology Collaboration creatinine equation (17).

Ultrasound assessments at baseline and definitions

An ultrasound assessment for joints and carotid arteries was conducted for each patient at baseline. All the ultrasound scanning was performed by two experienced rheumatologists endorsed by EULAR with over 10 years of experience. They were blinded to any clinical and laboratory data about the patients. A GE LOGIQ E9 (GE Healthcare, Waukesha, WI, USA) machine was used for all the scanning.

A musculoskeletal ultrasound assessment was performed for bilateral feet and ankles. Linear transducers, either with ML of 15–6 MHz or a small footprint array of 18–8 MHz were adopted. The scan procedures were based on standardized guidelines published by the Outcome Measures in Rheumatology Clinical Trials (OMERACT) task force (18). The domains for MSU crystal depositions include tophi, double contour sign, and aggregates. The articular inflammatory signs were indicated by the presence of a power Doppler (PD) signal locally.

Ultrasound assessment for bilateral carotid arteries was performed following the Mannheim consensus (19), using a semi-automatic reading system (artery management system) with an 11-MHz linear vascular probe. Six carotid arterial segments were assessed to detect atheroma plaques and measure the intima-media thickness. Carotid plaque (CP) was defined as a cIMT of >1.5 mm or a focal narrowing of ≥ 0.5 mm of the surrounding lumen, or $>50\%$ of the surrounding carotid IMT value (19). Subclinical atherosclerosis was defined when CP was present. A patient with either the presence of CP or cIMT of >0.9 mm was considered to have a high risk of CVD.

To ensure intra- and interobserver reliability, two rheumatologists performed ultrasound assessment on five patients on the same day and repeated the examinations 2 weeks later. The Cohen's κ values for the intraobserver agreement were 0.76 for the double-contour sign ($p < 0.0001$), 0.70 for tophi ($p < 0.0001$), and 0.60 for aggregates ($p < 0.0005$), respectively. The mean κ values were 0.65–0.75 for the intraobserver agreement ($p < 0.001$) and 0.70 for the

interobserver concordance ($p < 0.0001$). These indicated a good level of agreement and reliability.

Assessment of cardiovascular risk at baseline

The FRS, the most widely used tool for estimating the 10-year CV risk was calculated according to the Framingham Heart Study (20). SCORE2, developed by the European Society of Cardiology, was calculated (21), and QRISK3 was calculated using by the QRISK3-2018 risk calculator with an adjustment for rheumatic diseases (22). These three scores representing the CV risk were evaluated in each patient at baseline. A patient with FRS of $>10\%$, SCORE2 of $>5\%$, and QRISK3 of $>20\%$ was considered to have an elevated risk of CVD.

Study outcomes and definitions

The occurrence of the first MACE during the follow-up was defined as the outcome of the study, including ischemic heart disease, nonfatal myocardial infarction, TIA, stroke, and death due to any of the above reasons (11). Myocardial infarction included ST-segment elevation or non-ST-segment elevation myocardial infarction. Cerebrovascular accidents included ischemic stroke and TIA. Cardiovascular death included sudden cardiac death or death from myocardial infarction, heart failure, cerebrovascular accident, a cardiovascular procedure, or other cardiovascular causes. MACE was adjudicated by two researchers independently.

Statistical analysis

The mean \pm standard deviation (SD) and median (interquartile range) were used to prescribe normally and non-normally distributed data, respectively. Student's *t*-test and Chi-squared (χ^2) test were conducted to compare the means and proportions of each group. A Cox proportional hazard regression was used to investigate the baseline CV risk scores, cIMT, CP, and the time to the first MACE occurrence. The effect of the presence of crystal deposition and CP at baseline on MACE-free survival was assessed using Kaplan–Meier survival analysis. The survival distributions were compared by using log-rank testing. Statistical analyses were performed with SPSS for Windows, v. 26.0 (SPSS Inc., Chicago, IL, USA). *p*-values of <0.05 were considered significant. *p*-values of <0.01 were considered highly significant.

Results

Patient characteristics and CVD risks at baseline

Table 1 summarizes the baseline characteristics of 240 gout patients. The average age was 43.3 ± 12.1 years, with a male

TABLE 1 Baseline characteristics of the entire cohort in patients with both carotid and bilateral foot and ankle ultrasound imaging.

Parameters	<i>n</i> = 240	<i>n</i> = 198 without diabetes and CKD	<i>p</i> -value
Age (years)	43.3 ± 12.1	42.1 ± 11.6	0.58
Men (<i>n</i> (%))	238 (99.2)	197 (99.5)	0.85
Height (cm)	174.7 ± 5.9	174.2 ± 5.2	0.81
Weight (kg)	80.9 ± 14.9	80.7 ± 14.2	0.46
Presence of conventional CVD risk factors			
BMI (kg/m ²)	26.6 ± 3.6	26.8 ± 3.8	0.78
Hypertension (<i>n</i> (%))	88 (36.7)	62 (31.3)	0.72
Diabetes mellitus (<i>n</i> (%))	23(9.6)	0	–
Dyslipidemia (<i>n</i> (%))	94 (39.2)	79 (39.9)	0.56
Smoker (<i>n</i> (%))	66 (27.5)	55 (27.8)	0.62
Gout-related disease characteristics			
Disease duration in months	47.7 ± 25.4	47.2 ± 25.9	0.93
Number of involved joints	3 (0–4)	3 (0–4)	0.82
Number of flares last year	4 (2–13)	4 (2–13)	0.94
Presence of tophi	112 (46.7)	98 (49.5)	0.78
Patient global (0–100)	40 ± 23	40 ± 21	0.85
Physician global (0–100)	40 ± 21	40 ± 20	0.87
Alcohol intake (<i>n</i> (%))	95 (39.6)	84 (42.4)	0.63
Serum uric acid (μmol/L)	482.5 ± 130.7	502.3 ± 126.3	0.81
Creatinine (μmol/L)	95.3 ± 13.6	93.6 ± 13.5	0.75
eGFR (ml/min)	86.8 ± 15.5	87.7 ± 14.7	0.69
Chronic kidney disease			
eGFR <60 ml/min (<i>n</i> (%))	23 (9.6)	0	–
eGFR <30 ml/min (<i>n</i> (%))	1 (0.4)	0	–
Fasting glucose (mmol/L)	5.4 ± 0.3	5.4 ± 0.9	0.47
Cholesterol (mmol/L)	4.9 ± 1.0	4.9 ± 1.0	0.46
HDL (mmol/L)	1.1 ± 0.2	1.1 ± 0.2	0.39
LDL (mmol/L)	3.4 ± 0.5	3.1 ± 0.6	0.82
Triglycerides (mmol/L)	2.1 ± 1.0	2.1 ± 1.0	0.95
HCY (μmol/L)	5.0 ± 0.5	5.0 ± 0.6	0.82
hsCRP (mg/L)	6.3 ± 2.8	6.2 ± 2.7	0.73
Cardiovascular risk scores			
FRS	10.6 ± 8.7	10.2 ± 8.5	0.76
SCORE2	2.8 ± 2.3	1.9 ± 1.0	0.85
QRISK3	1.9 ± 1.2	1.8 ± 1.2	0.78
Treatment at baseline			
Diuretics			
Current (<i>n</i> (%))	0 (0)	0 (0)	–
Past (<i>n</i> (%))	2 (0.8)	0 (0)	–

(Continued)

TABLE 1 Continued

Parameters	<i>n</i> = 240	<i>n</i> = 198 without diabetes and CKD	<i>p</i> -value
Never (<i>n</i> (%))	238 (99.2)	198 (100)	0.86
Statins			
Current (<i>n</i> (%))	18 (7.5)	9 (4.5)	0.65
Past (<i>n</i> (%))	6 (2.5)	1 (0.5)	0.14
Never (<i>n</i> (%))	216 (90.0)	188 (95.0)	0.46
Antiplatelet drugs			
Current (<i>n</i> (%))	0 (0.0)	0 (0.0)	–
Past (<i>n</i> (%))	2 (0.8)	2 (1.0)	0.45
Never (<i>n</i> (%))	238 (99.2)	196 (99.0)	–
Urate-lowering therapy			
Current (<i>n</i> (%))	0 (0.0)	0 (0.0)	–
Past (<i>n</i> (%))	2 (0.8)	2 (1.0)	0.53
Never (<i>n</i> (%))	238 (99.2)	196 (99.0)	–
NSAIDs			
Current (<i>n</i> (%))	8 (3.3)	7 (3.5)	0.32
Past (<i>n</i> (%))	28 (11.7)	20 (10.1)	0.54
Never (<i>n</i> (%))	204 (85.0)	171 (86.4)	0.62
Colchicine			
Current (<i>n</i> (%))	8 (3.3)	7 (3.5)	0.34
Past (<i>n</i> (%))	2 (0.9)	1 (0.5)	0.56
Never (<i>n</i> (%))	230 (95.8)	190 (96.0)	0.63
Corticosteroids			
Current (<i>n</i> (%))	2 (0.9)	1 (0.5)	0.71
Past (<i>n</i> (%))	0 (0.0)	0 (0.0)	–
Never (<i>n</i> (%))	238 (99.1)	197 (99.5)	0.62
Carotid ultrasound findings			
Carotid plaque (<i>n</i> (%))	45(18.8)	32 (16.2)	0.57
TPA (cm ²)	64.2 ± 24.4	68.2 ± 28.8	0.72
Increased cIMT (<i>n</i> (%))	27 (11.3)	19 (9.6)	0.58
cIMT (mm)	0.91 ± 1.02	0.90 ± 1.11	0.69
Joint ultrasound parameters			
Positive PD signal (≥1)	55 (22.9)	49 (24.7)	0.64
Tophi (≥2)	16 (6.7)	11 (5.6)	0.87
Double-contour sign	83 (34.6)	70 (35.4)	0.75
Aggregates	22 (9.2)	18 (9.1)	0.69
Erosion	53 (22.1)	43 (21.7)	0.77

CVD, cardiovascular disease; BMI, body mass index; PD, power Doppler; eGFR, estimated glomerular filtration rate; HDL, high-density lipoprotein; LDL, low-density lipoprotein; HCY, homocysteine; hsCRP, highly sensitive C-reactive protein; FRS, Framingham risk score; NSAIDs, nonsteroidal anti-inflammatory drugs; IMT, intima-media thickness; TPA, total plaque area; CIMT, carotid intima-media thickness; N/A, not available.

predominance (238, 99.2%). At baseline, the median disease duration was 3.0 (IQR, 1.0–6.0) years. There were 219 (91.3%) patients having traditional cardiovascular risk factors, with 87 (36.3%), 64 (26.7%), 44 (18.3%), and 24 (10.1%) having with 1, 2, 3, and >3 risk factors, respectively; 99/240 (41.3%) patients were classified as having elevated risk for CV events defined by FRS >10%, 25/240 (10.4%) by SCORE2, and 11/240 (4.6%) by QRISK3, respectively.

For diabetes and chronic kidney disease to favor the development of atherosclerosis and cardiovascular disease, patients with diabetes or chronic kidney disease (eGFR level below 60 ml/min/1.73 m²) were compared with the entire cohort. There was no significant difference in clinical and laboratory parameters between the diabetes and chronic kidney disease group and the entire group at baseline (Table 1).

Ultrasound findings at carotid arteries at baseline

Regarding the carotid scans, atheroma plaques were present in 45 individuals (18.8%) and were found bilaterally in 24 (10.0%). The mean TPA (total plaque area) was 64.2 ± 24.4 cm². Twenty-seven (11.3%) participants showed increased IMT. The mean cIMT was 0.91 ± 1.02 mm.

Musculoskeletal ultrasound findings at baseline

The typical crystal deposition was found by ultrasound in 143 (59.6%) patients, presenting as tophi in 132 (55.0%) patients, DCS (double contour sign) in 83 (34.6%) patients, and aggregates in 22 (9.2%) patients. PD signal was observed in 22.9% (55/240) and bone erosions in 22.1% (53/240) patients, all in MTP1 joints. Among the 143 patients, the crystal deposition was most commonly located in MTP1 (first metatarsophalangeal) joint (87, 60.8%), Achilles tendon (49, 34.3%), ankle joint (7, 5.0%), and other regions. Among the 132 patients with tophi, four (3.0%) had four tophi, 12 (9.1%) had two tophi, and 116 (87.9%) had one tophus in the bilateral foot and ankle region.

MACE during follow-up

A total of 2,441 patient-years of follow-up were available for analysis. The median follow-up period was 10.3 (6.0–14.0) years, and 187 (77.9%) patients were followed up for more than 10 years. During follow-up, 28 (11.7%) patients experienced MACE (1.1 events per 100 patient-years), with stroke (18, 7.5%), acute myocardial infarction (six, 2.5%), TIA (five, 2.1%), and acute myocardial infarction along with stroke (one, 0.4%).

Compared to 212 MACE-free patients, those experiencing MACE during follow-up were older, more likely to have hypertension, diabetes, dyslipidemia, and higher FRS and QRISK3 scores at baseline. Moreover, the patients with MACE had a longer

duration of gout, more joint involvement, and more tophi on ultrasound (Table 2).

The predictors for MACE in gout patients

Among 28 patients who experienced MACE, there were 14 (50.0%), two (7.1%), and 23 (82.1%) patients identified as having elevated CV risk, respectively, defined by FRS, SCORE2, and QRISK3 at baseline.

The association of MACE occurrence with gouty arthritis, such as the number of flares from baseline in the previous, the presence of tophi, the double-contour sign, and the PD signal on ultrasound, is shown in Table 3. MACE was significantly more common in patients with tophi than those without by physical examination (91/212 (42.9%) vs. 21/28 (75.0%); $p = 0.001$), in patients with at least two tophi than less than two tophi on ultrasound (4/212 (1.9%) vs. 12/28 (42.9%); $p = 0.001$), and in patients with CP than those without CP (27/212 (12.7%) vs. 18/28 (64.3%); $p = 0.001$).

Univariable Cox regression analysis revealed that a higher number of gout flares in the previous year before enrollment (HR, 1.05 (95% CI, 1.02–1.09); $p < 0.05$), presence of at least two tophi (HR, 7.53 (95% CI, 7.92–38.8); $p = 0.001$), carotid plaque (HR, 7.36 (95% CI, 3.36–16.1); $p = 0.001$) on ultrasound were associated with a higher risk of developing MACE. Although in univariate analysis, the variables associated with MACE were hypertension, age, disease duration, diabetes, alcohol intake, and smoking, in the multivariate model, only the presence of at least two tophi was associated with MACE, with an HR of 9.63, and this effect was independent of other variables. There is no significant association of mean carotid IMT or maximum carotid IMT with MACE ($p = 0.23$; $p = 0.061$) (Table 3).

In the multivariable model, at least two tophi and carotid plaque were both independent predictors of MACE after adjusting for all CVD risk scores (HR ranged from 2.12 to 5.25 and 3.72 to 4.01; $p < 0.05$) in three models separately (Table 4).

A significant difference in MACE-free survival was observed between patients with at least two tophi and less than two tophi (Figure 1). The Kaplan–Meier survival curve indicated that the MACE-free survival was significantly lower in patients with CP compared with those without (Figure 2).

Discussion

MACE, CVD in particular, has been the leading cause of morbidity and mortality. Prospective studies demonstrating that the predictive CV tools designed for the general population underestimate the CV risk in patients with inflammatory diseases are scarce, and this is the first study confirming this point in gout. Patients with gout have a higher risk of CVD, independent of traditional cardiovascular risk factors (23). In this cohort study, we demonstrate that the baseline disease burden, as reflected by the presence of at least two tophi, is an independent predictive factor for incident MACE after adjusting for traditional cardiovascular risk scores. To the best of our knowledge, this is the first study reporting

TABLE 2 Clinical characteristics of patients with and without MACE in the entire cohort ($n = 240$).

	Entire cohort ($n = 240$; median (IQR) or mean \pm SD or n (%))		
	MACE- ($n = 212$)	MACE+ ($n = 28$)	p -value
Clinical demographic parameters			
Age (years)	39.3 \pm 11.5	44.6 \pm 12.1	0.029*
Men (n (%))	210 (99.0)	28 (100)	0.606
Gout duration (years)	3.0 (1.0, 6.0)	5.5 (2.0, 8.0)	0.009*
Cardiovascular risk factors			
BMI (kg/m^2)	26.4 \pm 3.8	27.1 \pm 2.1	0.131
Hypertension (n (%))	66 (31.1)	22 (78.6)	0.001*
Diabetes (n (%))	17 (8.0)	6 (21.4)	0.050*
Dyslipidemia (n (%))	74 (34.9)	20 (71.4)	0.001*
Smoker (n (%))	51 (24.1)	15 (53.6)	0.001*
Gout-related disease characteristics			
Number of involved joints	1 (1, 2)	1 (1, 3)	0.621
Number of flares last year	4.0 (2.0, 12.0)	10.0 (4.5, 17.5)	0.001*
Presence of tophi	91 (42.9)	21 (75.0)	0.001*
Patient global (0–100)	50 (20, 40)	60 (20, 50)	0.358
Physician global (0–100)	20 (10, 30)	20 (10, 30)	0.309
Alcohol intake (n (%))	75 (35.4)	20 (71.4)	0.001*
Fasting glucose (mmol/L)	5.5 \pm 0.8	6.3 \pm 1.2	0.050*
Serum uric acid ($\mu\text{mol}/\text{L}$)	489.2 \pm 130.8	568.8 \pm 96.7	0.002*
Creatine ($\mu\text{mol}/\text{L}$)	96.4 \pm 15.1	122.5 \pm 12.6	0.151
eGFR (ml/min)	85.1 \pm 16.3	79.5 \pm 12.1	0.245
Chronic kidney disease			
GFR <60 ml/min (n (%))	19 (9.0)	4 (14.3)	0.368
GFR <30 ml/min (n (%))	0 (0.0)	1 (3.6)	0.006*
Cholesterol (mmol/L)	4.8 \pm 1.0	4.7 \pm 1.1	0.491
HDL (mmol/L)	1.1 \pm 0.2	0.8 \pm 0.2	0.001*
LDL (mmol/L)	2.7 \pm 0.7	3.1 \pm 0.8	0.038*
Triglycerides (mmol/L)	2.1 \pm 1.0	2.7 \pm 0.9	0.132
HCY ($\mu\text{mol}/\text{L}$)	18.4 \pm 6.8	20.5 \pm 13.9	0.314
hsCRP	4.1 \pm 2.8	8.9 \pm 2.4	0.289
Cardiovascular risk scores			
FRS	10.5 \pm 8.3	15.0 \pm 11.0	0.040*
SCORE2	2.8 \pm 2.6	2.6 \pm 2.9	0.792
QRISK3	1.6 \pm 1.0	4.2 \pm 1.3	0.001*
Current treatment at baseline			
NSAIDs (n (%))	5 (2.4)	3 (10.7)	0.053
Steroid (n (%))	1 (0.5)	1 (3.5)	0.312

(Continued)

TABLE 2 Continued

	Entire cohort (<i>n</i> = 240; median (IQR) or mean \pm SD or <i>n</i> (%))		
	MACE- (<i>n</i> = 212)	MACE+ (<i>n</i> = 28)	<i>p</i> -value
Statin (<i>n</i> (%))	17 (8.0)	1 (3.6)	0.401
Carotid ultrasound parameters			
Carotid plaque (<i>n</i> (%))	27 (12.7)	18 (64.3)	0.001*
Mean carotid IMT (mm)	0.8 \pm 0.2	1.4 \pm 0.4	0.01*
Maximum carotid IMT (mm)	0.9 \pm 0.3	1.6 \pm 0.5	0.01*
Increased cIMT (<i>n</i> (%))	85 (40.1)	17 (60.7)	0.001*
TPA (cm ²)	20.6 \pm 3.7	131.9 \pm 85.8	0.03*
Joint ultrasound parameters			
Positive PD signal (≥ 1)	52 (24.5)	3 (10.7)	0.102
Tophi (≥ 2)	4 (1.9)	12 (42.9)	0.001*
Double-contour sign	69 (32.5)	14 (50.0)	0.068
Aggregates	19 (9.0)	3 (10.7)	0.651
Erosion	43 (20.3)	10 (35.7)	0.060

*Significant at $p \leq 0.05$.

BMI, body mass index; eGFR, estimated glomerular filtration rate; hsCRP, highly sensitive C-reactive protein; HCY, homocysteine; MACE+, patients who developed cardiovascular event; MACE-, patients who did not develop cardiovascular event; FRS, Framingham risk score; SCORE2, Systematic Coronary Risk Evaluation 2; HDL, high-density lipoprotein; LDL, low-density lipoprotein; IMT, intima-media thickness; TPA, total plaque area; N/A, not available; NSAIDs, nonsteroidal anti-inflammatory drugs; PD, power Doppler.

the association of the presence of at least two tophi and carotid plaque on ultrasound with MACE in addition to traditional cardiovascular risk factors in a long-term follow-up cohort of gout patients. Ultrasound evaluations in joints and carotid

arteries are especially useful for detecting subclinical tophi and subclinical arteriosclerosis and significantly improving cardiovascular risk assessment in gout patients. It supports the need to use additional validated tools like carotid US to improve CV

TABLE 3 Univariate and multivariate Cox regression analyses for parameters as predictors for MACE (*n* = 240).

	Univariate analysis		Multivariate analysis	
	HR (95% CI)	<i>p</i> -value	HR (95% CI)	<i>p</i> -value
Age	1.03 (1.01, 1.23)	0.321		
Disease duration	1.23 (1.03, 1.42)	0.587		
Hypertension	2.14 (1.42, 5.18)	0.002*		
Alcohol intake	1.92 (1.72, 3.32)	0.002*		
eGFR <60ml/min	2.58 (0.89, 7.52)	0.083		
Diabetes	1.42 (1.24, 1.72)	0.001*		
Dyslipidemia	1.11 (1.02, 2.56)	0.459		
Smoker	2.18 (1.43, 4.93)	0.003*		
Number of flares last year	1.05 (1.02, 1.09)	0.004*		
Patient global (0–100)	1.01 (1.00, 1.04)	0.123		
Physician global (0–100)	1.00 (0.99, 1.01)	0.871		
Presence of tophi	3.15 (1.34, 7.42)	0.009*		
Positive PD signal (≥ 1)	0.42 (0.13, 1.38)	0.152		
Tophi (≥ 2)	7.53 (7.92, 38.8)	0.001*	9.63 (6.12, 39.8)	0.001*
Double-contour sign	1.74 (0.81, 3.72)	0.154		

*Significant at $p \leq 0.05$.

TABLE 4 Multivariable Cox regression model for predicting MACE (n=240).

	Model 1 ^a		Model 2 ^b		Model 3 ^c	
	HR (95% CI)	p-value	HR (95% CI)	p-value	HR (95% CI)	p-value
Carotid plaque	3.72 (1.26–10.90)	0.017*	4.01 (1.64–10.30)	0.001*	3.92 (1.29–10.10)	0.011*
Tophi (≥2)	5.25 (2.55–26.72)	0.001*	3.42 (3.23–7.13)	0.003*	2.12 (2.11–9.31)	0.050*
FRS	1.05 (1.01–1.09)	0.005*	–			
SCORE2	–		2.15 (1.82–4.23)	0.432		
QRISK3	–				2.71 (1.67–2.99)	0.014*

*Significant at $p \leq 0.05$.
^aAdjusted for FRS.
^bAdjusted for SCORE2.
^cAdjusted for QRISK3.
FRS, Framingham risk score; SCORE2, Systematic Coronary Risk Evaluation 2.

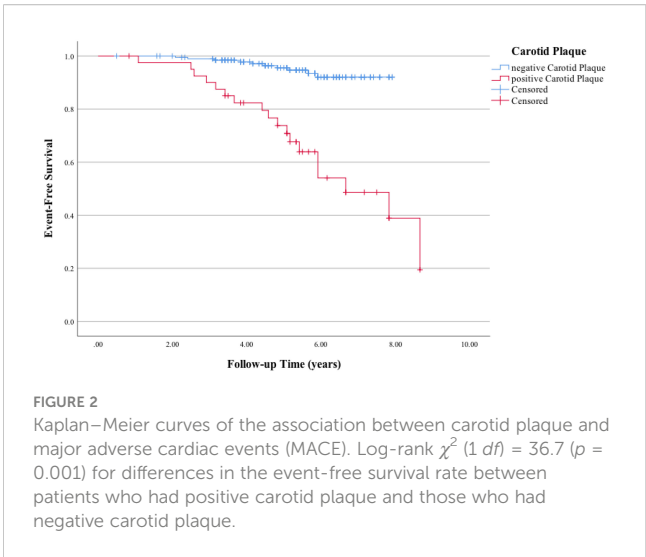
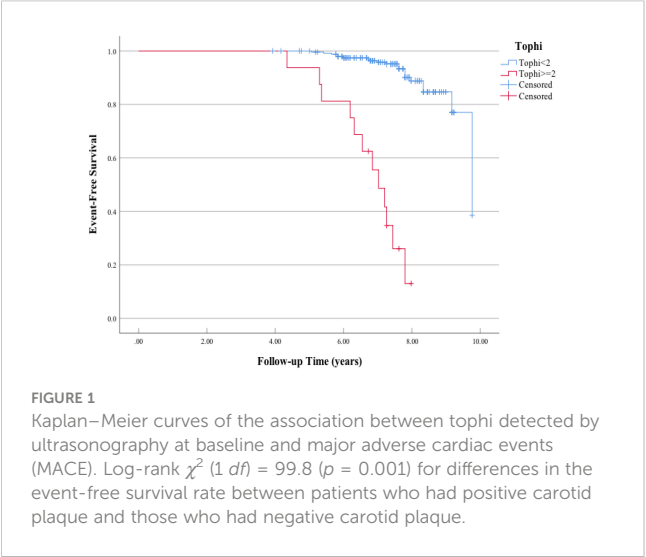
estimation in inflammatory conditions in general and in particular in gout; the presence of carotid plaques also allows for the reclassification of several patients into very-high CV risk.

Gout flares are characterized by neutrophil-rich acute inflammation due to NLRP-3 inflammasome activation (24). A recently published study based on a large nationwide database of gout patients suggested that gout flares were associated with a subsequently transient increase in cardiovascular events (25). Our results showed that the frequency of gout flares in the previous year of the baseline was also associated with subsequent MACE. Neutrophilic inflammation has been confirmed to be associated with instability and rupture of atherosclerotic plaque (26). Activated intraplaque inflammatory cells can upregulate the response proteins, including metalloproteinases and peptidases, and further promote oxidative stress, all of which contribute to plaque destabilization (27). This may explain the association of cardiovascular events with prior gout flares. A randomized clinical trial has demonstrated that blocking the NALP3 inflammasome indeed prevented recurrent cardiovascular events (28).

In this study, we found that those traditional cardiovascular risk scores appeared to be suboptimal as risk assessment tools in patients

with gout, although the performance of FRS and QIRSK3 was better than the SCORE2. A previous study showed that both FHS and SCORE appeared to underestimate the presence of carotid plaque in newly diagnosed gout patients (5). EULAR recommends screening for CVD risk in all patients with inflammatory arthritis and states that rheumatologists should be responsible for risk evaluation in 2022 (29). Unfortunately, no study has ever investigated the accuracy of these CVD prediction tools in patients with gout (29). Our data showed that FRS and QRISK3 can be used in gout patients in future clinical practice. With respect to this, a recent study proposed the combined use of QRISK3 and EULAR-modified SCORE2 as an alternative to the assessment of carotid plaques by ultrasound to identify patients with rheumatoid arthritis at high risk of cardiovascular disease (30). Therefore, it could be an option to be assessed in patients with gout when an ultrasound study is not available.

Clinically detectable tophi have been confirmed to be predictive of long-term MACE. Importantly, our study for the first time revealed that an equal or more than two tophi shown on ultrasound can also predict long-term MACE in gout patients. The number of tophi counted *via* ultrasound was the key predictive



factor for the incident MACE as a comorbidity of gout. This provides a new understanding of the role of MSU crystal burden in cardiovascular risk. Similar to our results, the volume of MSU crystals measured by dual-energy computed tomography has also been identified as a biomarker for the risk of developing new cardiometabolic diseases and all-cause mortality (31). Persistent deposition of MSU crystals can induce chronic inflammation (32). Controlling the chronic subclinical inflammation might improve cardiovascular mortality with medications, such as colchicine (33) and canakinumab (28). MSU crystallization can form by templated nucleation, and inflammatory cells rapidly react to the subclinical tophi (34). Ultrasound is definitely more sensitive than physical examination in detecting subcutaneous tophi, especially in joints (35). The exuberant inflammation surrounding large crystals in tophi was the largest source of chronic inflammation and may explain the link between gout and increased cardiovascular risk. Our study suggests that the overall crystal burden, including the subclinical tophi detected by ultrasonography, has a great impact on chronic inflammation and drives most of the MACE in gout. An observational study investigated specimens of coronary arteries from an explanted heart by polarization microscopy and found urate crystal deposition in about 10% of coronary arteries (36). Whether crystal deposition in the vessels contributes to a higher cardiovascular risk needs to be verified in the future.

In the analysis, we also found that ultrasound measurements of carotid atherosclerosis, as presented by carotid plaque, are an independent risk factor for MACE in gout. The presence of carotid plaque was associated with an approximately threefold increase in the risk of developing incident MACE after adjusting for traditional cardiovascular risks, which is comparable with that reported in patients with RA (37) or PsA (38). A prospective 5-year follow-up study confirmed that the presence of carotid plaques predicted the development of cardiovascular events and death in patients with RA (39). A recent study showed that the presence of tophi and a positive power Doppler signal were significantly associated with atheroma plaques in 103 Spanish gout patients (40). Also, the increased IMT measurement showed no association with MSU crystal, which is similar to our study. There is no correlation between the percentage of positive PD signals and MACE in our study. Differences in ethnicity, the severity of gout such as young age, a lower percentage of conventional CVD risk factors (such as diabetes and hypertension), as well as the acute or intercritical phase to acquire the inflammation in the US can be confounding factors. Moreover, hsCRP at baseline is not a risk factor or a PD signal in our study. Previous data remind us that baseline CRP level is a predictor of CV mortality and CV events in rheumatoid arthritis patients (41). Further study showed that while a single isolated determination of CRP may not be associated with subclinical atherosclerosis (increased carotid intima-media thickness) in patients with rheumatoid arthritis (42), the average CRP value over an extended long period of follow-up may reflect the chronicity of the inflammatory. Both tophi and carotid plaque were accumulated effects of gout; data from the cross-sectional study at baseline or follow-up points cannot explain the incidence of MACE.

The underlying pathophysiological mechanisms, such as systemic inflammation, elevated oxidative stress, endothelial

dysfunction, and changes in lipid profiles, might contribute to a higher CVD risk in gout patients. Two retrospective cohort studies suggested a protective effect of statins on mortality in patients with gout compared to those without statins (43, 44). In our cohort, we did not find a relationship between statin use and MACE.

There are several strengths of the present study. First, this is the first prospective study to investigate the added value of MSU crystal deposition and abnormal carotid manifestations for predicting incidents of MACE in subclinical CVD gout patients. In the study, ultrasound assessment of the carotid arteries and joints enabled us to compare the subclinical characteristics. Second, the follow-up period was long in the study, with a median of 10.3 (6.0–14.0) years and more than 10 years in 187 (71.3%) patients. Events can occur late, and the long-term follow-up and low loss of data guarantee this dataset may be best available in the future. Third, the analyses were adjusted for widely used CVD risk predictive tools. This supports the notion that subclinical atherosclerosis is on the causal pathway rather than a confounder. As the Chinese population has a lower CVD risk in general (45), the European low-risk chart was adopted using SCORE2. Most of the previous studies did not adjust the analysis to determine the predictive value of their findings compared to existing clinical tools. As this is a middle-aged population without a high degree of established comorbidity, the new incidence of MACE prompts the importance of detecting tophi and carotid plaque by ultrasonography in daily clinical practice.

We acknowledge some limitations. First, MACE as the primary outcome occurred in a limited number of patients. There were only 28 patients who developed incident MACE, but this has already been the only longitudinal study with a 10-year follow-up. Future studies with longer follow-ups are warranted. Second, this was a single-center study, and the results may be not generalized to other populations. Third, the CV risk algorithms calculated in this study have not been designed for Asian populations. Last, since the follow-up period was long, we were not able to list and discuss the choice and effect of urate-lowering therapy.

In conclusion, ultrasonography can detect atherosclerosis and crystal deposits in joints and surrounding tissues. This study shows the presence of at least two tophi and carotid plaque on ultrasound, which independently predicted incident MACE in addition to conventional cardiovascular risk factors. Combining ultrasound assessment on carotid arteries can improve the accuracy of cardiovascular risk based on traditional cardiovascular risk factors in patients with gout.

Data availability statement

The raw data supporting the conclusions of this article will be made available by the authors, without undue reservation.

Ethics statement

The studies involving human participants were reviewed and approved by Clinical Research Ethics Committees of Peking

University First Hospital. Written informed consent for participation was not required for this study in accordance with the national legislation and the institutional requirements.

Author contributions

All authors had access to the data and played a role in writing the manuscript. ZZ designed the research protocol and critically revised the manuscript. XD and XZ extracted the ultrasound data. YW designed the research protocol, had full access to all data collection, performed the statistical analysis, and wrote the manuscript. All authors contributed to the article and approved the submitted version.

Funding

This work was supported by the National High Level Hospital Clinical Research Funding (Interdepartmental Clinical Research Project of Peking University First Hospital) (2022CR10).

Acknowledgments

The authors would like to thank all members of the Department of Rheumatology at Peking University First Hospital for their assistance with data acquisition. The authors would also like to thank the rest of the research team at the rheumatology clinic as well as the health

professionals and nurses who facilitated our work. Finally, many thanks to all the participants who took part in the study and made this research possible. Thanks Weiwei Liu and Lu Chen for extracting data from the medical records system and interpreted the data.

Conflict of interest

The authors declare that the research was conducted in the absence of any commercial or financial relationships that could be construed as a potential conflict of interest.

Publisher's note

All claims expressed in this article are solely those of the authors and do not necessarily represent those of their affiliated organizations, or those of the publisher, the editors and the reviewers. Any product that may be evaluated in this article, or claim that may be made by its manufacturer, is not guaranteed or endorsed by the publisher.

Supplementary material

The Supplementary Material for this article can be found online at: <https://www.frontiersin.org/articles/10.3389/fimmu.2023.1151782/full#supplementary-material>

References

- Dehlin M, Jacobsson L, Roddy E. Global epidemiology of gout: prevalence, incidence, treatment patterns and risk factors. *Nat Rev Rheumatol* (2020) 16(7):380–90. doi: 10.1038/s41584-020-0441-1
- Liu R, Han C, Wu D, Xia X, Gu J, Guan H, et al. Prevalence of hyperuricemia and gout in mainland China from 2000 to 2014: A systematic review and meta-analysis. *BioMed Res Int* (2015) 2015:762820. doi: 10.1155/2015/762820
- Vargas-Santos AB, Neogi T, da Rocha Castelar-Pinheiro G, Kapetanovic MC, Turkiewicz A. Cause-specific mortality in gout: Novel findings of elevated risk of non-Cardiovascular-Related deaths. *Arthritis Rheumatol* (2019) 71(11):1935–42. doi: 10.1002/art.41008
- Andrés M, Quintanilla MA, Sivera F, Sánchez-Payá J, Pascual E, Vela P, et al. Silent monosodium urate crystal deposits are associated with severe coronary calcification in asymptomatic hyperuricemia: An exploratory study. *Arthritis Rheumatol* (2016) 68(6):1531–9. doi: 10.1002/art.39581
- Andrés M, Bernal JA, Sivera F, Quilis N, Carmona L, Vela P, et al. Cardiovascular risk of patients with gout seen at rheumatology clinics following a structured assessment. *Ann Rheum Dis* (2017) 76(7):1263–8. doi: 10.1136/annrheumdis-2016-210357
- Richette P, Perez-Ruiz F, Doherty M, Jansen TL, Nuki G, Pascual E, et al. Improving cardiovascular and renal outcomes in gout: what should we target? *Nat Rev Rheumatol* (2014) 10(11):654–61. doi: 10.1038/nrrheum.2014.124
- Drivelegka P, Forsblad-d'Elia H, Angeräs O, Bergström G, Schmidt C, Jacobsson LTH, et al. Association between serum level of urate and subclinical atherosclerosis: results from the SCAPIS pilot. *Arthritis Res Ther* (2020) 22(1):37. doi: 10.1186/s13075-020-2119-0
- Gonzalez-Gay MA, Gonzalez-Juanatey C, Vazquez-Rodriguez TR, Gomez-Acebo I, Miranda-Filloy JA, Paz-Carreira J, et al. Asymptomatic hyperuricemia and serum uric acid concentration correlate with subclinical atherosclerosis in psoriatic arthritis patients without clinically evident cardiovascular disease. *Semin Arthritis Rheumatol* (2009) 39(3):157–62. doi: 10.1016/j.semarthrit.2008.06.001
- Conroy RM, Pyörälä K, Fitzgerald AP, Sans S, Menotti A, De Backer G, et al. Estimation of ten-year risk of fatal cardiovascular disease in Europe: the SCORE project. *Eur Heart J* (2003) 24(11):987–1003. doi: 10.1016/S0195-668X(03)00114-3
- Agca R, Heslinga SC, Rollefstad S, Heslinga M, McInnes IB, Peters MJL, et al. EULAR recommendations for cardiovascular disease risk management in patients with rheumatoid arthritis and other forms of inflammatory joint disorders: 2015/2016 update. *Ann Rheumatic Diseases* (2017) 76(1):17–28. doi: 10.1136/annrheumdis-2016-209775
- Stone NJ, Robinson JG, Lichtenstein AH, Baurey Merz CN, Blum CB, Eckel RH, et al. 2013 ACC/AHA guideline on the treatment of blood cholesterol to reduce atherosclerotic cardiovascular risk in adults: A report of the American college of Cardiology/American heart association task force on practice guidelines. *J Am Coll Cardiol* (2014) 63(25, Part B):2889–934. doi: 10.1016/j.jacc.2013.11.002
- Neogi T, Jansen TLTA, Dalbeth N, Fransen J, Schumacher HR, Berendsen D, et al. 2015 Gout classification criteria: an American college of Rheumatology/European league against rheumatism collaborative initiative. *Ann Rheum Dis* (2015) 74(10):1789–98. doi: 10.1136/annrheumdis-2015-208237
- Bild DE, Bluemke DA, Burke GL, Detrano R, Diez Roux AV, Folsom AR, et al. Multi-ethnic study of atherosclerosis: objectives and design. *Am J Epidemiol* (2002) 156(9):871–81. doi: 10.1093/aje/kwf113
- 2018 practice guidelines for the management of arterial hypertension of the European society of hypertension and the European society of cardiology: ESH/ESC task force for the management of arterial hypertension: Erratum. *J Hypertens* (2019) 37(2):456. doi: 10.1097/HJH.0000000000002026
- Pearson TA, Palaniappan LP, Artinian NT, Carnethon MR, Criqui MH, Daniels SR, et al. American Heart association guide for improving cardiovascular health at the community level, 2013 update: a scientific statement for public health practitioners, healthcare providers, and health policy makers. *Circulation* (2013) 127(16):1730–53. doi: 10.1161/CIR.0b013e31828f8a94
- Expert panel on detection, evaluation, and treatment of high blood cholesterol in adults. executive summary of the third report of the national cholesterol education program (NCEP) expert panel on detection, evaluation, and treatment of high blood cholesterol in adults (Adult treatment panel III). *JAMA* (2001) 285(19):2486–97. doi: 10.1001/jama.285.19.2486
- Levey AS, Stevens LA, Schmid CH, Zhang YL, Castro AF, Feldman HI, et al. A new equation to estimate glomerular filtration rate. *Ann Intern Med* (2009) 150(9):604–12. doi: 10.7326/0003-4819-150-9-200905050-00006

18. Terslev L, Gutierrez M, Christensen R, Balint PV, Bruyn GA, Delle Sedie A, et al. Assessing elementary lesions in gout by ultrasound: Results of an OMERACT patient-based agreement and reliability exercise. *J Rheumatol* (2015) 42(11):2149–54. doi: 10.3899/jrheum.150366
19. Touboul PJ, Hennerici MG, Meairs S, Adams H, Amarenco P, Bornstein N, et al. Mannheim Carotid intima-media thickness and plaque consensus (2004-2006-2011). an update on behalf of the advisory board of the 3rd, 4th and 5th watching the risk symposia, at the 13th, 15th and 20th European stroke conferences, Mannheim, Germany, 2004, Brussels, Belgium, 2006, and Hamburg, Germany, 2011. *Cerebrovasc Dis* (2012) 34(4):290–6. doi: 10.1159/000343145
20. D'Agostino RB, Vasan RS, Pencina MJ, Wolf PA, Cobain M, Massaro JM, et al. General cardiovascular risk profile for use in primary care: the framingham heart study. *Circulation* (2008) 117(6):743–53. doi: 10.1161/CIRCULATIONAHA.107.699579
21. SCORE2 working group and ESC cardiovascular risk collaboration. SCORE2 risk prediction algorithms: new models to estimate 10-year risk of cardiovascular disease in Europe. *Eur Heart J* (2021) 42(25):2439–54. doi: 10.1093/eurheartj/ehab309
22. Hippisley-Cox J, Coupland C, Brindle P. Development and validation of QRISK3 risk prediction algorithms to estimate future risk of cardiovascular disease: prospective cohort study. *BMJ* (2017) 357:j2099. doi: 10.1136/bmj.j2099
23. Choi HK, Curhan G. Independent impact of gout on mortality and risk for coronary heart disease. *Circulation* (2007) 116(8):894–900. doi: 10.1161/CIRCULATIONAHA.107.703389
24. Martinon F, Pétrilli V, Mayor A, Tardivel A, Tschopp J. Gout-associated uric acid crystals activate the NALP3 inflammasome. *Nature* (2006) 440(7081):237–41. doi: 10.1038/nature04516
25. Cipolletta E, Tata LJ, Nakafero G, Avery AJ, Mamas MA, Abhishek A. Association between gout flare and subsequent cardiovascular events among patients with gout. *JAMA* (2022) 328(5):440–50. doi: 10.1001/jama.2022.11390
26. Ionita MG, van den Borne P, Catanzariti LM, Moll FL, de Vries JPPM, Pasterkamp G, et al. High neutrophil numbers in human carotid atherosclerotic plaques are associated with characteristics of rupture-prone lesions. *Arteriosclerosis Thrombosis Vasc Biol* (2010) 30(9):1842–8. doi: 10.1161/ATVBAHA.110.209296
27. Musher DM, Abers MS, Corrales-Medina VF. Acute infection and myocardial infarction. *N Engl J Med* (2019) 380(2):171–6. doi: 10.1056/NEJMra1808137
28. Ridker PM, Everett BM, Thuren T, MacFadyen JG, Chang WH, Ballantyne C, et al. Antiinflammatory therapy with canakinumab for atherosclerotic disease. *N Engl J Med* (2017) 377(12):1119–31. doi: 10.1056/NEJMoa1707914
29. Drosos GC, Vedder D, Houben E, Boekel L, Atzeni F, Badreh S, et al. EULAR recommendations for cardiovascular risk management in rheumatic and musculoskeletal diseases, including systemic lupus erythematosus and antiphospholipid syndrome. *Ann Rheum Dis* (2022) 81(6):768–79. doi: 10.1136/annrheumdis-2021-221733
30. Corrales A, Vegas-Revenga N, Atienza-Mateo B, Corrales-Selaya C, Prieto-Peña D, Rueda-Gotor J, et al. Combined use of QRISK3 and SCORE as predictors of carotid plaques in patients with rheumatoid arthritis. *Rheumatol (Oxford)* (2021) 60(6):2801–7. doi: 10.1093/rheumatology/keaa718
31. Marty-Ané A, Norberciak L, Andrès M, Houvenagel E, Ducoulombier V, Legrand J, et al. Crystal deposition measured with dual-energy computed tomography: association with mortality and cardiovascular risks in gout. *Rheumatology* (2021) 60(10):4855–60. doi: 10.1093/rheumatology/keaa920
32. Dalbeth N, Gosling AL, Gaffo A, Abhishek A. Gout. *Lancet* (2021) 397(10287):1843–55. doi: 10.1016/S0140-6736(21)00569-9
33. Tardif JC, Kouz S, Waters DD, Bertrand OF, Diaz R, Maggioni AP, et al. Efficacy and safety of low-dose colchicine after myocardial infarction. *N Engl J Med* (2019) 381(26):2497–505. doi: 10.1056/NEJMoa1912388
34. Pascual E, Addadi L, Andrés M, Sivera F. Mechanisms of crystal formation in gout—a structural approach. *Nat Rev Rheumatol* (2015) 11(12):725–30. doi: 10.1038/nrrheum.2015.125
35. Lee YH, Song GG. Diagnostic accuracy of ultrasound in patients with gout: A meta-analysis. *Semin Arthritis Rheumatol* (2018) 47(5):703–9. doi: 10.1016/j.semarthrit.2017.09.012
36. Park JJ, Roudier MP, Soman D, Mokadam NA, Simkin PA. Prevalence of birefringent crystals in cardiac and prostatic tissues, an observational study. *BMJ Open* (2014) 4(7):e005308. doi: 10.1136/bmjopen-2014-005308
37. Ajeganova S, de Faire U, Jogestrand T, Frostegård J, Hafström I. Carotid atherosclerosis, disease measures, oxidized low-density lipoproteins, and atheroprotective natural antibodies for cardiovascular disease in early rheumatoid arthritis – an inception cohort study. *J Rheumatol* (2012) 39(6):1146–54. doi: 10.3899/jrheum.111334
38. Lam SHM, Cheng IT, Li EK, Wong P, Lee J, Yip RML, et al. DAPSA, carotid plaque and cardiovascular events in psoriatic arthritis: a longitudinal study. *Ann Rheum Dis* (2020) 79(10):1320–6. doi: 10.1136/annrheumdis-2020-217595
39. Corrales A, Vegas-Revenga N, Rueda-Gotor J, Portilla V, Atienza-Mateo B, Blanco R, et al. Carotid plaques as predictors of cardiovascular events in patients with rheumatoid arthritis. results from a 5-year-prospective follow-up study. *Semin Arthritis Rheumatol* (2020) 50(6):1333–8. doi: 10.1016/j.semarthrit.2020.03.011
40. Calabuig I, Martinez-Sanchis A, Andrés M. Sonographic tophi and inflammation are associated with carotid atheroma plaques in gout. *Front Med (Lausanne)* (2021) 8:795984. doi: 10.3389/fmed.2021.795984
41. Gonzalez-Gay MA, Gonzalez-Juanatey C, Lopez-Diaz MJ, Piñeiro A, Garcia-Porrua C, Miranda-Fillooy JA, et al. HLA-DRB1 and persistent chronic inflammation contribute to cardiovascular events and cardiovascular mortality in patients with rheumatoid arthritis. *Arthritis Rheumatol* (2007) 57(1):125–32. doi: 10.1002/art.22482
42. Gonzalez-Gay MA, Gonzalez-Juanatey C, Piñeiro A, Garcia-Porrua C, Testa A, Llorca J. High-grade c-reactive protein elevation correlates with accelerated atherogenesis in patients with rheumatoid arthritis. *J Rheumatol* (2005) 32(7):1219–23.
43. Keller SF, Rai SK, Lu N, Oza A, Jorge AM, Zhang Y, et al. Statin use and mortality in gout: A general population-based cohort study. *Semin Arthritis Rheumatol* (2018) 48(3):449–55. doi: 10.1016/j.semarthrit.2018.03.007
44. Garcia-Gil M, Comas-Cufi M, Ramos R, Martí R, Alves-Cabreros L, Parramon D, et al. Effectiveness of statins as primary prevention in people with gout: A population-based cohort study. *J Cardiovasc Pharmacol Ther* (2019) 24(6):542–50. doi: 10.1177/1074248419857071
45. Chiu M, Austin PC, Manuel DG, Tu JV. Comparison of cardiovascular risk profiles among ethnic groups using population health surveys between 1996 and 2007. *CMAJ* (2010) 182(8):E301–310. doi: 10.1503/cmaj.091676



OPEN ACCESS

EDITED BY

Wilfried Le Goff,
Institut National de la Santé et de la
Recherche Médicale (INSERM), France

REVIEWED BY

I-Shiang Tzeng,
National Taipei University, Taiwan
Aleksandra Klisic,
Primary Health Care Center Podgorica,
Montenegro

*CORRESPONDENCE

Lian Liu
✉ 02417@zjhu.edu.cn

RECEIVED 21 November 2022

ACCEPTED 06 March 2023

PUBLISHED 28 April 2023

CITATION

Ren Z, Luo S and Liu L (2023) The positive
association between white blood cell
count and metabolic syndrome is
independent of insulin resistance
among a Chinese population: a
cross-sectional study.
Front. Immunol. 14:1104180.
doi: 10.3389/fimmu.2023.1104180

COPYRIGHT

© 2023 Ren, Luo and Liu. This is an open-
access article distributed under the terms of
the [Creative Commons Attribution License](#)
(CC BY). The use, distribution or
reproduction in other forums is permitted,
provided the original author(s) and the
copyright owner(s) are credited and that
the original publication in this journal is
cited, in accordance with accepted
academic practice. No use, distribution or
reproduction is permitted which does not
comply with these terms.

The positive association between white blood cell count and metabolic syndrome is independent of insulin resistance among a Chinese population: a cross-sectional study

ZhongYu Ren¹, Shi Luo¹ and Lian Liu^{2*}

¹School of Physical Education, Southwest University, Chongqing, China, ²School of Physical Education, Huzhou University, Huzhou, China

Background: The association between white blood cells (WBCs) and metabolic syndrome (MS) has been consistently reported in previous studies using regional samples. However, it remains unclear whether this relationship has urban–rural differences and is independent of insulin resistance using a large-scale representative sample. Additionally, accurate risk prediction in patients with MS is crucial for developing targeted interventions to enhance the quality of life and prognosis of patients.

Aims: The aims of this study were (1) to examine the cross-sectional association between WBCs and MS among the national population and analyze the urban–rural difference and whether insulin resistance plays a moderator effect in this association and (2) to describe the performance to predict MS using machine learning (ML) models.

Design: A cross-sectional study was performed using 7,014 data from the China Health and Nutrition Survey (CHNS).

Methods: WBCs were analyzed using an automatic hematology analyzer and MS was defined according to the criteria of the American Heart Association scientific statements of 2009. Variables on sociodemographic characteristics (sex, age, and residence), clinical laboratory (BMI and HOMA-IR), and lifestyle characteristics (smoking and drinking status) were used to construct ML models to predict MS [logistic regression (LR) and multilayer perceptron (MLP) neural network].

Results: We found that 21.1% of participants (1,479/7,014) were classified as having MS. In multivariate logistic regression (including insulin resistance), the result revealed a significant positive association between WBCs and MS. The odds ratios (95% CI) for MS with increasing WBC level were 1.00 (reference), 1.65 (1.18, 2.31), and 2.18 (1.36, 3.50) (p for trend: 0.001). For two ML algorithms, two models showed adequate calibration and good discrimination, but the MLP showed better performance (AUC-ROC = 0.862 and 0.867).

Conclusion: With the aim of confirming the association between WBCs and MS, this cross-sectional study is the first to show that maintaining normal WBC count levels is helpful to prevent the development of MS, and this association is independent of insulin resistance. The results also showed that the MPL algorithm represented a more prominent predictive performance to predict MS.

KEYWORDS

cross-sectional study, insulin resistance, white cell counts, metabolic syndrome, Chinese population

Introduction

Metabolic syndrome (MS) is a pro-inflammatory disease characterized by a constellation of cardiovascular risk factors, including central obesity, elevated blood pressure (BP), dyslipidemia, and impaired glucose tolerance (1). With socio-economic development and lifestyle changes, the prevalence of MS has shown an increasing trend worldwide. Currently, approximately 25% of the global population suffers from MS (2). Therefore, exploring convenient, effective, and available methods for determining systemic inflammation statuses and diagnosing MS is urgently needed.

Numerous inflammatory markers have been widely used to assess systemic inflammatory statuses in clinical practice and public health practices. These markers included soluble adhesion molecules (such as E-selectin, P-selectin, intracellular adhesion molecule-1, and vascular cell adhesion molecule-1), cytokines (such as interleukin-1 β , -6, -8, and -10, and tumor necrosis factor- α), acute-phase reactants [such as fibrinogen, serum amyloid A protein, and high sensitive C-reactive protein (hsCRP)], and white blood cell (WBC) count (3). Among these inflammatory markers, peripheral WBC counts are assayed in routine blood routine examination and used to diagnose systemic infection, tissue damage, and other conditions associated with inflammation (4). Furthermore, prior cross-sectional and cohort studies have shown that peripheral WBC count is associated with MS risk over the past decade (4–7). However, there are conflicting findings in recent studies. For example, two (8, 9) of the three studies (8–10) confirmed the cross-sectional and prospective findings. The association between WBC counts and MS may be different as there are urban–rural differences that have been observed in inflammation (11) and prevalence of MS (2). Additionally, insulin resistance plays an important pathophysiological role in the development of MS (12); however, it is unclear whether insulin resistance plays a moderator effect in this association (7, 13).

The recent progression of computer science has led to the development of machine learning (ML), a powerful tool that has been widely used to identify the risk factors of outcome variables. ML has provided the ability to compare the accuracy of the ML approaches and the traditional logistic regression in predicting the outcome variables (14). Therefore, in this study, we used a large-scale representative sample to comprehensively examine the association

between WBC count and MS risk among the general Chinese population, and analyzed the urban–rural difference and whether insulin resistance plays a moderator effect in this association.

Methods

Study population

The China Health and Nutrition Survey (CHNS), established in 1989, is an ongoing prospective cohort study. A previous study has published a detailed study design (15). In brief, the multi-stage random cluster sampling method was used to select 4,400 households and 19,000 participants, which covers nine provinces (Guizhou, Guangxi, Heilongjiang, Henan, Hubei, Hunan, Liaoning, Jiangsu, and Shandong). So far, the CHNS has completed data collection from 11 waves (1989, 1991, 1993, 1997, 2000, 2004, 2006, 2009, 2011, 2015, and 2018). The CHNS has obtained clinical, dietary, anthropometric, and all other individual data from each household member. Because the collection and analysis of blood samples were only conducted and released in 2009, we therefore used data from the 2009 wave of the CHNS. A detailed study design has been described in a previous study (16).

We analyzed 12,178 individuals who agreed to participate and gave informed consent for analysis of their data. This study included participants aged ≥ 18 years who participated in the 2009 survey wave. Participants were excluded if they met any of the following criteria: (1) a history of diabetes ($n = 131$), hypertension ($n = 1094$), apoplexy ($n = 38$), or myocardial infarction ($n = 28$); and (2) incomplete data ($n = 1963$). After excluding these incomplete data, this study finally included 7,014 individuals (3,253 men and 3,761 women). In order to show that the sample size of this study has sufficient statistical power, sample size was calculated based on a previous study that determined the prevalence rate of MS [control group = 0.14 (514/3,556); experimental group = 0.39 (194/495)] in a Chinese population-based study (7). Statistical power for a two-sample proportion chi-squared test indicated that a total of 156 participants were included in this study, which could achieve 95% statistical power. Ethics approval was obtained from the Institutional Review Board of the University of North Carolina at Chapel Hill and the National Institute for Nutrition and Health, Chinese Center for Disease Control and Prevention.

Blood biochemical measurement

Fasting blood samples were collected in blood collection tubes and tested in a national central lab in Beijing. Fasting blood glucose (FBG) and lipids [triglyceride (TG) and high-density lipoprotein cholesterol (HDL-C)] were analyzed using an automatic biochemical analyzer (Hitachi 7600 automated analyzer, Tokyo, Japan). Insulin was measured by an ELISA Kit (Millipore Corporation, Billerica, MA, USA). The homeostasis model assessment for insulin resistance (HOMA-IR) score was calculated using the following formula: fasting insulin (mU/L) * fasting glucose (mmol/L)/22.5 (17).

In order to determine all the above biochemical markers, FBG was measured by the glucose oxidase method. TG and HDL-C were measured by the enzymatic method.

Assessment of WBC count

Fasting blood samples were drawn from the cubital vein for routine blood detection. WBC count was analyzed using an automatic hematology analyzer (Beckman Coulter LH751, Beckman Coulter, USA). Generally, an individual who maintains a very low leukocyte count level is healthier. We grouped the subjects into three categories—low level (subnormal level: ≤ 3.9), middle level (normal level: 3.91–9.94), and high level (above normal level: ≥ 10.0). We aimed to examine the association between a subnormal WBC count and risk of MS.

Assessment of covariates

Anthropometric measurements (height, body weight, and waist circumference) were made using standard protocols. Body mass index (BMI) was calculated as the ratio of weight (kg) and height (m) squared. BP was measured three times after participants quietly sat for at least 5 min, and the maximum values of the first two of three readings were considered as the final BP values. All participants were also asked to fill in a standard questionnaire, which included demographic variables [sex, age, residence (city, suburban, town or county, capital city, and rural village)] and lifestyle variables [smoking status (smoker or not) and drinking status (drinker or not)].

Definition of MS

According to the criteria of the American Heart Association scientific statements of 2009 (1), if a participant suffered from three or more of the following syndromes, he/she will be defined as having MS:

- (1) Central obesity (≥ 90 cm in men, ≥ 80 cm in women);
- (2) Elevated triglycerides (TG ≥ 1.7 mmol/L);

- (3) Reduced HDL cholesterol (<1.0 mmol/L in men, <1.3 mmol/L in women);
- (4) Elevated BP [systolic BP (SBP) ≥ 130 mmHg or diastolic BP (DBP) ≥ 85 mmHg]; and
- (5) Elevated fasting glucose (≥ 5.6 mmol/L).

Statistical analysis

All continuous variables were expressed as median [interquartile range (IQR)] because of non-normal distribution, and categorical variables were expressed as percentage. To examine differences in participants' characteristics between WBC count category, Kruskal–Wallis test and chi-square test were applied for continuous variables and categorical variables, respectively. We examine the hypothesis of logistic regression analysis prior to its use. Firstly, to examine the independence of observation variables, interactions were tested by adding the respective multiplicative terms in the models simultaneously. There were significant interactions of WBC with age, residence, apoplexy, and insulin resistance on MS (p for interaction: <0.001 , 0.038, <0.001 , and 0.015, respectively) (Appendix Table 1). Based on the above findings, we also carried out subgroup analysis based on sex, age (age <65 years, age ≥ 65 years), residence (city, suburb, town, and village), apoplexy (yes or no), and insulin resistance (yes or no). Secondly, variance inflation factors (VIFs) were used to examine multicollinearity among explanatory variables, and the result shows that the VIFs of explanatory variables range from 1.02 to 1.91, which means that there is no multicollinearity between explanatory variables (Appendix Table 2). Thirdly, Cook's distance was used to identify extreme outliers, and the results showed that Cook's distance of each variable is less than or equal to 0.06, showing that no extreme outliers were found. Fourth, to initially assess whether there are linear relationships between continuous independent variables and dependent variable logit conversion values, the Box–Tidwell method was used (transformation of the independent variables). The results of the line test found nonlinear relationships between all continuous independent variables (age, BMI, and insulin resistance) and the dependent variable logit conversion values. To linearize relationships, all continuous variables were converted into ordinal categorical variables. To examine the association between WBC count and MS, multivariate logistic regression analyses were applied to calculate risk of MS in different WBC count categories when several potential confounding factors were adjusted. We adjusted for sex, age (continuous variable), BMI (continuous variable), residence (categorical variable), smoking and drinking status (categorical variable), and HOMA-IR.

To examine the robustness of the above-mentioned results, a sensitivity analyses was further conducted as follows: we excluded participants who was excessively thin and obese [BMI (<18 or >40 kg/m²)]. We also used receiver operating characteristic (ROC) curve analysis, precision, specificity, and sensitivity through ML including multilayer perceptron (MLP) and logistic regression (LR)

to compare the predictive performance of the MS risk model. In all two-sided tests, p -values of <0.05 were defined as statistically significant. Stata 16.0 software (Stata Corp LP, College Station, TX, USA) was used for all tests.

Results

Participants' characteristics according to WBC category

Participants' characteristics according to WBC category are shown in [Table 1](#); 3.4% of participants have a higher WBC level. Participants with a higher WBC level were more likely to be male, to be younger, and to live in a rural village. In addition, BMI and HOMA-IR increased statistically across different WBC categories. The proportion of participants with above-normal WBC count, who were cigarette smokers and alcohol drinkers, was statistically higher. However, there was no significant difference for other participants' characteristics between WBC categories.

Association of WBC category with MS and its components

In all 7,014 participants, 1,479 were diagnosed with MS. The prevalence rates of MS in the low level, middle level, and high level were 12.1% (48 of 397), 21.4% (1,368 of 6,380), and 26.6% (63 of 237), respectively. [Figure 1](#) shows a positive association between WBC count and risk of MS and its components. After adjustment for a potential confounder, the adjusted ORs for MS across WBC category were 1.00 (reference) for low level, 1.65 (95%CI: 1.18, 2.31) for middle level, and 2.18 (95%CI: 1.36, 3.50) for high level (p for

trend, 0.001). Similar significant relationships were also found when components of MS were analyzed respectively ([Figure 1](#)). In addition, a higher WBC level was also associated with increased risk of MS in both male and female ([Figure 2](#)).

Subgroup analyses stratified by sex, age, residence, smoking status, drinking status, BMI, and insulin resistance

Another purpose of this study was to examine the associations of WBC category and MS by the following subgroups: age (<65 or ≥ 65 years), residence (city, suburban, town, or rural village), smoking status (smoker or non-smoker), drinking status (drinker or non-drinker), BMI (<25 kg/m² or ≥ 25 kg/m²), and insulin resistance (yes or no). The strength of the association between WBC count and MS increased with age (OR, 1.42 [95%CI, 1.10–1.83] for adults aged <65 years; 1.85 [95%CI, 1.06, 3.21] for those aged ≥ 65 years). The strength of the association between WBC count and MS was weaker in participants who resided in a rural village (OR, 1.22 [95% CI, 0.90–1.66]) compared with other residences. The association between WBC count and MS was stronger in non-smokers (OR, 1.55 [95% CI, 1.19–2.03]) and non-drinkers (OR, 1.56 [95% CI, 1.19–2.04]) compared with smokers (OR, 1.34 [95%CI, 0.83–2.14])/drinkers (OR, 1.35 [95% CI, 0.86–2.12]). The association between WBC count and MS was stronger in normal/underweight participants compared with overweight/obese participants (OR, 1.71 [95% CI, 1.27–2.30] vs. 1.20 [95% CI, 0.82–1.74]) and was equivalent whether there was insulin resistance or not (OR, 1.54 [95% CI, 1.12–2.10] vs. 1.42 [95% CI, 1.01–1.99]). The detailed results has been showed in [Figures 3–5](#). Distribution of components of MS according to WBC category is also shown in violin plots ([Figure S1](#)).

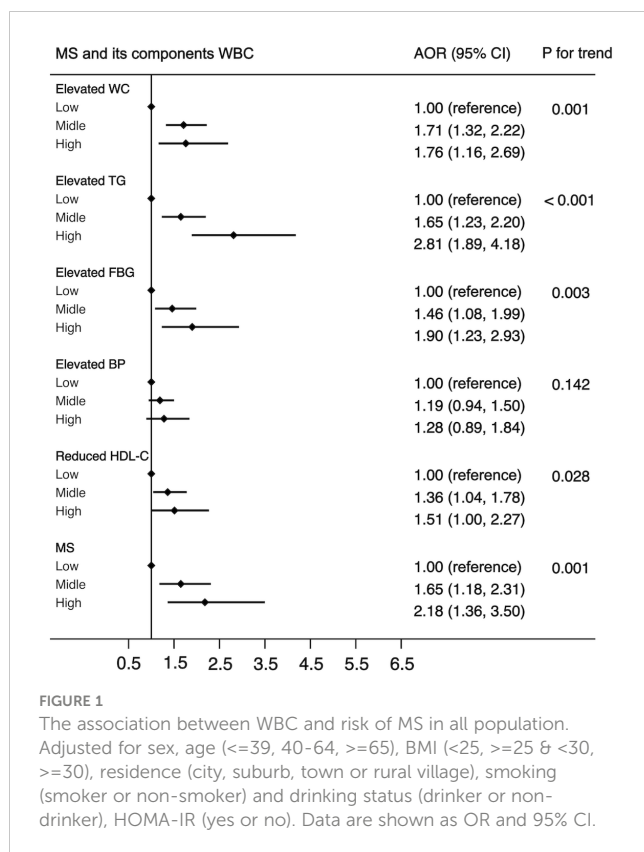
TABLE 1 Participants' characteristics according to WBC counts category 1.

N= 7014	Low level (≤ 3.9)	middle level (3.91–9.94)	high level (≥ 10.0)	P value ²
N	397	6380	237	—
Sex, (males,%)	28.5	47.2	54.0	<0.001
Age, years	52.0 (40.0, 59.0)	47.0 (38.0, 58.0)	45.0 (33.0, 57.0)	0.001
Residence, %				
City	11.3	12.8	8.0	0.069
Suburb	15.9	18.2	15.2	0.269
Town	17.1	16.1	13.1	0.385
Rural village	55.7	52.9	63.7	0.003
BMI, Kg/m ²	21.9 (20.0, 24.1)	23.1 (21.0, 25.6)	23.7 (21.3, 26.3)	<0.001
Cigarette smoker, %	14.6	31.3	40.1	<0.001
Alcohol drinker, %	22.4	34.4	35.9	<0.001
HOMA-IR	2.0 (1.4, 3.0)	2.3 (1.6, 3.4)	2.4 (1.6, 4.7)	<0.001

BMI = body mass index; HOMA-IR = homeostasis model assessment of insulin resistance.

¹ Continuous variables are expressed as medians (interquartile range) and categorical variables are expressed as percentages.

² P value were assessed using Kruskal Wallis test for continuous variables and chi-square test for categorical variables.



Sensitivity analyses

The aforementioned findings remained stable in a sensitivity analysis (Table S1). The results remained significant with the exclusion of excessively thin and obese participants [BMI (< 18 or > 40 kg/m²)].

To assess the predictive performance of predictive models, we selected MLP and logistic regression to compare their accuracy. The AUROC was calculated both in the 70% of training set and in the 30% of test set. It is generally accepted that an AUROC curve greater than 0.5 indicated having an adequate predictive performance. The results showed that the MLP algorithm represented a more prominent predictive performance (AUROC in the training set: 0.814; AUROC in the testing set: 0.842) compared to other algorithms (Table S2).

Discussion

In this study, we comprehensively examined the association between WBC count and the risk of MS in a representative Chinese population, and the results revealed that participants with a higher WBC count had a higher risk of MS and its components than those with a lower WBC count after adjusting for potential confounders. This study obtained the following novel results: (1) the significant associations between WBC count and risk of MS occur in participants living in suburbs or cities but not in towns or rural villages; (2) these significant associations were independent of insulin

resistance; and (3) the two models showed adequate calibration and good discrimination, but the MLP showed better performance.

The current cross-sectional study is consistent with the results of previous cross-sectional and cohort studies (4–7), which suggested that a higher WBC count level was related to an increased risk of MS. However, the association with WBC count varied between components of MS. Overall, the previous cross-sectional and prospective studies were heterogeneous, with differences in WBC count category, confounding factor adjustments, and sample selections. Nevertheless, the robust significant positive association between WBC count and MS was retained, despite the challenges introduced by these heterogeneities. This study harmonized fasting blood sample and other data across nine provinces, which largely attenuated these heterogeneities. Insulin resistance is an important marker for MS and its components; therefore, the significant positive associations of WBC count with the risk of MS and its components remained unchanged after adjusting for insulin resistance.

There are several plausible mechanisms that explain how WBC count may increase MS risk. Firstly, it is well known that insulin resistance is considered to be the root cause of MS (12); therefore, insulin resistance may mediate the association between WBC count and MS. Pro-inflammatory cytokines may lead to the activation of protein kinases and subsequently negatively regulate insulin receptor substrate and reduce the expression of glucose transporter 4 (18, 19); this inhibits the efficiency of blood glucose uptake (20). Therefore, compensatory hypersecretion of insulin can induce insulin resistance. However, the results of the current study suggest that elevated WBC count may increase the risk of MS in Chinese adults, even after adjusting for insulin resistance.

Secondly, it has been suggested that pro-inflammatory cytokines can increase hepatic fatty acid synthesis and stimulate lipolysis, which promotes the movement of free fatty acids to the liver (21). The above two mechanisms will subsequently enhance the production and secretion of triglycerides in the liver, resulting in hypertriglyceridemia (21).

Thirdly, the observed association between WBC count and elevated BP may be related to impaired endothelial function. Inflammation causes vasodilation, and the antithrombotic and antiatherosclerotic functions of the vascular endothelium are prevented by limiting the production of nitric oxide and prostacyclin (22). In contrast, the WBCs bind to the vascular endothelium, which may cause an increase in leukocytosis in capillaries, subsequently inducing capillary stenosis and increasing vascular pressure (23, 24), which may eventually lead to elevated BP.

Fourth, accumulated visceral fat can induce elevated fasting glucose levels compared to subcutaneous fat. This is because excessive free fatty acids produced by visceral fat through catabolism will overflow from adipose tissue into islet cells and induce fat ectopic deposition, causing insulin resistance in the muscle, liver, and pancreatic β cells, which subsequently can result in impaired glucose uptake (25). An imbalance between glucose production and uptake generally leads to elevated fasting glucose levels.

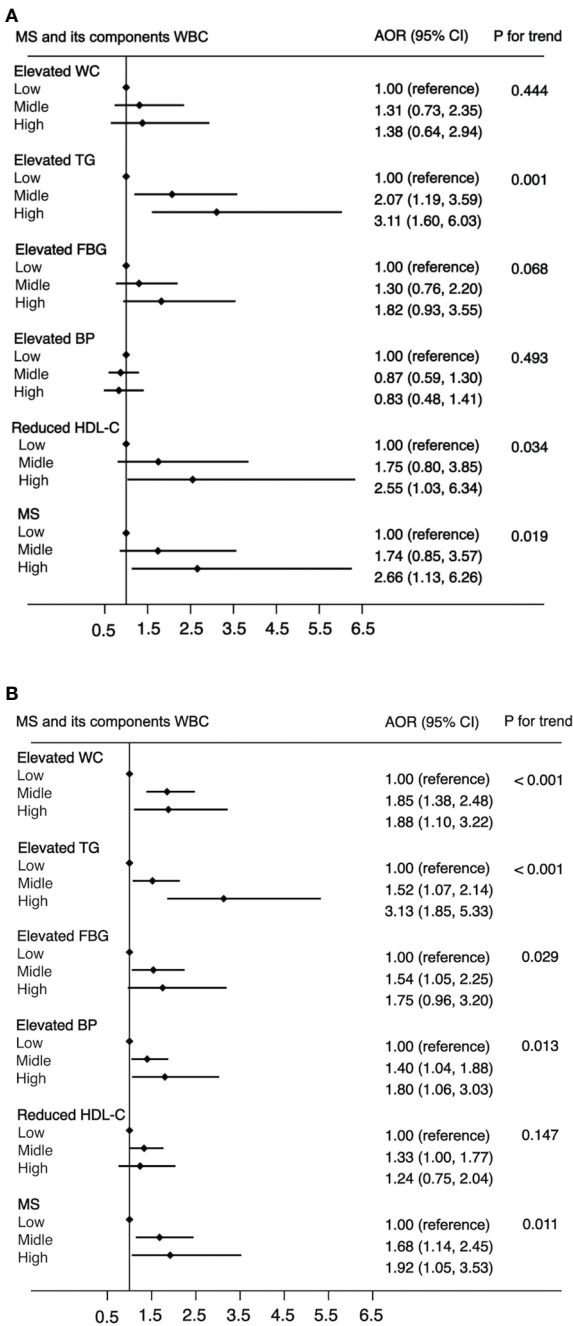
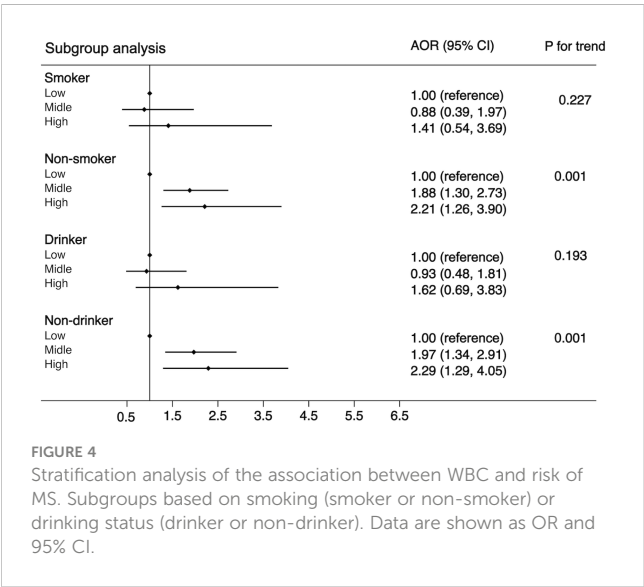
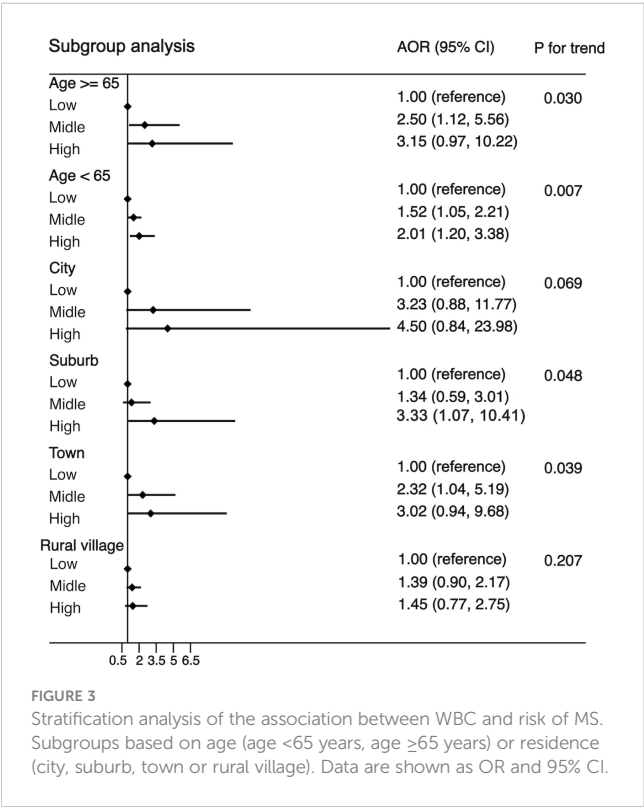


FIGURE 2
The association between WBC and risk of MS in male (A) and female (B). Adjusted for age (<=39, 40-64, >=65), BMI (<25, >=25 & <30, >=30), residence (city, suburb, town or rural village), smoking (smoker or non-smoker) and drinking status (drinker or non-drinker), HOMA-IR (yes or no). Data are shown as OR and 95% CI.

Logistic regression is a linear model widely used to analyze the linear association between independent and dependent variables (dichotomous variables), while ignoring the complex relationship between independent variables. MPL is composed of an input layer, one or more hidden layers, and an output layer, and can analyze the complex and potential associations among variables, rather than being limited to the linear relationship between the input and output (26). The results of this study indicated that the MPL algorithm had superior performance in predicting MS compared to logistic regression, indicating that the MPL algorithm is more suitable for predicting MS.

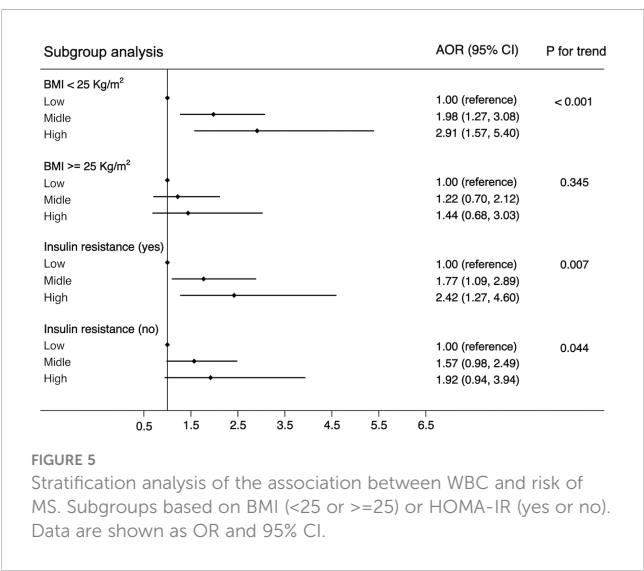
This study has several limitations. Firstly, the cross-sectional design of this study made it difficult to confirm the causal relationship between WBC count and MS and its components. Secondly, because there are fewer participants with a higher WBC level, this study therefore found seemingly inflated OR in Figures 2, 3, indicating that there are some sparse effects that may increase the probability of monotonic likelihood (27). Thirdly, the cross-sectional studies had Neyman bias because we could not identify whether the participants had suffered from MS in the past or only in the present. Therefore, the results of this



study may be affected by prevalence–incidence (Neyman’s) bias (28, 29). Further prospective cohort studies, which select the newly identified cases as study participants, will effectively avoid Neyman bias.

Conclusion

This study reveals representative evidence of positive associations between WBC counts and MS as well as its



components in a Chinese population. The findings of this study indicate that WBC count, as a convenient and routine examination, could be potentially used as a risk marker in the early identification and prevention of MS.

Data availability statement

Publicly available datasets were analyzed in this study. This data can be found here: <https://www.cpc.unc.edu/projects/china>.

Ethics statement

Ethics approval was obtained from the Institutional Review Board of the University of North Carolina at Chapel Hill and the National Institute for Nutrition and Health, Chinese Center for Disease Control and Prevention. The patients/participants provided their written informed consent to participate in this study.

Author contributions

ZR and LL designed this study, performed the statistical analyses, and wrote the manuscript. ZR and LL revised the manuscript. ZR and SL provided constructive and editorial feedback on drafts of the manuscript. All authors contributed to the article and approved the submitted version.

Funding

This study was supported by the Fundamental Research Funds for the Central Universities (Grant Nos. SWU1909734) and the

Funds for Administration of Sport of Chongqing (Grant No. B2019027).

Acknowledgments

We thank the CHNS database for providing a platform and the contributors for uploading their representative national datasets. We also thank all participants and the staff who participated in this study.

Conflict of interest

The authors declare that the research was conducted in the absence of any commercial or financial relationships that could be construed as a potential conflict of interest.

References

- Alberti KGMM, Eckel RH, Grundy SM, Zimmet PZ, Cleeman JI, Donato KA, et al. Harmonizing the metabolic syndrome: a joint interim statement of the international diabetes federation task force on epidemiology and prevention; national heart, lung, and blood institute; American heart association; world heart federation; international atherosclerosis society; and international association for the study of obesity. *Circulation* (2009) 120(16):1640–5. doi: 10.1161/CIRCULATIONAHA.109.192644
- Saklayen MG. The global epidemic of the metabolic syndrome. *Curr Hypertens Rep* (2018) 20(2):1–8. doi: 10.1007/s11906-018-0812-z
- Pearson TA, Mensah GA, Alexander RW, Anderson JL, Cannon RO, Criqui M, et al. Markers of inflammation and cardiovascular disease application to clinical and public health practice - a statement for healthcare professionals from the centers for disease control and prevention and the American heart association. *Circulation* (2003) 107(3):499–511. doi: 10.1161/01.CIR.0000052939.59093.45
- Babio N, Ibarrola-Jurado N, Bullo M, Angel Martinez-Gonzalez M, Waernberg J, Salaverria I, et al. White blood cell counts as risk markers of developing metabolic syndrome and its components in the predimed study. *PloS One* (2013) 8(3):1–11. doi: 10.1371/journal.pone.0058354
- Oda E, Kawai R. The prevalence of metabolic syndrome and diabetes increases through the quartiles of white blood cell count in Japanese men and women. *Internal Med* (2009) 48(13):1127–34. doi: 10.2169/internalmedicine.48.2138
- Meng W, Zhang C, Zhang Q, Song X, Lin H, Zhang D, et al. Association between leukocyte and metabolic syndrome in urban han Chinese: A longitudinal cohort study. *PloS One* (2012) 7(11):1–7. doi: 10.1371/journal.pone.0049875
- Sun S, Wu H, Zhang Q, Wang C, Guo Y, Du H, et al. Subnormal peripheral blood leukocyte counts are related to the lowest prevalence and incidence of metabolic syndrome: Tianjin chronic low-grade systemic inflammation and health cohort study. *Mediators Inflammation* (2014) 2014:1–12. doi: 10.1155/2014/412386
- Liu C-C, Ko H-J, Liu W-S, Hung C-L, Hu K-C, Yu L-Y, et al. Neutrophil-to-lymphocyte ratio as a predictive marker of metabolic syndrome. *Medicine* (2019) 98(43):1–12. doi: 10.1097/MD.00000000000017537
- Yang X-J, Tian S, Ma Q-H, Sun H-P, Xu Y, Pan C-W. Leukocyte-related parameters in older adults with metabolic syndrome. *Endocrine* (2020) 68(2):312–9. doi: 10.1007/s12020-020-02243-2
- Lin H-Y, Zhang X-J, Liu Y-M, Geng L-Y, Guan L-Y, Li X-H. Comparison of the triglyceride glucose index and blood leukocyte indices as predictors of metabolic syndrome in healthy Chinese population. *Sci Rep* (2021) 11(1):1–7. doi: 10.1038/s41598-021-89494-9
- Thompson AL, Houck KM, Adair L, Gordon-Larsen P, Popkin B. Multilevel examination of the association of urbanization with inflammation in Chinese adults. *Health Place* (2014) 28:177–86. doi: 10.1016/j.healthplace.2014.05.003
- Nolan CJ, Prentki M. Insulin resistance and insulin hypersecretion in the metabolic syndrome and type 2 diabetes: Time for a conceptual framework shift. *Diabetes Vasc Dis Res* (2019) 16(2):118–27. doi: 10.1177/1479164119827611
- Zhou P, Meng Z, Liu M, Ren X, Zhu M, He Q, et al. The associations between leukocyte, erythrocyte or platelet, and metabolic syndrome in different genders of Chinese. *Medicine* (2016) 95(44):1–7. doi: 10.1097/MD.0000000000005189
- Desai RJ, Wang SV, Vaduganathan M, Evers T, Schneeweiss S. Comparison of machine learning methods with traditional models for use of administrative claims with electronic medical records to predict heart failure outcomes. *JAMA Netw Open* (2020) 3(1):1–15. doi: 10.1001/jamanetworkopen.2019.18962
- Popkin BM, Du S, Zhai F, Zhang B. Cohort profile: The China health and nutrition survey-monitoring and understanding socio-economic and health change in China, 1989–2011. *Int J Epidemiol* (2010) 39(6):1435–40. doi: 10.1093/ije/dyp322
- He T, Wang M, Tian Z, Zhang J, Liu Y, Zhang Y, et al. Sex-dependent difference in the association between frequency of spicy food consumption and risk of hypertension in Chinese adults. *Eur J Nutr* (2019) 58(6):2449–61. doi: 10.1007/s00394-018-1797-8
- Matthews DR, Hosker JP, Rudenski AS, Naylor BA, Treacher DF, Turner RC. Homeostasis model assessment - insulin resistance and beta-cell function from fasting plasma-glucose and insulin concentrations in man. *Diabetologia* (1985) 28(7):412–9. doi: 10.1007/BF00280883
- de Luca C, Olefsky JM. Inflammation and insulin resistance. *FEBS Lett* (2008) 582(1):97–105. doi: 10.1016/j.febslet.2007.11.057
- Kunz HE, Hart CR, Gries KJ, Parvizi M, Laurenti M, Dalla Man C, et al. Adipose tissue macrophage populations and inflammation are associated with systemic inflammation and insulin resistance in obesity. *Am J Physiol-Endocrinol Metab* (2021) 321(1):E105–E21. doi: 10.1152/ajpendo.00070.2021
- Kahn SE, Hull RL, Utzschneider KM. Mechanisms linking obesity to insulin resistance and type 2 diabetes. *Nature* (2006) 444(7121):840–6. doi: 10.1038/nature05482
- Feingold KR, Doerrler W, Dinarello CA, Fiers W, Grunfeld C. Stimulation of lipolysis in cultured fat-cells by tumor-necrosis-factor, interleukin-1, and the interferons is blocked by inhibition of prostaglandin synthesis. *Endocrinology* (1992) 130(1):10–6. doi: 10.1210/endo.130.1.1370149
- Sinialo J, Paronen J, Mattila KJ, Syrjala M, Alfthan G, Palosuo T, et al. Relation of inflammation to vascular function in patients with coronary heart disease. *Atherosclerosis* (2000) 149(2):403–11. doi: 10.1016/S0021-9150(99)00333-0
- Harlan JM. Leukocyte endothelial interactions. *Blood* (1985) 65(3):513–25. doi: 10.1182/blood.V65.3.513.513
- Shankar A, Klein BEK, Klein R. Relationship between white blood cell count and incident hypertension. *Am J Hypertens* (2004) 17(3):233–9. doi: 10.1016/j.amjhyper.2003.11.005
- Hajer GR, van Haften TW, Visseren FLJ. Adipose tissue dysfunction in obesity, diabetes, and vascular diseases. *Eur Heart J* (2008) 29(24):2959–71. doi: 10.1093/eurheartj/ehn387

Publisher's note

All claims expressed in this article are solely those of the authors and do not necessarily represent those of their affiliated organizations, or those of the publisher, the editors and the reviewers. Any product that may be evaluated in this article, or claim that may be made by its manufacturer, is not guaranteed or endorsed by the publisher.

Supplementary material

The Supplementary Material for this article can be found online at: <https://www.frontiersin.org/articles/10.3389/fimmu.2023.1104180/full#supplementary-material>

SUPPLEMENTARY FIGURE 1

Violin plot of components of MS based on different WBC category among all participants.

26. Li C-p, Zhi X-y, Ma J, Cui Z, Zhu Z-l, Zhang C, et al. Performance comparison between logistic regression, decision trees, and multilayer perceptron in predicting peripheral neuropathy in type 2 diabetes mellitus. *Chin Med J* (2012) 125(5):851–7. doi: 10.3760/cma.j.issn.0366-6999.2012.05.022
27. Tzeng IS. To handle the inflation of odds ratios in a retrospective study with a profile penalized log-likelihood approach. *J Clin Lab Anal* (2021) 35(7):1–2. doi: 10.1002/jcla.23849
28. Neyman J. STATISTICS - SERVANT OF ALL SCIENCES. *Science* (1955) 122 (3166):401–6. doi: 10.1126/science.122.3166.401
29. Anzai T, Grandinetti A, Katz AR, Hurwitz EL, Wu YY, Masaki K. Paradoxical association between atrial fibrillation/flutter and high cholesterol over age 75 years: The kuakini Honolulu heart program and Honolulu-Asia aging study. *J Electrocardiol* (2021) 65:37–44. doi: 10.1016/j.jelectrocard.2020.12.008



OPEN ACCESS

EDITED BY

Wilfried Le Goff,
Institut National de la Santé et de la
Recherche Médicale (INSERM), France

REVIEWED BY

Madhumita Chatterjee,
Department of Pharmacology,
Experimental Therapy and Toxicology,
Germany
John Eleftheriades,
Yale University, United States
Fabrizio Salucci,
Independent Researcher,
Vercelli, Italy

*CORRESPONDENCE

Delong Jiang
✉ 20201108@cmu.edu.cn
Xinyang Li
✉ lixinyang199704@sina.com

RECEIVED 02 November 2022

ACCEPTED 14 April 2023

PUBLISHED 03 May 2023

CITATION

Tian Z, Zhang P, Li X and Jiang D (2023)
Analysis of immunogenic cell death in
ascending thoracic aortic aneurysms based
on single-cell sequencing data.
Front. Immunol. 14:1087978.
doi: 10.3389/fimmu.2023.1087978

COPYRIGHT

© 2023 Tian, Zhang, Li and Jiang. This is an
open-access article distributed under the
terms of the [Creative Commons Attribution
License \(CC BY\)](#). The use, distribution or
reproduction in other forums is permitted,
provided the original author(s) and the
copyright owner(s) are credited and that
the original publication in this journal is
cited, in accordance with accepted
academic practice. No use, distribution or
reproduction is permitted which does not
comply with these terms.

Analysis of immunogenic cell death in ascending thoracic aortic aneurysms based on single-cell sequencing data

Zemin Tian¹, Peng Zhang², Xinyang Li^{1*} and Delong Jiang^{1*}

¹Department of Vascular and Thyroid Surgery, The First Affiliated Hospital of China Medical University, Shenyang, Liaoning, China, ²Department of Neurology, The First Affiliated Hospital of Kunming Medical University, Kunming, Yunnan, China

Background: At present, research on immunogenic cell death (ICD) is mainly associated with cancer therapy. Little is known about the role of ICD in cardiovascular disease, especially in ascending thoracic aortic aneurysms (ATAA).

Method: ATAA single-cell RNA (scRNA) sequencing data were analyzed to identify the involved cell types and determine their transcriptomic characteristics. The chi-square test, Gene Ontology (GO) and Kyoto Encyclopedia of Genes and Genomes (KEGG) enrichment analyses, Gene Set Enrichment Analysis (GSEA), and CellChat for cell-to-cell communication analysis from the Gene Expression Omnibus (GEO) database were used.

Result: A total of 10 cell types were identified, namely, monocytes, macrophages, CD4 T/NK (CD4+ T cells and natural killer T cells), mast cells, B/Plasma B cells, fibroblasts, endothelial cells, cytotoxic T cells (CD8+ T cells, CTLs), vascular smooth muscle cells (vSMCs), and mature dendritic cells (mDCs). A large number of inflammation-related pathways were present in the GSEA results. A large number of ICD-related pathways were found in the KEGG enrichment analysis of differentially expressed genes in endothelial cells. The number of mDCs and CTLs in the ATAA group was significantly different from that in the control group. A total of 44 pathway networks were obtained, of which 9 were associated with ICD in endothelial cells (CCL, CXCL, ANNEXIN, CD40, IL1, IL6, TNF, IFN-II, GALECTIN). The most important ligand–receptor pair by which endothelial cells act on CD4 T/NK cells, CTLs and mDCs is CXCL12–CXCR4. The most important ligand–receptor pair by which endothelial cells act on monocytes and macrophages is ANXA1–FPR1. The most important ligand–receptor pair by which CD4 T/NK cells and CTLs act on endothelial cells is CCL5–ACKR1. The most important ligand–receptor pair that myeloid cells (macrophages, monocytes and mDCs) act on endothelial cells is CXCL8–ACKR1. Moreover, vSMCs and fibroblasts mainly promote inflammatory responses through the MIF signaling pathway.

Conclusion: ICD is present in ATAA and plays an important role in the development of ATAA. The target cells of ICD may be mainly endothelial cells,

in which the aortic endothelial cell ACKR1 receptor can not only promote T-cell infiltration through the CCL5 ligand but also promote myeloid cell infiltration through the CXCL8 ligand. ACKR1 and CXCL12 may become target genes for ATAA drug therapy in the future.

KEYWORDS

ICD (immunogenic cell death), ATAA (ascending thoracic aortic aneurysms), ACKR1, CXCL12 (SDF-1 α), CTL (cytotoxic T cells)

1 Introduction

It is well known that ascending thoracic aortic aneurysms (ATAA) are asymptomatic until complications such as rupture and dissection are present (1–3). The adventitia and media of the thoracic aortic wall contain high levels of inflammatory cells. In particular, studies have demonstrated that macrophages and T lymphocytes are prevalent in the thoracic aortas of patients with sporadic ATAA (4–6). Apoptosis, a type of regulatory cell death, has been shown to be significantly increased in smooth muscle cells (SMCs) in ATAA (7, 8). This observation also implies that there is regulated cell death in ATAA, and we explore the role of immunogenic cell death (ICD) in ascending thoracic aortic aneurysms in this study.

ICD, a type of regulated cell death, can lead to an inflammatory response, which triggers cytotoxic T lymphocyte (CTL)-driven adaptive immunity, as well as long-term immunological memory (9). It is well known that ICD occurs mainly in three types of cells: dying cells, antigen-presenting cells (APCs), and cytotoxic T cells. Moreover, three conditions need to be met for ICD to occur: antigenicity, adjuvanticity, and favorable microenvironment (10).

In this study, we first demonstrated the existence of ICD in ATAA. Second, we identified that the target cells for ICD were mainly endothelial cells of the ascending aorta. Finally, we identified the most important ligands released by endothelial cells and the most important receptors expressed by endothelial cells that cause ICD. In conclusion, investigating ICD in ATAA may provide new ideas for ATAA targeted therapy.

2 Methods

2.1 scRNA sequencing data processing

ATAA cells were collected by flow cytometry sorting and submitted to a 10X Chromium System with an Illumina NovaSeq 6000 (1). To generate the barcode, gene, and expression matrix files, the cleaned data (GSE155468) were aligned to the human reference genome (GRCh38 transcriptome) using Cell Ranger (version 3.0.2, 10X Genomics). In the GSE155468 dataset, there were samples from 11 individuals, including 8 samples in the experimental ATAA group and 3 samples in the control group (The protocol for collecting human tissue samples was approved by the Institutional Review Board at

Bayer College of Medicine (1)). In the Seurat R package, we first used PCA to reduce the dimensionality of the downstream data and then used t-distributed stochastic neighbor embedding (t-SNE) analysis to reduce the dimensionality of the data again (11). We removed cells with fewer than 200 genes, more than 7,000 genes, and more than 10% mitochondrial genes. Analysis was performed on 48128 filtered cells. Subsequent analysis was performed on 48128 filtered cells. Using the “LogNormalize” function, gene expression was normalized and scaled. Each sample possessed 2000 highly variable genes (HVGs) using the vst method after data normalization. After identifying significant principal components (PCs), PCA was applied. Batch correction was performed using the “Harmony” R package (version 0.1.0) (12) to avoid batch effects resulting from sample identity that could disrupt downstream analysis. Finally, 50 PCs were selected for t-SNE analysis. A total of 60 distinct clusters were created using FindClusters function at 4.0 resolution, and these clusters were then grouped into 10 cell types using marker genes, and the results of the “FindAllMarkers” function were manually checked for match with marker gene results. In each cluster, differentially expressed genes (DEGs) were identified using the “FindAllMarkers” function with logfc.threshold = 0.25 (13). Thirty-four ICD marker genes were selected, and a heatmap was constructed using the 10 identified cell types (14).

2.2 Gene ontology (GO) and Kyoto encyclopedia of genes and genomes (KEGG) analyses and gene set enrichment analysis (GSEA)

Significantly differentially expressed genes in each cell group relative to the other groups were identified and subjected to GSEA. The GO and KEGG enrichment analysis of the obtained smooth muscle cell differentially expressed genes and the obtained endothelial cell differentially expressed genes were performed using the GSE155468 dataset (logfc.threshold = 0, P_{val}adj<0.05), and the GO and KEGG enrichment results of the differentially expressed genes between the two cell populations were compared (15).

2.3 Statistical analysis

Differences between the ATAA group and control group were evaluated with a chi square (χ^2) test or Fisher exact test for all

categoric variables. Data were analyzed using IBM SPSS Statistics 2 software (version 26.0; IBM Corp, Armonk, NY, USA).

2.4 Cellchat in ATAA

First, in the ATAA data, we used the CellChat and patchwork packages to create CellChat objects, set up the ligand–receptor interaction database, and preprocessed the expression data for cell communication analysis.

Second, we used CellChat to infer biologically meaningful communication, and used the “trimean” function to calculate communication probability and infer the CellChat network. Then, we extracted the inferred CellChat network as a data frame; used the signaling pathway level to infer communication; and computationally integrated cellular communication networks (Supplementary Figure 1).

Third, we used circle plots to visualize signal paths that may be related to ICDs (Supplementary Figures 2–10). We calculated the contribution of each ligand–receptor pair to these signaling pathways, and visualized cellular communication regulated by individual ligand–receptor pairs. Signal gene expression distributions were plotted using violin plots for these communications.

Fourth, a systematic analysis of cellular communication networks was performed to identify the signaling roles of cell groups (e.g., dominant transmitter, receiver) as well as the main contributing signals. We identified the signals that contributed the most to the efferent or afferent signaling of certain cell groups (Figures 1A, C, D).

We compared the ICD-related pathways in which endothelial cells act as ligands on other cells, and identified the most important pathways. We used the same method to compare macrophages, monocytes, mDCs, CD4 T/NK cells and cytotoxic T cells (Figure 2). Protein–protein interaction (PPI) networks were constructed using

the most important ligand and receptor genes and visualized using Cytoscape software (Figure 1B).

3 Results

3.1 ATAA scRNA profiling

After filtering the data, there were a total of 48,128 cells in the scRNA sequencing dataset (GSE155468), including 39,651 cells from patients with ATAA and 8,477 cells from control individuals (Tables 1–5). After PCA, and Harmony, and t-SNE processing of the dataset (Figures 3A, B), we examined results (Figure 3C).

Sixty clusters could be assigned to known cell lineages through marker genes (Supplementary List 1), according to a previous study. We used t-SNE analysis to visualize the 10 clusters (Figure 3D) and identify marker genes in the 10 cell-type populations (Supplementary List 2). The expression of cell type marker genes is shown in the dot plot (Figure 4M). We observed 10 cell clusters (CD4T/NK: clusters 1, 6, 8, 9, 11, 17, 20, 22, 31, 35, 45, 46 and 52; expressing CD3D (16) (Figures 3E, I), CD7 (17) (Figures 3F, J), IL7R (interleukin 7 receptor) (18) (Figures 3G, K); CTL: clusters 0, 7, 16, 19, 23, 26, 37, 47, 49, 55 and 59; expressing CD8A (19) (Figures 3H, L); Endothelial: clusters 40 and 44; expressing vWF (20) (von Willebrand factor) (Figures 3M, Q); Fibroblast: clusters 24, 25, 56 and 58; expressing LUM (Lumican) (21) (Figures 3N, R); vSMC: clusters 2, 5, 14, 15, 21, 28, 30, 34, 41 and 42; expressing ACTA2 (actin alpha 2, smooth muscle) (22) (Figures 3O, S); B/Plasma_B: clusters 33 and 48; expressing CD79A (23) (Figures 3P, T); Macrophage: clusters 3, 4, 10, 12, 13, 18, 27, 32, 36, 39, 43, 53 and 54; expressing FCGR3A (24) (Figures 4A, E); Mast: cluster 50; expressing CPA3 (25) (Figures 4B, F); Monocytes: clusters 38 and 51, expressing S100A9 (26) (Figures 4C, G); mDCs: clusters 29 and

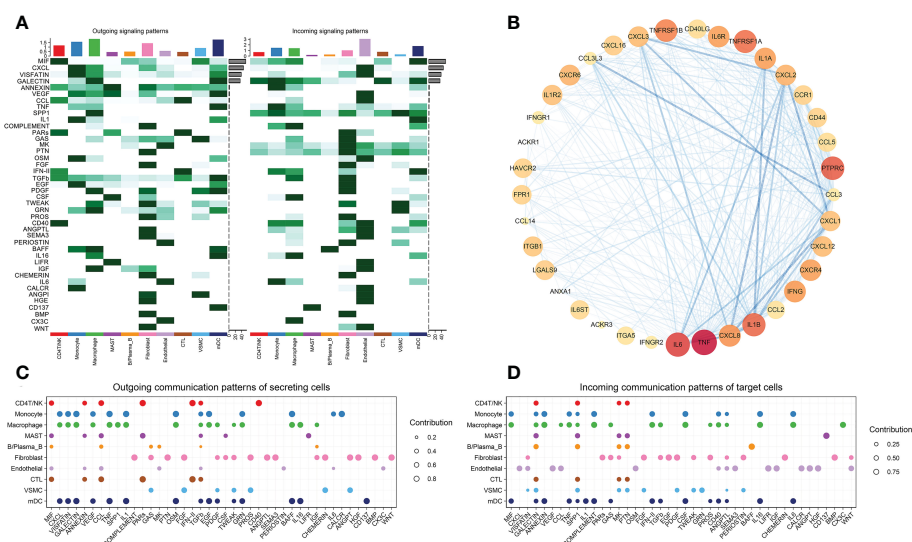


FIGURE 1

(A) Identified signals that contribute the most to the outgoing or incoming signaling of individual cell groups. (B) PPI analysis of ICD signaling pathway genes. (C) Outgoing communication patterns of secreting cells. (D) Incoming communication patterns of target cells.

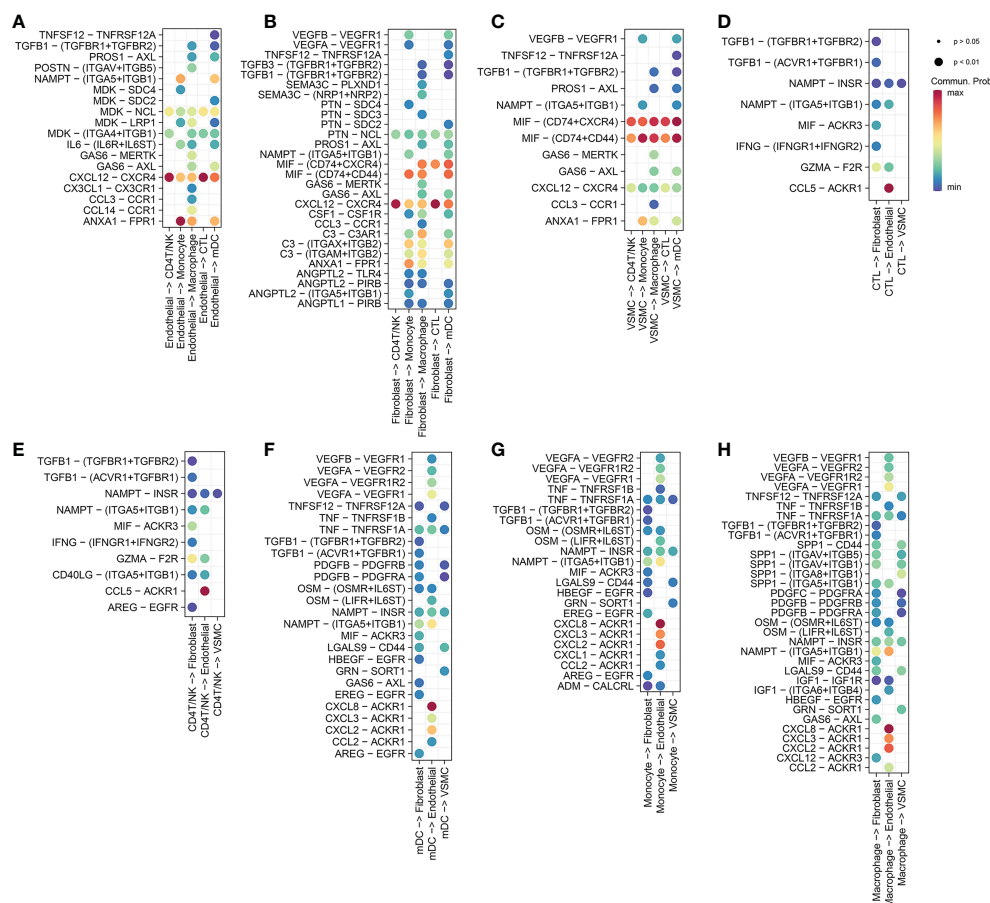


FIGURE 2

(A) Endothelial cells release ligands that act on myeloid cells (macrophages, monocytes and dendritic cells) and T cells (CD4 T/NK cells and cytotoxic T cells). (B) Fibroblasts release ligands that act on myeloid cells and T cells. (C) VSMCs release ligands that act on myeloid cells and T cells. (D) Cytotoxic T cells release ligands that act on nonimmune cells (fibroblasts, VSMCs, endothelial cells). (E) CD4 T/NK cells release ligands that act on nonimmune cells. (F) Mature dendritic cells release ligands that act on nonimmune cells. (G) Monocytes release ligands that act on nonimmune cells. (H) Macrophages release ligands that act on nonimmune cells.

57; expressing CD1C (27) (Figures 4D, H), CLEC9A (28) (Figures 4I, K), CD83 (29) (Figures 4J, L).

According to the results in Table 4 and Table 5, T-cells accounted for 51.97% of all ATAA cells (Figures 4N, O). This finding suggests that T-cell infiltration plays a very important role in the pathogenesis of ATAA. In ATAA, the number of endothelial cells was significantly reduced, accounting for only 1.42%.

3.2 The results of GO and KEGG analyses and GSEA

In nonimmune cells, 34 ICD-related marker genes were mainly expressed in endothelial cells (Figure 5A). In Figure 5B, we only showed the top 50 most important pathways, which could be mainly divided into several categories, such as metabolism-related, oxidative respiration-related, inflammation-related, and apoptosis-related, etc. At present, it is well known that the occurrence of cardiovascular disease was closely related to the abnormal expression of these

pathways. Inflammation plays an important role in the occurrence and development of ATAA. When we compared the GO enrichment results of endothelial cells and VSMCs, we found that the pathways enriched in endothelial cells were mainly related to transcription, while the pathways enriched in VSMCs were mainly related to the oxidative respiratory chain (Figure 5C). When we compared the KEGG results, we found that differentially expressed genes in endothelial cells were enriched in a large number of ICD-related pathways (Figure 5D; Supplementary List 3).

3.3 Chi-square test results of the number of mDCs and cytotoxic T cells

The number of mature dendritic cells was significantly correlated with the formation of ATAA, K^2 (mDC) = 136.86, P ($K^2 > 10.828$) < 0.001 (Table 6). The number of cytotoxic T cells was significantly correlated with the formation of ATAA, K^2 (CTL) = 1601.41, P ($K^2 > 10.828$) < 0.001 (Table 7).

TABLE 1 Demographic characteristics of patients and controls (1).

Variable	ATAA1	ATAA2	ATAA3	ATAA4	ATAA5	ATAA6	ATAA7	ATAA8	Control4	Control6	Control9
Sex	F	F	M	M	F	F	M	M	F	M	F
Ethnicity	Non-Hispanic	Non-Hispanic	Non-Hispanic	Non-Hispanic	Non-Hispanic	Non-Hispanic	Non-Hispanic	Non-Hispanic	Non-Hispanic	Non-Hispanic	Hispanic
Race	White	White	White	White	White	White	White	White	White	Black	Latino
Age (y)	75	78	59	62	75	67	69	56	63	61	62
Diagnosis/Comments	ATAA	ATAA	ATAA with root aneurysm	ATAA	ATAA with root aneurysm	ATAA with arch and DTAA	ATAA with root aneurysm	ATAA with root aneurysm	Heart transplant recipient	Heart transplant recipient	Lung transplant donor
Aortic diameter (cm)	5.2	4.9	5	5.2	5.8	4.9	5.2	5.2	NA	NA	2.2
Smoking status	Past (quit before 1990)	Never	Never	Never	Past (quit 1999)	Never	Never	Never	Never	Past	Current
Diabetes	No	No	Yes	Yes	No	No	No	No	No	No	Yes
Hypertension	Yes	Yes	Yes	Yes	Yes	Yes	Yes	Yes	No	Yes	Yes
COPD	No	Yes	No	No	Yes	No	No	No	No	No	No
Aortic valve regurgitation	No	No	Yes	Yes	Yes	Yes	No	Yes	No	No	No
BAV	No	Yes	Yes	No	No	No	NA	No	NA	NA	No
Re-operation	No	No	Yes *	No	No	No	Yes **	No	No	No	No

*Previous arch debranching before stent graft repair of arch and descending thoracic aorta.

**Previous aortic valve replacement.

NA, not available.

3.4 The ATAA CellChat results

We obtained a total of 44 cell-to-cell communications. Among nonimmune cells, the cells that sent the most cellular signals were fibroblasts, while the ones that received the most signals were endothelial cells (Figure 1A). This finding suggests that although VSMCs and fibroblasts may also trigger ICD through the MIF signaling pathway (Figures 2B, C), endothelial cells may be the main cells responsible for ICD. Therefore, we mainly explored ICD in endothelial cells. The 9 pathway networks are ANNEXIN signaling pathway network, CXCL signaling pathway network, CCL signaling pathway network, IFN-II signaling pathway network, IL1 signaling pathway network, IL6 signaling pathway network, GALECTIN signaling pathway network, TNF signaling pathway network, and CD40 signaling pathway network. Cells associated with these pathways were mainly endothelial cells, myeloid cells, CD4 T/NK cells and cytotoxic T cells (Figures 1C, D).

Endothelial cells acted as ligands in the ICD-related pathways of myeloid cells, including the ANNEXIN signaling pathway network (Supplementary Figure 2), CXCL signaling pathway

network (Supplementary Figure 3), CCL signaling pathway network (Supplementary Figure 4) and IL6 signaling pathway network (Supplementary Figure 10).

In the ANNEXIN signaling pathway network, there was only one ligand-receptor pair, ANXA1-FPR1 pathway (Supplementary Figure 2A), and ANXA1 ligands were highly expressed in all cells except B/Plasma_B cells (Supplementary Figure 2E). The receptor FPR1 was only expressed in myeloid cells (Supplementary Figure 2E). Among all the ICD-related pathways in which endothelial cells acted as ligands for myeloid cells (macrophage, monocyte and mDC), ANXA1-FPR1 was the most contributing pair (Figure 2A).

In the CXCL signaling pathway network, a total of seven ligand-receptor pairs were obtained, namely CXCL8-ACKR1, CXCL12-CXCR4, CXCL2-ACKR1, CXCL3-ACKR1, CXCL16-CXCR6, CXCL12-ACKR3, and CXCL1-ACKR1 (Supplementary Figure 3A). Among them, CXCL8-ACKR1 contributed the most to the CXCL signaling pathway network. The CXCL8 ligand was highly expressed in myeloid cells, while the ACKR1 receptor was only expressed in endothelial cells (Supplementary Figure 3K).

TABLE 2 Dataset features.

Datasets	Type	Platform	Sample size (Control/ATAA)
GSE155468	scRNA sequencing	Illumina NovaSeq 6000 (Homo sapiens)	3,8

TABLE 3 Single sample data features.

Sample name	Raw data	Data filtering (200<nFeature-RNA<7000,percent.mt<10)
GSM31 (Control 4: 63 years)	3377	3377
GSM32 (Control 6: 61 years)	1193	1193
GSM33 (Control 9: 62 years)	3907	3907
GSM34 (ATAA 1: 75 years)	6686	6686
GSM35 (ATAA 2: 78 years)	4598	4598
GSM36 (ATAA 3: 59 years)	3622	3622
GSM37 (ATAA 4: 62 years)	6384	6384
GSM38 (ATAA 5: 75 years)	4802	4802
GSM39 (ATAA 6: 67 years)	3526	3526
GSM40 (ATAA 7: 69 years)	6997	6997
GSM41 (ATAA 8: 56 years)	3036	3036
All (ATAA: 67.6±8.1 years, Control: 62±1 years)	48128	48128

Among all the ICD-related pathways in which myeloid cells (macrophages, monocytes and mDC) acted as ligands to endothelial cells, CXCL8-ACKR1 was the most contributing pair (Figures 2F, G, H). Among all the ICD-related pathways in which endothelial cells and fibroblasts acted as ligands to T cells (CD4T/NK cells and cytotoxic T cells), CXCL12-CXCR4 was the most contributing pair (Figures 2A, B).

In the CCL signaling pathway network, we obtained a total of 7 ligand-receptor pairs, namely CCL5-ACKR1, CCL2-ACKR1, CCL3-CCR1, CCL14-ACKR1, CCL3L1-CCR1, CCL5-CCR1, and CCL14-CCR1 (Supplementary Figure 4A). Among these pairs, CCL5-ACKR1 contributed the most to the CCL signaling pathway network. As a ligand, CCL5 was only highly expressed in CD4T/NK cells and cytotoxic T cells, while the ACKR1 receptor was only expressed in endothelial cells (Supplementary Figure 4K). Among all the ICD-related pathways in which T cells (CD4T/NK

cells and cytotoxic T cells) acted as ligands to endothelial cells, CCL5-ACKR1 was the most contributing pair (Figures 2D, E).

Myeloid cells (macrophage, monocyte and mDC) acted as ligands on the ICD-related pathways of T cells (CD4T/NK and CTL), including the CXCL signaling pathway network (CXCL16-CXCR6) (Supplementary Figure 3), TNF signaling pathway network (TNF-TNFRSF1B) (Supplementary Figure 6), and GALECTIN signaling pathway network (LGALS9-CD44 and LGALS9-CD45) (Supplementary Figure 5; Figures 5B, D, E). Among them, the contribution of the LGALS9-CD45 (PTPRC) pathway was the largest.

4 Discussion

ICD has not been reported in ATAA before, and almost all recent studies have mainly focused on ICD in the context of cancer therapy (30–32). In our study, we found that the marker genes of ICD were highly expressed in endothelial cells, and KEGG enrichment analysis results showed that the differentially expressed genes were enriched in a large number of ICD-related pathways. Based on the cell-to-cell communication results, we found that endothelial cells received the most signals and that there were numerous signaling pathways associated with ICD. This result suggests that dying endothelial cells in ATAA may contribute to the progression of ATAA through ICD. We identified the most important ligand–receptor pair leading to endothelial cell ICD, and according to these results, found that endothelial cells mainly acted on APCs and T cells by releasing ANXA1 and CXCL12 chemokines, respectively. The chemokine CXCL8 released by APCs and the chemokine CCL5 released by T cells bind to ACKR1 expressed by endothelial cells.

It is well known that ICD requires the simultaneous satisfaction of three conditions: antigenicity, adjuvanticity, and microenvironment (10, 33). First, we explored antigenicity in ATAA. In the field of oncology, it is currently believed that dying

TABLE 4 Data characteristics of the control group.

cell types	number of cells	ratio(%)
CD4T/NK	582	6.87
Monocyte	77	0.91
Macrophage	1917	22.61
MAST	61	0.72
B/Plasma_B	57	0.67
Fibroblast	319	3.76
Endothelial	364	4.29
CTL	338	3.99
VSMC	4674	55.14
mDC	88	1.04
All	8477	100

TABLE 5 Data characteristics of the ATAA group.

cell types	number of cells	ratio (%)
CD4T/NK	11852	29.89
Monocyte	725	1.83
Macrophage	9724	24.52
MAST	207	0.52
B/Plasma_B	859	2.17
Fibroblast	1557	3.93
Endothelial	565	1.42
CTL	8754	22.08
VSMC	4719	11.9
mDC	689	1.74
All	39651	100

tumor cells can provide antigenicity by conventional methods of generating epitopes (10). However, in nontumor cells, cellular oxidation could also cause enzymatic or nonenzymatic posttranslational modifications (PTMs) that generate epitopes that initiate ICD (34). In cardiovascular disease, endothelial cell dysfunction caused by oxidative stress stimulates abnormal proinflammatory and prothrombotic phenotypes of the endothelial cells lining the lumen of blood vessels (35, 36). This observation partly suggests that dying endothelial cells in ATAA can indeed generate epitopes that initiate ICD. The proinflammatory capacity of dysfunctional endothelial cells also provides a favorable microenvironment for the occurrence of ICD.

Finally, we explored the adjuvant substances in ATAA. According to the latest ICD research, the main role of adjuvant substances is to trigger chemotactic immune cells to migrate to the site of vascular lesions (10). According to the chi-square test results, in ATAA, we found that the numbers of the two most important immune cells involved in ICD [CTLs and mDCs (the strongest

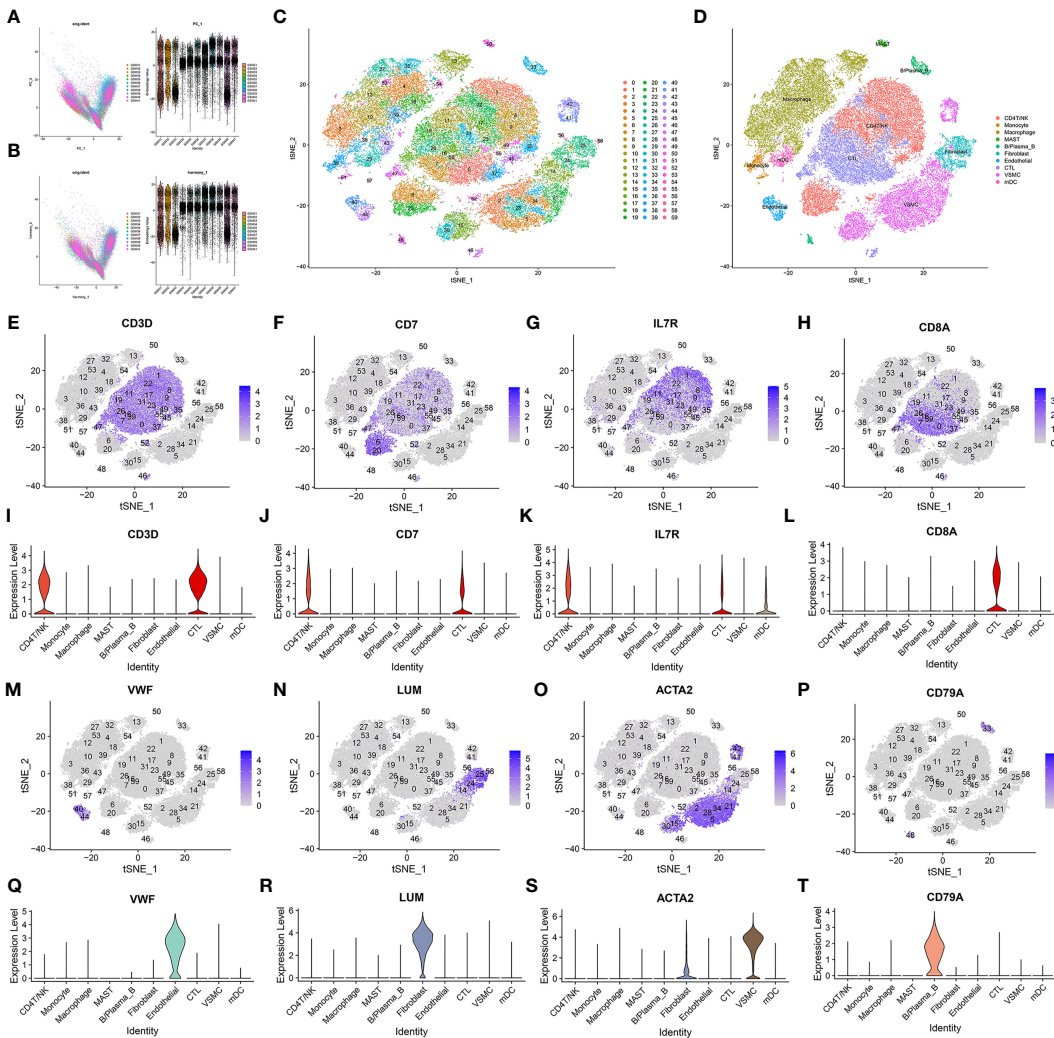


FIGURE 3 Data processing and defining cell types. (A, B) Harmony package sample batch effect elimination and PCA dimensionality reduction. (C) t-SNE dimensionality reduction. (D) The t-SNE results were divided into 10 cell populations using marker genes. (E–T) Sixty clusters defined using marker genes.

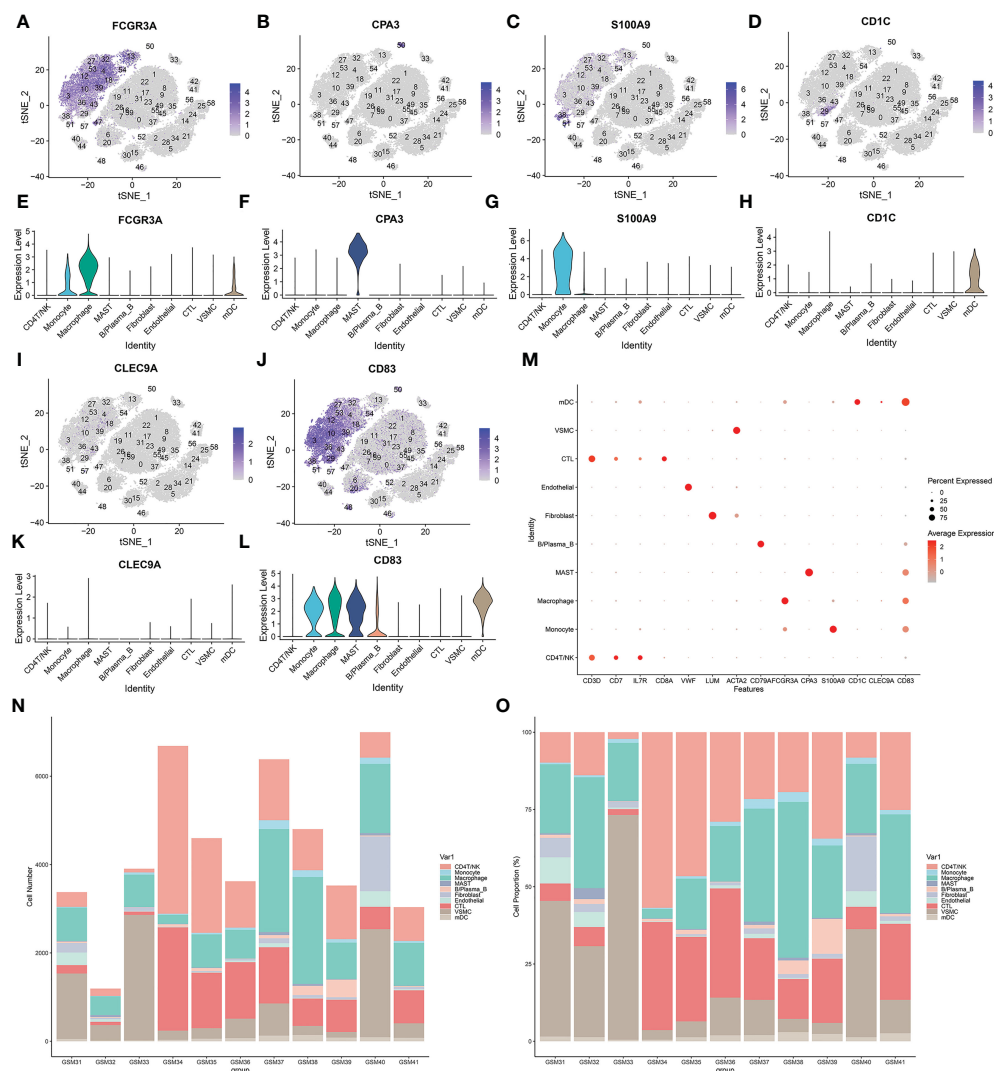


FIGURE 4

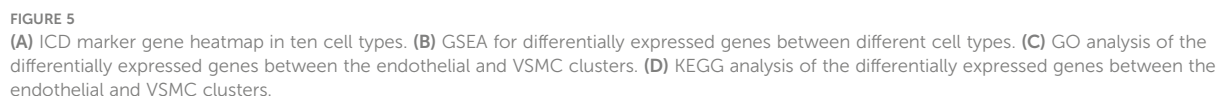
(A–L) Sixty clusters defined using marker genes. (M) The expression of cell type marker genes is shown in the dot plot. (N–O) Proportion of various types of cells in each sample.

antigen-presenting cells (37)) were much higher than those in the control group. This finding indirectly suggested the presence of adjuvant substances in ATAA. We identified a total of 9 signaling pathways that may be related to ICD, and we discussed the most important pathway related to endothelial cell ICD here. According to the latest ICD research, the primary role of ANXA1-FPR1 in tumor cells is to direct APCs to dying cells (38). ANXA1-FPR1 most likely plays the same role in ATAA. In our study, a large amount of APC infiltration was observed in ATAA samples, and this result was also consistent with many current literature reports (4).

CXCL12 interacts with glycosaminoglycans on endothelial cells before it can be stably presented to leukocytes (39, 40). It mainly attracts NK cells and T-lymphocytes (41). In cardiovascular disease, it has been shown that CXCL12 is proatherogenic in the development and progression of atherosclerosis (41, 42). Atherosclerosis is primarily responsible for ATAA in elderly individuals (2). The mean age of ATAA patients in this study was 67.6 ± 8.1 years, which was also in line with other reports in the

literature. Stéphanie Michineau et al. showed that CXCL12/CXCR4 axis is upregulated in human and mouse AAAs (abdominal aortic aneurysms), and the CXCR4 gene knockout can inhibit the expansion of abdominal aortic aneurysm through anti-inflammatory effect (43). This finding suggests that CXCL12/CXCR4 may play an important role in the formation of ATAA.

In the **Supplementary Figure 3K**, the ACKR1 gene was obviously expressed in endothelial cells. ACKR1 (typical chemokine receptor 1), also known as DARC, binds to more than 20 different inflammatory chemokines, mainly CC and CXC subfamilies (44). In previous studies, the ACKR1 gene was found to be mainly expressed on the surface of red blood cells and to a lesser extent in vascular endothelial cells and adipocytes (45). Mice with global DARC knockout had a significantly lower probability of developing atherosclerosis than wild-type mice (46). Many African Americans carry mutations in the gene encoding this receptor, resulting in a loss of its expression. This mutation resulted in a lower incidence of coronary heart disease in African Americans



diseases, it has been found that the interaction CXCL8/ACKR1 between macrophages and endothelial cells is enhanced, and the purpose of this interaction is to recruit immune cells to inflammatory sites in order to fight the infection (49). In the latest published article, ACKR1+ ECs (Endothelial cells) highly engaged in leukocyte recruitment into orbital connective tissue (OCT) in (thyroid-associated ophthalmopathy) TAO and that the recruitment process may be influenced by the interaction of

TABLE 7 CTL Chi-square test.

	CTL	other cells	
ATAA	8754	30897	39651
Normal	338	8139	8477
	9092	39036	48128

Conclusion: The number of CTL is associated with the formation of ATAA.

CXCL8/ACKR1 (50). Overall, CXCL8/ACKR1 axis has reported its recruitment effect on immune cells in various diseases. This axis may also play an important role in the occurrence and development of ATAA.

As well as its function in regulating CCL2 and CCL5 activity, ACKR1 is also reported to be involved in translocating these chemokines across the endothelial barrier after it binds to them (51, 52). In the Hashimoto's thyroiditis (HT), one study has proved that CCL5/ACKR1 axis facilitated the trans-endothelial migration of lymphocytes (53). According to our studies, the ACKR1 gene of endothelial cells in the aorta could not only promote T-cell infiltration through the CCL5 ligand but also promote myeloid cells infiltration through the CXCL8 ligand. ACKR1 could become a target gene for ATAA drug therapy in the future.

Our study has confirmed that ICD was present in ATAA and played an important role in the development of ATAA. And we used CellChat to screen three important ligand-receptor pairs (CXCL8-ACKR1, CCL5-ACKR1, CXCL12-CXCR4), and obtained two special genes expressed by endothelial cells, namely ACKR1 and CXCL12.

5 Conclusion

ICD is present in ATAA and plays an important role in the development of ATAA. The target cells of ICD are mainly endothelial cells, which communicate with chemotactic T cells and mature dendritic cells mainly through CXCL12-CXCR4 and myeloid cells through ANXA1-FPR1. The ACKR1 gene expressed by endothelial cells promotes the development of ATAA through the CCL5 ligand expressed by T cells and the CXCL8 ligand expressed by myeloid cells. The CXCL12 gene expressed by endothelial cells promotes the development of ATAA through the CXCR4 receptor expressed by T cells and mature dendritic cells. Overall, ACKR1 and CXCL12 may become target genes for ATAA drug therapy in the future.

Data availability statement

Publicly available datasets were analyzed in this study. This data can be found here: <https://www.ncbi.nlm.nih.gov/geo/query/acc.cgi?acc=GSE155468>.

References

- Li Y, Ren P, Dawson A, Vasquez HG, Ageedi W, Zhang C, et al. Single-cell transcriptome analysis reveals dynamic cell populations and differential gene expression patterns in control and aneurysmal human aortic tissue. *Circulation* (2020) 142(14):1374–88. doi: 10.1161/CIRCULATIONAHA.120.046528
- Aschacher T, Salameh O, Enzmann F, Messner B, Bergmann M. Telomere biology and thoracic aortic aneurysm. *Int J Mol Sci* (2017) 19(1):3. doi: 10.3390/ijms19010003
- Lavall D, Schäfers HJ, Böhm M, Laufs U. Aneurysms of the ascending aorta. *Deutsches Arzteblatt Int* (2012) 109(13):227–33. doi: 10.3238/arztebl.2012.0227
- El-Hamamsy I, Yacoub MH. Cellular and molecular mechanisms of thoracic aortic aneurysms. *Nat Rev Cardiol* (2009) 6(12):771–86. doi: 10.1038/nrcardio.2009.191
- He R, Guo DC, Estrera AL, Safi HJ, Huynh TT, Yin Z, et al. Characterization of the inflammatory and apoptotic cells in the aortas of patients with ascending thoracic aortic aneurysms and dissections. *J Thorac Cardiovasc Surg* (2006) 131(3):671–8. doi: 10.1016/j.jtcvs.2005.09.018
- Ruvolo G, Pisano C, Candore G, Lio D, Palmeri C, Maresi E, et al. Can the TLR-4-mediated signaling pathway be "a key inflammatory promoter for sporadic TAA"? *Med Inflamm* (2014) 2014:349476. doi: 10.1155/2014/349476

Ethics statement

The data for this study were obtained from public databases and no additional ethical approval was required.

Author contributions

The manuscript has been read and approved by all authors. DJ, conceptualization, funding acquisition, project administration, supervision, writing – review and editing, linguistic editing, and proofreading. XL and PZ, review and editing. ZT, data curation, formal analysis, writing – original draft, visualization, software, methodology, validation, writing – review and editing. All authors contributed to the article and approved the submitted version.

Acknowledgments

We thank the GEO database for allowing us free access.

Conflict of interest

The authors declare that the research was conducted in the absence of any commercial or financial relationships that could be construed as a potential conflict of interest.

Publisher's note

All claims expressed in this article are solely those of the authors and do not necessarily represent those of their affiliated organizations, or those of the publisher, the editors and the reviewers. Any product that may be evaluated in this article, or claim that may be made by its manufacturer, is not guaranteed or endorsed by the publisher.

Supplementary material

The Supplementary Material for this article can be found online at: <https://www.frontiersin.org/articles/10.3389/fimmu.2023.1087978/full#supplementary-material>

7. Pisano C, Maresi E, Balistreri CR, Candore G, Merlo D, Fattouch K, et al. Histological and genetic studies in patients with bicuspid aortic valve and ascending aorta complications. *Interactive Cardiovasc Thorac Surg* (2012) 14(3):300–6. doi: 10.1093/icvts/ivrl114
8. Pisano C, Maresi E, Merlo D, Balistreri CR, Candore G, Caruso M, et al. A particular phenotype of ascending aorta aneurysms as precursor of type a aortic dissection. *Interactive Cardiovasc Thorac Surg* (2012) 15(5):840–6. doi: 10.1093/icvts/ivs347
9. Galluzzi L, Buqué A, Kepp O, Zitvogel L, Kroemer G. Immunogenic cell death in cancer and infectious disease. *Nat Rev Immunol* (2017) 17(2):97–111. doi: 10.1038/nri.2016.107
10. Galluzzi L, Vitale I, Warren S, Adjemian S, Agostinis P, Martinez AB, et al. Consensus guidelines for the definition, detection and interpretation of immunogenic cell death. *J Immunother Cancer* (2020) 8(1):e000337. doi: 10.1136/jitc-2019-000337
11. Hao Y, Hao S, Andersen-Nissen E, Mauck WM3rd, Zheng S, Butler A, et al. Integrated analysis of multimodal single-cell data. *Cell* (2021) 184(13):3573–3587.e3529. doi: 10.1016/j.cell.2021.04.048
12. Korsunsky I, Millard N, Fan J, Slowikowski K, Zhang F, Wei K, et al. Fast, sensitive and accurate integration of single-cell data with harmony. *Nat Methods* (2019) 16(12):1289–96. doi: 10.1038/s41592-019-0619-0
13. Sinha D, Kumar A, Kumar H, Bandyopadhyay S, Sengupta D. dropClust: efficient clustering of ultra-large scRNA-seq data. *Nucleic Acids Res* (2018) 46(6):e36. doi: 10.1093/nar/gky007
14. Garg AD, De Ruyscher D, Agostinis P. Immunological metagene signatures derived from immunogenic cancer cell death associate with improved survival of patients with lung, breast or ovarian malignancies: a large-scale meta-analysis. *Oncotarget* (2016) 5(2):e1069938. doi: 10.1080/2162402X.2015.1069938
15. Kuleshov MV, Jones MR, Rouillard AD, Fernandez NF, Duan Q, Wang Z, et al. Enrichr: a comprehensive gene set enrichment analysis web server 2016 update. *Nucleic Acids Res* (2016) 44(W1):W90–97. doi: 10.1093/nar/gkw377
16. Noutsias M, Rohde M, Göldner K, Block A, Blunert K, Hemaian L, et al. Expression of functional T-cell markers and T-cell receptor β gene repertoire in endomyocardial biopsies from patients presenting with acute myocarditis and dilated cardiomyopathy. *Eur J Heart failure* (2011) 13(6):611–8. doi: 10.1093/eurjhf/hfr014
17. Kim SH, McQueen PG, Lichtman MK, Shevach EM, Parada LA, Misteli T. Spatial genome organization during T-cell differentiation. *Cytogenetic Genome Res* (2004) 105(2–4):292–301. doi: 10.1159/000078201
18. Gupta B, Iancu EM, Gannon PO, Wiekowski S, Baitsch L, Speiser DE, et al. Simultaneous coexpression of memory-related and effector-related genes by individual human CD8 T cells depends on antigen specificity and differentiation. *J Immunother (Hagerstown Md 1997)* (2012) 35(6):488–501. doi: 10.1097/CJI.0b013e31826183a7
19. Mitchell KG, Diao L, Karpinets T, Negrao MV, Tran HT, Parra ER, et al. Neutrophil expansion defines an immunoinhibitory peripheral and intratumoral inflammatory milieu in resected non-small cell lung cancer: a descriptive analysis of a prospectively immunoprofiled cohort. *J Immunother Cancer* (2020) 8(1):e000405. doi: 10.1136/jitc-2019-000405
20. Pusztaszeri MP, Seelentag W, Bosman FT. Immunohistochemical expression of endothelial markers CD31, CD34, von Willebrand factor, and flt-1 in normal human tissues. *J Histochem Cytochem* (2006) 54(4):385–95. doi: 10.1369/jhc.4A6514.2005
21. Chang PC, Chen Y, Lai MT, Chang HY, Huang CM, Liu HP, et al. Association analysis of polymorphisms in lumican gene and systemic lupus erythematosus in a Taiwan Chinese han population. *J Rheumatol* (2011) 38(11):2376–81. doi: 10.3899/jrheum.101310
22. Owens GK. Regulation of differentiation of vascular smooth muscle cells. *Physiol Rev* (1995) 75(3):487–517. doi: 10.1152/physrev.1995.75.3.487
23. Chu PG, Arber DA. CD79: a review. *Appl immunohistochem Mol morphol AIMM* (2001) 9(2):97–106. doi: 10.1097/00022744-200106000-00001
24. Ochoa MC, Minute L, Rodriguez I, Garasa S, Perez-Ruiz E, Inogés S, et al. Antibody-dependent cell cytotoxicity: immunotherapy strategies enhancing effector NK cells. *Immunol Cell Biol* (2017) 95(4):347–55. doi: 10.1038/icb.2017.6
25. Finlin BS, Zhu B, Confides AL, Westgate PM, Harfmann BD, Dupont-Versteegden EE, et al. Mast cells promote seasonal white adipose beiging in humans. *Diabetes* (2017) 66(5):1237–46. doi: 10.2337/db16-1057
26. Åberg AM, Bergström SH, Thysell E, Tjon-Kon-Fat LA, Nilsson JA, Widmark A, et al. High monocyte count and expression of S100A9 and S100A12 in peripheral blood mononuclear cells are associated with poor outcome in patients with metastatic prostate cancer. *Cancers* (2021) 13(10):2424. doi: 10.3390/cancers13102424
27. Heger L, Hofer TP, Bigley V, de Vries IJM, Dalod M, Dudziak D, et al. Subsets of CD11c(+) DCs: dendritic cell versus monocyte lineage. *Front Immunol* (2020) 11:559166. doi: 10.3389/fimmu.2020.559166
28. Chen YP, Yin JH, Li WF, Li HJ, Chen DP, Zhang CJ, et al. Single-cell transcriptomics reveals regulators underlying immune cell diversity and immune subtypes associated with prognosis in nasopharyngeal carcinoma. *Cell Res* (2020) 30(11):1024–42. doi: 10.1038/s41422-020-0374-x
29. Gouwy M, Struyf S, Leutenze L, Pörtner N, Sozzani S, Van Damme J. Chemokines and other GPCR ligands synergize in receptor-mediated migration of monocyte-derived immature and mature dendritic cells. *Immunobiology* (2014) 219(3):218–29. doi: 10.1016/j.imbio.2013.10.004
30. Kroemer G, Galluzzi L, Kepp O, Zitvogel L. Immunogenic cell death in cancer therapy. *Annu Rev Immunol* (2013) 31:51–72. doi: 10.1146/annurev-immunol-032712-100008
31. Ahmed A, Tait SWG. Targeting immunogenic cell death in cancer. *Mol Oncol* (2020) 14(12):2994–3006. doi: 10.1002/1878-0261.12851
32. Fucikova J, Kepp O, Kasikova L, Petroni G, Yamazaki T, Liu P, et al. Detection of immunogenic cell death and its relevance for cancer therapy. *Cell Death Dis* (2020) 11(11):1013. doi: 10.1038/s41419-020-03221-2
33. Procureur A, Simonaggio A, Bibault JE, Oudard S, Vano YA. Enhance the Immune Checkpoint Inhibitors Efficacy with Radiotherapy Induced Immunogenic Cell Death: A Comprehensive Review and Latest Developments. *Cancers* (2021) 13(4):678. doi: 10.3390/cancers13040678
34. Raposo B, Merky P, Lundqvist C, Yamada H, Urbonaviciute V, Niaudet C, et al. T Cells specific for post-translational modifications escape intrathymic tolerance induction. *Nat Commun* (2018) 9(1):353. doi: 10.1038/s41467-017-02763-y
35. Incalza MA, D'Oria R, Natalicchio A, Perrini S, Laviola L, Giorgino F. Oxidative stress and reactive oxygen species in endothelial dysfunction associated with cardiovascular and metabolic diseases. *Vasc Pharmacol* (2018) 100:1–19. doi: 10.1016/j.vph.2017.05.005
36. Siti HN, Kamisah Y, Kamsiah J. The role of oxidative stress, antioxidants and vascular inflammation in cardiovascular disease (a review). *Vasc Pharmacol* (2015) 71:40–56. doi: 10.1016/j.vph.2015.03.005
37. Wculek SK, Cueto FJ, Mujal AM, Melero I, Krummel MF, Sancho D. Dendritic cells in cancer immunology and immunotherapy. *Nat Rev Immunol* (2020) 20(1):7–24. doi: 10.1038/s41577-019-0210-z
38. Shakeel S, Rajendra E, Alcón P, O'Reilly F, Chorev DS, Maslen S, et al. Structure of the fanconi anaemia monoubiquitin ligase complex. *Nature* (2019) 575(7781):234–7. doi: 10.1038/s41586-019-1703-4
39. Cui Y, Zhou F, Wei L, Song Q, Tan J, Zeng Z, et al. *In Situ* Endothelialization promoted by SEMA4D and CXCL12 for titanium-based biomaterials. *Semin Thromb Hemostasis* (2018) 44(1):70–80. doi: 10.1055/s-0037-1605569
40. Hara T, Tanegashima K. CXCL14 antagonizes the CXCL12–CXCR4 signaling axis. *Biomolecular concepts* (2014) 5(2):167–73. doi: 10.1515/bmc-2014-0007
41. Murad HAS, Rafeeq MM, Alqurashi TMA. Role and implications of the CXCL12/CXCR4/CXCR7 axis in atherosclerosis: still a debate. *Ann Med* (2021) 53(1):1598–612. doi: 10.1080/07853890.2021.1974084
42. Döring Y, Pawig L, Weber C, Noels H. The CXCL12/CXCR4 chemokine ligand/receptor axis in cardiovascular disease. *Front Physiol* (2014) 5:212. doi: 10.3389/fphys.2014.00212
43. Michineau S, Franck G, Wagner-Ballon O, Dai J, Allaire E, Gervais M. Chemokine (C-X-C motif) receptor 4 blockade by AMD3100 inhibits experimental abdominal aortic aneurysm expansion through anti-inflammatory effects. *Arteriosclerosis thrombosis Vasc Biol* (2014) 34(8):1747–55. doi: 10.1161/ATVBAHA.114.303913
44. Gencer S, van der Vorst EPC, Aslani M, Weber C, Döring Y, Duchene J. Atypical chemokine receptors in cardiovascular disease. *Thromb Haemostasis* (2019) 119(4):534–41. doi: 10.1055/s-0038-1676988
45. Guha A, Wang X, Harris RA, Nelson AG, Stepp D, Klaassen Z, et al. Obesity and the bidirectional risk of cancer and cardiovascular diseases in African americans: disparity vs. *Ancestry Front Cardiovasc Med* (2021) 8:761488. doi: 10.3389/fcvm.2021.761488
46. Wan W, Liu Q, Lionakis MS, Marino AP, Anderson SA, Swamydas M, et al. Atypical chemokine receptor 1 deficiency reduces atherogenesis in ApoE-knockout mice. *Cardiovasc Res* (2015) 106(3):478–87. doi: 10.1093/cvr/cvv124
47. Bild DE, Detrano R, Peterson D, Guerci A, Liu K, Shahar E, et al. Ethnic differences in coronary calcification: the multi-ethnic study of atherosclerosis (MESA). *Circulation* (2005) 111(10):1313–20. doi: 10.1161/01.CIR.0000157730.94423.4B
48. Darbonne WC, Rice GC, Mohler MA, Apple T, Hébert CA, Valente AJ, et al. Red blood cells are a sink for interleukin 8, a leukocyte chemotaxin. *J Clin Invest* (1991) 88(4):1362–9. doi: 10.1172/JCI115442
49. Reynolds G, Vegh P, Fletcher J, Poyner EFM, Stephenson E, Goh I, et al. Developmental cell programs are co-opted in inflammatory skin disease. *Sci (New York NY)* (2021) 371(6527):eaba6500. doi: 10.1126/science.aba6500
50. Li Z, Wang M, Tan J, Zhu L, Zeng P, Chen X, et al. Single-cell RNA sequencing depicts the local cell landscape in thyroid-associated ophthalmopathy. *Cell Rep Med* (2022) 3(8):100699. doi: 10.1016/j.xcrm.2022.100699
51. Novitzky-Basso I, Rot A, Duffy Antigen receptor for chemokines and its involvement in patterning and control of inflammatory chemokines. *Front Immunol* (2012) 3:266. doi: 10.3389/fimmu.2012.00266
52. Nibbs RJ, Graham GJ. Immune regulation by atypical chemokine receptors. *Nat Rev Immunol* (2013) 13(11):815–29. doi: 10.1038/nri3544
53. Zhang QY, Ye XP, Zhou Z, Zhu CF, Li R, Fang Y, et al. Lymphocyte infiltration and thyrocyte destruction are driven by stromal and immune cell components in hashimoto's thyroiditis. *Nat Commun* (2022) 13(1):775. doi: 10.1038/s41467-022-28120-2



OPEN ACCESS

EDITED BY

Nadine Suffee,
Sorbonne Universités, France

REVIEWED BY

Aleksandr E. Vendrov,
University of Michigan, United States
David Lloyd,
Cardiff University, United Kingdom
Francisco Javier Sánchez-García,
National Polytechnic Institute (IPN), Mexico

*CORRESPONDENCE

Shaoqing Lei
✉ shqlei@whu.edu.cn

[†]These authors have contributed
equally to this work

RECEIVED 11 January 2023

ACCEPTED 24 April 2023

PUBLISHED 05 May 2023

CITATION

Jin Z, Ji Y, Su W, Zhou L, Wu X, Gao L,
Guo J, Liu Y, Zhang Y, Wen X, Xia Z-Y,
Xia Z and Lei S (2023) The role of circadian
clock-controlled mitochondrial dynamics
in diabetic cardiomyopathy.
Front. Immunol. 14:1142512.
doi: 10.3389/fimmu.2023.1142512

COPYRIGHT

© 2023 Jin, Ji, Su, Zhou, Wu, Gao, Guo, Liu,
Zhang, Wen, Xia, Xia and Lei. This is an
open-access article distributed under the
terms of the [Creative Commons Attribution
License \(CC BY\)](#). The use, distribution or
reproduction in other forums is permitted,
provided the original author(s) and the
copyright owner(s) are credited and that
the original publication in this journal is
cited, in accordance with accepted
academic practice. No use, distribution or
reproduction is permitted which does not
comply with these terms.

The role of circadian clock-controlled mitochondrial dynamics in diabetic cardiomyopathy

Zhenshuai Jin^{1†}, Yanwei Ji^{1†}, Wating Su^{1†}, Lu Zhou¹,
Xiaojing Wu¹, Lei Gao¹, Junfan Guo¹, Yutong Liu¹,
Yuefu Zhang¹, Xinyu Wen¹, Zhong-Yuan Xia¹,
Zhengyuan Xia^{2,3} and Shaoqing Lei^{1*}

¹Department of Anesthesiology, Renmin Hospital of Wuhan University, Wuhan, China, ²Department of Anesthesiology, Affiliated Hospital of Guangdong Medical University, Zhanjiang, China, ³Faculty of Chinese Medicine, State Key Laboratory of Quality Research in Chinese Medicine, Macau University of Science and Technology, Taipa, Macao SAR, China

Diabetes mellitus is a metabolic disease with a high prevalence worldwide, and cardiovascular complications are the leading cause of mortality in patients with diabetes. Diabetic cardiomyopathy (DCM), which is prone to heart failure with preserved ejection fraction, is defined as a cardiac dysfunction without conventional cardiac risk factors such as coronary heart disease and hypertension. Mitochondria are the centers of energy metabolism that are very important for maintaining the function of the heart. They are highly dynamic in response to environmental changes through mitochondrial dynamics. The disruption of mitochondrial dynamics is closely related to the occurrence and development of DCM. Mitochondrial dynamics are controlled by circadian clock and show oscillation rhythm. This rhythm enables mitochondria to respond to changing energy demands in different environments, but it is disordered in diabetes. In this review, we summarize the significant role of circadian clock-controlled mitochondrial dynamics in the etiology of DCM and hope to play a certain enlightening role in the treatment of DCM.

KEYWORDS

diabetic cardiomyopathy, clock circadian, mitochondrial dynamics, mitochondrial fusion, mitochondrial fission

1 Introduction

The incidence of diabetes mellitus is increasing, and now more than 350 million people are reported to suffer from diabetes worldwide (1). The population and condition of diabetes mellitus have become more and more juvenile and complicated (2). Patients with diabetes may develop cardiovascular complications, especially diabetic cardiomyopathy (DCM), which is prone to heart failure with preserved ejection fraction (HFpEF). This type

of heart failure was first reported in 1972 in patients with type 2 diabetes, who had no risk factors for heart failure, such as hypertension and coronary artery disease (3). Subsequent clinical and experimental studies gradually revealed the main pathophysiological mechanisms of DCM, such as inflammation, lipid accumulation, myocardial fibrosis, cardiac hypertrophy, cardiac apoptosis, microvascular damage, etc. (4, 5) The main clinical features of DCM are cardiac hypertrophy, diastolic dysfunction, and myocardium stiffening (6). At the late stage of DCM, the myocardial systolic function is also affected, leading to dilated cardiomyopathy (6). However, the pathophysiological mechanisms of DCM remain complex and unclear.

Increasing studies suggest the involvement of dysfunctional mitochondria in the pathophysiology of DCM. The dysfunctional mitochondria result in myocardial metabolic disorders, oxidative stress, Ca^{2+} overload, myocardial systolic/diastolic dysfunction, and myocardial stiffness (7, 8). Mitochondria are the centers of energy metabolism that are extremely essential for maintaining the function of the heart, an organ with high energy requirements. Mitochondria are highly dynamic in response to environmental changes through mitochondrial dynamics, including mitochondrial fusion and fission. Noteworthy, mitochondrial dynamics has a circadian rhythm throughout the day. The circadian rhythm of mitochondrial dynamics is regulated by circadian clock genes that mediate the expression of mitochondrial dynamic molecules and affect mitochondrial morphology and function (9). When circadian clock genes are mutated or disrupted, mitochondrial dynamics may lose circadian rhythm and become disordered, resulting in insulin resistance, cardiac lipotoxicity, excessive production of mitochondrial reactive oxidative species (ROS), mitochondrial Ca^{2+} mishandling, decreased mitochondrial membrane potential (MMP), impaired mitophagy, and endoplasmic reticulum (ER) stress, which are associated with the pathophysiology of DCM (9–11). Thus, recent advances in understanding clock-controlled mitochondrial dynamics and its implication for the pathophysiology of DCM may open up novel therapeutic avenues.

2 Mitochondrial dynamics

Mitochondria are highly dynamic organelles, constantly changing their morphology, from tubular (fusion) to fragmented (fission). The balance between mitochondrial fusion and division is important for the proper functioning of cells. Disruptions in mitochondrial dynamics affect mitochondrial morphology and function, leading in the development of disease, DCM.

2.1 Mitochondrial fusion

Mitochondria have an outer mitochondrial membrane (OMM) and an inner mitochondrial membrane (IMM) (12). The progress of mitochondrial fusion includes OMM fusion and IMM fusion. Mitofusin1/2 (MFN1/2), belongs to the family of GTPases, and

primarily orchestrates OMM fusion (12). As a transmembrane protein anchored to the OMM, MFN1/2 contains the N-terminal GTPase domain and heptad-repeat regions (HR1 and HR2) (13). When the tips of two mitochondria meet in the cytoplasm, MFN1/2 as a tether interacts with another mitochondrion, and forms the MFN homodimer or heterodimer, then alters the conformation of the HR2 region depending on GTPase, resulting in the fusion of OMM. In fact, MFN1 plays a leading role in the process of mitochondrial fusion, the role of MFN2 remains elusive, which primarily participated in the site of OMM interacting with other organelles (particularly the ER) (14, 15).

After OMM fusion, the IMM subsequently starts to fusion, and optic atrophy (OPA1) as a pivotal factor mainly participated in the process of IMM fusion. OPA1 consists of long OPA1 (L-OPA1) and short OPA1 (S-OPA1). L-OPA1 interacts with cardiolipin on the IMM to facilitate the fusion of the IMM. S-OPA1, which is produced by the degradation of L-OPA1 by proteolytic enzymes OMA1 and YME1-like ATPase (YME1L) (12), is mainly to promote mitochondrial fusion by assisting L-OPA1. However, when S-OPA1 over-accumulates, it will suppress the role of L-OPA1 (12), leading to mitochondrial division and disruption of mitochondrial dynamics (Figure 1) (16). OPA1 is not only participated in IMM fusion but also plays an important role in the remodeling of mitochondrial cristae, which is the site of oxidative phosphorylation (OXPHOS) and ATP synthase (17). The left-turned assemblies at the cristate (the structure of OPA1 is involved in the right- or left-turned helical assemblies) could prevent cytochrome C entering from the matrix into the intermembranous mitochondria by tightening mitochondrial crista and diminishing crista lumen. When OPA1 is reduced or destroyed, a large amount of cytochrome C enters into the intermembrane, then enters into the cytoplasm through the permeable out membrane, and finally induces cell apoptosis (12, 18). Overall, OPA1 has extensive effects on mitochondrial function, and different aspects of its function need to be further refined.

2.2 Mitochondrial fission

The proteins involved in the mitochondrial fission process mainly include dynamin-related protein1 (DRP1) and mitochondrial fission factor (MFF)/fission protein 1 (FIS1). DRP1 performs a critical role in mitochondrial fission by translocation to mitochondrial membranes and binding to receptors. In the cytoplasm, the activity of DRP1 is regulated by many factors, such as cAMP-dependent serine/threonine-specific protein kinase A (PKA). PKA phosphorylates the tryptophan of DRP1, stabilizing DRP1 in the cytoplasm and promoting mitochondrial elongation (19, 20). Besides, DRP1 is dephosphorylated by Ca^{2+} -dependent phosphate calcineurin, which promotes DRP1 translocation to OMM and binding to the receptor (21). MFF/FIS1 are primary receptors located on the OMM and perform a vital role in recruiting DRP1 (22). Mitochondrial dynamics proteins of 49 kDa and 51 kDa (MID49 and MID51) also recruit and bind to DRP1, when MFF/

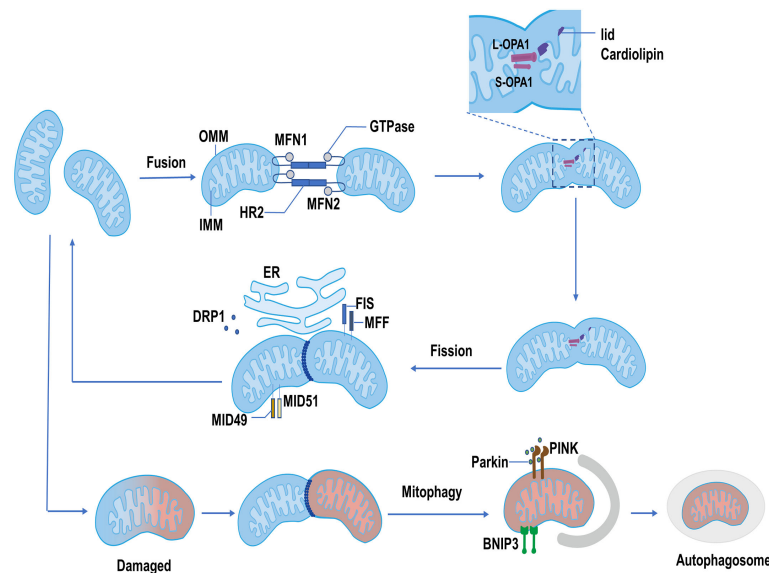


FIGURE 1

The process of mitochondrial dynamics. Mitochondrial fusion: MFN1 and MFN2 form homodimer or heterodimer, then alter the conformation of the HR2 region depending on GTPase, resulting in the fusion of OMM. IMM fusion is mainly orchestrated by OPA1. The L-OPA1 interacts with lipid cardiolipin and facilitates the fusion of the IMM. The S-OPA1 interacts with L-OPA1 and promotes IMM fusion. Mitochondrial fission: The dephosphorylated DRP1 is recruited at the mitochondrial membrane by its receptors, mainly including FIS and MFF. MID49 and MID51 also recruit DRP1 when the MFF/FIS1 is not available. Recruited DRP1 combined with the receptor, forming a ring-like structure to shear the mitochondria and promote the completion of mitochondrial fission. Mitophagy: Damaged mitochondria are degraded by autophagosomes through PINK1/Parkin and BNIP3 pathways.

FIS1 is not available (23). DRP1 is massively recruited and combined with the receptor, forming a ring-like structure to shear the mitochondria and promote the completion of mitochondrial fission (24). Mitochondrial fission usually occurs at the interface between mitochondria and the ER (Figure 1). This contact site is an extremely critical interface. It not only leads to the occurrence of mitochondrial fission but also is related to the rebuilds of mitochondrial cristae driven by transporting Ca^{2+} from the ER to the mitochondria (12).

The fission and fusion of mitochondria are dynamic and continuous processes. The balance between fission and fusion is very critical in maintaining the normal function of mitochondria. When the balance of mitochondrial dynamics is compromised, the mitochondrial dysfunction may disrupt normal metabolism through cytochrome C release, Ca^{2+} influx, excessive production of ROS, and mitochondrial protein efflux, causing cell damage and death (12, 25). For damaged mitochondria, however, mitochondrial fission can split this part of mitochondria out, and degrade or eliminate it through mitophagy pathways such as the PTEN-induced kinase 1 (PINK1)/Parkin or Bcl-2 19-kDa interacting protein 3 (BNIP3) (Figure 1) (26). In the process of resolving damaged mitochondria, mitochondrial fusion also exhibits a beneficial role by allowing the transmission of proteins, metabolites, and DNA across the network and attempting to restore and replenish mitochondrial function in exchange (27). Finally, mitochondrial fission, fusion, and mitophagy together operate the healthy mitochondrial pool. Disrupted mitochondrial dynamics would affect mitochondrial function and lead to the occurrence of diseases such as diabetic cardiomyopathy (28, 29).

3 Circadian clock and mitochondrial dynamics

3.1 Circadian clock

The circadian clock is temporal progress influenced by Earth's rotation. Many activities of living organisms including gene expression (30), metabolism (31), immune and endocrine function (32, 33), as well as behavior (34), are controlled by day and night clocks. Circadian clock is composed of master pacemaker and peripheral clocks. The central, master clocks are located in the suprachiasmatic nucleus (SCN) of the hypothalamus. The peripheral clocks are virtually located in all the tissues and cells of the body (35). The circadian clock can synchronize internal 24-hour timing with a 24-hour solar day through a hierarchical network of master and peripheral oscillators.

The molecular circadian clock in mammals is formed by a transcription-translation feedback loop (TTFL). The main TTFL is driven by the transcription factors CLOCK-BMAL1 and their negative regulators including the period (PER) and cryptochrome (CRY), as well as some other regulators such as casein kinases (CKI α , CKI δ , and CKI ϵ) and phosphatases (PP1, PP5), which regulate the stability and localization of these integral circadian proteins (36). The CLOCK-BMAL1 complexes directly combine with DNA to regulate E-BOX and induce the expression of negative regulators (37). The negative regulators PER and CRY form heterodimeric in the cytoplasm and translocate into the nucleus to inhibit the transcription of CLOCK-BMAL1. When the levels of PER and CRY decline through ubiquitin-dependent degradation, a

new CLOCK-BMAL1-driven transcription cycle begins with 24-hour periodicity. The casein kinases and phosphatases also play a key role in the circadian period by controlling the activity of the PER-CRY dimer and the rate at which it enters the nucleus. In addition to the main feedback loop, the second feedback loop also plays an important role. The main components of the second feedback loop are the nuclear receptors REV-ERB α/β (38), retinoid-related orphan receptor α (ROR α) (39), and CLOCK-BMAL1. Like the main loop, REV-ERB α/β and ROR α are also activated by CLOCK-BMAL1. REV-ERB α/β negatively regulates *BMAL1* transcription, but ROR α positively regulates *BMAL1* transcription (40). REV-ERB α/β and ROR α compete for binding REV-ERB-ROR response elements in the promoter and enhancer regions of the target gene, and make a rhythmic expression of the *BMAL1* gene (41). The primary function of the second feedback loop is to provide additional robustness to the oscillatory mechanism and counter surrounding disturbances to help circadian keep accurate timing (Figure 2) (36, 42).

The circadian clock is an internal and predictable mechanism that predicts the energy demands and metabolic changes through synchronization with light and temperature cycles (37). In this process, clock rhythm affects various cells or tissues, and confers various tissue-specific functions to circadian rhythmicity, such as the core body temperature with peak levels during the day and trough in the early morning, more oxidation delivered to the cell in active but less in inactive, and the melatonin secretion cycle that is inhibited by light (43). There is growing evidence that circadian disruption is involved in metabolic abnormalities. The liver-specific *BMAL1* knockout (KO) mice had higher levels of triglyceride, cholesterol, and free fatty acids than that in wild-type mice, and their livers contained lower levels of OXPHOS protein and complex

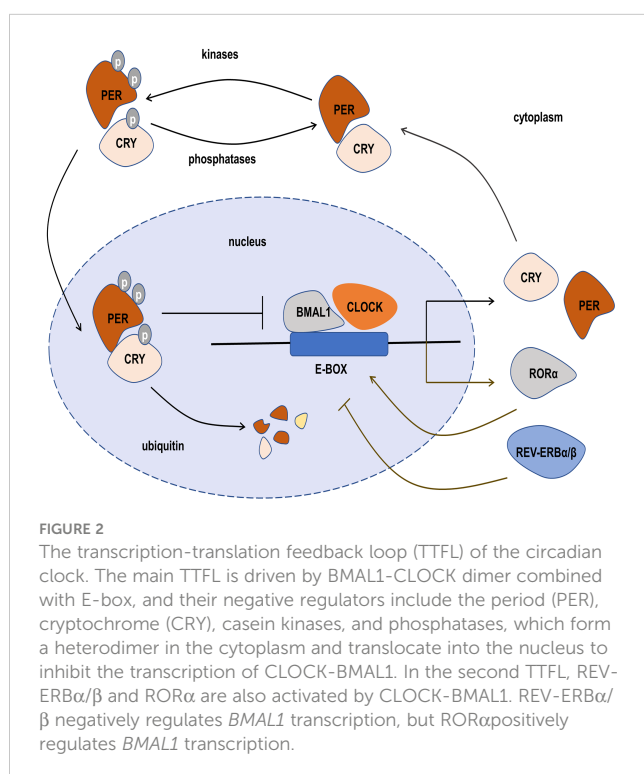
I (10). Likewise, if the internal clock of an organism is uncoupled with the natural clock circadian, the individual will have deleterious effects on nutrient metabolism, such as increasing the risk of developing diabetes (44) and cardiovascular disease (45).

3.2 Effects of the clock on mitochondrial dynamics

The highly dynamic morphology of mitochondria is closely regulated by the circadian clock. It was shown that the mitochondria in cultured hepatocytes exhibited circadian alteration that the number of the tubular structure of mitochondria rhythmically decreased from the light to the dark (46). In cultured fibroblasts, the mitochondrial structure also showed rhythmic oscillations, a synchronous transformation from the tubular structure at 16 h after serum shock to a fragmented network at 28 h after serum shock (9). This rhythmic alteration of mitochondrial morphology is affected by circadian clock disruption. In the liver-specific *BMAL1* KO mice, the dynamic morphology of mitochondria lost rhythmic oscillation at different zeitgeber points (10). These mitochondria manifested bigger and rounder, and maintained a similar pattern throughout the day and night, whereas wild-type mice showed a cyclical change in morphology according to the surrounding changes (10).

Aiming to illustrate the rhythmic changes in mitochondrial dynamics, the molecules related to mitochondrial dynamics have been studied in recent years. Calcineurin, which has a strong circadian rhythm (47), can dephosphorylate DRP1 at ser637 and promote the transfer of DRP1 from the cytoplasm to the mitochondrial membrane. Although the protein expression of calcineurin is constant throughout the day, its activation is under circadian regulation (47). Thus, the Ser637-phosphorylated DRP1 (P-DRP1) level exhibits circadian rhythm (9). The oscillations of DRP1 phosphorylation bring different levels of mitochondrial metabolism to adapt to environmental changes (9). It is also shown that CLOCK can accelerate the degradation of DRP1 mRNA through competitively inhibiting PUF60 function, a splicing factor that can improve DRP1 mRNA stability (48). The loss of CLOCK activity may release PUF60, resulting in increased DRP1 level and fragmented mitochondria (Figure 3) (48).

There are some other mediators linking mitochondria dynamics to the clock, such as AMP-activated protein kinase (AMPK), sirtuins (SIRT) (9). AMPK is a serine/threonine kinase, whose activity, subunit composition, and localization depend on the circadian clock (49). For mitochondrial dynamics, AMPK not only enhances mitochondrial fission and mitophagy by phosphorylating MFN and recruiting DRP1 from cytoplasm under energy stress (50), but also increases mitochondrial fusion by increasing MFN2 expression during the fasting period, thereby improving the efficiency of ATP generation (51). In addition, the activated AMPK could phosphorylate PER2 and CRY, leading to the efficient expression of CLOCK and BMAL1 and shorting the period of the circadian clock (Figure 3) (52–54). SIRT, a family of NAD⁺ (nicotinamide adenine dinucleotide)-dependent protein deacetylases, also play a significant role in the clock and



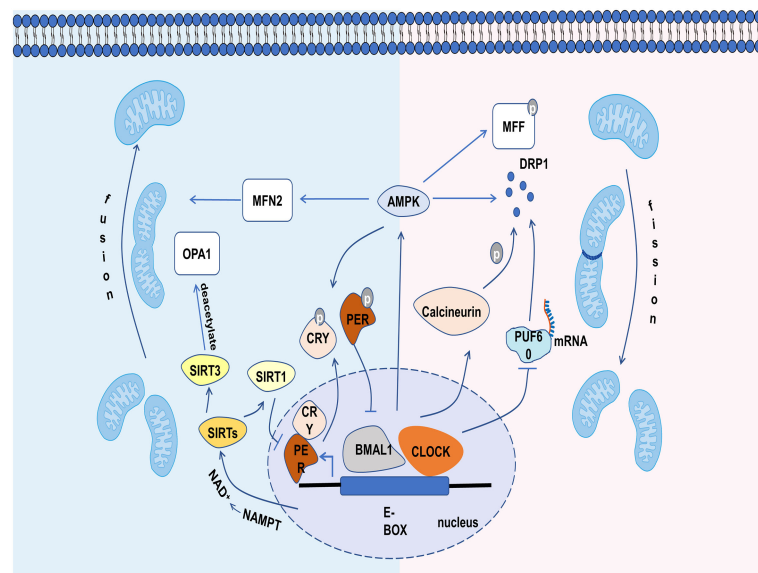


FIGURE 3

The relevant mechanisms by which circadian clock controls mitochondrial dynamics. The circadian clock regulates mitochondrial dynamics through influencing the molecules involved in it, including calcineurin, PUF60, AMPK, SIRT1 and SIRT3.

mitochondrial dynamics. SIRT1 can promote the deacetylation and degradation of PER2 by binding to the CLOCK-BMAL1 heterodimers, thus participating in the regulation of circadian rhythm (55). Conversely, the CLOCK-BMAL1 can also influence the level of SIRT1 by regulating the gene expression of nicotinamide phosphoribosyl transferase (NAMPT), an important enzyme for the production of NAD^+ (56). Recent studies have shown that the circadian clock can regulate the level of deacetylated OPA1 through the NAD^+ /SIRT3 pathway (Figure 3) (54). Cardiac OPA1 is hyperacetylated during pathological stress, and this modification reduces its activity of GTPase, resulting in mitochondrial fusion disorder (57). SIRT3 can deacetylate and activate OPA1, and eventually restore mitochondrial dynamics (57). Overall, mitochondrial dynamics are closely controlled by the clock and exhibit a circadian rhythm.

4 Clock-controlled mitochondrial dynamics in DCM

The clock-controlled mitochondrial dynamics are susceptible to energy stress. Many studies have reported that circadian clock and mitochondrial dynamics are disordered in the diabetic state (58–61). The disordered clock-controlled mitochondrial dynamics adversely affect cardiomyocytes through several underlying mechanisms, including insulin resistance, cardiac lipotoxicity, ROS, mitochondrial Ca^{2+} mishandling, decreased MMP, impaired mitophagy and ER stress, which ultimately lead to the development and progression of DCM (Figure 4).

4.1 Clock-controlled mitochondrial dynamics and insulin resistance

Insulin resistance is a critical pathophysiological abnormality associated with DCM. Insulin resistance has many detrimental effects on cardiomyocytes, such as decreased glucose uptake, elevated lipid metabolites, and increased glycation reactions. These harmful effects may lead to myocardial stiffness, reduced ejection fraction, and heart failure (62). Insulin resistance is closely related to mitochondrial dynamics disorder. In insulin-resistant cardiomyocytes, mitochondrial dynamics are disordered, manifested as decreased MFN1-mediated mitochondrial fusion and increased DRP1-mediated mitochondrial division, resulting in mitochondrial dysfunction and excessive ROS production (63). The disordered mitochondrial dynamics also affect insulin secretion and insulin signaling pathways. The overexpression of MFN1 or MFN2 can promote mitochondrial fusion, accompanied by improvement of insulin receptor substrate 1 (IRS1)-Akt signaling and insulin-stimulated glucose absorption (64). On the contrary, promoting mitochondrial division by overexpression of DRP1 and FIS1 show the opposite behavior (64). MFN1/2 are also demonstrated to be pivotal for glucose-stimulated insulin secretion by controlling mitochondrial DNA content and may be promising targets to restore glucose control in diabetes (65). Thus, mitochondrial dynamics play a critical role in the physiological function of insulin by impacting the insulin signaling pathway and insulin secretion.

It is worth noting that insulin resistance is closely related to circadian alteration. Under normal physiological conditions, insulin

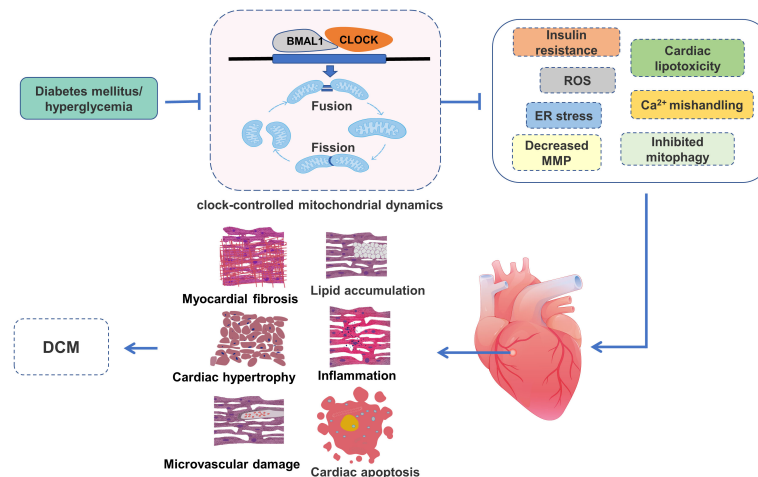


FIGURE 4

The role of clock-controlled mitochondrial dynamics in DCM. The disturbed clock-controlled mitochondrial dynamics may affect insulin signaling, lipid metabolism, mitochondrial ROS production, Ca^{2+} processing, MMP, mitophagy and ER stress, resulting in lipid accumulation, inflammation, myocardial fibrosis, cardiac hypertrophy, cardiac apoptosis and microvascular damage, and ultimately participate in the development of DCM.

secretion and insulin receptor sensitivity have a certain rhythm, that is insulin secretion increasing during the day and decreasing during the night, and insulin receptor sensitivity reaching a peak during the day (66, 67). Nonetheless, the mice with circadian rhythm disturbances induced by *BMAL1* and *CLOCK* mutations showed impaired glucose tolerance, reduced insulin secretion, and damaged islet size and proliferation, which progressively worsened with age (44). The insulin signaling pathways are also influenced by the circadian system. A large number of insulin signaling proteins (e.g. IRS1, *Pik3r1*, *Akt1*, and *Akt2*) in cardiomyocytes from clock mutant mice are significantly reduced compared with that in wild-type mice, which is consistent with the decreased insulin regulation of glucose metabolism (68). Recently, by using chromatin immunoprecipitation sequencing, researchers have found that *CLOCK* and *BMAL1* could bind to inner-mitochondrial genes related to insulin sensitivity, suggesting that the relationship between circadian rhythm and insulin resistance may be related to mitochondrial dynamics (69). Jacobi and his colleagues also observed insulin resistance when they studied changes in mitochondrial dynamics by knocking out the *BMAL1* gene (10). Consistently, Ye et al. observed that *BMAL1* inhibition resulted in mitochondrial dynamics disorder, as well as impaired insulin signaling in pancreatic beta cells (70). Thus, mitochondrial dynamics are inherently influenced by clock rhythm, and the disordered clock-controlled mitochondrial dynamics may lead to insulin resistance and promote DCM.

4.2 Clock-controlled mitochondrial dynamics and cardiac lipotoxicity

Lipid accumulation is a common feature of the diabetic heart. Lipids that exceed the storage and oxidation capacity of the heart may produce a variety of lipotoxic intermediates, including ceramides, diacylglycerol, and oxidized phospholipids, which are

detrimental to cardiac morphology and function (71). The lipotoxic intermediates contribute to the development of DCM by triggering cellular signaling (such as cellular metabolism, growth, and proliferation) and modifications of proteins and lipids (72). It is worth noting that the accumulation of lipids and the production of lipotoxic intermediates in the heart is associated with abnormal mitochondrial dynamics (73). Carnitine palmitoyl transferase 1 (*CPT1*) is the rate-limiting enzyme of β -oxidation that determines the rate of fatty acid entry into mitochondria. Wang et al. have shown that the abnormal activation of *DRP1* in mice deficient in low-density lipoprotein receptor-related protein 6 could inhibit the activity of the *CPT1* transcription factors *CTCE* and *c-Myc*, leading to fatty acid accumulation and heart failure (74). Ceramides are more directly related to mitochondrial dynamics. A large accumulation of ceramides may lead to mitochondrial fragmentation and mitochondrial apoptotic pathways, thereby promoting cell death and insulin resistance (75, 76). Recent studies have shown that the increased ceramide synthase 6, a key enzyme in ceramide synthesis, is associated with fragmented mitochondria and insulin resistance in high-fat diet induced obese mouse models (77, 78), and that inhibition of ceramide synthase 6 improves mitochondrial function and insulin signaling (78). Similarly, downregulation of *DRP1* decreases mitochondrial fission and protects H9C2 cells from lipotoxicity (79). These findings provide evidence that abnormal mitochondrial dynamics are closely associated with cardiac lipotoxicity in diabetes.

It is not surprising that the lipid uptake and oxidation are controlled by circadian clock. Under physiological conditions, the myocardium rhythmically takes up and utilizes lipid in response to variable environmental conditions (80). Disruption of circadian rhythms induced by genetic or environmental perturbation results in abnormal cardiac lipid metabolism, imbalances in lipid availability, and lipid oxidation rates, leading to the accumulation of intercellular lipotoxic derivatives (81, 82). Peroxisome proliferator-activated receptor (*PPAR*) α is a master nuclear

receptor, which plays a critical role in lipid metabolism through regulating lipid transport, esterification, and oxidation. Abnormal expression of PPAR α in the heart is thought to be an important player in cardiac lipotoxicity (83). This conception is supported by previously published experimental data showing that overexpression of PPAR α leads to lipid accumulation and the development of DCM (84), and that pharmacological inhibition of PPAR α reduces cardiac lipotoxicity in diabetes (84, 85). Recent studies have shown that the PPAR α gene can be transactivated by the CLOCK/BMAL1 heterodimer *via* an E-BOX-dependent mechanism (86). The mutation of BMAL1/CLOCK increases PPAR α mRNA N6-methyladenosine, which affects PPAR α stability and increases lipid accumulation (86–88), suggesting that the circadian clock is also involved in lipid metabolism. However, under diabetic condition, the disturbed circadian clock is frequently accompanied by disordered mitochondrial dynamics and cardiac lipotoxicity (71, 89, 90). Collectively, currently available research findings suggest that restoring clock-controlled mitochondrial dynamics may be an effective way to reduce DCM by reducing cardiac lipotoxicity.

4.3 Clock-controlled mitochondrial dynamics and mitochondria-generated ROS

The role of mitochondria-generated ROS in DCM is well-established (91). It is well demonstrated in diabetes that cardiomyocytes from animal models and patients display mitochondrial dysfunction and overproduction of ROS (92–94). Large amounts of ROS result in the damage of cardiomyocyte proteins, lipids, and DNA, eventually leading to the development of DCM (91). It is worth noting that abnormal mitochondrial morphology is intricately linked to the excessive production of ROS. Increasing studies have shown large amounts of fragmented mitochondria in diabetic cardiomyocytes, accompanied by excessive ROS production, which is reduced by inhibition of mitochondrial fission through decreasing DRP1 expression (95, 96). Additionally, improving OPA1 expression could decrease mitochondrial ROS generation by stabilizing oligomers and activity of ATPase, which is a key enzyme in ATP generation using electron potential energy to produce ATP (28, 97). Notably, the excessive mitochondrial ROS in the heart could promote mitochondrial fission by decreasing DRP1 phosphorylation and decrease mitochondrial fusion by altering OPA1 hydrolysis (98). Thus, it is understandable that the fragmented mitochondria induced by hyperglycemia can be restored with ROS scavenger (99). Therefore, the disordered mitochondrial dynamics and excessive ROS production may interact with each other, and it is a vicious cycle in diabetes.

ROS production in the process of mitochondrial metabolism in the physiological state has a circadian oscillation rhythm. Mitochondria generate more ROS at sleep onset relative to the wake period, due to higher levels of the clock genes BMAL1 and CLOCK at sleep onset (100). A recent study has indicated the decay of circadian genes (PER, TIM, CLOCK) oscillation with elevated ROS levels in diabetes (101). The disruption of clock

components can impact ROS production. In the pancreatic β -cell line, BMAL1 knockdown triggers an increase of the ROS content and impairs glucose-stimulated insulin secretion, the hallmark of the pancreas islet function in diabetes (102). Similarly, the loss of *CLOCK* gene increased ROS production and impaired cardiac structure and function (103). PER1-deficient mice also show impaired ROS-production rhythm with lower glutathione peroxidase activity and higher ROS level (104). In addition to affecting ROS production, the circadian clock also affects the anti-oxidative system. BMAL1 interacts with HSPB1, a small heat shock protein that resists ROS *via* S-thiolated modification, to reduce oxidative damage in cardiomyocytes (105). PER interacts with glutathione peroxidase to withstand oxidative stress, and reduced PER expression will diminish the activity of glutathione peroxidase (104). Recent studies have indicated that a disordered circadian clock may increase ROS generation or weaken antioxidant activity and is often accompanied by mitochondrial dynamics dysfunction. The disruption of functional *CLOCK* gene in cardiac myocytes impaired the expression of mitochondrial fusion proteins OPA1 and MFN2, resulting in fragmented mitochondria and the accumulation of mitochondria-generated ROS (103). Further study indicated the *CLOCK* could improve mitochondrial dynamics and function by stabilizing DRP1 mRNA expression (48). In *CLOCK* mutation mice, abnormal accumulation of DRP1 leads to fragmented mitochondria and increased ROS levels (48). Together, these results suggest that mitochondria-generated ROS is impacted by circadian-controlled mitochondrial dynamics and plays an important role in DCM.

4.4 Clock-controlled mitochondrial dynamics and mitochondrial Ca²⁺ handling

The abnormal Ca²⁺ signaling is a critical feature of DCM, notably mitochondrial Ca²⁺ mishandling (106). Mitochondrial Ca²⁺ handling normally provides a basis for normal excitation-contraction coupling and mitochondrial energy supply, but the disordered Ca²⁺ concentration in the mitochondrial matrix in diabetes contributes to decreased ATP generation and increased cardiomyocyte damage (8, 106, 107). Mitochondrial Ca²⁺ mishandling is affected by abnormal mitochondrial dynamics. In cultured cardiomyocytes, FIS1-induced mitochondrial fragmentation could reduce mitochondrial Ca²⁺ uptake (108). A similar observation is made later in the myofibers, where the inhibition of DRP1 could increase Ca²⁺ concentration in the mitochondrial matrix during the phase of electrical stimulation, and increase the expression of mitochondrial calcium uniporter (MCU), an important channel for mitochondrial Ca²⁺ uptake (109). The mitochondria-associated ER membrane (MAM), a critical regulator affecting mitochondrial Ca²⁺ handling, is also demonstrated to be affected by mitochondrial dynamics. In fly fruit hearts, MFN2 deficiency impair the physical contact between mitochondria and ER and decrease the protein content associated with MAM, resulting in reduced mitochondrial Ca²⁺ uptake (110). A further study has also shown that the disordered MAM induced

by MFN2 knockdown impairs ER Ca^{2+} release and decreases ATP generation in ventricular myocytes (111). Additionally, the mutation of OPA1 could reduce the distance between ER and mitochondria, suggesting OPA1 is necessary for mitochondrial Ca^{2+} handling (112).

Notably, mitochondrial Ca^{2+} handling itself has circadian oscillations and is controlled by clock system. A recent study applied calcium pulses to isolate mitochondria in mouse hearts at different periods to assess the calcium retention capacity and calcium uptake rate of mitochondria, showing mitochondria have higher calcium retention capacity and calcium absorption rate during the sleep stage (100). For some critical proteins of mitochondrial Ca^{2+} handling, MCU and sodium/calcium exchanger had higher expression levels at sleep onset relative to the wake phase (100). And, other proteins participated in mitochondrial Ca^{2+} handling are also influenced by the circadian clock, such as ryanodine receptors (RyR). The circadian complex CLOCK/BMAL1 can bind to the E-box of the RyR gene and impact its gene expression (113). In the suprachiasmatic nucleus of BMAL1 KO mice, the levels of RyR mRNA and RyR protein are significantly reduced, as well as the decreased intracellular Ca^{2+} concentration (114). In the models of disordered circadian clock, dysfunctional mitochondrial dynamics and mitochondrial Ca^{2+} mishandling are well observed (9, 100). Hyperglycemia is inherently a critical player, causing circadian clock disturbance, dysfunctional mitochondrial dynamics and mitochondrial Ca^{2+} mishandling (89, 90, 106). These findings provide important insights that clock-controlled mitochondrial dynamics may regulate mitochondrial Ca^{2+} handling and influence the development of DCM.

4.5 Clock-controlled mitochondrial dynamics and mitochondrial membrane potential

Mitochondria produce ATP through the electron transport chain, which creates an electrochemical gradient and generates mitochondrial membrane potential (MMP) (115). MMP is an important parameter for evaluating mitochondrial function and activity (116). Normal MMP is the key condition for mitochondrial oxidative phosphorylation, and its stability contributes to maintaining normal physiological function of the cells (115, 117). The abnormality of MMP may be attributable to apoptosis, ROS, and abnormal autophagy (118, 119). Mitochondrial dynamics is closely linked to MMP. In diabetic hearts, both abnormal MMP and dysfunctional mitochondrial dynamics are commonly observed. Diabetic hearts from db/db mice show excessive fragmented mitochondria and decreased MMP. Increased fusion events through reconstituting MFN2 in DCM restored the MMP and mitochondrial function (120). The lipotoxic hearts also exhibit impaired mitochondrial fusion due to decreased OPA1 expression and abnormal MMP (98). Further studies have revealed that the specific mechanism by which OPA1 changes MMP may be related to changes in mitochondrial cristae architecture (117). Moreover, the loss of MMP destabilizes the L-OPA1 structure, leading to increased OPA1 cleavage and consequent impact on mitochondrial

fusion (121). Likewise, in cardiomyocytes treated with high glucose, the inhibitors of DRP1, Mdivi-1, not only decreased excessive mitochondrial fission but also alleviated the decreased MMP (122).

MMP is also influenced by the circadian clock. Under normal physiological conditions, MMP has certain oscillatory patterns and is also associated with mitochondrial activity. A study shows that, in the suprachiasmatic nucleus of rats, MMP is higher during the light period than the dark period (123). In semi-anaerobic yeast cells, MMP is oscillating, and this oscillation may be related to mitochondrial metabolic activity (124). Further research indicates that this oscillatory pattern correlates with mitochondrial dynamics, mitochondrial fusion along with high MMP (125). Disruption of circadian rhythm leads to abnormal MMP and imbalance in mitochondrial dynamics. In pancreatic beta cells, the loss of BMAL1 decreased the expression of MNF1/2 and increased the expression of FIS1, accompanied by decreased MMP and impaired pancreatic function (70). Similarly, CLOCK-deficient cardiac myocytes showed excessive mitochondrial fission, loss of MMP, and impaired cardiac structure (103). Therefore, it can be speculated that the disordered clock rhythm under diabetic conditions can lead to the dysfunction of mitochondrial dynamics and the decrease of MMP, thereby increasing myocardial damage.

4.6 Clock-controlled mitochondrial dynamics and mitophagy

Hyperglycemia can easily lead to mitochondrial damage in diabetes. The progressive mitochondrial damage in cardiomyocytes leads to lipid accumulation and excessive oxidative stress, resulting in the development of DCM (126). To prevent damage to dysfunctional mitochondria, a selective degradation system referred to as “mitophagy” is activated to remove dysfunctional mitochondria (126). However, increasing studies demonstrate impaired mitophagy in diabetes (127, 128). Although the molecular mechanism of impaired mitophagy in DCM has not been fully clarified, recent findings imply that abnormal mitochondrial dynamics are involved. PINK/Parkin are critical molecules in ubiquitin-dependent mitophagy (129). In mouse cardiomyocytes, the OMM guanosine triphosphatase MFN2 could mediate Parkin recruitment to the damaged mitochondria *via* a PINK-dependent manner (130). Downregulation of MNF2 expression prevents depolarization-induced translocation of Parkin to the damaged mitochondria and inhibits mitophagy (130), which contributes to the development of DCM (120). Likewise, DRP1 disruption in cardiomyocytes leads to imbalanced mitochondrial dynamics, and suppresses mitophagy *via* reducing the formation of autophagosomes, resulting in cardiac dysfunction (131). In cultured H9C2 cardiomyocytes, the overexpression of OPA1 promotes mitochondrial fusion and stimulates mitophagy, thereby attenuating high glucose-induced cardiomyocytes injury (132). These findings suggest that mitochondrial dynamics are involved in the regulation of mitophagy and thus influence the development of DCM.

Mitophagy is also demonstrated to be regulated by circadian clock. The key regulators of mitophagy, PINK/Parkin, are

rhythmically expressed under clock control in response to environmental changes (103). The disruption of clock rhythm reduces the expression levels of PINK/Parkin, leading to suppressed mitophagy and myocardial dysfunction (103). BNIP3 is one of the important molecules of receptor-dependent mitophagy (129). It has been shown that BMAL1 binds to the E-BOX element in the promoter region of BNIP3 gene and regulates the level of BNIP3 protein oscillation in human embryonic stem cell-deprived cardiomyocytes (133). Downregulating BMAL1 expression directly reduces BNIP3 expression, leading to compromised mitophagy and cardiomyocyte dysfunction (133). Recently, Jacobi et al. have indicated that mitochondrial fission and mitophagy proteins show a similar diurnal pattern in the livers of WT mice (10). However, their levels fail to cycle and are significantly reduced in BMAL1 KO mice, and mitochondrial fission and mitophagy-related genes *DRP1*, *FIS1*, *PINK1*, and *BNIP3* are also greatly reduced, manifested by fragmented mitochondria and suppressed mitophagy (10). In cardiomyocytes, similarly, the loss of *CLOCK*/*BMAL1* expression may impair mitochondrial dynamics and suppress mitophagy, leading to dysfunctional mitochondria and cardiac injury (103, 133). Thus, the disordered circadian clock-controlled mitochondrial dynamics contributes to compromised mitophagy, which promotes the development of DCM.

4.7 Clock-controlled mitochondrial dynamics and ER stress

The main function of ER is protein folding and assembly. Hyperglycemia and hyperlipidemia in diabetes impair ER function, leading to the accumulation of unfolded proteins (134). This process can be prevented by a quality control system termed unfolded protein response (UPR), a signal transduction pathway alleviating the accumulation of abnormal proteins in the ER lumen (135). If the UPR is not able to process these unfolded proteins within a certain time lapse, it will induce cardiomyocyte apoptosis and promote the progress of DCM (136). In animal models of diabetes, ER stress has been shown to contribute to cardiac apoptosis, as evidenced by the induction of UPR signaling proteins and ER stress-associated apoptosis signaling proteins (71). UPR mainly contains three signaling pathways, protein kinase RNA-like ER kinase/activating transcriptional factor 4 (PERK/ATF4), inositol-requiring protein1 α /X-box binding protein (IRE1 α /XBP1), and activating transcriptional factor 6 (ATF6) pathways (134), which are demonstrated to be influenced by mitochondrial dynamics. The overactivated UPR branches such as PERK and ATF6 in hyperglycemia-treated cardiomyocytes can be alleviated by reducing MFN2 expression (137), and downregulation of MFN2 could attenuate mitochondrial dysfunction and ER-stress induced cardiomyocytes apoptosis (138). An opposite finding performed by other researchers suggests that MNF2 can suppress PERK activity through direct interaction under basal conditions, but hyperglycemia inhibits MFN2 expression and promotes the reduction of MNF2-PERK interaction, thereby MNF2 overexpression could alleviate the abnormal activation of PERK pathway, cardiomyocytes apoptosis and mitochondrial dysfunction (139, 140). In addition, DRP1 is also involved in ER stress- induced

pancreatic β -cell apoptosis through the process of mitochondrial fission, cytochrome c release, ROS generation and caspase-3 activation (141).

It is worth noting that many proteins related to UPR and ER stress are closely regulated by circadian rhythms (142). The circadian clock can coordinate the rhythmic activation of IRE1 α in 12-hour cycles to respond to the metabolic demands of organism. However, in *Cry1/Cry2* KO mice liver, the rhythmic activation of IRE1 α was lost, accompanied by disrupted lipid metabolism (143). A similar study was conducted in *CLOCK* mutant mice, showing the UPR-related genes in liver such as *PERK*, *IRE1 α* , and *ATF6*, were significantly up-regulated as compared to the WT mice (142). Additionally, the disruption of circadian rhythms caused by sleep deprivation or gene mutant in pancreas contributed to ER stress, resulting in the loss of pancreatic beta-cells and the development of diabetes (144, 145). Recent studies have shown that disturbing circadian clock can lead to ER stress and affect UPR-related protein expression, accompanied by disturbed mitochondrial dynamics (145, 146). Considering that the circadian clock is inherently susceptible to hyperglycemia (89), and that there exists disturbed mitochondrial dynamics and ER stress in diabetic myocardium (90, 134), it can be speculated that restoring the clock-controlled mitochondrial dynamics may inhibit ER stress and alleviate the development of DCM.

5 Clock-controlled mitochondrial dynamics as a novel therapeutic target in DCM

There is a lack of effective therapeutic approaches for DCM due to its complex etiology. However, glycemic control is still the core part. In healthy subjects, the combination of basal glucose production and insulin-mediated suppression of glucose production, in alliance with oscillatory insulin levels, keeps glycemia stable throughout the day (147). The glycemia in patients with diabetes has a special oscillatory pattern, manifested as increased glycemic variability with specific circadian characteristics (148, 149). Epidemiological evidence suggests that irregular eating habits, reduced light exposure, increased night shift hours, nocturnal light exposure, and sleep deprivation disrupt the circadian clock and increase the risk of diabetes (150, 151). Thus, it is understandable that enhancing circadian clock rhythms through adjusting lifestyle contributes to prevention and treatment of diabetes-associated complications (152).

The potential novel drugs targeting clock-controlled mitochondrial dynamics are also imminent. The first circadian clock-based drug was melatonin, a hormone secreted by the pineal gland (153). Exogenous melatonin supplementation increased ROR levels in diabetic myocardium, and prevented the development of DCM *via* reducing dysfunctional mitochondria, ER stress, myocardial apoptosis, autophagy dysfunction, and oxidative stress damage (60, 153, 154). In recent years, a number of small-molecule chemical enhancers targeting the circadian system have been developed, such as Nobiletin, CRY activator (KL001), Rev-

TABLE 1 Summary of potential interventions involving clock-controlled mitochondrial dynamics in DCM.

Potential drugs	Effects on clock circadian/mitochondrial dynamics	Other effects on DCM	References
Melatonin	Increase ROR α expression Increase DRP1 expression	Decrease myocardial apoptosis Reduce oxidative stress Mitigate myocardial hypertrophy and cardiac fibrosis Improve cardiac diastolic function	(60, 153, 155)
Nobiletin	Enhance amplitude of circadian rhythms Enhance ROR α / γ transcriptional activity Increase BMAL1 expression	Improve glucose tolerance and insulin sensitivity Increase insulin secretion	(155, 156)
KL001	Increase CRY level	Suppress glucose production	(157)
SR9011/ SR9009	Increase REV-ERB α / β expression	Decrease triglyceride synthesis Increase lipid and glucose oxidation Mitigate cardiac fibroblasts	(158, 159)
Mitochondrial fusion promoter-M1	Increase OPA1 expression	Improve mitochondrial function Inhibit myocardial apoptosis Decrease ROS generation	(28)
Nicotinamide riboside	Increase MFN2 expression	Reduce cardiomyocyte apoptosis Decrease ROS generation	(120, 160)

ERB- α / β agonist (especially SR9011/SR9009), and so on (The mechanism of their action is given in Table 1). These chemical compounds restored cardiac circadian rhythms and oscillatory patterns of metabolic gene expression, resulting in phenotypical improvements in insulin resistance, lipotoxicity, oxidative stress, and dysfunctional mitochondrial dynamics (153, 155–158, 161–163). Notably, improving mitochondrial dynamics is also a critical approach to restore myocardial function in diabetes. It is well demonstrated that inhibiting mitochondrial fission or increasing mitochondrial fusion has beneficial effects on diabetic hearts. Ding et al. suggest that the administration of mitochondrial fusion promoter-M1 can restore mitochondrial dynamics balance and attenuate DCM *via* an OPA1-dependent way (28). Similarly, Hu et al. have shown that reconstitution of MFN2 in diabetic myocardium inhibits mitochondrial fission and prevents DCM progress (120). In a mouse model of diabetes, increasing MFN2 expression could improve mitochondrial function, inhibit mitochondrial oxidative stress, and reduce cardiomyocyte apoptosis (160). In addition, melatonin attenuates the development of diabetes-induced cardiac dysfunction by preventing DRP1-mediated mitochondrial fission through the SIRT1-PGC1 α pathway (164). Therefore, the interventions involving in circadian clock and mitochondrial dynamics are promising approaches for the treatment of DCM (The summary of potential drugs were shown in Table 1).

6 Conclusion

Circadian clock-controlled mitochondrial dynamics are critical for the normal structure and function of the heart. Alternations in the circadian clock and mitochondrial dynamics in diabetes play an important role in the pathophysiological process of DCM. In this review, we summarize the relevant pathways of circadian clock-

controlled mitochondrial dynamics and discuss how the disruption of circadian clock and mitochondrial dynamics impact multiple etiologies of DCM, including insulin resistance, cardiac lipotoxicity, mitochondria-generated ROS, mitochondrial Ca²⁺ handling, MMP, mitophagy, and ER stress. This study also provides a strong rationale for targeting the circadian clock and mitochondrial dynamics in the treatment and prevention of DCM. Further studies are urgently needed to identify and characterize the mechanisms of action of novel chemical and endogenous modulators of the circadian clock and mitochondrial dynamics to prevent heart damage in diabetic states.

Author contributions

ZJ, YJ, and WS wrote the manuscript and performed the validation. LZ, XJW, LG, and JG carried literature research. YL, YZ, XYW, and Z-YX performed manuscript review. ZX and SL contributed to the conception of the manuscript and contributed significantly to manuscript preparation. All authors contributed to the article and approved the submitted version.

Conflict of interest

The authors declare that the research was conducted in the absence of any commercial or financial relationships that could be construed as a potential conflict of interest.

Publisher's note

All claims expressed in this article are solely those of the authors and do not necessarily represent those of their affiliated

organizations, or those of the publisher, the editors and the reviewers. Any product that may be evaluated in this article, or

claim that may be made by its manufacturer, is not guaranteed or endorsed by the publisher.

References

- Lotfy M, Adeghate J, Kalasz H, Singh J, Adeghate E. Chronic complications of diabetes mellitus: a mini review. *Curr Diabetes Rev* (2017) 13(1):3–10. doi: 10.2174/1573399812666151016101622
- Ma RCW. Epidemiology of diabetes and diabetic complications in China. *Diabetologia* (2018) 61(6):1249–60. doi: 10.1007/s00125-018-4557-7
- Rubler S, Dlugash J, Yuceoglu YZ, Kumral T, Branwood AW, Grishman A. New type of cardiomyopathy associated with diabetic glomerulosclerosis. *Am J Cardiol* (1972) 30(6):595–602. doi: 10.1016/0002-9149(72)90595-4
- Ritchie RH, Abel ED. Basic mechanisms of diabetic heart disease. *Circ Res* (2020) 126(11):1501–25. doi: 10.1161/CIRCRESAHA.120.315913
- Avagimyan A, Popov S, Shalnova S. The pathophysiological basis of diabetic cardiomyopathy development. *Curr Probl Cardiol* (2022) 47(9):101156. doi: 10.1016/j.cpcardiol.2022.101156
- Zhao X, Liu S, Wang X, Chen Y, Pang P, Yang Q, et al. Diabetic cardiomyopathy: clinical phenotype and practice. *Front Endocrinol (Lausanne)* (2022) 13:1032268. doi: 10.3389/fendo.2022.1032268
- Cieluch A, Uruska A, Zolinska-Ziolkiewicz D. Can we prevent mitochondrial dysfunction and diabetic cardiomyopathy in type 1 diabetes mellitus? pathophysiology and treatment options. *Int J Mol Sci* (2020) 21(8):2852. doi: 10.3390/ijms21082852
- Jia G, Hill MA, Sowers JR. Diabetic cardiomyopathy: an update of mechanisms contributing to this clinical entity. *Circ Res* (2018) 122(4):624–38. doi: 10.1161/CIRCRESAHA.117.311586
- Schmitt K, Grimm A, Dallmann R, Oettinghaus B, Restelli LM, Witzig M, et al. Circadian control of Drp1 activity regulates mitochondrial dynamics and bioenergetics. *Cell Metab* (2018) 27(3):657–66.e5. doi: 10.1016/j.cmet.2018.01.011
- Jacobi D, Liu S, Burkewitz K, Kory N, Knudsen NH, Alexander RK, et al. Hepatic Bmal1 regulates rhythmic mitochondrial dynamics and promotes metabolic fitness. *Cell Metab* (2015) 22(4):709–20. doi: 10.1016/j.cmet.2015.08.006
- Mezhnina V, Ebeigbe OP, Poe A, Kondratov RV. Circadian control of mitochondria in *ros* homeostasis. *Antioxid Redox Signal* (2022) 37(10–12):647–63. doi: 10.1089/ars.2021.0274
- Giacomello M, Pyakurel A, Glytsou C, Scorrano L. The cell biology of mitochondrial membrane dynamics. *Nat Rev Mol Cell Biol* (2020) 21(4):204–24. doi: 10.1038/s41580-020-0210-7
- Santel A, Fuller MT. Control of mitochondrial morphology by a human mitofusin. *J Cell Sci* (2001) 114(Pt 5):867–74. doi: 10.1242/jcs.114.5.867
- Ishihara N, Eura Y, Mihara K. Mitofusin 1 and 2 play distinct roles in mitochondrial fusion reactions *Via* gtpase activity. *J Cell Sci* (2004) 117(Pt 26):6535–46. doi: 10.1242/jcs.01565
- de Brito OM, Scorrano L. Mitofusin 2 tethers endoplasmic reticulum to mitochondria. *Nature* (2008) 456(7222):605–10. doi: 10.1038/nature07534
- Anand R, Wai T, Baker MJ, Kladt N, Schauss AC, Rugarli E, et al. The I-aaa protease Yme1 and Oma1 cleave Opa1 to balance mitochondrial fusion and fission. *J Cell Biol* (2014) 204(6):919–29. doi: 10.1083/jcb.201308006
- Vogel F, Bornhord C, Neupert W, Reichert AS. Dynamic subcompartmentalization of the mitochondrial inner membrane. *J Cell Biol* (2006) 175(2):237–47. doi: 10.1083/jcb.200605138
- Faelber K, Dietrich L, Noel JK, Wollweber F, Pfitzner AK, Muhleip A, et al. Structure and assembly of the mitochondrial membrane remodeling gtpase Mgm1. *Nature* (2019) 571(7765):429–33. doi: 10.1038/s41586-019-1372-3
- Chang CR, Blackstone C. Cyclic amp-dependent protein kinase phosphorylation of Drp1 regulates its gtpase activity and mitochondrial morphology. *J Biol Chem* (2007) 282(30):21583–7. doi: 10.1074/jbc.C700083200
- Cribbs JT, Strack S. Reversible phosphorylation of Drp1 by cyclic amp-dependent protein kinase and calcineurin regulates mitochondrial fission and cell death. *EMBO Rep* (2007) 8(10):939–44. doi: 10.1038/sj.embor.7401062
- Cereghetti GM, Stangherlin A, Martins de Brito O, Chang CR, Blackstone C, Bernardi P, et al. Dephosphorylation by calcineurin regulates translocation of Drp1 to mitochondria. *Proc Natl Acad Sci U S A* (2008) 105(41):15803–8. doi: 10.1073/pnas.0808249105
- Yoon Y, Galloway CA, Jhun BS, Yu T. Mitochondrial dynamics in diabetes. *Antioxidants Redox Signaling* (2010) 14(3):439–57. doi: 10.1089/ars.2010.3286
- Loson OC, Song Z, Chen H, Chan DC. Fis1, mff, Mid49, and Mid51 mediate Drp1 recruitment in mitochondrial fission. *Mol Biol Cell* (2013) 24(5):659–67. doi: 10.1091/mbc.E12-10-0721
- Kalia R, Wang RY, Yusuf A, Thomas PV, Agard DA, Shaw JM, et al. Structural basis of mitochondrial receptor binding and constriction by Drp1. *Nature* (2018) 558(7710):401–5. doi: 10.1038/s41586-018-0211-2
- Rizwan H, Pal S, Sabnam S, Pal A. High glucose augments *ros* generation regulates mitochondrial dysfunction and apoptosis *Via* stress signalling cascades in keratinocytes. *Life Sci* (2020) 241:117148. doi: 10.1016/j.lfs.2019.117148
- Marinkovic M, Novak I. A brief overview of Bnip3l/Nix receptor-mediated mitophagy. *FEBS Open Bio* (2021) 11(12):3230–6. doi: 10.1002/2211-5463.13307
- Sato A, Nakada K, Hayashi J. Mitochondrial dynamics and aging: mitochondrial interaction preventing individuals from expression of respiratory deficiency caused by mutant mtdna. *Biochim Biophys Acta* (2006) 1763(5–6):473–81. doi: 10.1016/j.bbamer.2006.03.001
- Ding M, Liu C, Shi R, Yu M, Zeng K, Kang J, et al. Mitochondrial fusion promoter restores mitochondrial dynamics balance and ameliorates diabetic cardiomyopathy in an optic atrophy 1-dependent way. *Acta Physiol (Oxf)* (2020) 229(1):e13428. doi: 10.1111/apha.13428
- Ketenci M, Zablocki D, Sadoshima J. Mitochondrial quality control mechanisms during diabetic cardiomyopathy. *JMA J* (2022) 5(4):407–15. doi: 10.31662/jmaj.2022-0155
- Hsu PY, Harmer SL. Global profiling of the circadian transcriptome using microarrays. *Methods Mol Biol* (2014) 1158:45–56. doi: 10.1007/978-1-4939-0700-7_3
- Dyar KA, Lutter D, Artati A, Ceglia NJ, Liu Y, Armenta D, et al. Atlas of circadian metabolism reveals system-wide coordination and communication between clocks. *Cell* (2018) 174(6):1571–85.e11. doi: 10.1016/j.cell.2018.08.042
- Hergenhan S, Holtkamp S, Scheiermann C. Molecular interactions between components of the circadian clock and the immune system. *J Mol Biol* (2020) 432(12):3700–13. doi: 10.1016/j.jmb.2019.12.044
- Jouffe C, Weger BD, Martin E, Atger F, Weger M, Gobet C, et al. Disruption of the circadian clock component Bmal1 elicits an endocrine adaption impacting on insulin sensitivity and liver disease. *Proc Natl Acad Sci U S A* (2022) 119(10):e2200083119. doi: 10.1073/pnas.2200083119
- Jagannath A, Taylor L, Wakaf Z, Vasudevan SR, Foster RG. The genetics of circadian rhythms, sleep and health. *Hum Mol Genet* (2017) 26(R2):R128–R38. doi: 10.1093/hmg/ddx240
- Ko CH, Takahashi JS. Molecular components of the mammalian circadian clock. *Hum Mol Genet* (2006) 15(2):R271–7. doi: 10.1093/hmg/ddl207
- Partch CL, Green CB, Takahashi JS. Molecular architecture of the mammalian circadian clock. *Trends Cell Biol* (2014) 24(2):90–9. doi: 10.1016/j.tcb.2013.07.002
- Cox KH, Takahashi JS. Circadian clock genes and the transcriptional architecture of the clock mechanism. *J Mol Endocrinol* (2019) 63(4):R93–R102. doi: 10.1530/JME-19-0153
- Preitner N, Damiola F, Lopez-Molina L, Zakany J, Duboule D, Albrecht U, et al. The orphan nuclear receptor rev-erbalpha controls circadian transcription within the positive limb of the mammalian circadian oscillator. *Cell* (2002) 110(2):251–60. doi: 10.1016/s0092-8674(02)00825-5
- Sato TK, Panda S, Miraglia LJ, Reyes TM, Rudic RD, McNamara P, et al. A functional genomics strategy reveals *rora* as a component of the mammalian circadian clock. *Neuron* (2004) 43(4):527–37. doi: 10.1016/j.neuron.2004.07.018
- Solt LA, Kojetin DJ, Burris TP. The *rev-erbs* and *rors*: molecular links between circadian rhythms and lipid homeostasis. *Future Med Chem* (2011) 3(5):623–38. doi: 10.4155/fmc.11.9
- Patke A, Young MW, Axelrod S. Molecular mechanisms and physiological importance of circadian rhythms. *Nat Rev Mol Cell Biol* (2020) 21(2):67–84. doi: 10.1038/s41580-019-0179-2
- Brown SA, Kowalska E, Dallmann R. (Re)Inventing the circadian feedback loop. *Dev Cell* (2012) 22(3):477–87. doi: 10.1016/j.devcel.2012.02.007
- Kalsbeek A, Yi CX, Cailotto C, la Fleur SE, Fliers E, Buijs RM. Mammalian clock output mechanisms. *Essays Biochem* (2011) 49(1):137–51. doi: 10.1042/BSE0480137
- Marcheva B, Ramsey KM, Buhr ED, Kobayashi Y, Su H, Ko CH, et al. Disruption of the clock components *clock* and *Bmal1* leads to hypoinsulinemia and diabetes. *Nature* (2010) 466(7306):627–31. doi: 10.1038/nature09253
- Xie M, Tang Q, Nie J, Zhang C, Zhou X, Yu S, et al. Bmal1-downregulation aggravates porphyromonas gingivalis-induced atherosclerosis by encouraging oxidative stress. *Circ Res* (2020) 126(6):e15–29. doi: 10.1161/CIRCRESAHA.119.315502
- Uchiyama Y. Circadian alterations in tubular structures on the outer mitochondrial membrane of rat hepatocytes. *Cell Tissue Res* (1981) 214(3):519–27. doi: 10.1007/BF00233492

47. Huang CC, Ko ML, Vernikovskaya DI, Ko GY. Calcineurin serves in the circadian output pathway to regulate the daily rhythm of l-type voltage-gated calcium channels in the retina. *J Cell Biochem* (2012) 113(3):911–22. doi: 10.1002/jcb.23419
48. Xu L, Lin J, Liu Y, Hua B, Cheng Q, Lin C, et al. Clock regulates Drp1 mrna stability and mitochondrial homeostasis by interacting with Puf60. *Cell Rep* (2022) 39 (2):110635. doi: 10.1016/j.celrep.2022.110635
49. Jordan SD, Lamia KA. Ampk at the crossroads of circadian clocks and metabolism. *Mol Cell Endocrinol* (2013) 366(2):163–9. doi: 10.1016/j.mce.2012.06.017
50. Toyama EQ, Herzig S, Courchet J, Lewis TL Jr., Loson OC, Hellberg K, et al. Metabolism. amp-activated protein kinase mediates mitochondrial fission in response to energy stress. *Science* (2016) 351(6270):275–81. doi: 10.1126/science.aab4138
51. Canto C, Jiang LQ, Deshmukh AS, Matak C, Coste A, Lagouge M, et al. Interdependence of ampk and Sirt1 for metabolic adaptation to fasting and exercise in skeletal muscle. *Cell Metab* (2010) 11(3):213–9. doi: 10.1016/j.cmet.2010.02.006
52. Um JH, Yang S, Yamazaki S, Kang H, Viollet B, Foretz M, et al. Activation of 5'-Amp-Activated kinase with diabetes drug metformin induces casein kinase iepsilon (Ck1epsilon)-dependent degradation of clock protein Mper2. *J Biol Chem* (2007) 282 (29):20794–8. doi: 10.1074/jbc.C700070200
53. Lamia KA, Sachdeva UM, DiTacchio L, Williams EC, Alvarez JG, Egan DF, et al. Ampk regulates the circadian clock by cryptochrome phosphorylation and degradation. *Science* (2009) 326(5951):437–40. doi: 10.1126/science.1172156
54. Sardon Puig L, Valera-Alberni M, Canto C, Pilon NJ. Circadian rhythms and mitochondria: connecting the dots. *Front Genet* (2018) 9:452. doi: 10.3389/fgenet.2018.00452
55. Asher G, Gattfield D, Stratmann M, Reinke H, Dibner C, Kreppel F, et al. Sirt1 regulates circadian clock gene expression through Per2 deacetylation. *Cell* (2008) 134 (2):317–28. doi: 10.1016/j.cell.2008.06.050
56. Ramsey KM, Yoshino J, Brace CS, Abrassart D, Kobayashi Y, Marcheva B, et al. Circadian clock feedback cycle through nampt-mediated nad⁺ biosynthesis. *Science* (2009) 324(5927):651–4. doi: 10.1126/science.1171641
57. Samant SA, Zhang HJ, Hong Z, Pillai VB, Sundaresan NR, Wolfgeher D, et al. Sirt3 deacetylates and activates Opa1 to regulate mitochondrial dynamics during stress. *Mol Cell Biol* (2014) 34(5):807–19. doi: 10.1128/MCB.01483-13
58. Tan X, Chen YF, Zou SY, Wang WJ, Zhang NN, Sun ZY, et al. Aldh2 attenuates ischemia and reperfusion injury through regulation of mitochondrial fusion and fission by Pi3k/Akt/Mtor pathway in diabetic cardiomyopathy. *Free Radic Biol Med* (2023) 195:219–30. doi: 10.1016/j.freeradbiomed.2022.12.097
59. Chang X, Li Y, Cai C, Wu F, He J, Zhang Y, et al. Mitochondrial quality control mechanisms as molecular targets in diabetic heart. *Metabolism* (2022) 137:155313. doi: 10.1016/j.metabol.2022.155313
60. Zhao Y, Xu L, Ding S, Lin N, Ji Q, Gao L, et al. Novel protective role of the circadian nuclear receptor retinoic acid-related orphan receptor-alpha in diabetic cardiomyopathy. *J Pineal Res* (2017) 62(3):e12378. doi: 10.1111/jpi.12378
61. Skrcel I, Milic J, Cilensek I, Petrovic D, Wagner J, Peterlin B. Circadian clock genes and myocardial infarction in patients with type 2 diabetes mellitus. *Gene* (2019) 701:98–103. doi: 10.1016/j.gene.2019.03.038
62. Jia G, DeMarco VG, Sowers JR. Insulin resistance and hyperinsulinaemia in diabetic cardiomyopathy. *Nat Rev Endocrinol* (2016) 12(3):144–53. doi: 10.1038/nrendo.2015.216
63. Montaigne D, Marechal X, Coisne A, Debry N, Modine T, Fayad G, et al. Myocardial contractile dysfunction is associated with impaired mitochondrial function and dynamics in type 2 diabetic but not in obese patients. *Circulation* (2014) 130 (7):554–64. doi: 10.1161/CIRCULATIONAHA.113.008476
64. Lin HY, Weng SW, Chang YH, Su YJ, Chang CM, Tsai CJ, et al. The causal role of mitochondrial dynamics in regulating insulin resistance in diabetes: link through mitochondrial reactive oxygen species. *Oxid Med Cell Longev* (2018) 2018:7514383. doi: 10.1155/2018/7514383
65. Sidarala V, Zhu J, Levi-D'Ancona E, Pearson GL, Reck EC, Walker EM, et al. Mitofusin 1 and 2 regulation of mitochondrial DNA content is a critical determinant of glucose homeostasis. *Nat Commun* (2022) 13(1):2340. doi: 10.1038/s41467-022-29945-7
66. Boden G, Ruiz J, Urbain JL, Chen X. Evidence for a circadian rhythm of insulin secretion. *Am J Physiol* (1996) 271(2 Pt 1):E246–52. doi: 10.1152/ajpendo.1996.271.2.E246
67. Luo Q, Xiao Y, Alex A, Cummins TR, Bhatwadekar AD. The diurnal rhythm of insulin receptor substrate-1 (Irs-1) and Kir4.1 in diabetes: implications for a clock gene Bmal1. *Invest Ophthalmol Vis Sci* (2019) 60(6):1928–36. doi: 10.1167/iovs.18-26045
68. McGinnis GR, Tang Y, Brewer RA, Brahma MK, Stanley HL, Shanmugam G, et al. Genetic disruption of the cardiomyocyte circadian clock differentially influences insulin-mediated processes in the heart. *J Mol Cell Cardiol* (2017) 110:80–95. doi: 10.1016/j.yjmcc.2017.07.005
69. Gabriel BM, Altintas A, Smith JAB, Sardon-Puig L, Zhang X, Basse AL, et al. Disrupted circadian oscillations in type 2 diabetes are linked to altered rhythmic mitochondrial metabolism in skeletal muscle. *Sci Adv* (2021) 7(43):eabi9654. doi: 10.1126/sciadv.abi9654
70. Ye L, Wu H, Xu W. Deletion of Bmal1 impairs pancreatic beta-cell function via mitochondrial signaling pathway. *BioMed Res Int* (2020) 2020:9803024. doi: 10.1155/2020/9803024
71. Bugger H, Abel ED. Molecular mechanisms of diabetic cardiomyopathy. *Diabetologia* (2014) 57(4):660–71. doi: 10.1007/s00125-014-3171-6
72. Nakamura M, Sadoshima J. Cardiomyopathy in obesity, insulin resistance and diabetes. *J Physiol* (2020) 598(14):2977–93. doi: 10.1111/JP276747
73. Kretschmar T, Wu JMF, Schulze PC. Mitochondrial homeostasis mediates lipotoxicity in the failing myocardium. *Int J Mol Sci* (2021) 22(3):1498. doi: 10.3390/ijms22031498
74. Wang Y, Yin C, Chen Z, Li Y, Zou Y, Wang X, et al. Cardiac-specific Lrp6 knock-out induces lipid accumulation through Drp1/Cpt1b pathway in adult mice. *Cell Tissue Res* (2020) 380(1):143–53. doi: 10.1007/s00441-019-03126-3
75. Parra V, Eisner V, Chiong M, Criollo A, Moraga F, Garcia A, et al. Changes in mitochondrial dynamics during ceramide-induced cardiomyocyte early apoptosis. *Cardiovasc Res* (2008) 77(2):387–97. doi: 10.1093/cvr/cvm029
76. Bikman BT, Summers SA. Ceramides as modulators of cellular and whole-body metabolism. *J Clin Invest* (2011) 121(11):4222–30. doi: 10.1172/JCI57144
77. Raichur S, Brunner B, Bielohuby M, Hansen G, Pfenninger A, Wang B, et al. The role of C16:0 ceramide in the development of obesity and type 2 diabetes: Cers6 inhibition as a novel therapeutic approach. *Mol Metab* (2019) 21:36–50. doi: 10.1016/j.molmet.2018.12.008
78. Hammerschmidt P, Ostkotte D, Nolte H, Gerl MJ, Jais A, Brunner HL, et al. Cers6-derived sphingolipids interact with mff and promote mitochondrial fragmentation in obesity. *Cell* (2019) 177(6):1536–52.e23. doi: 10.1016/j.cell.2019.05.008
79. Chen CY, Li SJ, Wang CY, Mersmann HJ, Ding ST. The impact of Drp1 on myocardial fibrosis in the obese minipig. *Eur J Clin Invest* (2020) 50(3):e13204. doi: 10.1111/eci.13204
80. Durgan DJ, Moore MW, Ha NP, Egbejimi O, Fields A, Mbawuke U, et al. Circadian rhythms in myocardial metabolism and contractile function: influence of workload and oleate. *Am J Physiol Heart Circ Physiol* (2007) 293(4):H2385–93. doi: 10.1152/ajpheart.01361.2006
81. Durgan DJ, Trexler NA, Egbejimi O, McElfresh TA, Suk HY, Petterson LE, et al. The circadian clock within the cardiomyocyte is essential for responsiveness of the heart to fatty acids. *J Biol Chem* (2006) 281(34):24254–69. doi: 10.1074/jbc.M601704200
82. Pan X, Mota S, Zhang B. Circadian clock regulation on lipid metabolism and metabolic diseases. *Adv Exp Med Biol* (2020) 1276:53–66. doi: 10.1007/978-981-15-6082-8_5
83. Szanto M, Gupte R, Kraus WL, Pacher P, Bai P, Parps in lipid metabolism and related diseases. *Prog Lipid Res* (2021) 84:101117. doi: 10.1016/j.plipres.2021.101117
84. Wang L, Cai Y, Jian L, Cheung CW, Zhang L, Xia Z. Impact of peroxisome proliferator-activated receptor-alpha on diabetic cardiomyopathy. *Cardiovasc Diabetol* (2021) 20(1):2. doi: 10.1186/s12933-020-01188-0
85. Chen W, Xia Y, Zhao X, Wang H, Chen W, Yu M, et al. The critical role of astragalus polysaccharides for the improvement of pparalpha [correction of pparalpha]-mediated lipotoxicity in diabetic cardiomyopathy. *PLoS One* (2012) 7(10):e45541. doi: 10.1371/journal.pone.0045541
86. Oishi K, Shirai H, Ishida N. Clock is involved in the circadian transactivation of peroxisome-proliferator-activated receptor alpha (Pparalpha) in mice. *Biochem J* (2005) 386(Pt 3):575–81. doi: 10.1042/BJ20041150
87. Canaple L, Rambaud J, Dkhissi-Benyahya O, Rayet B, Tan NS, Michalik L, et al. Reciprocal regulation of brain and muscle arnt-like protein 1 and peroxisome proliferator-activated receptor alpha defines a novel positive feedback loop in the rodent liver circadian clock. *Mol Endocrinol* (2006) 20(8):1715–27. doi: 10.1210/me.2006-0052
88. Zhong X, Yu J, Frazier K, Weng X, Li Y, Cham CM, et al. Circadian clock regulation of hepatic lipid metabolism by modulation of M(6)a mrna methylation. *Cell Rep* (2018) 25(7):1816–28.e4. doi: 10.1016/j.celrep.2018.10.068
89. Young ME, Wilson CR, Razeghi P, Guthrie PH, Taegtmeier H. Alterations of the circadian clock in the heart by streptozotocin-induced diabetes. *J Mol Cell Cardiol* (2002) 34(2):223–31. doi: 10.1006/jmcc.2001.1504
90. Galloway CA, Yoon Y. Mitochondrial dynamics in diabetic cardiomyopathy. *Antioxid Redox Signal* (2015) 22(17):1545–62. doi: 10.1089/ars.2015.6293
91. Tang Z, Wang P, Dong C, Zhang J, Wang X, Pei H. Oxidative stress signaling mediated pathogenesis of diabetic cardiomyopathy. *Oxid Med Cell Longev* (2022) 2022:5913374. doi: 10.1155/2022/5913374
92. Anderson EJ, Kypon AP, Rodriguez E, Anderson CA, Lehr EJ, Neuffer PD. Substrate-specific derangements in mitochondrial metabolism and redox balance in the atrium of the type 2 diabetic human heart. *J Am Coll Cardiol* (2009) 54(20):1891–8. doi: 10.1016/j.jacc.2009.07.031
93. Jarosz J, Ghosh S, Delbridge LM, Petzer A, Hickey AJ, Crampin EJ, et al. Changes in mitochondrial morphology and organization can enhance energy supply from mitochondrial oxidative phosphorylation in diabetic cardiomyopathy. *Am J Physiol Cell Physiol* (2017) 312(2):C190–C7. doi: 10.1152/ajpcell.00298.2016

94. Kaluderac N, Di Lisa F. Mitochondrial ros formation in the pathogenesis of diabetic cardiomyopathy. *Front Cardiovasc Med* (2020) 7:12. doi: 10.3389/fcvm.2020.00012
95. Yu T, Sheu SS, Robotham JL, Yoon Y. Mitochondrial fission mediates high glucose-induced cell death through elevated production of reactive oxygen species. *Cardiovasc Res* (2008) 79(2):341–51. doi: 10.1093/cvr/cvn104
96. Yu T, Robotham JL, Yoon Y. Increased production of reactive oxygen species in hyperglycemic conditions requires dynamic change of mitochondrial morphology. *Proc Natl Acad Sci U S A* (2006) 103(8):2653–8. doi: 10.1073/pnas.0511154103
97. Quintana-Cabrera R, Manjarres-Raza I, Vicente-Gutierrez C, Corrado M, Bolanos JP, Scorrano L. Opa1 relies on cristae preservation and atp synthase to curtail reactive oxygen species accumulation in mitochondria. *Redox Biol* (2021) 41:101944. doi: 10.1016/j.redox.2021.101944
98. Tsushima K, Bugger H, Wende AR, Soto J, Jensen GA, Tor AR, et al. Mitochondrial reactive oxygen species in lipotoxic hearts induce post-translational modifications of Akap121, Drp1, and Opa1 that promote mitochondrial fission. *Circ Res* (2018) 122(1):58–73. doi: 10.1161/CIRCRESAHA.117.311307
99. Makino A, Scott BT, Dillmann WH. Mitochondrial fragmentation and superoxide anion production in coronary endothelial cells from a mouse model of type 1 diabetes. *Diabetologia* (2010) 53(8):1783–94. doi: 10.1007/s00125-010-1770-4
100. Abdel-Rahman EA, Hosseiny S, Aaliya A, Adel M, Yasseen B, Al-Okda A, et al. Sleep/Wake calcium dynamics, respiratory function, and ros production in cardiac mitochondria. *J Adv Res* (2021) 31:35–47. doi: 10.1016/j.jare.2021.01.006
101. Nayak N, Mishra M. High fat diet induced abnormalities in metabolism, growth, behavior, and circadian clock in drosophila melanogaster. *Life Sci* (2021) 281:119758. doi: 10.1016/j.lfs.2021.119758
102. de Jesus DS, Bargi-Souza P, Cruzat V, Yechoor V, Carpinelli AR, Pelicari-Garcia RA. Bmal1 modulates ros generation and insulin secretion in pancreatic beta-cells: an effect possibly mediated Via Nox2. *Mol Cell Endocrinol* (2022) 555:111725. doi: 10.1016/j.mce.2022.111725
103. Rabinovich-Nikitin I, Rasouli M, Reitz CJ, Posen I, Margulets V, Dhingra R, et al. Mitochondrial autophagy and cell survival is regulated by the circadian clock gene in cardiac myocytes during ischemic stress. *Autophagy* (2021) 17(11):3794–812. doi: 10.1080/15548627.2021.1938913
104. Sun Q, Yang Y, Wang Z, Yang X, Gao Y, Zhao Y, et al. Per1 interaction with Gpx1 regulates metabolic homeostasis under oxidative stress. *Redox Biol* (2020) 37:101694. doi: 10.1016/j.redox.2020.101694
105. Liu X, Xiao W, Jiang Y, Zou L, Chen F, Xiao W, et al. Bmal1 regulates the redox rhythm of Hspb1, and homoxidized Hspb1 attenuates the oxidative stress injury of cardiomyocytes. *Oxid Med Cell Longev* (2021) 2021:5542815. doi: 10.1155/2021/5542815
106. Dia M, Gomez L, Thibault H, Tessier N, Leon C, Chouabe C, et al. Reduced reticulum-mitochondria Ca(2+) transfer is an early and reversible trigger of mitochondrial dysfunctions in diabetic cardiomyopathy. *Basic Res Cardiol* (2020) 115(6):74. doi: 10.1007/s00395-020-00835-7
107. Diaz-Juarez J, Suarez JA, Dillmann WH, Suarez J. Mitochondrial calcium handling and heart disease in diabetes mellitus. *Biochim Biophys Acta Mol Basis Dis* (2021) 1867(1):165984. doi: 10.1016/j.bbdis.2020.165984
108. Frieden M, James D, Castelbou C, Danckaert A, Martinou JC, Demareux N. Ca (2+) homeostasis during mitochondrial fragmentation and perinuclear clustering induced by Hfist1. *J Biol Chem* (2004) 279(21):22704–14. doi: 10.1074/jbc.M312366200
109. Favaro G, Romanello V, Varanita T, Andrea Desbats M, Morbidoni V, Tezze C, et al. Drp1-mediated mitochondrial shape controls calcium homeostasis and muscle mass. *Nat Commun* (2019) 10(1):2576. doi: 10.1038/s41467-019-10226-9
110. Mohan S, Nair A, Poornima MS, Raghu KG. Vanillic acid mitigates hyperinsulinemia induced σ stress mediated altered calcium homeostasis, mams distortion and surplus lipogenesis in Hepg2 cells. *Chem Biol Interact* (2023), 375:110365. doi: 10.1016/j.cbi.2023.110365
111. Chen Y, Csordas G, Jowdy C, Schneider TG, Csordas N, Wang W, et al. Mitofusin 2-containing mitochondrial-reticular microdomains direct rapid cardiomyocyte bioenergetic responses Via interorganelle Ca(2+) crosstalk. *Circ Res* (2012) 111(7):863–75. doi: 10.1161/CIRCRESAHA.112.266585
112. Seidlmayer LK, Mages C, Berber A, Eder-Negrin P, Arias-Loza PA, Kaspar M, et al. Mitofusin 2 is essential for Ip3-mediated Sr/Mitochondria metabolic feedback in ventricular myocytes. *Front Physiol* (2019) 10:733. doi: 10.3389/fphys.2019.00733
113. Cartes-Saavedra B, Macuada J, Lagos D, Arancibia D, Andres ME, Yu-Wai-Man P, et al. Opa1 modulates mitochondrial Ca(2+) uptake through er-mitochondria coupling. *Front Cell Dev Biol* (2021) 9:774108. doi: 10.3389/fcell.2021.774108
114. Pfeffer M, Muller CM, Mordel J, Meissl H, Ansari N, Deller T, et al. The mammalian molecular clockwork controls rhythmic expression of its own input pathway components. *J Neurosci* (2009) 29(19):6114–23. doi: 10.1523/JNEUROSCI.0275-09.2009
115. Pelletier-Galarneau M, Detmer FJ, Petibon Y, Normandin M, Ma C, Alpert NM, et al. Quantification of myocardial mitochondrial membrane potential using pet. *Curr Cardiol Rep* (2021) 23(6):70. doi: 10.1007/s11886-021-01500-8
116. Chen LB. Mitochondrial membrane potential in living cells. *Annu Rev Cell Biol* (1988) 4:155–81. doi: 10.1146/annurev.cb.04.110188.001103
117. Wolf DM, Segawa M, Kondadi AK, Anand R, Bailey ST, Reichert AS, et al. Individual cristae within the same mitochondrion display different membrane potentials and are functionally independent. *EMBO J* (2019) 38(22):e101056. doi: 10.15252/emboj.2018101056
118. Lemasters JJ, Qian T, He L, Kim JS, Elmore SP, Cascio WE, et al. Role of mitochondrial inner membrane permeabilization in necrotic cell death, apoptosis, and autophagy. *Antioxid Redox Signal* (2002) 4(5):769–81. doi: 10.1089/152308602760598918
119. Korshunov SS, Skulachev VP, Starkov AA. High protonic potential actuates a mechanism of production of reactive oxygen species in mitochondria. *FEBS Lett* (1997) 416(1):15–8. doi: 10.1016/s0014-5793(97)01159-9
120. Hu L, Ding M, Tang D, Gao E, Li C, Wang K, et al. Targeting mitochondrial dynamics by regulating Mfn2 for therapeutic intervention in diabetic cardiomyopathy. *Theranostics* (2019) 9(13):3687–706. doi: 10.7150/tno.33684
121. Song Z, Chen H, Fiket M, Alexander C, Chan DC. Opa1 processing controls mitochondrial fusion and is regulated by mrna splicing, membrane potential, and Yme1l. *J Cell Biol* (2007) 178(5):749–55. doi: 10.1083/jcb.200704110
122. Wu QR, Zheng DL, Liu PM, Yang H, Li LA, Kuang SJ, et al. High glucose induces Drp1-mediated mitochondrial fission Via the Ora1 calcium channel to participate in diabetic cardiomyocyte hypertrophy. *Cell Death Dis* (2021) 12(2):216. doi: 10.1038/s41419-021-03502-4
123. Isobe Y, Hida H, Nishino H. Circadian rhythm of metabolic oscillation in suprachiasmatic nucleus depends on the mitochondrial oxidation state, reflected by cytochrome c oxidase and lactate dehydrogenase. *J Neurosci Res* (2011) 89(6):929–35. doi: 10.1002/jnr.22609
124. Andersen AZ, Poulsen AK, Brasen JC, Olsen LF. On-line measurements of oscillating mitochondrial membrane potential in glucose-fermenting saccharomyces cerevisiae. *Yeast* (2007) 24(9):731–9. doi: 10.1002/yea.1508
125. Oliva-Ramirez J, Moreno-Altamirano MM, Pineda-Olvera B, Cauch-Sanchez P, Sanchez-Garcia FJ. Crosstalk between circadian rhythmicity, mitochondrial dynamics and macrophage bactericidal activity. *Immunology* (2014) 143(3):490–7. doi: 10.1111/imm.12329
126. Zheng H, Zhu H, Liu X, Huang X, Huang A, Huang Y. Mitophagy in diabetic cardiomyopathy: roles and mechanisms. *Front Cell Dev Biol* (2021) 9:750382. doi: 10.3389/fcell.2021.750382
127. Kobayashi S, Patel J, Zhao F, Huang Y, Kobayashi T, Liang Q. Novel dual-fluorescent mitophagy reporter reveals a reduced mitophagy flux in type 1 diabetic mouse heart. *J Am Osteopath Assoc* (2020) 120(7):446–55. doi: 10.7556/jaoa.2020.072
128. Yu LM, Dong X, Xue XD, Xu S, Zhang X, Xu YL, et al. Melatonin attenuates diabetic cardiomyopathy and reduces myocardial vulnerability to ischemia-reperfusion injury by improving mitochondrial quality control: role of Sirt6. *J Pineal Res* (2021) 70(1):e12698. doi: 10.1111/jpi.12698
129. Fritsch LE, Moore ME, Sarraf SA, Pickrell AM. Ubiquitin and receptor-dependent mitophagy pathways and their implication in neurodegeneration. *J Mol Biol* (2020) 432(8):2510–24. doi: 10.1016/j.jmb.2019.10.015
130. Chen Y, Dorn GW2nd. Pink1-phosphorylated mitofusin 2 is a parkin receptor for culling damaged mitochondria. *Science* (2013) 340(6131):471–5. doi: 10.1126/science.1231031
131. Ikeda Y, Shirakabe A, Maejima Y, Zhai P, Sciarretta S, Toli J, et al. Endogenous Drp1 mediates mitochondrial autophagy and protects the heart against energy stress. *Circ Res* (2015) 116(2):264–78. doi: 10.1161/CIRCRESAHA.116.303356
132. Wang Y, Han Z, Xu Z, Zhang J. Protective effect of optic atrophy 1 on cardiomyocyte oxidative stress: roles of mitophagy, mitochondrial fission, and Mapk/Erk signaling. *Oxid Med Cell Longev* (2021) 2021:3726885. doi: 10.1155/2021/3726885
133. Li E, Li X, Huang J, Xu C, Liang Q, Ren K, et al. Bmal1 regulates mitochondrial fission and mitophagy through mitochondrial protein Bnip3 and is critical in the development of dilated cardiomyopathy. *Protein Cell* (2020) 11(9):661–79. doi: 10.1007/s13238-020-00713-x
134. Yang L, Zhao D, Ren J, Yang J. Endoplasmic reticulum stress and protein quality control in diabetic cardiomyopathy. *Biochim Biophys Acta* (2015) 1852(2):209–18. doi: 10.1016/j.bbdis.2014.05.006
135. Hetz C, Zhang K, Kaufman RJ. Mechanisms, regulation and functions of the unfolded protein response. *Nat Rev Mol Cell Biol* (2020) 21(8):421–38. doi: 10.1038/s41580-020-0250-z
136. Xu J, Zhou Q, Xu W, Cai L. Endoplasmic reticulum stress and diabetic cardiomyopathy. *Exp Diabetes Res* (2012) 2012:827971. doi: 10.1155/2012/827971
137. Zhang J, Zhang F, Wang Y. Mitofusin-2 enhances mitochondrial contact with the endoplasmic reticulum and promotes diabetic cardiomyopathy. *Front Physiol* (2021) 12:707634. doi: 10.3389/fphys.2021.707634
138. Yuan M, Gong M, Zhang Z, Meng L, Tse G, Zhao Y, et al. Hyperglycemia induces endoplasmic reticulum stress in atrial cardiomyocytes, and mitofusin-2 downregulation prevents mitochondrial dysfunction and subsequent cell death. *Oxid Med Cell Longev* (2020) 2020:6569728. doi: 10.1155/2020/6569728
139. Cao Y, Chen Z, Hu J, Feng J, Zhu Z, Fan Y, et al. Mfn2 regulates high glucose-induced mams dysfunction and apoptosis in podocytes Via perk pathway. *Front Cell Dev Biol* (2021) 9:769213. doi: 10.3389/fcell.2021.769213

140. Munoz JP, Ivanova S, Sanchez-Wandelmer J, Martinez-Cristobal P, Noguera E, Sancho A, et al. Mfn2 modulates the upr and mitochondrial function Via repression of perk. *EMBO J* (2013) 32(17):2348–61. doi: 10.1038/emboj.2013.168
141. Peng L, Men X, Zhang W, Wang H, Xu S, Xu M, et al. Dynamin-related protein 1 is implicated in endoplasmic reticulum stress-induced pancreatic beta-cell apoptosis. *Int J Mol Med* (2011) 28(2):161–9. doi: 10.3892/ijmm.2011.684
142. Yuan G, Hua B, Cai T, Xu L, Li E, Huang Y, et al. Clock mediates liver senescence by controlling er stress. *Aging (Albany NY)* (2017) 9(12):2647–65. doi: 10.18632/aging.101353
143. Cretenet G, Le Clech M, Gachon F. Circadian clock-coordinated 12 hr period rhythmic activation of the Ire1alpha pathway controls lipid metabolism in mouse liver. *Cell Metab* (2010) 11(1):47–57. doi: 10.1016/j.cmet.2009.11.002
144. Gale JE, Cox HI, Qian J, Block GD, Colwell CS, Matveyenko AV. Disruption of circadian rhythms accelerates development of diabetes through pancreatic beta-cell loss and dysfunction. *J Biol Rhythms* (2011) 26(5):423–33. doi: 10.1177/0748730411416341
145. Lee J, Liu R, de Jesus D, Kim BS, Ma K, Moulik M, et al. Circadian control of beta-cell function and stress responses. *Diabetes Obes Metab* (2015) 17 Suppl 1:123–33. doi: 10.1111/dom.12524
146. Zhu B, Zhang Q, Pan Y, Mace EM, York B, Antoulas AC, et al. A cell-autonomous mammalian 12 hr clock coordinates metabolic and stress rhythms. *Cell Metab* (2017) 25(6):1305–19.e9. doi: 10.1016/j.cmet.2017.05.004
147. Ding G, Li X, Hou X, Zhou W, Gong Y, Liu F, et al. Rev-erb in gabaergic neurons controls diurnal hepatic insulin sensitivity. *Nature* (2021) 592(7856):763–7. doi: 10.1038/s41586-021-03358-w
148. Vasquez-Munoz M, Arce-Alvarez A, von Igel M, Veliz C, Ruiz-Esqueda G, Ramirez-Campillo R, et al. Oscillatory pattern of glycemic control in patients with diabetes mellitus. *Sci Rep* (2021) 11(1):5789. doi: 10.1038/s41598-021-84822-5
149. Vasquez-Munoz M, Arce-Alvarez A, Alvarez C, Ramirez-Campillo R, Crespo FA, Arias D, et al. Dynamic circadian fluctuations of glycemia in patients with type 2 diabetes mellitus. *Biol Res* (2022) 55(1):37. doi: 10.1186/s40659-022-00406-1
150. Sankaranarayanan C, Subramanian P. Molecular mechanisms interlinking biological clock and diabetes mellitus: effective tools for better management. *Diabetes Metab Syndr* (2022) 16(11):102639. doi: 10.1016/j.dsx.2022.102639
151. Khan S, Nabi G, Yao L, Siddique R, Sajjad W, Kumar S, et al. Health risks associated with genetic alterations in internal clock system by external factors. *Int J Biol Sci* (2018) 14(7):791–8. doi: 10.7150/ijbs.23744
152. Jakubowicz D, Landau Z, Tsameret S, Wainstein J, Raz I, Ahren B, et al. Reduction in glycated hemoglobin and daily insulin dose alongside circadian clock upregulation in patients with type 2 diabetes consuming a three-meal diet: a randomized clinical trial. *Diabetes Care* (2019) 42(12):2171–80. doi: 10.2337/dc19-1142
153. Javed N, Matveyenko AV. Circadian etiology of type 2 diabetes mellitus. *Physiol (Bethesda)* (2018) 33(2):138–50. doi: 10.1152/physiol.00003.2018
154. Shen S, Liao Q, Wong YK, Chen X, Yang C, Xu C, et al. The role of melatonin in the treatment of type 2 diabetes mellitus and alzheimer's disease. *Int J Biol Sci* (2022) 18(3):983–94. doi: 10.7150/ijbs.66871
155. Rakshit K, Matveyenko AV. Induction of core circadian clock transcription factor Bmal1 enhances beta-cell function and protects against obesity-induced glucose intolerance. *Diabetes* (2021) 70(1):143–54. doi: 10.2337/db20-0192
156. He B, Nohara K, Park N, Park YS, Guillory B, Zhao Z, et al. The small molecule nobiletin targets the molecular oscillator to enhance circadian rhythms and protect against metabolic syndrome. *Cell Metab* (2016) 23(4):610–21. doi: 10.1016/j.cmet.2016.03.007
157. Hirota T, Lee JW, St John PC, Sawa M, Iwasako K, Noguchi T, et al. Identification of small molecule activators of cryptochrome. *Science* (2012) 337(6098):1094–7. doi: 10.1126/science.1223710
158. Solt LA, Wang Y, Banerjee S, Hughes T, Kojetin DJ, Lundasen T, et al. Regulation of circadian behaviour and metabolism by synthetic rev-erb agonists. *Nature* (2012) 485(7396):62–8. doi: 10.1038/nature11030
159. Luo X, Song S, Qi L, Tien CL, Li H, Xu W, et al. Rev-erb is essential in cardiac fibroblasts homeostasis. *Front Pharmacol* (2022) 13:899628. doi: 10.3389/fphar.2022.899628
160. Hu L, Guo Y, Song L, Wen H, Sun N, Wang Y, et al. Nicotinamide riboside promotes Mfn2-mediated mitochondrial fusion in diabetic hearts through the Sirt1-Pgc1alpha-Pparalpha pathway. *Free Radic Biol Med* (2022) 183:75–88. doi: 10.1016/j.freeradbiomed.2022.03.012
161. Dusabimana T, Kim SR, Kim HJ, Park SW, Kim H. Nobiletin ameliorates hepatic ischemia and reperfusion injury through the activation of sirt-1/Foxo3a-Mediated autophagy and mitochondrial biogenesis. *Exp Mol Med* (2019) 51(4):1–16. doi: 10.1038/s12276-019-0245-z
162. Humphries PS, Bersot R, Kincaid J, Mabery E, McCluskie K, Park T, et al. Carbazole-containing sulfonamides and sulfamides: discovery of cryptochrome modulators as antidiabetic agents. *Bioorg Med Chem Lett* (2016) 26(3):757–60. doi: 10.1016/j.bmcl.2015.12.102
163. Andersen PAK, Petrenko V, Rose PH, Koomen M, Fischer N, Ghiasi SM, et al. Proinflammatory cytokines perturb mouse and human pancreatic islet circadian rhythmicity and induce uncoordinated beta-cell clock gene expression via nitric oxide, lysine deacetylases, and immunoproteasomal activity. *Int J Mol Sci* (2020) 22(1):83. doi: 10.3390/ijms22010083
164. Ding M, Feng N, Tang D, Feng J, Li Z, Jia M, et al. Melatonin prevents Drp1-mediated mitochondrial fission in diabetic hearts through Sirt1-Pgc1alpha pathway. *J Pineal Res* (2018) 65(2):e12491. doi: 10.1111/jpi.12491



OPEN ACCESS

EDITED BY

Ping Zeng,
Xuzhou Medical University, China

REVIEWED BY

Kevin Sean Kimbro,
Morehouse School of Medicine,
United States
Jacqueline Valverde-Villegas,
UMR5535 Institut de Génétique
Moléculaire de Montpellier (IGMM), France

*CORRESPONDENCE

Ronghuai Zhang
✉ science_game@126.com

RECEIVED 27 February 2023

ACCEPTED 12 May 2023

PUBLISHED 25 May 2023

CITATION

Wei T, Zhu Z, Liu L, Liu B, Wu M, Zhang W,
Cui Q, Liu F and Zhang R (2023) Circulating
levels of cytokines and risk of
cardiovascular disease: a Mendelian
randomization study.
Front. Immunol. 14:1175421.
doi: 10.3389/fimmu.2023.1175421

COPYRIGHT

© 2023 Wei, Zhu, Liu, Liu, Wu, Zhang, Cui,
Liu and Zhang. This is an open-access article
distributed under the terms of the [Creative
Commons Attribution License \(CC BY\)](#). The
use, distribution or reproduction in other
forums is permitted, provided the original
author(s) and the copyright owner(s) are
credited and that the original publication in
this journal is cited, in accordance with
accepted academic practice. No use,
distribution or reproduction is permitted
which does not comply with these terms.

Circulating levels of cytokines and risk of cardiovascular disease: a Mendelian randomization study

Tao Wei¹, Zhanfang Zhu², Lin Liu¹, Bo Liu¹, Min Wu³,
Wei Zhang¹, Qianwei Cui¹, Fuqiang Liu¹ and Ronghuai Zhang^{1*}

¹Department of Cardiology, Shaanxi Provincial People's Hospital, Xi'an, China, ²Department of General Internal Medicine, Xi'an Jiaotong University Hospital, Xi'an, China, ³Shaanxi Provincial Key Laboratory of Infection and Immune Diseases, Shaanxi Provincial People's Hospital, Xi'an, China

Background: Epidemiological studies have linked various circulating cytokines to cardiovascular disease (CVD), which however remains uncertain whether these relationships represent causality or are due to bias. To address this question, we conducted a Mendelian randomization (MR) analysis to systematically investigate the causal effects of circulating cytokine levels on CVD development.

Methods: This study leveraged the summary statistic from respective genome-wide association study (GWAS) of 47 cytokines and four types of CVD. The *cis*-quantitative trait locus (*cis*-QTL) definition, derived from a GWAS meta-analysis comprising 31,112 participants of European descent, served as instruments for cytokines. A two-sample MR design was employed, followed by comprehensive sensitivity analyses to validate the robustness of results.

Results: The results of inverse-variance weighted method using *cis*-protein QTL (*cis*-pQTL) instruments, showed the causal effects of four cytokines (i.e., IL-1ra, MCSF, SeSelectin, SCF) on the risk of coronary artery disease (CAD). We also identified causal relationships between two cytokines (i.e., IL-2ra, IP-10) and heart failure (HF), as well as two cytokines (i.e., MCP-3, SeSelectin) and atrial fibrillation (AF), after controlling for false discovery rate (FDR). The use of *cis*-expression QTL (*cis*-eQTL) revealed additional causal associations between IL-1a, MIF and CAD, between IL-6, MIF, and HF, as well as between FGFBasic and AF. No significant sign was survived for stroke with FDR applied. Results were largely consistent across sensitivity analyses.

Conclusion: The present study provides supportive evidence that genetic predisposition to levels of certain cytokines causally affects the development of specific type of CVD. These findings have important implications for the creation of novel therapeutic strategies targeting these cytokines as a means of preventing and treating CVD.

KEYWORDS

circulating cytokines, cardiovascular disease, Mendelian randomization, *cis*-quantitative trait locus, European

Introduction

Cardiovascular disease (CVD), a cluster of disorders that impact the heart and/or blood vessels, is a foremost cause of death and disability worldwide. In 2019, it is estimated that 17.9 million deaths were attributed to CVD, ranking the first leading cause of all global death (1). CVD has a complex etiology and often develops over decades before an obvious symptomatic event. Early intervention is vital to reduce morbidity and mortality from CVD, which would produce a far-reaching influence on the public health burden. Therefore, improved understanding of the causal effect of different risk factors, especially at the microscale and molecular levels, can refine prevention strategies and enable novel targets for therapeutic intervention in CVD.

Cytokines act a crucial part in regulating the inflammatory response, altering vasoconstriction and impeding endothelium-dependent vasodilation, and therefore, they may offer potential targets for preventing CVD (2). Extensive epidemiological evidence has documented strong associations between cytokines and CVD. For instance, a meta-analysis comprising 29 cohort studies demonstrated that several cytokines, such as interleukin-6 (IL-6), IL-18, and tumour necrosis factor alpha (TNF- α), each were associated with the risk of developing coronary artery disease (CAD), in an approximately log-linear manner, independent of traditional risk factors (3). Another study involving 17,180 individuals found the positive relationship of circulating levels of monocyte chemoattractant protein-1 (MCP-1) with long-term risk of stroke (4). However, classical observational designs are prone to reverse causation and confounding that hinder causal inference, and conducting clinical trials on cytokine interventions are challenging.

Mendelian randomization (MR) is a robust technology that can address the limitations accompanying observational studies mentioned above and provides the highest level of evidence hierarchy other than randomized controlled trials by leveraging genetic variants as instrumental variables (IVs) (5). This method, when certain assumptions are satisfied, could determine causality of a

given exposure-outcome association. Indeed, two successive MR analyses have helped identify the causal effect of IL-6 on the development of CAD and total CVD, indicating that IL-6 blockade may serve as a novel therapeutic target (6, 7). And the extent of this benefit may be directly proportional to the degree of reduction in levels of high-sensitivity C-reactive protein (hsCRP) (6, 7). Additionally, several MR studies have also explored the causal impact of circulating cytokines on stroke (8, 9). However, the most of existing efforts were focused on one particular type of CVD or a single pro-inflammatory cytokine, leaving other cardiovascular events such as heart failure (HF) and atrial fibrillation (AF) less explored. Herein, we applied a two-sample MR framework to systematically ascertain whether there was a causality between a broad range of cytokines and the risk of CVD which encompasses CAD, HF, AF, and stroke.

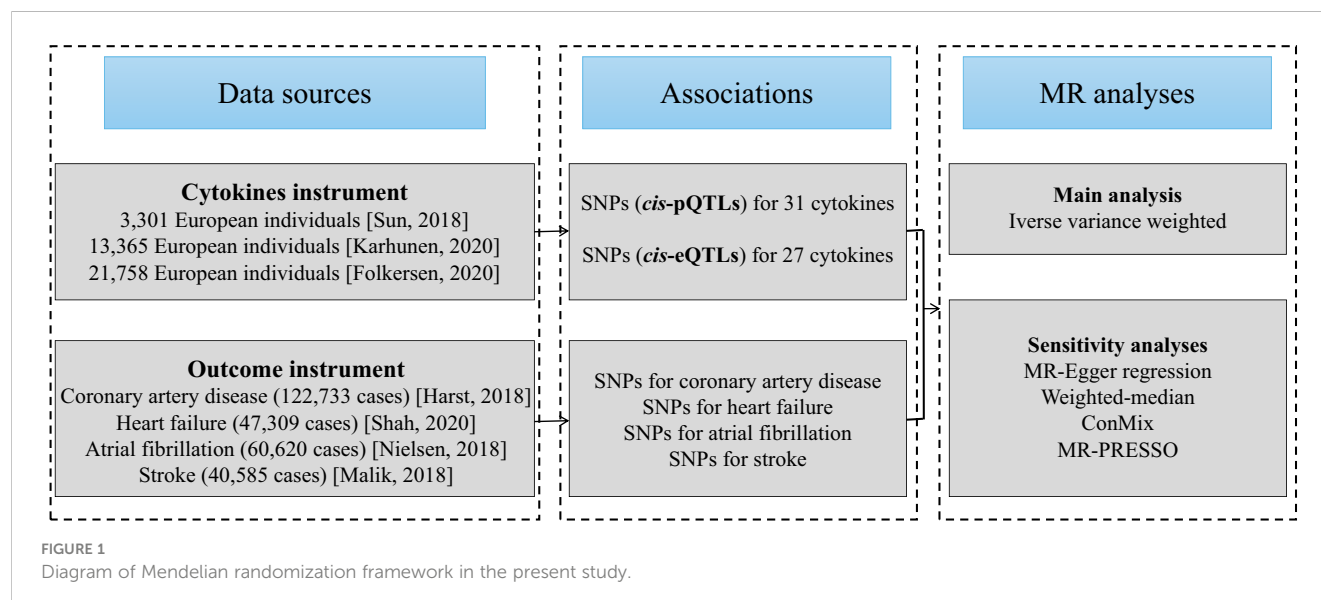
Methods

Study design

The flowchart of the current work is outlined in Figure 1. To begin, we selected genetic variants as IVs for circulating cytokines. Next, latest summary statistics from the corresponding genome-wide association studies (GWASs) for CAD, HF, AF, and stroke were collected. Then, we performed a two-sample MR study with inverse-variance weighted (IVW) method as our primary analysis. Finally, a series of sensitivity analyses were followed, including MR-Egger regression, weighted-median, contamination mixture (ConMix), and MR-Pleiotropy Residual Sum and Outlier (MR-PRESSO).

Data sources and instrumental variable selection

The present study relies on publicly available summary statistics from published studies, and therefore no additional



ethical approval from the institutional review board was required. The characteristics of data used in this study are shown in [Table 1](#).

For the cytokines as exposures, we acquired the IVs from the most up-to-date GWAS meta-analysis of three independent sources (10) [i.e., the SCALLOP consortium (11), the INTERVAL study (12), and a the Northern Finland Birth Cohort 1966 (13)], which include a total of 31,112 subjects of European ancestry. Details on the methods of SNP selection and meta-analysis can be found in the original paper (10).

For the outcomes, the summary-level data for CAD (122,733 cases and 424,528 controls), HF (47,309 cases and 930,014 controls), AF (60,620 cases and 970,216 controls), and stroke (40,585 cases and 40,6111 controls) were derived from CARDIoGRAMplusC4D Consortium (14), HERMES Consortium (15), a GWAS conducted by Nielsen et al. (16), and MEGASTROKE Consortium (17), respectively. These study populations were predominantly of European descent. There is no obvious sample overlap between the GWAS meta-analyses of cytokines and four investigated cardiovascular diseases.

MR relies on three IV assumptions to ensure the accuracy of causal inferences (1): IVs must truly be associated with exposures (2), independent of confounders, and (3) affect outcomes solely through exposures, not through any other pathways. To better ensure that the selected IVs satisfy the above three assumptions, especially for the first and the third, we here used *cis* quantitative trait locus (QTLs) as IVs to enhance instrument strength, including *cis*-protein QTLs (*cis*-pQTLs, gene range \pm 500kb) and *cis*-expression QTLs (*cis*-eQTLs, gene range \pm 500kb). These *cis*-QTLs, located at or close to the gene of origin, naturally have a stronger correlation with the gene expression and thereafter protein concentrations than other variants. For our main analysis, we used *cis*-pQTLs as the IVs, and for complementary analysis, we used *cis*-eQTLs since *cis*-eQTLs may capture the effects of pQTLs through gene expression, although not all pQTLs are represented by eQTLs (18). Specifically, *cis*-pQTLs and *cis*-eQTLs were associated with the circulating cytokine levels and their gene expression aggregated across tissues, respectively, both met a significant threshold of $1E-4$. Of note, to better balance the number and strength of instrumental variables and obtain potentially informative results, a relatively

loose threshold of $1E-4$ was selected as an alternative to the $5E-8$ threshold used in traditional GWAS. We excluded palindromic variants with a minor allele frequency (MAF) greater than 0.05 and performed clumping by setting a pairwise linkage disequilibrium (LD) cutoff of $r^2 < 0.1$. The alleles of the QTLs were harmonized between the exposure and the outcome to ensure proper alignment of effects. Detailed information on the characteristics of the QTLs used as IVs can be found in the [Supplementary Tables 1, 2](#).

Statistical analyses

We incorporated separate analyses using two different sets of IVs (*cis*-pQTL and *cis*-eQTL) to assess the links between genetically predicted circulating cytokine levels and the risk of each CVD outcome. For cases where there exists only one single QTL, the classic Wald ratio was adopted to gain MR estimates. Otherwise, the random-effects IVW model using a meta-analysis approach was performed to combine the Wald ratios of multiple QTLs to obtain overall MR estimates (19). IVW is generally considered to provide unbiased estimates of the causal effect of the exposure on the outcome, provided that the three assumptions mentioned above are met. Furthermore, we conducted sensitivity analyses using four pleiotropy-robust methods, namely MR-Egger regression (20), weighted-median method (21), ConMix (22), and MR-PRESSO (23). Different methods could yield valid results under different model assumptions with the criterion relaxed to some extent. The weighted-median estimator is capable of providing a valid estimation even when 50% IVs are invalid. The MR-Egger regression is sensitive to the presence of horizontal pleiotropy across IVs, but it depends on the Instrument Strength Independent of Direct Effect (InSIDE) assumption, where the genetic variant used as an instrument affects the outcome only through the exposure of interest and not through any other pathway that could confound the association between the exposure and the outcome. The method ConMix could estimate the causal effect with implicitly distinguishing valid and invalid IVs using an underlying mixture model. MR-PRESSO can obtain consistent causal estimates by horizontal pleiotropic outlier (if it is noted) removal. These

TABLE 1 Characteristics of data in this study.

Phenotype	PMID	Available year	Source	Sample size	Ancestry
Exposures					
Cytokines	33067605	2020	SCALLOP Consortium	21,758	100% European
	–	2020	Karhunen et al.	13,365	100% European
	29875488	2018	INTERVAL Study	3,301	100% European
Outcomes					
Coronary artery disease	29212778	2018	CARDIoGRAMplusC4D Consortium	122,733 cases and 424,528 controls	77% European
Heart failure	31919418	2020	HERMES Consortium	47,309 cases and 930,014 controls	100% European
Atrial fibrillation	30061737	2018	Nielsen et al.	60,620 cases and 970,216 controls	100% European
Stroke	29531354	2018	MEGASTROKE Consortium	40,585 cases and 40,6111 controls	100% European

methods rely on different assumptions to each other which are difficult to prove, and if the results from all of these different analyses are largely consistent, then the investigator can be more confident in drawing conclusions regarding causality. Moreover, the Cochran's Q test in the IVW and the intercept from MR-Egger method were deployed to test the heterogeneity and horizontal pleiotropy, with a P -value < 0.05 , respectively. The original paper provided information on the proportion of variance (R^2) that each cytokine has explained by the QTLs and F -statistics that quantified the strength of the IVs (10). We further calculated the cumulative F -statistics and an F -statistic > 10 was considered to avoid weak instrument bias (24). The statistical power of our entire MR analyses was estimated utilizing the non-centrality parameter-based approach proposed by Brion et al. on the online tool (<https://shiny.cnsgenomics.com/mRnd/>) (25). Lastly, correlation analysis was done to illustrate the mutual corroboration or complementary of results under two instruments strategies.

All statistical analyses were implemented using the "TwoSampleMR" (version 0.5.6), "MendelianRandomization"

(version 0.6.0), and "MR-PRESSO" (version 1.0) packages in R (version 4.1.2). To address the issue of multiple comparisons for the numerous cytokines, we performed the stratified false discovery rate (FDR) approach using Benjamini-Hochberg procedure for IVW analysis, i.e., estimating adjusted P -value separately for each CVD outcome (26). Additionally, we also utilized the aggregated FDR correction to complement our results. The statistical significance was defined using a threshold of adjusted P -value $< 10\%$.

Results

To unravel the causal effect of all analyzable cytokines (shown in Table 2) on the risk of four types of CVD (i.e., CAD, HF, AF, stroke), two-sample MR tests were carried out. Of 35 cytokines analyzed, 31 cytokines possessed *cis*-pQTL instruments, explaining 0.1% to 28.9% of the phenotypic variance, and 27 cytokines possessed *cis*-eQTL instruments, explaining 0.04% to 13.0% of the phenotypic variance. Cumulative F -statistics of *cis*-pQTL for 29 out

TABLE 2 Instruments for each studied cytokine in the *cis*-pQTL and *cis*-eQTL analyses.

Cytokine	Gene	<i>cis</i> -pQTL			<i>cis</i> -eQTL		
		No. SNPs	R^2	F -statistic	No. SNPs	R^2	F -statistic
activePAI	SERPINE1	1	0.003	16	–	–	
bNGF	NGF	–	–		1	0.002	7
CTACK	CCL27	3	0.060	75	2	0.041	77
Eotaxin	CCL11	6	0.015	29	4	0.010	30
FGFBasic	FGF2	–	–		2	0.002	8
GROa	CXCL1	11	0.272	186	1	0.127	993
HGF	HGF	6	0.010	19	–	–	
IL-16	IL16	18	0.037	44	6	0.031	114
IL-18	IL18	5	0.051	71	2	0.024	86
IL-1a	IL1A	–	–		3	0.003	5
IL-1ra	IL1RN	18	0.075	79	2	0.017	165
IL-2ra	IL2RA	14	0.260	72	4	0.130	128
IL-6	IL6	1	0.002	16	1	0.001	8
IL-7	IL7	1	0.005	16	–	–	
IL-8	CXCL8	1	0.004	72	2	0.005	41
IL-12p70	IL12A	1	0.002		–	–	
IL-12p70	IL12B	1	0.002		–	–	
IP-10	CXCL10	5	0.020	35	–	–	
MCP-1	CCL2	28	0.006	4	3	0.001	8
MCP-3	CCL7	13	0.289	77	–	–	
MCSF	CSF1	13	0.049	62	3	0.018	93
MIF	MIF	2	0.019	34	5	0.020	14

(Continued)

TABLE 2 Continued

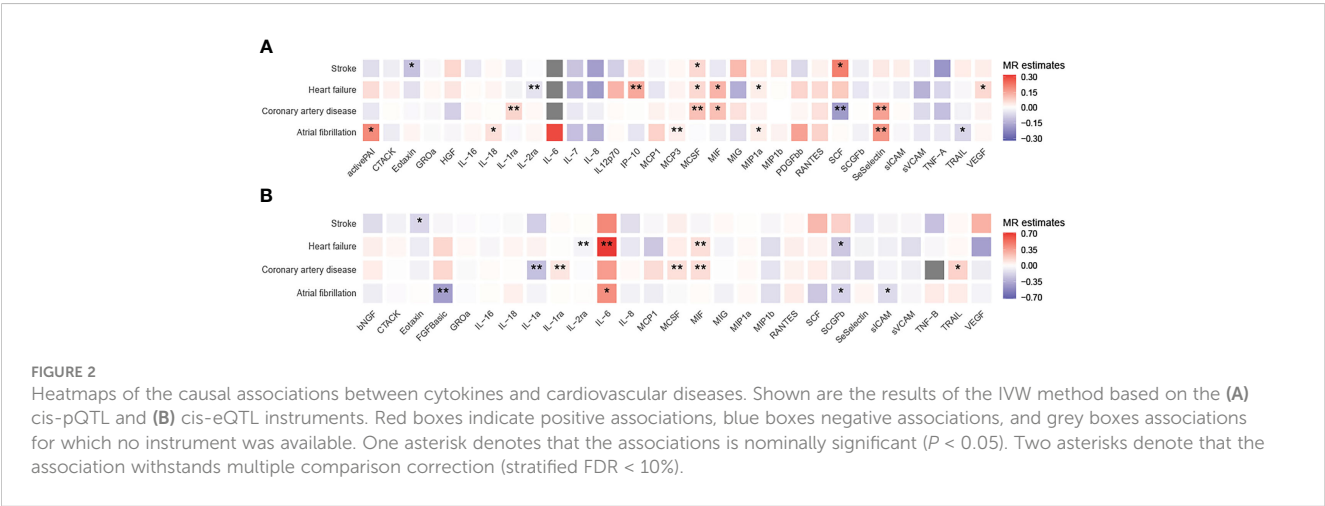
Cytokine	Gene	<i>cis</i> -pQTL			<i>cis</i> -eQTL		
		No. SNPs	R ²	F-statistic	No. SNPs	R ²	F-statistic
MIG	CXCL9	1	0.011	41	2	0.008	15
MIP1a	CCL3	34	0.217	111	1	0.059	1194
MIP1b	CCL4	26	0.147	67	3	0.003	12
PDGFbb	PDGFB	1	0.001	18	–	–	
RANTES	CCL5	1	0.009	31	1	0.009	31
SCF	KITLG	3	0.006	30	2	0.001	7
SCGFb	CLEC11A	2	0.016	57	1	0.004	28
SeSelectin	SELE	2	0.008	91	2	0.002	7
sICAM	ICAM1	25	0.168	35	2	0.004	11
sVCAM	VCAM1	1	0.003	16	1	0.003	16
TNF-A	TNF	2	0.004	19	–	–	
TNF-B	LTA	–	–		1	0.001	5
TRAIL	TNFSF10	46	0.027	7	5	0.006	14
VEGF	VEGFA	21	0.073	105	1	0.0004	10

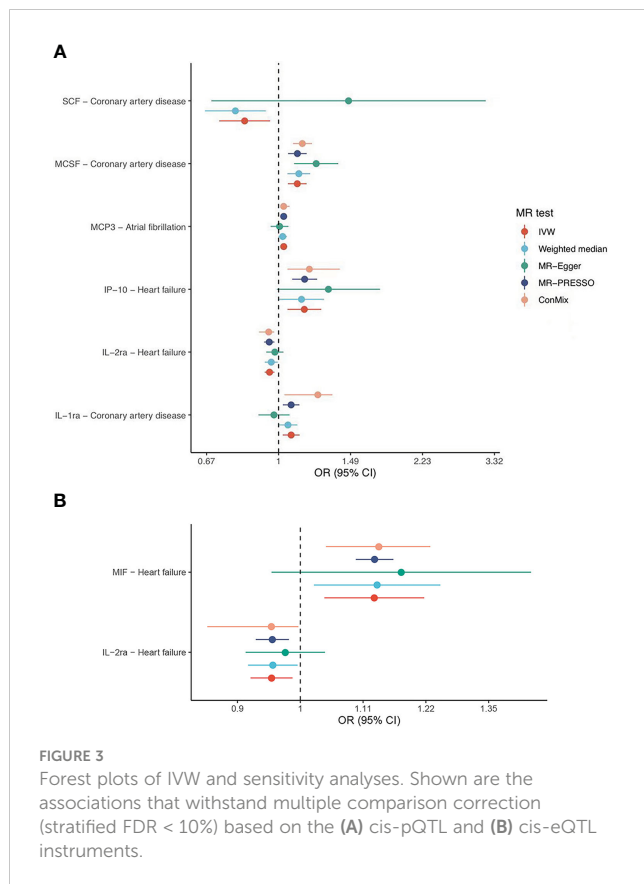
activePAI, active plasminogen activator inhibitor-1; bNGF, beta nerve growth factor; CTACK, cutaneous T-cell attracting chemokine; FGFBasic, basic fibroblast growth factor; GROa, growth-regulated oncogene-alpha; HGF, hepatocyte growth factor; IL, interleukin; ra, receptor antagonist; IP-10, interferon gamma-induced protein 10; MCP-1, monocyte chemotactic protein-1; MCP-3, monocyte chemotactic protein-3; MCSF, macrophage colony-stimulating factor; MIF, macrophage migration inhibitory factor; MIG, monokine induced by interferon-gamma; MIP, macrophage inflammatory protein; PDGFbb, platelet-derived growth factor BB; SCF, stem cell factor; SCGFb, stem cell growth factor beta; SeSelectin, soluble E-selectin; sICAM, soluble intercellular adhesion molecule; sVCAM, soluble vascular cell adhesion molecule; TNF, tumour necrosis factor; TRAIL, TNF-related apoptosis inducing ligand; VEGF, vascular endothelial growth factor.

of 31 cytokines were greater than 10, proving the good strength of genetic instruments (Table 2). Detailed MR results for the causal relationship of interests are shown in Supplementary Table 3 (based on the *cis*-pQTL instruments) and Supplementary Table 4 (based on the *cis*-eQTL instruments). The visualization of all IVW results is presented in Figure 2 and only significant IVW results (stratified FDR < 10%) with sensitivity analyses are shown in Figure 3. Furthermore, the results of the two correction strategies (stratified FDR vs. aggregated FDR) did not differ significantly.

Using the *cis*-pQTL instruments in IVW analysis, genetic predicated higher levels of four cytokines had a suggestive

association with an increased risk of CAD, including IL-1ra (interleukin-1 receptor antagonist, odds ratio [OR]: 1.07, 95% confidence interval [CI]: 1.02-1.12, *P*: 0.004), MCSF (macrophage colony-stimulating factor, OR: 1.11, 95% CI: 1.05-1.17, *P*: 8.88E-05), MIF (macrophage inflammatory protein, OR: 1.11, 95% CI: 1.02-1.22, *P*: 0.021), SeSelectin (soluble E-selectin, OR: 1.17, 95% CI: 1.04-1.31, *P*: 0.007), while one cytokine, SCF (stem cell factor, OR: 0.83, 95% CI: 0.72-0.95, *P*: 0.009), to a lower risk of CAD. After stratified FDR correction, the significance of MIF results was not remained. As expected, when using the *cis*-eQTL instruments and similarly estimated by IVW, most of findings from our main





analysis including IL-1ra, MCSF were replicated, yet the MIF (OR: 1.13, 95% CI: 1.06-1.22, P : 4.15E-04) maintained notable significant relationship with CAD risk. In addition, we observed the novel evidence regarding IL-1a (OR: 0.77, 95% CI: 0.64-0.92, P : 0.004).

Likewise, tested by IVW method using the *cis*-pQTL instruments, six cytokines (IL-2ra, IP-10 [interferon gamma-induced protein 10], MCSF, MIF, MIP1a, and VEGF [vascular endothelial growth factor]) showed suggestive association with the risk of HF, six cytokines (activePAI [active plasminogen activator inhibitor-1], IL-18, MCP-3, MIP1a, SeSelectin, and TRAIL [TNF-related apoptosis inducing ligand]) with AF, and three cytokines (Eotaxin, MCSF, and SCF) with stroke. When considering the stratified FDR of 10% or less, only two cytokines, IL-2ra (OR: 0.95, 95% CI: 0.93-0.98, P : 2.93E-04) and IP-10 (OR: 1.15, 95% CI: 1.05-1.27, P : 0.003), reached a statistical significance (stratified FDR < 10%) for HF, as well as two cytokines, MCP-3 (OR: 1.03, 95% CI: 1.01-1.05, P : 0.003) and SeSelectin (OR: 1.19, 95% CI: 1.07-1.32, P : 0.002), for AF. No significant sign was survived for stroke after stratified FDR correction. With *cis*-eQTL instruments and stratified FDR adjustment applied, the additional associations between IL-6 (OR: 2.01, 95% CI: 1.27-3.17, P : 0.003), MIF (OR: 1.13, 95% CI: 1.04-1.22, P : 0.004) and HF, as well as FGFBasic (basic fibroblast growth factor) and AF (OR: 0.66, 95% CI: 0.5-0.84, P : 0.001) were captured.

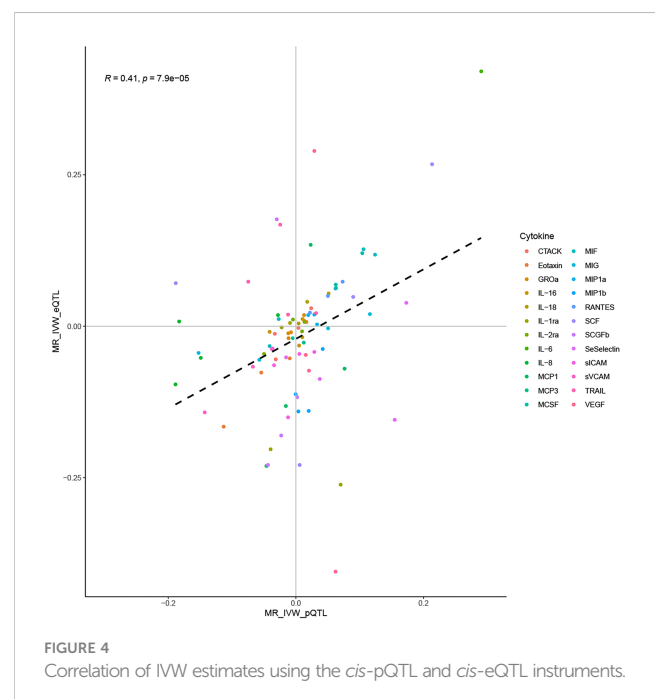
Focused on the associations that withstand multiple comparison correction (stratified FDR < 10%), their corresponding sensitivity analyses indicated roughly the same estimates although several methods yield wide CIs due to less statistical power (refer to

Figure 3). Further examination revealed little evidence of heterogeneity (majority of P -value of Cochran Q statistic > 0.05) or horizontal pleiotropy (majority of P -value of MR-Egger intercept > 0.05), as shown in the Supplementary Tables 5, 6.

Correlation analysis suggested a moderate correlation of IVW estimates obtained using the *cis*-pQTL and *cis*-eQTL instruments (correlation coefficient: 0.41, P : 7.9E-05, Figure 4). Their moderate correlation, combined with the biological background foreshadowed earlier, validated the rationality of using *cis*-pQTL instruments for the main analysis and *cis*-eQTL as a complement. Furthermore, sufficient statistical power was achieved in our MR study to detect the causal associations of cytokines with CVD outcomes, provided they were true. By complementing the statistical power of the two instruments, we attained a power of 100% to detect an OR of 1.2/0.83 for the majority of the associations (Supplementary Tables 7, 8).

Discussion

In our MR analysis, we systematically assessed the causal roles of circulating cytokine levels in the four CVD outcomes. The results provided the strong evidence in favor of the causal relationships of genetic predicted levels of IL-1ra, MCSF, SCF, and SeSelectin with CAD, genetic predicted levels of IL-2ra and IP-10 with HF, as well as genetic predicted levels of MCP-3 and SeSelectin with AF. There was also suggestive evidence supporting causal effect of IL-1a, MIF concentrations on CAD, of IL-6, MIF concentrations on HF, as well as of FGFBasic concentrations on AF. The relationship of circulating cytokine concentrations with stroke were attenuated after correction for multiple comparisons. Using the power of molecular genetic markers as IVs, particularly through the use of



both pQTL and eQTL instruments, our study was able to overcome potential biases and confounders that arise in observational studies. Our results support the hypothesis that manipulating cytokine levels may represent a promising therapeutic strategy for CVD.

Our findings strengthened or extended existing observational evidence, pointing to an essential role played by certain cytokines, including IP-10, IL-6, IL-1ra, and SCF, in the development of CVD. A study combining data from two prospective cohorts suggested that higher concentration of IP-10 was related to the elevated risk of HF but not CAD or stroke, which largely aligns with our own results (27). In addition, our findings regarding IL-6, based on the eQTL instruments, in relation to HF was in line with the results from a case-cohort study (28). A meta-analysis of six population-based cohorts reported that serum IL-1ra level was positively related to the risk of total CVD (29). A 19.2-year follow-up study with 4,742 participants demonstrated that individuals with high levels of SCF have a decreased risk of cardiovascular events (30). Our results add further specificity to these findings, indicating that the IL-1ra and SCF were more likely to represent the causal factors for CAD risk. This conclusion was also confirmed by a recent MR study that used a different set of IVs (31). Nevertheless, the aforementioned MR analysis gave the evidence for the involvement of IL-6 on CAD and AF, which was also consistent with the findings from two previous MR studies that we foreshadowed in the introduction section (6, 7). Due to the limited availability of valid pQTLs for IL-6 and a single SNP as the only eQTL instrument, our study may be underpowered to fully establish its relationship with CVD outcomes. Georgakis et al. found that genetic predicted circulating levels of MCP-1 was positively associated with stroke risk (8), while our study failed to capture this signal. This may be due to different sources of IVs (three independent cohorts v.s. two independent cross-sectional surveys) (32) and different selection criteria ($P < 1e-4$ v.s. $FDR < 5\%$). More studies are needed to further explore. Notably, our study offered some novel insights regarding MCP-3, MCSF, and SeSelectin, which have not been previously found or minimally explored in direct relation to CVD.

Cytokines may have both direct and indirect effects on the cardiovascular system. Direct effects include alterations in the function of the heart and blood vessels such as increased heart rate, reduced blood flow, and changed blood pressure regulation (33, 34). The relationship between cytokines and CVD is complex and multilayered, with the key indirect mechanism mainly being inflammation and oxidative stress (2, 35). Inflammatory cytokines like TNF and IL-6 activate immune cells, such as monocytes and macrophages. On the one hand, activated macrophages release various inflammatory molecules and reactive oxygen species (ROS) which lead to inflammation, oxidative stress, and ultimately, endothelial dysfunction (36). On the other hand, this accumulation of immune cells and other degenerative material in the inner layer of artery walls could lead to the development of atheroma, contributing to cardiovascular events (37). More seriously, oxidative stress and inflammation have a mutually reinforcing positive feedback loop (38, 39). In contrast, anti-inflammatory cytokines like IL-1ra, which was also supported by our study, has ability to block inflammatory signals from IL-1 by binding to the IL-1 receptor (40). In addition, thrombosis caused by platelet activation and increased heart rate

and blood pressure caused by adrenergic activation were also believed to be potential causative pathways induced by cytokines in the development of CVD.

One main strength of the current study is the broad scope of cytokines that we covered, as well as the substantial sample size for each trait of interest that we used, especially for cytokines, which is larger than previously used GWAS (31,112 v.s. 8,293) (32). Another important strength is the utilization of QTLs as IVs, which are in close proximity to the encoding gene region, minimizing the likelihood of horizontal pleiotropy (41). Several limitations should be acknowledged. Firstly, as mentioned early, although a relatively lenient threshold was applied, the limited number of instruments for several cytokines, such as IL-6 and/or MIF, due to the *cis*-instrument definition approach, may result in a less statistical power, especially for MR sensitivity analysis which requires a higher number of instruments. Additionally, because of the high correlation between cytokines, particularly within a category, such as the ILs family, as well as correlations among four types of CVD, the naive multiple comparison adjustment may be excessive, further affecting the false negative. We hereby reminded that even in cases of negative results, complete exclusion of causality cannot be ensured and thus such results should be interpreted with caution. Secondly, the expression of certain cytokines can be influenced by age and the changing external setting, such as a bimodal curve that has been described for IL-1ra expression throughout the life stage (42). The estimates of a lifetime effect of cytokines on CVD provided by MR may not deliver much clinical meaningful for age-specific interventions. There may be non-linear effects or interactions between cytokines that are not captured by the present study. An age-specific MR analysis especially with individual-level data was warranted in future endeavors. Thirdly, even though a wide panel of cytokines was investigated, some other important kinds of cytokines like IL-1 β (43) and IL-10 (44), known for their direct role in targeting inflammation in atherosclerosis, were not analyzed in our study due to the lack of available QTL instruments for these cytokines. Lastly, due to the inaccessibility of the full summary statistics for cytokines, we were unable to conduct the colocalization analysis, which are valuable in strengthening the observed MR associations in helping identify associations that may have arisen due to confounding by LD. Further studies are warranted to strengthen our findings with colocalization when full summary statistics for cytokines are available.

Conclusion

To conclude, based on innovative IVs that incorporate gene expression relevance and large genetic association data, this MR study comprehensively examined the causal influence of circulating cytokine levels on four major CVDs. Our MR study provides robust evidence that the levels of certain cytokines were associated with the development of CVD and highlights the importance of considering cytokines as potential targets for the prevention and management of CVD. Further research, if possible, clinical trials, are necessary to validate these findings and delve into the underlying biological mechanisms specifically at the specific cytokine level.

Data availability statement

The original contributions presented in the study are included in the article/**Supplementary material**. Further inquiries can be directed to the corresponding author.

Ethics statement

Ethical review and approval was not required for the study on human participants in accordance with the local legislation and institutional requirements. The patients/participants provided their written informed consent to participate in this study.

Author contributions

RZ and TW were the major contributors in conceptualisation. TW, ZZ and LL analyzed the data. ZZ, BL, MW, WZ, QC, and FL verified the correctness of the data. TW, ZZ and RZ were major contributors in writing the manuscript. All authors contributed to the article and approved the submitted version.

Funding

This study was supported by the Qin Chuangyuan Traditional Chinese Medicine Innovation Research and Development Transformation Project (No.2022-QCYZH-022), Key Program for the Traditional Chinese Medicine Inheritance and Innovation and “Qin Medicine” Development [No. 2021-03-22-001], the Key Basic Natural Science Foundation of Shaanxi Province [No. 2022JZ-47], the Key Industrial Innovation Chain Project in Shaanxi Province of China [No. 2021ZDLSF02-03 and 2020ZDLSF01-08], the Shaanxi Provincial Health and Health Research Fund Project [No.

2022D024], and the Natural Science Foundation of Shaanxi Province [No.2023-YBSF-086 and No.2021JQ-911].

Acknowledgments

The data analyzed in this study was provided by Bouras's Lab, SCALLOP Consortium, Karhunen's Lab, INTERVAL Study, CARDIoGRAMplusC4D Consortium, HERMES Consortium, Nielsen's Lab, and MEGASTROKE Consortium. We gratefully acknowledge their contributing studies and the participants in the corresponding studies without whom this effort would not be possible.

Conflict of interest

The authors declare that the research was conducted in the absence of any commercial or financial relationships that could be construed as a potential conflict of interest.

Publisher's note

All claims expressed in this article are solely those of the authors and do not necessarily represent those of their affiliated organizations, or those of the publisher, the editors and the reviewers. Any product that may be evaluated in this article, or claim that may be made by its manufacturer, is not guaranteed or endorsed by the publisher.

Supplementary material

The Supplementary Material for this article can be found online at: <https://www.frontiersin.org/articles/10.3389/fimmu.2023.1175421/full#supplementary-material>

References

- Roth GA, Mensah GA, Fuster V. The global burden of cardiovascular diseases and risks: a compass for global action. *J Am Coll Cardiol* (2020) 76(25):2980–1. doi: 10.1016/j.jacc.2020.11.021
- Amin MN, Siddiqui SA, Ibrahim M, Hakim ML, Ahammed MS, Kabir A, et al. Inflammatory cytokines in the pathogenesis of cardiovascular disease and cancer. *SAGE Open Med* (2020) 8:2050312120965752. doi: 10.1177/2050312120965752
- Kaptoge S, Seshasai SR, Gao P, Freitag DF, Butterworth AS, Borglykke A, et al. Inflammatory cytokines and risk of coronary heart disease: new prospective study and updated meta-analysis. *Eur Heart J* (2014) 35(9):578–89. doi: 10.1093/eurheartj/ehz367
- Georgakis MK, Malik R, Bjorkbacka H, Pana TA, Demissie S, Ayers C, et al. Circulating monocyte chemoattractant protein-1 and risk of stroke: meta-analysis of population-based studies involving 17 180 individuals. *Circ Res* (2019) 125(8):773–82. doi: 10.1161/CIRCRESAHA.119.315380
- Davies NM, Holmes MV, Davey Smith G. Reading mendelian randomisation studies: a guide, glossary, and checklist for clinicians. *BMJ* (2018) 362:k601. doi: 10.1136/bmj.k601
- Interleukin-6 Receptor Mendelian Randomisation Analysis C, Swerdlow DJ, Holmes MV, Kuchenbaecker KB, Engmann JE, Shah T, et al. The interleukin-6 receptor as a target for prevention of coronary heart disease: a mendelian randomisation analysis. *Lancet* (2012) 379(9822):1214–24. doi: 10.1016/S0140-6736(12)60110-X
- Georgakis MK, Malik R, Richardson TG, Howson JMM, Anderson CD, Burgess S, et al. Associations of genetically predicted IL-6 signaling with cardiovascular disease risk across population subgroups. *BMC Med* (2022) 20(1):245. doi: 10.1186/s12916-022-02446-6
- Georgakis MK, Gill D, Rannikmae K, Traylor M, Anderson CD, Lee JM, et al. Genetically determined levels of circulating cytokines and risk of stroke. *Circulation* (2019) 139(2):256–68. doi: 10.1161/CIRCULATIONAHA.118.035905
- Li Y, Lu J, Wang J, Deng P, Meng C, Tang H. Inflammatory cytokines and risk of ischemic stroke: a mendelian randomization study. *Front Pharmacol* (2021) 12:779899. doi: 10.3389/fphar.2021.779899
- Bouras E, Karhunen V, Gill D, Huang J, Haycock PC, Gunter MJ, et al. Circulating inflammatory cytokines and risk of five cancers: a mendelian randomization analysis. *BMC Med* (2022) 20(1):3. doi: 10.1186/s12916-021-02193-0
- Folkersen L, Gustafsson S, Wang Q, Hansen DH, Hedman AK, Schork A, et al. Genomic and drug target evaluation of 90 cardiovascular proteins in 30,931 individuals. *Nat Metab* (2020) 2(10):1135–48. doi: 10.1038/s42255-020-00287-2
- Sun BB, Maranville JC, Peters JE, Stacey D, Staley JR, Blackshaw J, et al. Genomic atlas of the human plasma proteome. *Nature* (2018) 558(7708):73–9. doi: 10.1038/s41586-018-0175-2
- Karhunen V, Gill D, Malik R, Ponsford M, Ahola-Olli A, Papadopolou A, et al. Genetic study of circulating cytokines offers insight into the determinants,

cascades and effects of systemic inflammation. *medRxiv* (2020). doi: 10.1101/2020.10.26.20219477

14. van der Harst P, Verweij N. Identification of 64 novel genetic loci provides an expanded view on the genetic architecture of coronary artery disease. *Circ Res* (2018) 122(3):433–43. doi: 10.1161/CIRCRESAHA.117.312086
15. Shah S, Henry A, Roselli C, Lin H, Sveinbjornsson G, Fatemifar G, et al. Genome-wide association and mendelian randomisation analysis provide insights into the pathogenesis of heart failure. *Nat Commun* (2020) 11(1):163. doi: 10.1038/s41467-019-13690-5
16. Nielsen JB, Thorolfsdottir RB, Fritsche LG, Zhou W, Skov MW, Graham SE, et al. Biobank-driven genomic discovery yields new insight into atrial fibrillation biology. *Nat Genet* (2018) 50(9):1234–9. doi: 10.1038/s41588-018-0171-3
17. Malik R, Chauhan G, Traylor M, Sargurupremraj M, Okada Y, Mishra A, et al. Multiancestry genome-wide association study of 520,000 subjects identifies 32 loci associated with stroke and stroke subtypes. *Nat Genet* (2018) 50(4):524–37. doi: 10.1038/s41588-018-0058-3
18. Consortium GT. The GTEx consortium atlas of genetic regulatory effects across human tissues. *Science* (2020) 369(6509):1318–30. doi: 10.1126/science.aaz1776
19. Burgess S, Butterworth A, Thompson SG. Mendelian randomization analysis with multiple genetic variants using summarized data. *Genet Epidemiol* (2013) 37(7):658–65. doi: 10.1002/gepi.21758
20. Burgess S, Thompson SG. Interpreting findings from mendelian randomization using the MR-egger method. *Eur J Epidemiol* (2017) 32(5):377–89. doi: 10.1007/s10654-017-0255-x
21. Bowden J, Davey Smith G, Haycock PC, Burgess S. Consistent estimation in mendelian randomization with some invalid instruments using a weighted median estimator. *Genet Epidemiol* (2016) 40(4):304–14. doi: 10.1002/gepi.21965
22. Burgess S, Foley CN, Allara E, Staley JR, Howson JMM. A robust and efficient method for mendelian randomization with hundreds of genetic variants. *Nat Commun* (2020) 11(1):376. doi: 10.1038/s41467-019-14156-4
23. Verbanck M, Chen CY, Neale B, Do R. Detection of widespread horizontal pleiotropy in causal relationships inferred from mendelian randomization between complex traits and diseases. *Nat Genet* (2018) 50(5):693–8. doi: 10.1038/s41588-018-0099-7
24. Burgess S, Thompson SG, Collaboration CCG. Avoiding bias from weak instruments in mendelian randomization studies. *Int J Epidemiol* (2011) 40(3):755–64. doi: 10.1093/ije/dyr036
25. Brion MJ, Shakhbazov K, Visscher PM. Calculating statistical power in mendelian randomization studies. *Int J Epidemiol* (2013) 42(5):1497–501. doi: 10.1093/ije/dyt179
26. Sun L, Craiu RV, Paterson AD, Bull SB. Stratified false discovery control for large-scale hypothesis testing with application to genome-wide association studies. *Genet Epidemiol* (2006) 30(6):519–30. doi: 10.1002/gepi.20164
27. Leavitt C, Zakai NA, Auer P, Cushman M, Lange EM, Levitan EB, et al. Interferon gamma-induced protein 10 (IP-10) and cardiovascular disease in African americans. *PLoS One* (2020) 15(4):e0231013. doi: 10.1371/journal.pone.0231013
28. Chia YC, Kieneker LM, van Hassel G, Binnenmars SH, Nolte IM, van Zanden JJ, et al. Interleukin 6 and development of heart failure with preserved ejection fraction in the general population. *J Am Heart Assoc* (2021) 10(11):e018549. doi: 10.1161/JAHA.120.018549
29. Herder C, de Las Heras Gala T, Carstensen-Kirberg M, Huth C, Zierer A, Wahl S, et al. Circulating levels of interleukin 1-receptor antagonist and risk of cardiovascular disease: meta-analysis of six population-based cohorts. *Arterioscler Thromb Vasc Biol* (2017) 37(6):1222–7. doi: 10.1161/ATVBAHA.117.309307
30. Björkbacka H, Yao Mattsson I, Wigren M, Melander O, Fredrikson GN, Bengtsson E, et al. Plasma stem cell factor levels are associated with risk of cardiovascular disease and death. *J Intern Med* (2017) 282(6):508–21. doi: 10.1111/joim.12675
31. Yuan S, Lin A, He QQ, Burgess S, Larsson SC. Circulating interleukins in relation to coronary artery disease, atrial fibrillation and ischemic stroke and its subtypes: a two-sample mendelian randomization study. *Int J Cardiol* (2020) 313:99–104. doi: 10.1016/j.ijcard.2020.03.053
32. Ahola-Olli AV, Wurtz P, Havulinna AS, Aalto K, Pitkanen N, Lehtimäki T, et al. Genome-wide association study identifies 27 loci influencing concentrations of circulating cytokines and growth factors. *Am J Hum Genet* (2017) 100(1):40–50. doi: 10.1016/j.ajhg.2016.11.007
33. Prabhu SD. Cytokine-induced modulation of cardiac function. *Circ Res* (2004) 95(12):1140–53. doi: 10.1161/01.RES.0000150734.79804.92
34. Vila E, Salaices M. Cytokines and vascular reactivity in resistance arteries. *Am J Physiol Heart Circ Physiol* (2005) 288(3):H1016–1021. doi: 10.1152/ajpheart.00779.2004
35. Mehra VC, Ramgopal VS, Bender JR. Cytokines and cardiovascular disease. *J Leukoc Biol* (2005) 78(4):805–18. doi: 10.1189/jlb.0405182
36. Higashi Y. Roles of oxidative stress and inflammation in vascular endothelial dysfunction-related disease. *Antioxidants (Basel)* (2022) 11(10):1958. doi: 10.3390/antiox11101958
37. Hansson GK, Hermansson A. The immune system in atherosclerosis. *Nat Immunol* (2021) 12(3):204–12. doi: 10.1038/nri.2001
38. Voigt A, Rahnefeld A, Kloetzel PM, Kruger E. Cytokine-induced oxidative stress in cardiac inflammation and heart failure-how the ubiquitin proteasome system targets this vicious cycle. *Front Physiol* (2013) 4:42. doi: 10.3389/fphys.2013.00042
39. Bondia-Pons I, Ryan L, Martinez JA. Oxidative stress and inflammation interactions in human obesity. *J Physiol Biochem* (2012) 68(4):701–11. doi: 10.1007/s13105-012-0154-2
40. Volarevic V, Al-Qahtani A, Arsenijevic N, Pajovic S, Lukic ML. Interleukin-1 receptor antagonist (IL-1Ra) and IL-1Ra producing mesenchymal stem cells as modulators of diabetogenesis. *Autoimmunity* (2010) 43(4):255–63. doi: 10.1019/08916930903305641
41. Davey Smith G, Hemani G. Mendelian randomization: genetic anchors for causal inference in epidemiological studies. *Hum Mol Genet* (2014) 23(R1):R89–98. doi: 10.1093/hmg/ddu328
42. Decker ML, Grobusch MP, Ritz N. Influence of age and other factors on cytokine expression profiles in healthy children-a systematic review. *Front Pediatr* (2017) 5:255. doi: 10.3389/fped.2017.00255
43. Libby P. Interleukin-1 beta as a target for atherosclerosis therapy: biological basis of CANTOS and beyond. *J Am Coll Cardiol* (2017) 70(18):2278–89. doi: 10.1016/j.jacc.2017.09.028
44. Yilmaz MI, Solak Y, Saglam M, Cayci T, Acikel C, Unal HU, et al. The relationship between IL-10 levels and cardiovascular events in patients with CKD. *Clin J Am Soc Nephrol* (2014) 9(7):1207–16. doi: 10.2215/CJN.08660813



OPEN ACCESS

EDITED BY

Nadine Suffee,
Sorbonne Universités, France

REVIEWED BY

Xuanyou Liu,
Mayo Clinic, United States
Vinod Kumar,
The University of Queensland, Australia
Jonathan David Turner,
Luxembourg Institute of Health,
Luxembourg

*CORRESPONDENCE

Jorge Suarez
✉ jsuarez@health.ucsd.edu
Wei Ying
✉ weying@health.ucsd.edu

[†]These authors have contributed equally to this work

RECEIVED 03 May 2023

ACCEPTED 27 June 2023

PUBLISHED 13 July 2023

CITATION

Gao H, Wang K, Suarez JA, Jin Z, Rocha KCe, Zhang D, Farrell A, Truong T, Tekin Y, Tan B, Jung HS, Kempf J, Mahata SK, Dillmann WH, Suarez J and Ying W (2023) Gut lumen-leaked microbial DNA causes myocardial inflammation and impairs cardiac contractility in ageing mouse heart. *Front. Immunol.* 14:1216344. doi: 10.3389/fimmu.2023.1216344

COPYRIGHT

© 2023 Gao, Wang, Suarez, Jin, Rocha, Zhang, Farrell, Truong, Tekin, Tan, Jung, Kempf, Mahata, Dillmann, Suarez and Ying. This is an open-access article distributed under the terms of the [Creative Commons Attribution License \(CC BY\)](#). The use, distribution or reproduction in other forums is permitted, provided the original author(s) and the copyright owner(s) are credited and that the original publication in this journal is cited, in accordance with accepted academic practice. No use, distribution or reproduction is permitted which does not comply with these terms.

Gut lumen-leaked microbial DNA causes myocardial inflammation and impairs cardiac contractility in ageing mouse heart

Hong Gao^{1†}, Ke Wang^{1†}, Jorge A. Suarez^{1†}, Zhongmou Jin², Karina Cunha e Rocha¹, Dinghong Zhang¹, Andrea Farrell², Tyler Truong², Yasemin Tekin², Breanna Tan², Hyun Suh Jung², Julia Kempf², Sushil K. Mahata^{3,4}, Wolfgang H. Dillmann¹, Jorge Suarez^{1*} and Wei Ying^{1*}

¹Division of Endocrinology and Metabolism, Department of Medicine, University of California San Diego, San Diego, CA, United States, ²Division of Biological Sciences, University of California San Diego, San Diego, CA, United States, ³the Veterans Affairs San Diego Healthcare System, San Diego, CA, United States, ⁴Division of Nephrology and Hypertension, Department of Medicine, University of California San Diego, San Diego, CA, United States

Emerging evidence indicates the critical roles of microbiota in mediating host cardiac functions in ageing, however, the mechanisms underlying the communications between microbiota and cardiac cells during the ageing process have not been fully elucidated. Bacterial DNA was enriched in the cardiomyocytes of both ageing humans and mice. Antibiotic treatment remarkably reduced bacterial DNA abundance in ageing mice. Gut microbial DNA containing extracellular vesicles (mEVs) were readily leaked into the bloodstream and infiltrated into cardiomyocytes in ageing mice, causing cardiac microbial DNA enrichment. Vsig4⁺ macrophages efficiently block the spread of gut mEVs whereas Vsig4⁺ cell population was greatly decreased in ageing mice. Gut mEV treatment resulted in cardiac inflammation and a reduction in cardiac contractility in young Vsig4^{-/-} mice. Microbial DNA depletion attenuated the pathogenic effects of gut mEVs. cGAS/STING signaling is critical for the effects of microbial DNA. Restoring Vsig4⁺ macrophage population in ageing WT mice reduced cardiac microbial DNA abundance and inflammation and improved heart contractility.

KEYWORDS

microbial DNA, extracellular vesicle, Vsig4 + macrophage, inflammaging, cardiac contractility

Introduction

Ageing and the incidence of heart failure (HF) are tightly intertwined. Humans older than 65 years have an increased propensity for HF (e.g. 11/1000 persons), and the risk of HF is increased further with increased age (e.g. 43/1000 in humans > 80 years old) (1–4). This is of critical significance to the ageing population since HF is always

associated with recurrent hospitalization, decreased quality of life, and a reduction in life span (5). Despite the extensive body of research, the mechanisms that determine cardiac dysfunction in ageing are incompletely understood. Consequently, translation of the findings to improve cardiac function and life span in ageing has been unsuccessful, suggesting that there is a gap in our knowledge of the molecular foundations of ageing-related cardiac impairment.

A progressive increase in the proinflammatory status referred to as “inflamm-ageing” is characteristic of the ageing process (6–12). As the hallmark of inflammageing, immune response abnormalities are evident, such as a reduction in macrophage-dependent phagocytosis (13–15). While several mechanisms such as mitochondrial disorder and senescence have been implicated in the pathogenesis of ageing-associated HF (16–19), whether the initiation and amplification of inflammation results in these cellular disorders in cardiomyocytes are unknown.

Previous studies have shown the absence of an increase in pro-inflammatory cytokines in the bloodstream and better longevity of germ-free ageing mice than their conventional counterparts, suggesting that microbiota play critical roles in promoting inflammageing phenotypes (20, 21). However, the mechanisms whereby microbiota modulates inflammageing phenotypes are not completely understood. Ageing is accompanied by gut barrier breach, allowing the translocation of microbiota-derived products into host circulation and distal tissues (20, 22). Previous studies have demonstrated that, in the context of gut leakage, microbiota-derived extracellular vesicles (EVs) act as important carriers spreading microbial DNA into host tissues, subsequently triggering host cellular inflammatory responses (23). Thus, these findings lead to the hypothesis that the infiltration of microbiota-derived microbial DNA containing EVs (mEVs) into the heart could cause myocardial inflammation and contractility abnormalities in ageing mice.

Here, we report that ageing-associated gut leakage and reduction of V-set and immunoglobulin domain containing 4 expressing (Vsig4⁺) macrophage population result in the translocation of gut mEVs into cardiomyocytes, leading to myocardial bacterial DNA enrichment. Bacterial DNA is the key cargo contributing to the pathogenic effects of gut EVs on inducing ageing-related cardiac abnormalities through a cGAS/STING-dependent mechanism. Finally, recovering the Vsig4⁺ macrophage population remarkably diminishes the levels of bacterial DNA in mouse ageing hearts, concomitant with decreased levels of cardiac inflammatory responses and improved myocardial contractility.

Results

Ageing hearts are characterized by microbial DNA accumulation

An impaired and defective intestinal barrier is observed in ageing (20, 22). Consistently, the electron microscope analysis shows that 100–108 weeks (wks) old ageing mice had an impaired gut integrity, as evidenced by increases in the length and/or

diameter in adherens junctions, tight junctions, or desmosomes (Figure S1A). In addition, the expression of key genes associated with gut gap junction was significantly repressed in ageing mice (Figure S1B). After 1 hour of oral administration of FITC dextran to ageing mice, plasma FITC fluorescent intensity was markedly elevated, demonstrating increased intestinal permeability in ageing mice (Figure S1C). The abundance of IgA, which plays a critical role in preventing the leakage of microbiota (24), was significantly lower in ageing mouse gut, compared to young mice (Figure S1D). These results demonstrate that ageing is accompanied by the impairment of gut integrity.

Previous studies have demonstrated that microbial DNA-containing gut extracellular vesicles (mEVs) are readily translocated through an impaired gut barrier into host circulation and distal tissues (23). Consistently, the ageing-associated leaky gut resulted in the enrichment of mEVs in plasma, whereas, bacterial DNA was barely detected in the plasma EVs collected from young lean WT mice (Figure 1A). More importantly, as shown in Figures 1B, C and S1E, 16s rRNA was readily detected in both ageing human and mouse cardiomyocytes. To further assess whether gut mEVs are leaky from the gut lumen into host circulation and hearts in ageing mice, red fluorescent dye PKH26-labeled gut mEVs (5 × 10⁹ EVs/mouse) were injected into the ileum section of either young or ageing WT recipient mice. After 16 hours, PKH26 signals were readily detected in the cardiomyocytes of ageing recipient mice, thus suggesting the leakage of injected mEVs from the ageing gut (Figure 1D). In contrast, PKH26 fluorescence was barely detectable in young mouse hearts (Figure 1D).

To examine if bacterial DNA enriched in ageing heart is derived from microbiota, ageing WT mice were orally given antibiotics for 2 wks. Compared to ageing controls treated with saline, antibiotic treatment resulted in a remarkable reduction in bacterial DNA abundance in the circulation and heart (Figures 1E, F). We also compared the bacterial DNA species accumulated in the heart with the microbial composition of ageing WT mice. The 16s rRNA seq analysis indicates that phylum *Firmicutes* were the dominant microbial species in the ileum section of ageing gut (Figures 1G, S1F–S1G, Tables S1, S2). Consistently, the bacterial DNA enriched in ageing hearts was mainly derived from phylum *Firmicutes* (Figure 1G). Taken together, these data suggest that microbiota-derived mEVs are readily shuttled from the impaired intestinal barrier into the heart in the context of ageing.

Ageing is accompanied by a loss of Vsig4⁺ macrophages

Liver Vsig4⁺ Kupffer cells (KCs) are important sentinel cells that remove bacteria and their products from the bloodstream (23, 25). We observed that ageing livers contained a significantly lower amount of Kupffer cells (Clec4f⁺F4/80⁺) than young lean mouse livers, concomitant with markedly lower Vsig4 abundance on ageing KCs (Figures 2A, B). Previous studies have shown that Vsig4⁺ macrophages can efficiently clean gut mEVs from the bloodstream (23). After injecting PKH26-labeled gut mEVs into

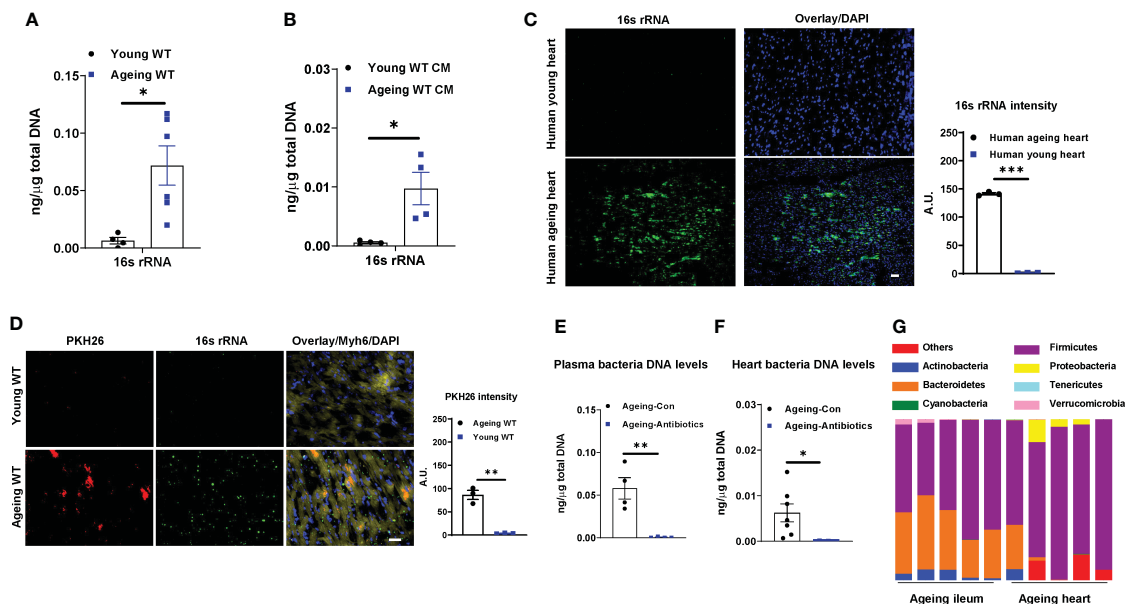


FIGURE 1

Bacterial DNA is enriched in ageing hearts. 16s rRNA abundance in plasma EVs (A) and cardiac myocytes (CM; B) isolated from young (8–12 wks old) or ageing (100–108 wks old) WT mice. (C) 16s rRNA levels in human hearts. Scale bar=25μm. (D) The appearance of PKH26 red fluorescent signals in the hearts after 16 hours of injecting PKH26-labeled gut microbial DNA containing extracellular vesicles (mEVs) into the ileum section of young or ageing WT mice. Scale bar=50μm. 16s rRNA abundance in plasma (E) and heart (F) of ageing WT mice after 2 wks of treatment with a mixture of antibiotics. Control ageing mice were treated with sterile water. (G) The microbial DNA species detected in ileum sections and hearts of ageing WT mice. Data are presented as mean ± SEM. * $P < 0.05$, ** $P < 0.01$, *** $P < 0.001$, Student's t -test.

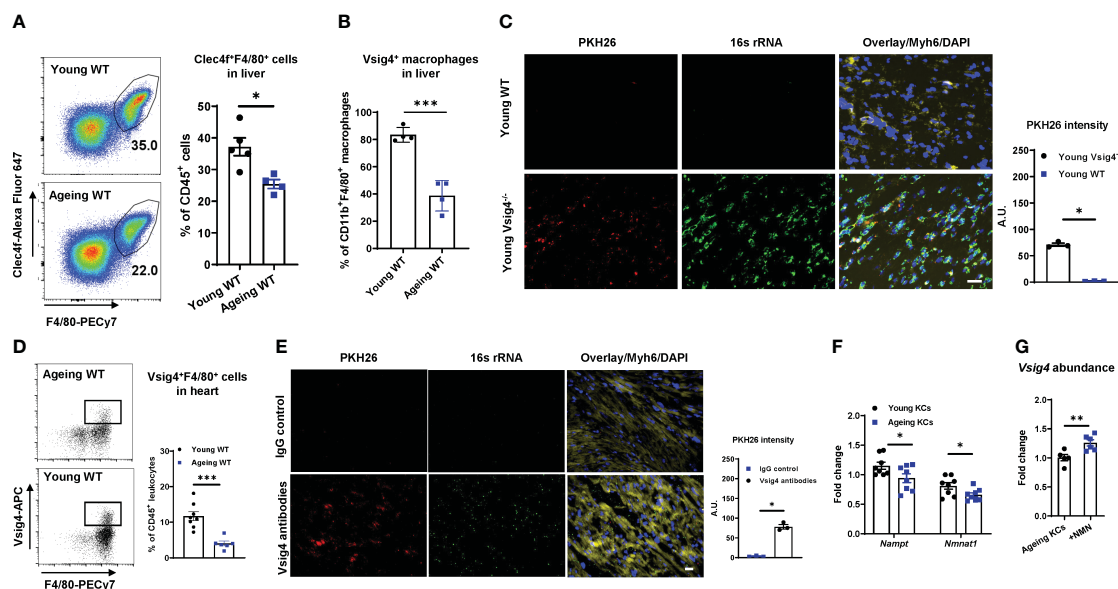


FIGURE 2

Vsig4⁺ macrophage population is remarkably decreased in ageing mice. The population of Kupffer cells (KCs, Clec4e⁺F4/80⁺; A) and Vsig4⁺ macrophages (B) in the livers of young or ageing WT mice was analyzed by flow cytometric assays. (C) The abundance of PKH26 signals in the hearts of young WT or Vsig4^{-/-} mice after 16 hours of tail vein injection with PKH26-labeled gut mEVs. Scale bar=50μm. (D) Vsig4⁺ macrophage population in hearts was analyzed by flow cytometric assays. (E) PKH26 intensity in hearts after 16 hours injection of gut mEVs into jugular vein of young WT mice pre-treated with either IgG or Vsig4 antibodies. Images are representative of three experiments. Scale bar=25μm. (F) The expression of key genes associated with NAD homeostasis in KCs was analyzed by qPCR assays. (G) qPCR analysis of Vsig4 abundance in ageing KCs after *in vitro* treatment with nicotinamide mononucleotide (NMN). Data are presented as mean ± SEM. * $P < 0.05$, ** $P < 0.01$, *** $P < 0.001$, Student's t -test.

the tail vein of young lean *Vsig4*^{-/-} mice to mimic ageing-associated high levels of mEVs in circulation, robust red fluorescent PKH26 signals were present in the heart (Figure 2C). We also observed that PKH26 signals were diminished after 48 hours injection and almost gone after 72 hours (Figure S2A). Conversely, young lean WT mice showed few PKH26 fluorescence in cardiomyocytes after 16 hours injection of PKH26 mEVs, thus demonstrating the critical role of *Vsig4*⁺ cells in preventing the infiltration of mEVs into the heart (Figure 2C).

In addition to the liver, *Vsig4*⁺ macrophages also reside in other tissues such as pancreatic islets and adrenal glands (26–28). Consistently, we found that ~20% of cardiac macrophages (CD11b⁺F4/80⁺) were *Vsig4* positive in young mice (Figure S2B), whereas, ageing hearts harbored less population of *Vsig4*⁺ macrophages than young mice or humans (Figures 2D, S2C). In addition, ageing results in a significant reduction in the cardiac macrophage population (Figure S2D). To further assess the ability of cardiac *Vsig4*⁺ macrophages to block the infiltration of gut mEVs into cardiomyocytes, we depleted Kupffer cells by injecting diphtheria toxin (DT) to young *Clec4eCre*⁺DTR⁺ mice (KCKO; 10–12wks old) and then intravenously injected PKH26-labeled gut mEVs into these young KCKO mice (Figures S2E, S2F) (29). After 24 hours, no PKH26 signal was detected in young KCKO mice treated with PKH26 EVs (Figure S2G). In addition, injecting gut mEVs (5 × 10⁸ EVs/mouse) into the jugular vein of young WT mice did not cause bacterial DNA accumulation in the hearts (Figure 2E). In contrast, pre-treating *Vsig4* antibodies into jugular vein blocked the function of heart *Vsig4*⁺ macrophages of young WT mice,

subsequently resulting in the infiltration of gut mEVs into cardiomyocytes (Figure 2E). Thus, these data suggest that cardiac macrophages exert a profound function in cleaning gut EVs.

Previous studies have demonstrated that NAD deficiency leads to ageing-associated macrophage dysfunction (14, 30). We also found that both ageing KCs and cardiac macrophages contained less abundance of key enzymes associated with the NAD salvage pathway than young mice (Figures 2F, S2H). To assess the effect of NAD homeostasis on *Vsig4* expression, KCs isolated from ageing WT mice were treated with biosynthetic NAD precursor, NMN. After 24 hours, NMN treatment led to a significant increase in *Vsig4* abundance in ageing KCs (Figure 2G).

Microbial DNA accumulation results in ageing-associated cardiac contractility defects

Ageing is concomitant with impaired cardiac contraction. To demonstrate the regulation of microbiota on ageing cardiac functions, ageing WT mice were treated with antibiotics (Figure S3A). After 2 wks of treatment, we found that depletion of microbiota led to an improvement of cardiac contraction, as demonstrated by elevated levels of left ventricular systolic pressure, the derivative of pressure over time maximum, and dP/dt (the derivative of pressure over time) minimum (min) in the hearts of antibiotic-treated ageing mice (Figures 3A–C). In addition, the abundance of Serca2, which is critical for cardiac calcium

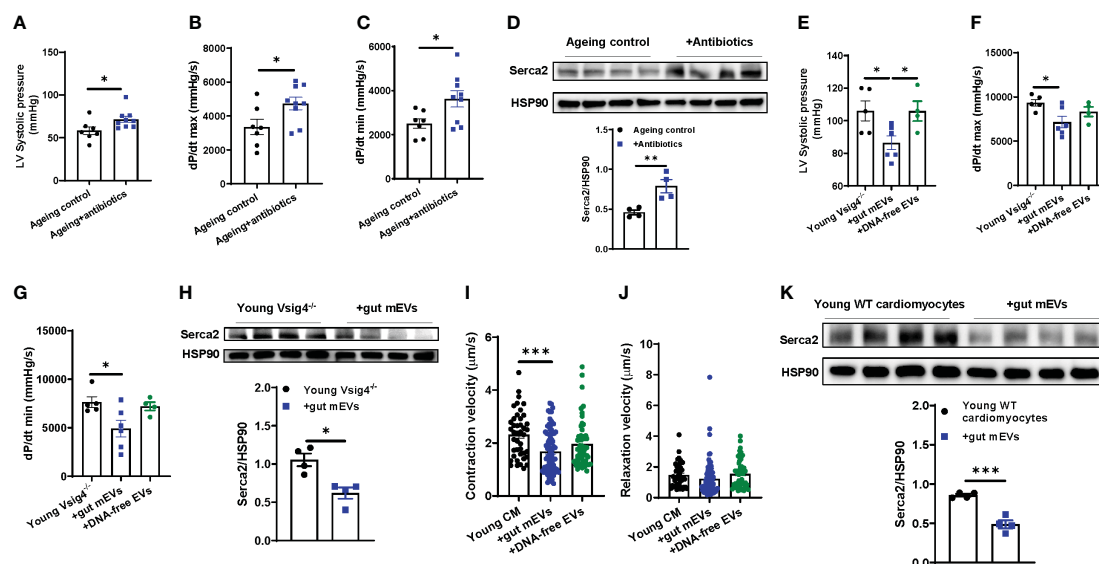


FIGURE 3

Microbial DNA accumulation impairs cardiac contractility. Left ventricular (LV) systolic pressure (A) maximal rate of rise of left ventricular pressure (dP/dt max; B) and maximum rate of ventricular pressure decrease (dP/dt min; C) of antibiotic-treated ageing WT mice were measured by *in vivo* cardiac contractility with the Millar catheter. (D) Serca2 abundance in the hearts of ageing WT mice after 2 wks of antibiotic treatment. After 4 wks of treatment with either gut mEVs or DNA-free EVs, the cardiac contractility of young *Vsig4*^{-/-} mice was evaluated by the levels of the left ventricular systolic pressure (E) maximal rate of rise of left ventricular pressure (F) and maximum rate of ventricular pressure decrease (G). (H) Serca2 abundance in the hearts of young *Vsig4*^{-/-} mice after 4 wks of treatment of gut mEVs. After *in vitro* treatment with either gut mEVs or DNA-free EVs for 36 hours, the contractile function of young WT cardiac myocytes was evaluated by the levels of both contraction (I) and relaxation velocity (J). (K) Serca2 abundance in young WT cardiomyocytes after 36 hours of treatment with gut mEVs. Data are presented as mean ± SEM. **P* < 0.05, ***P* < 0.01, ****P* < 0.001, Student's *t*-test.

handling for contractility, was elevated in ageing hearts after 2 wks of antibiotic treatment (Figure 3D).

Given that the leakage of microbiota-derived mEVs leads to microbial DNA accumulation in cardiomyocytes in ageing mice (Figure 1), we next assessed the pathogenic effects of microbial DNA enrichment on cardiac functions. Young lean *Vsig4*^{-/-} mice were intravenously injected with gut mEVs (5×10^9 EVs/mouse). After 4 wks of mEV treatment, bacterial DNA levels in the hearts of young lean *Vsig4*^{-/-} mice were comparable to those of ageing WT mouse hearts (Figure S3B). More importantly, gut mEV treatment resulted in impaired cardiac functions, as evidenced by decreased levels of left ventricle (LV) systolic pressure, dP/dt max, and dP/dt min in the hearts of gut mEV-treated young lean *Vsig4*^{-/-} mice (Figures 3E–G). In addition, *Serca2* expression was reduced in the heart after gut mEV treatment (Figure 3H). In contrast, depletion of microbial DNA cargo from gut mEVs led to non-significant changes in bacterial DNA levels in heart and cardiac functions of young lean *Vsig4*^{-/-} mice, thus demonstrating that microbial DNA is the key pathogenic cargo contributing to the effects of gut mEVs on cardiac responses (Figures S3B, 3E–G). In addition, after 3 wks withdrawn from gut mEV treatment, heart *Serca2* levels were restored (Figure S3C). We also found that *Vsig4* knockout didn't affect heart phenotypes in young mice (Figures S3D–F).

To assess the direct effects of microbial DNA on inducing cardiomyocyte dysfunction, cardiomyocytes isolated from young WT mice were *in vitro* treated with either gut mEVs or DNA-free EVs (Figure S3G). Following gut mEV-induced microbial DNA accumulation, young WT cardiomyocytes displayed a marked reduction in rates of contraction (Figures S3H, 3I, J). We also evaluated the state of calcium handling in cardiomyocytes after gut

mEV treatment. Microbial DNA accumulation blunted the ability of young cardiomyocytes to mediate calcium homeostasis for contraction (Figure 3K). In contrast, depletion of microbial DNA cargos markedly reduced these effects of gut mEVs on cardiomyocyte responses (Figures S3H, 3I, J). Taken together, these results demonstrate that microbial DNA is a pathogenic factor inducing ageing-associated cardiac contractility abnormalities.

Microbial DNA enrichment induces cardiomyocyte inflammation in ageing mice

Previous studies have demonstrated that the infiltration of microbial DNA triggers mammalian cell inflammatory responses (23). Concomitant with a marked accumulation of microbial DNA in ageing hearts, ageing cardiomyocytes displayed greater levels of inflammation than young lean cardiac myocytes, as shown by a higher abundance of proinflammatory mediators, including *Il1b*, *Ccl2*, *Ifng*, and *Il6*, in ageing cells (Figure 4A). In contrast, microbiota-depleted ageing mice displayed attenuated inflammation in the heart, compared to ageing control mice (Figure 4B). We also found that heart abnormalities were restored in ageing WT mice after recovering microbiota from 2 wks antibiotic withdrawal (Figures S3A, S4A, B). To further demonstrate that microbial DNA shuttled by gut mEVs is a pathogenic factor inducing ageing-related cardiac inflammation, either young lean *Vsig4*^{-/-} or KCKO mice were intravenously injected with gut mEVs. The control young mice were treated with DNA-free EVs. After 4 wks treatment, the hearts of young

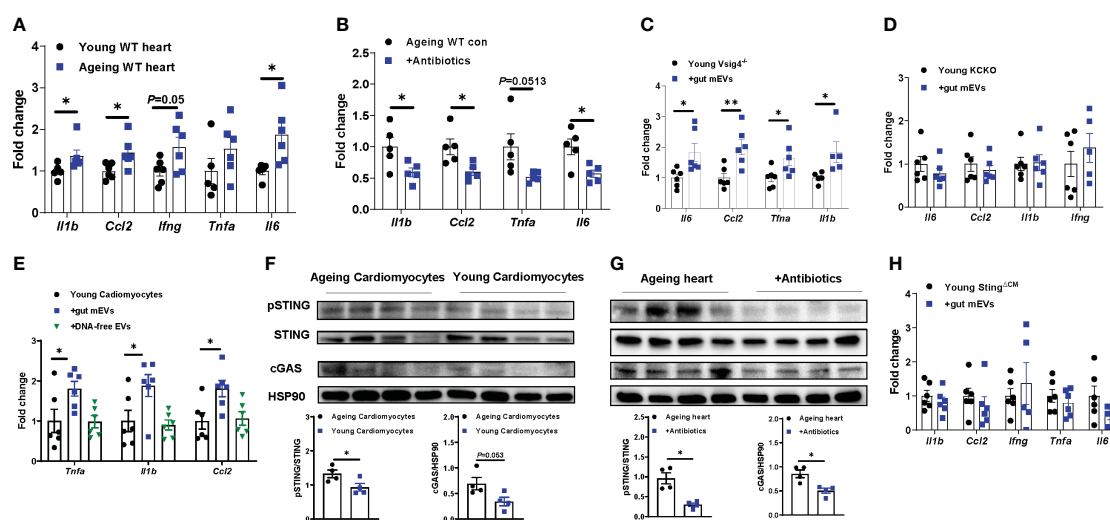


FIGURE 4

Microbial DNA enrichment triggers inflammation in cardiomyocytes. (A) qPCR analysis of proinflammatory gene abundance in the hearts of young vs. ageing WT mice. (B) Effect of antibiotic treatment on the expression of proinflammatory genes in ageing hearts. Inflammatory responses in young *Vsig4*^{-/-} mouse hearts (C) or the cardiomyocytes of young Kupffer cell depletion (KCKO) mice (D) after 4 wks of treatment with gut mEVs. The control young mice were treated with DNA-free EVs. (E) After *in vitro* treatment with gut mEVs or DNA-free EVs for 24 hours, qPCR analysis of proinflammatory gene expression in young WT cardiomyocytes. (F) The levels of cGAS and phosphorylated STING in cardiomyocytes isolated from young vs. ageing WT mice. (G) Effect of antibiotic treatment on the activation of cGAS/STING signaling in ageing WT mouse hearts. (H) qPCR analysis of proinflammatory gene abundance in the hearts of young cardiomyocyte-specific *Sting* knockout (*Myh6Cre*⁺*Sting*^{f/f}, *Sting*^{ΔCM}) mice after 4 wks of treatment with gut mEVs. Data are presented as mean ± SEM. **P* < 0.05, ***P* < 0.01, Student's *t*-test.

Vsig4^{-/-} mice injected with gut mEVs expressed greater levels of proinflammatory cytokines than that in control mice injected with DNA-free EVs, indicating that microbial DNA cargo within gut mEVs elevate heart inflammatory responses (Figure 4C). In addition, microbial DNA was barely accumulated in the cardiomyocytes of young lean KCKO mice after 4wks of intravenous treatment with gut mEVs, thus leading to comparable inflammatory responses in cardiomyocytes among young lean KCKO mice (Figures S2F, 4D). After the injection of gut mEVs into jugular vein of Vsig4 antibodies-pretreated young WT mice, heart inflammation levels were elevated (Figure S4C). We also found that *in vitro* treatment with gut mEVs directly promoted an inflammatory state in young WT cardiac cells, whereas, depletion of microbial DNA cargo blunted these effects of gut mEVs (Figure 4E).

The cGAS/STING signaling is critical to sense bacterial DNA and subsequently trigger host cellular responses (31, 32). We found that ageing cardiomyocytes expressed greater levels of cGAS and phosphorylated STING (pSTING) than young cardiac myocytes, whereas, the activation of cGAS/STING signaling in the heart was blunted after depletion of microbiota and reducing heart microbial DNA accumulation in ageing mice (Figures 4F, G). We also demonstrated that microbial DNA shuttled by gut mEVs plays a critical role in inducing cGAS/STING signaling activation in cardiomyocytes, as shown by elevated cGAS and pSTING in gut mEVs-treated cardiomyocytes but not in DNA-free gut EV-treated cells (Figures S4D, E). To further assess the importance of cGAS/STING signaling on the ability of microbial DNA to induce cardiomyocyte inflammation, young lean cGAS^{-/-} (cGAS knockout) cardiac cells were treated with gut mEVs *in vitro*. After 24 hours of treatment, the cellular inflammation state was

comparable among all cGAS^{-/-} cells (Figures S4F, G). While microbial DNA was accumulated, gut mEV treatment had minimal effects on the heart inflammation of young lean cardiomyocyte-specific Sting knockout (Myh6Cre⁺Sting^{f/f}; Sting^{ΔCM}) mice pre-treated with Vsig4 antibodies (Figures 4H, S4H, I). Taken together, these data suggest that microbial DNA induces ageing-related cardiac inflammation through the activation of cGAS/STING signaling.

Microbial DNA-induced inflammation impairs cardiac contraction

Previous studies have demonstrated that inflammation is an important factor initiating heart dysfunctions (33, 34). While microbial DNA enrichment occurred in the cardiomyocytes of ageing cGAS^{-/-} mice, these cGAS^{-/-} ageing cardiac cells displayed lower levels of inflammation but better contractile activity than ageing WT cardiomyocytes (Figures S5A, 5A–C). In addition, ageing cGAS^{-/-} cardiomyocytes contained less pSTING than ageing WT cells (Figure S5B). Knockout of cGAS also blunted the effects of ageing on cardiac calcium handling, as evidenced by greater Serca2 abundance in ageing cGAS^{-/-} cardiomyocytes (Figure 5D). We next assessed the importance of cGAS/STING-induced inflammation on the ability of microbial DNA to induce ageing-related cardiac dysfunctions. In young lean Sting^{ΔCM} mice, concomitant with their blunted inflammatory responses to microbial DNA accumulation, gut mEV treatment had minimal effects on Serca2 abundance and contractility in the heart (Figures S4F, 5E–G). Thus, these data suggest that cGAS/STING-mediated inflammation plays a critical role in microbial DNA-induced ageing cardiac dysfunctions.

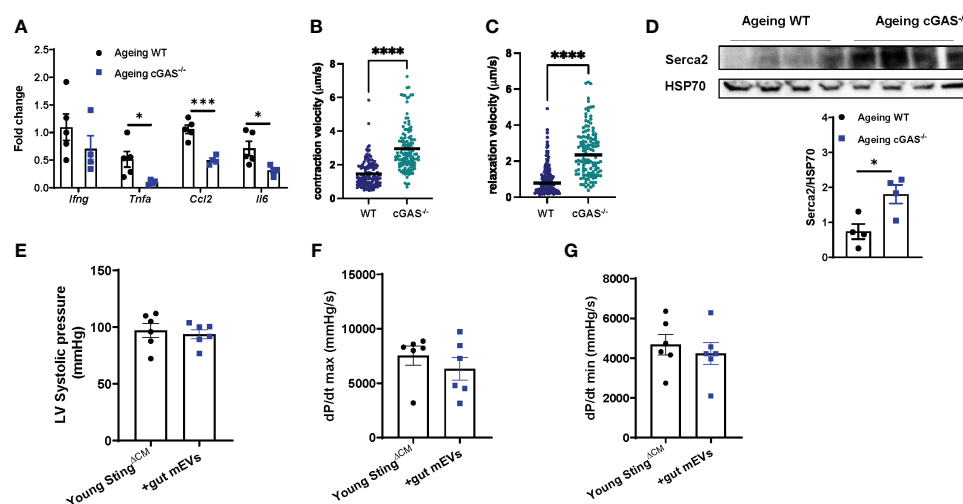


FIGURE 5
Microbial DNA-induced inflammatory responses reduce cardiac contraction capacity. The levels of proinflammatory gene expression (A), contractility (B, C), and Serca2 abundance (D) of the cardiomyocytes isolated from ageing WT vs cGAS^{-/-} mice. After 4 wks of treatment with gut mEVs, the cardiac contractility of young Sting^{ΔCM} mice was evaluated by the levels of the left ventricular systolic pressure (E), maximal rate of rise of left ventricular pressure (F), and maximum rate of ventricular pressure decrease (G). Data are presented as mean ± SEM. *P < 0.05, ***P < 0.001, ****P < 0.0001, Student's *t*-test.

Recovery of Vsig4⁺ macrophages is sufficient to attenuate ageing-associated cardiac abnormalities

Given that Vsig4⁺ macrophages efficiently clean bacterial products from the bloodstream, we next evaluated the effects of Vsig4 overexpression on ageing-associated heart microbial DNA accumulation and cardiac functions. To overexpress Vsig4, ageing WT mice were intravenously injected with lentivirus carrying the VPR system (including three transcriptional activators VP64, p65, and Rta) linked to the C-terminal end of deactivated Cas9 (dCas9) and gRNA-Vsig4 TSS (Transcription start site; Vsig4oe). After 2 wks of injection with these lentiviruses, Vsig4 abundance was elevated in the livers and hearts of ageing mice (Figures S6A, B). Following the recovery of the Vsig4⁺ macrophage population, we observed that the bacterial DNA abundance was significantly reduced in the hearts of ageing mice, concomitant with lower levels of cGAS/STING activation and proinflammatory cytokines in the heart (Figures 6A–C). In addition, ageing mice displayed improved cardiac contraction and Serca2 abundance in the heart after restoring Vsig4⁺ macrophages (Figures 6D–G). Therefore, these data demonstrate that restoration of the Vsig4⁺ macrophage population is an efficient way to blunt microbial DNA-induced heart dysfunction in ageing mice.

Discussion

In this study, we have assessed the effects of microbial DNA enrichment on the development of ageing-associated cardiac

abnormalities. In specific, we find that the hearts of both ageing humans and mice harbor a robust abundance of bacterial DNA. The intestinal mEVs are readily translocated from gut lumen into the circulation and heart in ageing mice, whereas the intact gut barrier of healthy young mice prevents the leakage of intestinal mEVs. Ageing is accompanied by a significant reduction in the population of Vsig4⁺ macrophages which efficiently remove gut mEVs from the bloodstream. In the absence of Vsig4⁺ macrophages, enrichment of gut mEVs in the circulation by intravenous injection results in microbial DNA accumulation and inflammatory responses in cardiomyocytes of young Vsig4^{-/-} mice, concomitant with impaired calcium handling and cardiac contraction. In contrast, depletion of microbial DNA cargo diminishes these pathogenic effects of gut EVs on cardiac functions. The activation of cGAS/STING signaling is critical for the effects of microbial DNA, as demonstrated by non-significant changes in cardiac responses in both *in vivo* and *in vitro* experiments with cGAS or STING-KO mice after gut mEV treatment. We also demonstrate that restoring the Vsig4⁺ macrophage population remarkably decreases the levels of bacterial DNA and inflammatory responses in ageing mouse hearts, accompanied by an improvement in cardiac functions.

As one of the striking phenotypes of this study, both human and mouse hearts contained a great abundance of bacterial DNA, which was barely detected in healthy young hearts. In addition, ageing bloodstream was enriched with bacterial DNA. Previous studies have suggested that microbiota could be the origins of bacterial DNA accumulated in host tissues in the scenario of the impaired gut barrier, for example, obesity-induced gut leakage (23, 35, 36). Indeed, the 16s rRNA sequencing analysis indicates that the bacterial DNA profile in ageing hearts shares some similarities,

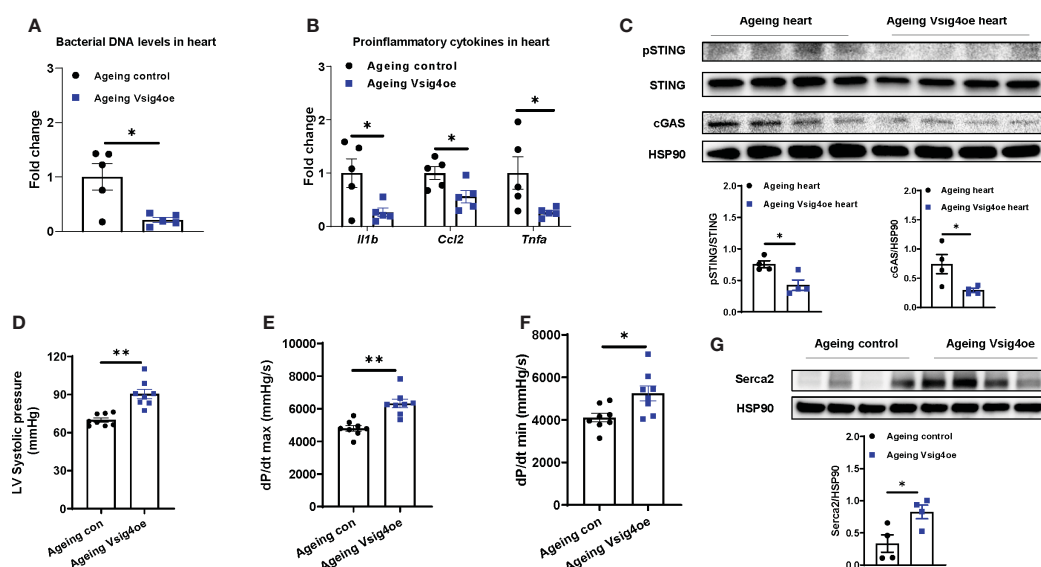


FIGURE 6

Restoring Vsig4⁺ macrophage population attenuates microbial DNA-induced cardiac abnormalities in ageing mice. The levels of bacterial DNA (A) and proinflammatory genes (B) in the hearts of ageing mice after 2 wks of injection with lentivirus carrying deactivated Cas9-VPR (VP64, p65, and Rita) and gRNA-Vsig4 transcriptional start site (TSS; Vsig4oe). Control ageing mice were injected with lentivirus carrying deactivated Cas9-VPR only. After recovery of Vsig4 expression, the levels of cGAS/STING activation (C), left ventricular systolic pressure (D), maximal rate of rise of left ventricular pressure (E), maximum rate of ventricular pressure decrease (F), and Serca2 abundance (G) in the hearts of ageing mice were measured. Data are presented as mean \pm SEM. * P < 0.05, ** P < 0.01, Student's *t*-test.

for example, phylum *Firmicutes*, with the microbiome composition in ageing ileum section. The microbiota in other intestinal sections may also contribute to the microbial DNA accumulation in ageing heart. It would be interesting to evaluate whether circulating bacterial DNA species could be related to the development of ageing-associated abnormalities. In addition, gut barrier breach occurs in both ageing humans and mice (12), thus likely allowing the leakage of microbiota-derived products into host circulation and distant organs. The impairment of ageing-related gut barrier functions could be due to reduced mucus thickness and functions and abnormal intestinal structure (22, 37, 38). In concordance with these earlier findings, we also observed decreased IgA abundance and impaired gut barrier structure. Previous studies have demonstrated that, in the context of obesity-induced gut leakage, microbiota-derived mEVs are readily translocated into the host bloodstream and various tissues (23, 26, 27). Consistently, we found that the ageing mouse gut barrier did not efficiently block the leakage of gut mEVs, as evidenced by strong red fluorescent signals in the hearts after an injection of PKH26-labeled gut EVs into the ileum section of ageing WT mice. With respect to the manners in which gut mEVs interact with target cells, several mechanisms, including integrin-dependent tropism and endocytosis, have been implicated (39, 40). However, how microbiota-derived EVs enter host cells is still unknown.

In addition to the protection of the gut barrier, the complement immune system plays critical roles in cleaning up bacterial products from the bloodstream in both humans and mice (25, 41). *Vsig4*⁺ macrophages are important components of the host complement immunity (25). Previous studies have demonstrated that *Vsig4*⁺ macrophages can prevent the spread of gut mEVs into host tissues (23). While *Vsig4*⁺ macrophages mainly reside in the liver, we also found that a portion of cardiac macrophages was *Vsig4* positive in the young heart. In the young KCKO mouse models, an intravenous injection of gut mEVs did not efficiently infiltrate into hearts, suggesting the protective roles of cardiac *Vsig4*⁺ macrophages. However, we found that the population of *Vsig4*⁺ macrophages in both liver and heart was diminished in ageing humans and mice. It has been reported that the impairment in NAD homeostasis and metabolism contributes to the functional abnormalities of ageing macrophages (14, 30, 42). In our studies, we also observed a significant reduction in the expression of key enzymes involving the NAD salvage pathway in ageing KCs and cardiac macrophages. In addition, supplementation of NMN restored *Vsig4* expression in ageing macrophages, suggesting the importance of NAD homeostasis for macrophages to maintain *Vsig4* abundance. The beneficial effects of NAD homeostasis or *Vsig4*⁺ macrophage restoration should be further validated *in vivo* in both ageing humans and mice. Interestingly, in 2 years old chromogranin A deficient mice, liver *Vsig4* abundance were greater than WT ageing mice, accompanied by less bacterial DNA abundance and remarkable reduction in bacterial DNA-induced inflammation (43). A previous study by Hall et al. observed an increase in *Vsig4*⁺ cell population in the fat pad of ageing mice (44). The discrepancy in *Vsig4* abundance in ageing liver, fat, and heart may be attributed to the distinct tissue microenvironment.

Ageing heart is characterized by elevated inflammatory responses, which result in impaired cardiac contractility (19, 45). In this study, we have shown that the treatment of gut mEVs in young *Vsig4*^{-/-} mice led to the accumulation of microbial DNA in cardiomyocytes, concomitant with an elevated cellular inflammatory response and reduced contractility. In contrast, depletion of microbial DNA cargo abolished these effects of gut EVs, thus demonstrating the pathogenic roles of microbial DNA in inducing ageing-associated cardiomyocyte inflammation and abnormal contraction. In line with the importance of cGAS/STING signaling activation on the ability of microbial DNA in host cells (31, 32), knockout of either cGAS or STING minimized the pathogenic effects of microbial DNA accumulation on cardiac myocyte responses. Previous studies have shown that cellular senescence is a causal factor driving ageing-related cardiac inflammation (46, 47). However, the connection between the microbial DNA-induced cGAS/STING activities and the incidence of cellular senescence in cardiac myocytes is still unclear. We also observed that microbial DNA accumulated in other cell types in the ageing heart. The effects of microbial DNA on these non-cardiomyocyte cell responses would be explored in future studies.

In summary, we find that microbial DNA is transported by EVs from the gut lumen into distant cardiomyocytes in the context of ageing, resulting in elevated cardiac inflammation and contractility defects. *Vsig4*⁺ macrophages in both the liver and heart are critical to prevent microbial DNA accumulation in cardiomyocytes, whereas ageing macrophages display a significant reduction in *Vsig4* expression. Recovery of *Vsig4* expression effectively attenuates the pathogenic impacts of microbial DNA on cardiac functions in ageing mice. Based on these studies, we suggest a new mechanism whereby microbial DNA accumulation induces cardiac inflammation and decreased contractility in ageing.

Methods

Animal care and use

cGAS^{-/-} (Stock No. 026554) Sting-flox (Stock No. 031670), iDTR (Stock No. 007900; Cre-inducible expression of diphtheria toxin receptor), Myh6-Cre (Stock No. 011038), Clec4f-Cre (Stock No. 033296) mice were received from the Jackson Laboratory. *Vsig4*^{-/-} mice (C57BL/6J-*Vsig4*^{em1Smoc}) were received from Shanghai model organisms. *Vsig4* wild-type (WT) mice were produced by crossing *Vsig4* heterozygous mice together. Ageing mice used in these studies were 100–108 wks old, and young mice were 8–12 wks old. To block *Vsig4* function, young Myh6Cre⁺Sting^{fl/fl} male mice were injected with purified *Vsig4* antibodies before gut mEV treatment, through tail vein injection. All mice were maintained on a 12/12 hr light-dark cycle. All animal procedures were performed in accordance with the University of California, San Diego Research Guidelines for the Care and Use of Laboratory Animals, and all animals were randomly assigned to cohorts when used.

EV purification and characterization

The intestinal EVs were prepared from small intestine lumen contents of ageing WT mice with sterile tools. Debris and dead cells in the lumen contents were removed by centrifugation at 1,000 x g for 10 min and then passed through a 0.2 μ m filter. Then, the supernatant was added with a mixture of antibiotics (0.5 mg/mL vancomycin HCl, 1 mg/mL ampicillin sodium salt, 1 mg/mL metronidazole, 1 mg/mL neomycin sulfate, and 1mg/mL gentamycin sulfate; Sigma) and then ultracentrifuged at 100,000 x g for 4 hours at 4°C with a Type 70 Ti fixed-angle rotor (Beckman Coulter). The EV-containing pellet was resuspended in 1 mL of sterile PBS and passed through a 0.2 μ m filter to remove large particles in a sterile hood. The particle size and concentration of intestinal EVs were detected by NanoSight analysis (Malvern Instruments).

Red fluorescent dye PKH26-labeled gut mEVs

PKH26 fluorescent dye using the PKH26 fluorescent cell linker kit (Cat. No. PKH26GL-1KT, Sigma). After PKH26 staining, the EVs were washed with sterile PBS and collected by ultracentrifugation (100,000 x g for 2 hours) at 4°C. Finally, PKH26 labeled EVs were resuspended in sterile PBS and passed through a 0.2 μ m filter.

In vivo EV trafficking assays

PKH26-labeled EVs (5×10^9 EVs per mouse) were delivered to either young or ageing WT recipient mice through injection into the ileum section. After anesthetized, the ileum section was exposed through making a small incision at the abdominal area, and then 150 μ L of saline containing EVs were injected into ileum. Following closure of incisions, sites will be treated with 10% povidone-iodine solution. After 16 hours of injection, hearts were collected to detect PKH26 red fluorescent signals.

Jugular vein cannulation and antibody injection

Mice will be anesthetized with ketamine (25 mg/kg), acepromazine (1 mg/kg) and xylazine (2 mg/kg) via intramuscular injection. Incision sites will be shaved and cleaned with isopropyl alcohol and a 10% povidone-iodine solution. The right jugular vein will be cleared of surrounding tissue and a sterilized dual microrethane catheter (Type MRE-025) filled with heparinized saline (100 U/mL) will be inserted ~1 cm into vessel and secured with double silk ligatures. Catheter ends will then be tunneled subcutaneously to the mid-scapular region, externalized, placed in a protective silastic tubing (0.18 cm), and sutured to the skin. Following closure of incisions, sites will be treated with 10% povidone-iodine solution and animals will be given 1cc 0.9% sterile

saline subcutaneously for rehydration. Lidocaine (2.5%) will be administered twice a day for 5 days post-surgery. To block the function of Vsig4+ macrophage in hearts, Vsig4 antibodies (0.5 mg/ml) were injected into heart through the jugular vein catheter. Control mice were injected with IgG antibodies. After 24 hours, PKH26-labeled gut mEVs (5×10^8 EVs/mouse) were injected into the jugular vein catheter of these antibodies-treated mice.

In vivo FITC dextran assay

Mice were fasted for 6 hours and then orally gavaged with FITC dextran (600mg/Kg body weight; Sigma) from a 125mg/mL solution (48, 49). Plasma samples were collected after 1 hour FITC dextran treatment and used to measure the intensity of FITC by fluorescence spectroscopy (excitation at 485nm and emission at 535nm) relative to a linear standard curve made using diluted FITC dextran solution in plasma from untreated mice.

Depletion of microbial DNA cargo from gut EVs

The isolated gut EVs from ageing WT mice were resuspended in sterile PBS. Then, as previously described (23, 50–52), these EVs were loaded into a Gene Pulser/micropulser Cuvettes (Bio-Rad) for electroporation (GenePulser Xcell electroporator, Bio-Rad) and treated with DNase I (300U) for 30 mins, 37°C.

Isolation of adult ventricular cardiomyocytes

Calcium-tolerant adult cardiomyocytes were isolated from ventricular tissue of mice by standard enzymatic digestion (53, 54). Briefly, isolated hearts were perfused using a Ca^{2+} -free Tyrode solution containing (in mM) 126 NaCl, 4.4 KCl, 1.2 MgCl_2 , 0.12 NaH_2PO_4 , 4.0 NaHCO_3 , 10 HEPES, 30 2,3-butanedione monoxime, 5.5 glucose, 1.8 pyruvate, and 5.0 taurine (pH 7.3) for 5 min, followed by 0.9–1.0 mg/mL collagenase (type II, Worthington) for 20 min. Hearts were transferred to tubes containing fresh collagenase for an additional 10 min in a 37°C water bath. The heart tissue was mechanically dispersed and rinsed with gradually increasing extracellular calcium to 1 mM. The cells were plated on 24×50 -mm, No. 1 glass coverslips coated with laminin.

Invasive hemodynamic measurements

After anesthetized and endotracheal intubation, mice were connected to a volume-cycled rodent ventilator. The anterior neck and abdomen were shaved. A subcostal incision was performed in the abdomen. The diaphragm was incised by a transverse substernal approach leaving the pericardium intact. The left ventricle was entered through an apical stab with a 25 1/2 G needle, followed immediately by a 1F Millar conductance-

micromanometer (Millar Instruments). The catheter was positioned in the left ventricle and monitored to verify correct placement. Pressure recordings were obtained and analyzed to obtain left ventricular pressure (LVP), rate of contraction (dP/dt max) and rate of relaxation (dP/dt min).

Contractility measurements *in vitro*

Cardiac myocyte (CM) contractility is measured with a state-of-the-art integrated myocyte contractility workstation (IonOptix LLC). This method combines brightfield imaging with a high-speed camera recording system, along with sarcomere and cell-length detection algorithms, and application-specific analysis software to output reliable quantification of cardiomyocyte contractile function at the sarcomere level. Analysis outputs include determination of $\pm\Delta L/\Delta t$ (dL/dt), representing peak shortening/relengthening velocities, and percent shortening for both sarcomere and cell length. CM contractility was measured after 36 hours of treatment with gut EVs.

In vitro assays with Kupffer cells

KCs (Clec4f⁺F4/80⁺) isolated from ageing WT mice were seeded in a 24-well plate (0.5x10⁵/well) and cultured with nicotinamide mononucleotide (NMN; 1mM). After 24 hours, cells were used for qPCR assays.

16s rRNA sequencing and bioinformatics analysis

Bacterial DNA was isolated from ileum lumen content and heart samples using the ZymoBIOMICS DNA extraction kits. Bacterial 16s ribosomal RNA gene targeted sequencing was performed using the Quick-16STM NGS Library Pre Kit (Zymo Research). The bacterial 16s primers amplified the V3-V4 region of the 16s rRNA gene. The final PCR products were quantified with qPCR fluorescence readings and pooled together based on equal molarity. The final pooled library was cleaned with the Select-a-Size DNA Clean & ConcentratorTM (Zymo Research), then quantified with TapeStation[®] (Agilent Technologies) and Qubit[®] (Thermo Fisher). The final library was sequenced on an Illumina MiSeq with a v3 reagent kit (600 cycles). The sequencing was performed with 10% PhiX spike-in. For bioinformatics analysis, unique amplicon sequences variants were inferred from raw reads using the DADA2 pipeline (55). Potential sequencing errors and chimeric sequences were also removed with the DADA2 pipeline. Chimeric sequences were also removed with the DADA2 pipeline. Taxonomy assignment was performed using Uclust from Qiime v.1.9.1 with the Zymo Research Database, a 16s database that is internally designed and curated. Composition visualization, alpha-diversity, and beta-diversity analysis were performed with Qiime v.1.9.1 (56). If applicable, a taxonomy that has significant abundance among different groups was identified by LEfSe using default settings (57).

Sequencing raw data supporting these studies can be found in the Sequence Read Archive database under accession number PRJNA859808.

Kupffer cell-depleted (KCKO) mice

To deplete Kupffer cells, diphtheria toxin (DT) was intraperitoneally (i.p.) injected into Clec4fCre⁺DTR⁺ lean mice (crossbreeding Clec4fCre mice and iDTR mice) daily for three days (200 ng/mouse). Thereafter, these mice were injected with DT (200 ng/mouse) every two days to prevent KC recovery (26).

CRISPR-Cas9 system for transcriptional activation

Plasmids containing deactivated Cas9-VPR (VP64, p65, and Rta) system (Cat. No. CAS11915) or guide RNA for Vsig4 TSS (Cat. No. GSGM11893-247477006) were obtained from Horizon Discovery (58–60). The lentivirus packing these plasmids were prepared by the UCSD Vector core. 100wks old ageing WT mice were intravenously injected with these lentiviruses (1x10⁸ particles/mouse). Control mice were treated with lentivirus containing dCas9-VPR only. After 2 wks, Vsig4 expression in livers and hearts was evaluated by Western blot analysis.

In vivo antibiotic treatment

Ageing WT mice (100–108wks old) were subject to oral gavage (twice per week; 200 μ L per mouse) with a mixture of broad-spectrum antibiotics (0.5 mg/mL vancomycin HCl, 1 mg/mL ampicillin sodium salt, 1 mg/mL metronidazole, 1 mg/mL neomycin sulfate, and 1mg/mL gentamycin sulfate; Sigma) (48). Control mice were treated with water alone. The ageing WT mice in the antibiotic withdrawal group were fed ad libitum without antibiotic treatment for another 2 wks.

Quantification of bacterial DNA using real-time PCR

Bacterial DNA was assessed by qPCR using a Femto Bacterial DNA Quantification Kit by following the manufacturer's instructions. Briefly, Bacterial DNAs were extracted from cells, tissues, or plasma samples using the ZymoBIOMICS DNA extraction kits according to the manufacturer's instructions. The concentration of bacterial DNA in each sample was calculated from the standard curve.

Immunofluorescence staining

Mouse hearts were snap frozen in optimum cutting temperature (O.C.T., Fisher Healthcare) with dry ice. Tissue cryo-sections were

prepared and fixed with pre-cold acetone for 20 min. Slides were blocked with 5% normal donkey serum for 60 min at RT. Then, the samples were incubated with antibodies diluted 1:100 in PBS at 4°C overnight. After washing, nuclei were stained with DAPI (4',6-Diamidino-2-28 phenylindole dihydrochloride) for 10 min at room temperature. Mounting media and coverslips were then added to slides for imaging. Images were acquired on a Keyence Fluorescent Microscope and were processed with ImageJ (NIH, Bethesda, MD).

RNAscope *in situ* hybridization combined with immunofluorescence

We performed RNAscope ISH to detect 16s rRNA. Mouse hearts were frozen in O.C.T with dry ice. Human heart sample information is presented in [Table S3](#). Tissue sections were fixed with 4% PFA for 15 min at 4°C and then dehydrated with 50%, 70%, and 100% ethyl alcohol gradients for 5 min each at room temperature. Next, tissue sections were treated with hydrogen peroxide and protease IV at room temperature for 10 min each. 16s RNA probes (Cat. No. 464461, Advanced Cell Diagnostics) were then added for 2 hours at 40°C. Signal amplification and detection reagents were applied sequentially and incubated in AMP 1, AMP 2, AMP 3, HRP-C1 (RNAscope® Multiplex fluorescent reagent kit v2, Cat. No. 323100, Advanced Cell Diagnostics), Opal 520 (Cat. No. PNFP1487001KT, Akoya Biosciences), or Opal 690 (Cat. No. FP1497001KT, Akoya Biosciences). Then, slides were immediately processed for immunofluorescence, and images were taken with a Leica SP8 Confocal microscope.

Flow cytometry analysis

The liver and heart were perfused to get single cells which were then stained with fluorescence-tagged antibodies. KCs were CD45⁺Clec4f⁺F4/80⁺ cells, and cardiac macrophages were CD45⁺CD11b⁺F4/80⁺ cells. These cells were analyzed by an MA900 flow cytometer (SONY). Data were analyzed using Flowjo software. Clec4f (Cat. No. 156804), F4/80 (Cat. No. 123114), CD11b (Cat. No. 101235), and CD45 (Cat. No. 103116) antibodies were received from Biolegend, and Vsig4 antibody (Cat. No. 17-5752-82) was from ThermoFisher Scientific. The concentration of antibodies (0.25 µg per 10⁶ cells) for sample staining were used.

Quantitative reverse transcriptase-polymerase chain reaction analysis

Total RNA was extracted using the RNA extraction protocol according to the manufacturer's instructions. cDNA was synthesized using MultiScribe Reverse Transcriptase and random primers (High-capacity cDNA reverse transcription kit, Cat. No. 4368813, ThermoFisher Scientific). qPCR was carried out in 10 µl reactions using iTaq SYBR Green supermix (Cat. No. 172-5125, Bio-Rad) on a StepOnePlus Real-Time PCR Systems (ThermoFisher Scientific). The data presented correspond to the

mean of 2-ΔΔCt from at least three independent experiments after being normalized to β-actin.

Western blot analysis

Cells or tissues were homogenized in 1x RIPA buffer supplemented with protease and phosphatase inhibitors. Equal amounts of cell lysate proteins (30 µg protein per lane for detection) from each biological replicate were subjected to western blotting. Using the ChemiDoc XRS imaging system (BioRad), the protein bands on blots were detected with the SuperSignal West Pico Chemiluminescent Substrate (Cat. No. 34077, ThermoFisher Scientific). Protein bands were analyzed using Image Lab software (BioRad). We normalized phosphorylated protein to total protein bands or normalized protein expression to housekeeping protein bands. Western blot data in figures and supplemental figures are all representatives of more than three independent experiments. pSTING (Cat. No. 72971), STING (Cat. No. 50494), cGAS (Cat. No. 316595), and Serca2 (Cat. No. 4388S) antibodies were bought from Cell Signaling Technology. Vsig4 antibody (Cat. No. 17-5752-82) was obtained from ThermoFisher Scientific. All primary antibodies were diluted at 1:1000.

Lentivirus production

Production of lentivirus vectors: HIV1-based lentivirus vectors were produced by transient co-transfection of 293T cells maintained in Dulbecco's modified Eagle's medium (DMEM) with 10% FCS. 293T cells in ten 150 mm dishes were co-transfected by the polyethyleneimine method with gRNA vector plasmid, pLP1 (gal-pol) and pLP2 (Rev) (Invitrogen), and pCMV-G (61). Conditioned media on day 1, 2, and 3 post-transfection were collected, filtered through a 0.45 µm filter, and concentrated by centrifugation at 7000 rpm for 16 hours at 4°C with Sorvall GS-3 rotor. The resulting pellets were resuspended with buffer containing 10 mM Tris HCl, pH 7.8, 1 mM MgCl₂, and 3% sucrose. Titering of HIV1 vectors by real-time Q-PCR: HIV1-CMV-GFP vector (1x10⁹ iu/mL) was used as the standard. HEK293 cells in a 6-well plate were infected with different amounts of viruses in the presence of polybrene (4 µg/mL). Infected cells were passaged once every 4 days and cell DNAs were prepared on day 14 post-infection by the DNeasy Blood & Tissue kit (Qiagen Science, MD). Real-time Q-PCR was performed using a primer set selected from the WPRE sequence.

Statistical analysis

To assess whether the means of two groups are statistically different from each other, an unpaired two-tailed Student's *t*-test was used for statistical analyses using Prism8 software (GraphPad software v8.0; Prism, La Jolla, CA). *P* values of 0.05 or less would be considered to be a significant difference. Degrees of significance was indicated in each of the figure legends.

Data availability statement

The datasets presented in this study can be found in online repositories. The names of the repository/repositories and accession number(s) can be found below: PRJNA859808 (SRA).

Ethics statement

The animal study was reviewed and approved by University of California, San Diego Research Guidelines for the Care and Use of Laboratory Animals.

Author contributions

WY and JS designed the studies and HG, KW, and JAS performed most of the experiments. ZJ, AF, TT, YT, BT, HJ, JK, assisted with mouse genotyping and tissue collection. KR performed jugular vein cannulation. ZL assisted with ISH staining. SM helped with EM and imaging. WD, JS, and WY supervised the project. HG, KW, JAS, WD, JS, and WY analyzed and interpreted the data, and HG, JAS, JS, and WY wrote the manuscript. All authors contributed to the article and approved the submitted version.

Funding

This study was funded by the UCSD School of Medicine Microscopy Core grant (P30 NS047101), the Department of Veterans Affairs Merit Review grant (I01 BX003934 to SM), and

the U.S. National Institutes of Health awards (R00DK115998, R21HD107516, and R01DK125560 to WY).

Acknowledgments

We thank Jennifer Santini for the confocal microscope analysis; the UCSD vector core for lentivirus preparation.

Conflict of interest

The authors declare that the research was conducted in the absence of any commercial or financial relationships that could be construed as a potential conflict of interest.

Publisher's note

All claims expressed in this article are solely those of the authors and do not necessarily represent those of their affiliated organizations, or those of the publisher, the editors and the reviewers. Any product that may be evaluated in this article, or claim that may be made by its manufacturer, is not guaranteed or endorsed by the publisher.

Supplementary material

The Supplementary Material for this article can be found online at: <https://www.frontiersin.org/articles/10.3389/fimmu.2023.1216344/full#supplementary-material>

References

1. Curtis LH, Whellan DJ, Hammill BG, Hernandez AF, Anstrom KJ, Shea AM, et al. Incidence and prevalence of heart failure in elderly persons, 1994–2003. *Arch Intern Med* (2008) 168(4):418–24. doi: 10.1001/archinternmed.2007
2. Roger VL, Go AS, Lloyd-Jones DM, Benjamin EJ, Berry JD, Borden WB, et al. Heart disease and stroke statistics–2012 update: a report from the American heart association. *Circulation* (2012) 125(1):e2–e220. doi: 10.1161/CIR.0b013e31823ac046
3. Mosterd A, Hoes AW. Clinical epidemiology of heart failure. *Heart* (2007) 93(9):1137–46. doi: 10.1136/hrt.2003.025270
4. Benjamin EJ, Muntner P, Alonso A, Bittencourt MS, Callaway CW, Carson AP, et al. Heart disease and stroke statistics–2019 update: a report from the American heart association. *Circulation* (2019) 139(10):e56–e528. doi: 10.1161/CIR.0000000000000659
5. Solomon SD, Anavekar N, Skali H, McMurray JJV, Swedberg K, Yusuf S, et al. Influence of ejection fraction on cardiovascular outcomes in a broad spectrum of heart failure patients. *Circulation* (2005) 112(24):3738–44. doi: 10.1161/CIRCULATIONAHA.105.561423
6. Franceschi C, Bonafè M, Valensin S, Olivieri F, De Luca M, Ottaviani E, et al. Inflamm-aging: an evolutionary perspective on immunosenescence. *Ann New York Acad Sci* (2000) 908(1):244–54. doi: 10.1111/j.1749-6632.2000.tb06651.x
7. Ferrucci L, Semba RD, Guralnik JM, Ershler WB, Bandinelli S, Patel KV, et al. Proinflammatory state, hepcidin, and anemia in older persons. *Blood* (2010) 115(18):3810–6. doi: 10.1182/blood-2009-02-201087
8. Cohen HJ, Pieper CF, Harris T, Rao KM, Currie MS. The association of plasma IL-6 levels with functional disability in community-dwelling elderly. *J Gerontol A Biol Sci Med Sci* (1997) 52(4):M201–8. doi: 10.1093/gerona/52a.4.m201
9. Newman AB, Sanders JL, Kizer JR, Boudreau RM, Odden MC, Hazzouri A, et al. Trajectories of function and biomarkers with age: the CHS all stars study. *Int J Epidemiol* (2016) 45(4):1135–45. doi: 10.1093/ije/dyw092
10. Ferrucci L, Fabbri E. Inflammageing: chronic inflammation in ageing, cardiovascular disease, and frailty. *Nat Rev Cardiol* (2018) 15(9):505–22. doi: 10.1038/s41569-018-0064-2
11. Walker KA, Basisty N, Wilson DM 3rd, Ferrucci L. Connecting aging biology and inflammation in the omics era. *J Clin Invest* (2022) 132(14):e158448. doi: 10.1172/JCI158448
12. Franceschi C, Garagnani P, Parini P, Giuliani C, Santoro A. Inflammaging: a new immune-metabolic viewpoint for age-related diseases. *Nat Rev Endocrinol* (2018) 14(10):576–90. doi: 10.1038/s41574-018-0059-4
13. Oishi Y, Manabe I. Macrophages in age-related chronic inflammatory diseases. *NPJ Aging Mech Dis* (2016) 2:16018. doi: 10.1038/npjamd.2016.18
14. Covarrubias AJ, Kale A, Perrone R, Lopez-Dominguez JA, Pisco AO, Kasler HG, et al. Senescent cells promote tissue NAD(+) decline during ageing via the activation of CD38(+) macrophages. *Nat Metab* (2020) 2(11):1265–83. doi: 10.1038/s42255-020-00305-3
15. Mogilenko DA, Shchukina I, Artyomov MN. Immune ageing at single-cell resolution. *Nat Rev Immunol* (2022) 22(8):484–98. doi: 10.1038/s41577-021-00646-4
16. Dai DF, Santana LF, Vermulst M, Tomazela DM, Emond MJ, MacCoss MJ, et al. Overexpression of catalase targeted to mitochondria attenuates murine cardiac aging. *Circulation* (2009) 119(21):2789–97. doi: 10.1161/CIRCULATIONAHA.108.822403
17. Picca A, Mankowski RT, Burman JL, Donisi L, Kim J, Marzetti E, et al. Mitochondrial quality control mechanisms as molecular targets in cardiac ageing. *Nat Rev Cardiol* (2018) 15(9):543–54. doi: 10.1038/s41569-018-0059-z
18. Schriener SE, Linford NJ, Martin GM, Treuting P, Ogburn CE, Emond M, et al. Extension of murine life span by overexpression of catalase targeted to mitochondria. *Science* (2005) 308(5730):1909–11. doi: 10.1126/science.1106653

19. Li H, Hastings MH, Rhee J, Trager LE, Roh JD, Rosenzweig A. Targeting age-related pathways in heart failure. *Circ Res* (2020) 126(4):533–51. doi: 10.1161/CIRCRESAHA.119.315889
20. Thevaranjan N, Puchta A, Schulz C, Naidoo A, Szamosi JC, Verschoor CP, et al. Age-associated microbial dysbiosis promotes intestinal permeability, systemic inflammation, and macrophage dysfunction. *Cell Host Microbe* (2017) 21(4):455–66.e4. doi: 10.1016/j.chom.2017.03.002
21. Parker A, Romano S, Ansorge R, Aboulnour A, Gall GL, Savva GM, et al. Fecal microbiota transfer between young and aged mice reverses hallmarks of the aging gut, eye, and brain. *Microbiome* (2022) 10(1):68. doi: 10.1186/s40168-022-01243-w
22. Sovran B, Hugenholtz F, Elderman M, Van Beek AA, Graversen K, Huijskes M, et al. Age-associated impairment of the mucus barrier function is associated with profound changes in microbiota and immunity. *Sci Rep* (2019) 9(1):1437. doi: 10.1038/s41598-018-35228-3
23. Luo Z, Ji Y, Gao H, Reis F, Bandyopadhyay G, Jin Z, et al. CRIG(+) macrophages prevent gut microbial DNA-containing extracellular vesicle-induced tissue inflammation and insulin resistance. *Gastroenterology* (2021) 160(3):863–74. doi: 10.1053/j.gastro.2020.10
24. Cerutti A, Rescigno M. The biology of intestinal immunoglobulin A responses. *Immunity* (2008) 28(6):740–50. doi: 10.1016/j.immuni.2008.05.001
25. Helmy KY, Katschke KJ Jr., Gorgani NN, Kljavin NM, Elliott JM, Diehl L, et al. CRIG: a macrophage complement receptor required for phagocytosis of circulating pathogens. *Cell* (2006) 124(5):915–27. doi: 10.1016/j.cell.2005.12.039
26. Gao H, Jin Z, Tang K, Ji Y, Suarez J, Suarez JA, et al. Microbial DNA enrichment promotes adrenomedullary inflammation, catecholamine secretion, and hypertension in obese mice. *J Am Heart Assoc* (2022) 11(4):e024561. doi: 10.1161/JAHA.121.024561
27. Gao H, Luo Z, Ji Y, Tang K, Jin Z, Ly C, et al. Accumulation of microbial DNAs promotes to islet inflammation and beta cell abnormalities in obesity in mice. *Nat Commun* (2022) 13(1):565. doi: 10.1038/s41467-022-28239-2
28. Fu W, Wojtkiewicz G, Weissleder R, Benoist C, Mathis D. Early window of diabetes determinism in NOD mice, dependent on the complement receptor CRIG, identified by noninvasive imaging. *Nat Immunol* (2012) 13(4):361–8. doi: 10.1038/ni.12233
29. Sakai M, Troutman TD, Seidman JS, Ouyang Z, Spann NJ, Abe Y, et al. Liver-derived signals sequentially reprogram myeloid enhancers to initiate and maintain kupffer cell identity. *Immunity* (2019) 51(4):655–70.e8. doi: 10.1016/j.immuni.2019.09.002
30. Minhas PS, Liu L, Moon PK, Joshi AU, Dove C, Mhatre S, et al. Macrophage *de novo* NAD(+) synthesis specifies immune function in aging and inflammation. *Nat Immunol* (2019) 20(1):50–63. doi: 10.1038/s41590-018-0255-3
31. Ahn J, Barber GN. STING signaling and host defense against microbial infection. *Exp Mol Med* (2019) 51(12):1–10. doi: 10.1038/s12276-019-0333-0
32. Ablasser A, Chen ZJ. cGAS in action: expanding roles in immunity and inflammation. *Science* (2019) 363(6431):eaat8657. doi: 10.1126/science.aat8657
33. Kelly RA, Smith TW. Cytokines and cardiac contractile function. *Circulation* (1997) 95(4):778–81. doi: 10.1161/01.cir.95.4.778
34. Klingenberg R, Luscher TF. Inflammation in coronary artery disease and acute myocardial infarction - is the stage set for novel therapies? *Curr Pharm Des* (2012) 18(28):4358–69. doi: 10.2174/138161212802481219
35. Oh TG, Kim SM, Caussy C, Fu T, Guo J, Bassirian S, et al. A universal gut-Microbiome-Derived signature predicts cirrhosis. *Cell Metab* (2020) 32(5):878–888. doi: 10.1016/j.cmet.2020.06.005
36. Ortiz S, Zapater P, Estrada JL, Enriquez P, Rey M, Abad A, et al. Bacterial DNA translocation holds increased insulin resistance and systemic inflammatory levels in morbid obese patients. *J Clin Endocrinol Metab* (2014) 99(7):2575–83. doi: 10.1210/jc.2013-4483
37. Elderman M, Sovran B, Hugenholtz F, Graversen K, Huijskes M, Houtsma E, et al. The effect of age on the intestinal mucus thickness, microbiota composition and immunity in relation to sex in mice. *PLoS One* (2017) 12(9):e0184274. doi: 10.1371/journal.pone.0184274
38. Moorefield EC, Andres SF, Blue RE, Van Landeghem L, Mah AT, Santoro MA, et al. Aging effects on intestinal homeostasis associated with expansion and dysfunction of intestinal epithelial stem cells. *Aging (Albany NY)* (2017) 9(8):1898–915. doi: 10.18632/aging.101279
39. Isaac R, Reis FCG, Ying W, Olefsky JM. Exosomes as mediators of intercellular crosstalk in metabolism. *Cell Metab* (2021) 33(9):1744–62. doi: 10.1016/j.cmet.2021.08.006
40. Hoshino A, Costa-Silva B, Shen TL, Rodrigues G, Hashimoto A, Mark MT, et al. Tumour exosome integrins determine organotropic metastasis. *Nature* (2015) 527(7578):329–35. doi: 10.1038/nature15756
41. Reis ES, Mastellos DC, Hajishengallis G, Lambris JD. New insights into the immune functions of complement. *Nat Rev Immunol* (2019) 19(8):503–16. doi: 10.1038/s41577-019-0168-x
42. Pajuelo D, Gonzalez-Juarbe N, Tak U, Sun J, Orihuela CJ, Niederweis M. NAD(+) depletion triggers macrophage necroptosis, a cell death pathway exploited by mycobacterium tuberculosis. *Cell Rep* (2018) 24(2):429–40. doi: 10.1016/j.celrep.2018.06.042
43. Liu MA, Shahabi S, Jati S, Tang K, Gao H, Jin Z, et al. Gut microbial DNA and immune checkpoint gene Vsig4/CRIG are key antagonistic players in healthy aging and age-associated development of hypertension and diabetes. *Front Endocrinol (Lausanne)* (2022) 13:1037465. doi: 10.3389/fendo.2022.1037465
44. Hall BM, Gleiberman AS, Strom E, Krasnov PA, Fresco D, Vujcic S. Immune checkpoint protein Vsig4 as a biomarker of aging in murine adipose tissue. *Aging Cell* (2020) 19(10):e13219. doi: 10.1111/acer.13219
45. Liberale L, Montecucco F, Tardif JC, Libby P, Camici GG. Inflamm-aging: the role of inflammation in age-dependent cardiovascular disease. *Eur Heart J* (2020) 41(31):2974–82. doi: 10.1093/eurheartj/ehz961
46. Lewis-McDougall FC, Ruchaya PJ, Domenjo-Vila E, Teoh TS, Prata L, Cottle BJ, et al. Aged-senescent cells contribute to impaired heart regeneration. *Aging Cell* (2019) 18(3):e12931. doi: 10.1111/acer.12931
47. Walaszczyk A, Dookun E, Redgrave R, Taul-Chalot S, Victorelli S, Spyridopoulos I, et al. Pharmacological clearance of senescent cells improves survival and recovery in aged mice following acute myocardial infarction. *Aging Cell* (2019) 18(3):e12945. doi: 10.1111/acer.12945
48. Wollam J, Riopel M, Xu YJ, Johnson AM, Ofrecio JM, Ying W, et al. Microbiota-produced n-formyl peptide fMLF promotes obesity-induced glucose intolerance. *Diabetes* (2019) 68(7):1415–26. doi: 10.2337/db18-1307
49. Johnson AM, Costanzo A, Gareau MG, Armando AM, Quehenberger O, Jameson JM, et al. High fat diet causes depletion of intestinal eosinophils associated with intestinal permeability. *PLoS One* (2015) 10(4):e0122195. doi: 10.1371/journal.pone.0122195
50. Lamichhane TN, Raiker RS, Jay SM. Exogenous DNA loading into extracellular vesicles via electroporation is size-dependent and enables limited gene delivery. *Mol Pharmacol* (2015) 12(10):3650–57. doi: 10.1021/acs.molpharmaceut.5b00364
51. Lamichhane TN, Jay SM. Production of extracellular vesicles loaded with therapeutic cargo. *Methods Mol Biol* (2018) 1831:37–47. doi: 10.1007/978-1-4939-8661-3_4
52. Usman WM, Pham TC, Kwok YY, Vu LT, Ma V, Peng B, et al. Efficient RNA drug delivery using red blood cell extracellular vesicles. *Nat Commun* (2018) 9(1):2359. doi: 10.1038/s41467-018-04791-8
53. Suarez J, McDonough PM, Scott BT, Suarez-Ramirez A, Wang H, Fricovsky ES, et al. Sorcin modulates mitochondrial Ca(2+) handling and reduces apoptosis in neonatal rat cardiac myocytes. *Am J Physiol Cell Physiol* (2013) 304(3):C248–56. doi: 10.1152/ajpcell.00039.2012
54. Diaz-Juarez J, Suarez J, Cividini F, Scott BT, Diemer T, Dai A, et al. Expression of the mitochondrial calcium uniporter in cardiac myocytes improves impaired mitochondrial calcium handling and metabolism in simulated hyperglycemia. *Am J Physiol Cell Physiol* (2016) 311(6):C1005–C13. doi: 10.1152/ajpcell.00236.2016
55. Callahan BJ, McMurdie PJ, Rosen MJ, Han AW, Johnson AJA, Holmes SP. DADA2: high-resolution sample inference from illumina amplicon data. *Nat Methods* (2016) 13(7):581–3. doi: 10.1038/nmeth.3869
56. Caporaso JG, Kuczynski J, Stombaugh J, Bittinger K, Bushman FD, Costello EK, et al. QIIME allows analysis of high-throughput community sequencing data. *Nat Methods* (2010) 7(5):335–6. doi: 10.1038/nmeth.f.303
57. Segata N, Izard J, Waldron L, Gevers D, Miropolsky L, Garrett WS, et al. Metagenomic biomarker discovery and explanation. *Genome Biol* (2011) 12(6):R60. doi: 10.1186/gb-2011-12-6-r60
58. Cheng AW, Wang H, Yang H, Shi L, Katz Y, Theunissen TW, et al. Multiplexed activation of endogenous genes by CRISPR-on, an RNA-guided transcriptional activator system. *Cell Res* (2013) 23(10):1163–71. doi: 10.1038/cr.2013.122
59. Gilbert LA, Horlbeck MA, Adamson B, Villalta JE, Chen Y, Whitehead EH, et al. Genome-scale CRISPR-mediated control of gene repression and activation. *Cell* (2014) 159(3):647–61. doi: 10.1016/j.cell.2014.09.029
60. Konermann S, Brigham MD, Trevino AE, Joung J, Abudayeh OO, Barcena C, et al. Genome-scale transcriptional activation by an engineered CRISPR-Cas9 complex. *Nature* (2015) 517(7536):583–8. doi: 10.1038/nature14136
61. Yee JK, Miyanojara A, LaPorte P, Bouic K, Burns JC, Friedmann T. A general method for the generation of high-titer, pantropic retroviral vectors: highly efficient infection of primary hepatocytes. *Proc Natl Acad Sci U S A* (1994) 91(20):9564–8. doi: 10.1073/pnas.91.20.9564

Frontiers in Immunology

Explores novel approaches and diagnoses to treat immune disorders.

The official journal of the International Union of Immunological Societies (IUIS) and the most cited in its field, leading the way for research across basic, translational and clinical immunology.

Discover the latest Research Topics

[See more →](#)

Frontiers

Avenue du Tribunal-Fédéral 34
1005 Lausanne, Switzerland
frontiersin.org

Contact us

+41 (0)21 510 17 00
frontiersin.org/about/contact

